

BOOK OF ABSTRACTS

13th EARSeL

16 - 19 April 2024, València, Spain



EUROPEAN ASSOCIATION
OF REMOTE SENSING LABORATORIES



VNIVERSITAT
D VALÈNCIA



KEYNOTE SESSIONS

NEW VEGETATION PRODUCTS FROM IMAGING SPECTROSCOPY: PHYSICAL MEANING, QUANTITATIVE INFORMATION, UNCERTAINTIES AND VALIDATION

Jose F. Moreno

Faculty of Physics, University of Valencia, 46100 Burjassot, Valencia, Spain – Jose.Moreno@uv.es

Advanced scientific usage of satellite vegetation products in global models of carbon and water cycles, and climate models with improved predictive capabilities, as well as the usage of vegetation products in emerging applicators (precision agriculture, food security, phenotyping, biodiversity) are demanding new vegetation products that can provide the necessary inputs. Such new products must satisfy four main characteristics: have a precise physical meaning, represent quantitative well-defined information, have quantitative estimates of uncertainties and be subject to a systematic rigorous validation. Among the new products recently introduced, or to be soon available from new satellite systems are: chlorophyll fluorescence emission spectrum, decomposition of light absorption by elementary pigments, dynamical changes in leaf pigments with stress adaptations and energy dissipation cycles (xanthophylls), plus more precise quantification of biochemical constituents and more precise structural information, and high-level products such as actual photosynthetic (electron transport) rates and vegetation stress indicators (potential versus actual photosynthesis, photoprotection adaptations, non-photochemical energy dissipation). The combined usage of such products in dynamical models of vegetation will also allow derivation of improved estimates of carbon assimilation (Gross Primary Productivity) and evapotranspiration rates, with an explicit coupling of dynamical effects in the combined energy-water-carbon cycles.

Among the different new products mentioned above, the chlorophyll fluorescence emission deserves special interest as new type of information, particularly when the full spectral emission is available, with direct implications for improvements in the modelling of photosynthesis light reactions and quantitative estimation of stress effects reducing photosynthetic capacity.

The possibility to derive such new type of information, in a consistent and systematic manner from satellite data with global coverage, will be made possible with several new satellite systems currently under development, in particular the Fluorescence Explorer (FLEX) mission, but also exploiting in parallel ESA Copernicus Sentinel systems, like Sentinel-2/3 and CHIME, and other satellite systems.

All such new vegetation products are not yet operative, some are more mature and some are still in an early state of prototype development. Then, it is very important to provide each product with a proper estimate of the corresponding uncertainties, with explicit confidence intervals, using the corresponding statistical distribution for each product. Special care is put in deriving the corresponding uncertainties at each processing step and propagating the uncertainties from one step to the next by using the full covariance matrices. Explicit separation of systematic and random uncertainties are considered at each processing step and separately propagated in the derivation of the final uncertainties. This strategy is relevant for all users and applications, but results of special interest for those applications exploiting data assimilation into dynamical models of land processes, which is one of the key targets for all such developments. A proper, quantitative, and statistically sound validation of such new vegetation products has to be developed, where the associated uncertainties in satellite products and field data are consistently considered.

A complete set of activities are taking place to provide the new products in an operational manner in the coming years, opening new perspectives towards science and applications.

Assessing the State of Aquatic Ecosystems with 5 Years of PRISMA Observations

Claudia Giardino

¹ National Research Council, Institute for Electromagnetic Sensing of the Environment, Italy

Keywords (5): PRISMA, atmospheric correction, validation, hyperspectral water reflectance, aquatic ecosystems

Abstract

Hyperspectral technology has led to a giant leap in the field of remote sensing. The increasing demand for hyperspectral images across the globe and their adoption in several research applications has raised their visibility. For the large thematic domain dealing with research and applications for aquatic ecosystems, imaging spectrometry offers clear advantages due to the narrow spectral features that water components cause on observed reflectance. The availability of a contiguous spectrum makes algorithms more effective in a wide variety of waters with varying water column depths and bottom reflectance and lead to more successful retrieval of a larger number of properties to derive meaningful information of aquatic ecosystems conditions.

Since several decades, imaging spectroscopy have been used for aquatic ecosystem mapping for the retrieval of parameters describing water quality, aquatic vegetation diversity, floating matter and benthic substrate types. Following the launch of Hyperion, a new generation of spaceborne hyperspectral sensors is now available (e.g., EnMAP) for improving water resources monitoring, while future missions are also under development (e.g., CHIME). Along with such class of hyperspectral missions, typically covering the 400-2500 nm wavelength range with a spatial detail of about 30 m, other missions as PACE for oceans or FLEX for terrestrial vegetation are going to provide novel data for observing aquatic ecosystems status and health.

In such a context, this contribution aims to review the exploitation of data gathered from the PRecursore IperSpettrale della Missione Applicativa (PRISMA), after 5 years of operation for studying aquatic ecosystems. To the aim, an overview of standard PRISMA products at 30 m spatial resolution, including both top-of-atmosphere radiance and bottom-of-atmosphere reflectance is presented along with the common challenges of remote sensing of water quality, such as the non-covarying water constituents, adjacent effects and the complexity of the atmosphere. The contribution then focuses on the community efforts for developing and testing ad-hoc procedures for correcting PRISMA data by atmospheric and adjacency effects, as well as for sun glint contamination. The results are evaluated against reference measurements of water reflectance, gathered from both in situ infrastructures and airborne campaigns acquired over globally distributed inland and marine waters. The developing and testing of algorithms for the estimation of water constituents, phytoplankton pigments diversity, bottom properties and floating matter, such as aquatic vegetation and scum, are then presented as use cases. These uses cases are presented thanks to the recent achievements of the hyperspectral water community for a variety of sites including rivers, lakes, artificial reservoirs, lagoons, estuaries and coastal waters, located both in Italy and at international sites. Finally, the synergistic use of PRISMA with different types of sensors is discussed to demonstrate the need for a multi-scale/multi-sensor approach for studying water resources and for developing applications of societal importance, such as the areas of water quality hazards and of regional biodiversity hot spots.

**Mapping and Monitoring Peatlands with
Spaceborne Imaging Spectroscopy Data –
Opportunities and Challenges**

Sebastian van der Linden

University of Greifswald, Germany, Partner in the Greifswald Mire Centre

Keywords: Imaging Spectroscopy, EnMAP, PRISMA, Peatland

Abstract

The new and upcoming spaceborne imaging spectroscopy missions offer new ways for analysing and monitoring terrestrial ecosystems. A better understanding of the processes related to ecosystem changes will contribute to a more sustainable land management and, hence, to climate change mitigation. Peatlands play an important role in the context of global climate change, but especially peatlands under agricultural land use are often overlooked in Earth observation research with regard to their role as carbon sink, storage or source. While intact peatlands are carbon sinks and represent an important carbon storage, peatland degradation leads to high carbon emissions, due to the mineralisation of the organic soil layer that is characteristic to the peatland. In Europe, for example, 50 % of the peatlands are degraded, especially through drainage, and contribute 5% of the total greenhouse gas emissions. Only the conservation of (near-) natural peatlands and the rewetting of degraded peatlands will lead to positive effects regarding climate change mitigation. Both, the conservation and the process of rewetting require detailed spatial information, e.g. on the vegetation composition or biomass, and a consistent monitoring, e.g. of vegetation drought periods or shrub encroachment. Time series of imaging spectroscopy data can support such mapping and monitoring and complement existing time series of multispectral or microwave data. However, especially the monitoring of rewetted peatlands and the processes of these novel ecosystems calls for new or adapted approaches for analysing the imaging spectroscopy time series. In this talk, a brief introduction into the role of peatlands within global climate change research is given, followed by an overview of peatland related imaging spectroscopy research in combination with other related Earth observation products. The talk concludes with ideas for next steps in bringing the newly available data and existing challenges together.

**Them.Sess. 1-1: Preparing for the
Copernicus Hyperspectral
Imaging Mission for the
Environment (CHIME)**

THE COPERNICUS HYPERSPECTRAL IMAGING MISSION FOR THE ENVIRONMENT (CHIME): CURRENT STATUS

[Marco Celesti](#)¹, Kevin Alonso², Valentina Boccia³, Laurent Despoisse⁴, Antonio Gabriele⁴, Ferran Gascon³, Nafiseh Ghasemi⁴, Claudia Isola⁴, Giuseppe Ottavianelli³, Anke Schickling³, Helene Strese⁴, Heidrun Weber⁴, Jens Nieke⁴

¹ HE Space for ESA - European Space Agency, European Space Research and Technology Centre (ESA-ESTEC), Noordwijk, The Netherlands

² RHEA for ESA - European Space Agency, European Space Research Institute (ESA-ESRIN), Frascati, Italy

³ European Space Agency, European Space Research Institute (ESA-ESRIN), Frascati, Italy

⁴ European Space Agency, European Space Research and Technology Centre (ESA-ESTEC), Noordwijk, The Netherlands

Keywords (5): Earth Observation, Imaging Spectroscopy, Copernicus, Agriculture, Raw materials

As part of the European Copernicus Programme, the Copernicus Hyperspectral Imaging Mission for the Environment (CHIME) will provide routine hyperspectral observations globally over land and coastal zones in support to European Union policies for the management of natural resources, ecosystem services and societal benefits. This unique visible-to-shortwave infrared spectroscopy-based observatory will provide key unique contributions in fulfilling user requirements in many domains including for example sustainable raw materials exploitation, resilient agriculture with a focus on soil protection and soil-health restoration, correct use of nutrients, effective water management, food security and the protection of biodiversity. By sampling many specific absorption features of the surface and the atmosphere, and by exploiting the information content of the full continuous VSWIR spectral signature, CHIME measurements and derived Level-2 products will be diagnostic for geophysical surface properties such as plant functional traits (e.g., nitrogen content, leaf water content), soil properties (e.g., soil organic carbon content) and minerals abundance (e.g., kaolinite). Moreover, several secondary applications will benefit from the routine provision of CHIME Level-1 and Level-2 products, e.g., coastal and inland water quality monitoring (e.g., phytoplankton pigments), methane and CO₂ emission detection from point sources, snow and ice light absorbing impurities. A thorough analysis of the user requirements as expressed by the Copernicus users has been performed since the early development stage of the mission. Building on that, a set of mission requirements for the space and ground segment traceable to these user needs has been defined by ESA and the CHIME Mission Advisory Group in the Mission Requirements Document (MRD).

For the development of the Space Segment Contract (Phase B2/C/D/E1) Thales Alenia Space (France) as Satellite Prime and OHB (Germany) as Instrument Prime were selected. Currently there are two satellites foreseen and each of the satellites will embark a HyperSpectral Instrument (HSI) which is a pushbroom-type grating Imaging Spectrometer with high Signal-to-Noise Ratio (SNR), high radiometric accuracy and data uniformity. HSI is characterised by a single telescope, and three single-channel

spectrometers covering each one-third of the total swath of ~130 km. Each spectrometer has then a single detector covering the entire spectral range from 400 to 2500 nm. With two satellites in orbit, the mission will provide global coverage of land and coastal areas every 11 days with a spatial resolution of 30 m (Figure 1). This baseline is compliant with the mission requirements defined in the MRD and traceable to the requirements expressed by the Copernicus users.

CHIME data will be pre-processed onboard the satellite within the dedicated Data Processing Unit, allowing cloud detection and compression using machine learning techniques. Once transmitted via Ka-Band antenna to the ground, the CHIME data will be processed by the Copernicus Ground Segment and disseminated through the Copernicus Data Space Ecosystem (Level-1 and Level-2 core products; <https://dataspace.copernicus.eu/>). Additional demonstration products and higher-level prototype products related to key vegetation, soil and raw material properties are also being prototyped. A full-fledged End-to-End (E2E) simulator is being developed to support the CHIME mission development. It embeds the Observation Performance Simulator (OPSI) and includes a full forward and inverse modelling of CHIME data products and preliminary retrieval algorithms, with the main aim of assessing the CHIME performance with respect to the requirements set in the MRD and flowed down in the System Requirements Document. In parallel to the CHIME E2E, a specific relevant activity was kicked-off in 2023 for the development of the future operational processors of the CHIME Level-2 products. These activities will exploit data collected during the CHIME campaigns in 2018, 2020 and 2021 with a combination of airborne and (in 2020 and 2021) spaceborne spectrometers deployed by ESA, NASA, DLR and ASI, supported by ground teams from numerous European institutes.

In this contribution, the main outcomes of the CHIME activities carried out in Phase A/B1 and B2, as well as the ongoing and planned activities for Phase C/D/E will be presented, covering the scientific support studies, the technical developments, and the user community preparatory activities. The status of the ongoing cooperation between ESA, ASI, DLR and NASA towards increasing synergies of current and future imaging spectroscopy missions in space will be reported as well.

CHIME Key Specifications



- Carpet-mapping observations of land and coastal areas (current mask: up to 370 km offshore)
- SZA < 84°
- Spectral range: 400 – 2500 nm
- FWHM ≈ 10 nm, SSI ≈ 8.4 nm
- Ground Resolution: 30 m
- Swath ≈ 130 km
- Revisit 11 days (w/ 2 satellites)
- High radiometric accuracy and SNR, low spectral/spatial mis-registration

Core data products:

- Top-of-atmosphere (TOA) radiance in sensor geometry
- Ortho-rectified TOA reflectance
- Bottom-of-atmosphere (BOA) land surface and aquatic reflectance in sensor and ortho-rectified geometry

>> with associated uncertainties

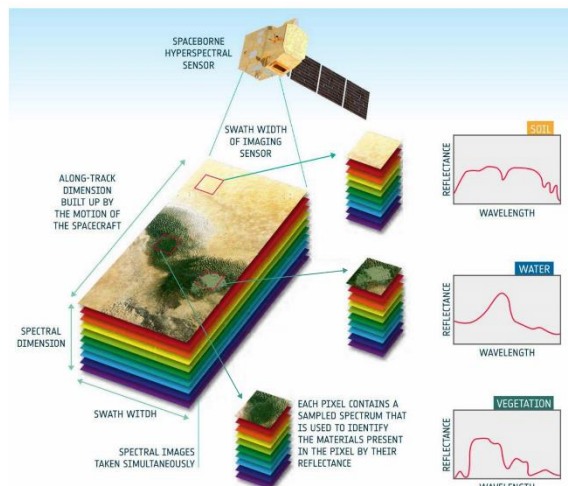


Figure 1 CHIME Key Specifications

CHIME Level 2A and 2B: Atmospheric Correction and Higher-Level Processing

Tobias Storch¹, Raquel de los Reyes¹, Peter Schwind¹, Maximilian Langheinrich¹, David Marshall Ingram¹, Andreas Hueni², Pieter de Vis³, Nicolas Lamquin⁴, Vincent Levasseur⁴, Jérôme Louis⁵, Sébastien Saunier⁵, Martin Bachmann¹, Jochem Verrest⁶, Katja Berger⁶, Stéphane Guillaso⁷, Karl Segl⁷, Luigi Agrimano⁸, Lucie Homolová⁹, Kevin Alonso¹⁰, Ferran Gascon¹¹, Valentina Boccia¹¹

¹ German Aerospace Center (DLR), Earth Observation Center (EOC), Germany

² University of Zurich (UZH), Department of Geography, Switzerland

³ National Physical Laboratory (NPL), United Kingdom

⁴ ACRI-ST, France

⁵ Telespazio, France

⁶ University of Valencia (UV), Image Processing Laboratory (IPL), Spain

⁷ GFZ German Research Centre for Geosciences, Germany

⁸ Planetek Italia, Italy

⁹ Czechglobe, Global Change Research Institute (CAS), Czech Republic

¹⁰ Rhea System, Italy

¹¹ European Space Agency (ESA), ESA Centre for Earth Observation (ESRIN), Italy

Keywords: Earth Observation, Copernicus, Hyperspectral Imaging, Atmospheric Correction, Higher-Level Processing

Challenge

CHIME (Copernicus Hyperspectral Imaging Mission for the Environment), planned to be launched in 2028, aims to complement the existing Copernicus satellites for observing land and coastal areas. The mission is synergetic with Sentinel-1, -2, -3 and LSTM, and also with other international hyperspectral missions such as SBG, EnMAP (by DLR) and PRISMA (by ASI).

The imaging spectrometer covers the visible, near and shortwave infra-red spectral range from 400 nm to 2500 nm at intervals of at most 10 nm and at spatial resolutions of at most 30 m. These Earth observation capabilities will in particular support services for food security, agriculture and raw materials.

Based on Top-Of-Atmosphere (TOA) radiances in cartographic or sensor geometry, Bottom-Of-Atmosphere (BOA) reflectance will be generated fulfilling the CEOS ARD surface and aquatic reflectance specifications. Also, a range of higher-level high priority products related to canopy & leaf level and soil & mineralogy will be provided.

Methodology

CHIME Level 2A and 2B processors will be provided as open source and integrated in the Copernicus Expansion Mission Product Algorithms Laboratory (CEM-PAL) and for Level 2A in ESA's operational processing environments for systematic product generation and distribution to users.

The CHIME Level 2A processor will use several features of PACO (Python-based Atmospheric COrrrection), duly optimized for CHIME, and optimized atmospheric corrections for land and water surfaces. First, it masks pixels, e.g. land-water, cloud-haze-cirrus-clear. It then derives atmospheric parameters based on mission-external Copernicus Atmosphere Monitoring Service (CAMS) and mission-internal instrument data. Next, it determines the reflectance for all types of terrain using the Copernicus DEM and based on Look-

Up-Tables containing various atmospheric profiles and radiative transfers using libRadTran. Finally, the surface anisotropy quantified by Bidirectional Reflectance Distribution Function (BRDF) models is corrected.

The CHIME Level 2B processor will apply well-established approaches for the retrieval of Canopy and Leaf Nitrogen and Water Content, Leaf Mass per Area for vegetated pixels, and Soil Organic Carbon (SOC) content and Kaolinite abundance for non-vegetated pixels. Due to the influence of cover fractions of green photosynthetic active vegetation (PV), dry non-photosynthetic vegetation (NPV) and bare soil per pixel, these will be estimated by an improved and tailored pixel masking.

Results

To derive the atmospheric profile, air temperature and total ozone columns are extracted based on CAMS. Aerosol Optical Thickness (AOT) retrieval is based on dark reference areas in different wavelength ranges, e.g. 2100 nm, 660 nm, 470 nm for land and 850 nm, 660 nm for water, and especially in typical spectral relations. Water Vapour (WV) is estimated based on absorption regions at 945 nm, 1130 nm. Other molecular absorbers are expected to have constant mixing ratios.

Vegetation products are based on a hybrid model blending the physics described by coupled canopy-leaf radiative transfers related to multiple states of vegetation characteristics and the efficiency of machine learning regression algorithms. For SOC content products, first dominant soil pixels are selected and then a SOC reference soil database is used for the parametrization of the machine learning retrieval model. For kaolinite abundance products, first kaolinite-bearing pixels are selected and then the kaolinite abundance and uncertainty are determined using machine learning techniques.

The uncertainty analysis for the outputs considers the input uncertainties and uncertainty tree diagrams for the processing to account precisely for error contributors and to achieve consistency for Level 2A and 2B. Propagation is performed through analytical or Monte Carlo methods, depending on the applicability of assumptions on Gaussian probability distributions and linear measurement functions in the range of errors.

Outlook for the future

L2H/F (harmonized / fused) extends Level 2A processing based on CHIME and SBG Level 1C products by considering co-registration to a reference image, inter-calibration, and spectral band adjustment, to obtain denser (and longer) time series.

The realization of Level 2A and 2B processors will start by Q4/2023 and first prototypical versions are expected for Q4/2024 and Q2/2026, respectively, and final operational versions one year before CHIME satellite launch.

In particular after launch, the Calibration and Validation (Cal/Val) of Level 2A and 2B products will extensively consider uncertainty information to ensure the mission performs within specified limits and to verify the accuracy of the derived products, usually by comparing it to a reference standard traceable to the International System of Units (SI) or to other internationally accepted standards and to independent ground-based measurements, e.g. RadCalNet and AERONET, or other mission products like NASA SBG and ESA TRUTH.

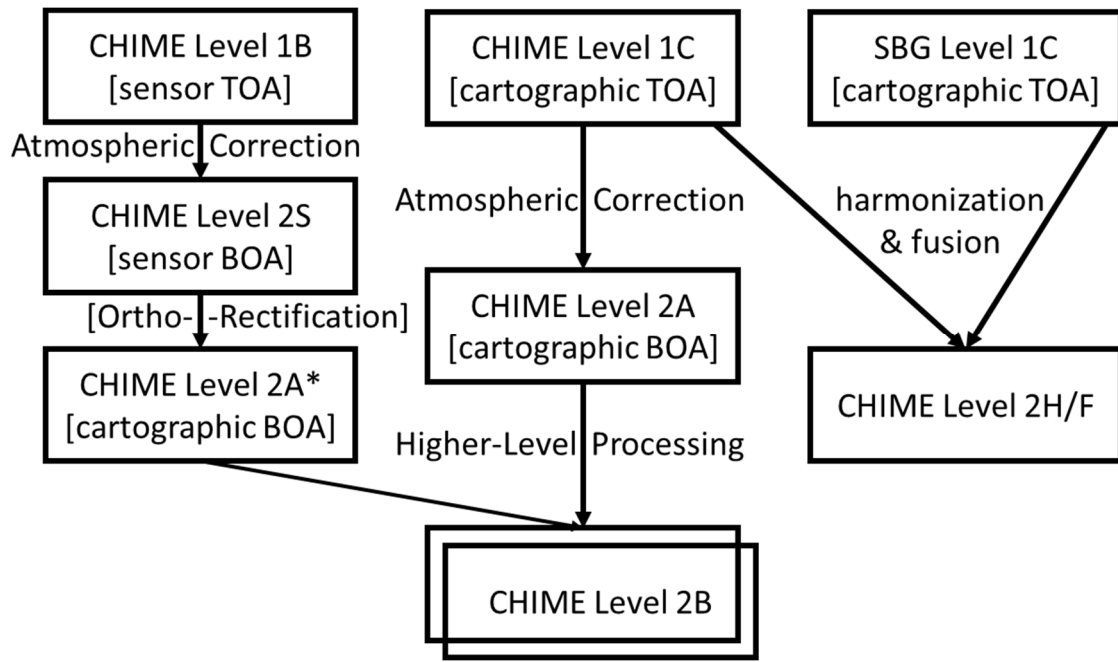


Figure Illustration of Product Levels

Progress in the development of the L2B mineral module for the CHIME E2E Simulator (CHEES).

[Karl Segl](#)¹, Stéphane Guillaso¹, Saeid Asadzadeh¹, Massimo Musacchio², Ana Maria Sánchez Montero³

¹ Helmholtz Centre Potsdam GFZ German Research Centre for Geosciences, Potsdam Germany

² National Institute of Geophysics and Volcanology, Rome, Italy

³ GMV, Madrid, Spain

Keywords: CHIME, Hyperspectral, Geology, Kaolinite, E2E Simulation

Challenge

Kaolinite abundance is one of the high-priority spectral products defined by the CHIME Mission Advisory Group. Within the CHIME E2E consortium, GFZ is responsible for the development of a suitable retrieval module that also provides uncertainties. This task contains two major challenges: (i) Kaolinite often occurs together with other spectrally similar clay minerals such as illite and smectite as well as the members of the kaolin group including dickite and halloysite. This results in the overlapping of diagnostic absorption features of kaolinite (i.e., at around 2165 and 2207 nm) with the noted minerals, making spectral-based identification and quantification a challenge (ii) There is no agreement on the meaning of "abundance" in the geologic remote sensing community. The term "spectral abundance" refers to the proportion of a pre-defined endmember within a pixel spectrum. In our development, we aim to minimize the impact of the selection and yield areal abundance maps by considering the spectral variability and intimate mixtures of kaolinite. Furthermore, we investigate the possibilities and limitations for deriving volumetric abundance (or proportion), which is the most sought-after parameter for kaolinite and other clay minerals considering the limitations imposed by the coating effects of kaolinite.

Methodology

To meet these challenges, we use a two-step approach. In the first step, we pre-select pixels that contain a minimum proportion of kaolinite. A sequence of various selection steps is applied to CHIME L2A data considering available information about surface type, data quality, and reflectance uncertainty. The most important step is the classification of kaolinite-bearing pixels using an artificial neural network (multilayer perceptron). The model was trained in advance by using an enriched spectral library, generated by linearly mixing the main surface cover types and minerals with kaolinite. The fraction of kaolinite in the training data ranges between 5-100 %.

In the second step, pixel spectra are analyzed for their kaolinite content. For this purpose, two methods are currently implemented. The first method is based on a spectral feature, which is composed of the triangle area (TRF) defined by the BOA reflectance at 2193, 2210, and 2219 nm. Tests showed that this feature is less sensitive to spectral mixtures with other clays compared to, for instance, the commonly used continuum-removed absorption depth of kaolinite at around 2200 nm. The second method is based on Gaussian process regression (GPR). Both methods are also trained in advance using synthetic mixtures.

For the derivation of the required uncertainty products, classical error propagation is performed for the TRF method, whereas for the GPR method, the uncertainties are taken directly from the model.

Results

The validation of the two processing steps shows excellent results. For example, a classification accuracy of over 98% was achieved for the preselection step considering independent synthetically mixed spectra. Figure 1 shows the results for the two implemented kaolinite abundance retrieval methods. The R^2 for the TRF and GPR methods are 0.874 and 0.976, with the RMSE of 0.086 and 0.037, respectively. Here, the machine-learning approach is still more convincing, but this remains to be verified by real applications.

The new L2BM module was also tested with EnMAP data. For this purpose, the retrieval models were trained separately with EnMAP resampled spectra. Figure 2 (left) shows the EnMAP sub-scene and the map of the areal abundance of kaolinite. The results look very reasonable, but cannot be easily validated in the field.

Therefore, a further step in the direction of volumetric abundance would be important, since XRD can be used to determine the actual kaolinite abundance from field samples. Figure 3 (right) shows the first result by comparing areal and volumetric abundances. As expected, volumetric abundance above 20% cannot be really derived using areal abundance. Kaolinite coatings of e.g. quartz grains pretend a much higher abundance to the satellite sensor in comparison to XRD analyses, where the samples are crushed to powder. This can also be seen in the saturation of kaolinite absorption.

Outlook for the future

Methodologically, we will extend the training and validation data, in particular, and supplement it with direct field measurements. In the case of volumetric abundance, we plan to analyze and model the important range of 0-20% in more detail. For this purpose, comprehensive mixing experiments in the laboratory are planned.

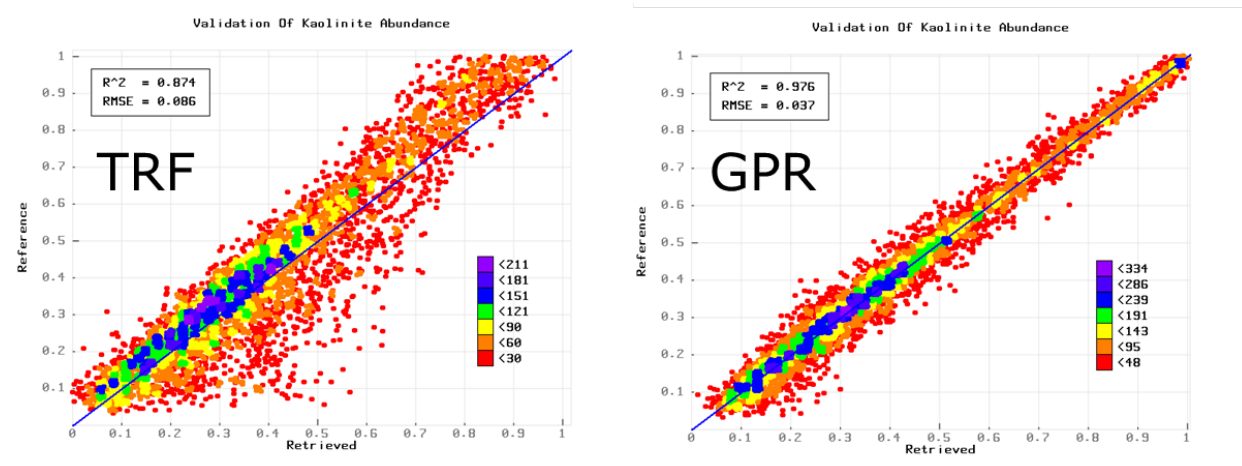


Figure 1: (a) Accuracy assessment of TRF and GPR methods.

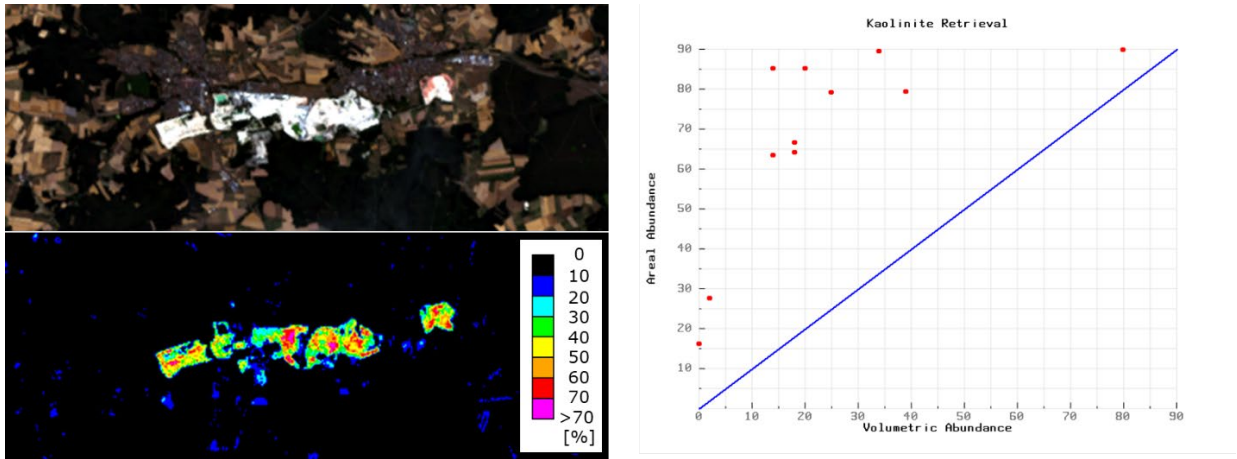


Figure 2: EnMAP RGB (subset) and retrieved areal kaolinite abundance (kaolinite open pit mine, Hirschau, Germany) (left) and areal versus volumetric abundance correlation plot of field and product samples (right).

[Formatting guidelines for abstract submission]

EARSeL Valencia 2024
Abstract

Corresponding Author:

[stephane.guillaso@gfz-potsdam.de]

Progress in the Development of the L2B Soil Module for the CHIME-E2E Simulator

Stéphane Guillaso¹, Karl Segl¹, Robert Milewski¹, Stefano Pignatti², Raffaele Casa³, Ana Maria Sánchez Montero⁴

¹ Helmholtz Centre Potsdam GFZ German Research Centre for Geoscience, Potsdam, Germany

² National Research Council (CNR-IMAA), Potenza, Italy

³ University Tuscia, DAFNE Dep., Viterbo, Italy

⁴ GMV, Madrid, Spain

Keywords (5): CHIME, Hyperspectral, Soil, SOC, E2E Simulation

Challenge (800 - 1000 characters incl. spaces)

Soil Organic Carbon (SOC) is, according to the United Nations, one of the most relevant soil properties directly related to the climate change. It is one of the high-priority products defined by the CHIME Mission Advisory Group. In the frame of the development of CHIME activities, an international consortium is developing an End-to-end (E2E) simulator including a suitable SOC content retrieval module. This task is confronted to the following challenges: (i) the assumption of pure bare soil is difficult to be assessed within a spatial resolution of 30 m. (ii) The 110 km swath is introducing variation in the viewing angle and effects such shaded soil fraction. (iii) Currently, research on SOC is considered only at local scale and is based on the use of a local database to parametrize the machine learning retrieval model. (iv) Finally, the proposed approach should be robust enough and not increase uncertainties that might be present in the input data.

The L2BS module implements the algorithms for retrieval SOC content that minimize the impact of the different challenges. We investigate the potential and limitations of different parametrization of machine learning model and compare it with a band analysis method. The latest status of the L2BS module is presented as tested on PRISMA and ENMAP images acquired on selected test areas.

Methodology (1200 – 1500 characters incl. spaces)

The proposed method to meet challenges (iii) and (iv) is a two steps approach. First a pixel preselection sub-module is applied to CHIME L2A data by applying different spectral analysis in order to identify non-water (NDRBI), non-green (NDBI) /dry (NCAI) vegetation, no moisture pixel (NSMI). The different indices are calculated and compared to a threshold to remove non desired pixel. After this step, we consider that the pixel is a pure bare soil pixel.

The second step is the SOC retrieval approach. Two methods are currently implemented. The first method is extracted a spectral feature which corresponds to the inverse of the slope defined by the BOA reflectance at 400 and 600 nm. The SOC content is estimated by calculating linear regression parameters (Gain and offset) using a local database. With this mathematical approach, uncertainties can be calculated and propagated through the module. The second method is using the Gaussian process regression (GPR) which allows to retrieve uncertainties directly from the model. Both methods are trained in advance using local database including variability in the input spectrum to “simulate” errors in the input data.

Results (1200 – 1500 characters incl. spaces)

The validation of the two processing steps shows encouraging results. Our preliminary estimation using synthetic scene has a R^2 of 0.8 and a RMSE < 3. We also use a real dataset that has been acquired by HySpex sensor and was provided with courtesy from the EnMAP Preparatory Flight Campaign. The data serves as input for the SGM and after running the E2E phase A/B1 simulator, a CHIME L2A data has been generated and finally the L2BS module has been applied using SOC ground truth data for model calibration. Figure 1 shows a visual comparison between SOC map prediction using two-step PLSR approach applied to HySpex airborne imagery (a) and the SOC map prediction using simulated CHIME data and the L2BS module (b). Similar spatial patterns are clearly visible and areas with very high SOC content are correctly depicted. We also obtained a RMSE of 3.22 over the whole region of interest which is reduced to 1.86 using all pixel having a square of errors less then 15 corresponding to 80% of the selected region. We have also implemented the GPR method to retrieve SOC content and we obtain a R^2 of 0.89 with a RMSE of 2.31 proving that the machine-learning approach is more convincing and needs to be verified by real applications.

Outlook for the future (800 - 1000 characters incl. spaces)

Based on the ongoing work and preliminary results, future work will be devoted to i) expand the number of test areas using EnMAP/PRISMA images to test the SOC retrieval algorithm including a wider range of variability in soil characteristics (e.g., texture) than the amount of SOC; ii) generalize the SOC retrieval methods to achieve performance that is less dependent on local SSL and local pixel conditions (e.g., soil moisture); (iii) refine the procedure to select bare soil pixels by minimizing the effects of photosynthetic vegetation, moisture, and non-photosynthetic vegetation (e.g., crop residues); (iv) evaluate the impact of observation angle in SOC recovery.

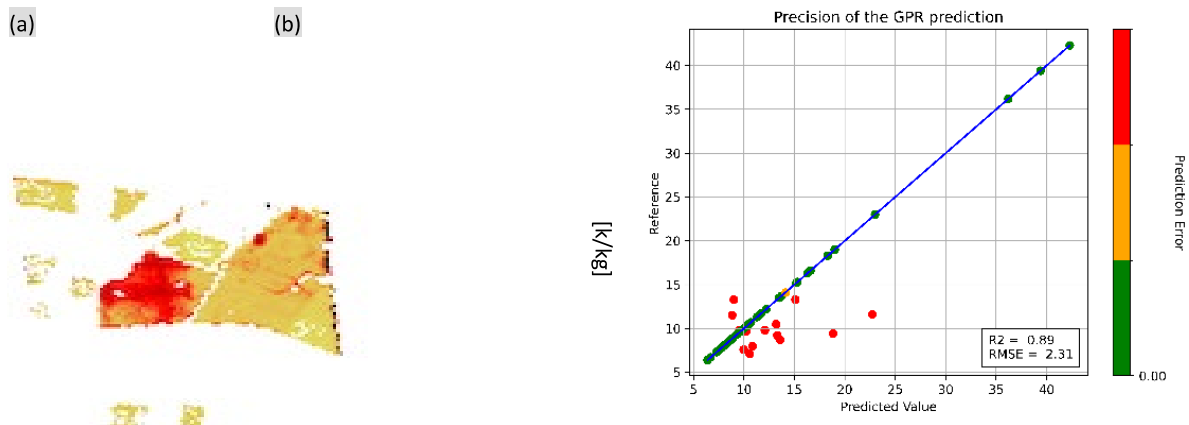


Figure 1 Left: SOC maps for airborne HySpex (a) using the two-step PLSR approach (b) simulated CHIME imagery. Right: Accuracy assessment of the GPR method.

Latest status of the vegetation traits retrieval processor and models in the context of CHIME mission preparation

José Luis García-Soria¹, Miguel Morata¹, Jochem Verrelst¹, Ana Belén Pascual-Venteo¹, Katja Berger¹, Cinzia Panigada², Giulia Tagliabue², Ana María Sánchez Montero³

¹ University of Valencia, Image Processing Laboratory (IPL), Spain

² University of Milano-Bicocca, Department of Earth and Environmental Science, Italy

³ GMV, Spain

Keywords (5): Imaging Spectroscopy, Vegetation, CHIME, Retrieval, Machine Learning

Challenge

The forthcoming Copernicus Hyperspectral Imaging Mission for the Environment (CHIME) is an imaging spectrometer satellite mission that can capture reflected radiation from the visible to the shortwave infrared (400–2400 nm). CHIME will routinely acquire hyperspectral imagery across the globe to support, among others, cropland and biodiversity monitoring applications. While the mission will process spectral data from levels 1 to 2A (bottom-of-atmosphere reflectance), it also plans to produce prototype higher-level surface products, such as a diversity of vegetation products.

In preparation for CHIME, ESA has initiated a full end-to-end (E2E) performance simulator called CHEES. This E2E aims to provide realistic synthetic datasets that go through all essential processing modules, including validation of the generated products. Specifically, the L2B Vegetation Processor (L2BV) is responsible for retrieving a set of leaf and canopy vegetation traits. CHIME's Mission Advisory Group (MAG) has identified a set of priority vegetation traits: leaf nitrogen content (LNC), leaf mass area (LMA), leaf water content (LWC), canopy nitrogen content (CNC), and canopy water content (CWC). The L2BV Processor is also prepared to retrieve the following vegetation traits: leaf chlorophyll content (LCC), leaf area index (LAI), canopy chlorophyll content (CCC), fractional vegetation cover (FVC), and fraction of absorbed photosynthetically active radiation (FAPAR). This presentation reports on the latest status of the CHEES L2BV Processor.

Methodology

Starting with the reflectance product processed by L2A, the purpose of the L2BV module is to quantify a collection of vegetation traits. To achieve this, so-called hybrid models were developed. Hybrid models take advantage of the physical soundness of radiative transfer models (RTM) and the flexibility of machine learning regression algorithms (MLRA) to build nonlinear relationships between spectra and vegetation traits. As RTM, the latest version of SCOPE (v.2.1) was used to generate training datasets. The training data was further optimised both in the spectral and sampling domains. The key steps of the pursued workflow are summarised below:

1. With SCOPE v.2.1, we generated a dataset with 2000 simulations for training, covering a broad variability for all the selected leaf and canopy traits.

2. To account for spectral collinearity, the spectral dimension of the training dataset was reduced through principal component analysis (PCA). To account for redundancy in the sampling domain, the training dataset was then optimised, and reduced, through active learning (AL). The AL step works as follows: for a portion of the training dataset, the AL technique evaluates the training dataset against real data, i.e. coming from airborne and field campaigns over croplands. It then keeps only the simulations that improve the validation of the model. Additionally, a diversity of bare soil samples was added to the final training dataset in order to account for non-vegetated surface pixels.
3. Three different MLRAs were trained in order to take the top-performing one when compared to simulated scenes. Gaussian process regression (GPR) was selected as a benchmark algorithm given its excellent performance and the provision of associated uncertainty estimates. As backup algorithms, kernel ridge regression (KRR) and neural networks (NN) were additionally evaluated as appealing algorithms. For these two algorithms, associated uncertainty is calculated through bootstrapping. The L2BV Processor has been prepared to run these three algorithms, but the best-performing model is selected as the baseline model.
4. The different versions of the models are evaluated against a reference scene consisting of L2A-like reflectance with associated input layers. The scene comprises three vegetated classes (scarce, medium, and dense), wherein all soil, leaf, canopy, and geometry variables were ranged. In this way, the model's predictive accuracy can be evaluated, either for the entire scene, per class, within variable limits, or as a function of an NDVI filter. A normalised root mean squared error (NRMSE) of 10% was set as a mission requirement (MR) for a variable to consider the model as pass to acceptance.

An overview of the developed workflow is provided below, in Figure 1.

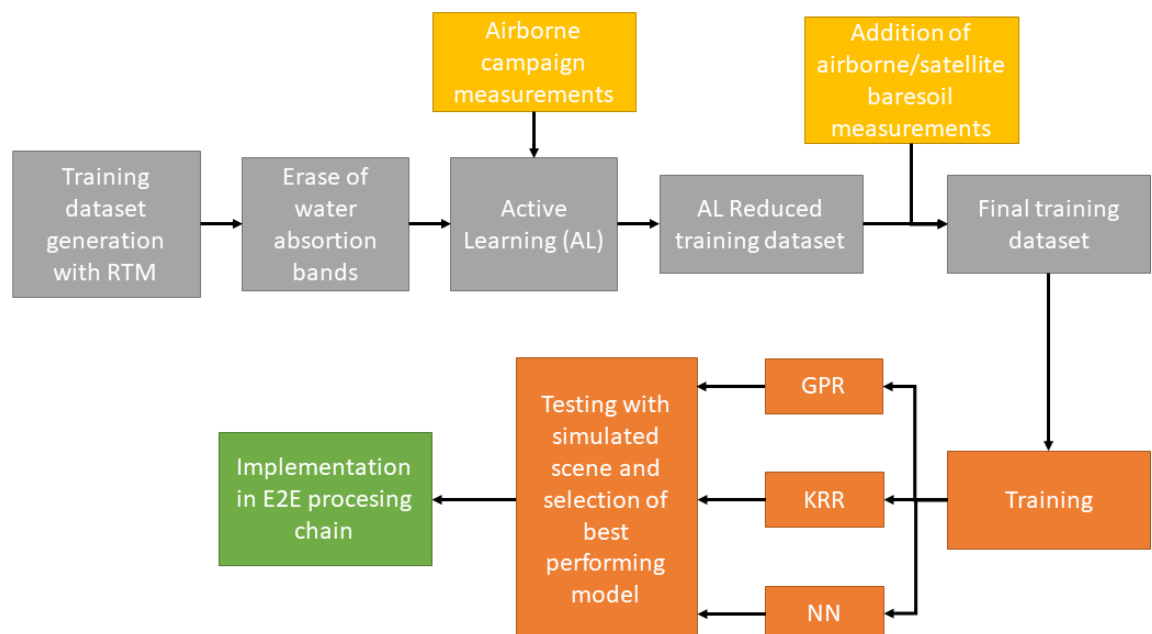


Figure 1. Workflow of the methodology used to train and select best performing models for the E2E simulator.

Results

The latest version of the models was evaluated against the simulated CHIME-like L2A reference scene. Scatterplots of the leaf and canopy variables are shown in Figure 2. Maps obtained from the reference scene are shown in Figure 3.

Regarding the leaf variables, both the priority variable LWC and also LCC passed the MR with NRMSE of 10% ($R^2: 0.94$) and 10% ($R^2: 0.95$), respectively. However, the priority variables LNC and LMA totally failed. Those models cannot be considered valid, and alternative retrieval strategies are under exploration.

Regarding the canopy variables, these models are more successful. In part, thanks to the contribution of LAI in the upscaling of the leaf variables to canopy. LAI approached the MR threshold with a NRMSE of 10.2% ($R^2: 0.87$). CWC passed the MR with a NRMSE of 9.4% ($R^2: 0.94$) and CCC is close to passing the MR with a NRMSE of 11.4% ($R^2: 0.94$). Also the priority canopy variable CNC is in the direction of reaching the MR, with a NRMSE of 13.7 ($R^2: 0.78$). Finally, FVC was also close to passing the MR, with a NRMSE of 11.4% ($R^2: 0.86$).

An important remark is that the reference scene ranged in LAI from 0 to 8, which might be considered excessively high, especially in the context of croplands. Restricting the reference scene to a LAI maximum of 6 resulted in a general improvement for the remaining variables, with notable cases occurring for CCC and LAI, which decreased their NRMSEs to 7.6% ($R^2: 0.96$) and 9.1% ($R^2: 0.92$), respectively, well below the MR.

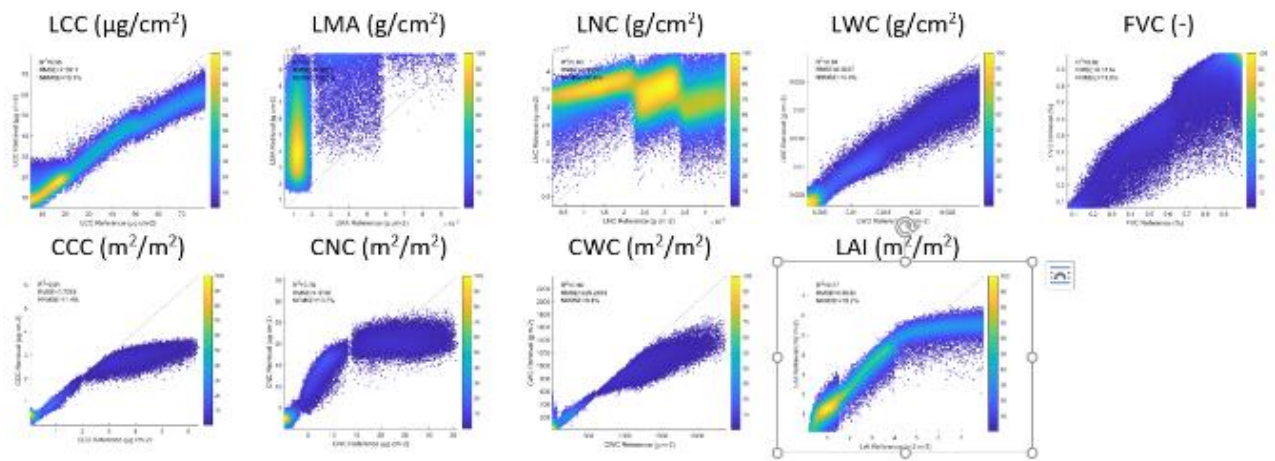


Figure 2. Scatterplots of the assessment of the models v2.1 versus the simulated scene.

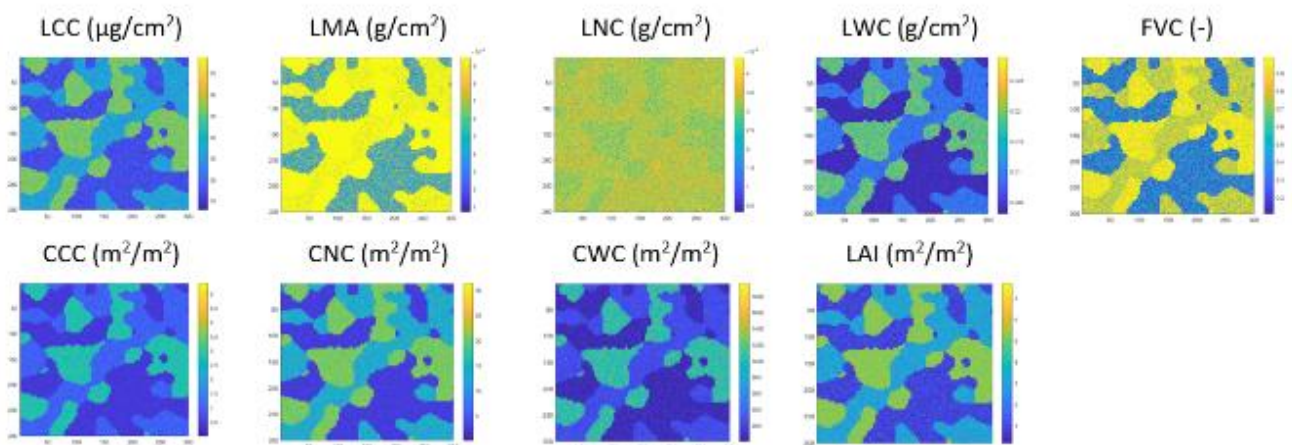


Figure 3. Retrieved maps over L2A-like synthetic 300x300 scene with the models v2.1.

Outlook for the future

With respect to ongoing developments, dedicated efforts are planned to improve the leaf priority variables LNC and LMA. The following strategies will be pursued:

- Exploring alternative spectral processing methods, such as spectral transformations, band selection, and alternative dimensionality reduction strategies, in combination with available MLRAs.
- Collecting additional campaign data to improve model tuning.

Another important aspect of improving the hybrid models is to explore their predictive power for more heterogeneous surfaces, such as forests and natural vegetation. This would involve including simulations from 3D radiative transfer models (RTMs), such as DART, as well as tuning and validating against field data collected from those surfaces. We expect to present initial results in these directions.

How Accurately and How Frequently Must We Retrieve Snow Properties from Imaging Spectroscopy?

EARSel Valencia 2024

Abstract

Corresponding Author: dozier@ucsb.edu

Jeff Dozier¹, David R. Thompson², U. Niklas Bohn², Edward H. Bair³

¹ University of California, Santa Barbara, USA

² Jet Propulsion Laboratory, USA

³ Leidos Inc., USA

Keywords: Snow, Hyperspectral, Net Radiation, Albedo

Challenge

In most climates, absorbed solar radiation primarily drives a snowpack's energy balance. Snow albedo, the most important intrinsic snow property to retrieve, depends on the size of snow grains and concentration, size, and optical properties of light-absorbing particles. In Earth's middle latitudes, mountains cover about a quarter of the land area but provide half the water resources. Therefore, retrieval of mountain snow properties must account for variations in reflectivity that the topography causes and deal with the likelihood that most mountain snow pixels are mixed with vegetation, soil, or rock. We must thus estimate the albedo by retrieving snow properties and modeling albedo, rather than measure the pixel albedo directly with the spectrometer.

How accurately and how frequently must snow properties be estimated? Will future missions CHIME and SBG meet these accuracy requirements? Can supporting imagery from multispectral sensors help meet needs for frequent retrievals?

Methodology

The U.S. National Academies' *Thriving on Our Changing Planet* (2018) clarifies a specific need for measurement of snow albedo: "Spectral albedo of subpixel snow and glaciers at weekly intervals to an accuracy to estimate absorption of solar radiation to 10%." We adopt this specification as a benchmark need for snow albedo. Note that estimating **absorption** to $\pm 10\%$ is a more stringent requirement than estimating **albedo** to that accuracy.

We simulated the broadband absorptivity ($1 - \text{albedo}$), over a range of solar zenith angles, local illumination angles, and snow grain sizes for both clean and dirty snow. The delta-Eddington radiative transfer algorithm calculated the spectral albedo, assuming deep snow. Grain radii ranged from 50 μm to 1800 μm . For the dirty snow, the simulation combined a 100 $\mu\text{g/g}$ concentration of San Juan Dust of radius 2.5 μm with a 100 ng/g concentration of black carbon of radius 0.25 μm .

For the atmospheric radiation, we used a mid-latitude winter atmosphere at 3000 m elevation. The solar zenith and local illumination angles are separately included because they affect the spectral snow albedo and the spectral distributions of the direct and diffuse irradiance.

To examine the temporal variability of snow albedo, we examined seven years of measurements from the Mammoth Mountain snow study site. With interpolating splines, we estimated all noontime measurements for the snow-covered seasons of each year, and we identified the "peaks" (local maxima) and "valleys" (local minima) in the time series.

Results

Figure 1, for solar zenith 60° and local illumination 50°, provides an example of useful information for setting performance criteria in the design of spectroscopy missions. Setting the accuracy on grain size retrievals to the square root rather than the value itself takes advantage of the relationship of spectral albedo to square root of grain radius being closer to linear than to grain radius itself.

The right-hand graph in Figure 1 shows that at these solar zenith and local illumination angles, getting the RMS error of the square root of grain radius to ~20% for clean snow and ~15% for dirty snow would enable estimating net solar radiation to 10% RMS error. The reason for the slightly tighter criterion for dirty snow lies in the combined effect of snow grain size and light-absorbing particles extending over the whole solar spectrum, whereas grain size itself has negligible effect on albedo of clean snow in the visible spectrum. We also find that existing retrieval algorithms can estimate snow properties at fractional snow cover values of 0.3 or greater, at illumination angles less than 65°-70°.

Analysis of in situ data from the Mammoth Mountain snow study site (Figure 2) shows that changes in albedo average 5-day recurrence intervals. In the seven snow seasons (1,555 days) analyzed, we identified 163 peaks (local maxima) and 157 valleys (local minima).

Outlook for the future

To extend the analysis, we need to translate the measurement accuracies of top-of-atmosphere radiances to the retrieval algorithms and ascertain whether the CHIME and SBG designs meet the necessary accuracy and precision. We must cover the full range of solar zenith and local illumination angles, atmospheric properties, topographic surfaces, and surface roughness, so that we can clarify the conditions under which we can estimate net solar radiation to 10% RMS error. Finally, we need to explore the trade-offs between using mission-provided surface reflectance retrievals versus specific forward atmospheric models that account for bright surfaces.

Also ripe for exploration is the fusion of hyperspectral with multispectral data to obtain information about albedo changes during intervals between CHIME and SBG overpasses.

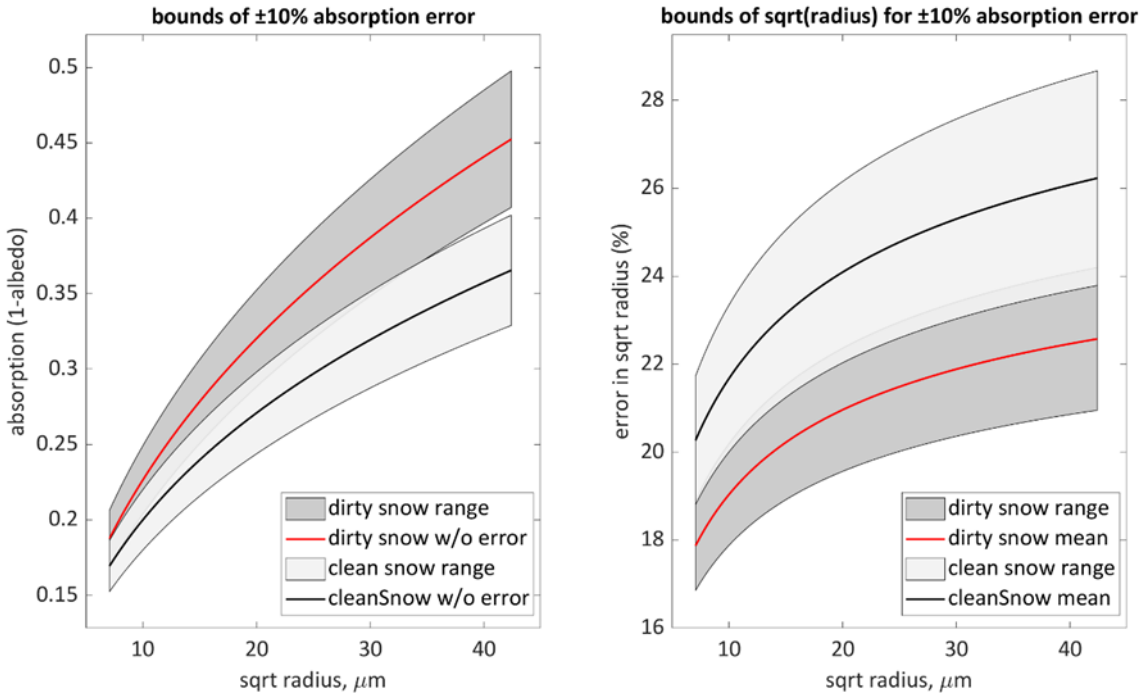


Figure 1. Left graph shows the broadband absorption with ±10% error for a range of snow grain radii from 50 μm to 1800 μm. The right graph shows the percent error in the square root of the grain size that meets the ±10% error criterion. The x-axes use the square root of the grain size because the relationship with albedo is closer to linear than with grain size itself.

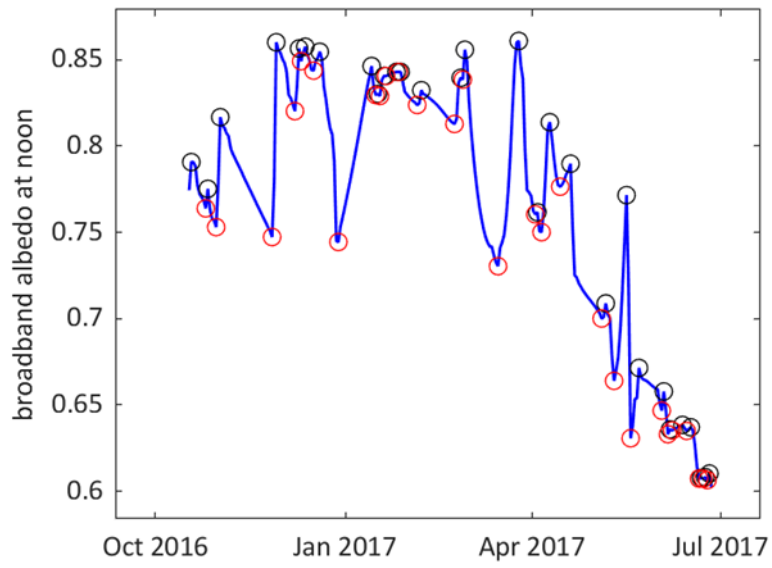


Figure 2. Progression of broadband albedo at the Mammoth Mountain snow study site for water year 2017. The black circles show the peaks (local maxima) in the albedo time series, the red circles show the valleys (local minima).

**Them.Sess. 1-2: Advancements in
field and laboratory
measurements of vegetation
spectra**

An innovative UAV-HSI integration for the validation of current and upcoming space-borne spectroscopy platforms reflectance products.

J. Pablo Arroyo-Mora¹, Margaret Kalacska², Oliver Lucanus², Raymond J. Soffer¹, Maximilian Brell³

¹ National Research Council of Canada, Flight Research Laboratory, Canada

² Applied Remote Sensing Laboratory, McGill University, Canada

³ German Centre for Geosciences (Gfz), Germany

Keywords (5): Hyperspectral, Drones, Mer Bleue Cal/Val Supersite, Reflectance, EnMAP

Challenge (800 - 1000 characters incl. spaces)

Hyperspectral space-borne sensors represent the next generation of EO technologies which are crucial to map and model the rapid ecosystem changes due to anthropogenic activities and climate change. Central to the effective use of the information generated from these systems by the user community, is the validation of, for example, satellite surface reflectance products for various terrestrial and aquatic ecosystems. Cutting edge *in-situ* validation efforts now focus on the use of unmanned aerial vehicles with hyperspectral imager payloads (UAV-HSI), which provide rich spectral data at ultra-high spatial resolution (e.g. 3-10 cm). Here we reveal a new UAV-HSI integration taking advantage of the payload and flight capacity of the DJI T30 Agras. We modified the payload of the T30 to integrate a full range HSI (400-2500 nm), the Mjolnir VS-620. Our second objective is to showcase the superb geometric and radiometric quality of the HSI data acquired over three large areas at the Mer Bleue Peatland Observatory Cal/Val Supersite.

Methodology (1200 – 1500 characters incl. spaces)

Our integration of the HySpex Mjolnir VS-620 hyperspectral sensor (6.7kg) and other components such as the inertial navigation system (INS) antenna, HSI power source and radio link, required a modification of the DJI T30 payload. The T30 with the original payload of a 30L tank designed for agricultural spraying, is capable of heavy lifting and precise flight control. Following aerospace design and fabrication guidelines, a plate capable of integrating the different components, including a gimbal for the sensor was developed. After the full integration of the system, wind tunnel, vibration and endurance tests were performed. To assess the radiometric and geometric quality of the HSI data, a flight plan was developed in ArcGIS 10.7.1 to acquire three 150m x 150m areas (2.25 ha each) at Mer Bleue, near-coincidentally with an EnMAP overpass. As the system total weight was >25 kg, a Special Flight Operation Certificate from Transport Canada was required. The day of the UAV-HSI data acquisition, near-Lambertian 1%, 5% and 40% panels previously characterized in the laboratory, were deployed. In addition, an in-situ field spectra of representative hummocks and hollows were collected with an ASD FieldSpec3 along the Mer Bleue boardwalk. The VS-620 imagery was processed to the bottom of the atmosphere reflectance using manufacturer applications (HySpex RAD, HySpex NAV), POSPac 9.0, PARGE and DROACOR packages. The FieldSpec data were processed with the ASDToolkit.

Results (1200 – 1500 characters incl. spaces)

The total weight of RPAS HSI system is ~ 43 kg, which allows for a data collection time of around 15 minutes, with only 60-70% of the drone battery depleted (i.e. safety measure). Wind tunnel results showed that the system is stable with a wind tolerance up to 14 m/s, but given the requirement of low winds for UAV-HSI data acquisition due to safety and data quality considerations, the system would only be used with wind speeds up to 7 m/s. The vibration test showcased the importance of the gimbal and dampener implementation, which shows a decrease in the vibrational forces from 0.699g to 0.075g between the plate and the HSI. During the Mer Bleue UAV-HSI campaign, despite partial cloud cover, we were able to complete the HSI data collection for the 3 areas, and repeat one area during an EnMAP overpass, for a total of 9 hectares. Figure 1A shows a mosaic of Area 1 resampled to 10 cm pixel size with 390 spectral bands, which in practical terms represents more than 500,000 individual spectra useful for the validation of the EnMAP reflectance product. Figure 1B reveals the panel reflectance generated from the nominal reflectance panels. Finally, Figure 1C shows a preliminary evaluation of the spectra from the system, revealing key spectral features around 550 nm for the hummocks composed of shrubs and other green vascular plants, and the 650 nm peak for moss vegetation dominated hollows.

Outlook for the future (800 - 1000 characters incl. spaces)

The validation of satellite reflectance products for satellite systems like Sentinel-2 are evolving towards maturity. However, the complexities and challenges of novel space-borne hyperspectral systems like EnMAP and PRISMA, and future missions like CHIME (ESA), would greatly benefit from systems like the one we developed. Covering areas at the hectometre scale, and capturing the spatial- spectral variability in various ecosystem, would improve the confidence in the products generated by these space-borne systems. Moreover, efforts like ESA's Fiducial Reference Measurements for Vegetation (FRM4VEG) provide a framework to develop protocols required for traceable *in-situ* measurements of vegetation-related parameters for validation purposes, for example. We believe the upscaling methodology implemented by our research group at Mer Bleue provides a clear example of practical traceable measurements from lab to field, field to manned and unmanned airborne systems, and airborne to satellite validation.

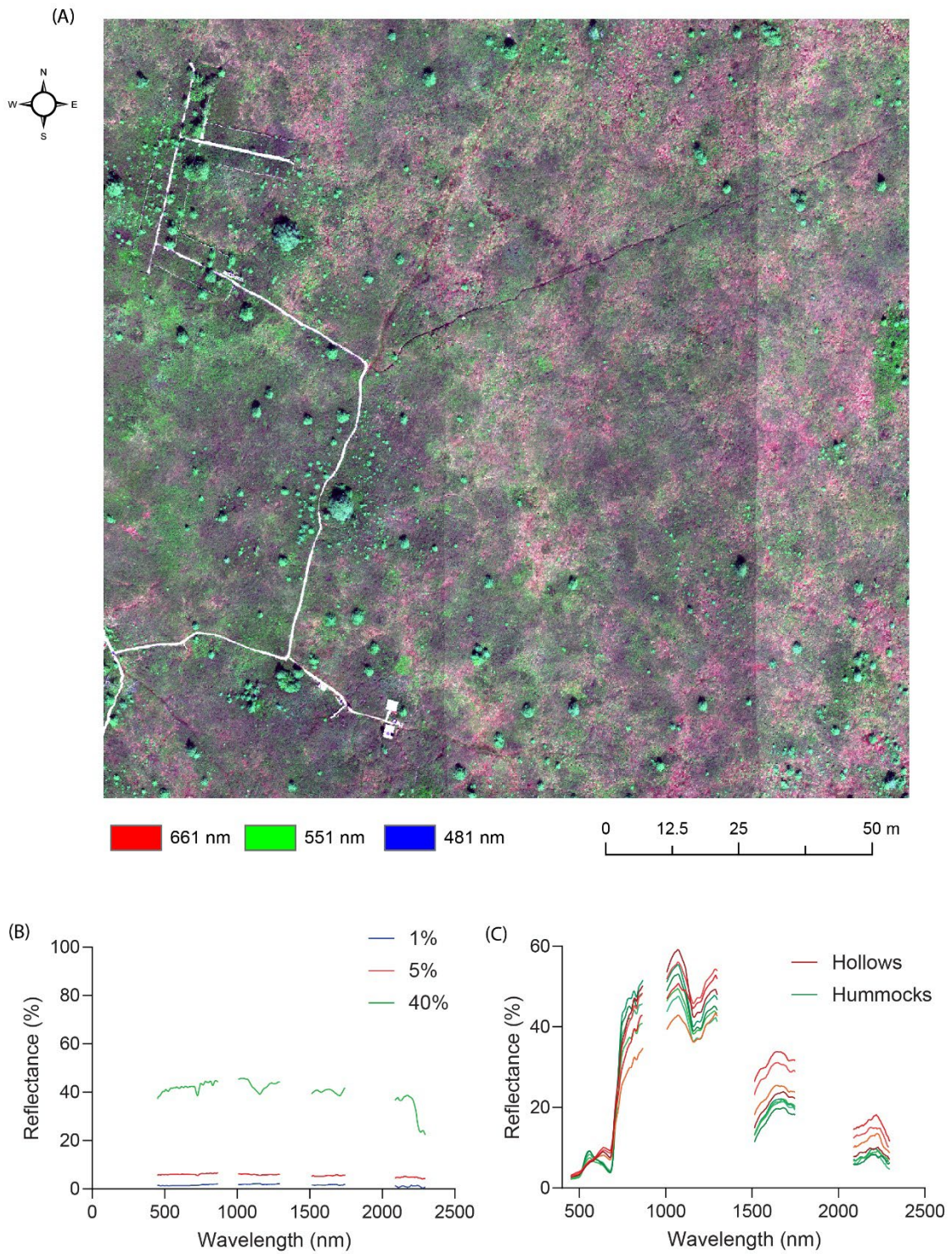


Figure 1 (A) UAV-HSI mosaic for Mer Bleue Peatland Observatory at 10cm spatial resolution and 390 spectral bands from UAV HSI data acquired on July 24, 2023. (B) Nominal near-Lambertian target spectra (C) Example of spectra for hollows and hummocks vegetation.

Spectral invariant-based illumination correction of shaded and sunlit surfaces in close-range imaging spectroscopy data

EARSeL Valencia 2024

Abstract

Corresponding Author: olli.ihalainen@vtt.fi

Olli Ihalainen¹, Theresa Sandmann^{2,3}, Matti Möttöus¹, Uwe Rascher³

¹VTT Technical Research Centre of Finland Ltd, Finland

²University of Bonn, Germany

³Forschungszentrum Jülich GmbH, Germany

Keywords (5): Illumination correction, Hyperspectral, Spectral invariant, Radiative transfer, Machine learning

Challenge

The varying illumination conditions within a vegetation canopy pose a major challenge for the assessment of leaf traits via close-range imaging spectroscopy. The conventional approach of computing reflectance with respect to the top-of-canopy (TOC) surface yields values which can be drastically different from the optical properties of the leaves in the image due to the differences between the illumination conditions at the TOC and at the leaf-level. This, in turn, will lead to errors in the estimation of leaf biophysical and -chemical traits. The theory of spectral invariants can be used to solve this problem as it links the TOC reflectance to the true leaf reflectance via spectrally invariant parameters related to the canopy structure and illumination conditions. Recently, the theory has been used to perform illumination correction for sunlit leaves in close-range TOC reflectance images. We present a new formulation of the theory that applies also to any surface, sunlit or shaded, in a vegetation canopy. In addition, we demonstrate a fast and efficient implementation of the illumination correction with random forest (RF) regression.

Methodology

We formulated the reflectance signal recorded in a pixel of an ultra-high spatial resolution image with six spectrally invariant parameters quantifying the illumination conditions on the leaf surface. To test the theory, we generated synthetic images of vegetation canopies with Monte Carlo ray tracing (MCRT) using the measured spectra of leaves, bark, understory, and artificial materials from various spectral libraries in the simulated scenes. Next, we trained a RF algorithm on the MCRT output for estimating the spectral invariants, which, in turn, were used to retrieve the true leaf reflectance. Different images were used for training and validating the RF algorithm.

Finally, the performance of the RF algorithm was evaluated on real-life imaging spectroscopy data in the visible and near-infrared range. The data were collected from a *Diervilla Lonicera* Mill. shrubbery in August 2022, Otaniemi, Finland using a Specim IQ camera (Fig. 1a), and from 5 different Brassica phenotypes under drought stress conditions during June 2023 in Bonn, Germany, using the HyScreen imaging system. The targets in the image were plant leaves and artificial surfaces (colored paper, plastic) inserted in the canopy. The spectral properties of the materials in the images were determined using an Avantes AVASPEC-ULS 2048x64TEC-EVO spectrometer with a bare fiber optic and a Spectral Evolution NaturaSpec spectrometer attached to an Avantes AvaSphere integrating sphere.

Results

The RMSE between the TOC reflectance produced by the MCRT program and the spectral invariant theory were between 0.01 % and 1.00 % for each pixel, showing excellent agreement between the model and the measurement. The main contributor to RMSE was the digital noise in the MCRT data. The illumination-corrected spectra were computed using the spectral invariant parameters from the RF algorithm (Fig. 1) which showed good agreement with the field-measured reflectance (Fig. 2). The RMSE for the RF-retrieved spectral reflectance factors of sunlit leaves and artificial surfaces the measured images were between 0.3 % and 5.0 %. For the shaded pixels, RMSE ranged between 2.4 % and 19.7 %. The proposed illumination-correction method is computationally efficient, with a computation time of less than 1 s for a 512x512 image with 152 bands on a 12-core, 1600 MHz, Intel® i5 processor.

Outlook for the future

Our results demonstrate that the illumination effects in close-range images can be corrected for with the spectral invariant theory, and the true physical reflectance signals can be retrieved robustly and efficiently. Existing methods, e.g., leaf reflectance models, can be used to determine leaf biophysical and –chemical traits. This can lead to significant improvements in applications requiring rapid acquisition of the spectral characteristics of plant leaves, e.g., in high-throughput plant phenotyping. We demonstrated that the theory of spectral invariants can be extended to pixels containing non-green materials allowing for a better remote characterization of materials within or below vegetation.

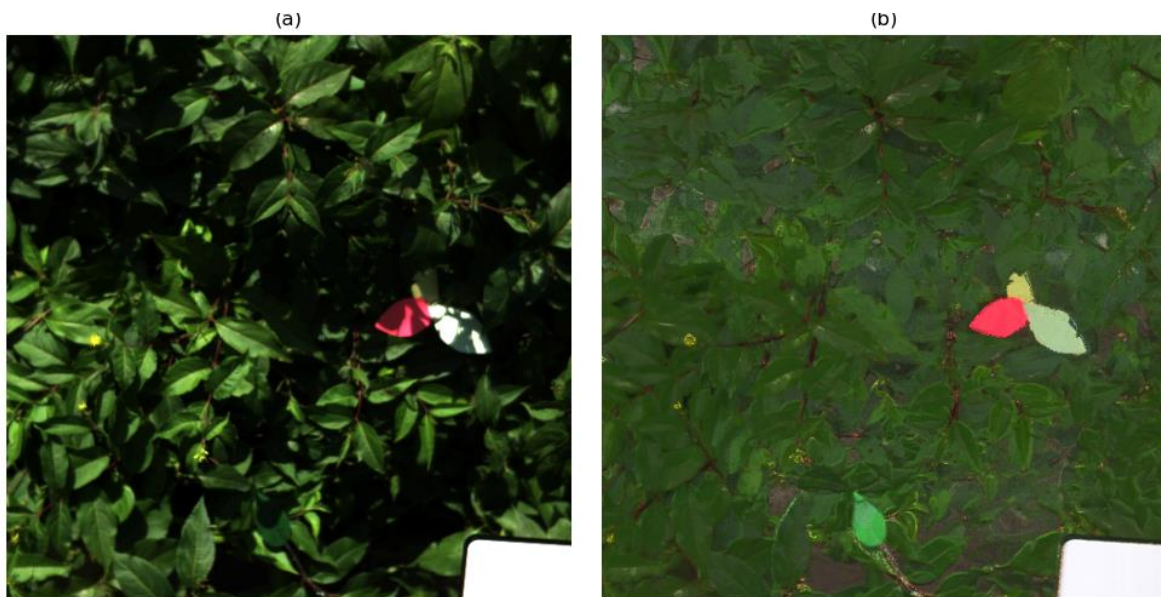


Figure 1. (a) TOC reflectance image in RGB and (b) the corresponding illumination-corrected reflectance image. The scene contains plant leaves, a plastic leaf and red, green, and yellow paper.

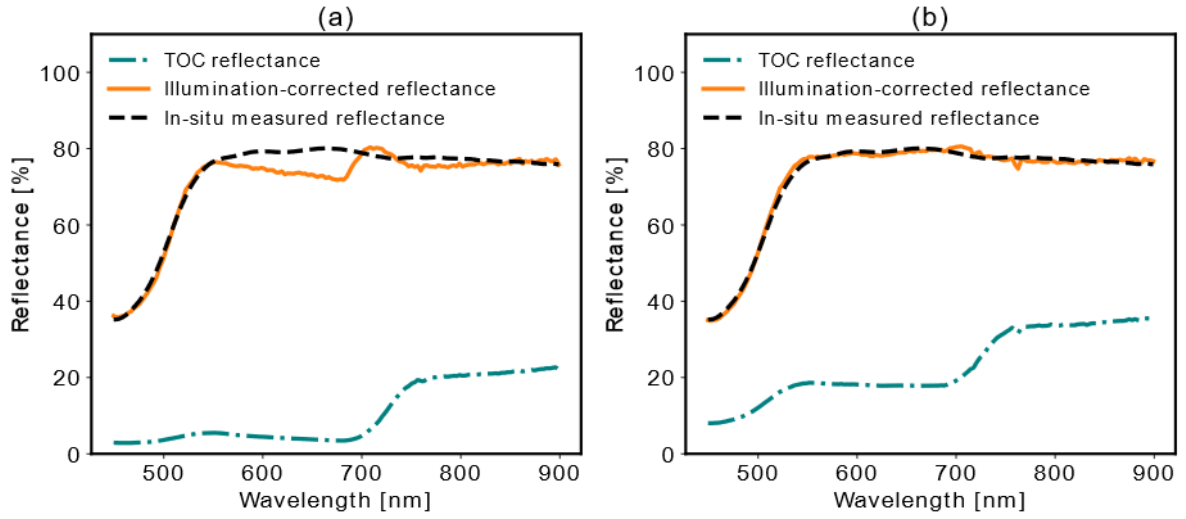


Figure 2. The TOC, illumination-corrected and true reflectance of yellow paper in a vegetation canopy in (a) shaded and (b) sunlit pixels.

Variability in biochemical and optical traits of coniferous and deciduous tree species - implications for validation of remote sensing products

Petr Lukeš¹, Lucie Homolová¹, Zuzana Lhotáková², Eva Neuwirthová², Aarne Hovi³

¹ GLOBAL CHANGE RESEARCH INSTITUTE OF THE CZECH ACADEMY OF SCIENCES (CZECHGLOBE), CZECH REPUBLIC

² CHARLES UNIVERSITY, FACULTY OF SCIENCE, DEPARTMENT OF PLANT EXPERIMENTAL BIOLOGY, CZECH REPUBLIC

³ AALTO UNIVERSITY, DEPARTMENT OF BUILT ENVIRONMENT, FINLAND

KEYWORDS: LEAF TRAITS, VARIABILITY, PRODUCT VALIDATION, PHENOLOGY, UPSCALING

Challenge

With the advent of new hyperspectral satellite missions, we will be able to map global vegetation parameters on a regular time scale. However, quantitative vegetation products, such as chlorophyll, carotenoids and water content require robust validation to determine their uncertainties. To achieve this, appropriate sampling campaigns should be designed to capture the variability of the traits between vegetation types, within canopy positions or during different phenological phases. The variability of these traits also controls the optical properties of the leaves, which are parameterized in radiative transfer (RT) models. In nature, we observe large functional differences between evergreen tree species such as Norway spruce and deciduous tree species. The fundamental question we ask is what is the variability in traits of these broad forest types with respect to their phenology, canopy position, or intra-specific variability among individuals of the same species. This will allow the design of appropriate protocols for the validation and parameterization of RT models.

Methodology

In this study, we make use of a rich dataset of ground-based leaf-level traits collected at CzechGlobe at several sites between 2006 and 2020. Deciduous species were sampled in 2019 and 2020 in the vicinity of the ecosystem station ICOS Lanžhot. In total, seven campaigns were organized at different phenological phases for 5 dominant tree species - Quercus, Carpinus, Fraxinus, Tilia and Populus. Data on optical and biochemical traits of Norway spruce were collected during several campaigns in the Czech Republic, Finland, and Estonia between 2006 and 2020. These measurements also allowed us to investigate geographical and temporal variability. All campaigns followed similar protocol - sampling was performed by a tree-climber, who always sampled the whole branch from two locations - the illuminated and the shaded part of the canopy. For conifer samples, we distinguished three age classes of needles - current year, previous year and older, while for deciduous samples we sampled both larger and smaller leaves. Leaf samples were collected from branches and analysed in the laboratory for chlorophyll, carotenoids, water, leaf mass per area (LMA) and equivalent water thickness (EWT), while their optical properties (reflectance - HCRF and transmittance HCRT) were measured in the ASD RTS-3ZC integrating sphere. For spruce needles, we used the gap fraction method, which is unavoidable when measuring small samples in special carriers.

Results

For Norway spruce conifer samples, the trait data (leaf chlorophylls, carotenoids, water content and leaf mass per area) show large variability within a single tree crown due to needle age-classes and vertical sampling positions (sun-exposed needles vs. shaded needles). The within-tree variability of spruce traits is often greater than or comparable to the variability between-tree averages. Analysis of more than 300 spruce trees of different ages and growing conditions showed that 50% of tree-averaged leaf chlorophyll a+b content falls within a narrow range between 40 and 50 $\mu\text{g}/\text{cm}^2$. Interestingly, we did not observe a strong seasonal trend in spruce biochemical traits and leaf optical properties, the only notable differences being in the visible range of the current year's needles. Our measurements of needle optical properties also show little geographical and temporal variation. In contrast, broadleaves showed clear phenological trends in both biochemical and optical traits; as with spruce needles, variability among individuals was low, and no significant differences were observed between canopy positions.

Outlook for the future

The results of this study provide new insights into the validation of future quantitative remote sensing products over forest ecosystems, particularly for global products from hyperspectral satellite systems. We propose a ground-based survey data collection method for robust validation that takes into account the specificities of individual tree species and the variability of their biochemical and optical traits. Ground survey data for plant trait validation are scarce, especially when multi-temporal observations are involved. Activities within the in-situ component of COPERNICUS should take this into account and develop their own initiative for a pan-European data collection system for the validation of vegetation products from current and future (e.g., CHIME) missions.

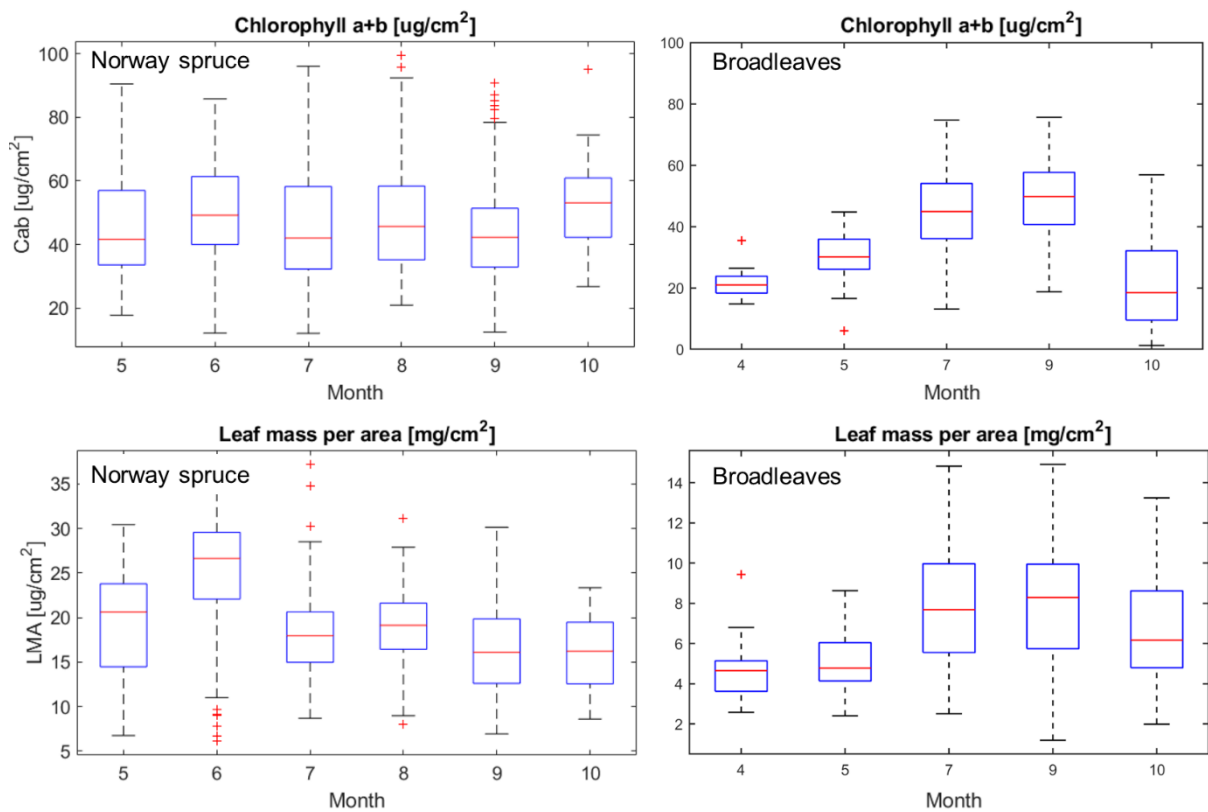


Figure 1. Variability in leaf-level traits of Norway spruce (left) and broadleaves (right) across vegetation season. Upper – chlorophyll content, lower – leaf mass per area (LMA).

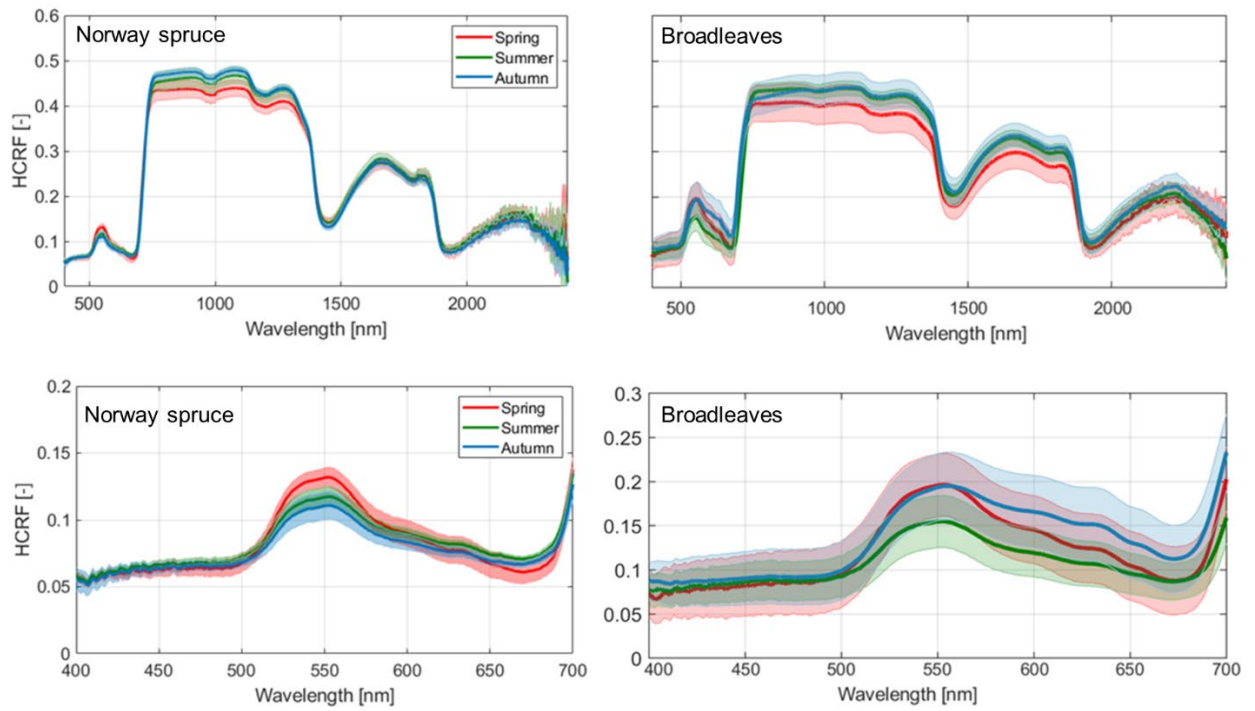


Figure 2. Seasonal trends of leaf optical properties of Norway spruce (left) and broadleaves (right) as measured in spring (red), summer (green) and autumn (blue). Bold line shows the average leaf reflectance (HCRF) value and the corresponding area its standard deviation. Top column shows the entire spectral range from 400 to 2400 nm, while the bottom column highlights the VIS region from 400 to 700 nm.

Assessment of heavy metals contamination of selected tree species using imaging spectroscopy

Dominik Kopeć^{1,2}, *Marlena Kycko*³, *Daniel Okupny*⁴, *Ryszard Borówka*⁴, *Dominik Żmuda*²

¹ University of Lodz, Department of Biogeography, Paleoecology and Nature Conservation, Poland

² MGGP Aero, Poland

³ University of Warsaw, Department of Geoinformatics, Cartography and Remote Sensing, Poland

⁴ University of Szczecin, Institute of Marine and Environmental Sciences, Poland

Keywords: hyperspectral, field spectroscopy, heavy metals, vegetation indices, biogeochemistry

Challenge

One of the major environmental threats associated with industrial development is heavy metal (HM) contamination. A challenge that is being undertaken in remote sensing in recent years is the development of a method that can quickly identify sites polluted by HM. One method of monitoring HM contamination is to analyze their content in plant tissues. Among the plants considered as indicators of HM content, trees are an important group. The identification of trees with higher metal content is based on the assumption that increased HM concentrations interfere with the basic metabolism of plants, which is reflected in the internal structure of the leaves, as well as in individual physiological, biophysical and biochemical parameters. We can analyze these parameters in the form of spectral reflectance curves, as well as vegetation indices.

The aim of the study was to answer the following research questions:

(i) Is there a relationship between the content of HM (Cr, Cu, Fe, Mn, Ni, Pb and Zn) in the leaves of selected tree species (*Acer negundo*, *Betula pendula*, *Salix caprea*) and their spectral signature in the range from 350 - 2500 nm?

(ii) Which spectral bands between 350 and 2500 nm have the greatest potential for identifying HM in tree leaves?

Methodology

The study area included two dye industry waste dumps and an inactive ash and gypsum dump located in the direct neighborhood of the former "Boruta" S.A plant (Poland, Zgierz cities (N 51°50'52"; E19°23'17")). Three tree species were surveyed: goat willow (*Salix caprea*), box elder (*Acer negundo*) and silver birch (*Betula pendula*). The field work was conducted in September 2022. The field studies included: (i) selecting 30 trees from each of the three study species; (ii) collecting 100 leaves from the crown tops of each tree; (iii) measuring the spectral reflectance curve of selected leaves using an ASD FieldSpec 4 spectrometer and Plant Probe in the spectral range of 350-2500 nm.

Then in the laboratory dried leaves were transferred to Teflon bombs, and the wet digestion was performed using a mixture of HNO₃, HCl and H₂O₂. The concentrations of metals (Cr, Cu, Fe, Mn, Ni, Pb and Zn) were determined using the AAS method with Unicam 969 spectrometer. The mercury (Hg) content was determined using a DMA-80 Analyser (Milestone Company).

Next, the first-order derivative and the second-order derivative were calculated from the spectral curves. Then correlation of the content of each heavy metal with the spectral reflectance curve was performed. Spectral ranges depicting the changes in the spectral reflectance curve caused by high concentrations of each heavy metal for each tree species studied separately were derived.

Expected results

The results obtained indicate that it is possible to determine spectral ranges for individual tree species in which changes in reflectance values due to HM contamination are apparent. For example Cr contamination, significant changes in the spectral curves were observed for *Acer negundo* in the 410-673, 688-731 nm ranges for *Salix caprea* in the 420-508, 596-692, 731-1887, 2038-2399 nm ranges. Research is currently underway to indicate whether these ranges are universal or dependent on the tree species and metal studied.

Outlook for the future

The results of the analyses indicate that it is possible to use imaging spectroscopy to identify trees with higher levels of heavy metals in their leaves. The next planned step will be to perform the analysis using aerial hyperspectral data. Thus, the goal of further research will be to perform using hyperspectral data and machine learning to mapping trees with higher heavy metal content.

Diversification of the fAPAR: Retrieval of leaf energy dissipation mechanisms based on spectral unmixing

Shari Van Wittenberghe¹, Eatidal Amin¹, Sara Pescador¹, Ana Belen Pascual⁴, Adrian Moncholi¹, M^oPilar Cendrero-Mateo¹, Jose Moreno¹

¹ University of Valencia, Laboratory of Earth Observation, Spain

Keywords (5): Photoprotection, xanthophylls, pigment absorption, energy partitioning, photosynthesis

Challenge (800 - 1000 characters incl. spaces)

Recent and upcoming high-spectral resolution and imaging spectroscopy satellites for vegetation are bringing opportunities to refine existing global vegetation products and define new ones. In this regard, protocols to quantitatively assess the light partitioning within the photosynthetic antenna could be further refined by the retrieval of effective pigment (f)APAR products. Besides Chl a, other photosynthetic pigments are involved in the photosynthetic light absorption, either with an energy harvesting or energy dissipation function. The latter involves the non-photochemical quenching (NPQ) of excessive energy. Quantifying the partial energy balance mechanisms in an absolute manner has remained, however, a challenging task, even at the leaf level. The reasons for this are (1) the strong spectral overlap of the pigment's absorption, (2) their unknown exact absorption behaviour in vivo, and (3) the relatively small NPQ-related absorption changes compared to the spectrally more dominant Chl changes.

Methodology (1200 – 1500 characters incl. spaces)

In this work we address the issue of spectral overlap of the different photosynthetic pigments at the leaf level, as a first step to define the effective pigment absorbances of Chl a, Chl b, beta-carotene and xanthophylls. To achieve this, we propose a bottom-up spectral unmixing approach at the leaf level to decouple the individual pigment APAR contributions and to extract quantitative information on the distribution of absorbed light based on leaf spectral data, matching expected spectral inputs similar to the FLEX-FLORIS spectral configuration.

To address the unknown NPQ-related absorption mechanisms, controlled leaf spectroscopy experiments were performed. We used light transients to observe the smooth xanthophyll-related absorption changes upon the induction of NPQ. Both quick and slow absorbance changes were observed in the 500-800 nm region and argued to be related to the pigment-protein dynamics whereby spectral properties of the pigment bed are fine-tuned due to modified interactions between the chromophores. Gaussian fitting of the quick 531-nm peak showed the kinetic behaviour driven by antheraxanthin.

Further, we developed a linear unmixing model to retrieve the effective absorption coefficients of the different pigments. In this model we fit the effective absorbance A_{eff} as defined by the Beer-Lambert law, i.e., where the extinction of light, measured by the sum of the scattered light, follows an exponential decay according to an attenuation coefficient $\mu(\lambda)$ multiplied by a factor b .

Expected results (1200 – 1500 characters incl. spaces)

Using a pigment-based spectral unmixing of the estimated absorbance, a new strategy for the disentangling the different fractions of absorbed photosynthetically active radiation at the leaf level is presented. The effective energy absorbed by Chl a was used to calculate the fluorescence quantum

efficiency, which expresses the photon fate of emission versus the absorption, as a first early stress indicator of the photosynthetic light reactions. Focussing on the retrieval of early-stress and photosynthesis-related products, the specific aims here were (1) the quantitative retrieval of an APAR Chl a product to further derive the fluorescence quantum efficiency (FQE), and (2) to test the retrieval of the subtle Xan-driven absorption, indicative of the activation of the quick photoprotective mechanisms. Apart from the extraction of the spectrally-dominant Chl a absorbance, our method demonstrates a first attempt and proof of concept for the retrieval of the subtle NPQ-driven absorption behavior by the xanthophylls in the 500-600 nm region. It is shown that this small feature, which overlaps with all other pigment absorptions, can be retrieved for leaves with a certain minimum threshold of Xan/Chl a accumulation.

Outlook for the future (800 - 1000 characters incl. spaces)

Upscaling the proposed spectral unmixing to larger spatial scales presents the difficulty of increased signal complexity and consideration of structural effects. In particular, the background contribution to the signal, including soil effects that add absorption in the blue-green region of the spectral range, is strongly manifested and can lead to unrealistic fitting of the pigment endmembers. The current retrieval of Xan-driven absorption in the green region therefore needs to be further improved, for example by incorporating stricter constraints based on a priori weight settings and additional soil-based endmember approaches.

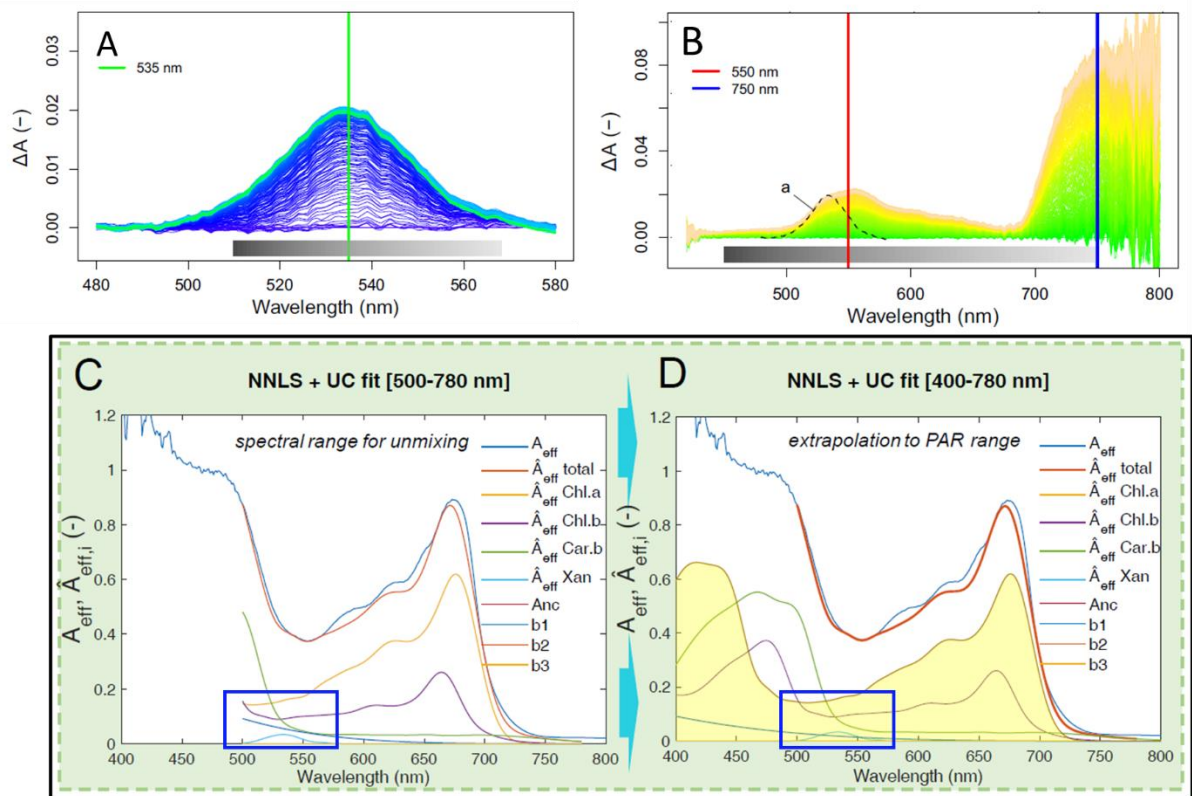


Figure Identified quick (a) and slow (b) absorption features related to controlled energy dissipation by xanthophylls and non-negative least squares (NNLS) linear unmixing of the various pigment absorptions (c,d)

UAV- and handheld-hyperspectral imaging for *Sphagnum* discrimination and vegetation modelling

Franziska Wolff¹, Pasi Korpelainen¹, Anette Eltner², Timo Kumpula¹, Sandra Lorenz³.

¹ University of Eastern Finland, Department of Geographical and Historical Studies, Finland

² Technische Universität Dresden, Institute of Photogrammetry and Remote Sensing, Germany

³ Division Exploration Technology, Helmholtz-Zentrum Dresden-Rossendorf, Helmholtz-Institute Freiberg for Resource Technology (HZDR-HIF), Germany

Keywords: Spectral library, Peatland, Spectral Angle Mapper, Water Index, Multi-source

Challenge

Sensor development advances accurate vegetation classification, enhancing a comprehensive understanding of species spatial distribution and diversity. Applying hyperspectral imaging particularly benefits the understanding of biodiversity based on the spectral properties acquired over a larger, spatial scale. This is interesting for mire ecosystems, where especially *Sphagnum* mosses pose a challenge regarding spectral separability. The separability of peat mosses can help to assess the current state and dynamics in peatland ecosystems, which in turn reveal information about ecological processes, such as carbon storage. This study examined the spectral variation of dominant *Sphagnum* mosses using multi-source, multi-scale concepts as enabled by two hyperspectral sensors to model dominant *Sphagnum* class distribution in an aapa mire in North Karelia, Finland.

Methodology

Using vegetation plot imagery of 32 plots captured with Specim IQ hyperspectral handheld camera (400 – 1000 nm) and species inventory, we established spectral libraries containing species and plot-spectra. The study site was further recorded with a hyperspectral sensor (Specim AFX 10, 400 – 1000 nm) mounted at a UAV resulting in hyperspectral image of approximately 8 cm spatial resolution. Another plot-level spectral library was created using this data by extracting the reflectance values of the plots. We examined the spectral characteristics of the same species and plot types to understand the variation as enabler or challenge for subsequent image analysis. We used the spectral library entries and the recorded hyperspectral imagery to model dominant *Sphagnum* classes and mixed vegetation across the study site using the Spectral Angle Mapper (SAM) algorithm. In addition to the vegetation inventory, we measured the water table depth (WTD) at each plot. We investigate the relationship between those measurements and a calculated Water Index (WI) using the near-infrared region provided by the UAV-hyperspectral image. The WI served as a second part of this study to evaluate the classification performance, as moisture has a significant impact on spectral reflectance and species tend to grow along a wetness gradient.

Expected results

Our study has shown that *Sphagnum* species can be clearly distinguished from other peatland vegetation. The data reveals further clear differences among the different drying stages of mosses as recorded in the field. Among the genus *Sphagnum*, the separation is most evident for the visible region. However, the first derivatives calculated from the reflectance data indicates only little variation suggesting difficulties for further image classification. The SAM classification reached only moderate accuracies; the best result with an accuracy of 0.55 was obtained when using a combination of all three libraries (i.e., species-, plot-, and UAV-plot libraries). A closer look highlights the varying performance

among the dominant *Sphagnum* classes: mosses that grow at a larger hydrological range as indicated by WTD and WI, that is, in the transition area from dry to wet, are prone to misclassification. Lawns consisting of *Sphagnum balticum* were classified with 0.78 and hummock-forming *Sphagnum fuscum* with 0.72 very well.

Outlook for the future

This study considered particularly *Sphagnum* mosses to form spectral libraries with sufficient entries at species and plot level. Further studies should include also other vegetation, such as graminoid species, and recording from different climatic conditions to highlight the hydrological influence on spectral signatures. To enhance the discrimination and classification results, the inclusion of shortwave-infrared (SWIR) would be beneficial.

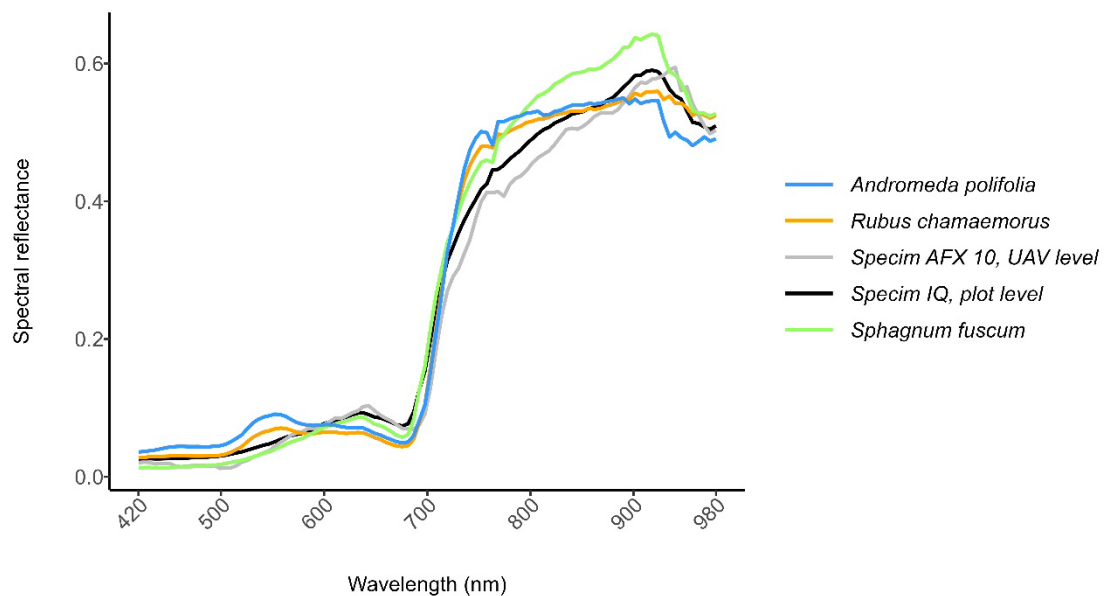


Figure (a) Spectral reflectance profile recorded with a hyperspectral handheld camera (Specim IQ) of three mire species present in one vegetation plot of 30 x 30 cm. Additional, average reflectance spectra of the entire plot recorded with the same device and with the hyperspectral UAV (Unmanned Aerial Vehicle) sensor Specim AFX 10.

**Them.Sess. 1-3: Assessment of
Advancing Water Quality
Monitoring with Hyperspectral
Satellite Imagery and Explainable
Machine Learning**

First Look at Mondrian Forests for Hyperspectral Secchi Depth Estimation

Sivert Bakken¹, Geir Johnsen², Tor Arne Johansen¹

¹Norwegian University of Science and Technology, Department of Engineering Cybernetics

²Norwegian University of Science and Technology, Department of Biology

Keywords (5): Reflectance, Water Quality, Hyperspectral, Machine Learning, Secchi Depth

Challenge (800 - 1000 characters incl. spaces)

The Secchi depth is a measure of the transparency of water. This measure has been taken for centuries and is one of the longest-standing water quality records. Secchi disks are a simple, low-cost tool for obtaining this measurement. However, the Secchi disk approach is best suited to cover smaller areas. Estimated Secchi Depth from Earth Observation can reduce this limitation. Hyperspectral measurements of ocean colour are valuable due to their ability to reveal ecologically essential characteristics to derive geophysical ocean properties and develop new applications. Estimating the Secchi depth from hyperspectral water leaving reflectance can be an asset in water resource management and decision support. These activities can be further supported by quantified uncertainty, giving a better foundation for policy decisions.

Methodology (1200 – 1500 characters incl. spaces)

The work is based on the GLORIA data set of Secchi Depths. Constructing a robust estimation model for Secchi Depth is challenging due to nonlinear responses to optical properties and complex physical and biogeochemical processes in different waters. Past research has demonstrated the feasibility of using machine learning techniques to effectively enhance remote sensing estimation of Secchi disk depth in global lakes and reservoirs. Machine Learning models that can represent nonlinear responses well, such as random forests (RF), have shown favourable performance. Mondrian Forests (MF) is a machine learning algorithm utilized for regression tasks that belong to the family of RFs. Unlike standard decision tree implementations, MFs do not restrict themselves to the leaf when making predictions. Instead, they consider the entire tree structure, making them a variant of random forests. MFs are especially beneficial for large-scale regression problems where uncertainty plays a role. They can measure the uncertainty linked with each prediction, which is helpful in real-world regression problems. This work investigates the performance of MFs in estimating from hyperspectral reflectance. The MF model performance is compared with other relevant ML models.

Results (1200 – 1500 characters incl. spaces)

The expected result of this study is a better understanding of the application of Mondrian Forests (MF) to derive bio geophysical parameters of interest, exemplified by Secchi Depth, from hyperspectral remote sensing reflectance of ocean colour. The expected results also include insight into how well the MF approach compares with other Machine Learning approaches that attempt to quantify uncertainty. When put alongside conventional ML methods that do not quantify uncertainty, the cost associated with uncertainty quantification will also be discussed.

Outlook for the future (800 - 1000 characters incl. spaces)

The study aims to construct an improved estimation model using machine learning techniques to estimate Secchi depth with uncertainty assessments from hyperspectral water-leaving reflectance. The expected outcome is a better understanding of the application of Mondrian Forests (MF) to derive biogeochemical parameters of interest, such as Secchi Depth, from hyperspectral remote sensing reflectance of ocean color. The results can form a basis for similar model structures adapted to specific regions or satellites. With a successful adaptation, the derived results from this study can provide a better foundation for decision support. Future studies will look at if this approach can be adapted to existing earth observation systems.

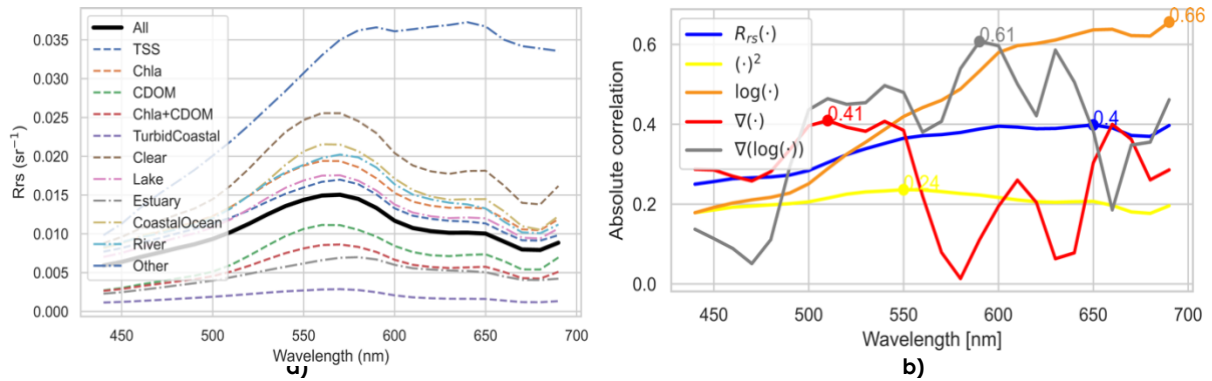


Figure a) Mean wavelength of remote sensing reflectance from the GLORIA data set, where each water type and water body type, as defined in the GLORIA publication, has been plotted as one signal. b) The absolute value of the correlation coefficient between each wavelength vector of various static preprocessing methods and the directly measured Secchi Depth.

Advancing Phytoplankton Primary Production Modeling through Hyperspectral Neural Network-Based Uncertainty Quantification

EARSeL Valencia 2024

Abstract

Corresponding Author:

mortimer.werther@eawag.ch

Mortimer Werther¹, Daniel Odermatt^{1,2}, Arun M. Saranathan³, Nima Pahlevan^{3,4}, Sundarabalan V. Balasubramanian^{5,6}, Daniela Gurlin⁷, Jonas Wydler^{1,2}, Olivier Burggraaff⁸

¹ Swiss Federal Institute of Aquatic Science and Technology (EAWAG) – Department of Surface Waters - Research and Management, Dübendorf, Switzerland

² Department of Geography, University of Zürich, 8057 Zürich, Switzerland

³ Science Systems and Applications (SSAI), Lanham 20706, MD, USA

⁴ NASA Goddard Spaceflight Center, Greenbelt 20771, MD, USA

⁵ University of Maryland Baltimore-County, Baltimore, MD 21250, USA

⁶ Geo-Sensing and Imaging Consultancy, Trivandrum, Kerala 695001, India

⁷ Wisconsin Department of Natural Resources, Madison, WI, USA

⁸ Institute of Environmental Sciences (CML), Leiden University, Leiden, The Netherlands

Keywords: Phytoplankton, IOPs, Neural Networks, Uncertainty, Hyperspectral

Challenge

In the study of lake and coastal water ecology, dependable measurements are paramount, and phytoplankton primary production (PP) stands out as a key variable. Satellite remote sensing is widely used to obtain surface PP estimates. Obtaining these estimates typically involves a sequence of algorithms, each with its own level of uncertainty, beginning with the atmospheric correction (AC) of satellite-measured top-of-atmosphere radiance. The AC process generates remote sensing reflectance (R_{rs}), the foundation for extracting inherent optical properties (IOPs). These IOPs, specifically phytoplankton absorption and particulate backscattering, are subsequently employed in PP models. While advanced hyperspectral missions such as NASA's Plankton, Aerosol, Cloud, ocean Ecosystem (PACE) are engineered to improve the fidelity of both R_{rs} and IOPs, they cannot fully negate intrinsic uncertainties. Traditional algorithms like Lee et al.'s, 2002 Quasi-Analytical Algorithm (QAA) fall short in these optically complex waters, limiting their utility in PP models where understanding the propagation of uncertainty is crucial for model design, optimization, and evaluation.

Methodology

Recent research has explored neural networks (NNs) like Mixture Density Networks and Bayesian Neural Networks (O'Shea et al., 2023; Pahlevan et al., 2022; Saranathan et al., 2023; Werther et al., 2022). These networks employ probabilistic modeling techniques to improve the IOP retrieval and estimate associated uncertainty. While promising, discrepancies have emerged in how well each network's intrinsic uncertainty aligns with actual retrieval errors (Saranathan et al., (in prep.)). This raises questions: Are different probabilistic NNs comparably reliable in identical aquatic scenarios? Or are the uncertainty estimates model-specific?

To clarify these aspects, our study undertakes a comparative analysis of six distinct probabilistic NNs based on ensemble, mixture model, and variational inference frameworks. We target four key objectives: 1) uniform evaluation of IOP retrieval uncertainties using a consistent model and

dataset configuration, 2) assessment of the calibration quality across various NNs, 3) differentiation between aleatoric (data-driven) and epistemic (model-driven) uncertainties, and 4) investigation into methods for recalibrating poorly aligned uncertainty estimates.

Expected results

Anticipated results suggest that the NNs under evaluation will show effectiveness in retrieving IOPs, with expected inter-model error rate discrepancies ranging from 3% to 15%. Despite likely similar retrieval accuracy, we expect the quality of uncertainty calibration to vary significantly among the tested models. By separating these uncertainties into aleatoric and epistemic components, we will identify variations that appear to be model-specific. Some models are expected to produce high-confidence yet misaligned uncertainty estimates, while others will likely be more accurately calibrated but with higher uncertainties. We plan to demonstrate that these substantial calibration misalignments can be improved using a re-calibration approach with an independent hold-out dataset.

These expected results carry multiple implications: they will highlight the inconsistent capability of probabilistic NNs to provide well-calibrated uncertainties for IOP retrievals and underscore the importance of choosing the appropriate architecture for specific applications. Moreover, we intend to show that recalibration techniques will be effective across different architectures, provided a separate hold-out dataset is available.

Outlook for the future

The integration of estimated IOP uncertainties into PP models offers distinct advantages. PP models are inherently sensitive to input parameters like phytoplankton absorption and total particulate backscattering. Using NNs that excel in estimating these parameters improves the robustness of PP models. The calibrated uncertainties permit the modeling of a distribution of PP outcomes, quantifying the model's output uncertainty. This contributes directly to the robustness of long-term ecological, food web, and climate change studies. Differentiating between epistemic and aleatoric uncertainties helps understanding whether limitations in PP models originate from input observations or the model architecture, guiding research efforts in targeted model development. Additionally, the use of calibrated uncertainties allows for a quantitative assessment of the expected benefits using hyperspectral resolutions.

References

- Lee, Z., Carder, K.L., Arnone, R.A., 2002. Deriving inherent optical properties from water color: a multiband quasi-analytical algorithm for optically deep waters. *Appl. Opt.* 41, 5755–5772. <https://doi.org/10.1364/AO.41.005755>
- O'Shea, R.E., Pahlevan, N., Smith, B., Boss, E., Gurlin, D., Alikas, K., Kangro, K., Kudela, R.M., Vaičiūtė, D., 2023. A hyperspectral inversion framework for estimating absorbing inherent optical properties and biogeochemical parameters in inland and coastal waters. *Remote Sensing of Environment* 295, 113706. <https://doi.org/10.1016/j.rse.2023.113706>
- Pahlevan, N., Smith, B., Alikas, K., Anstee, J., Barbosa, C., Binding, C., Bresciani, M., Cremella, B., Giardino, C., Gurlin, D., Fernandez, V., Jamet, C., Kangro, K., Lehmann, M.K., Loisel, H., Matsushita, B., Hà, N., Olmanson, L., Potvin, G., Simis, S.G.H., VanderWoude, A., Vantrepotte, V., Ruiz-Verdù, A., 2022. Simultaneous retrieval of selected optical water quality indicators from Landsat-8, Sentinel-2, and Sentinel-3. *Remote Sensing of Environment* 270, 112860. <https://doi.org/10.1016/j.rse.2021.112860>
- Saranathan, A.M., Smith, B., Pahlevan, N., 2023. Per-Pixel Uncertainty Quantification and Reporting for Satellite-Derived Chlorophyll-a Estimates via Mixture Density Networks. *IEEE*

- Transactions on Geoscience and Remote Sensing 61, 1–18.
<https://doi.org/10.1109/TGRS.2023.3234465>
- Saranathan, A.M., Pahlevan, N., Werther, M., Balasubramanian, S.V., Odermatt, D., 2024. Assessment of density-based neural networks for the dual estimation of water quality indicators and uncertainties from multi- and hyperspectral remote sensing. *In preparation*.
- Werther, M., Odermatt, D., Simis, S.G.H., Gurlin, D., Lehmann, M.K., Kutser, T., Gupana, R., Varley, A., Hunter, P.D., Tyler, A.N., Spyrakos, E., 2022. A Bayesian approach for remote sensing of chlorophyll-a and associated retrieval uncertainty in oligotrophic and mesotrophic lakes. *Remote Sensing of Environment* 283, 113295.
<https://doi.org/10.1016/j.rse.2022.113295>

Machine Learning-Based Assessment of Cyanobacteria concentration with hyperspectral In-situ data: Implications and insights for Remote Sensing Applications

Jorge García-Jiménez^{1,2}, Katalin Blix³, Ana B. Ruescas², Julia Amorós-López², Dagmar Müller¹, Carole Lebreton¹, Kerstin Stelzer¹.

¹ Brockmann Consult GmbH, Germany

² Image Processing Laboratory, University of València, Spain

³ UiT The Arctic University of Norway, Norway

Keywords (5): Cyanobacteria, Water Quality, Hyperspectral, Machine learning, Earth Observation.

Challenge (800 - 1000 characters incl. spaces)

Cyanobacteria Harmful Algal Blooms (cHABs) cause environmental problems in aquatic ecosystems and water quality. Monitoring initiatives, such as the LIFE project CyanoBloom, aim to establish algal alert warning systems based on satellite and ground-based measurements for rapid response to detect high levels of cHABs. When using optical instruments for monitoring and analysis, Chlorophyll-a (Chl-a) and Phycocyanin (PC) are the primary fingerprints of cyanobacteria. While Chl-a is a ubiquitous pigment in all phytoplankton communities, PC is solely in cyanobacteria. Different approaches, from band ratios to neural networks, have been developed to isolate the contribution of cyanobacteria to the total Chl-a and quantify PC concentration. Technical advances in in-situ equipment allow us to measure the concentration of different phytoplankton groups together with radiometric data, enabling the creation of large databases for developing machine-learning algorithms that can improve the detection of cyanobacteria and determine the alert levels.

Methodology (1200 – 1500 characters incl. spaces)

This research utilises two databases that contain collocated radiometric data (converted to Rrs: Remote sensing reflectance) along with cyanobacteria and Chl-a concentration ($\mu\text{g/l}$) *in-situ* measurements from spectrofluorimeters. The first database comprises data from a diverse range of inland water bodies in Germany (SpecWa from Maier et al., 2020); while the second database consists of various measurements taken within Lake Balaton in Hungary. These two databases offer a wide range of optical and trophic conditions of the lakes. One of the objectives of this study is to serve as a proof of concept for hyperspectral satellite sensors. To achieve this, we conducted a spectral convolution using the spectral response function (SRF) of the EnMAP sensor, allowing us to simulate and identify the relevant wavelengths of the sensor. To fully exploit the potential of machine learning, we evaluate different regression algorithms to estimate Chl-a and cyanobacteria, including linear and non-linear models like Random Forest, XGBoost, Gaussian Processes and Neural Nets.

Results (1200 – 1500 characters incl. spaces)

The results of the study are focused on different issues: i) dataset preparation and analysis; ii) application of the machine learning models, including feature selection and hyperparameter tuning; iii) model comparison through regression performances, accuracy of the models and statistical analysis. We will perform a comparison with other methods of cyanobacteria detection based on semi-analytical procedures, like band ratios. Derivative algorithms, based on the quantification of the curvature in the spectra due to absorption and scattering, will also be evaluated.; iv) application of the models on EnMAP imagery. The results will offer insights into the performance of data-driven models when handling high-dimensional data. They will also determine whether the improvements, by including the entire wavelength spectrum, can outperform the methods based on specific wavelength selection.

Outlook for the future (800 - 1000 characters incl. spaces)

Derivation of water quality parameters and associated products from remote sensing is critical for the rapid and extensive monitoring of inland and coastal waters. Operational products and services based on multispectral data are a reality, but further work could be done on the accuracy of the estimations. Hyperspectral sensors like PRISMA, EnMAP and future missions like CHIME or PACE will add new spectral information and hopefully help to better understand some essential features in determining cyanobacteria concentration and other types of HABs. With this work, we expect to also improve the identification of phytoplankton communities by better accounting for concentrations of algae types or cell sizes/structures with specific functions.

PHYTOPLANKTON RECOGNITION IN MODELLED HYPERSPECTRAL DATA USING MACHINE LEARNING AND CLASSICAL DATA ANALYSIS METHODS

EARSel Valencia 2024
Abstract
Corresponding Author:
esmee.oudijk@ntnu.no

Oudijk, Adriënne Esmeralda; Flores-Romero, Alvaro; Justo, Jon Alvarez; Hasler, Oliver Kevin; Johansen, Tor Arne; Alver, Morten Omholt

NORWEGIAN UNIVERSITY OF SCIENCE AND TECHNOLOGY, DEPARTMENT OF
ENGINEERING CYBERNETICS, NORWAY

Keywords (5): Ocean Observation, Light Interaction Modelling, Hyperspectral data, Phytoplankton Recognition, Multi-Target Regression

Challenge (800 - 1000 characters incl. spaces)

To study primary production in oceans and lakes it is of great importance to distinguish phytoplankton species. One possible tool to study this on large spatial scale is hyperspectral imaging (HSI) from space. For distinguishing phytoplankton groups like diatoms and flagellates in HSI data, the challenge lies in identifying the optimal (combinations of) spectral bands. In this work we focus on trying to detect the presence of the diatoms and flagellates groups in spectral signatures coming from HSI. Machine learning algorithms (ML) are possible candidates to identify phytoplankton groups from spectral signatures. The performance of ML and other classical data analysis methods are evaluated in this paper. Once we can distinguish phytoplankton groups in HSI data, the HSI observations can be used to correct ocean models. These models can give insight into the ecosystems on high spatiotemporal dimensions.

Methodology (1200 – 1500 characters incl. spaces)

To train ML networks, large, labelled datasets (thousands of spectra) are needed. Creating such datasets using *in situ* data to label phytoplankton functional groups in the ocean is challenging. This is because the coverage of HSI from space (~km) does not align with sample point coverage (~m to cm). To address this, we simulate labelled, hyperspectral point measurements using the state-of-the-art light model Ecolight-S, provided by Sequoia Scientific.

We generate N random water column examples, each with vertical profiles of key constituents: flagellate and diatom groups, and coloured dissolved organic matter (cdom). We specify absorbance and scattering coefficients for each wavelength and constituent. Ecolight-S solves the radiative transfer equations through the water column's optical layers, and calculates the above-surface, nadir-viewing, water-leaving radiance, and the spectral-irradiance down. We then derive the remote sensing reflectance (RRS) in air. The dataset comprises N examples of water column constituents and their calculated RRS.

The dataset utilized in ML and classic data processing methods includes 1D RRS arrays (400 to 700 nm, 5 nm steps). These are associated with 1D label arrays denoting the maximum concentrations and depths for flagellates, diatoms and cdom. Fig. 1 shows the concentration data. We focus on this limited regression problem due to the substantial impact of constituents on RRS when peak values occur in the top layers or at high concentrations.

Results (1200 – 1500 characters incl. spaces)

The large dataset will be used in different ML and classic data processing methods to find which constituents can be observed with remote sensing and which (combination of) spectral bands are relevant to distinguish the different constituents. Hyperspectral imaging offers an advantage over multispectral imaging by enabling to take the derivatives of the RRS, potentially identifying critical spectral

features for classification. The first data analysis method is Principle Component Analysis (PCA), which we use to find the orthogonal components that explain the spectral variability. We apply PCA on the original RRS as well as on its first and second derivative (RRS' and RRS''). The RRS'' is shown in Fig. 2. Then, we correlate the eigenvectors with the largest eigenvalues (the components that determine most of the variability), to the diatom, flagellate and cdom concentrations, to determine if PCA is a suited first approach for classifying RRS. Second, we use Partial Least Square Regression (PLSR) on RRS' and RRS'' to find which (combination of) wavelengths (features) are important for flagellate and diatom groups and cdom. Last, we explore ML for feature selection on wavelength combinations. The optimal feature for each constituent is used to predict the depth at which the maxima values occur (classification), and its concentration (regression). Evaluation metrics include precision and accuracy for classification and Mean Absolute Error and historical average error for regression.

Outlook for the future (800 - 1000 characters incl. spaces)

The goal is to identify relevant wavelengths for recognizing phytoplankton functional groups. The current light model set-up lacks atmospheric effects. To use the modelling set-up in remote sensing from space we need to incorporate this. Then, we can test our models using real satellite data, for example from the HYPSON-1 satellite of our university. HYPSON-1 images coastal areas and provides hyperspectral data of a spectral resolution of 5 nm in the visible light spectrum.

To be able to train ML algorithms, a high-quality dataset is prerequisite, but the feasibility is not given, and we have to test further whether the algorithms are successful. Currently, the concentrations of diatoms, flagellates, and cdom are generated independently. In reality, phytoplankton concentrations are physically and ecologically dependent. The coupled physical-biological ocean model SINMOD captures these dependencies. In future training datasets SINMOD simulations could be used for generating the datasets.

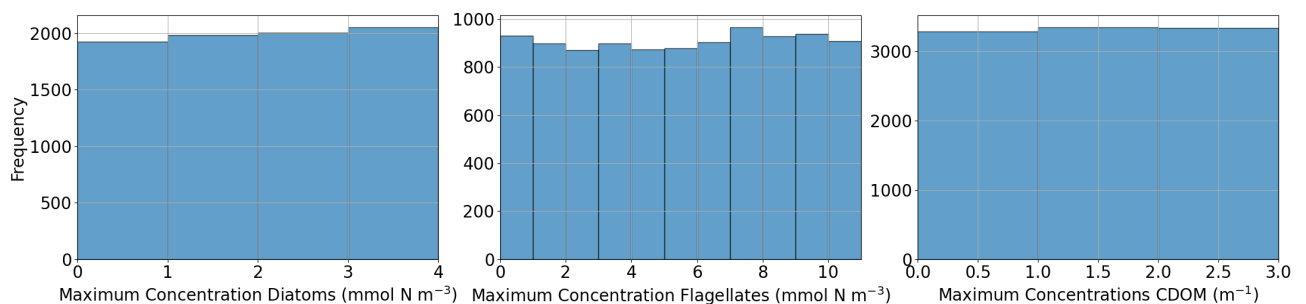


Figure 1 These histograms show the maximum concentration distributions of the different constituents.

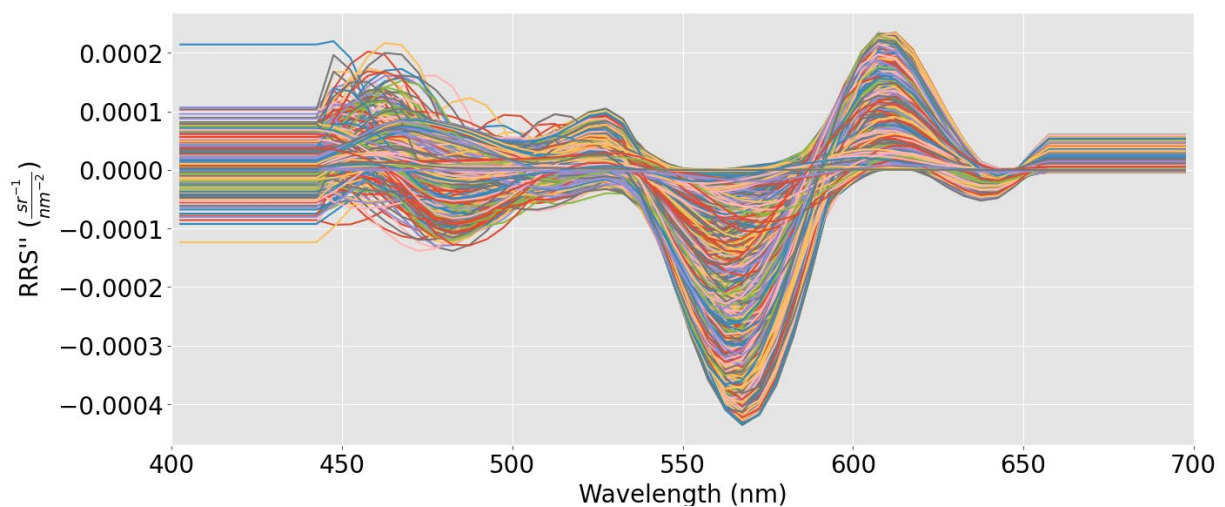


Figure 2 The second derivative of the RRS.

Advances in ocean surface modeling to correct for sun and sky glint contributions in imaging spectroscopy measurements

EARSel Valencia 2024

Abstract

Corresponding Author: urs.n.bohn@jpl.nasa.gov

Niklas Bohn¹, Philip G. Brodrick¹, John Chapman¹, Adam Chlus¹, Regina Eckert¹, Robert O. Green¹, Marcel König², Jeremy Kravitz³, Kelly Luis¹, Jouni Susiluoto¹, David R. Thompson¹

¹Jet Propulsion Laboratory, California Institute of Technology, USA

²Center for Global Discovery and Conservation Science, Arizona State University, Tempe, USA

³NASA Ames Research Center, Moffett Field, USA

Keywords (5): PRISM, imaging spectroscopy, ocean remote sensing, glint, SBG

Challenge

Remote sensing of water bodies is critical for monitoring ecosystems of open oceans and coastal zones. It helps to assess the impacts of climate change on natural resources and global carbon budgets. Remote estimates of, e.g., chlorophyll concentration or phytoplankton blooms can provide valuable insights into environmental processes. Imaging spectroscopy measurements feature the spectral resolution to detect and quantify water constituents. However, one of the challenging factors impacting the accuracy of these retrievals is surface glint that occurs at the air-water interface. It can be separated into sun and sky glint. Existing remote sensing literature emphasizes sun glint over sky glint. Furthermore, glint correction algorithms are commonly applied as a post-hoc method after retrieving water-leaving reflectance from radiance measurements, introducing substantial uncertainties, especially in the case of challenging illumination conditions.

Methodology

We present a new approach that couples a physics-based surface model, which incorporates the effects of both sun and sky glint, with simulations of atmospheric radiative transfer to estimate glint-corrected water-leaving reflectance directly from measured at-sensor radiance. We exclude wind speed and structure of wave facets from our glint model by solely optimizing for both a direct and a diffuse component of scattered sky radiance being reflected at the air-water interface. We combine an analytical three-component water surface reflectance model (3C) with a synthetic spectral library from the Spectral Water Inversion Processor and Emulator (SWIPE), and obtain required atmospheric functions from the MODTRAN radiative transfer code. We use SWIPE to build glint-free simulations of water-leaving reflectance, which is essential to inform a prior-based Optimal Estimation (OE) approach. The needed separation of downwelling direct and diffuse transmittance is achieved by calculating path radiance and transmittance from multiple MODTRAN runs with different surface reflectance magnitudes. Our model is integrated into the open-source ISOFIT codebase, so that atmosphere and surface parameters are optimized simultaneously, and validated with measurements from the airborne PRISM imaging spectrometer.

Results

Results from selected PRISM flightlines acquired during the S-MODE campaign in both fall 2022 and spring 2023 show that magnitude and shape of estimated remote sensing reflectance significantly improves as the contribution of both sun and sky glint is removed. Near-infrared reflectance is reduced to a minimum, which is expected for ocean water surfaces. At the same time, the simultaneous inversion of aerosol optical depth (AOD) and surface glint improves reflectance in the shortest visible wavelengths as a general overestimation of surface-reflected radiation is removed by attributing more scattering to atmospheric aerosols. The use of glint-free SWIPE-based priors further enhances the accuracy of retrieved spectral shape and magnitude. Almost residual-free radiance fits confirm the validity of our expanded forward model. A more detailed investigation of optimized sky radiance reveals that the contribution of sun glint is up to six orders of magnitude higher and varies significantly more than the diffuse sky glint component. The latter is rather a constantly underlying spectrum, present with nearly the same

magnitude in all analyzed examples. On the other hand, we find that sky glint can also exceed sun glint in the blue visible wavelengths, indicating increased Rayleigh and aerosol scattering, which is confirmed by larger AOD values in these cases.

Outlook for the future

We present a new approach to model the effects of both sun and sky glint in spectroscopic measurements over water surfaces. Instead of removing glint post-hoc from water-leaving reflectance or entirely excluding glint pixels from any retrievals, we simultaneously estimate atmospheric parameters and surface properties using a simplified assumption about sky radiance reflected at the water surface. First results confirm improved performance by reducing NIR reflectance to a minimum. Although impacts on downstream products such as chlorophyll concentration or phytoplankton blooms still have to be investigated and a comprehensive validation with in-situ measurements is not yet completed, we see promising potential for future ocean remote sensing retrievals, with a particular outlook to the upcoming era of global spaceborne spectroscopic measurements from SBG and CHIME.

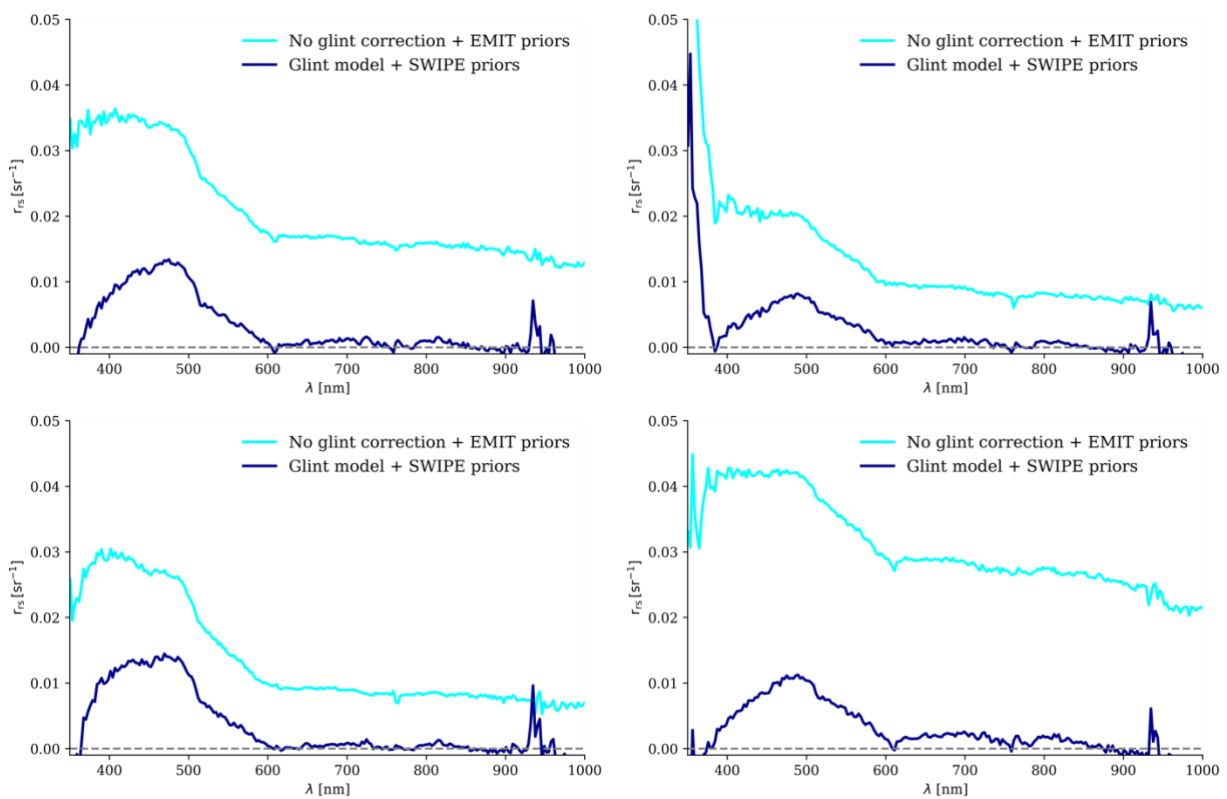


Figure 1. Examples of retrieved water-leaving reflectance from PRISM. The light blue lines show results without glint correction assuming standard EMIT priors, while dark blue lines highlight improved reflectance after applying the new sun and sky glint model in combination with glint-free SWIPE priors.

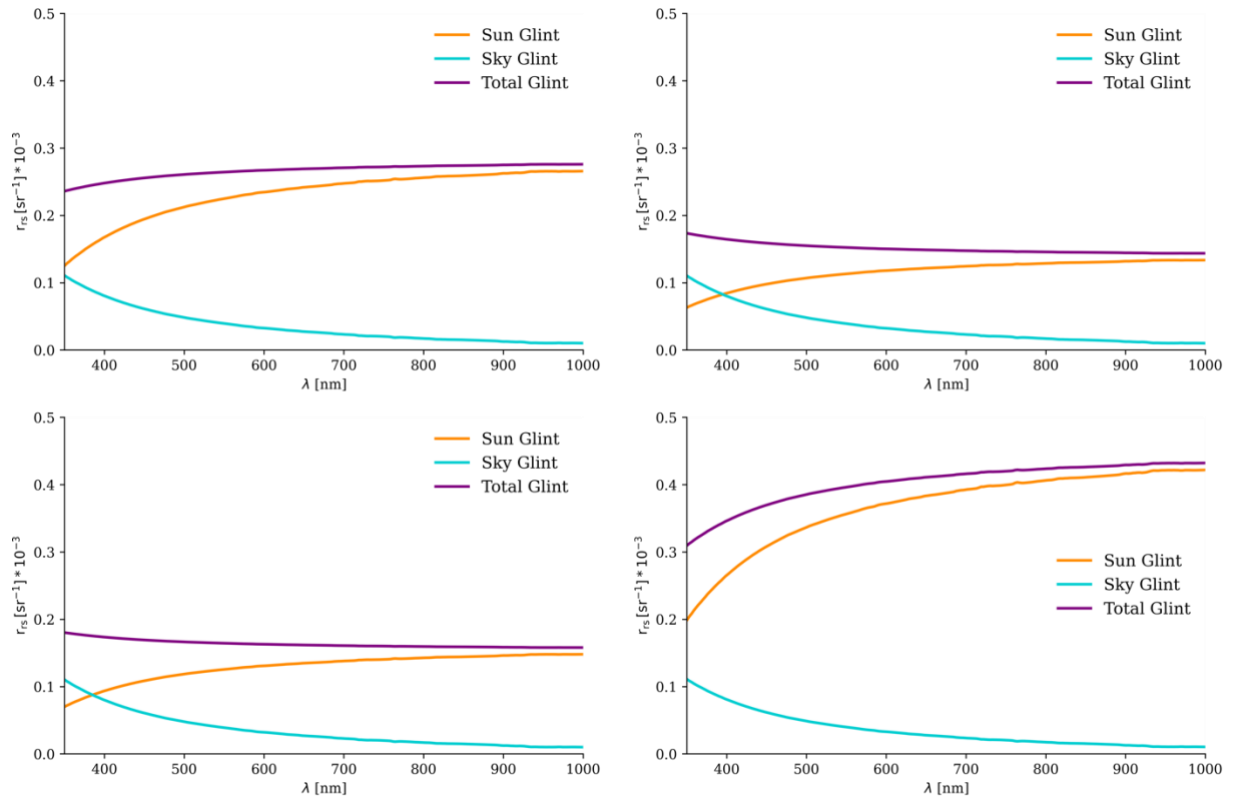


Figure 2. Absolute contributions of sun, sky, and total glint for the dark blue spectra in Figure 1.

Estimating Aquatic Plant Diversity Using Spectral Metrics from Drone Hyperspectral Imaging

Paolo Villa¹, Andrea Berton², Rossano Bolpagni^{1,3}, Michele Caccia^{4,5}, Maria Beatrice Castellani⁶, Andrea Coppi⁶, Alice Dalla Vecchia^{1,3}, Francesca Gallivanone^{4,5}, Lorenzo Lastrucci⁷, Erika Piaseri^{1,8}

¹ National Research Council, Institute for Electromagnetic Sensing of the Environment, Italy

² National Research Council, Institute of Geosciences and Earth Resources, Italy

³ University of Parma, Dept of Chemistry, Life Sciences and Environmental Sustainability, Italy

⁴ National Research Council, Institute of Molecular Bioimaging and Physiology, Italy

⁵ National Biodiversity Future Center (NBFC), Italy

⁶ University of Florence, Department of Biology, Italy

⁷ University of Florence, Natural History Museum, Italy

⁸ Politecnico di Milano, Department of Civil and Environmental Engineering, Italy

Keywords: Macrophytes, Functional diversity, Generalized Additive Model (GAM), Functional traits, Ultra-high resolution

Challenge

Due to their morpho-physiological peculiarities and wide phenotypic plasticity, aquatic plants occupy the extremes of the global spectrum of vegetation forms; such heterogeneity results in them exhibiting contrasting patterns of diversity along ecological and geographical gradients. In the last decade, high-throughput imaging spectroscopy has emerged as a feasible and efficient option for assessing plant diversity based on spectral proxies directly related to morphological and biochemical traits, which we define as spectro-functional traits. Linking spectral traits with plant species diversity to characterise plant communities can further advance this topic. In this study, we explored the use of spectral features extracted from centimetre resolution hyperspectral images collected by a drone to estimate functional diversity using generalized additive models (GAMs) within communities of floating hydrophytes and helophytes sampled across a trophic gradient.

Methodology

Hyperspectral imagery was acquired over target aquatic plant communities in five wetland sites in Italy during summer 2021 using a Nano-Hyperspec sensor (Headwall Photonics), resulting in 3 cm nominal resolution georeferenced surface reflectance data cubes.

Spectral diversity features were derived from the hyperspectral data cubes under four different dimensions: i) spectral species functional diversity (SSFD); ii) Rao's quadratic entropy from selected spectral features (RaoQ); iii) spectro-functional traits (SFT); and iv) the first 5 spectral principal components (PC). For each dimension, synthetic metrics were derived as mean, standard deviation. For each data cube, only green material pixels were retained by setting a minimum greenness index threshold, i.e. $WAVI > 0.4$, and the mean, standard deviation, coefficient of variation and distance from the multidimensional centroid were calculated over all green pixels falling within a circular area of 4 m radius centred on the in situ surveyed plant communities (Fig. 1).

In addition to the drone flights, in situ data were collected from boat-based surveys covering species abundance and individual functional traits of 90 target plant communities divided into two groups with

different water affinity: 41 of floating and emergent hydrophytes and 49 of riparian helophytes. Functional diversity of the sampled plant communities was calculated using n-dimensional kernel-based hypervolumes using the R package *bat*, and expressed in terms of richness (FDrich), divergence (FDdiv) and evenness (FDeven).

Results

After excluding mutually correlated features (Pearson's $\rho < -0.7$ or > 0.7) within each dimension, a set of spectral metrics was used as input to GAMs (R package *mgcv*) to predict functional diversity across all target communities in terms of FDrich, FDdiv and FDeven (log-transformed to reduce distribution skewness). Only metrics showing moderately significant effects in multidimensional linear models ($p < 0.1$) were used as inputs for non-linear GAMs, and no input interactions were considered. GAMs were calibrated separately using selected input metrics belonging to each spectral dimension (SSFD, RaoQ, SFT, PC) and by merging all spectral metrics that showed significant effects in dimension-specific models.

Our results (Table 1) show that hypervolume-based community richness (FDrich) is the functional diversity metric that is better estimated from spectral features in each dimension ($R^2 > 0.38$). The situation is similar for the community divergence metric (FDdiv), but with slightly lower precision compared to FDrich (difference in $R^2 \geq 0.04$). Functional evenness is the diversity metric with the lowest stability from spectral features ($R^2 < 0.41$).

Regarding the different spectral dimensions considered, spectral PC tends to be the best dimension in terms of modelling efficiency for richness and divergence ($R^2 = 0.70$ for FDrich, $R^2 = 0.66$ for FDdiv) and SFT performs best for evenness ($R^2 = 0.4$), while metrics derived from Rao's quadratic entropy underperform other dimensions for all FD outputs ($R^2 < 0.38$).

Outlook for the future

Preliminary results have shown that there is potential for estimating functional diversity in aquatic plant communities using centimetre resolution hyperspectral imagery, and that some spectral features are more efficient for estimating functional diversity than others. As merging the best spectral features (e.g. combining spectral species diversity features with spectral functional features and spectral PC) could further improve the performance of diversity modelling, future developments will focus on testing how to better design such integration.

In addition, future work will include testing the approach across spatial and spectral resolutions to assess upscaling capabilities, e.g. up to satellite hyperspectral data (PRISMA, EnMap).

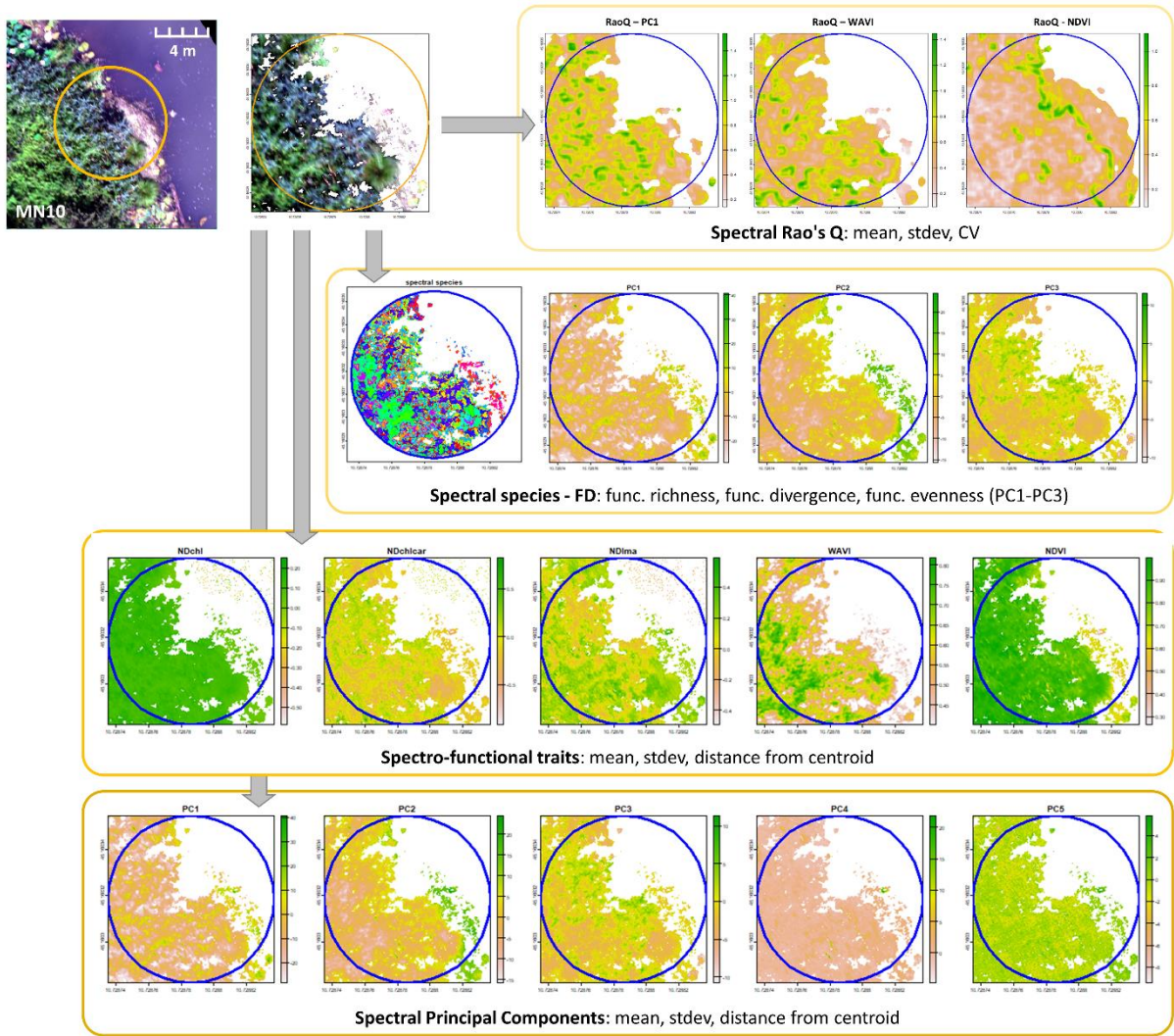


Figure 1 Example of spectral features/metrics derived from hyperspectral data over a target community (ID: MN10).

Table 1 Summary of GAM results with different input combinations (shaded cells identify input metrics used for each model, and show the significance of their effect in terms of p-value)

Model output	Spectral species FD			Spectral Rao's Q			Spectro-functional traits			Spectral principal components			Merged spectral features		
	FDirich	FDdiv	FDeven	FDirich	FDdiv	FDeven	FDirich	FDdiv	FDeven	FDirich	FDdiv	FDeven	FDirich	FDdiv	FDeven
Input features															
SSFD_rich	ns														
SSFD_even	***	**											***	***	
SSFD_div			ns												
SSFD_even	**	*	ns										***	***	
RaoQ_PC1_m				°	*										
RaoQ_PC1_sd					ns	ns									
RaoQ_PC1_CV					ns										
RaoQ_WAVI_CV				ns	ns										
RaoQ_NDVI_m				*	ns										
RaoQ_NDVI_sd				ns		ns									
RaoQ_NDVI_CV				ns	*										
NDchlar_m															
NDVI_m							ns								
NDchl_sd							*	°							
NDchlar_sd							°	ns							
NDVI_sd							*	°	°				***	***	ns
PC1_m										°	**				
PC3_m												°			*
PC4_m										***	***		***	***	
PC5_m											*				
PC4_sd										*					
PCdist_norm										°	ns	ns			
R²_{adj}	0.51	0.45	0.24	0.38	0.33	0.25	0.50	0.41	0.41	0.70	0.66	0.38	0.79	0.68	0.35

*** = p<0.001, ** = p<0.01, * = p<0.05, ° = p<0.1, ns = p≥0.1

Them.Sess. 1-4: Imaging spectroscopy for soil applications

Spaceborne hyperspectral time-series for soil properties mapping

Kathrin J. Ward^{1,2}, Saskia Foerster¹, Sabine Chabrillat^{1,2}

¹ German Research Centre for Geosciences Potsdam, Section Remote Sensing and Geoinformatics, Germany

² Leibniz University Hannover, Institute of Soil Science, Germany

KEYWORDS (5): SOIL PROPERTIES, SPACEBORNE, HYPERSPECTRAL, MULTITEMPORAL, SOC MAPS COMPOSITE

Challenge (800 - 1000 characters incl. spaces)

Mapping and monitoring of soil quality and soil degradation is recommended by the European Commission and within frameworks such as the SDGs. It is essential to face challenges such as food security and climate change. Our soils are the largest terrestrial carbon pool and provide many essential ecosystem services. We investigated the potential of using the recently launched spaceborne hyperspectral sensors to estimate soil properties in the uppermost soil layer. Therefore, we used the spectral information of bare soil pixels together with the chemically analysed soil property of a range of local soil samples. The new challenge is to investigate workflows how to combine hyperspectral time-series images of the same study site into one soil composite map of the investigated soil property. This enables producing spatially more complete soil property maps since imaging spectroscopy of soils is always dependent on bare soils being present at the surface, especially in the pixels corresponding to local soil samples.

Methodology (1200 – 1500 characters incl. spaces)

Our study site is located in the North-East of Germany within the long-term observatory of TERENO-NE and near the town of Demmin. More than 180 local soil samples were collected in this study site. Additionally, there is already a time-series of PRISMA acquisitions covering this site which has been analysed for its applicability for producing soil organic carbon (SOC) maps. We compared different machine learning and regression algorithms (Partial Least Squares Regression, Random Forest, Gaussian Process Regression). Furthermore, we tested some spectral feature analyses and a two-step local PLSR approach which uses the estimated instead of the measured SOC content based on a large-scale spectral library. In order to produce spatially more complete maps of the SOC content, we tested two workflows to combine the PRISMA time-series. The first workflow was adapted from the multispectral time-series analyses. In this workflow, we created a synthetic bare soil map composed of the median spectra of all available bare soil pixel within the time-series. Based on this synthetical image, models were trained, validated and applied in order to produce a SOC map. This bare soil composite workflow was compared to a new workflow named SOC maps composite. In this workflow SOC maps were produced for each image separately and combined in a last step.

Results (1200 – 1500 characters incl. spaces)

The results show medium to high quality models for most cases regarding the individual models for each date. The SOC maps composite was superior to the bare soil composite workflow leading to better results for all tested modelling approaches. Overall best results for the SOC maps composite were achieved

using the SOC spectral feature approach with a coefficient of determination $R^2 = 0.79$ and RPD = 2.21. When comparing the tested modelling approaches, the two-step local PLSR using estimated SOC contents performed in a similar range for the composite maps as the comparable traditional approach using measured SOC contents. Three out of seven investigated spectral features performed well to very well for most single images and overall best for the SOC maps composite. The spectral features were linked to the ground truth measurements in a linear regression and the transferability of this regression was tested in between the different dates. For dates with a small temporal difference of a few days the linear regressions could be transferred with high accuracies. For other cases the accuracy at least decreased or a transferability was not possible. These results show that imaging spectroscopy is a valid tool that can be used to support SOC mapping and monitoring at larger scales.

Outlook for the future (800 - 1000 characters incl. spaces)

Spectral feature analyses for SOC performed better than expected in this study and could provide a robust alternative to machine learning methods that could be valuable with regard to larger spatial and temporal datasets. The two tested multitemporal workflows present a start of finding one or multiple standard ways of producing more complete soil properties maps using time-series data. An advantage of the bare soil composite is that more samples fall into bare soil pixels to train the model, whereas the strength of the SOC maps composite is the possibility to adapt the model to the environmental conditions of the individual image leading to more accurate predictions but usually less samples being available per image.

The availability of spaceborne hyperspectral images that are suitable for soil monitoring is still limited and generating time-series is even more challenging. Depending on the availability of hyperspectral time series on further test sites, we plan to expand our studies to further sites and soil properties.

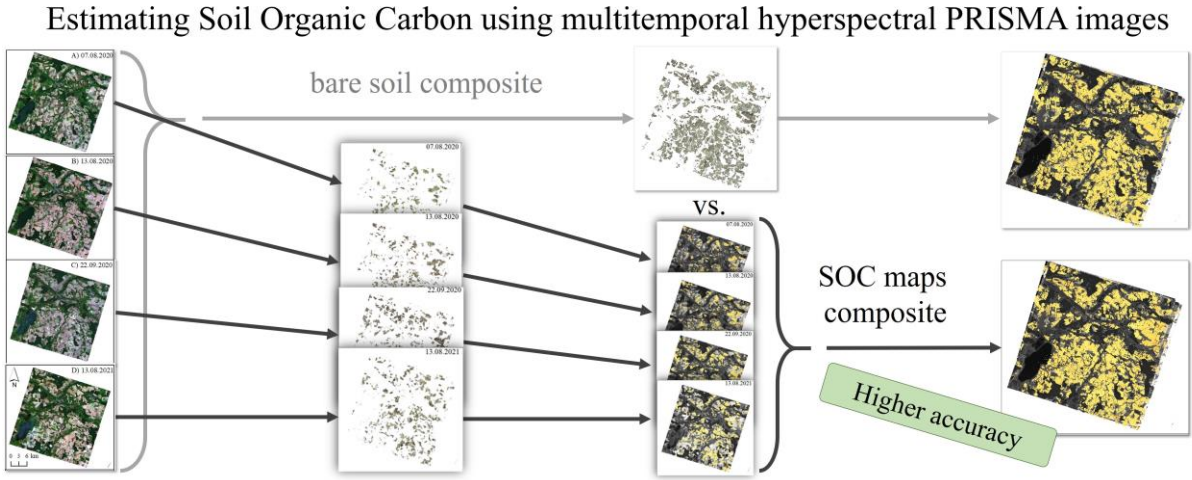


Figure Workflow for multitemporal SOC maps compositing (adapted from Ward et al., 2024, in rev.).

[Formatting guidelines for abstract submission]EARSel Valencia 2024
Abstract
Giacomo Lazzeri: giacomo.lazzeri@unifi.it**Hyperspectral remote sensing for soil salinization assessment**Giacomo Lazzeri¹, Robert Milewski², Saskia Förster², Sandro Moretti¹, Sabine Chabrillat^{2,3}¹ University of Florence, Department of Earth Sciences, Italy² Helmholtz Center Potsdam, GFZ German Research Centre for Geosciences, Germany³ Leibniz University Hannover, Institute of Soil Science, Germany**Keywords (5):** Hyperspectral, EnMAP, Soil salinization, Land abandonment, Narrow band index**Challenge (800 - 1000 characters incl. spaces)**

Climate change is altering seasonal weather patterns and dynamics, impacting terrestrial systems and soil properties. This results in less rain, higher temperatures, and more extreme precipitation events. Drought periods combined with augmented plant evapotranspiration will increase the need for man-managed crop irrigation. In coastal agricultural areas, the plant water deficit will be compensated with increased freshwater extraction, possibly resulting in salt water wedge intrusion and contamination of the freshwater reservoir by cations and anions. Repeated application of brackish water will result in salt build-up in the topsoil, leading to plant productivity reduction and in the end, land abandonment. To reduce the deterioration of a non-renewable resource as soil, this study aims at taking advantage of hyperspectral remote sensing to investigate soil salinization prior to the appearance of its effects on plant health.

Methodology (1200 – 1500 characters incl. spaces)

In this framework, this study takes advantage of the new insights obtained by soil spectroscopy and the new research possibilities offered by modern hyperspectral satellites (i.e. EnMAP, PRISMA). The datasets used for the analysis are so constituted: ancillary airborne AVIRIS-NG hyperspectral imagery (2018), salinization affected field soil spectral signatures, concomitant acquisitions of EnMAP and PRISMA data (2023), laboratory soil spectral signatures of the field samples and quantification of soil sample salt content via laboratory electrical conductivity measurements (EC). Both the field collected spectral signatures and the laboratory soil spectra were used for the computation of two sets of 2D correlograms to assess the wavelengths correlation with the measured soil EC. The performance of individuated wavelength couples was tested for three narrow-band spectral indexes. The index-band combination best correlated with EC was then applied to the selected bare soil pixels of the satellite images to test the capability of remotely sensed data to investigate soil salinization. Additionally, a machine learning (ML) model was implemented to assess the presence of salinization covariant parameters and their mapping capability compared to spectral indexes derived from 2D correlograms.

Expected results (1200 – 1500 characters incl. spaces)

Salt surface manifestation in soils is strongly related with salt content. Hyperspectral analysis and retrieval of this parameter poses challenges related to the absence of absorption features for salts as halite, reducing the characteristic spectral features available for the individuation of the phenomenon.

Nevertheless, the increased reflectance for salt affected soils and descriptive wavelengths obtained with the 2D correlograms might provide a satisfactory combination of parameters capable of mapping salinization via narrow-band indexes. On the other hand, the better understanding and individuation of covariant parameters resulting from the machine learning model can provide helpful indicators for salt-affected soil and their possible spatial distribution in topsoils. Furthermore, the ML model additional information regarding salinization related parameters can possibly reduce the uncertainty deriving from the computation of 2D correlograms for a target with low or absent related spectral features. Overall, combining the narrow-band indexes and the insights deriving from the ML model the expected results verge on the creation of salt affected soil maps or salinization hazard maps bearing enhanced information compared to both methods individually considered.

Outlook for the future (800 - 1000 characters incl. spaces)

The developed methodology will be further tested with additional case studies to assess the performance of the found narrow-band indexes, focussing on areas with different soil characteristics and salinization levels. In addition, the parameters individuated thanks to the ML model will be validated with field analysis, investigating their predictive capabilities for soil salinization and possibly defining the related descriptive wavelengths through the computation of new 2D correlograms. The obtained insights will contribute to the evaluation of the best performing technique, taking into account the sensing scale. If available, airborne hyperspectral data will be acquired to study the different performance of the methods here presented and the selected wavelengths. The introduction of this platform aims at providing a connection between the field and satellite sensed data and their different capabilities.

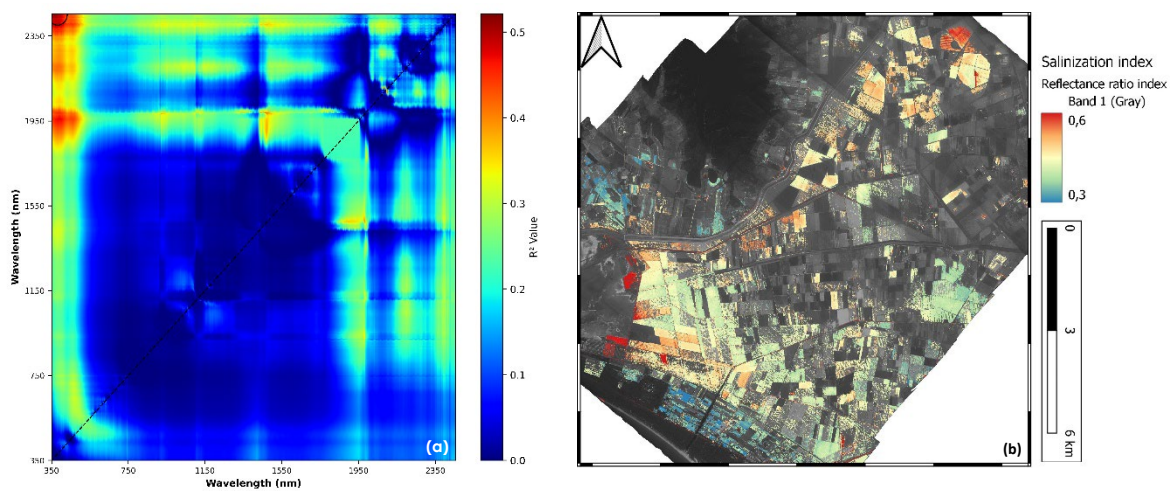


Figure (a) 2D correlogram for the reflectance Ratio index (b) AVIRIS-NG exploratory salinity mapping

Using Coupled Radiative Transfer Models to Improve Soil Organic Carbon Estimation at the EO Scale

Asmaa Abdelbaki¹, Robert Milewski¹, Sabine Chabrillat^{1,2}

¹ Section Remote Sensing, Helmholtz Centre Potsdam GFZ German Research Centre for Geosciences, Telegrafenberg, 14473 Potsdam, Germany

² Leibniz University Hannover, Institute of soil science, Herrenhäuser Str. 2, 30419 Hannover, Germany

Keywords (5): Earth Observation, Soil, Hyperspectral, Soil spectral library, convolutional neural network

Challenge (800 - 1000 characters incl. spaces)

Soils, as a carbon store, play a vital role in addressing global climate change and supporting agricultural systems. Remote sensing methods using hyperspectral data can precisely retrieve various soil physiochemical properties, including soil organic carbon (SOC), salinity, and nitrogen, which are valuable for mapping soil applications. However, accurately estimating soil attributes poses many challenges at the scale of Earth Observation (EO). These include high sensitivity to BRDF effects, and dynamic surface conditions such as residual vegetation cover, soil surface roughness, soil moisture (causing a mixed pixel signal in the sensor's Field of View), spatial and temporal coverage, and big data challenges. To address these challenges, the combined use of established radiative transfer models (RTM) and growing availability of soil spectral libraries (SSL) at continental to global scale is proposed to mimic the complex spectral composition found within a pixel at the EO scale. Compared to 3D ray-tracing simulations based on Monte Carlo theory, 1D-RTMs can determine the spectral signature for active photosynthetic vegetation (PV), non-active photosynthetic vegetation (NPV), surface soil moisture (SM), and soil surface roughness with less computational effort. The suggested approach integrates empirical data of the LUCAS soil spectral library with the MARMIT, and PRO4SAIL-2 RTMs to account for the effects of SM, PV and NPV. This study aims to investigate whether including these spectral variations found in real-world surface conditions, including variability of soil moisture, and green and dry vegetation residual cover, can enhance the precision of soil organic carbon estimation, and prospectively improve soil monitoring efforts at the EO scale.

Methodology (1200 – 1500 characters incl. spaces)

In this study the methodology is carried out in three steps: 1) The original version of the Soil-Leaf-Canopy (SLC) canopy radiative transfer model is modified by replacing the limited soil reflectance variation provided by the Hapke's model (1981) with extensive SSL of LUCAS. The LUCAS SSL integrates laboratory measured soil reflectances with chemical and physical soil properties from 23 Member States of the European Union (EU), 2) The Multilayer Radiative Transfer Model of soil reflectance (MARMIT) is used to simulate different moisture levels based on the LUCAS dry soil reflectance, and 3) Synthetic wet soil are coupled with the 4SAIL canopy reflectance model and the PROSPECT leaf optics model, creating synthetic PV and NPV mixtures for each bare and wet soil scenarios. The Initial testing for the integrated model is done with the LUCAS 2009 dataset, comprising 158 bare soil samples and their reflectance data in the 400 – 2500 nm range at 1 nm resolution. The dataset includes diverse SOC content and samples from different cropland soils distributed over the EU. In the forward mode, A look-up table is generated, encompassing 6,952 simulated spectra, 11 leaf area index scenarios (0.05 - 1 m²/m²) for PV and NPV, 158

bare soil samples, and three SM content scenarios (0.015 - 0.07 g/g). The model is also updated with the LUCAS 2015 database containing 35,765 soil spectra. Results are evaluated by comparing simulations from the integrated SLC-MARMIT approach with those from the senSCOPE model. Finally, the integrated model is employed to predict topsoil SOC using a hybrid machine learning-based retrieval method.

Expected results (1200 – 1500 characters incl. spaces)

We conducted simulations to evaluate the impact of dynamic soil surface conditions, including different levels of soil moisture, green vegetation, and dry plant residue, on the reflectance of bare soil surfaces. A comprehensive upscaled soil spectral library was created, forming the foundation for in-depth analysis. Spectrally, the results of the compiled simulation results seem reasonable, e.g., for the moisture affected soil reflectance modeled by coupled SLC-MARMIT, decreasing soil reflectance is observed most pronounced in the shortwave infrared region (>2000 nm) and less strong in visible wavelength. Spectra of green vegetation, both the visible and near-infrared parts of the spectrum changed significantly. Lastly, plant residue signals affected mostly the shortwave infrared portion of the spectrum, with minimal effects on visible regions, consistent with previous research that highlighted differences in spectral signatures between bare soil and crop residues in the shortwave infrared of the spectrum, rather than visible wavelengths. Analyses for the LUCAS soil database with 21,860 soil spectral data, were restricted to mineral soils with organic content less than 120 g/kg, as the distribution of SOC content displays a strong positive skew, with the majority of values falling below 519 g/kg and a mean SOC content of 17.62 g/kg and very low number of samples containing high SOC content. Preliminary results for SOC estimation using a convolutional neural network (1D-CNN) show encouraging results with $R^2 = 0.70$, RMSE= 6 (g/kg), and PRIQ around 1.6 for bare soil scenarios, and indicate strong loss of accuracies. This procedure will be applied for hybrid soil modeling with 82,2572 simulations to estimate SOC content.

Outlook for the future (800 - 1000 characters incl. spaces)

This study highlights the importance of accounting for dynamic surface conditions at the EO scale. Further research is clearly necessary to improve correction methods to support reliable soil monitoring of SOC and other important soil properties. In addition to the disturbance effects considered in this work, it is crucial to address additional factors such as soil crusting and surface roughness, e.g., by integrating photometric models recently proposed by Labarre S., et al., 2019 to account for multi-angular reflectance of soil surfaces. Our upcoming research will focus on assessing the scale dependency of the proposed approach, utilizing Unmanned Aerial Vehicle (UAV) hyperspectral data, and expanding its regional application through the incorporation of EnMAP imagery. Furthermore, the ongoing efforts to consolidate continental to global soil spectral libraries will significantly broaden the applicability of the proposed approach, extending its reach beyond the boundaries of the European Union.

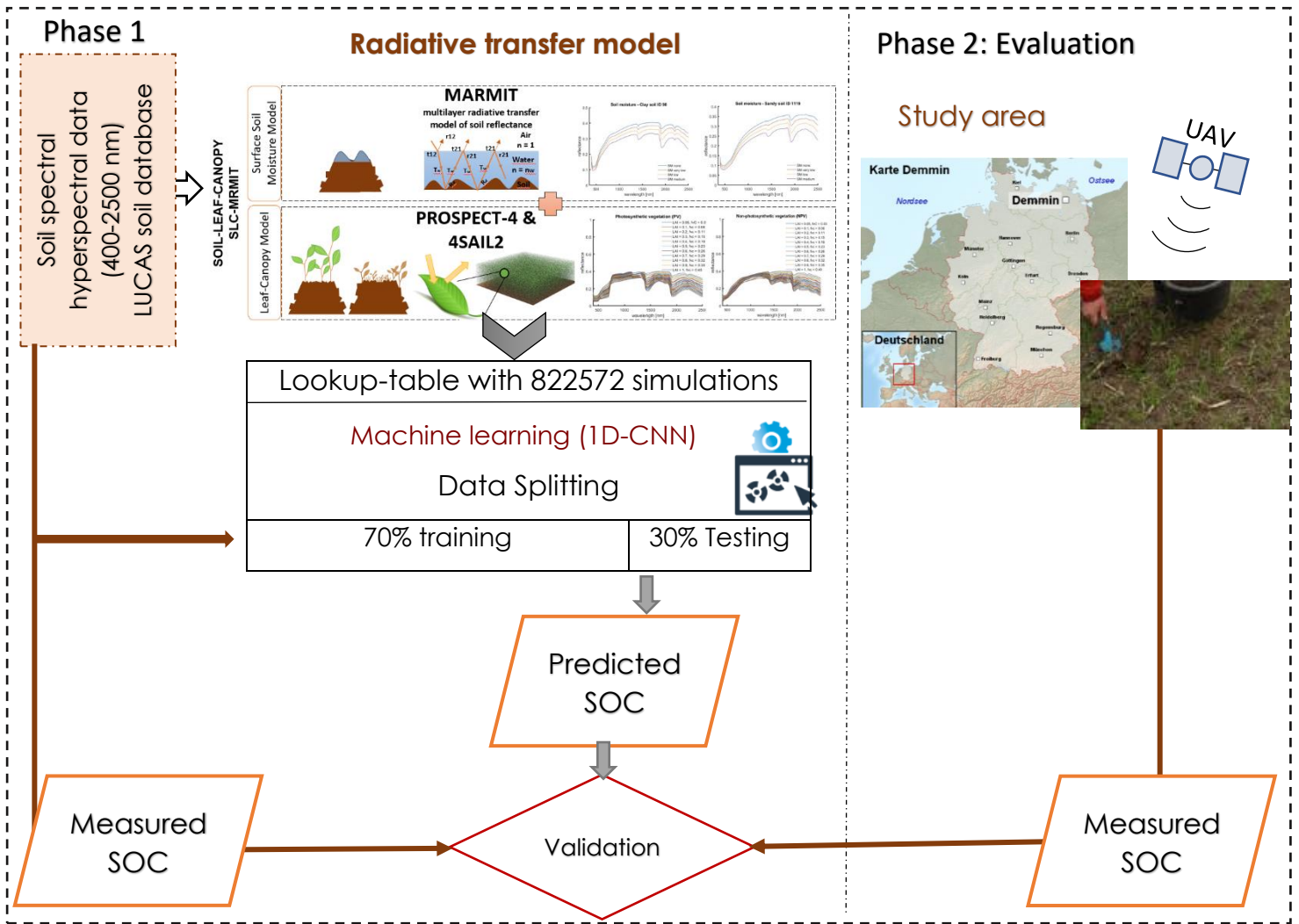


Figure (1) Flowchart on predicting SOC concentration from the SLC-MARMIT model.

Mapping Soil Microbiological Biodiversity Using Simulated CHIME Hyperspectral Data

EARSeL Valencia 2024

Abstract

Corresponding Author:

h.j.abdullah-1@utwente.nl

Andrew K. Skidmore¹, [Haidi Abdullah](#)¹, Andjin Siegenthaler¹, D.P. Adinigrat¹, Y. Duan¹, M.S.D. Rousseau¹, A. Torres Roriguez¹, R. Darvish¹, T. Wang¹, G. Arjen de Groot²

¹Faculty of Geo-Information Science and Earth Observation (ITC), University of Twente, P.O. Box 217, 7500 AE Enschede, The Netherlands.

²Wageningen Environmental Research, Wageningen UR, P.O. Box 46, 6700 AA, Wageningen, The Netherlands

Keywords (5): environmental DNA (eDNA), soil microbiome, CHIME, simulation, PLSR

Challenge

Microbial communities play a pivotal role within forest ecosystems, serving as linchpins for the overall health, structure, and sustainability of these vital environments. While recent advances in molecular research offer a promising means to study these often-neglected communities, they come with significant cost and labour demands, making large-scale assessments challenging. However, there is a glimmer of hope on the horizon. The emergence of spaceborne hyperspectral sensors in recent years has presented an innovative solution to bridge the gaps in our data. These sensors enable the extrapolation of environmental DNA (eDNA)-based microbial profiles across expansive regions. For instance, the impending launch of the next-generation CHIME satellite, known as the Copernicus Hyperspectral Imaging Mission for the Environment, will cater to the surging demand for hyperspectral data needed for expanding our understanding of microbial diversity based on eDNA analysis. CHIME promises to transform the field of biodiversity monitoring, especially in the context of microbial communities. It will empower researchers to identify thousands of taxonomic units directly from modest soil, water, or plant samples. Despite this groundbreaking capability, our understanding of the spatial distribution of microbiological biodiversity, and its critical contribution to ecosystem function, remains limited due to the scarcity of in-situ observations.

Methodology (1200 – 1500 characters incl. spaces)

In this study, our main goal was to assess whether CHIME data could effectively estimate soil alpha diversity. To achieve this, we initially created simulated hyperspectral imagery data using the AVIRIS-NG product, matching the band specifications of CHIME data. We resampled the AVIRIS reflectance data to resemble CHIME bands, considering theoretical Gaussian spectral response functions (equating to 210 bands with 10 nm bandwidth). We then removed bands affected by atmospheric water vapor absorption, resulting in a final CHIME-like spectral setup of 157 bands. For validating our retrieval models, we used CHIME-like reflectance spectra obtained from the original AVIRIS-NG data at the same locations where field measurements were taken. Furthermore, to showcase our mapping process, we spatially resampled the images to the expected CHIME spatial resolution of 30 meters using a cubic convolution algorithm. This allowed us to create realistic CHIME maps displaying estimated soil alpha diversity metrics.

To estimate soil alpha diversity, we employed a Partial Least Square Regression (PLSR) model, which considers the variability in both the explanatory and dependent variables. PLSR establishes a linear relationship between a set of dependent variables (in this case, in-situ measured soil alpha diversity) and a set of predictor variables (represented by CHIME spectral reflectance data simulated from AVIRIS-NG data).

Expected results (1200 – 1500 characters incl. spaces)

The study's findings reveal that hyperspectral data obtained from a simulated CHIME satellite can accurately estimate soil alpha diversity. It resulted in a root mean square error (RMSE_{cv}) of 18.43, 21.05, and 20.16, along with cross-validated coefficient of determination (R²_{CV}) values of 0.56, 0.30, and 0.58 for functional richness, Shannon index, and phylogenetic diversity, respectively. Additionally, when we compared these findings to our prior results using DESIS image spectroscopy data on the same dataset, it became evident that the simulated CHIME data significantly enhanced the accuracy of the estimated alpha diversity metrics (see Table 1).

Outlook for the future (800 - 1000 characters incl. spaces)

This study illustrates how spaceborne next-generation CHIME hyperspectral data can be harnessed to accurately predict potential microbial functions. By generating maps and models of significant value to the field of forest ecology and management, this approach holds the potential to revolutionize the utilization and expansion of environmental DNA (eDNA) point-based information. It introduces groundbreaking solutions to tackle ecological challenges on a global scale, thereby opening up new horizons for the conservation and sustainable management of forest ecosystems.

Table 1 : Comparison of Estimated Soil Alpha Diversity Metrics from DESIS and Simulated CHIME Data

Alpha Diversity Metrics	R ² _{CV}	
	Simulated CHIME spectra	DESIS
Shannon	0.30	0.24
Functional Richness	0.58	0.38
Phylogenetic Diversity	0.56	0.40

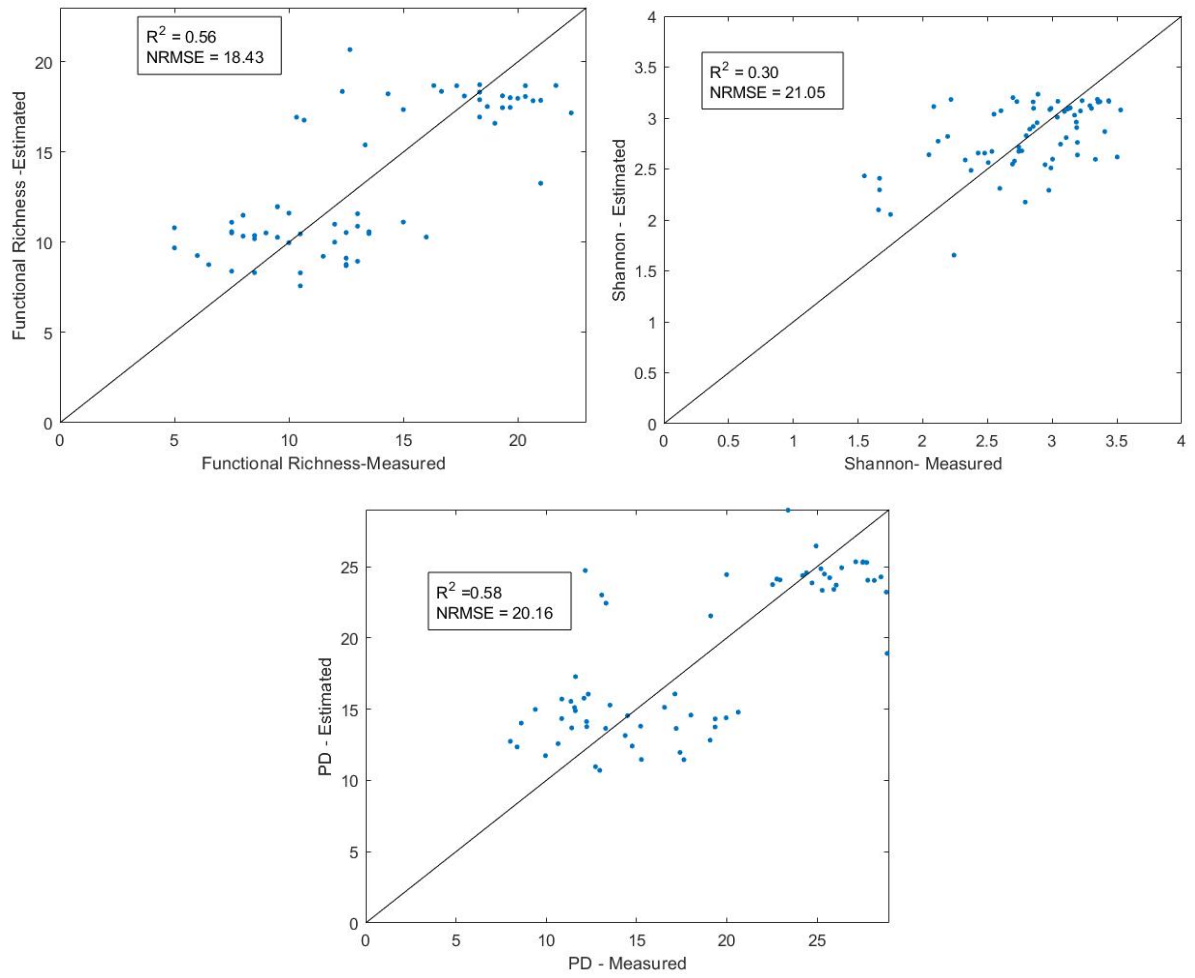


Figure 1: Scatter plot for measured and estimated soil fungi alpha diversity metrics (Shannon, functional richness, and PD).

Modeling of Soil Parameters in the Atacama Desert Based on the New EnMAP Sensor

Christopher Loy¹, Robert Milewski¹, Jens Boy², Diana Boy², Sabine Chabrilat¹

¹ Helmholtz Center Potsdam, GFZ German Research Center for Geosciences, Potsdam, Germany

² Leibniz University Hannover, Institute of Soil Science, Hannover, Germany

Keywords (5): Atacama, Soil, EnMAP, Machine Learning, Field Spectroscopy

Challenge

The Atacama desert in Chile is a unique and remote landscape, characterized by extreme environmental conditions. Our primary objective is to gain valuable insights into landscape processes, like erosion and transportation, within this challenging environment. Accurately assessing the distribution of crucial soil properties, including Calcium Carbonate, Sand, and Clay, is essential for understanding such processes. Yet, the vastness and remoteness of the desert render traditional soil sampling and analysis methods ineffective. Here, hyperspectral remote sensing provides new possibilities, enabling us to observe the landscape in detail which wasn't possible with more conventional methods. Innovations must address these complex challenges and use a larger-scale observation approach for the effect mapping of the landscape.

Methodology

To address this challenge, we sampled different sites in the Atacama desert. We collected soil spectra and samples along an aridity gradient, spanning from the Mediterranean-like southern part of the desert to the hyperarid north. In addition, we acquired hyperspectral satellite images from EnMAP for all the study sites, integrating field spectra with spaceborne data and enabling us to create a comprehensive dataset for analysis. The Atacama desert provided perfect atmospheric conditions, rarely achieved outside a laboratory. This also led to ideal conditions for comparing field and EnMAP satellite spectra.

We employed various machine learning approaches, including Random Forest, XGBoost, and Partial Least Squares Regression (PLSR). These models were trained and validated using the field-collected soil data. To improve the model's performance, we used multiple preprocessing techniques such as Principal Component Analysis (PCA), parameter scaling, and spectral smoothing. The combination of these methods resulted in accurate models for predicting Soil Parameters.

With these well-performing machine learning pipelines, we expanded our analysis to predict the distribution of these soil properties across entire EnMAP satellite scenes, covering an area of 30 by 90 kilometers for six sites in the Atacama desert. This comprehensive approach allowed us to map critical soil properties on a large scale, providing insights into the landscape formation processes.

Expected

We anticipate several significant outcomes from our project. Firstly, we aim to produce high-resolution maps of different soil parameters across the Atacama desert. These maps will provide valuable information on landscape processes, such as erosion and transportation, that shaped this environment.

Secondly, our study will contribute to a deeper understanding of the relationships between soil properties and aridity gradients in the Atacama desert. By using advanced machine learning techniques and hyperspectral satellite data, we aim to uncover previously undiscovered patterns and insights.

Preliminary model results show especially good results for Calcium Carbonate modeling using a Scaled Dataset with PCA in a Random Forest Model ($R^2 = 0.81$, RMSE = 0.513 %). For Sand and Clay, a preliminary PLSR model achieved the best results.

Also, due to the excellent quality of field spectra and spaceborne spectra, we have the chance to evaluate the quality of EnMAP soil spectra and draw comparisons to other sensors. That should make it possible to assess even small substance concentrations.

Finally, we want to provide a basis for further work in the Atacama desert. With this knowledge, future site visits will allow us to establish new sampling schemes for addressing other questions, including those related to the parent rock and microbial life. This should lead to more understanding of the formation, landscape evolution, and ecosystem properties in this unique place.

Outlook for the future

The next step will involve a revisiting of the desert's sites to establish new and more efficient sampling schemes. These schemes will facilitate the investigation of additional questions, particularly in the areas of soil science, geology, and geomorphology, as well as microbiology, to give a better understanding of this landscape and its formation. Also, in further research, tracking the impact of elevation changes into perspective since this study only dealt with a North-South gradient. Furthermore, applying this approach to a temporal scale might also lead to tracking surface changes in the desert, like desert blooming after flood events.

Hyperspectral remote sensing allows in-depth analysis of landscape parameters for places in harsh environments. This approach could be an example for other comparable regions with uncovered soils.

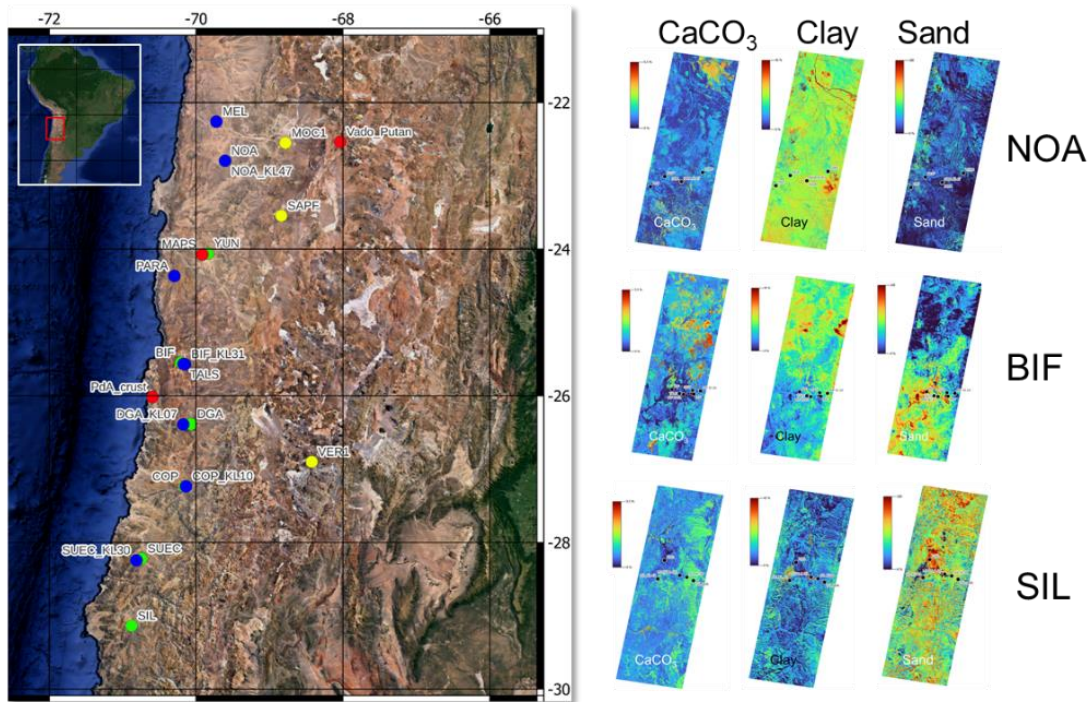


Figure: Left: Location of the study area and sampling from the February expedition 2023, Right: Preliminary quantitative mapping results from EnMAP in 3 regions each 30 km wide x 90 km along acclimate gradient from Mediterranean climate in southern site (SIL) to most hyperarid areas in the northern sites (NOA)

Assessment of EnMAP Imaging Spectroscopy Data for the Estimation of Soil Properties in Mediterranean Croplands

EARSel Valencia 2024

Abstract

Corresponding Author: Robert Milewski
[milewski@gfz-potsdam.de]

Robert Milewski¹, Sabine Chabrillat^{1,2}, Nikos Tziolas³, Thomas Schmid⁴

¹ Helmholtz Center Potsdam GFZ German Research Center for Geosciences, Section 1.4 Remote Sensing and Geoinformatics, Germany

² Leibniz University Hannover, Institute of soil science, Germany

³ University of Florida, Department of Soil and Water Sciences, USA

⁴ Department of Environment, Centro de Investigaciones Energéticas, Medioambientales y Tecnológicas (CIEMAT), Spain

Keywords (5): Earth Observation, Hyperspectral, Soil Properties, EnMAP, Mediterranean Croplands

Challenge

Soils are vital for food production and ecosystem services, e.g., storing 30% of global terrestrial carbon. Mapping and monitoring soil properties are essential for assessing soil quality and supporting policies like the European Soil Protection Directive, in line with initiatives like the European Green Deal. Soil spectroscopy covering the VNIR-SWIR (400-2500 nm) spectral range, has proven effective for precise soil property determination at controlled laboratory conditions and from high resolution and carefully processed airborne survey data. Hyperspectral spaceborne sensors like EnMAP are expected to contribute to regular monitoring and reporting tasks of cropland soil properties at the regional to global scale. However, their potential and limitations for soil property mapping at a 30 m GSD need further assessment.

Methodology

This contribution presents results for topsoil property estimation based on EnMAP spaceborne imaging spectroscopy data acquired during its first year of operation over two Mediterranean agricultural regions located in Central Spain (Province of Toledo) and Northern Greece (Western Macedonia). These areas exhibit diverse terrain and geological backgrounds, resulting in a wide range of soil properties, making them ideal test sites for evaluating EnMAP's capabilities in soil property estimation and mapping. In this work, EnMAP data quality related to soil spectral features is assessed and compared to in-situ data acquisition using ASD field spectrometers. Key soil properties, such as soil texture, iron-oxide, organic and inorganic carbon content are derived using linear and nonlinear machine learning techniques, e.g., PLS, RF, SVM, and GP regression techniques. In addition, the impact of different spectral transformation and pre-processing techniques such as PCA, Continuum Removal, Standard Normal Variate, Detrend, and higher derivatives of absorbance and reflectance are tested and evaluated in cross-validation. Results are presented and compared previous work based on high resolution hyperspectral airborne imagery.

Expected results

The initial findings demonstrate promising levels of accuracy, underscoring the potential of EnMAP imagery for the global mapping and monitoring of soil properties. In the model estimations, the determination of soil carbonate content yielded excellent results using PLSR and absorbance transformation, achieving an R^2 of 0.86 and an RMSE of 5.8%. In addition, soil organic matter estimation

was effectively carried out using GPR in continuum-removed spectral space, with an R^2 of 0.83 and an RMSE of 0.45%. For soil texture analysis, the estimation of sand and silt content produced satisfactory model accuracies, with R^2 values of 0.73 and 0.56, and RMSE values of 7.3% and 5.3%, respectively. However, the estimation of clay content, which is relatively low, was less successful, resulting in an R^2 of 0.43 and an RMSE of 6.9%. Soil iron-oxide content was determined with an R^2 of 0.61 and an RMSE of 0.09% through GPR analysis of the first spectral derivative. These results underscore the importance of spectral pre-treatment and the choice of machine learning algorithms in achieving successful soil property modelling. Furthermore, the spatial distribution of the results matches the expected patterns of soil properties at the landscape and field plot scale. For instance, the mapping of organic-rich and clay-rich alluvial soils at the Northern Greece test site, and the sandy colluvial deposits, as well as highly eroded, carbonate-rich soils of degraded field plots of the study area in Central Spain.

Outlook for the future

The results of this study show that the high spectral resolution and excellent quality of EnMAP data can exploit the well-defined spectral absorption features characteristically linked to the functional sets in the VNIR and SWIR associated to soil properties, including the carbonate spectral feature at 2.3 μm which is usually affected by stronger noise levels. Furthermore, the usually less accurately derived featureless sand fraction could be estimated with good accuracies. Deriving this information at the EO scale can support relevant agricultural assessments, e.g., regarding soil fertility, water availability and the classification of erosional potential at the regional level. Future work will focus on improving spectral modelling techniques to account for dynamic surface conditions at the scale of Earth Observation, such as soil moisture affected soils, and mixed soil-vegetation scenarios. It can be concluded that hyperspectral data from the EnMAP sensor and forthcoming satellite missions such as CHIME and SBG have high potential to advance the mapping and monitoring of soil properties.

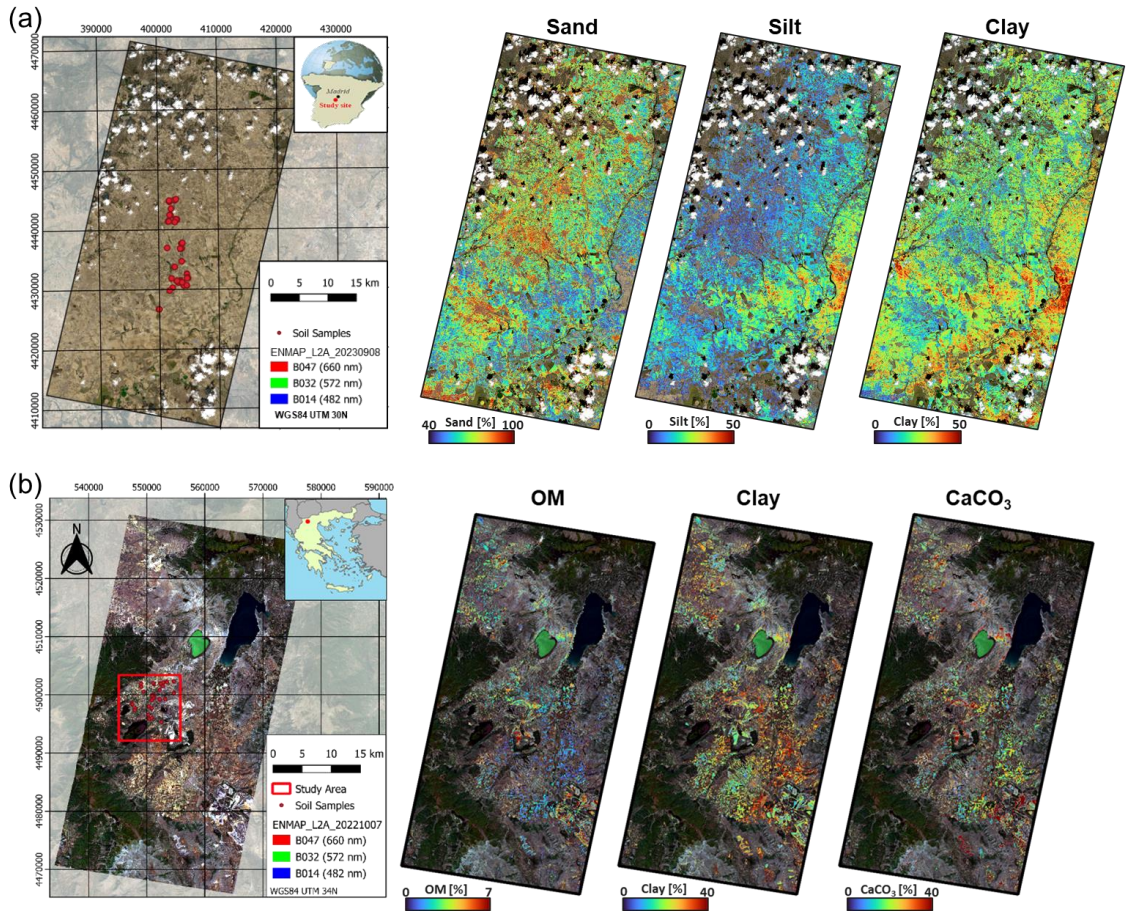


Figure EnMAP derived soil property mapping of (a) soil texture information (Sand, Silt Clay), Central Spain and (b) Organic Matter, Clay, and Carbonate content of cropland soils in Northern Greece

**Them.Sess. 1-5: Machine learning
and emulation for imaging
spectroscopy applications**

Multi-fidelity Gaussian Process Emulation for Atmospheric Radiative Transfer Models

EARSel Valencia 2024

Abstract

Corresponding Author: jorge.vicent@uv.es

Jorge Vicent Servera¹, Luca Martino², Jochem Verrelst¹, Gustau Camps-Valls¹

¹ University of VALENCIA, IMAGE PROCESSING LABORATORY (IPL), SPAIN

² University REY JUAN CARLOS, MADRID, SPAIN

Keywords (5): Atmospheric correction, emulation, hyperspectral, multi-fidelity Gaussian processes, radiative transfer models

Challenge

Atmospheric radiative transfer models (RTMs) are widely used in imaging spectroscopy applications. While interpolating look-up tables (LUTs) is common practice, their exponential growth makes them impractical for accurate atmospheric correction of hyperspectral data. Emulators offer an accurate alternative to approximate RTMs at a fraction of their runtime and reduced LUT size. To further enhance their accuracy whilst reducing runtime, we integrate multi-fidelity methods with Gaussian Process regression and dimensionality reduction into a unified framework. Multi-fidelity combines simulations of an accurate but computationally expensive model with a larger dataset from a fast but less accurate model. We compared several emulators in terms of accuracy and performance, and applied them for atmospheric correction of PRISMA data. Our approach is generic and valid for multiple RTMs. We provide an automated workflow and tools for developing emulators applicable to real-world applications.

Methodology

The multi-fidelity emulation consists of a sequence of fidelity layers, where each layer is a statistical model that approximates the difference between the predictions of the previous layer and the high-fidelity RTM, i.e. $\hat{g}_{t+1}(x) = c \cdot \hat{g}_t(x) + \delta_t(x)$. For the lowest fidelity layer, $\hat{g}_0(x)$, a polynomial fitting of RTM simulations is used. Then, we calculate the difference between the training data and the predictions of the polynomial fitting, $\delta_0(x) = g(x) - \hat{g}_0(x)$, and use this difference to train a GP emulator. The first higher fidelity layer is the sum of the polynomial model and the Gaussian Process emulator, $\hat{g}_1(x) = \hat{g}_0(x) + \delta_0(x)$. This process is repeated t times to create a sequence of fidelity layers.

To test our method, we generated datasets of MODTRAN6 simulations using a Latin Hypercube Sampling with a wide range of input conditions. Three training datasets with 100, 500, and 1000 samples were generated to test the impact of training dataset size on the emulator accuracy. We studied the impact in accuracy and runtime of varying the number of PCA components (3 to 15) in the GP emulators and the number of fidelity layers (0 to 5). The accuracy was evaluated in terms of atmospheric correction over a reference dataset of 10000 samples. The entire workflow (MODTRAN6 simulations and emulation) was automated using the Atmospheric Look-up table Generator (ALG) toolbox.

Results

We first conducted a systematic performance assessment of multi-fidelity GP emulators. We found that adding multi-fidelity layers and PCA components improves the accuracy of the emulators at the expense of an increased runtime. The higher errors associated with a low number of PCA components are somewhat compensated by adding extra layers in the multi-fidelity emulator. This improvement reaches a saturation limit after 3 layers but it can be reached with fewer fidelity layers when adding more PCA components. The best-balanced emulator (in terms of accuracy and runtime) uses 5 PCA components

and one multi-fidelity layer, and is trained on 500 samples. This emulator achieves an average relative error of 0.54%, with the highest errors (2%) occurring in the 400-500 nm spectral range.

We then tested the utility of emulators in atmospheric correction by applying them to PRISMA Level-1 data. We found that the best-balanced emulator was able to accurately invert the surface reflectance from the PRISMA data, with consistent results with the official PRISMA Level-2C product. The processing of 10^6 PRISMA pixels were achieved in less than 4 min. Some discrepancies were visible above 2250 nm likely due to wrong implementation of the Level-2 processor where a residual H₂O absorption is still observed. Overall, the results of the test suggest that emulators can be a useful tool for atmospheric correction. However, it is important to be aware of the limitations of the data being used.

Outlook for the future (800 - 1000 characters incl. spaces)

Several research activities are ongoing. First, we are exploring active learning techniques to improve the accuracy and speed of the emulator. These techniques can identify the most important regions of the input parameter space to focus on when generating the training dataset. Second, we are developing a fast semi-empirical atmospheric RTM for the lowest fidelity layer to improve the explainability of the emulator.

In terms of optimizing emulators for operational applications, we can think of various strategies. First, GPUs can significantly improve the speed of an emulator as they are well-suited for the large matrix multiplication operations required by the emulator. Second, we can optimize the number of PCA components to improve the speed of the emulator. This is because the number of PCA components affects the size of the kernel matrix, which is a key factor in the runtime of the emulator. Finally, the use of macro-pixels (large image areas with nearly constant input conditions) instead of individual pixels, will reduce the number of emulator predictions and thus processing time.

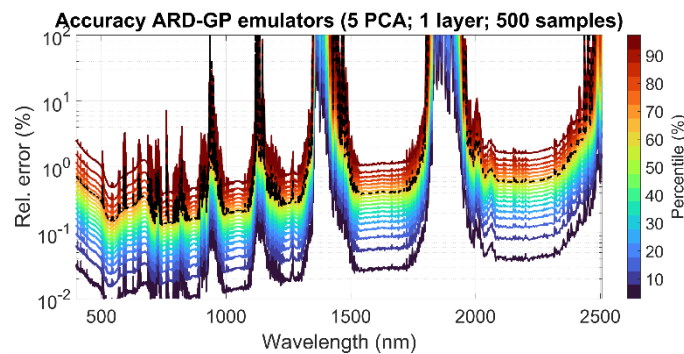


Figure 1 Relative error histogram (in %) (see colour bar) and mean error (black dashed line) between reference and inverted surface reflectance with a multifidelity emulator with 500 training samples, 5 PCA components and 1 layer.

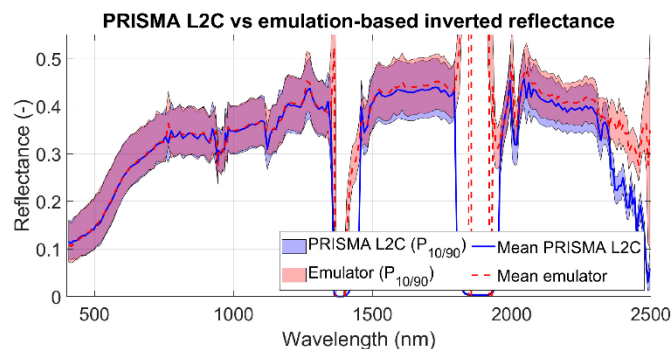


Figure 2 Average surface reflectance from PRISMA L2C product and inverted from emulation (blue and red dashed lines respectively) and percentiles (Px) 10% and 90% (shaded areas). Overlapping areas are seen in purple colour.

Local linear emulators accelerate atmospheric correction

David R. Thompson, Regina Eckert, Philip Brodrick, U. Niklas Bohn, Nimrod Carmon, Robert O. Green

Jet Propulsion Laboratory, California Institute of Technology

This presentation describes a clever trick, first described in Thompson et al. (2022, <https://doi.org/10.1029/2021JG006711>) for accelerating atmospheric correction by exploiting the local spatial smoothness of the atmospheric state. The computational efficiency of atmospheric correction is an important problem because many state of the art methods are iterative algorithms based on nonlinear optimization. This can be too time consuming to perform on each pixel independently. Fortunately, most imaging spectrometers spatially oversample the smooth atmosphere, making it unnecessary to solve each spectrum of the image independently. Our approach uses a set of spatially sparse solutions to develop local linear emulators of the atmospheric radiative transfer relationship between surface reflectance and radiance at sensor. In effect, it is a collection of local *empirical line* solutions similar to those often used when in situ reflectances are available. These emulators can be inverted analytically in closed form, making it trivially easy to calculate the reflectances for each pixel in their local neighborhood. We describe how this approach can be implemented in topographically-flat terrain, as well as scenes where there is topographic variability and a changing balance of direct and diffuse downwelling radiation.

For our case study, the approach reduces computational requirements by approximately two orders of magnitude without meaningful accuracy penalty. The actual speed benefits depend on the lengthscales of atmospheric variability; near-constant atmospheres yield large performance gains, while topographic or atmospheric variability reduces the computational benefits. We then describe validation on a series of airborne datasets acquired by NASA's Next Generation Airborne Visible InfraRed Imaging Spectrometer (AVIRIS-NG). In the EMIT science data system and those of our airborne instruments, this approach has already been superseded by other more model-based spatial inference approaches with stronger optimality guarantees (Eckert et al., Remote Sensing of Environment, in review). However, the generality of this approach means it is still useful as an approach for speeding up nearly any atmospheric correction algorithm.

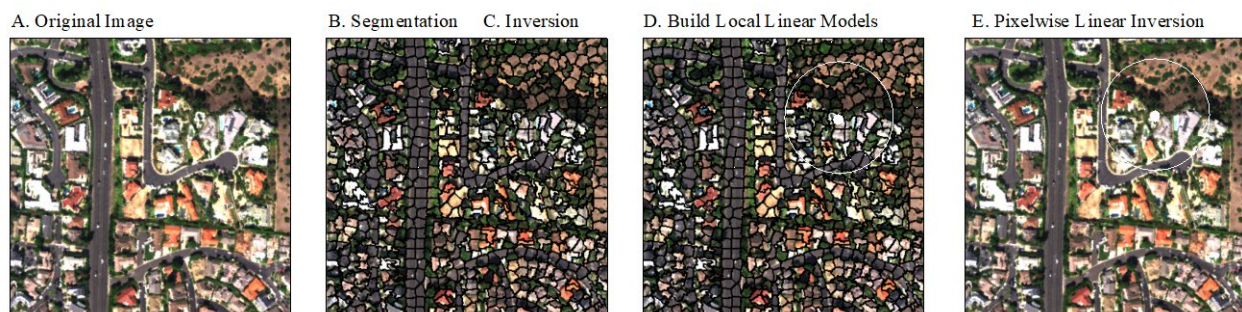


Figure: Method of local segmentation and linear emulation followed by a pixelwise inversion.

Copyright 2023 California Institute of Technology. All rights reserved. US Government Support Acknowledged.

Probabilistic radiative transfer emulation for imaging spectroscopy applications with Kernel Flows

EARSeL Valencia 2024

Abstract

Corresponding Author:

jouni.i.susiluoto@jpl.nasa.gov

Jouni Susiluoto¹, Amy Braverman¹, Philip G. Brodrick¹, Nimrod Carmon¹, Otto Lamminpää¹, Houman Owhadi², Michael Turmon¹

¹Jet Propulsion Laboratory, California Institute of Technology, USA

²California Institute of Technology, USA

Keywords (5): Gaussian process, emulator, cross validation, imaging spectroscopy, dimension reduction

Challenge

Solving the inverse problem for imaging spectroscopy retrievals with good quality requires repeated simulation of effects of atmosphere on measured radiance. This is due to the nature of the measurements: any light leaving Earth's surface needs to travel through the atmosphere to reach an instrument regardless to whether it is mounted on an air- or spaceborne platform. Radiative transfer modeling is, however, generally computationally demanding, which poses a significant problem with the data volumes that modern hyperspectral instruments produce. A back of the envelope calculation verifies this: assuming 10k measurements per second, one second for a single radiative transfer simulation, and 10 simulations per retrieval, we would need 100,000 computing cores for a brute-force computation. A standard workaround is to use look-up-tables (LUT); however, they often need to be re-generated due to changing conditions, which is still expensive. This slows down research, increases computational complexity, and makes carrying out fast analyses with new data difficult.

Methodology

We address the problem by using a modification of a specific Gaussian process (GP) formulation, "Kernel Flows", to address the issue. Kernel Flows differs from a standard GP in that it is trained using cross validation of the relative error over minibatches instead of maximum likelihood. We have further modified the algorithm to improve the performance in our specific case.

The enhancements include multi-level modeling, custom dimension reduction algorithms, a general but specifically parameterized form of kernel functions, modifications to the standard training algorithms, etc. The dimension reduction algorithms are used to reduce the dimension of the problem from thousands to tens.

We evaluate the effectiveness of the approach using cross-validated error metrics and compare them to alternative approaches. We also demonstrate how the emulator can be used in practice in an imaging spectroscopy retrieval framework.

The code is open source and written in the Julia programming language.

Expected results

We demonstrate how the emulator works by both looking at the cross-validated error of the radiative transfer quantities over randomly sampled input data, and by evaluating how the emulator performs in retrievals. The results show that compared to both a simple parameterized family of kernels or to a kernel learned with maximum likelihood we are able to achieve much better accuracy. We know that GP prediction can be made very fast, and that the amount of computation required scales linearly as a function of training data size. In practice cache size limits on compute nodes may pose challenges, and for this reason we will also compare this performance to LUT implementations, which are known to be very fast, but also to compromise accuracy.

Outlook for the future

The GP emulator that we present will be integrated as an optional component in retrieval frameworks such as our homegrown Julia-based framework, as well as the well-established ISOFIT framework. We envision the emulator being used both for LUT generation for large scenes, and for direct retrievals for smaller.

The GP emulation methodology is completely general and is not constrained to imaging spectroscopy missions, even though it is framed as such in this talk. If time permits, we will present additional results from radiative transfer emulation for inversions with Orbiting Carbon Observatory data. In principle, any input-output relation can be emulated, and we will briefly discuss some of these to provide an idea of the range of problems that can be tackled, along with limitations.

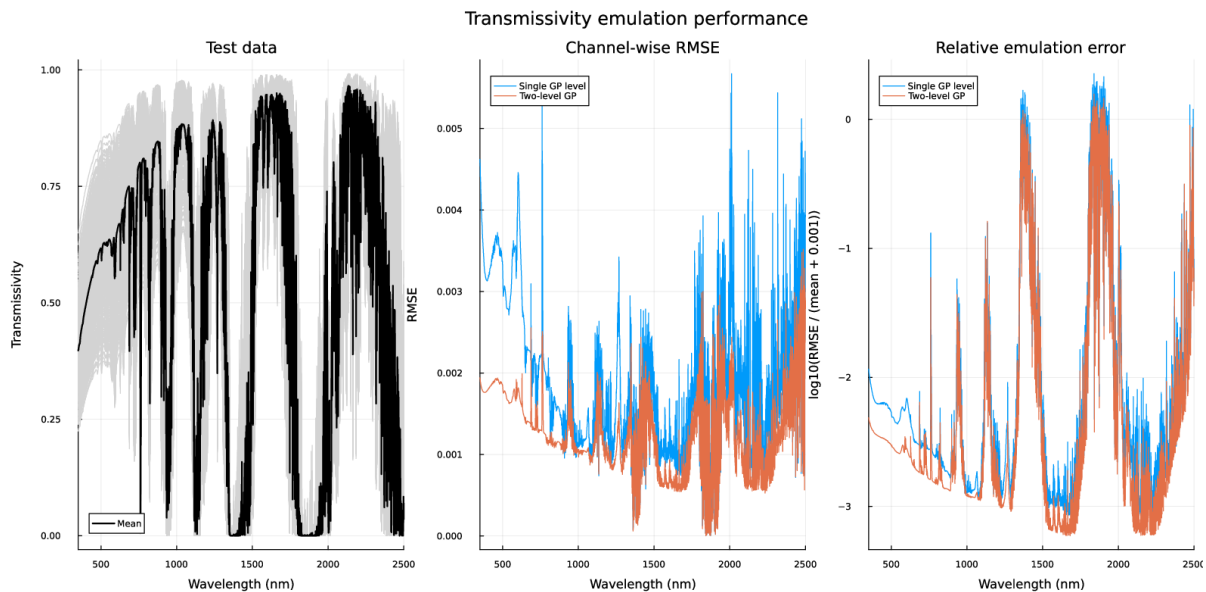


Figure. Example of radiative transfer emulation using the Kernel flows emulator. The data is on the left, and emulation RMSE over a test data set is shown in the middle and right-hand side plots. Multi-level emulation improves the results in this example.

Using Deep Learning To Generate Fractional Vegetation Cover From Multispectral Data

Peter Schwind¹, Kevin Kühl¹, David Marshall Ingram¹, Martin Bachmann¹, Uta Heiden¹

¹ German Aerospace Center (DLR), Earth Observation Center (EOC), Weßling, Germany

Keywords: Earth Observation, Fractional Vegetation Cover, Soils, Deep Learning, Hyperspectral

Challenge

The launch of hyperspectral missions such as EnMAP, DESIS, PRISMA and EMIT in recent years has led to substantial improvements in the measurement of soil and vegetation cover world-wide. Within the Earth Observation Center at DLR, an fCover processor has been developed, which extracts and classifies endmembers from hyperspectral data and, following a spectral unmixing step, generates soil and vegetation cover maps (containing fractions between 0-100% for active vegetation, non-photosynthetically active vegetation and bare soil).

Even though the availability of hyperspectral data has increased significantly, the overall world coverage and revisit times are not yet comparable to multispectral missions such as Sentinel-2 or Landsat 8. Ideally, a method should be devised which would exploit both the high spectral resolution of EnMAP data and the high spatial and temporal coverage of S2 data. In this work, such a method, based on deep learning vector regression, is presented.

Methodology

To generate fCover maps based on Sentinel-2 imagery, the following approach is proposed: A deep learning vector regression model was trained using fCover labels generated on EnMAP imagery and corresponding Sentinel-2 imagery as inputs. Several image segmentation/classification methods (U-Net, Res-Net, FSKNet, HybridsN) were adapted and tested to perform the required regression task. Out of these, HybridSN was evaluated more vigorously, since initial tests showed the most promising results. Even though originally designed for hyperspectral image classification, adapting HybridSN for a multispectral vector regression problem is straightforward: The kernel size of the three initial convolution layers has to be reduced in the third dimension to account for the lower amount of input bands and the final Softmax activation has to be replaced by a Linear activation step to obtain a vector with three scalars (see Figure 1).

To train the modified HybridSN algorithm, 40 EnMAP and Sentinel-2 pairs each acquired at approximately the same time were selected. Out of the 40 scene pairs, 37 were used to train the model and 3 were used for validation. After masking out cloudy, urban and water areas, the Sentinel-2 scenes were split into 24,081,056 training patches with a size of 25x25x10, with the corresponding (normalized) label vectors computed by fCover on the EnMAP imagery. The model was subsequently trained for ten epochs on a single NVIDIA GeForce RTX 2080 Ti.

Results

The training over 10 epochs took approximately 20 hours. The number of epochs could probably be reduced in the future as the training (0.015 MSE) and validation losses (0.021 MSE) already reached their minimum points at the second and third epochs, respectively. The weights obtained after the third epoch

were subsequently used for the creation of fCover maps from Sentinel-2 data. An example of such a map, created for an area not included in the training data, can be compared to an fCover map extracted using the fCover processor in Figure 2. Even though the DL based approach in this case somewhat underestimated the photosynthetically active vegetation, the two maps look very similar overall. The MSE between these two scenes is 0.031 and it took 18 minutes to extract the fCover map from a full Sentinel-2 tile (110x110 km²).

In a more detailed analysis of all the individual training images, it could be observed that the MSE ranges from 0.007 to 0.044. Some of the comparatively higher losses might be explained by the temporal distance between the training pairs, while in others it might indicate consistency problems within the used fCover references, which were so far created without absolute ground truth. The overall relatively low MSE for training and validation data however, indicates that the proposed method is well suited for the task of fCover generation from multispectral data.

Outlook for the future

While these first results already look very promising, there is potential for improvement. First of all, the currently used training data is not optimal as it is often not possible to find suitable EnMAP data for the corresponding Sentinel-2 scene. For example, some of the used training pairs have a temporal distance of more than 10 days, which might introduce inconsistencies (e.g. harvested fields) in the model training. The acquisition of more data over time by the relatively young EnMAP mission should improve the quality of these training pairs.

Concerning the method evaluation, so far, the predicted results were only compared to the fCover outputs without an absolute reference. It would also make sense to validate the fCover maps, both derived from EnMAP and Sentinel-2 data, with actual ground truth values.

Finally, optimizations in the used DL model itself should be investigated. While the used HybridSN model with minor adaptations already delivered very robust results, it should be kept in mind that this model was originally developed for a very different purpose (hyperspectral image classification). There are many parameters (band selection, patch size, kernel sizes, layers, etc.) which could be tuned to try to improve accuracy, robustness and runtime of the presented methodology.

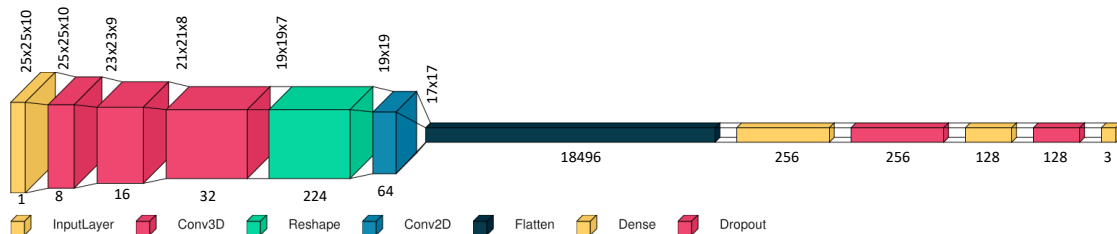


Figure 1 Adapted HybridSpectralNet (HybridSN) Model

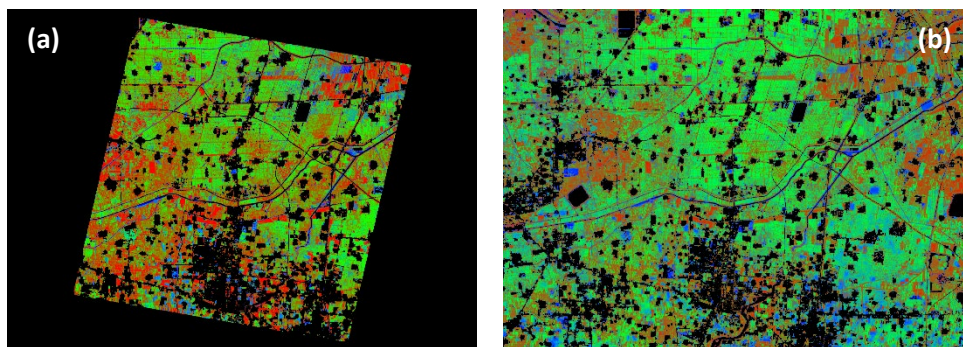


Figure 2 (a) fCover map derived from EnMAP scene using the fCover processor and (b) fCover map derived from Sentinel-2 scene using DL regression for the same region close to Binzhou, China (Legend: red: photosynthetically active vegetation (PV); green: non-photosynthetically active vegetation (NPV); blue: bare soil (BS). The intensity of the colours is related to the cover fractions.)

Comparison of Explainable Machine Learning Methods for Marine Vegetation Mapping by Using Hyperspectral Imagery

Katalin Blix¹, Jorge Garcia-Jimenez^{2,3}, Ana B. Ruescas², Julia Amorós², Galice G. Hoarau⁴, Eli Rinde⁵, Kasper Hancke⁵ and Martin H. Skjeltvareid⁶

¹ UiT University of Arctic of Norway, Department of Physics and Technology, Norway

² Image Processing Laboratory, University of València, Spain

³ Brockmann Consult GmbH, Germany

⁴ Nord University, Faculty of Biosciences and Aquaculture, Norway

⁵ The Norwegian Institute for Water Research (NIVA), Norway

⁶ UiT The Arctic University of Norway, Department of Computer Science and Computational Engineering, Norway

Keywords (5): Unmanned Aerial Vehicles, Arctic Sea, eXplainable Machine Learning, coastal waters, marine vegetation

Challenge

Marine vegetation plays an important ecological role in the coastal areas in Norway. Anthropogenic activity and environmental changes have had a significant impact on macroalgae. Remote sensing techniques opened the possibility for large-scale continuous monitoring. However, the currently freely available sensors onboard satellites might not have the required spatial and spectral resolution to estimate fine details of the marine vegetation. Recently, hyperspectral sensors on Unmanned Aerial Vehicles (UAV) have been applied for monitoring sea meadows. The acquired hyperspectral and the corresponding labelled data is used to train Machine Learning (ML) methods for classifying marine vegetation. Although ML methods have been shown to perform excellently for this task, the importance of the input features usually stays hidden. Therefore, the objective of this study is to compare methods in the field of explainable machine learning to assign relevance to the input hyperspectral bands.

Methodology

Explainable methodologies can uncover the importance of the input features, which can help us to explain the physical and chemical variables that affect the underwater meadows of the study area. This site is located at the coast of northern Norway at the bay called Juvika, where we collect hyperspectral imagery and corresponding ground truth data in the year of 2021 and 2022. Several surface classes were defined including sand, and several percentages of seagrass density, *Fucus Vesiculosus* (FV) and *Ascophyllum Nodosum* (AN). This might allow an insight of the underlying biophysical properties and prepare for more than probable climate change scenarios. We used the collected hyperspectral data to classify the five classes

by using ML methods. These methods include the Support Vector Machine (SVM), feed forward Neural Networks (NN) and Random Forests (RF). In order to assess feature relevance, we are going to apply the Sensitivity Analysis (SA) of the SVM and the gradient boost (XGBoost) model for decision trees.

A Sensitivity Analysis (SA) applied to the Support Vector Machine (SVM) classification problem is used to assess the relevance of the input features. The SA is a probabilistic approach, and it provides the expected value of the squared partial derivatives of the function. In this case, the function is the SVM classifier, where the kernel function is the Radial Basis Function (RBF). Note that the RBF was used to avoid optimisation difficulties with respect to the large number of hyperparameters in the hyperspectral data. The output of the SA is the sensitivity map, which holds the ranked features or the relative importance of the hyperspectral bands (input features).

Gradient boosting derives its name from setting target outcomes based on error gradients. New models aim to minimise prediction errors, adjusting predictions for each training case. XGBoost, a variant used here, provides feature and permutation importance like other tree-based models. Methods such as Shapley Value Sampling (SHAP) values can also be used to interpret feature importance and uncover hidden relationships.

Results

In previous tests, several classification algorithms were evaluated to estimate the five classes from the hyperspectral dataset. Decision trees and NN based methods had acceptable accuracy and efficient computational performance. The SVM has also comparable performance, however it requires long computational time. Figure 1 shows the RGB image of the study site (left), the labelled image (middle) and the result of the NN classification (right).

In the present case, we will apply SA to the classification of sea meadows by using SVM and the XGBoost mentioned before. Assessment by other methods like permutation importance will also be analysed. These techniques enable the development of more accurate and interpretable models for seagrass classification, crucial for monitoring and preserving marine ecosystems. With advancements in data collection (UAV) and model optimization, we can expect enhanced sensitivity analysis to uncover critical features and relationships, contributing to better-informed conservation efforts and ecological management practices.

Outlook for the future

On the one hand, collecting reliable data in coastal areas demands the use of many resources. However, increasing the training dataset enhances its diversity and representativeness, thus improving the learning of classification models and their generalisation capabilities. New measures and data from UAV (300 spectral bands from 400 -1000 nm) will surely help to improve the models. The study can also be extended to other areas to move from local to regional or even global models.

On the other hand, other SA methods can be used for seagrass classification using machine learning models. Exploring and comparing different SA methods can help to better understand the behaviour of the models, as well as see how the different features influence the results. This allows to improve model performance and to detect which are the main learning drivers for the seagrass classification problem.

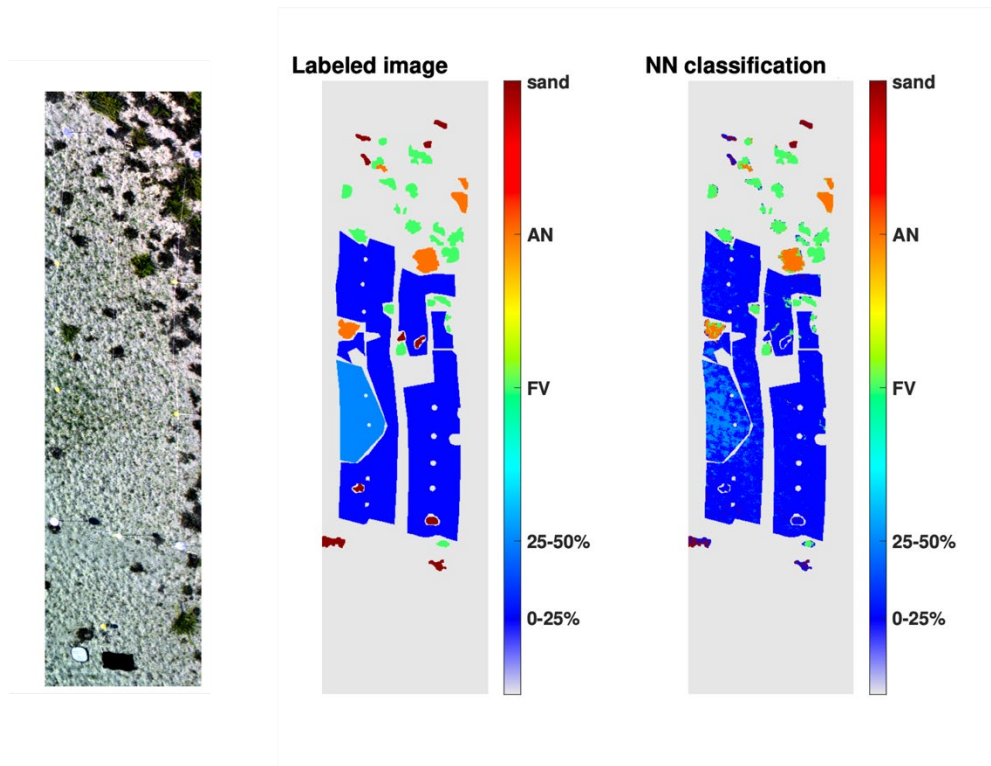


Figure 1. RGB image of the study site, the labelled image, and the results of the classification by using NN. It can be seen that the NN could successfully estimate the classes although there are some misclassifications.

**Them.Sess. 1-6: Imaging
Spectroscopy for climate robust
agriculture**

The SPAGHYTI project - Assessing the nitrogen status and monitoring the (a)biotic stress levels of winter wheat using hyperspectral satellite imagery

Louise Leclère¹, Yannick Curnel¹, Philippe Vermeulen², François Stevens², Vincent Baeten², Damien Malice¹, Anne-Michelle Faux³, Damien Eylenbosch³, Charlotte Bataille⁴, Benjamin Van Der Verren⁵, Nicolas Chamberland⁶, Maxime Troiani⁷, Pierre Defourny⁷, Viviane Planchon¹

¹ Walloon Agriculture Research Center (CRA-W), Agriculture Territory and Technologies integration Unit, Belgium

² CRA-W, Quality and Authentication of Agricultural products Unit, Belgium

³ CRA-W, Crop production Unit, Belgium

⁴ CRA-W, Crops and Forest health Unit, Belgium

⁵ Centre Pilote Céréales et Oléo-protéagineux (CePiCOP), Belgium

⁶ Constellr s.a., Belgium

⁷ UCLouvain - ELIE, Belgium

Keywords (5): Agriculture, Hyperspectral, Wheat, Nitrogen status, (A)biotic stresses

Challenge

Agriculture is at once a cause, a victim and a solution to climate change. A drastic evolution in agricultural practices is needed to mitigate their negative environmental impacts and ensure their resilience, while maintaining acceptable levels of productivity. Digital agriculture is a promising approach that brings together a wide range of modern technological tools like hyperspectral imaging. The SPAGHYTI project aims at developing services for agriculture in the form of applications that provide farmers with relevant and actionable information at the parcel level. These applications will rely on hyperspectral satellite imagery, enabling access to high-value information at a marginal cost with frequent revisits. Currently, two applications are defined in the user segment. These applications aim at assessing the nitrogen status and monitoring the (a)biotic stress levels of winter wheat.

Methodology

An intensive field campaign was organised in 2023 from March to July. Data were collected both in field trials and in farmers' fields located in Wallonia (southern part of Belgium). Field trials included fertilization trials, post-inscription variety trials (under conventional and organic management) and fungicide trials. Ground-based measurements included reflectance data acquired using a portable spectrometer working in the visible and near-infrared wavelength range (ASD FieldSpec 4), characterisation of canopy cover and LAI using digital hemispherical imagery, and disease severity scorings. Wheat samples were also collected and sent to the laboratory for the assessment of dry matter and total nitrogen using near infrared spectroscopy (FOSS NIR XDS). In parallel, satellite images were acquired from the EnMAP and PRISMA missions, depending on the weather conditions. The on-board sensors have a spatial resolution of 30 m and a revisit time of 4 to 27 days, depending on the tolerated off-nadir angle.

The development of the two applications are implemented using field data and hyperspectral data acquired by ASD and satellite sensors. First, the most relevant wavelengths, wavelength combinations and spectral indices are identified (Figure 1). Then, the different existing models are tested and assessed. Based on these two previous analyses, new algorithms are developed and calibrated.

Results

We initially focused on the assessment of the nitrogen status (nitrogen content) using ASD ground-based reflectance. The collected field data were divided into a training dataset (n=112; 3 trials) and an independent validation dataset (n=108; remaining trial and farmers' fields). A Generalized Additive Model (GAM) was used to model the nitrogen content (N) according to spectral variables. The spectral variables were preselected using the Pearson correlation. These variables corresponded to three wavelengths (645, 683 and 1656 nm), spectral indices of the literature (*NDVI_1220_610*) and new spectral indices (*R_747_988*, *NDVI_747_988* and *NDVI_550_1721*). The nitrogen content was predicted with a R^2 value of 0.88, a bias of 0.00 and a RMSE of 2.06 (Figure 2A). Concerning the independent validation, the accuracy was a little lower: the R^2 , the bias and the RMSE were equal to 0.32, 0.63 and 3.44, respectively (Figure 2B).

Outlook for the future

The next steps are going to focus on the assessment of the nitrogen status using satellite imagery and the monitoring of (a)biotic stress levels. The data processing from the first field campaign is still ongoing. Based on data collected in 2023, the potentialities of using hyperspectral data for monitoring (a)biotic stresses and for characterizing grain protein will be investigated. Preliminary results will also be presented at the conference.

In order to complete the field dataset and validate our first analyses, a second field campaign will be organized in 2024.

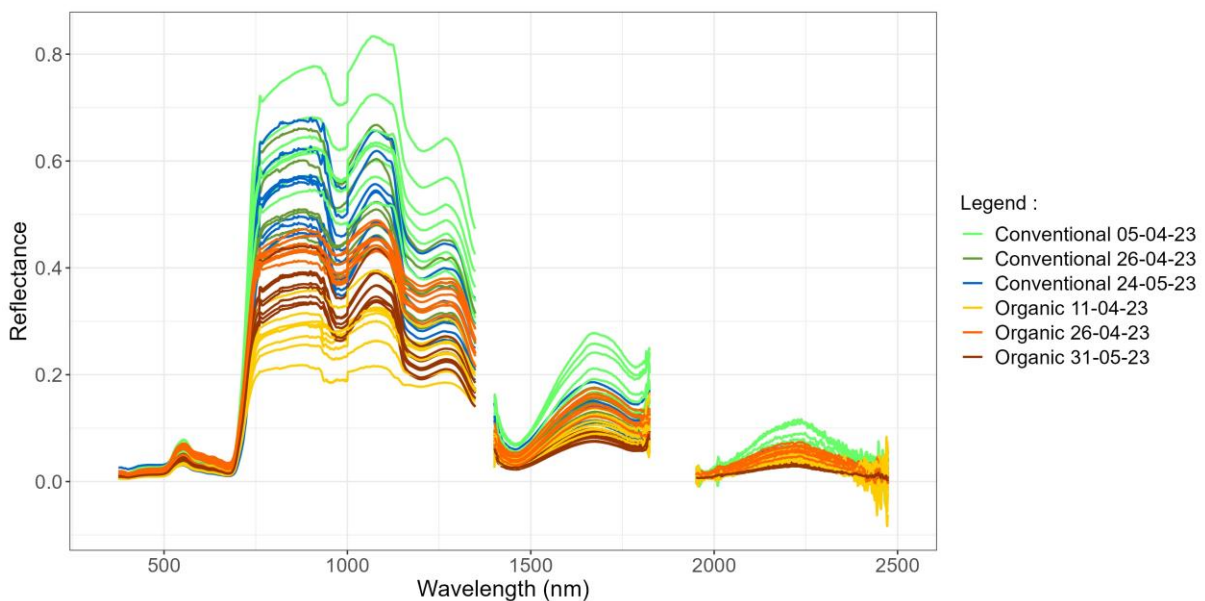


Figure 1. Spectra collected within variety trials under organic and conventional management during the fertilization application period using the ASD FieldSpec 4.

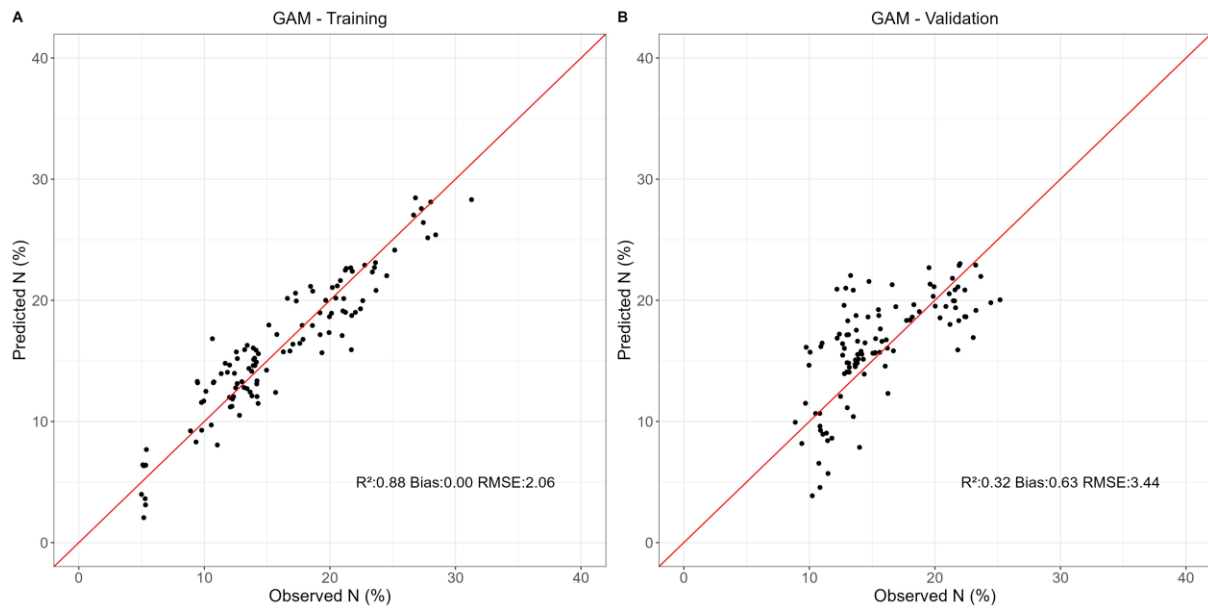


Figure 2. GAM accuracy for the training (A) and independent validation (B) datasets.

Hyperspectral remote sensing and 3D radiative transfer modelling for maize crop monitoring

Romain Démoulin¹, Jean-Philippe Gastellu-Etchegorry², Xavier Briottet³, Matthieu Marionneau¹, Zhijun Zhen², Karine Adeline³, Valérie Le Dantec²

¹ Hyperplan, France

² University of Toulouse 3 - Paul Sabatier, CESBIO UMR 5126, CNES, CNRS, IRD, INRAE, France

³ ONERA - The French Aerospace Lab, France

Keywords (4): Earth Observation, Crop monitoring, Hyperspectral, Radiative Transfer

Challenge

The cereal industry constantly has to imagine scenarios without knowing the harvest date nor the grain quantity or quality. This anticipation capacity becomes more and more difficult due to growing sources of uncertainties like climatic events or global market. A tighter monitoring of crops, spatially, temporally and qualitatively is thus essential. Satellite remote sensing (RS) offers a great potential for near real-time monitoring of crops at global scale. Upcoming hyperspectral missions (CHIME, BIODIVERSITY, SBG...) will give access to more information on crop development. Common approaches rely on the inversion of satellite data using radiative transfer models (RTM) that represent vegetation as a horizontal homogeneous medium, whereas crop fields like maize are often heterogeneous with slopes. This work focuses on the benefits of taking into account the 3D structure of the field for operational inversion.

Methodology

The study site includes maize fields, in Grosseto (42°49'47.02"N 11°04'10.27"E), Italy. The RS dataset consists of two HyPlant hyperspectral images (7 and 30 July 2018) of the ESA FLEXSENSE campaign. Maize crop functional traits were measured in the field at that time. Our work has two objectives:

- To choose the most appropriate radiative transfer model (RTM) and maize field model for the inversion of RS images, for flat and sloped terrain. This is done by comparing the widely used PROSAIL 1D RTM adapted to homogeneous horizontal canopies, and DART RTM that considers the 3D geometry of canopies, including local topography (Figure 1). The inversion is done on 10⁴ DART and PROSAIL simulated RS images. It consists in a training step (85% of dataset) and a testing step (15% of dataset) of a machine learning (ML) algorithm on the LUTs simulated by the two RTMs. Here, three Look-Up Tables (LUT) are simulated using a theoretical maize field and a wide range of instrumental (e.g., HyPlant-DUAL spectral bands) and experimental (e.g., Leaf Area Index: LAI) parameters: horizontal field (PROSAIL), 3D horizontal field (DART horizontal) and 3D sloped field (DART slope).
- Inversion of HyPlant images with ML algorithms to generate crop biophysical and biochemical maps. It uses LUTs simulated by the most appropriate RTM (i.e., DART) with a Grosseto maize field model. It is compared to previous PROSAIL inversion for the same site (Candiani et al., 2022, Remote Sens., 14(8)).

Results

Because the inversion is usually done with PROSAIL, and because DART is assumed to provide more exact RS signals than PROSAIL, it is important to quantify the inaccuracy of the PROSAIL-based inversion method using DART images as references of the RS signal. This is done using the three simulated LUTs "PROSAIL", "DART horizontal field" and "DART sloped field". Figure 2 presents the results of the three types of inversion

for seven functional traits (chlorophyll Cab, carotenoids Car, dry matter Cm, carbon-based constituent Cbc, protein content Cp, water content Cw, LAI):

Case 1: Training and Test with "DART sloped field" (**blue**). This is the most realistic and complex case. It shows the best overall performance and is used as the reference inversion result.

Case 2: Training with "PROSAIL" and Test with "DART horizontal field" (**orange**). Its inversion performance is lower than case 1, partly due to structural effects (e.g., angle between sun direction and row orientation).

Case 3: Training with "PROSAIL" and Test with "DART sloped field" (**green**). It has an even lower inversion performance than case 2. Prediction errors increase for steeper slope, in addition to the canopy structural effects.

The case {Training and test with "DART horizontal field"} will be done for the workshop.

This work shows the interest of DART for the inversion of maize functional traits. It also stresses the importance of realistic mock-ups (e.g., row orientation, topography, mean distance between rows, etc.)

Outlook for the future

Building realistic models of the site of interest will be made through the joint use of DART and the maize growth model DRSmaize (Figure 1). It will lead to more accurate plant structure, including the leaf angle distribution (LAD), the number of leaves at a given growth stage, etc. The model of the crop field will then be used to generate a LUT and apply the inversion method. Future work will compare retrieval performances of maize functional traits from hyperspectral and multispectral instruments. To do so, airborne images will be transformed by French space agency (CNES) into hyperspectral images of upcoming CNES sensor BIODIVERSITY (10m spatial resolution); Sentinel-2 images will be also simulated. Inversion performances will then be compared, and should show potential synergy of multi-/hyper-spectral spaceborne sensors in terms of spatial resolution, spectral sampling and revisit rate to address agri-food industry needs in terms of sustainability and competitiveness.

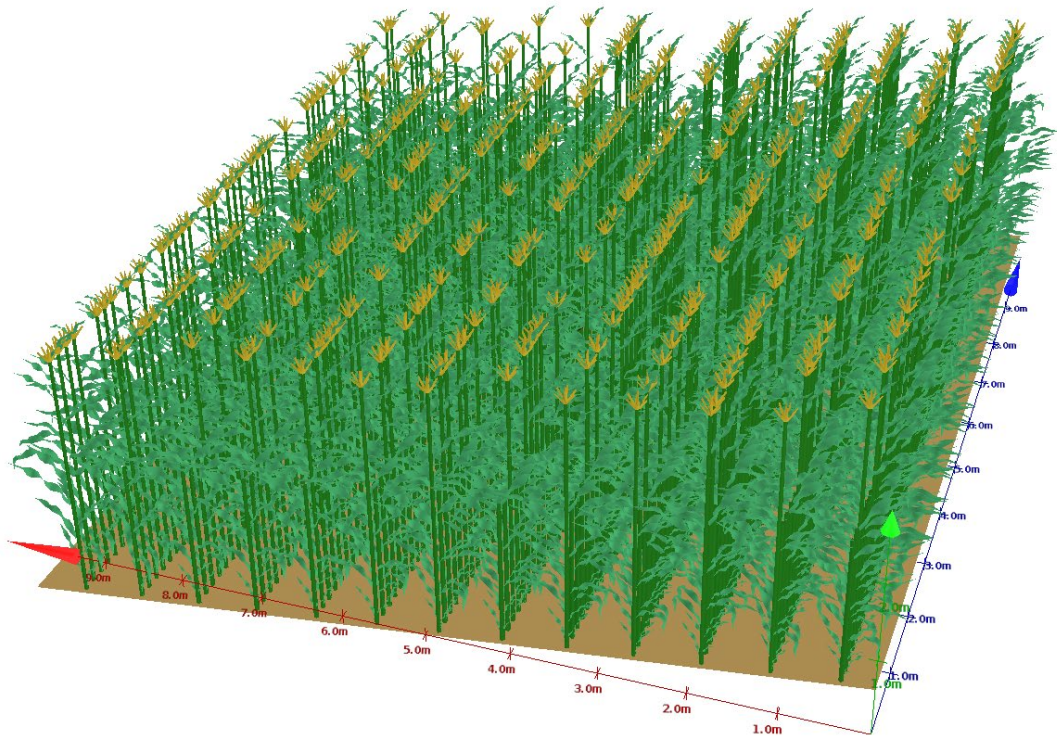


Figure 1: Implementation of 4D Dynamic Real Structure Maize Model (DRSmaize) controlled by degree days to the DART processing chain.

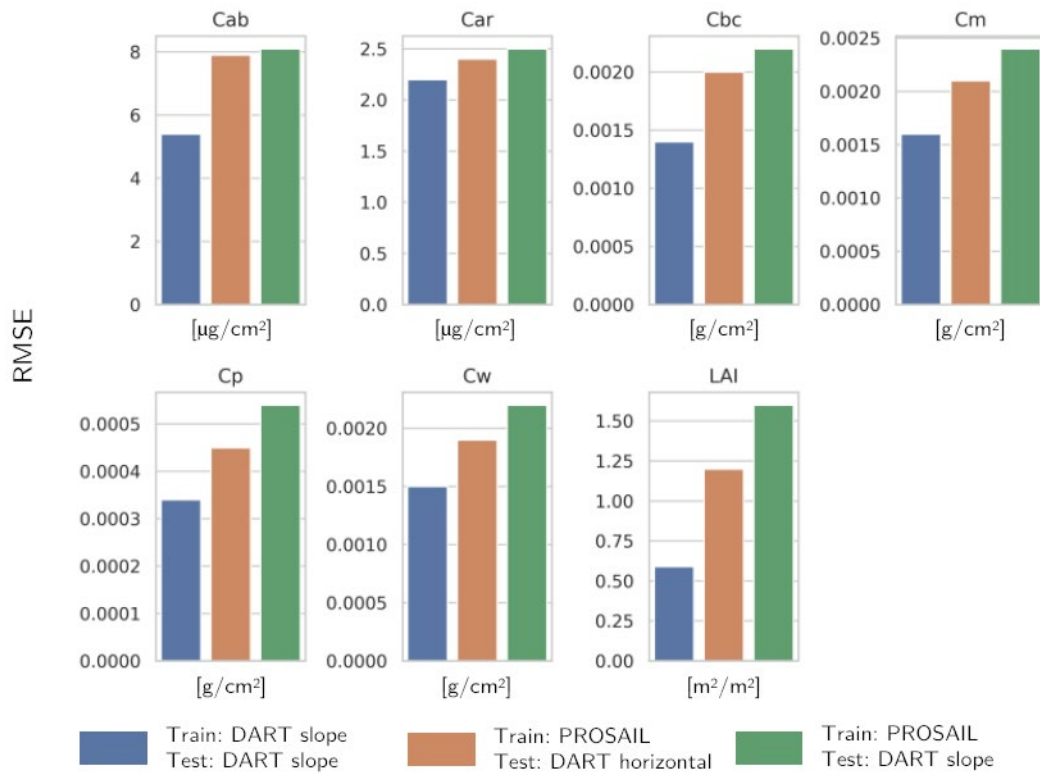


Figure 2: Inversion RMSE of target functional traits at leaf (Cab, Car, Cbc, Cm, Cp, Cw) and canopy (LAI) scale for three inversion cases.

Multi-year and multi-crop traits estimation through hybrid approach from PRISMA hyperspectral data

Candiani Gabriele¹, Alberto Crema¹, Ramin Heidarian Dehkordi¹, Francesco Nutini¹, Cinzia Panigada², Lorenzo Parigi¹, Monica Pepe¹, Marina Ranghetti¹, Giulia Tagliabue², Giulio Tellina¹, Mirco Boschetti¹

¹ Institute for the Electromagnetic Sensing of Environment, National Research Council, Milan, Italy

² University of Milano - Bicocca, Department of Earth and Environmental Sciences, Milan, Italy

Keywords: Leaf Area Index, Canopy Chlorophyll Content, Canopy Nitrogen Content, hybrid models, PRISMA

Challenge

In the next few years, several hyperspectral missions will increment the data stream already provided by the ASI PRISMA and DLR EnMap missions, enabling new research possibilities within the “agriculture and food security” domain. In order to efficiently exploit this upcoming hyperspectral data stream, there is a need to implement and test processing methods on comprehensive real dataset to allow a robust and independent validation of the retrieval approach. In the framework of ASI -PRISMASCIENZA project “PRIS4VEG”, a hybrid approach (HYB) and its variant, featuring sampling reduction through active learning (HAL), were tested on PRISMA hyperspectral data to evaluate estimation of crop traits, such as Leaf Area Index (LAI), chlorophyll content at leaf (LCC) and canopy (CCC) level as well as nitrogen content (LNC, CNC). A multi-year (2020-2023) and multi-crop dataset has been exploited to assess exportability and accuracy of tested approaches.

Methodology

From 2020 to 2023, several in-situ campaigns were carried out in the largest Italian farm, located in the North-East of Italy (Jolanda di Savoia - FE (44.855061 N, 11.952233 E). Field data were collected in different phenological periods to cover a wide range of crop traits and as close as possible to PRISMA acquisitions. During that period, 223 samples were collected for LAI, LCC and CCC and 198 samples for LNC and CNC. These data were split in training (data from 2020 to May 2021) and test dataset (data from June 2021 to 2023). Following a hybrid approach, the radiative transfer model PROSAIL-PRO was selected to simulate canopy reflectances, considering leaf and canopy crop parameters as well as background, illumination and viewing conditions (Sun–target–sensor geometry). To avoid unrealistic combinations of PROSAIL-PRO input variables, covariances between available crop traits acquired during field campaigns have been exploited. The generated Look-Up-Table (LUT), which included 2000 input-output pairs of crop traits and the related reflectance spectra simulations, was spectrally reduced through Principal Component Analysis, selecting the first 15 components. This LUT was used to train a GPR algorithm to model a predictive relation between reflectance spectra and crop traits (HYB). In addition, GPR was also tested considering the optimization of LUT samples through the Active Learning technique (HAL) and the standardization of LUT data (HAL_{STD}).

Results

Both HYB and HAL results showed the difficulty in estimating crop traits at leaf level. HYB failed in providing reliable estimation whereas HAL models, using either raw or standardised data, are able to estimate leaf

traits in the correct range but with moderate correlation to ground data: retrieval statistics provided $R^2 = 0.22$ and $nRMSE = 24\%$ for LCC and $R^2 = 0.02$ and $nRMSE = 26\%$ for LNC. On the contrary, canopy level assessment resulted reliable. The results reported in Figure 1 highlight the benefit of HAL approach with respect to HYB. HYB estimates were highly correlated with ground data (e.g. $R^2 = 0.69$, 0.65 and 0.60 for LAI, CCC and CNC, respectively) but with a significant overestimation of crop traits ($nRMSE = 36\%$, 34% and 28% for LAI, CCC and CNC). HAL, on the other hand, improved the results reducing estimation errors ($nRMSE = 13\%$, 15% and 16% for LAI, CCC and CNC, respectively). The standardisation of input (HAL_{STD}) provided mixed results when compared to HAL: LAI estimation showed a slight improvement (R^2 and regression slope increased from 0.73 to 0.75 and from 0.76 to 0.81 , respectively) whereas CCC retrievals showed lower accuracy (R^2 decreased from 0.63 to 0.59). In case of CNC, even if no significant change was observed comparing HAL and HAL_{STD}, it is interesting to notice a reduction of estimation uncertainty.

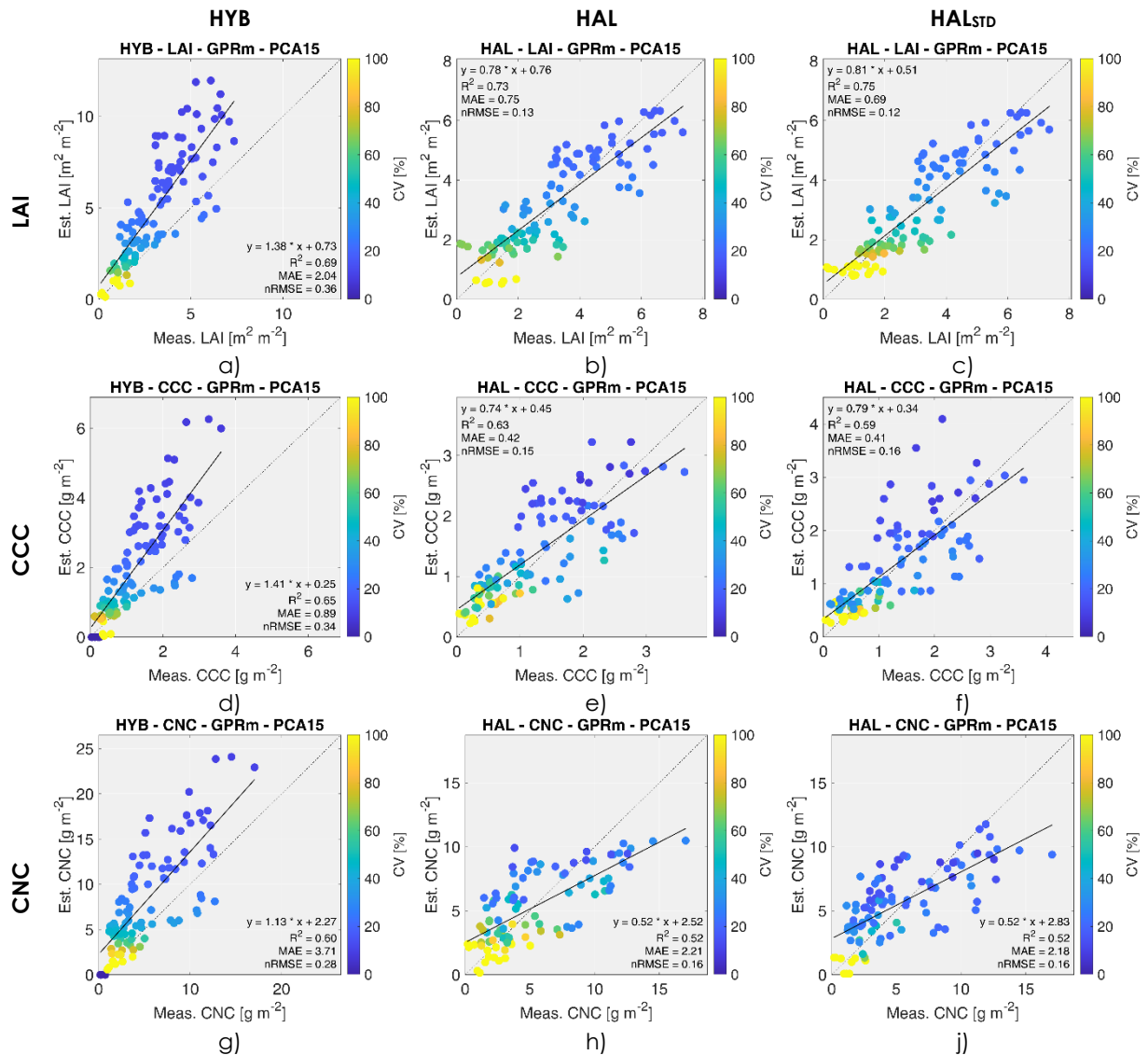


Figure 1. Results of crop trait estimation for LAI (panels a), b), c)), CCC (panels d), e); f)) and CNC (panels g), h), j)) using either HYB (left side) or HAL with two configurations: normal (centre) and standardised input (right side). The colours of the points represent the coefficient of variation estimated by the GPR algorithm.

Outlook for the future

HAL algorithms applied to PRISMA data showed satisfactory performances for the retrieval of crop traits at canopy level. The exploitation of a multi-year and multi-crop dataset allowed to assess the model performance, demonstrating the validity of the proposed approach and utility of PRISMA data. In the

future, several aspects will be investigated: i) data driven estimation of crop traits through MLRA as benchmark performance comparison; ii) application of developed HAL models to available EnMap data to assess solution transferability across sensors; iii) testing different artificial intelligence techniques for complex problem solution; iv) exploiting crop modelling to biologically constrain PROSAIL-PRO input; v) exploring the opportunity to fuse multispectral (i.e. Sentinel-2) and hyperspectral (i.e. PRISMA, EnMAP) data to enhance their spatial and temporal resolution.

Acknowledgements

This work is carried out within Contract "PRIS4VEG" n. 2022-5-U.0 (CUP F43C22000000005), funded by ASI in the "PRISMA SCIENZA" program. Some hybrid algorithms were developed in the frame of the project CHEES - Chime End to End Mission Performance Simulator, funded by ESA (Contract reference 4000137752/22/NL/NA).

Poster Day 1: Poster session

**[Formatting guidelines for
abstract submission]**

EARSeL Valencia 2024

Abstract

Corresponding Author:

[andrej.halabuk@gmail.com]

Title:

Towards quantification of non-photosynthetic vegetation from Copernicus Hyperspectral Imaging Mission for the Environment (CHIME_NPV)

Andrej Halabuk¹, Tomáš Rusňák¹, Svetlana Košťánová¹

¹ Institute of Landscape Ecology, Slovak Academy of Sciences, Slovakia

KEYWORDS (5): EARTH OBSERVATION, CHIME, NPV, CROP RESIDUE, RTM

Challenge

The mapping and quantification of Non-Photosynthetic Vegetation (NPV) represent a critical element in ecological and agricultural management, posing substantial challenges due to NPV's dynamic nature and heterogeneity. Recognized as a priority for upcoming space-borne imaging spectroscopy missions, especially the Copernicus Hyperspectral Imaging Mission for the Environment (CHIME), accurate NPV quantification is crucial for assessing carbon and nitrogen cycling, fire risks, and environmental monitoring. The limitations of past and current sensors in the shortwave infrared (SWIR) spectral range, coupled with the scarcity of in-situ NPV data, have hindered the progress of NPV biomass estimation from space. The advancement of CHIME's hyperspectral capabilities offers a unique opportunity to address these challenges with novel, efficient, and transferable methodologies.

Methodology

The methodological framework integrates a "hybrid" approach, leveraging leaf and canopy radiative transfer models (RTM) with machine learning (ML) regression techniques to develop a comprehensive workflow for NPV quantification using CHIME data. The methodology includes identifying NPV representation strategies within RTMs, crafting robust retrieval methods across diverse vegetation types, and creating a detailed spectral and crop trait database to aid CHIME's pre-launch campaigns and algorithm validations. Over 100 plot-based canopy spectral reflectance measurements using Fieldspec4, along with key vegetation parameters obtained from various experimental field platforms, are utilized for the optimization of commonly used Radiative Transfer Models (RTMs) such as PROSAIL or DART. Subsequently, machine learning (ML) models are trained using extensive simulations from the optimized RTMs and the resulting model input-output data space. After appropriate spectral resampling to match the forthcoming CHIME configuration, this framework and its models are prepared for deployment on spaceborne imagery. However, independent validation at a regional scale remains crucial.

Expected results

The proposed workflow aims to deliver retrieval methods that not only achieve high locally valid accuracy but also ensure robustness and efficiency across different agricultural landscapes and scales. Anticipated outcomes include an overall accuracy of at least 75% for NPV classification images and 80% for NPV masks, with NPV biomass quantification models expected to exhibit an R^2 of at least 0.5 and a relative RMSE of around 30%. This will significantly surpass the capabilities of existing methods, enabling plausible mapping of NPV biomass across varied conditions.

Outlook for the future

The success of this workflow will set a new precedent for the operational quantification of NPV using CHIME, contributing vitally to broad-scale environmental monitoring, fire risk management, and the enhancement of agricultural practices. By establishing a solid foundation of comprehensive databases and robust methodologies, this initiative is poised to revolutionize NPV assessment globally, offering invaluable insights for the launch and operational phases of CHIME. The CHIME_NPV project serves as a pioneering step in refining baseline requirements for NPV monitoring, with the potential to extend into the integration of operational algorithms that can provide robust and reliable NPV data for future hyperspectral missions.



Figure 1 NPV, crop residue and soil measurements sequence.

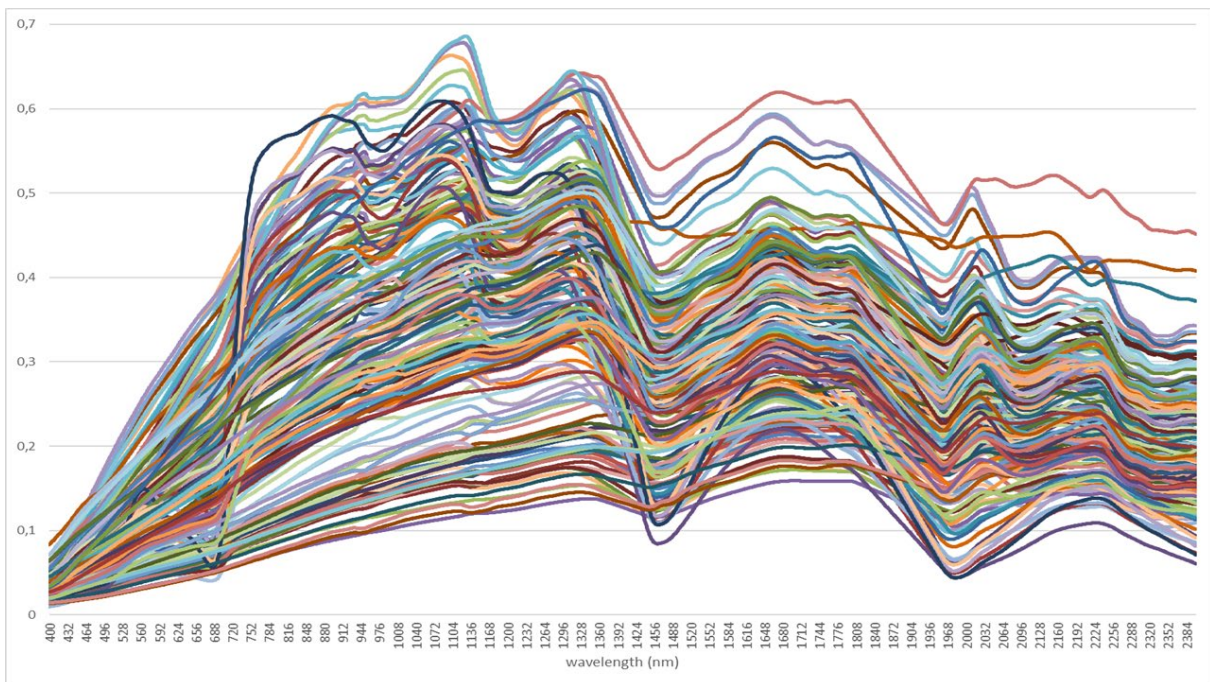


Figure 2 Spectral variability of the gradient of measured NPV targets. Spectral measurements with the Fieldspec4 spectroradiometer.

Cross Validation of Orbital Hyperspectral Sensors: A Case Study Using PRISMA, EnMAP, DESIS, and EMIT

Daniela Heller-Pearlshtien*¹ and Eyal Ben-Dor¹

Remote Sensing Laboratory, Geography Department, Porter School of the Environment and Earth Sciences,
Faculty of Exact Sciences, Tel Aviv University, Tel Aviv 699780, Israel;

Abstract

The pursuit of enhanced precision and complex applications has surged in this sensor era, marked by the increasing deployment of advanced hyperspectral orbital sensors. These HRS sensors must deliver advanced outputs tied to their reflectance calibration and specification. Comprehending the differentiating factors among these sensors becomes paramount for end-users aiming to select the optimal fit for their distinct application endeavors. This study compared four HRS orbital sensors at their very early stage in space : ASI's PRISMA, DLR's ENMAP and DESIS, and NASA JPL's EMIT, with a primary emphasis on their specifications, Level 2 atmospheric correction products, and their aptitude for mineral mapping. The results may be used as a marker to judge quality of these sensors in its operating time.

The Role of the Scene Generation Module (SGM) into the CHIME End-to-End Simulator (CHEES).

EARSel Valencia 2024

Abstract

Corresponding Author: carolina.tenjo@uv.es

Carolina Tenjo¹, Adrian Jacinto-Guillén¹, Antonio Ruiz-Verdú¹, José Moreno¹
(Style: Authors, presenting author underlined)

¹ UNIVERSITAT DE VALÈNCIA
(STYLE: AFFILIATIONS;)

Keywords (5): Earth Observation, CHIME, Hyperspectral, BRDF, SGM

Challenge (800 - 1000 characters incl. spaces)

The End-to-End Simulator (CHEES) plays a key role for the CHIME mission. It simulates the mission workflow, aiding in design, performance assessment, and data processing development. CHEES modules include Scene Generation, Observing Performance, Retrieval, and Performance Assessment.

The Scene Generation Module (SGM) within CHEES generates realistic 3D synthetic scenes, replicating surface properties, atmosphere conditions, and geometric characteristics in accordance with the physical processes of electromagnetic radiation interaction with natural surfaces. This includes the incorporation of Bidirectional Reflectance Distribution Function (BRDF) and adjacency effects. SGM build scenes with higher spatial and spectral resolution than the instrument, facilitating the assessment of data processing and the optimization of mission performance.

Methodology (1200 – 1500 characters incl. spaces)

The SGM is a tool that realistically simulates the natural world reproducing the physical properties, surface interactions, atmospheric effects, and the geometric relationships between the sun, the scene, and the observing instrument.

First, the SGM generates a common spatial scene that includes all three CHIME spectrometers' fields of view. Within this common grid, it distributes reflectances from various sources, depending on the simulation's objectives.

The SGM can incorporate reflectances from airborne scenes or pre-existing reflectance databases, or it can generate reflectances using a Radiative Transfer Model (RTM) with provided key parameters. SGM employs the SCOPE V 2.1 RTM (Van der Tol et al., 2009, Biogeosciences 6, 12) to simulate vegetation reflectances. Additionally, it includes a database created using the HydroLight RTM, which contains Bidirectional Reflectance Distribution Functions (BRDF) for water reflectances, enabling the simulation of the sunglint effect over water surfaces.

Additionally, the SGM models the atmosphere by distributing key atmospheric parameters within the scene, such as Water Vapour or Ozone, and clouds. Geometric and viewing features are also taken into account, including terrain altitude, latitude and longitude coordinates, solar geometry, and observation geometry.

After modelling these characteristics, the forward model simulates Top of Atmosphere (TOA) radiative propagation, following the methodology by Mousivand et al. (2015, Remote Sensing, 7).

Results (1200 – 1500 characters incl. spaces)

The SGM can simulate the topographic effect on TOA radiance and variable retrieval by quantifying various topographic components, such as sky view factor and terrain-reflected radiance, following the approach by Mousivand et al. (2015, Remote Sensing, 7). To illustrate the impact of topography on TOA radiance, we conducted the following exercises:

1. We simulated a homogeneous scene in terms of reflectance, incorporating a Digital Elevation Model (DEM) and modelling the atmosphere while considering variations in terrain altitude, without BRDF and adjacency effects. In Figure 1, TOA radiance at 720 nm (Water Vapour band) and 761 nm (O2A band) is displayed. As expected there is a correspondence in the TOA radiance spatial pattern with the DEM altitudes, due to the correlation of atmospheric thickness and oxygen and water vapour absorption intensities.

2. We repeated the same scene as in exercise 1 but included BRDF and adjacency effects, allowing us to compare it with the scene in exercise 1. Figure 2 illustrates the differences in TOA radiance at 650 nm between both scenes.

The results presented here demonstrate the SGM's capabilities to simulate realistic scenarios, enabling a more robust development of Level-2 retrieval models, including atmospheric correction.

Outlook for the future (800 - 1000 characters incl. spaces)

In the future, the SGM could make a substantial contribution to our understanding of complex natural environments, encompassing changes in land cover and interactions within the atmosphere. The integration of RTMs, alongside improved BRDF and adjacency effects modelling, further enhances the SGM's scene simulation capabilities.

As the demand for precise environmental data continues to grow, driven by challenges related to climate change and resource management, the SGM's role in supporting Level-2 retrieval models and atmospheric correction becomes indispensable. Its ability to replicate diverse scenarios, including topographic effects and sunglint over water surfaces, is invaluable to researchers. By enhancing our capacity to model Earth's dynamic systems, the SGM is shaping the future of environmental research and remote sensing applications.

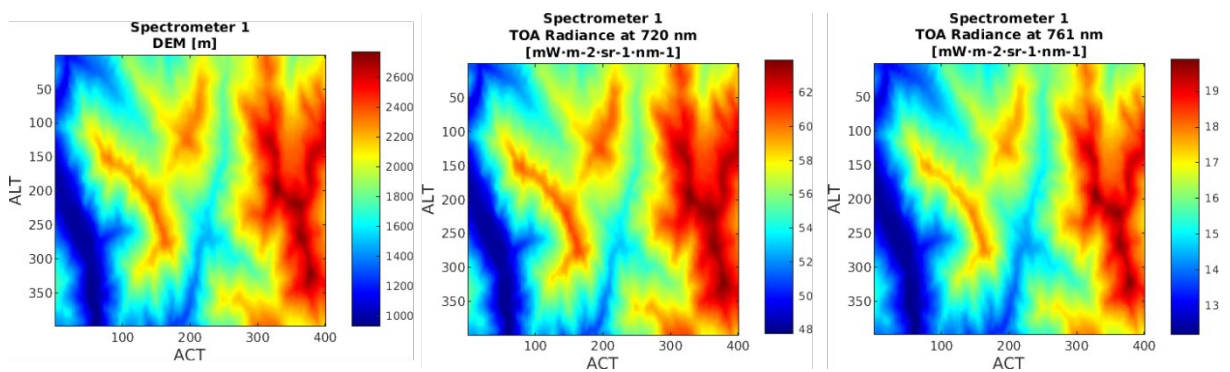


Figure 1 Comparison of TOA radiance at 720 nm (Water Vapour band) and at 761 nm (O2A band) and the DEM.

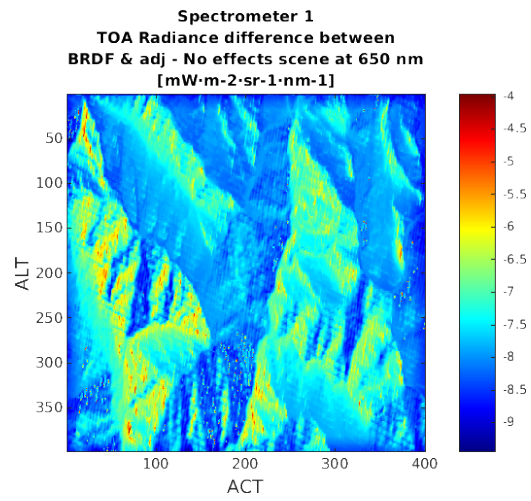


Figure 2 Difference in TOA radiance between a scene with BRDF and adjacency effects and a scene without these effects.

Towards global detection of methane plumes in hyperspectral data of EMIT with focus for on-board deployment

EARSel Valencia 2024
Abstract
Corresponding Author:
vit.ruzicka@cs.ox.ac.uk

Vít Růžička¹, Andrew Markham¹

¹ University of Oxford, Department of Computer Science, United Kingdom

Keywords (5): Methane detection, Machine Learning, Hyperspectral, EMIT, Earth Observation

Challenge

Recent research has shown that automated detection of methane plumes in hyperspectral, high-resolution remote sensing data is feasible. However, it has been demonstrated only over a limited localised area, as supported by the availability of the data.

Applying machine learning models globally requires first and foremost access to a diverse and global dataset. For detection of rare signals, such as methane plumes, enough labelled samples are also needed. With recent and upcoming hyperspectral satellites, it would take long time to wait for capturing real methane leak events. Quite uniquely, when working with hyperspectral data, we can realistically simulate methane plume events using raw clean hyperspectral data, the knowledge of the methane signature across different wavelengths and methane enhance product as a source of labels from other locations. With these, we can feasibly simulate a global methane plume dataset with reliable annotation for any upcoming hyperspectral sensor.

Methodology

We create the dataset using the recent hyperspectral sensor EMIT, which offers a near-global coverage of the arid regions of Earth and allows for public access to the data. We are also interested in the multi-temporal scenario, as an alternative to the single image detection. With weaker sensors and with smaller methane plumes, it has been shown that having access to multiple views of the sample location can improve the detection performance.

For simulating plume events we use methods detailed by the works of Gorroño et. al 2023 and others. Given the knowledge of methane transmittance, it is possible to use a source methane enhancement product from another source alongside with a clean hyperspectral cube of data to simulate sample with an event. As the source of real methane enhancement products, we use the STARCOP dataset of methane plumes released by Ruzicka et.al 2023.

Using a pair of collocated hyperspectral samples, and by simulating methane plume events in the latter of the pair, we can either frame the task mono-temporally as semantic segmentation, or multi-temporally as change detection. For this we could employ models such as U-Net, or SegFormer, and in the multi-temporal scenario, their Siamese variants. Furthermore, we'd like to explore the potential on-board deployment of the proposed models, highlighting the trade-offs between speed and accuracy of different approaches.

Expected results

Experimentally, we plan to compare the baseline of matched filter products (such as the magic method of Foote, M. D., et al. 2020), with a newer approach proposed by Ruzicka V. et al. 2023 that uses a learned U-Net model on top of these products. Additionally, we plan to explore end-to-end architectures, that would be able to detect methane directly from the hyperspectral datacubes without relying on manually crafted filters. So far, we have tested the time performance of these approaches on the constrained hardware provided by D-Orbit and Unibap - each machine with a quad-core x86 64-bit CPU processor, Intel Movidius Myriad X VPU and 2 GB RAM of memory.

Computing the methane enhancement product for a typical hyperspectral tile of 128x128px, using the iterative matched filter approach (mag1c) takes ~1.96 seconds. Additional pass through the learned model using a U-Net architecture increases this runtime to ~2.0 seconds. In our initial experiments, a similar U-Net based model processing the full hyperspectral tile without the matched filter product takes only ~0.16 seconds. This is in fact comparable with the time required to running the matched filter for only one iteration, which takes about ~0.12 seconds, and results in quite noisy image. All the measurements include the IO time needed to load the hyperspectral tile.

Importantly, we plan to run more experiments with these models trained on the proposed global dataset of simulated methane plume events.

Outlook for the future

We expect the proposed machine learning architectures to be relevant in many scenarios that range beyond satellite methane detection (for example for on-board processing in hand-held optical gas imaging (OGI) cameras). Furthermore, the planned global dataset should promote machine learning research when dealing with hyperspectral data – as typical, out of the box machine learning model, doesn't account for spectral dimensionality and thus may lose information during the processing. In future, we plan to use this dataset for further experiments to adapt novel architecture designs with the high spectral dimensionality in mind. As will be further explored, end-to-end models may also be beneficial in terms of the inference speed for on-board deployment. Finally, with the upcoming satellite missions, our methods of creating a global dataset of methane plume events from previously observed real events, can be used to speedily adapt models for new sensors.

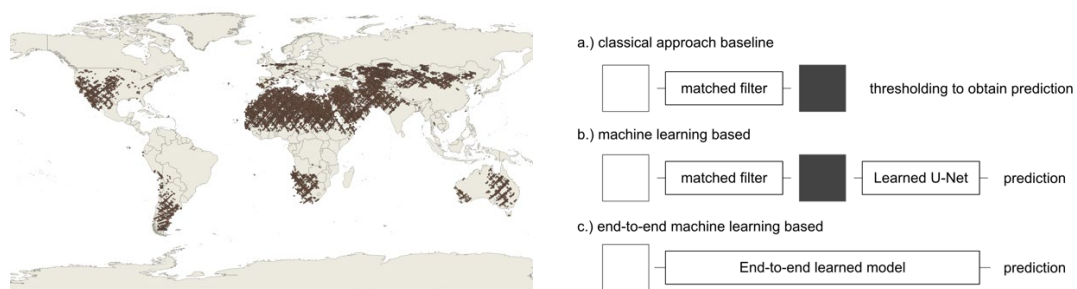


Figure (left) Locations of all intersections present in the EMIT data (resulting in 7791 intersections), which can be used to download samples with multi-temporal coverage. Likely these would need to be further filtered with cloud coverage. (right) Overview of the proposed methods for methane detection.

Advancing Topographic Correction in Hyperspectral Imaging: The Shape from Spectra Method

EARSel Valencia 2024
Abstract
Corresponding Author:
Nimrod.carmon@jpl.nasa.gov

[Nimrod Carmon](#)¹, Alexander Berk², Niklas Bohn¹, David R. Thompson¹, Philip G Brodrick¹, Charles Bachmann³.

¹ Jet Propulsion Laboratory, California Institute of Technology, USA

² Spectral Sciences Inc., USA

³ Rochester Institute of Technology, USA

Keywords (5): Earth Observation, Urban, Hyperspectral, Land Use, Copernicus

Challenge (800 - 1000 characters incl. spaces)

The challenge addressed here is the compensation for topographic effects—slope and aspect—in VSWIR spectroscopy, traditionally corrected post-atmospheric analysis. This method, assuming flat terrain initially, skews atmospheric state readings and introduces errors to subsequent topographic corrections. Complications arise using DEMs to ascertain local solar zenith angles for topographic adjustment. Mismatches between DEMs and radiance data can introduce spatial, temporal, and alignment errors into spectral inversions, escalating the uncertainty of reflectance maps. Such inaccuracies hinder high-precision applications that rely on accurate and precise spectral signatures in the VNIR such as plant trait estimation, snow and ice monitoring and iron oxide mineral mapping.

Methodology

Our methodology, termed 'Shape from spectra,' innovates by estimating topography directly from radiance data, without the need for external DEMs. It begins by calculating the decoupled direct/diffuse atmospheric transmittances for any given atmospheric state, utilizing the MODTRAN atmospheric radiative transfer engine. We then use a radiance model that distinguishes between direct and diffuse illumination, adjusting for the topography's influence on the amount of direct illumination, which has a significantly different spectral shape compared to the diffuse illumination.

For surface reflectance we employ a data-driven approach, leveraging a spectral library with a wide range of known endmember spectra. By applying dimension reduction techniques, we distill complex spectral data into simpler, more manageable forms. This process identifies the fundamental spectral signatures needed to represent the observed data accurately. With the reduced spectral library, we construct a multiple endmember linear mixture model. This model accounts for the varying proportions of different materials present in the pixel's instantaneous field of view (iFOV) and their unique spectral responses.

The crux of our methodology is the nonlinear optimization process. We use a trust region reflective algorithm—a robust nonlinear least squares solver—to iteratively adjust our estimates of topography, surface reflectance, and atmospheric parameters. By minimizing the difference between the modeled and observed radiance, we extract the topographic slope from the radiance spectra itself.

This integrated approach allows for simultaneous atmospheric and topographic corrections, providing a self-contained solution that is both accurate and aligned in space and time with the radiance measurements. Our methodology is poised to address the current limitations in VSWIR imaging spectroscopy, offering a path toward more accurate, topography-aware spectral analysis.

Expected results

Our initial results, benchmarked against high-resolution LIDAR data, demonstrate that our 'Shape from spectra' method delivers comparable performance in estimating topography. This outcome is a strong indicator that the expected results for remote sensing applications are highly promising. Our approach is particularly advantageous for analyses dependent on the VNIR spectral range, often employed in rugged and mountainous terrains where accurate topographic representation is crucial.

Current hyperspectral missions like EMIT, PRISMA, EnMAP, and DESIS could immediately leverage this methodology to enhance their data quality. These missions, which sometimes struggle with topographic corrections due to the challenges presented by complex landscapes, stand to gain from our more precise topographic estimations derived directly from radiance data.

Looking forward, forthcoming missions such as NASA's SBG and ESA's CHIME will also reap significant benefits. These missions are poised to utilize the most accurate reflectance maps for a variety of Earth observation purposes, and our method's ability to accurately capture the nuances of Earth's topography will be instrumental in their success. With our technique, we expect a new level of precision in remote sensing that aligns with the advancing demands of these future missions.

Outlook for the future

The outlook for our 'Shape from spectra' methodology is to broaden retrieval capabilities by combining robust physical formulations with cutting-edge machine learning techniques. By integrating physical Bidirectional Reflectance Distribution Function (BRDF) models, specifically those based on the pioneering work of Hapke, we aim to enhance the precision of our spectral signature retrievals from these remote sensing measurements.

These enhancements are expected to lead to a significant expansion in the retrieval capacities of remote sensing platforms. By refining the spectral data accuracy, especially in the VNIR range, we can achieve more precise environmental monitoring and resource management. This development holds the promise of propelling remote sensing into a new era of detailed Earth observation, underpinning advances in fields ranging from agriculture to climate science.

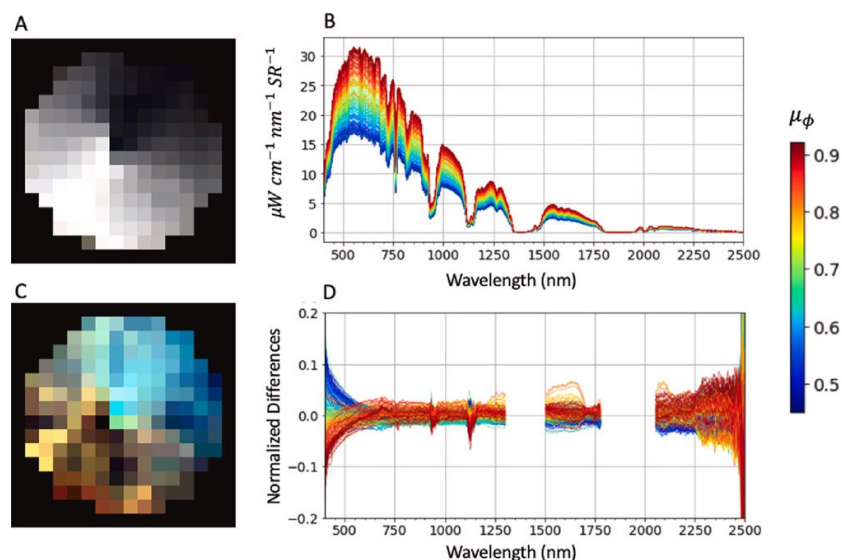


Figure The topographic slope variable has both a magnitude and a spectral shape effect on the measured radiance. Panel A shows a true color image from the radiance measurements, with individual spectra plotted in panel B, illustrating the magnitude effect. Panel C shows normalized differences in radiance, in true color, with the normalized spectra plotted in panel D, illustrating the spectral shape effect. Spectra in panels B and D are colored by the appropriate lidar-estimated topographic slope value. True color images in panels A and C are plotted with a linear min-max stretch.

Validation of the WORLDSOIL Organic Carbon Monitoring System in the area of Demmin, Germany: Comparison with in-situ and air and spaceborne hyperspectral imagery prediction

Asmaa Abdelbaki¹, Sabine Chabrilat^{1,2}, Robert Milewski¹, Kathrin Ward¹, Bas van Wesemael³, Marmar Sabetizadeh³, Asa Gholizadeh⁴, Daniel Žížala⁴, Nikolaos Tziolas⁵, Nikolaos Tsakiridis⁶, Uta Heiden⁷, Pablo d'Angelo⁷, Laura Poggio⁸, Eyal Ben-Dor⁹, Adrián Sanz¹⁰, María Julia Yagüe Ballester¹⁰

¹ Section Remote Sensing, Helmholtz Centre Potsdam GFZ German Research Centre for Geosciences, Telegrafenberg, 14473 Potsdam, Germany

² Leibniz University Hannover, Institute of soil science, Herrenhäuser Str. 2, 30419 Hannover, Germany

³ Earth and Life Institute, Université Catholique de Louvain, 1348 Louvain-la-Neuve, Belgium

⁴ Department of Soil Science and Soil Protection, Faculty of Agrobiology, Food and Natural Resources, Czech University of Life Sciences Prague, Kamycka 129, Prague, 16500, Czech Republic

⁵ Department of Soil, Water and Ecosystem Sciences, Institute of Food and Agricultural Sciences, University of Florida, 2685 State Rd 29N, Immokalee, FL 34142, USA

⁶ Laboratory of Remote Sensing, Spectroscopy, and GIS, Department of Agriculture, Aristotle University of Thessaloniki, 54124 Thessaloniki, Greece

⁷ German Aerospace Center (DLR), Remote Sensing Technology Institute (IMF), Oberpfaffenhofen, 82234 Wessling, Germany

⁸ ISRIC - World Soil Information, Droevendaalsesteeg 3, 6708 PB Wageningen (Building 101), the Netherlands

⁹ The Remote Sensing Laboratory, Tel Aviv University, Zelig 10, Tel Aviv 69978, Israel

¹⁰ GMV - Remote Sensing and Geospatial Analytics Division, Isaac Newton 11, P.T.M. Tres Cantos, E-28760 Madrid, Spain

Keywords: Exposed Soil Reflectance Composite, Time-series Sentinel-2 data, HySpex Imaging Hyperspectral data, Machine Learning, Soil Reference Databases

Challenge (800 - 1000 characters incl. spaces)

Soil organic carbon (SOC) is crucial for the global carbon balance, affecting climate change. Moreover, it is one of the indicators for soil quality, and ecosystem functions. Precise monitoring is essential to support policies and decision-making for soil protection and restoration. The ESA-funded WORLDSOILS Monitoring System (WOSOMS) project addresses this need by developing a pre-operational monitoring System providing high-resolution annual SOC estimations at a continental (Europe) scale, based on available multispectral spaceborne data. It leverages Earth Observation (EO) data and advanced modelling, hosted on an European cloud platform. Challenges include the accuracy of SOC mapping, limited soil exposure in satellite images, disturbance factors on soil surface, and limited spatial and spectral resolution. To study these challenges, the third phase of the WORLDSOILS project includes an intense validation of the SOC maps obtained at different test sites. In this study, we focus on evaluating SOC predictions at the local/regional scale in the Demmin test site, Germany, highlighting the difference between the Sentinel-2 and air- and spaceborne hyperspectral data predictions based on HySpex.

Methodology (1200 – 1500 characters incl. spaces)

SOC prediction utilises machine learning, integrating multi-temporal Sentinel-2 and Copernicus data linked to soil reference databases (LUCAS 2018 and WoSIS). The automated soil composite mapping processor (SCMaP) is an approach for processing Sentinel-2 satellite data to make the use of per-pixel reflectance composites mitigating the issue of limited soil exposure. The spectral composites are subsequently segmented at a spatial resolution of 50 m across Europe into two categories: cropland (bare soil) and permanent vegetation, leveraging data from multiple time series (2018-2020, 2019-2021, and 2020-2022). The analysis for predicting SOC products is divided into three steps:

1. For the bare soil pixels selected based on multitemporal soil composite and different indices, a 1-D CNN is applied to the exposed soil reflectance composite (SRC), partitioned into calibration and test sets using the conditioned latin hypercube sampling (cLHS) algorithm.
2. For the permanently vegetated soils, a quantile random forest (QRF) model utilises spectral composites and environmental covariates derived from multiple sources.
3. The final step merges the obtained results from both models, producing a unified SOC prediction at 50 m resolution for Europe, accompanied by an uncertainty map.

The models performance is validated internally through rigorous 10-fold cross-validation, ensuring generalization and mitigating overfitting risk. The predicted SOC product is externally validated in three pilot regions (Belgium, Czech Republic, and Greece) at a large regional scale. In addition, at a smaller scale, the Demmin region in Germany is considered for the validation purpose due to the availability of dense in-situ data and SOC prediction maps from variable EO data. Finally, the WORLDSOILS predicted SOC is compared with the HySpex airborne hyperspectral data prediction. The evaluation is done by using the assessment metrics (e.g., R^2 , RMSE, and so on).

Results (1200 – 1500 characters incl. spaces)

In the study area, 63 soil samples were collected at the topsoil layer from bare, exposed fields during the years 2013, 2016, and 2017. These sampling campaigns were specifically designed to validate EO SOC products, thus composite samples covering a 2 m radius were taken from the top surface (< 5 cm) in the middle of crop fields (Figure 1A). To validate the results, we extracted the predicted SOC values for the respective pixels in the geospatial dataset, with these sample selections aligning with the acquisition timeframe of the Sentinel-2 composite imagery. Table 1 reveals that these samples had relatively high variability in SOC contents (mean = 20.5 g kg⁻¹, standard deviation = 30.13 g kg⁻¹) and a limited SOC value range in the WORLDSOILS prediction compared to in-situ data. The model performed reasonably in case of R^2 and RPD, but showed high RMSE due to some high measured SOC contents (Table 2). The model is struggling to predict high SOC contents at a smaller scale. Figure 1B depicts the distribution of the predicted SOC map using the HySpex data. The high SOC contents appear in kettle holes in the glacial sediments, where shallow peat layers developed. These hotspots of high SOC content predicted less promising using the WORLDSOILS model at the 50 m spatial scale, as shown in Figure 1A.

Table 1 Summary statistics of the in-situ data and the mean of predictive SOC map (the final SOC prediction product)

Samples	SOC	Mean	Std.	Min	Max	C.V. (%)
N=63	Measured parameter	20.5	30.1	7.8	168.8	146.9
2018-2020	Predicted parameter	15.3	4.3	11.0	37	28.3
2019-2021	Predicted parameter	17.1	4.2	10.0	29	24.7
2020-2022	Predicted parameter	16.8	4.3	10.0	29	25.8

Table 2 Evaluation of WORLDSOILS SOC prediction versus in-situ data.

Year	R^2	RMSE (g kg ⁻¹)	NRMSE	CCC	Bias	NSE	RE (%)	RPD	RPIQ
2018-2020	0.6	28.0	0.2	0.3	5.8	0.2	26.9	1.1	0.7
2019-2021	0.5	28.3	0.2	0.2	3.5	0.7	16.8	1.1	0.7
2020-2022	0.4	29.7	0.2	0.7	4.9	0.1	22.5	1.1	0.7

Outlook for the future (800 - 1000 characters incl. spaces)

A future extension of this work will be the employment of data from spaceborne hyperspectral imaging satellites for such a comparison. The predicted SOC maps can be validated by not only by comparing the multi-temporal SRC based on Sentinel-2 time series data with airborne hyperspectral data but also by incorporating PRISMA to enhance the precision of monitoring SOC changes on regional, continental, and global scales. We are working on extending this work to compare with EnMAP and PRISMA SOC predictions. In the future, the WORLDSOILS monitoring system should be extended to hyperspectral spaceborne data that allows an improved selection of bare soil pixels through a better estimation of soil fraction vs non-photosynthetic vegetation cover.

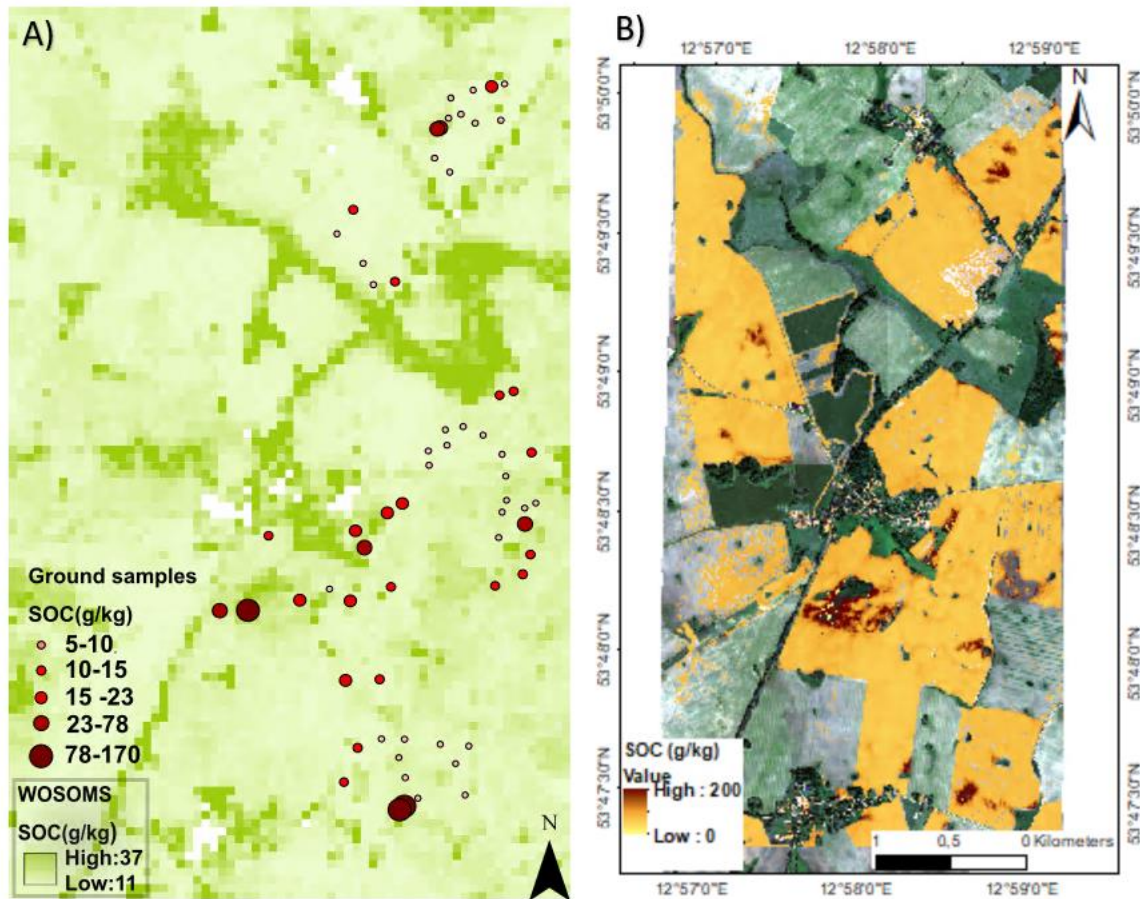


Figure 1: **A)** WORLDSOILS predicted SOC product (2018-2020) in the Demmin region with a 50 m spatial resolution along with the location of ground truth data (left) and **B)** SOC HySpex product of bare soil with a spatial resolution of 1.9 m for visible near-infrared (VNIR) range and 4 m for short-wave infrared (SWIR) range.

HYPERedu Online Learning Program: Concept, Implementation Status and Cooperation Opportunities

EARSeL Valencia 2024

Abstract

Corresponding Author: hyperedu@eo-college.org

[Arlena Brosinsky¹, Katrin Koch¹, Saskia Foerster^{1,2}, Robert Eckardt^{3,4}, Michael Bock⁵](#)

¹GFZ German Research Centre for Geosciences, Remote Sensing and Geoinformatics Section, Telegrafenberg, 14473 Potsdam, Germany

²UBA German Environment Agency, Wörlitzer Platz 1, 06844 Dessau-Roßlau, Germany

³Friedrich-Schiller-University of Jena, Department of Earth observation, Löbdergraben, 07743 Jena, Germany

⁴ignite education GmbH, Am Steinborn 2, 07749 Jena, Germany

⁵DLR German Aerospace Center, Space Agency, Königswinterer Str. 522-524, 53227 Bonn, Germany

Keywords (5): Hyperspectral, education, training, EnMAP, community, MOOC

Challenge

With the launch of hyperspectral satellites like PRISMA and EnMAP, the availability of imaging spectroscopy data is continuously increasing and the interest in hyperspectral data analyses is growing. However, training courses and educational resources on imaging spectroscopy are still scarce. Therefore, HYPERedu, an online learning initiative for hyperspectral remote sensing, was conceptualized and is implemented as part of the EnMAP science program since 2019.

Methodology

HYPERedu provides online learning resources on principles, methods and applications of imaging spectroscopy, addressing students as well as professionals in research, business, and public institutions. The resources comprise annotated slide collections, practical hands-on tutorials (based on the EnMAP-Box software), a number of educational videos (YouTube) and a series of Massive Open Online Courses (MOOCs). The first MOOC on the fundamentals of imaging spectroscopy (2021) was followed by shorter MOOCs on selected hyperspectral application fields. All resources are continuously revised and extended and increasingly used in training courses, university teaching and individual learning.

Results

The first MOOC on the basics of imaging spectroscopy titled "Beyond the Visible: Introduction to Hyperspectral Remote Sensing" was launched in November 2021. It teaches the principles of imaging spectroscopy, sensor technologies and data acquisition techniques as well as data sources and software, using state-of-the-art interactive eLearning approaches. The course is designed to take 5-8 hours to be completed at one's own pace. Upon successful completion, participants receive a certificate, as well as a listing of all course content in a diploma supplement. Following this basic MOOC, in 2022 a MOOC on agricultural applications and in 2023, both a MOOC on EnMAP data access and image preprocessing techniques and a MOOC on soil applications were/will be published. Further MOOCs on inland and coastal waters as well as forestry are under preparation or planned for the upcoming years. All MOOCs are available as interactive online versions as well as offline documents (PDF format), allowing participants to take the course even when a stable internet connection is lacking.

In addition, the HYPERedu YouTube channel has grown to host (as of October 2023) 55 Videos. Further resources include 9 slide collections and 3 hands-on tutorials.

Outlook for the future

All materials and courses are hosted on the EO College platform and are provided free of charge under a CC-BY License. EO College is a learning hub for online courses, open educational resources and discussion forum in the field of Earth Observation. Even though HYPERedu was initiated as part of the EnMAP science program, it is regarded as an initiative by and for the hyperspectral community.

This contribution aims to present and discuss the concept, implementation status and cooperation opportunities of HYPERedu.

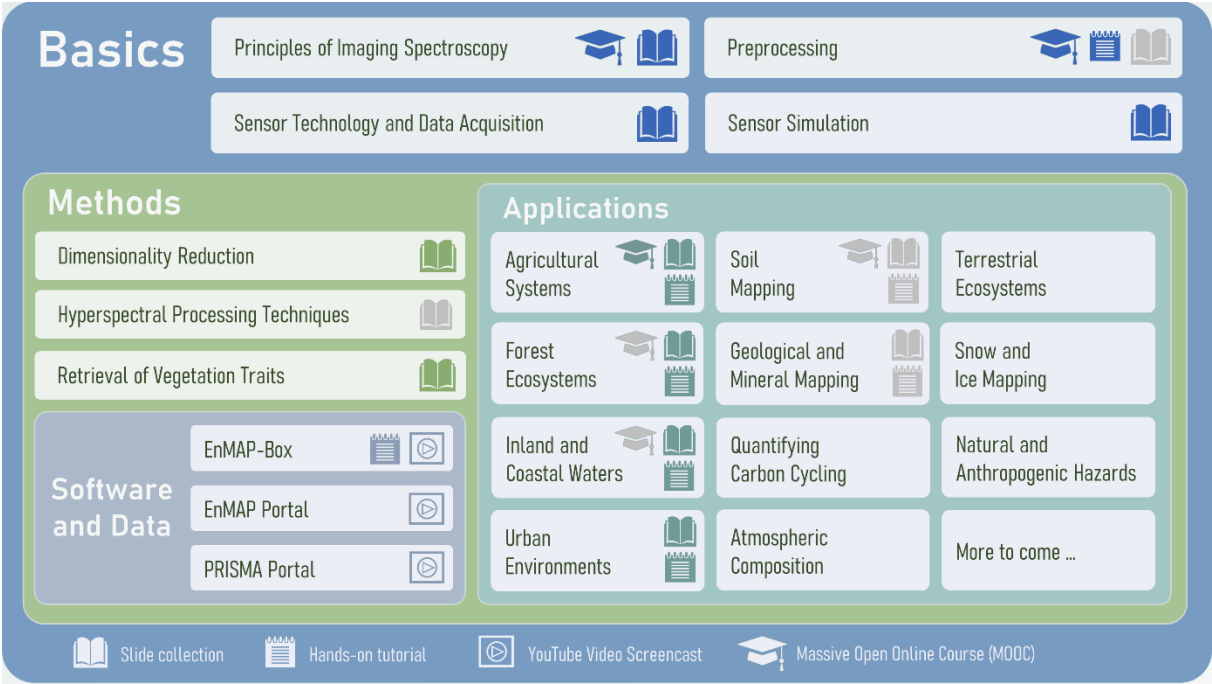


Figure Overview of available (coloured symbols) and planned (grey symbols) HYPERedu resource materials as of October 2023

Mineral mapping using EnMAP hyperspectral data: a comparison of selected machine learning algorithms

Anna Buczyńska¹, Saeid Asadzadeh ²

¹ WROCŁAW UNIVERSITY OF SCIENCE AND TECHNOLOGY, FACULTY OF GEOENGINEERING, MINING AND GEOLOGY, 50 – 370 WROCŁAW, POLAND

² HELMHOLTZ CENTRE POTSDAM, GFZ GERMAN RESEARCH CENTRE FOR GEOSCIENCES, 14473 POTSDAM, GERMANY

Keywords (5): EnMAP, Machine Learning, Mineral Mapping, Hyperspectral, Cuprite test site

Challenge

In recent years, a plethora of machine learning techniques and algorithms have been developed and applied for remote sensing image classification. While many of these methods are valuable for the general purpose of multi- and hyperspectral image classification, their potential applications (and limitations) for mineral classification and mapping have not yet been fully understood. The main challenge in this direction is that minerals often occur in close association with each other in geologic environment, resulting in mixed spectra within image pixels with many individual minerals exhibiting similar spectral behavior in the feature space. The Tetracorder expert system, developed by the US Geological Survey, is designed to address many of these complexities and as a result, it provides the most reliable mineral mapping results from hyperspectral remote sensing data, especially when it is applied to airborne AVIRIS data. With the advent of new hyperspectral imaging systems, such as EnMAP acquired from satellite platforms on a global scale, there is an increasing need for rapid and accurate image classification algorithms capable of mapping surface mineralogy with minimum training datasets on any given geologic site. To explore the potentials of machine learning methods for this purpose, we initiated a study at the well-known Cuprite test site in Nevada, USA. We aim to compare the performance of different machine learning-based classification algorithms against Tetracorder mapping results and identify the most effective techniques for processing EnMAP hyperspectral data.

Methodology

The research conducted in this study included the following steps: (1) acquisition of satellite hyperspectral imagery, (2) preprocessing of the acquired data, (3) development of training data for machine learning models, and (4) performance of supervised classification based on prepared training dataset. At the first step, the EnMAP data acquired on 07.07.2023 over the Cuprite hill was subjected to preliminary preprocessing, including the removal of overlapping channels (in the range of 902.0 nm - 993.3 nm), as well as bands registered in the region of strong atmospheric absorption (in the range of 1330.8 nm – 1461.1 nm). Mineral maps, generated by the Tetracorder expert system applied to AVIRIS data, were first georeferenced and the result was used as a basis to prepare the training dataset covering 19 classes of different minerals and mineral mixtures. The last stage of the work comprised supervised classification, which included using six classification algorithms (Extra Trees, Random Forest, Linear Support Vector, Naive Bayes, and K-Neighbors and Radial Basis Function Support Vector). Preprocessing of the acquired data, as well as supervised classification, was carried out in the ENVI software.

Expected results

Visual and qualitative comparison of the results indicated that the Radial Basis Function Support Vector algorithm yields results closest to the Tetracorder's mineral maps. Satisfactory results were also obtained by supervised classification of EnMAP imagery using the Random Forest and Extra Trees methods. The Naive Bayes and Linear Support Vector algorithms were identified as the least accurate classifiers because the mineral map obtained based on them was significantly different from the reference map. Analyzing the accuracy of the maps obtained in terms of individual classes of minerals, it can be concluded that all the applied classifications correctly indicated the location and extent of the following six mineral classes: alunite, calcite, alunite + kaolinite, dickite, hydrated silica, as well as kaolinite + white mica + alunite + halloysite. The lowest classification accuracy was achieved for the classes: white mica, Na – montmorillonite, and calcite + white mica. The preliminary results obtained so far are encouraging showing that the EnMAP data can be very effectively used to obtain high-accuracy mineral maps of highly altered areas characteristics of advanced argillic alteration.

Outlook for the future

Based on our promising initial results, we have outlined a comprehensive plan to advance our work in several key areas. Our primary objective is to conduct a rigorous quantitative comparison between various classification algorithms and training datasets. Additionally, we are in the process of assessing the impact of different preprocessing and data enhancement methods on the overall performance of each classifier. We are also considering including various deep-learning algorithms in the study. Furthermore, we plan to test the sensitivity of each technique to the quality and quantity of training. In the broader context, we plan to expand our research to encompass AVIRIS-NG and EMIT hyperspectral data, enabling a comprehensive comparison of the results both in terms of algorithms and sensor performance across the study area. For this aim, all datasets will be processed in parallel using the MICA expert system by the USGS.

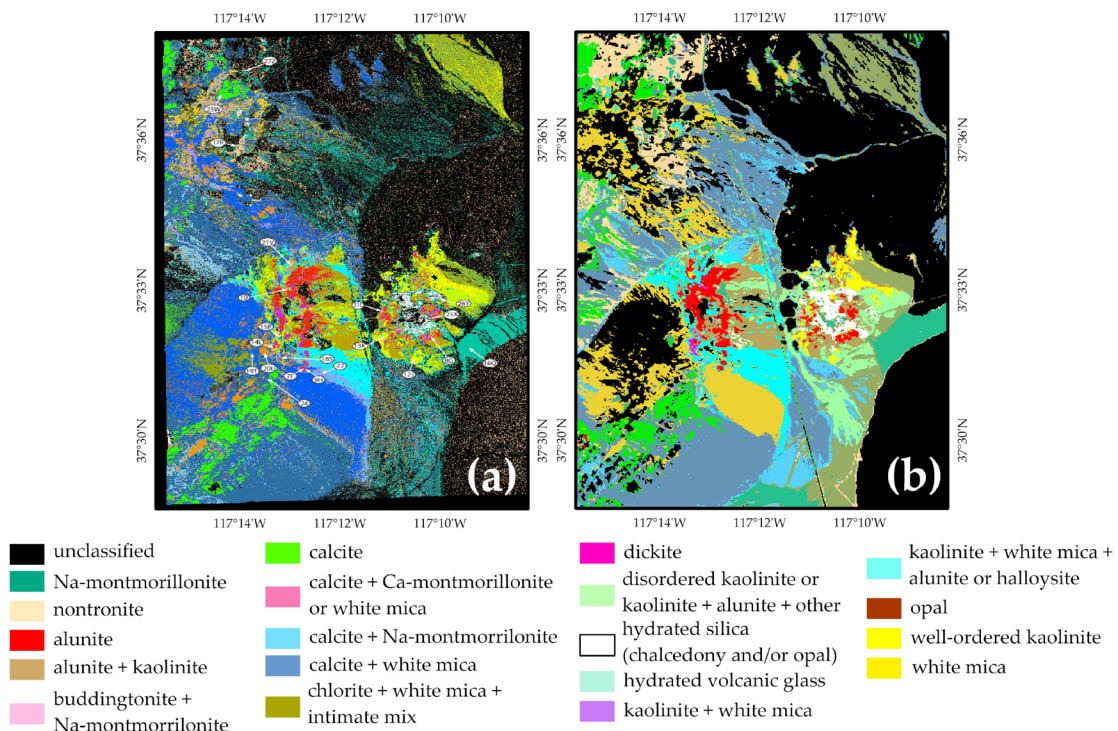


Figure Mineral classification map over the Cuprite Hills area (a) developed using the Tetracorder system and AVIRIS data (b) developed using the EnMAP image and the RBF Support Vector Classifier.

Mapping land surface covers of ice-free areas within the South Shetland Islands, Antarctica using hyperspectral imaging spectroscopy

EARSel Valencia 2024

Abstract

Corresponding Author:

[thomas.schmid@ciemat.es]

Thomas Schmid¹, Robert Milewski², Sabine Chabrilat^{2,3}, Claudia Giménez Poblador¹, Stéphane Guillaso², Juan Pablo Corella¹, Magaly Koch⁴, Jerónimo López-Martínez⁵

¹ CENTRO DE INVESTIGACIONES ENERGÉTICAS MEDIO AMBIENTALES Y TECNOLÓGICAS - CIEMAT, AVDA. COMPLUTENSE 40, 28040 MADRID, SPAIN.

² GFZ GERMAN RESEARCH CENTER FOR GEOSCIENCES, SECTION REMOTE SENSING AND GEOINFORMATICS, TELEGRAFENBERG, 14473 POTSDAM, GERMANY.

³ LEIBNIZ UNIVERSITY HANNOVER, INSTITUTE OF SOIL SCIENCE, 30419 HANNOVER, GERMANY.

⁴ CENTER FOR REMOTE SENSING, BOSTON UNIVERSITY, BOSTON, MA, USA.

⁵ FACULTAD DE CIENCIAS, UNIVERSIDAD AUTÓNOMA DE MADRID, 28049 MADRID, SPAIN.

Keywords (5): hyperspectral, EnMAP, ice-free areas, South Shetland Islands

Challenge (800 - 1000 characters incl. spaces)

Ice-free areas in the South Shetland Islands are primarily under the influence of glacial, periglacial and paraglacial processes. These ice-free areas contain fragile ecosystems with a potential biodiversity that are affected by natural causes such as climate change and by human induced influences. Studies show that nowadays summer thawing occurs earlier and stays thawed for a longer period. Therefore, the active hydrological cycle influences the chemical, physical and biological process that affects permafrost stability, causes surface erosion and is a boon to organisms that have to survive in these harsh conditions. The challenge of this work is to map different land surface covers of Byers Peninsula on Livingston Island, which is the largest ice-free area in the archipelago, using hyperspectral satellite data from the German Environmental Mapping and Analysis Program (EnMAP).

Methodology (1200 – 1500 characters incl. spaces)

Byers Peninsula (approx. 62° 37' S, 61° 06' W) is about 60 km² and is the most extensive ice-free area in the South Shetlands archipelago. The Rotch Dome glacier forms the eastern limit of the peninsula. Hyperspectral EnMAP data was acquired over the Byers Peninsula on the 15th of March 2023 and downloaded as level 2A format. It was necessary to carry out further stages of pre-processing, e.g., noise reduction, spectral smoothing and masking of clouds for a selected area covering 83 km². The cloud cover and cloud shadow reduced the area of interest by 28 km². A first step was to analyse image-derived spectra that were obtained from selected reference sites. These reference sites were visited in the field during the 2018 and 2022 austral summer campaigns when field spectra were taken with an ASD Field Spec3 combined in 2022 with a SoilPROII instrument. Later laboratory spectra were measured on the obtained soil and sediment samples. These spectra were compiled into an ongoing elaboration of the Northern Antarctic Peninsula region SPECTral library (NAPSPEC). In a second step, the Spectral Angle Mapper (SAM) method was applied and the image derived spectra were used to train the classifier. The processing was carried out using Matlab (version 2022a) and ENVI programs (version 5.2).

Expected Results (1200 – 1500 characters incl. spaces)

Although cloud cover affected the data, 11 different surface covers were mapped over an area of 55 km². Preliminary results show the variable lithological composition, differentiating the marine detrital deposits (4.6 km²) to the west and the non-marine volcanoclastics (8.3 km²) to the east. This also includes rock outcrops of sills, plugs and other marine igneous bodies (2.6 km²). Moraine deposits (3.5 km²) are mainly found along the glacier front, however, scattered deposits from past glacier stages were also identified. Due to the cloud coverage, successive elevated Holocene beaches (6.7 km²) were only mapped along the northern and southern coastline. Vegetation covers include moss carpets (2.7 km²) along the coast, lichen with moss forming communities (1.5 km²) on soils and extensive lichen vegetation (1.5 km²) covering stones and rocks. Although the latter two vegetation classes have a sparse coverage, the spectral signature differentiates them well. The glacier front (14.1 km²) occupies the largest area and is just a small part of the greater ice sheet that still covers Livingston Island. The glacier front is often partially covered by detrital particles and differentiates well from the highly reflective snow cover (4.1 km²). Water bodies were sparse, because they occur mainly in the cloud affected area. An overall accuracy of 71% was achieved, where accuracy for individual classes ranged from 49% for moraine deposits to 85% for the snow cover.

Outlook for the future (800 - 1000 characters incl. spaces)

This is the first time a preliminary mapping has been obtained using hyperspectral satellite data of this peninsula. The validation was carried out using waypoints that were gathered in the different campaigns as well as geomorphological and geological maps that were compiled in the past by our group. However, in the coming field campaign planned for February 2024, the distribution of the different classes will be checked, and further validation points will be obtained to improve the accuracy. The aim is to obtain further hyperspectral images of the area, ideally during the next field campaign and as much cloud free as possible. Having shown the importance of the hyperspectral data input, an integrated methodology is being worked on to combine different available data sources such as hyperspectral and synthetic aperture radar data as well as incorporating photogrammetric field data using machine learning techniques.

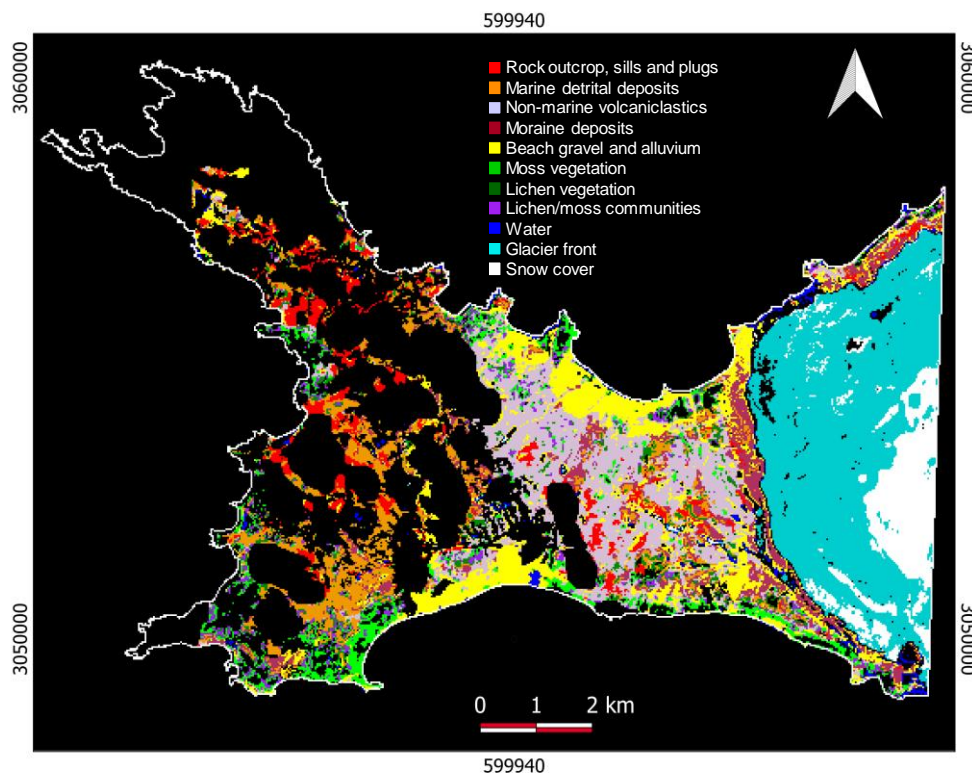


Figure Preliminary map of the land surface covers of Byers Peninsula

Assessment of atmospheric correction algorithms in PRISMA, DESIS, and EnMAP images in inland waters

Xavier Sòria-Perpinyà¹, Eduardo Vicente², Bárbara Alvado¹, Rebeca Pérez-González², Patricia Urrego¹, Gabriel Caballero¹, Carolina Tenjo¹, Antonio Ruíz-Verdú¹, Jesús Delegido¹, Juan Miguel Soria², José Moreno¹, María A. Rodrigo Alacreu²

¹ UNIVERSITAT DE VALÈNCIA, IMAGE PROCESSING LABORATORY, SPAIN

² UNIVERSITAT DE VALÈNCIA, Cavanilles Institute of Biodiversity and Evolutionary Biology, SPAIN

Keywords (5): Hyperspectral, water atmospheric correction, L2 products, ACOLITE, freshwater

Challenge

The RESSBIO (Remote Sensing Spectroscopy for Wetlands Biodiversity) project aims to investigate and exploit the capabilities of new Earth Observation satellite missions, equipped with hyperspectral sensors for assessing and monitoring the ecological status of lentic aquatic systems. The hyperspectral missions currently in orbit, such as PRISMA, DESIS, and EnMAP, provide the opportunity to study the organic matter and phytoplankton composition, differentiating between ecological status indicators groups (diatoms, chlorophyceae, cyanobacteria, dinoflagellates), as well as the organic matter composition (dissolved and particulate). However, to obtain accurate estimates of various limnological variables from reflectance spectra, the first essential step is to achieve an accurate atmospheric correction (AC). To achieve this goal, we conducted an evaluation of the AC algorithms specifically developed for these sensors, called L2 products, and other algorithm commonly used in inland waters, ACOLITE.

Methodology

During the first year of the RESSBIO project, three field campaigns were carried out, coincident with the acquisition of four hyperspectral images. Two of them matched with PRISMA images, one in the Bellús reservoir (turbid waters), and the other in the Benaixeve reservoir (clear waters). Additionally, one sampling campaign was conducted in the Albufera lake (turbid waters) three days after the EnMAP image acquisition and three days before the DESIS image acquisition. In this case, to assess the stability of the reflectance spectra between the image acquisition and the field data, the Rrs spectra of three Sentinel-3 images were compared, and the differences were determined using a t-test. In the field. The sampling points were georeferenced, and above-surface water radiometry was measured using an ASD FieldSpec® HandHeld 2 spectroradiometer. The in situ remote sensing reflectance (Rrs) was obtained with a 1 nm spectral sampling and then averaged to the band set of each sensor by using the specific spectral response functions. The Level 1C product, without AC, and L2 product, with their specific AC, labeled as 2A for DESIS and EnMAP and 2D for PRISMA, were downloaded. L2 products provide the Rrs values obtained with the specific AC algorithm of each sensor. In addition, the ACOLITE AC algorithm was applied to the L1C images. The Rrs values from L2 products and from L1C products corrected atmospherically with ACOLITE, were extracted using a 3x3 pixel window centred on the sampling points, and the mean value were then calculated. These values were validated using in-situ Rrs data, and several metrics, including R², RMSE, RRMSE, and bias, were calculated.

Expected results

The results obtained can be interpreted in several ways: as a whole, between different AC algorithms (Figures 1a and 2a), or by spectral zones (Figures 1b and 2b), comparing them either for a single AC or between AC algorithms. When comparing different algorithms of ACs, the expected results should demonstrate that L2 products ACs yield tighter Rrs values compared to generic ACs. However, for EnMAP images in this study, the ACOLITE algorithm provides better validation results than the EnMAP L2 image. This improvement is particularly noticeable for wavelengths longer than 600 nm compared to the EnMAP L2 image. The same holds true for the DESIS L2 image. If we focus on the comparison by spectral regions, the lowest results generally agree across different algorithms of ACs. Thus, for PRISMA images, acceptable results (approximately RRMSE of 10%) are obtained in the green and red areas of the spectrum for turbid waters, while for EnMAP and DESIS images, the lowest results are achieved with ACOLITE in the infrared region. In clear water, acceptable results for PRISMA images are only achieved with the PRISMA L2 image within the spectrum range of 500 to 600 nm. These findings suggest that the choice of AC may depend on the specific area of the spectrum we are interested in.

Outlook for the future

To enhance the validation of our results, we require more coincident field data alongside hyperspectral imagery in clear and turbid freshwaters. In this regard, we are striving to obtain in advance the image acquisition schedules for DESIS and EnMAP, as PRISMA already provides this information one or two days ahead. Additionally, we aim to implement and validate other AC algorithms, such as 6S and Polymer. Consequently, the primary challenges we need to address for the future include: (1) achieve more overlaps between in situ measurements and hyperspectral imagery, (2) acquiring advanced knowledge of the image acquisition schedules for DESIS and EnMAP sensors; (3) achieving an acceptable AC for clear water; (4) obtaining a satisfactory AC in the blue region to enable the study of organic matter.

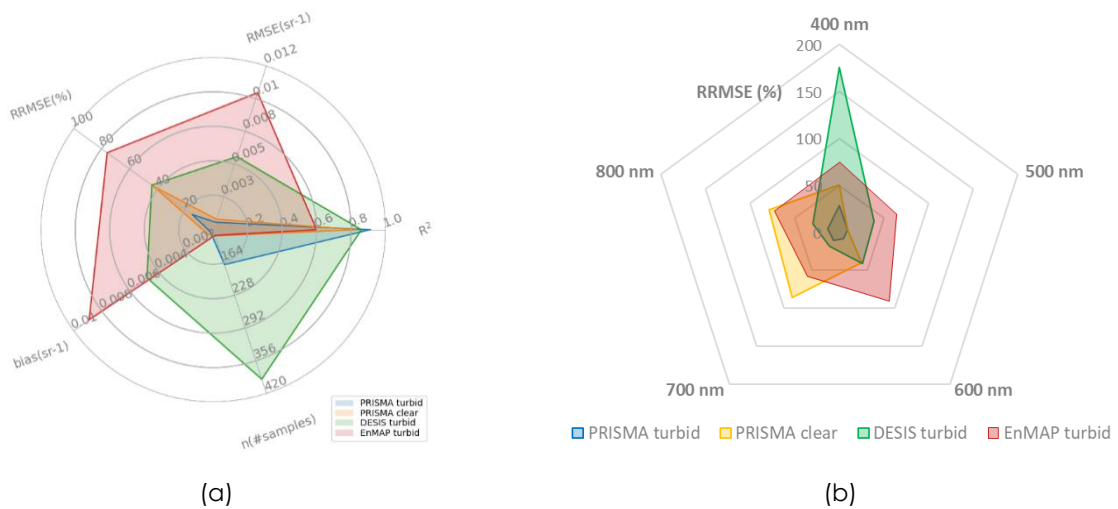
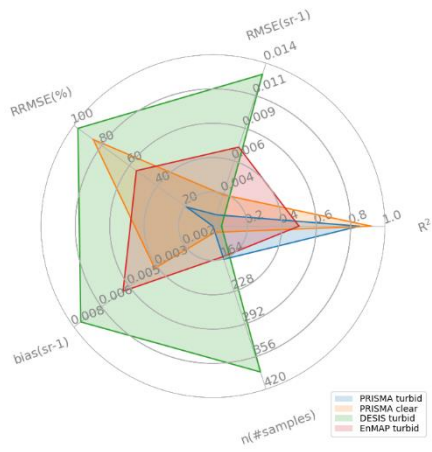
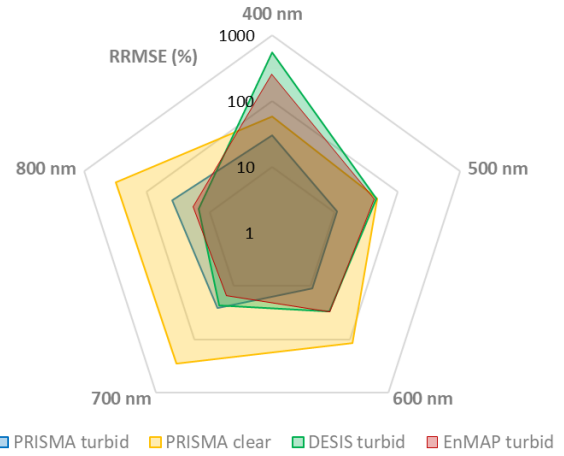


Figure 1 Validation results of the Level 2 products with a specific atmospheric correction. (a) using all data (b) by spectrum parts



(a)



(b)

Figure 2 Validation of the ACOLITE atmospheric correction algorithm. (a) using all data (b) by spectrum parts

Assessment of the influence of wildfires on water quality of lakes in ESA CCI global datasets by deep learning

EARSeL Valencia 2024
Abstract
Corresponding Author:
[\[stroppiana.d@irea.cnr.it\]](mailto:stroppiana.d@irea.cnr.it)

Lorenzo Parigi¹, [Daniela Stroppiana](#)¹, Gloria Bordogna¹, Claudia Giardino¹, Monica Pinardi¹, Giulio Tellina¹, Rossana Caroni¹, Mariano Bresciani¹, Clément Albergel²

¹ CNR – INSTITUTE FOR ELECTROMAGNETIC SENSING OF THE ENVIRONMENTAL, VIA A. CORTI 12, 20133 MILAN, ITALY

² EUROPEAN SPACE AGENCY (ESA) CLIMATE OFFICE, ECSAT, HARWELL CAMPUS, DIDCOT, OXFORDSHIRE, UNITED KINGDOM

Keywords (5): wildfires, chlorophyll-a, global datasets, Climate Change Initiative

Challenge

Lakes are an important natural resource providing relevant ecosystem services besides offering unique habitats for numerous species of plants and animals. Global warming and increasing aridity are leading to various responses of aquatic systems and lakes are considered as sentinels of climate change by, at the same time, increasing severity of wildfires. This study relies on global and long-term satellite datasets made available by the European Space Agency (ESA) Climate Change Initiative (CCI) to investigate the relationship between lake water quality and wildfire occurrence (burned area, BA). A large global dataset of lakes (Figure 1) is used to model, with Long Short-Term Memory (LSTM) network models, the relation between chlorophyll-a concentration (Chl-a) and meteo-climatic variables (precipitation, runoff, lake surface temperature, wind speed, surface solar radiance) with/without the contribution of fire. The time-period covered by the time series analysis is 2002-2020.

Methodology

Time series of Chl-a and lake water surface temperature were obtained from the LakeCCI project. Lake depth and surface area were identified using the HydroBASIN collection. Meteorological variables were extracted from the ERA5 dataset: total daily precipitation and surface runoff computed for the lake catchments. For the lake basin, daily aggregated surface solar radiance and wind speed were extracted. The FIRECCI51 provided, for each catchment, the total burned area that was split into forest and non-forest fires based on the landcover classification integrated in the dataset.

All datasets were aggregated at weekly time step and spline interpolation was applied to fill missing values. The lake database was split into burned and unburned basins, and then sorted based on the number of Chl-a weekly observations. The first 160 unburned catchments were selected to train a LSTM-NN model able to predict Chl-a concentration when lakes are not affected by fires. This model was tested on both the remaining 40 unburned catchments and 40 burned catchments to investigate if its prediction accuracy was different for the two cases. The rationale of this choice was to avoid generating a biased model due to an unbalanced training set containing less burned catchments than unburned ones. At the same time, we can assess if wildfires affect or not Chl-a concentration. After the training, the model was tested on both burned and unburned catchments and its predictive capabilities were compared.

Expected results

The LSTM-NN model is deemed able to predict Chl-a concentration, over the lakes of the global datasets, based on the meteo-climatic variables. In those lake catchments where wildfires occur, the model's performance is significantly worse (significance test was computed) than the unburned catchments, thus confirming the hypothesis that the presence of wildfires lake water quality worsens. In the future, we expect to define a general model trained over both burned and unburned catchments which is expected to improve when the burned area over the catchment is included among the model's predictors.

The model can be tested with different sets of input parameters, and, in this work, we test the performance with/without including lake characteristics (depth, area, trophic status) to investigate the influence of those parameters in lake response to meteorological conditions. The trophic status of lakes (oligotrophic, mesotrophic, eutrophic) is also included in the analysis to investigate to what extent it can influence the relationship of water quality response to fire occurrence in the lake basin. To this aim, model's performance can be analysed for burned and unburned catchments and split by trophic status that is deemed relevant in lake resilience to fire disturbance.

Outlook for the future

These results can contribute to studying the impacts of climate change on lake ecosystems given the expected trends in wildfire occurrence and severity. Further analyses are necessary to better investigate how lake water quality can change when wildfire occur in the lake catchment although this effect is expected to change with the lake and catchment characteristics. We will complement the analysis by also including water turbidity as predicted parameter in LSTM-NN models.

In the framework of climate change studies, it is also important to investigate the impact of change in lake characteristics such as trophic status that in this study has been assumed as not variable over the time period, while it might not be the case. The trophic status parameter could be hence included as predictor in the model. Finally, a study will be carried out to assess the impact of wildfires via atmospheric transportation and the same approach will be used by including relevant CCI datasets.

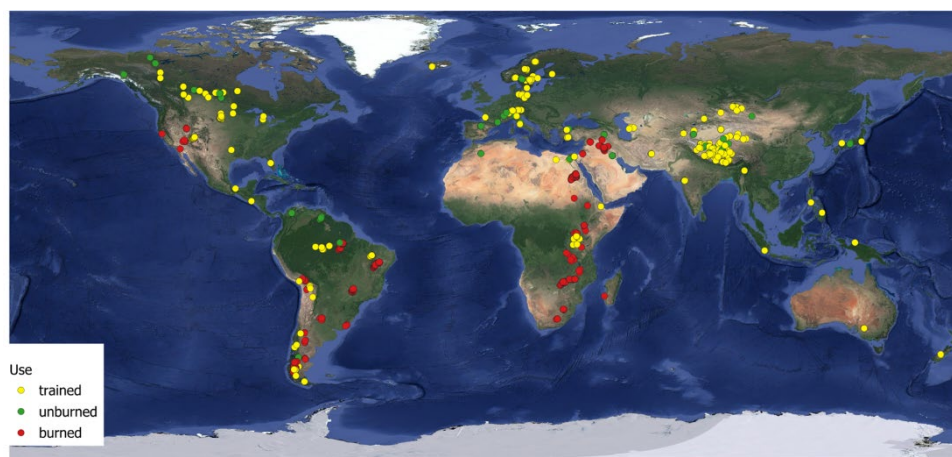


Figure 1 The location of the lakes used as study areas in this work and split into training and burned/unburned basins.

Imaging spectroscopy of phytoplankton species: Investigating the link between inherent optical properties and illumination conditions

Loé Maire^{1,2}, Alexander Damm-Reiser^{1,2}, Daniel Odermatt^{1,2}

¹ Eawag, Swiss Federal Institute of Aquatic Science & Technology, Surface Waters – Research and Management, Switzerland

² Department of Geography, University of Zurich, Switzerland

Keywords : Imaging spectroscopy, Inherent Optical Properties (IOPs), Inland waters, Light adaptation, Phytoplankton diversity

Challenge

Inland waters are subject to climate change and human-driven environmental pressures. Such pressures significantly contribute to the eutrophication, acidification, and warming of lakes. Phytoplankton play a crucial role in lake ecosystems, while their functional state and species composition are sensitive indicators of environmental change. Phytoplankton diversity in lakes can be analyzed via remote sensing, particularly thanks to new hyperspectral imaging spectroscopy sensors. Therefore, spectral signatures of common phytoplankton types are needed and typically obtained from laboratory experiments. However, environmental conditions like illumination, temperature, and nutrient supply impact phytoplankton growth and their inherent optical properties (IOP), which again affects these IOPs' representativeness for bio-optical modeling. This study evaluates the effect of illumination conditions on phytoplankton IOPs and possible implications for remote sensing of phytoplankton diversity.

Methodology

Research on species-specific IOPs requires the growth of monocultures of representative phytoplankton species under controlled environmental conditions. Some selected isolates from our test site Greifensee, a perialpine eutrophic lake in Switzerland, were grown as monocultures. Here we specifically focus on two common cyanobacteria species, *Microcystis aeruginosa* and *Planktothrix rubescens*. Different illumination conditions were particularly evaluated by growing replicates in the laboratory and in ponds under natural light.

Once cultures were adapted to light conditions, a Spectral Absorption and Attenuation Meter (AC-S-WETLabs) was used to measure the bulk absorption, attenuation, and scattering of the cultures, as well as their chlorophyll-a concentration according to the absorption line height algorithm [1]. The filter pad absorption method was then applied to derive the absorption spectra of each bulk absorption component [2], including absorption by colored dissolved organic matter (a_{CDOM}), non-algal particles (a_{NAP}), and phytoplankton (a_{ph}). Therefore, a volume of the cultures (between 50 and 300 mL) was filtered using a 25-mm diameter Whatman glass-fiber GF/F filter. Then, the filtrated substance was analyzed with a PerkinElmer LAMBDA 850+ UV/VIS spectrophotometer and a 150 mm InGaAs Integrating Spheres, to obtain the particulate absorption a_{PA} . The pigmented solutions were bleached for one hour with methanol before repeated analysis to obtain a_{NAP} .

Results

The spectral IOP measurements of *Microcystis aeruginosa* and *Planktothrix rubescens* monocultures grown in the laboratory show species-specific spectral signatures that allow identifying and differentiating them from one another.

The specific absorption spectra of *Microcystis aeruginosa* (Figure 1a) are similar among the evaluated replicates. The common peaks at 440 nm and 675 nm correspond to chlorophyll absorption [3]. In addition, Figure 1a shows a peak around 620 nm, corresponding to phycocyanin, the main light-harvesting pigment of *Microcystis aeruginosa* [4]. Similarly, the specific absorption spectra of *Planktothrix rubescens* (Figure 1b) also show comparable yet slightly less similar absorption spectra among replicates, and they compare well with results from previous studies [5]. Besides the common chlorophyll absorption features, other pigments can be detected such as phycoerythrin with its large peak around 560-575nm, and allophycocyanin with the one around 650nm [6], [7].

This first set of experiments shows that there is potential to distinguish phytoplankton species from IOP spectra. Additional experiments carried out in small ponds under natural illumination were not successful due to a too-large transition step from the laboratory to natural environmental conditions. Particularly the water temperature in the ponds increased above the expected seasonal levels, and above suitable levels for the monocultures.

Outlook for the future

In a next step, the ENVILAB setup developed by Göritz et al. [8] will be used to control gradients of environmental conditions (e.g. water temperature, light intensity, nutrient conditions) during phytoplankton growth. With similar measures to those described previously, such experiments will allow investigate deeper into the adaptation of pigments to light intensity and will further enhance our knowledge to facilitate phytoplankton retrievals from IOP spectra.

Using the radiative transfer model Hydrolight (Sequoia Scientific Inc., Bellevue, Washington, DC, USA) [9], we will then establish the link between derived IOP spectra and remote sensing reflectance from in situ and satellite measurements to advance the retrieval of phytoplankton species across scales. These activities contribute to the exploitation of upcoming imaging spectroscopy satellite missions for research and monitoring of inland water bodies.

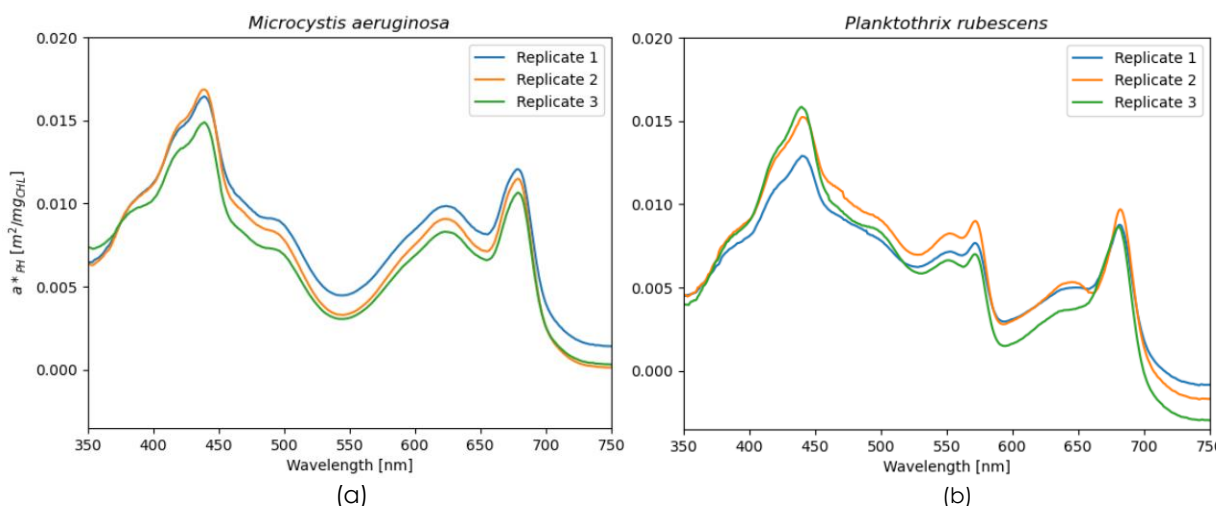


Figure 1 Chlorophyll-specific phytoplankton absorption coefficient of (a) *Microcystis aeruginosa* and (b) *Planktothrix rubescens* grown in the laboratory.

REFERENCES

- [1] Collin S. Roesler, Andrew H. Barnard, "Optical proxy for phytoplankton biomass in the absence of photophysiology: Rethinking the absorption line height," *Methods in Oceanography*, vol. 7, pp. 79-94, 2013.
- [2] IOCCG, "Inherent Optical Property Measurements and Protocols: Absorption Coefficient," IOCCG Ocean Optics and Biogeochemistry Protocols for Satellite Ocean Colour Sensor Validation, 2018.
- [3] Robert Bidigare, J. Morrow, Michael Ondrusek, Dale Kiefer, "In-vivo absorption properties of algal pigments," *Proc. SPIE.*, vol. 1302, 1990.
- [4] Kaylan Randolph, Jeff Wilson, Lenore Tedesco, Lin Li, Lani Pascual, Emmanuel Soyeux, "Hyperspectral remote sensing of cyanobacteria in turbid productive water using optically active pigments, chlorophyll a and phycocyanin," *Remote Sensing of Environment*, vol. 112, pp. 4009-4019, 2008.
- [5] Laura Oberhaus, Jean-François Briand, Christophe Leboulanger, Stéphan Jacquet, "Comparative effects of the quality and quantity of light and temperature on the growth of *Planktothrix agardhii* and *P. Rubescens*," *Journal of Phycology*, vol. 43, no. 6, pp. 1191-1199, 2007.
- [6] Martin Dokulil, Katrin Teubner, "Deep living *Planktothrix Rubescens* modulated by environmental constraints and climate forcing," *Hydrobiologia*, vol. 698, no. 1, pp. 29-46, 2012.
- [7] Bernhard Ernst, Stefan Hoeger, Evelyn O'Brien, Daniel Dietrich, "Abundance and toxicity of *Planktothrix Rubescens* in the pre-alpine Lake Ammersee, Germany," *Harmful Algae*, vol. 8, no. 2, pp. 329-342, 2009.
- [8] Anna Göritz, Stefan von Hoesslin, Felix Hundhausen, Peter Gege, "ENVILAB: Measuring phytoplankton in-vivo absorption and scattering properties under tunable environmental conditions," *Opt. Express*, vol. 25, no. 21, 2017.
- [9] Curtis D. Mobley, "A numerical model for the computation of radiance distributions in natural waters with wind-roughened surfaces," *Limnol. Oceanog.*, vol. 34, no. 8, pp. 1473-1483, 1989.

Autonomous Hyperspectral Radiometry Systems to support monitoring of Coastal and Inland Water Quality in Belgium.

Francesca Ortenzio¹, Heloise Lavigne¹, Quinten Vanhellemont¹, Clemence Goyens¹, Kevin Ruddick¹

¹ Royal Belgian Institute of Natural Sciences, REMSEM, Brussels - Belgium

Keywords (4): Hyperspectra, Waterhypernet, Radiometry, Water Monitoring

Challenge

Aquatic ecosystems preservation requires efficient monitoring. A source of data is represented by in situ measurements obtained from field campaigns that, although necessary to measure a wide range of parameters, suffer a lack of temporal and spatial coverage which might be in adapted to the time and spatial scales of certain environmental events. In fact, water quality parameters can change in a short time and space scale for reasons as currents, tides, plankton dynamics, meteorological events.

Here, we propose to explore the capabilities of autonomous high-frequency measurements hyperspectral radiometry systems - Panthyr (and Hypstar®) - to solve the temporal scale and help monitoring water quality parameters. As part of a network primary developed as support for satellite water reflection validation, these systems, in coastal and inland waters, have been proven useful for water monitoring, detecting chlorophyll-a, suspended sediment concentration and harmful algae blooms.

Methodology

Panthyr is a pointable autonomous hyperspectral radiometry system, part of the Waterhypernet network.

The system is programmed to take measurements every 20 minutes from sunrise to sunset, following an above-water radiometry acquisition well defined protocol. Measurements are acquired at 90° and/or 135° relative azimuth to sun to avoid sunglints and potentially both left and right of sun, depending on the geometry of the mounting structure and its shadows. For each azimuth angle measurements are made of downwelling irradiance, upwelling water radiance, downwelling sky radiance. There is a camera incorporated in the system that takes pictures of the target of the measures, as a back-up quality check in case of inconsistent data. Every measurement cycle lasts about 7 minutes.

As result of data processing and quality control, water leaving reflectance spectra are released. The system is equipped with a 4G router that allows to send data almost in real-time (4 times per day) but it is always possible to connect in remote and download raw data and pictures on demand.

The results from a PANTHYR system are hyperspectral spectra of water reflectance from which different water parameters can be calculated. Standards parameters include Turbidity and Chlorophyll-a concentration but thanks to hyperspectral data it is possible to detect also certain phytoplankton group or species such as *Phaeocystis globosa* in the Southern North Sea or cyanobacteria often blooming in inland waters bodies.

Expected results

Optical remote sensing has been in use for long time already, making it possible to acquire high-resolution spectral data and providing a valuable support in the understanding of key parameters of water quality, such as suspended sediment and dissolved organic matter or to support Harmful Algae Bloom monitoring, providing information on the total phytoplankton biomass with Chlorophyll-a concentration. However, remote sensing data are limited by cloud coverage reducing the temporal and spatial coverage in high latitude regions. It is also more complex to apply in coastal and inland waters because the atmospheric correction is more challenging (adjacency effects, positive water reflectance in the red-NIR). Plus, most of the ocean color remote sensing instruments are multispectral limiting the range of parameters that can be retrieved. It is then expected to complete gaps in satellite observations with autonomous in situ radiometers. Having continuous and real-time data provided by Panthyr we expect to have a better insight on the evolution and growth rate of algae in different places and time of the year. We can monitor the blooming of *Phaeocystis Globosa*, a not toxic algae with negative effects on higher trophic levels in the marine ecosystem and consequently on human activities. Real-time Panthyr data from a water reservoir can detect the appearance of phytoplankton blooms of the toxic Cyanobacteria and near real time data acquisition can be used for rapid water management.

Outlook for the future

The Waterhypernet Network has as main goal to provide water reflectance validation data at hyperspectral resolution every day for sites with diverse water types but at the same time is providing a big amount of high-resolution and high-quality data that can be used to support the management of the water resources. More systems will provide continuous dataset that can be used to fill the gap in time that comes from in-situ measurements that, even if essential, are limited and cannot provide continuous and real-time data. In a world that is heavily affected by climate change and pollution, it is essential to have a sustainable approach in the management of natural resources, as water. Together with the traditional methodology, the hyperspectral data coming from autonomous systems can be extremely useful in the monitoring of water bodies and provide decisional support for both for the economic and the environmental perspective.

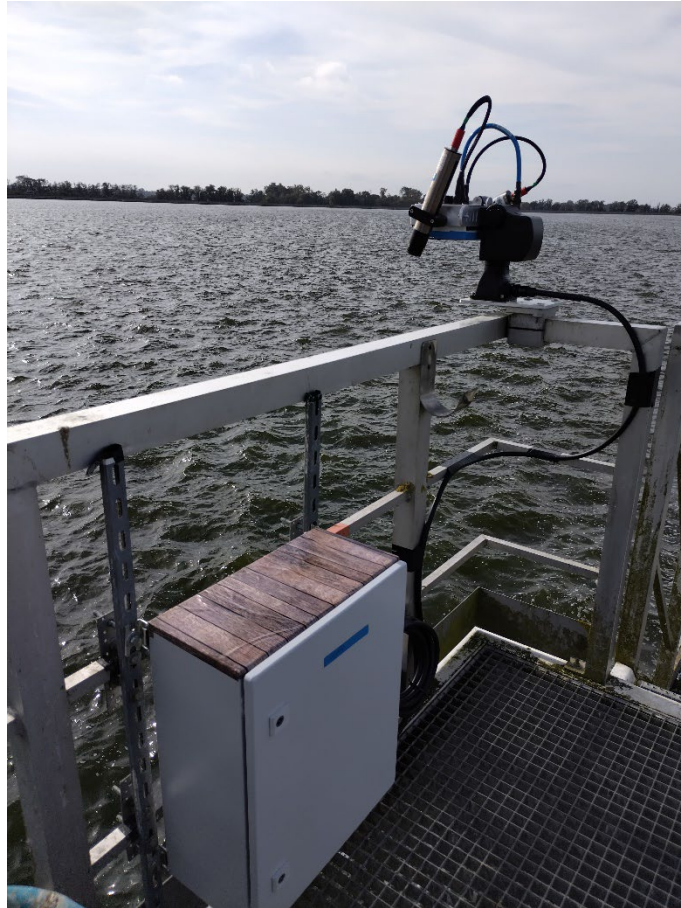


Figure 1 Panthyr System

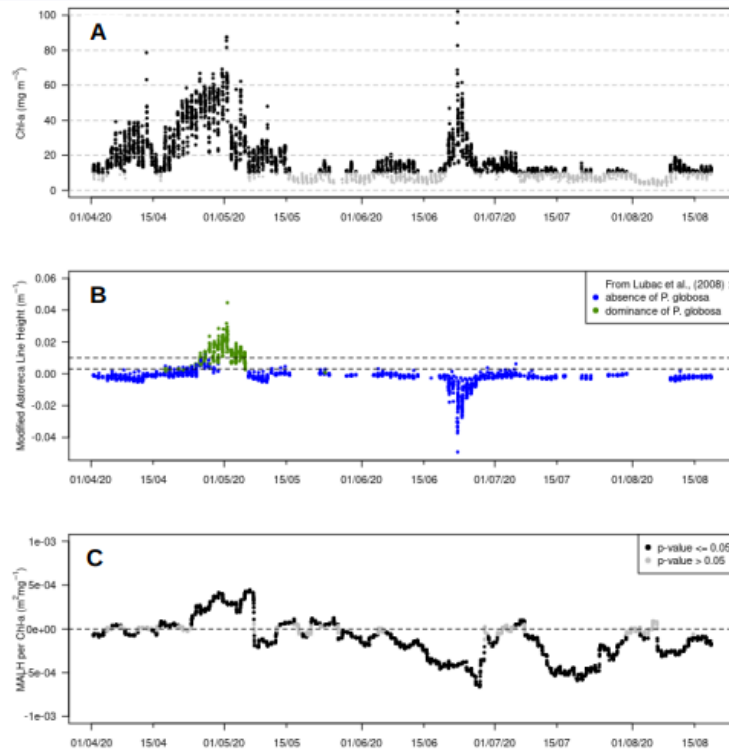


Figure 1 Chl-a and *P. globosa* at RT-1 Station (Ostend)

April to August 2020 - PANTHYR data

From hyper- to multi-spectral databases: training machine learning models for turbidity estimation

Masuma Chowdhury^{1,2}, Ana B. Ruescas³, Irene Laiz², Ignacio de la Calle¹

¹Quasar Science Resources, S.L., Madrid, Spain

²Universidad de Cádiz, Departamento de Física Aplicada, Spain

³Universitat de València, Image Processing Laboratory, Spain

Keywords: Ocean colour, complex water, turbidity, machine learning, feature importance.

Challenge

Turbidity measurements are a way to assess water clarity based on scattered light. Higher turbidity implies more scattered light due to various materials, including nutrients, bacteria, algae, and organic/inorganic particles. Higher turbidity affects marine ecosystems by impeding phytoplankton growth and indicates nutrient loading that can initiate eutrophication. Estimations of turbidity are essential for complying with the EU Marine Strategy Framework Directive. In this study, the GLORIA global dataset and Sentinel-2 (S2) satellite data are used to develop new algorithms for the estimation of turbidity using machine-learning approaches. Hyperspectral and turbidity in situ measurements, together with S2-Multipectral Imager (MSI) measurements are combined in a new dataset, which comprises representative data from where the models can learn and predict medium to very high turbidity up to 2200 FNU.

Methodology

The methodology used in the study involves data collection and pre-processing from the GLORIA dataset, which includes hyperspectral data from various water bodies around the world. S2 satellite data is also used. This data is pre-processed to ensure its suitability for analysis. The study performs a matchup analysis by comparing S2 and GLORIA data with a temporal window of ± 3 hours, which helps align the satellite data with the in situ measurements. The remote sensing reflectance (R_{rs}) obtained from the best-suited atmospheric correction method (ACOLITE) on the S2 data is combined with the convolved hyperspectral dataset. Single band, band ratios, band combinations and normalized difference indices were evaluated for feature selection. The study utilizes several linear and non-linear machine learning algorithms to develop turbidity models. The developed models are validated by comparing their predictions with in-situ measurements taken at the Guadalquivir estuary. After evaluation of the first results obtained, the input data for the models was separated by water type using three distinct water colours: blue, green and brown. The separation involved spectral analysis to categorize data points into these three water colours. The study explored all the developed machine learning algorithms for predicting turbidity within each water type. Factors like accuracy, model complexity, and performance were evaluated.

Results

The feature selection analysis revealed that the red (B4), red-edge (B5) and NIR (B8A) bands exhibited higher correlations with the target variables, indicating their potential significance in the modelling process. Besides, certain band combinations, especially combinations among the red (B4), red-edge (B5 – B7) and NIR (B8, B8A) bands also demonstrated elevated levels of correlation, implying the potential for improved predictive power when incorporating them into the machine learning regression models. Therefore, several machine learning regressors, such as lasso, kernel ridge, gradient boosting, random forest, and K-nearest neighbours were trained on the selected features -using grid searchCV and cross-validation techniques for defining hyperparameters- on the 75% of the combined dataset. The obtained models showed Pearson correlation coefficients ranging from 0.72 to 0.90 on the 25% of the remaining dataset (test data) and 0.85 to 0.95 on the validation data taken at the Guadalquivir estuary. Focusing on the brown waters, naturally closely related to the types of waters that can be found in the Guadalquivir estuary, the random forest regression model was found as the most suitable and stable machine learning model among others.

Outlook for the future

As the future outlook of the study, we intend to carry out a comparison between the developed machine learning models and the available empirical turbidity models to further validate our algorithms' robustness and applicability in various water bodies around the world. We will also focus on explainable AI, particularly with regard to feature importance per model to ensure the interpretability of our model as well as to gain a better understanding of why certain spectral features are crucial for the models' predictions. Lastly, we plan to adapt our models to harness the increased spectral resolution offered by the hyperspectral satellite data, especially PACE (Plankton, Aerosol, Cloud, ocean Ecosystem) and EnMAP. This advancement will enable us to extract more detailed information to address complex environmental challenges and support sustainable decision-making and resource management.

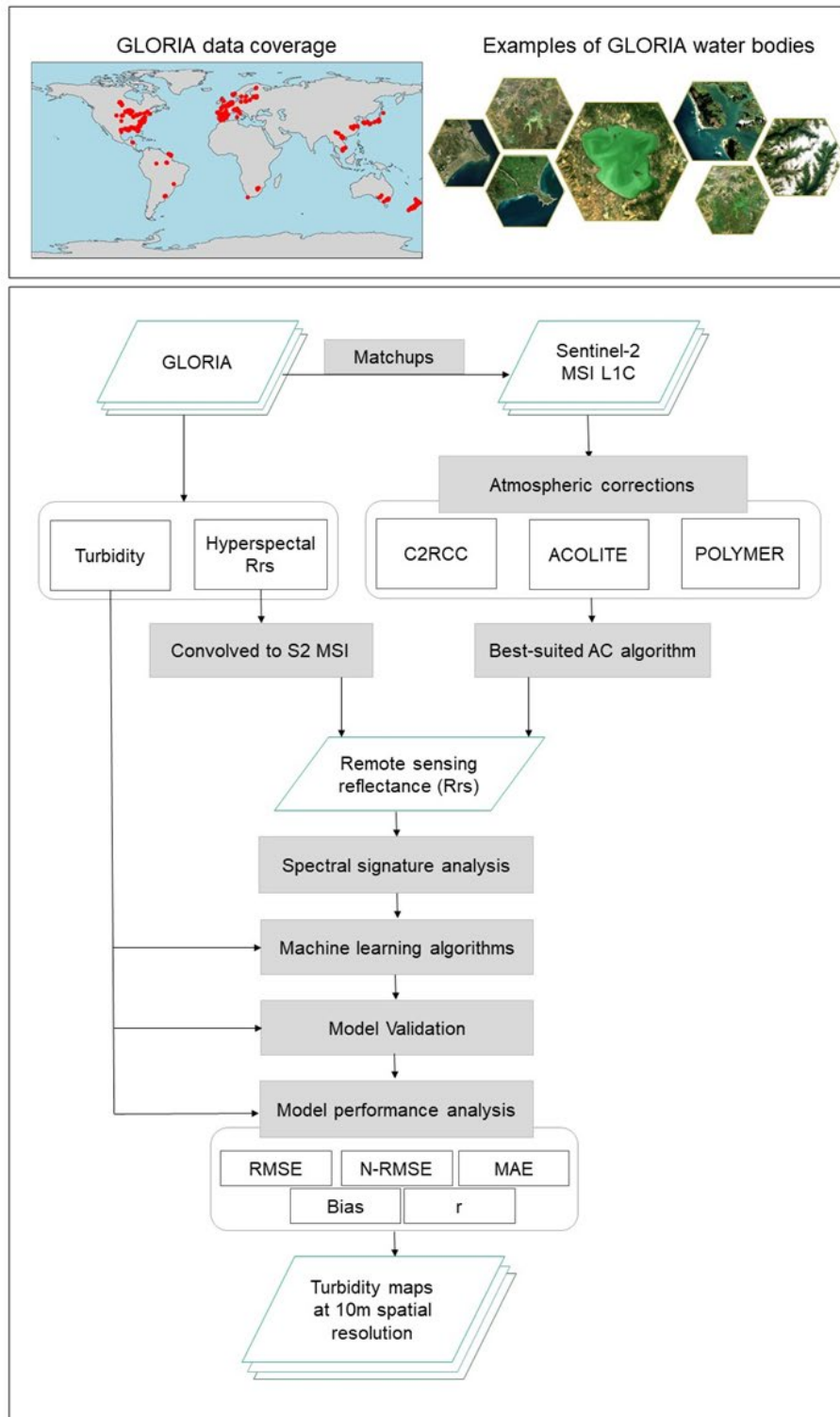


Figure 1. Schematic diagram of the methodology.

Advanced Training Material and Tools for The Next Generation of Marine Remote Sensing Experts

[\[ana.ruescas@brockmann-consult.de\]](mailto:ana.ruescas@brockmann-consult.de)

Ana B. Ruescas^{1,2}, Hayley Evers-King³, Benjamin Loveday^{3,4}, Juan Ignacio Gossn³, Vinca Rosmorduc⁵, Kevin Ruddick⁶, Gary Corlett³

¹ Image Processing Laboratory, Universitat de València, Spain

² Brockmann Consult GmbH, Hamburg, Germany

³ EUMETSAT, Darmstadt, Germany

⁴ Innoflair, Darmstadt, Germany

⁵ CLS, Toulouse, France

⁶ RBINS, Brussels, Belgium

Keywords (5): Marine Remote Sensing, Training, Hyperspectral, Copernicus, EUMETSAT

Challenge

To support the current and next generation of experts in the marine remote sensing community, EUMETSAT (European Organisation for the Exploitation of Meteorological Satellites) is facilitating the development of a range of advanced training material and tools. The material and tools cover a wide range of topics that can support current activities and equip the next generation of experts with the knowledge and skills needed to access and process data, conduct validation activities, and more. Development of material and tools is taking place through collaboration with current scientific studies and community projects, as well as through collaboration with community members during our marine training courses. Examples of current materials include:

- Advanced data access tools using Python based clients and APIs to navigate and access collections of Sentinel-3 and Sentinel-6 data
- Exploitation of the ThoMaS (Tool to generate Matchups of OC products with Sentinel-3/OLCI) toolkit
- Using the HyperCP community processor for above water *in situ* ocean colour radiometry processing
- Demonstration models for learning about:
 - Ocean colour inversion and algorithm development
 - Applying altimetry corrections.
 - Cloud masking for sea surface temperature products

Methodology

These tools are primarily developed as Python-based Jupyter notebooks and, in the case of the demonstration models, will be accompanied by guidance on how to use them to both learn and train.

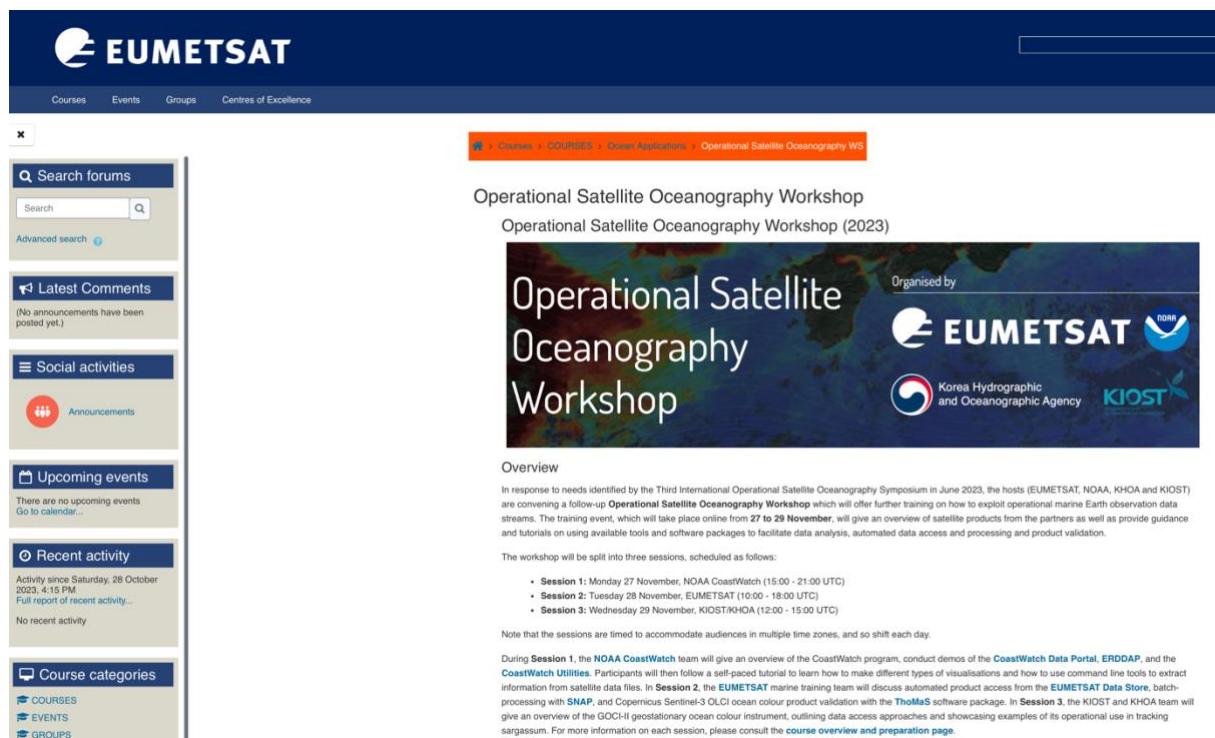
All material will be distributed via the EUMETSAT GitLab and made openly available for reuse by the community under open-source licences. EUMETSAT seeks both feedback on existing material, and requirements for defining future developments. Experts who wish to contribute and collaborate on the development of this material are welcomed.

Results

EUMETSAT offers training courses related to various aspects of meteorology and satellite data applications. This includes training courses focussed on topics relevant to marine applications, such as oceanography and marine data analysis. These courses, which centre on the use of Copernicus Sentinel-3 and Sentinel-6, aim to improve the understanding and utilization of satellite data for monitoring and studying marine environments. To get the most current and detailed information about EUMETSAT's marine training courses, it is recommended visiting the official EUMETSAT website (<https://training.eumetsat.int/course/index.php?categoryid=46>). The website provides information on available courses, schedules, and registration procedures.

Outlook for the future

Incorporating hyperspectral imaging (HSI) data, whether gathered through in-situ measurements or satellite imagery, holds great promise for advancing our understanding of marine ecosystems. By combining HSI with traditional multispectral approaches, we can unlock a wealth of information about underwater environments. To fully harness the potential of this technology, collaboration with HSI marine experts is essential. Working together on new case studies offers the opportunity to expand our knowledge and allow other researchers to contribute with new projects and ideas to the sustainable management of marine resources.



The screenshot displays the EUMETSAT website interface. At the top, the EUMETSAT logo and navigation menu (Courses, Events, Groups, Centres of Excellence) are visible. A search bar is located in the top right. The main content area is titled "Operational Satellite Oceanography Workshop" and "Operational Satellite Oceanography Workshop (2023)". Below the title is a banner image for the workshop, organized by EUMETSAT, NOAA, and KIOST. The banner includes the text "Operational Satellite Oceanography Workshop" and "Organised by EUMETSAT NOAA KIOST". Below the banner is an "Overview" section with the following text:

In response to needs identified by the Third International Operational Satellite Oceanography Symposium in June 2023, the hosts (EUMETSAT, NOAA, KHOA and KIOST) are convening a follow-up **Operational Satellite Oceanography Workshop** which will offer further training on how to exploit operational marine Earth observation data streams. The training event, which will take place online from **27 to 29 November**, will give an overview of satellite products from the partners as well as provide guidance and tutorials on using available tools and software packages to facilitate data analysis, automated data access and processing and product validation.

The workshop will be split into three sessions, scheduled as follows:

- **Session 1:** Monday 27 November, NOAA CoastWatch (15:00 - 21:00 UTC)
- **Session 2:** Tuesday 28 November, EUMETSAT (10:00 - 18:00 UTC)
- **Session 3:** Wednesday 29 November, KIOST/KHOA (12:00 - 15:00 UTC)

Note that the sessions are timed to accommodate audiences in multiple time zones, and so shift each day.

During **Session 1**, the NOAA CoastWatch team will give an overview of the CoastWatch program, conduct demos of the **CoastWatch Data Portal**, **ERDDAP**, and the **CoastWatch Utilities**. Participants will then follow a self-paced tutorial to learn how to make different types of visualisations and how to use command line tools to extract information from satellite data files. In **Session 2**, the EUMETSAT marine training team will discuss automated product access from the **EUMETSAT Data Store**, batch-processing with **SNAP**, and Copernicus Sentinel-3 OLCI ocean colour product validation with the **ThOMAS** software package. In **Session 3**, the KIOST and KHOA team will give an overview of the GOCH-1 geostationary ocean colour instrument, outlining data access approaches and showcasing examples of its operational use in tracking sargassum. For more information on each session, please consult the [course overview and preparation page](#).

Figure Example of one of the marine courses delivered by EUMETSAT

A TIR Data-Based Service Supporting The Identification Of Heat Mitigation Measures In Cities

Anita D. Bayer¹, Marco Spagnolli¹, Dietrich Kuhn², Stephan Holsten³

¹ OHB SYSTEM AG, WESSLING, GERMANY

² OHB DIGITAL SERVICES GMBH, BREMEN, GERMANY

³ OHB SYSTEM AG, BREMEN, GERMANY

Keywords (5): Land Surface Temperature, Urban Heat Islands, Urban Heat Mitigation, Simulation

Challenge

Increased heat in urban agglomerations (Urban Heat Island, UHI) has a significant influence on human health, habitability and labour productivity. Measures to mitigate UHIs have to identify the source of the problem and based on this find appropriate solutions. The EU Horizon 2020 project CityCLIM aims to provide practical and actionable information for the mitigation and adaptation to urban heat and air pollution to citizens and city administrations. One purely EO data-based service developed within CityCLIM targets the simulation and mitigation of urban heat by utilizing the land surface temperature (LST) as measured by TIR sensors as a proxy for the urban heat distribution. The service allows the user to modify urban characteristics (e.g., create an urban green space) on a web-based user interface and explore the effects of these modifications on LST in order to find the best urban heat mitigation option.

Methodology

We characterize the urban environment determining the urban heat distribution by (1) 2D land surface parameters, i.e. Normalized Difference Built-up and Vegetation Indices (NDBI and NDVI) derived from Sentinel-2 or Landsat 8/9 data, and the distance to water and vegetation derived from ESA Worldcover data and (2) by 3D urban morphology parameters (sky view factor, building volume density, building roof index) derived from high-resolution digital elevation models. These parameters are linked to the Landsat 8/9 LST product by calibrating a prediction model utilizing an artificial neuronal network (ANN). The performance of the LST prediction model is assessed with test set validation.

The LST prediction model builds the basis for the urban heat simulation service which, in its final setup, will be running on the CityCLIM open platform. A user-friendly GUI will allow the user to modify the urban land surface based on ESA Worldcover on 10m spatial resolution, for instance to counteract urban heat by the installation of urban green spaces or water surfaces or to explore the increased heat accumulation from the installation of new buildings. It is aspired that heat patterns can be explored for a typical and an extreme summer day, each over the past few years. The calibrated LST prediction model is used to simulate the effects of the user-made changes on LST. Results will be provided on 30m spatial resolution and shown as deviations from the original LST distribution. Additional statistics summarizing the simulated changes in LST will be provided which can be exported.

Results

LST prediction models set up for the four CityCLIM pilot cities (Valencia, Karlsruhe, Luxembourg, Thessaloniki) provide medium prediction accuracies (all models $R^2 > 0.58$ in testing with RMSE around 1K). NDBI and the distance to vegetation are the most important urban surface parameters in the prediction

models. Upon stylized scenarios, such as the sealing of a park with buildings or the installation of urban green instead of an aboveground train station, the models predict plausible changes in LST, as shown in Fig. 1 for these two examples in Valencia, Spain.

Changes in the simulated LST of any user-defined scenario will be checked for plausibility, so that, for instance, an increase in building density in comparison to open spaces correctly leads to an increase in LST while the creation of urban green spaces or water surfaces lead to a decrease in LST. In addition, we will make use of suitable examples of real construction work from the near past in the four pilot cities to compare the real changes in LST caused by the construction work to the changes in LST that were simulated by the scenario service.

Outlook for the future

The LST prediction models underly a service simulating the effects of user-made changes on the land surface temperature as a proxy for the urban heat distribution. The service contributes to a better understanding and design of urban planning and policies to mitigate unhealthy climate in cities. It will be part of the CityCLIM online platform addressing first of all city administrations and city planners and second the interested public. The service is initially developed for the four project pilot cities with the perspective of extension to any city worldwide with a low effort because it applies standard EO data (high-resolution city digital elevation models are optional). The next steps are the further refinement of the LST prediction model, the deployment of the methodology to the open CityCLIM platform and the following testing and iterative improvement of the user-friendliness of the implementation. Services such as the one presented here, will greatly benefit from future TIR missions providing LST on high spatial resolution and with high accuracy, like TRISHNA or LSTM.

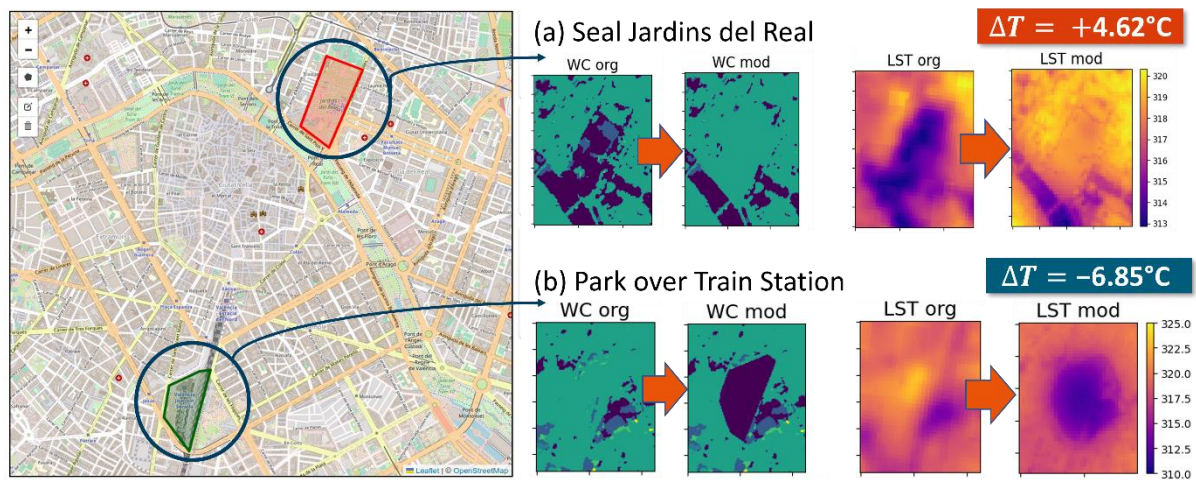


Figure 1 Example application of the Service on simulating and mitigating urban heat for Valencia, Spain. The user changes the urban land surface based on ESA Worldcover (WC) and then the land surface temperature (LST) is calculated with the calibrated prediction model for the new configuration. (a) An average-sized building placed in the urban park "Jardins del Real" leads to an average surface temperature increase within the modified area of more than 4°C (b) For the installation of an urban green space instead of an aboveground train station, a decrease in surface temperature of over 6°C is simulated in this area.

Airborne Hyperspectral Imaging for the Detection, Identification, and Quantification of Pollutant and Toxic Gas Emissions from Inefficient Methane Flaring

EARSel Valencia 2024
Abstract
Corresponding Author: Antoine Dumont
antoine.dumont@telops.com

Antoine Dumont¹, Frederick Marcotte¹, Stephane Boubanga¹, Hajera Kouser¹,

¹Telops, Canada

Keywords (5): Hyperspectral, Airborne, Gas Detection, Green House Gas

Challenge (800 - 1000 characters incl. spaces)

Detection, identification, and quantification of greenhouse gases is essential to ensure compliance with regulatory guidelines and mitigate damage associated with anthropogenic climate change. Over the last decades, technological progresses have allowed combining Fourier-transform spectrometer instruments with focal-plane array imaging in order to provide a combination of high spatial, spectral and temporal resolutions. Passive infrared hyperspectral imaging remote sensing can be used to identify the chemical nature of targets based on their unique infrared spectral signature, and spatially resolve multiple species within a same scene (such as a mixture of greenhouse gases). This offers a new reliable gas identification and quantification imaging method that represents an improvement to the current standard gas detection technologies. The Telops Hyper-Cam Airborne Mini Platform is an established system for aerial hyperspectral measurements for gas and mineral survey applications.

Methodology (1200 – 1500 characters incl. spaces)

The workflow is separated into three phases:

- 1) In Pre-flight, the user needs to determine which and how many assets they want to survey. The system can fly over all kinds of assets such as wells, gas plants, pipelines or flares. When the list of assets is finalized, Telops and its service partners create a KML file including the GPS coordinates of all the sites, which will allow full data visualization on a satellite map for each position where a measurement is obtained.
- 2) During the aerial surveys, the Hyper-Cam Airborne Mini sensor captures thermal data and visible HD imagery. **Error! Reference source not found.**1 shows typical imagery quality. Depending on the pre-set parameters, the system gathers data in either a mapping or a targeting mode. Mapping mode establishes a mosaic of images to have a large scale overview of a surveyed area. Targeting mode focuses on one location and can obtain multiple captures per flyover, which can help determine plume dynamics.
- 3) Collected thermal data is thoroughly processed and analysed. The hypercube data can be reprocessed as many times as required for as many chemical species investigated as it contains the complete spectral information. The IR signature for each pixel is authenticated with a compound library following the measurement parameters in the detection scenario.

Expected results (1200 – 1500 characters incl. spaces)

In the Winter of 2023, the Hyper-Cam Airborne Mini platform was flown above a water treatment methane flare gas release system to collect hyperspectral data for gas quantification analysis. This measurement campaign was performed to document the performance of the Hyper-Cam Airborne Mini methane quantification capabilities within a difficult scene. This talk introduces the principles behind the gas

detection, identification, and quantification algorithms and presents the motivations and results from these measurements in Winter 2023. While methane observation was at the core of the campaign, a post-processing analysis focused on a flare stack combustion revealed the presence of carbon dioxide, water vapor, sulfur dioxide and nitrous oxides emitted from the flare. These later two pollutant gases, coming from a sour or sweet gas input, can cause acid rain in the area and are typically avoided as much as possible by flare operators. Similarly to the input gas methane being detected in inefficient combustion, toxic gas hydrogen sulfide, the known combustible source of sulfur dioxide, was detected as a non-combusted emission.

Outlook for the future (800 - 1000 characters incl. spaces)

Methane is at the forefront of the fight against climate change and Telops airborne methane leaks detection makes it simple and efficient for the oil and gas industry to monitor and reduce emissions while improving safety and regulation compliancy. It is still important to consider other products from flare combustion that can have a severe impact on the environment. From a scientific perspective, the proper remote quantification of such emissions can be an essential tool in improving and confirming flaring combustion models. These types of measurements can also be shared with such facilities as feedback to help further refine their burn-off processes, improve the security of workers, and minimize the amount of unnecessary greenhouse gas released into the environment.

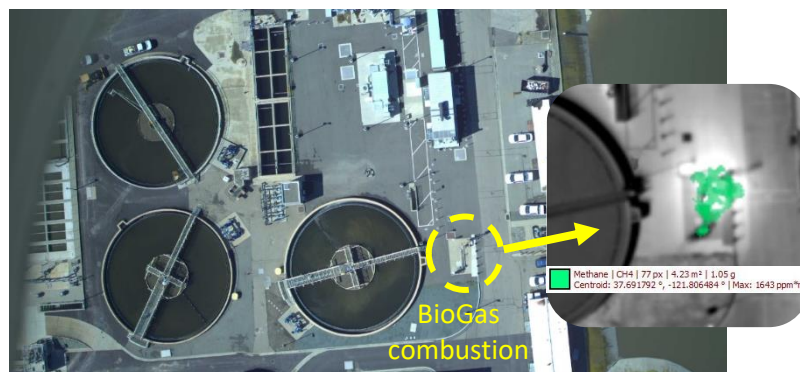


Figure Visible picture example at a flyover pass above a methane flare. Accompanied by the IR image obtained by the hyperspectral instrument, with methane identification and quantification.

[Formatting guidelines for abstract submission]

EARSeL Valencia 2024
Abstract

Corresponding Author:

[kopkane.d@czechglobe.cz]

Emissivity estimation of metal roofs from hyperspectral thermal data

Daniel Kopkáně¹, Jan Hanuš¹, Miroslav Píkl¹, Lucie Homolová¹

¹ Global Change Research Institute CAS, Department of Remote Sensing, Czech Republic

KEYWORDS URBAN, THERMAL HYPERSPECTRAL, METAL ROOFS, LOW EMISSIVITY

Challenge

Airborne thermal hyperspectral data can be used to assess urban thermal regimes and heat islands because their high spatial and spectral resolution is particularly well suited to resolving highly heterogeneous systems (in terms of variation in size and spectral properties of objects) such as urban environments. The post-processing of hyperspectral thermal data needs to solve the separation of emissivity and temperature to provide the final products: Land Surface Emissivity (LSE) and Land Surface Temperature (LST). Temperature Emissivity Separation (TES) algorithms are very useful for surfaces with an emissivity greater than 0.6. For lower emissivity surfaces, such as metal roofs, the algorithm fails by predicting LST typically 20 to 40 K below the actual surface temperature. We therefore present here a solution based on using the atmospheric 9-10 μm ozone feature to estimate the emissivity of each pixel, resulting in more accurate LST estimates.

Methodology

The enhanced pre-processing is designed for urban landscape datasets acquired by TASI 600 - a 32-band hyperspectral thermal sensor operating in the spectral range 8 - 11.5 μm (ITRES, Ltd.). Atmospheric corrections are based on the MODTRAN atmospheric model parameterised by ERA5 reanalyses. The hourly ERA5 data are interpolated in space and time domain to fit a given flight line. The atmospheric profile is used to estimate transmittance, upwelling and downwelling fluxes for individual sensor bands by MODTRAN 6. The workflow evaluates surfaces based on the shape of the land leaving radiance and classifies high and low emissivity surfaces. The high emissivity pixels are processed using the standardised TES algorithm. The low emissivity pixels are processed by searching for the emissivity value that gives the smoothest spectral radiance curve with respect to the ozone peak. The evaluation is based on the assumption that low emissivity metal roofs have essentially featureless spectra.

Expected results

The end result is an optimised algorithm for evaluating the emissivity of metal roofs (Figure 1). Errors in LST and LSE estimates increase with decreasing emissivity due to mismatch between modelled and real atmospheric features. This is because the shiny metal roofs tend to reflect the features of the real atmosphere, as the potential influence increases with increasing surface reflectance. For this reason, it is likely that the estimated LST will be prone to errors up to 5 K. In comparison, for the ordinary surfaces (emissivity >0.9) the typical accuracy is around 0.5 K. However, compared to the result of the standard TES algorithm, where errors can reach up to 40 K, this is a significant improvement.

Outlook for the future

Further improvements can be made by incorporating airborne laser scanning data to account for the tilt of individual roof pixels. Particularly for very low emissivity roofs, the specular part of the reflection will emphasise the effect of off-nadir downwelling radiation from the atmosphere. The challenge is the accurate modelling of atmospheric features, which can be improved by incorporating on-board measurements of atmospheric temperature to verify the ERA5 data.

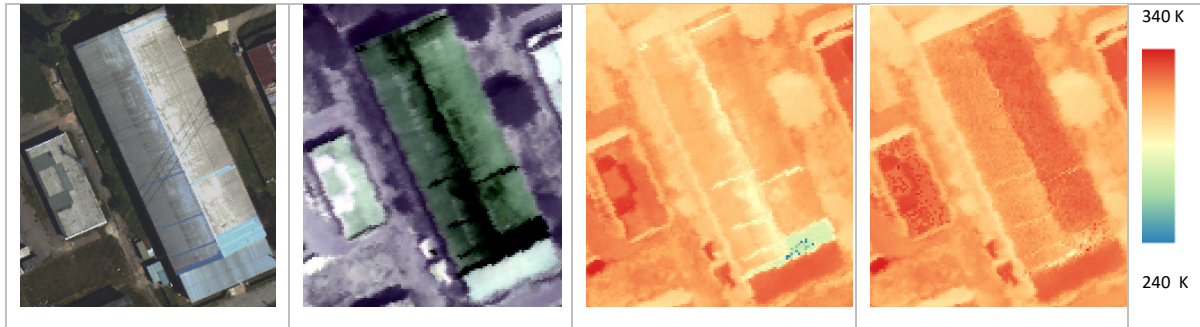


Figure 1 a) true color of a metal roof, b) at sensor radiance, c) LST estimated by standard TES algorithm, d) LST estimated by the improved algorithm

**Them.Sess. 2-1: EnMAP's first two
years in orbit- current status and
recent activities I**

EnMAP Mission Status

EARSel Valencia 2024
Abstract
Corresponding Author:
sebastian.fischer@dlr.de

Sebastian Fischer¹, Laura La Porta¹, Anke Schickling^{1,2}, Sabine Chabrilat³, Emiliano Carmona Flores⁴, Nicole Pinnel⁴

¹ German Space Agency at DLR, Germany

² ESA/ESRIN, Italy

³ GFZ Potsdam, Germany

⁴ German Aerospace Center (DLR), Germany

Keywords (5): Earth Observation, Urban, Hyperspectral, Land Use, EnMAP

Challenge

The Environmental Mapping and Analysis Program (EnMAP) is a spaceborne German hyperspectral satellite mission that aims at monitoring and characterizing the Earth's environment on a global scale. EnMAP core themes are environmental changes, ecosystem responses to human activities, and management of natural resources.

Methodology

EnMAP was launched on April 1st 2022 under the tip of a Falcon 9 rocket from Cape Canaveral in Florida. The commissioning phase of the instruments was successfully accomplished within 7 months and afterward the satellite started routine operations. Since November 2nd 2022 EnMAP data are available to the scientific community.

Results

This presentation will give an overview of the mission status, the current acquisitions strategy and open AO Calls.

Outlook for the future

This presentation will also give an outlook on upcoming AO calls to be considered for EnMAP high priority observations.

EnMAP: A breakthrough for Hyperspectral Earth Observation. Seen from the manufacturer of the satellite, 2 years after Launch

R. Feckl⁽¹⁾, M. Betz⁽¹⁾, S. Baur⁽¹⁾, M. Kuchler⁽¹⁾, W. Schmid⁽¹⁾, B. Sang⁽¹⁾, R. Wachter⁽¹⁾

¹ OHB, Manfred-Fuchs-Str. 1, 82234 Weßling (Germany)

Keywords (5): Earth Observation, Satellite, Hyperspectral

Challenge

OHB was the Industrial Prime contractor for Germany's DLR EnMAP (Environmental Mapping and Analysis Program) Mission and manufacturer of the Satellite. In this role OHB has not only developed and manufactured the Spacecraft Bus, but also the technologically demanding Hyper-Spectral Imager (HSI) instrument.

During this development it was required to overcome, together with our partners and suppliers, numerous technical & technological challenges.

The EnMAP Satellite was successfully launched on April 1st, 2022. After LEOP, IOT and Commissioning the Spacecraft was put successfully into routine operations in November 2022.

Methodology (1200 – 1500 characters incl. spaces)

This paper, for the EARSel 2024 will provide an overview on the planned and realized objectives and capabilities of the EnMAP Satellite with focus on HSI instrument in terms of:

- Timeline of key events since the Launch
- The manufacturers view on technical availability & achieved performance of the system:
 - Opto-mechanical stability and performance (Instrument Optical Unit comprising telescope, spectrometers and integrated sensors)
 - Achieved in-orbit performance of sensors key-parameters (compared with pre-flight characterization)
 - Performance of in-orbit calibration devices and activities (Absolute and relative radiometric, spectral and linear calibration)
 - Achieved overall image quality (geometric (incl. co-registration of sensors), spectral and radiometric accuracy)
- Encountered anomalies with focus on instrument sensors electro-optics
 - Unexpected characteristics of signal degradation on VNIR detector in commissioning phase
 - One trigger of latch-up protection circuit of the VNIR camera observed during an imaging
 - One configuration change in SWIR camera ROIC registers detected during an imaging

- Evolution
 - Implementation of requested change in transferred spectral bands showed high flexibility in implemented design

Results (1200 – 1500 characters incl. spaces)

Confirmation of expected performance by validation *in orbit*

- very low smile, very high quality of spectral knowledge, other parameters stable wrt on-ground characterization
- Radiometric accuracy, signal quality very good
- Geometric data quality beyond expectation, image quality high
- Confirmation of in-orbit calibration concepts and associated HW / ops
- Stability of instrument exceeding expectations
- Some real-world effects noticeable (but within specifications)
- striping / low signal non-linearity (possible improvements in L1 proc)
- VNIR / SWIR mismatching (recommendation to use SWIR data)
- VNIR response changes (not noticeable above L1c)

EnMAP data quality/performance successfully confirmed in operations

Outlook for the future (800 - 1000 characters incl. spaces)

OHB has gained enormously in terms of General Technology and Instrument Know-how from EnMAP:

- OHB had gained very valuable knowledge from ENMAP on technologies and manufacturing:
 - Optical Coatings,
 - Calibration references,
 - Gluing technologies,
 - Material properties, long term behavior etc.
 - Optical Alignment Technologies
 - Many more.....
- Which is of great importance for all future missions of optical instruments.
- This return of experience is applied on all currently ongoing OHB projects
 - One prominent example is optical alignment in MTG - Where we have repeated the EnMAP technology on 10 instruments (FCI & IRS)
 - A second prominent example is obviously CHIME the European ESA Hyperspectral Mission with OHB acting as instrument prime



Figure (a) EnMAP Satellite HSI Aperture Port View – during final AIT

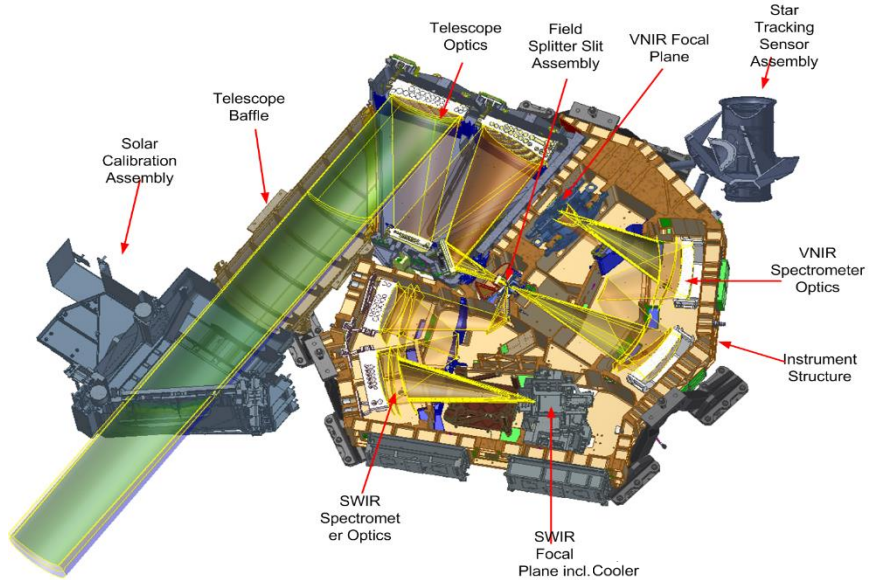
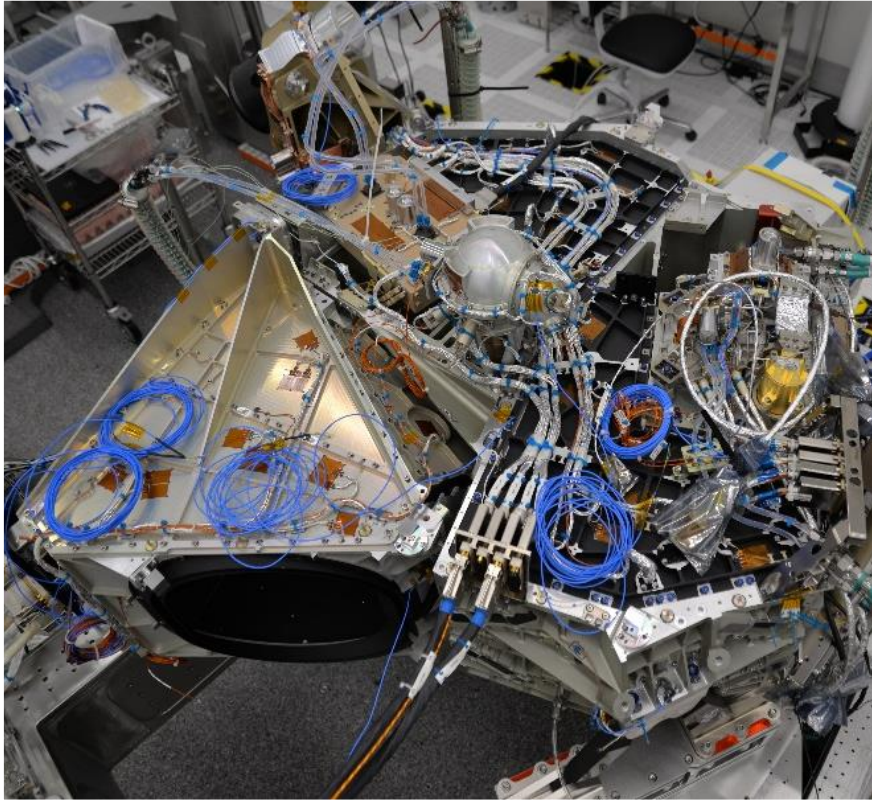


Figure (b) Core of the EnMAP hyper-spectral instrument: Instrument Optics Unit (IOU) Schematic



- **Figure** (c) Core of the EnMAP hyper-spectral instrument: Instrument Optics Unit (IOU) – during AIT

Two years of EnMAP Ground Segment Operations

EARSeL Valencia 2024

Abstract

Corresponding Author:

Emiliano.Carmona@dlr.de

[Emiliano Carmona](#)¹, Sabine Engelbrecht², Martin Habermeyer², Sebastian Hartung³, Lukas Hoffmann⁴, Helmut Mühle², Miguel Pato¹, Nicole Pinnel², Peter Schwind¹, Katrin Wirth⁴

¹ Remote Sensing Technology Institute, DLR, 82234 Weßling, Germany

² German Remote Sensing Data Center, DLR, 82234 Weßling, Germany

³ German Remote Sensing Data Center, DLR, 17235 Neustrelitz, Germany

⁴ German Space Operations Center, DLR, 82234 Weßling, Germany

Keywords (5): Earth Observation, Hyperspectral, Spaceborne Mission, Ground Segment, Operations

Challenge

Space-borne imaging spectroscopy has enormous potential to improve our understanding of the Earth's dynamic systems and the changes we face today. The ability to obtain spectra from any point on Earth can be used to obtain more precise and quantitative measurements for a variety of different applications. With this in mind, the EnMAP Mission was designed with the aim of providing the scientific community with high-quality hyperspectral data from space.

Operating a high-precision instrument in Space that generates a large volume of data, that must be commanded according to user requests and whose data has to be processed on demand according to different processing options, poses many challenges. The infrastructure responsible for the operation of the mission after launch and which must act as the interface between the users and the satellite, overcoming these challenges, is the Ground Segment (GS).

Methodology

EnMAP's GS is the responsibility of the German Aerospace Centre (DLR). It is designed to operate for 5 years and provide access to EnMAP data for another 10 years. The GS is composed of 3 systems:

Mission Operation System. It is responsible for controlling the satellite and the instrument. It is in charge of receiving telemetry data and sending telecommands, controlling the satellite's orbit, executing the necessary satellite maneuvers and planning the satellite's daily operations (imaging acquisitions, contacts with ground stations, etc.)

Payload Ground System. It is responsible for receiving, processing and archiving data, as well as providing the user interfaces for user registration, submission of proposals, instrument tasking and processing and downloading of the user EnMAP products.

Processor and Calibration/Validation System. It is responsible for developing and maintaining the processing chain that transforms the instrument raw data into the ordered products, by performing data calibration, orthorectification and atmospheric correction (levels 1B, 1C and 2A with ESA definition). It monitors and updates the radiometric, spectral and geometric calibration, performs quality control of the data and monitors the instrument to guarantee the quality of the delivered data.

Following the successful completion of the commissioning phase, the user community was granted access to EnMAP products, as well as the possibility to task the instrument by submitting a proposal.

Results

From its launch to September 30th 2023, the EnMAP mission has produced and archived over 39,000 Earth Data products (see figure) and 159 calibration data products. The interest in EnMAP data by the user community is demonstrated by the use of the GS services since it opened for user registration (2nd November 2023). As of September 30th 2023, a total of 1425 users from 85 countries around the world have registered. A total of 350 proposal submissions (100 more in preparation) show that the main areas of interest are vegetation, geology/soil and water applications. As of October 2023, the GS has processed and delivered more than 25,000 products from its catalogue.

The mission experienced an extended eight-week outage between December 2022 and February 2023 that was resolved with no impact on mission requirements, lifetime or redundancies. The GS has also introduced several improvements in areas such as the usability of the Instrument Planning tool, the integration of a new receiving station, the update of SWIR band configuration, the re-processing of archived commissioning data, as well as several improvements and bug fixes in the processing software (de-stripping of images, geometric accuracy improvements, correction of L2A-water adjacency, etc.). GS updates are announced in the news section of www.enmap.org if they affect EnMAP products, and are always reported on the Mission Quarterly reports, publicly available on the same web page.

Outlook for the future

Approaching two years of operation, the EnMAP mission has been able to achieve its goal of providing high-quality hyperspectral data to a growing number of users worldwide. During the operational time, the GS is works to keep all the services required for operations up and running and has introduced several service and data quality improvements. This period has not been without challenges, but the GS has been working to address them and minimize their impact on the mission. The GS is currently considering changes to the acquisition strategies and planning, with the aim of improving the tasking of EnMAP observations for a greater number of users and increasing the volume of data acquired over the areas with a very high user demand. Our goal for the coming years is to provide a larger number of users with a larger amount of the high-quality hyperspectral data that EnMAP can produce.

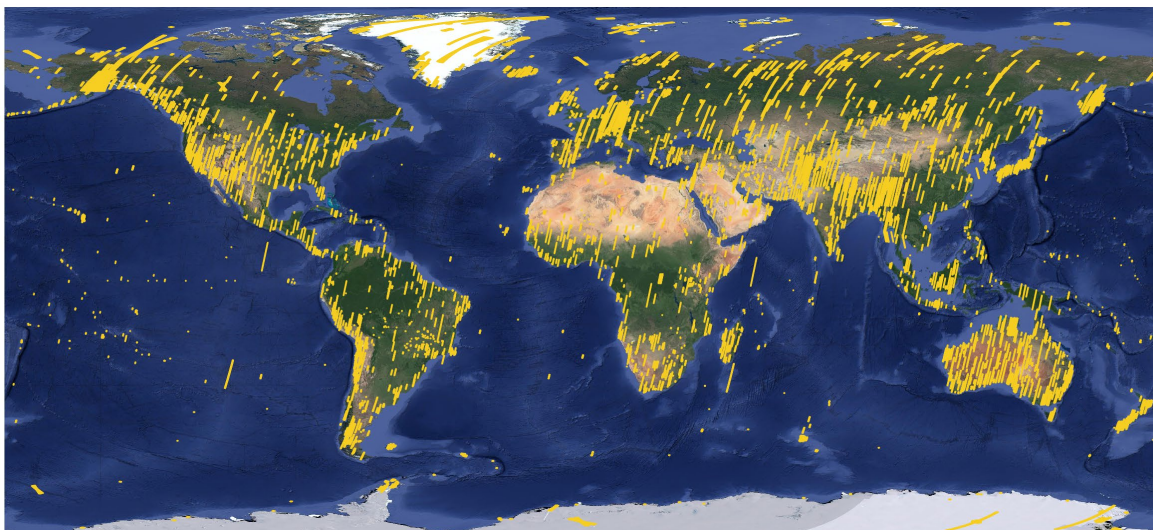


Figure Footprint of EnMAP acquisitions from April 1st, 2022 (launch date) until September 30th, 2023.

Status of EnMAP processor and calibration activities

Miguel Pato¹, Kevin Alonso², Martin Bachmann³, Simon Baur⁴, Maximilian Brell⁵, Raquel de los Reyes¹, Birgit Gerasch¹, Martin Habermeyer³, Stefanie Holzwarth³, Maximilian Langheinrich¹, David Marshall Ingram¹, Mathias Schneider¹, Peter Schwind¹, Helge Witt¹, Emiliano Carmona¹

¹ German Aerospace Center (DLR), Earth Observation Center, Remote Sensing Technology Institute, Oberpfaffenhofen, Germany

² RHEA Group c/o European Space Agency (ESA), Largo Galileo Galilei, Frascati, Italy

³ German Aerospace Center (DLR), Earth Observation Center, German Remote Sensing Data Center, Oberpfaffenhofen, Germany

⁴ OHB-System AG, Weßling, Germany

⁵ Helmholtz Center Potsdam, GFZ German Research Center for Geosciences, Potsdam, Germany

Keywords (5): Earth Observation, EnMAP, processing chain, in-flight calibration, quality control

Challenge

The Environmental Mapping and Analysis Program (EnMAP) mission, launched on April 1, 2022, has been acquiring high-quality hyperspectral measurements since the successful completion of the commissioning phase and start of operations in November 2022. EnMAP imagery for Earth observations consists of 30x30 km² tiles with a spatial resolution of 30 m and covers the full reflective range 418–2445 nm with 224 spectral channels of bandwidths between 5 nm and 12 nm. The correct processing and high quality of these data are ensured by the EnMAP Ground Segment (DLR) through the Processor and Calibration team, whose main operational tasks include the maintenance of the processing chain, in-flight calibration, data quality control and instrument monitoring. In this contribution, we give a detailed account of our activities since the beginning of the operational phase with a special focus on the improvements of relevance to users of EnMAP data.

Methodology

The EnMAP payload consists of two push-broom spectrometers covering the visible and near infrared (VNIR) and the short-wave infrared (SWIR) spectral ranges with requirements on radiometric accuracy and stability of 5% and 2.5% respectively and spectral accuracy of 0.5 nm for VNIR and 1 nm for SWIR. This performance is possible in EnMAP due to the extensive in-flight calibration equipment, which enables different calibration types: relative radiometric (white Spectralon®), absolute radiometric (Sun diffuser), spectral (doped Spectralon®), linearity (focal plane LEDs), deep space and dark frames (closed shutter). The EnMAP Ground Segment regularly schedules the calibration measurements in order to continuously calibrate and monitor the instrument. The EnMAP processing chain then incorporates the latest calibration tables to generate the Earth observation user products at three levels: L1B (top-of-atmosphere radiances), L1C (orthorectified top-of-atmosphere radiances) and L2A (orthorectified bottom-of-atmosphere reflectances). The processing chain is under active maintenance and is frequently updated to improve the delivered products. The radiometric, spectral and geometric quality of EnMAP products of all levels is controlled regularly and reported in the publicly available mission quarterly reports. The same report also includes a comprehensive overview of the life-limited items and other instrument parameters monitored.

Results

We briefly present selected results from the commissioning phase, which validated the products delivered by the EnMAP processing chain. At the start of the operational phase, three main EnMAP processing and calibration issues remained:

- VNIR degradation. A rapid sensitivity decay of the VNIR instrument was noticed soon after the first calibration acquisitions. The decay slowed down during 2022 and stopped in 2023 (see figure below). The issue was mitigated in March 2023 by applying dynamic coefficients between radiometric calibrations.
- Across-track striping. This effect was visible in both VNIR and SWIR, hampering the use of EnMAP data for certain applications. After thorough investigation, an image-based destriping algorithm developed by GFZ was implemented in March 2023 at L1B level. The algorithm is very effective in reducing striping in most situations.
- VNIR/SWIR co-registration. At the end of commissioning, the alignment between VNIR and SWIR images amounted to 0.7–0.8 pixels, above the requirement of 0.3 pixels. This was sequentially improved to 0.06 pixels by March 2023 through two geometric calibrations and a processor update.

All three issues have been solved and can be retroactively fixed in past scenes by re-ordering the products. Other issues fixed include L2A snow spectra (July 2023) and the adjacency correction in L2A water products (September 2023). In addition, a new SWIR band configuration in the instrument was uplinked in July 2023.

Outlook for the future

The EARSeL workshop in April 2024 will mark the second anniversary of EnMAP in orbit. During these two years, EnMAP has gradually acquired, delivered and archived tens of thousands of hyperspectral image products, filling an important gap in the needs of the global remote sensing community. The Processor and Calibration team within the EnMAP Ground Segment has routinely performed its operational tasks and in parallel solved the main issues affecting the quality of the end-user products. Additional minor issues (e.g., SWIR along-track striping and VNIR/SWIR radiometric consistency in overlapping spectral range) are being investigated at the moment. In this respect, the feedback provided by users (as well as by EnMAP Space Segment and Science Segment) remains crucial to improve the delivered products during the EnMAP mission lifetime and beyond.

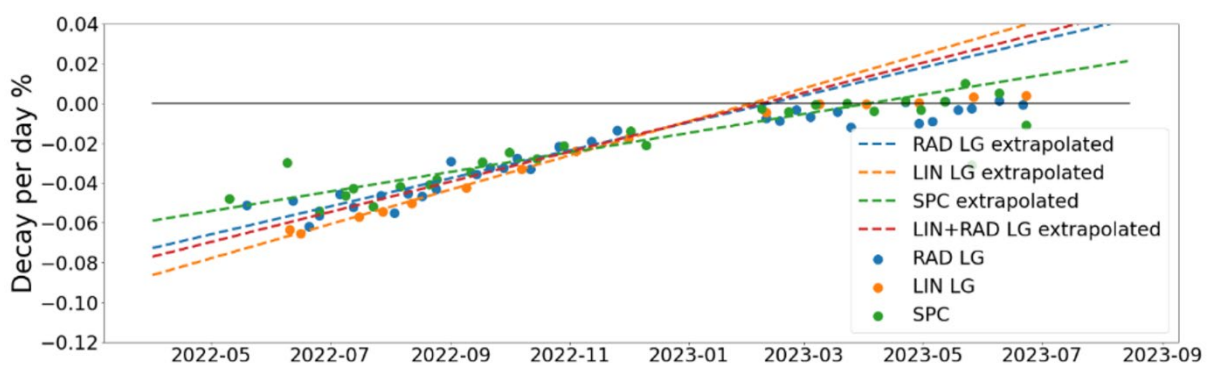


Figure VNIR degradation effect as a function of time. The decay rate was fast after launch, but it has gradually slowed down and essentially stopped by March 2023.

A Brief History of the Inflight Spectral and Radiometric Performance of EnMAP

[David Marshall Ingram](#)¹, Kevin Alonso², Martin Bachmann¹, Simon Baur³, Birgit Gerasch¹, Martin Habermeyer¹, Stefanie Holzwarth¹, Maximilian Langheinrich¹, Miguel Pato¹, Raquel de los Reyes¹, Mathias Schneider¹, Peter Schwind¹, Helge Witt¹, Emiliano Carmona¹

¹ German Aerospace Center (DLR), Earth Observation Center (EOC), Weßling, Germany

² RHEA Group c/o European Space Agency (ESA), Largo Galileo Galilei, Frascati, Italy

³ OHB-System AG, Weßling, Germany

Keywords: EnMAP, Earth Observation, Hyperspectral, Spectral Calibration, Radiometric Calibration

Challenge

The Environmental Mapping and Analysis Program (EnMAP) of the German Aerospace Center (DLR) was launched in April 2022 and provides users with hyperspectral imagery to monitor and study the dynamic processes on our planet. EnMAP covers a spectral range of 418 – 2445 nm with two sensors, one for the Visible and Near Infrared (VNIR) and one for Short-Wave Infrared (SWIR), at a spatial resolution of 30 m, a swath width of 30 km and a maximum coverage of 5000 km per day. The raw images captured by EnMAP are radiometrically corrected during L1 processing and, to ensure that high quality Earth observations are acquired, it is vital that accurate spectral and radiometric calibration tables are obtained. For this, EnMAP has five onboard calibration systems which are frequently used to assess and monitor the characteristics of the VNIR and SWIR sensors.

Methodology

The radiometric stability of the VNIR and SWIR sensors is assessed through observations of a white Spectralon® sphere as part of the On-Board Calibration Assembly Lamp (OBCA-Lamp). A second unit, the OBCA-Spectral, contains a doped Spectralon® sphere and separate lamps where an optimisation procedure uses the many spectral lines to calculate the central wavelengths in each channel. The radiometric calibration tables which are used in L1B processing are generated from absolute radiometric observations of the sun via a solar diffuser. By comparing the reference measurements to a solar model, the radiometric, response non-uniformity (RNU) and gain matching coefficients are hence derived. A set of LED lamps in front of the focal plane are measured at increasing integration times to assess the linearity behaviour of both sensors. Finally, as part of the Shutter Calibration Mechanism, dark measurements are made for every calibration and earth datatake and deep space measurements are made in order to determine the thermal contributions to the sensor. All calibration units are monitored regularly – weekly for OBCA-Lamp, fortnightly for OBCA-Spectral, and monthly intervals for the absolute radiometric, linearity and deep space calibration – to ensure the stability of the two sensors.

Results

Throughout the mission, the SWIR sensor has been remarkably stable, changing by <0.15% in sensitivity. On the other hand, the VNIR sensitivity has changed significantly over time. Between April 2022 and May 2023, the VNIR sensor degraded by approximately 9% with large variations across the detector (up to 18% in the centre and less than 3% at the edges). However, the speed of the degradation reduced over time: from 0.05% per day in August 2022 to a stable zero point in April 2023 (Figure 1). Since then, the central part of the sensor appears to have increased in sensitivity by about 0.3%. The VNIR radiometric coefficients

have changed over time due to the early degradation and more recently as a result of the increase in sensitivity. To mitigate for the VNIR degradation during 2022, dynamic coefficients were introduced whereby the VNIR radiometric and RNU coefficients were modelled over time with an exponential-polynomial function. Meanwhile, the SWIR radiometric coefficients have been relatively stable.

From the OBCA-Spectral, the VNIR sensor has 91 channels from 418 – 993 nm, an average spectral sampling distance (SSD) of 6.5 nm and an average full width at half maximum (FWHM) of 7.8 nm. For the SWIR sensor, the wavelength range is 902 – 2445 nm for 133 channels, the average SSD is 10 nm and the average FWHM is 9.6 nm. In orbit, both sensors have been spectrally stable with changes of less than 0.4 nm between April 2022 and September 2023 (Figure 2).

Outlook for the future

The performance of EnMAP is spectrally and radiometrically stable, performing within the 2.5% radiometric stability requirement and within the spectral stability requirements for VNIR (0.5 nm) and SWIR (1.0 nm) between consecutive calibration/OBCA measurements. Current calibration measurements suggest that the stability is much better than these requirements. The VNIR sensor has changed in sensitivity, resulting in updates to the radiometric coefficients in order to account for this behaviour. Additionally, the measured dark signal has also shown good temporal stability. A radiometric mismatch at low signals between the VNIR and SWIR sensors at 900 – 1000 nm has been observed in Earth observations and is currently under investigation for a calibration-based solution. The behaviour of both sensors will be constantly monitored and updates to the calibration tables will be made when necessary to ensure that EnMAP continues to provide high quality Earth observations.

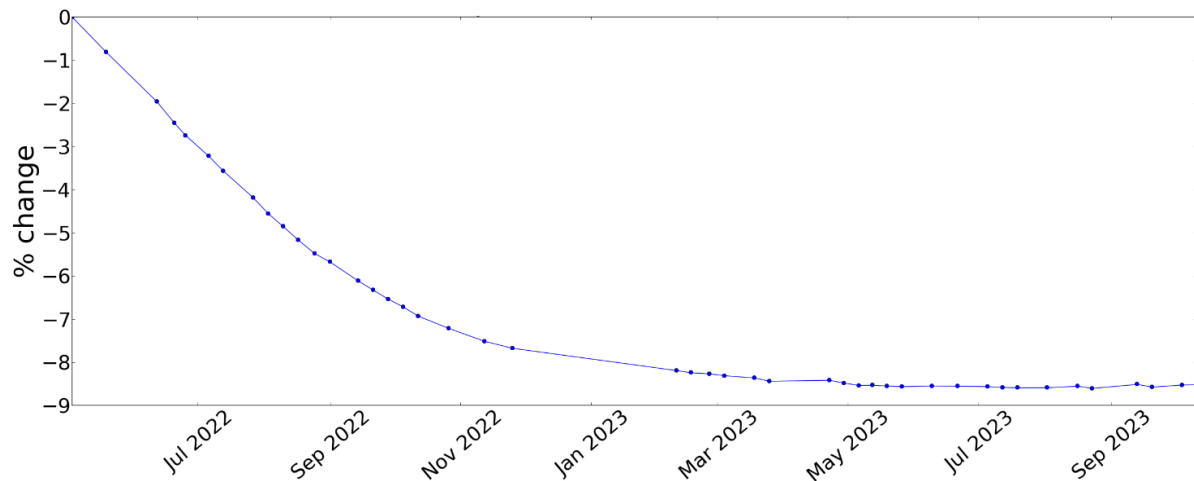


Figure 1 Average percentage change in VNIR low gain sensitivity over time based on measurements of the OBCA-Lamp of EnMAP

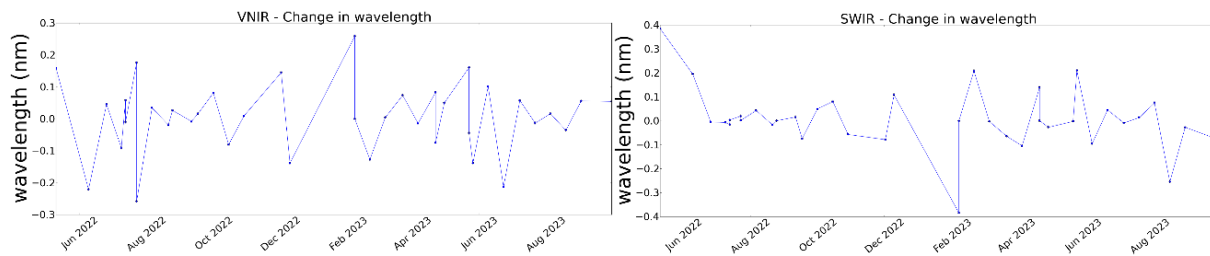


Figure 2 Average change in the central wavelengths for VNIR (left) and SWIR (right) over time based on measurements of the OBCA-Spectral of EnMAP

ENMAP PRODUCT VALIDATION: LESSONS LEARNED FROM TWO YEARS IN ORBIT

M. Brell¹, L. Guanter², D. Scheffler¹, K. Segl¹, N. Bohn¹, S. Chabrillat^{1,3}, M. Soppa⁴, A. Bracher⁴, M. Bachmann⁵, R. De Los Reyes⁵, M. Pato⁵, E. Carmona⁵, M. Bock⁶, L. La Porta⁶, S. Fischer⁶

¹ Helmholtz Center Potsdam, GFZ German Research Center for Geosciences, Potsdam, Germany

² Universitat Politècnica de València, Valencia, Spain

³ Leibniz University Hannover, Institute of soil science, Hannover, Germany

⁴ Alfred Wegener Institute, Helmholtz Center for Polar and Marine Research, Bremerhaven, Germany

⁵ Earth Observation Center (EOC), German Aerospace Center (DLR), Weßling, Germany

⁶ Space Agency, German Aerospace Center (DLR), Bonn, Germany

Keywords (5): CAL/VAL, In-Orbit Validation, EnMAP, In-situ data

Challenge

After two years in orbit of the hyperspectral EnMAP (Environmental Mapping and Analysis Program) satellite, the external EnMAP data product validation monitoring activities, led by the EnMAP science segment represented by GFZ and the EnMAP Science Advisory Group (EnSAG), have become an essential and integral part of the mission. Independent of the EnMAP Ground Segment (GS at DLR EOC) calibration and data quality control activities, the global and holistic GFZ product monitoring efforts intend to ensure high L2A product quality from a user- and scientific-driven perspective. With the collaboration and support of intensely international science field campaigns, CAL/VAL networks, and sites such as RadCalNet, HYPERNETS, AERONET, PICS, and the hyperspectral imaging community, emphasis is placed on covering the full relevant parameter range regarding surface and atmospheric conditions, altitude, and global distribution.

Methodology

The prerequisite for high data quality of the EnMAP L2A product is a consistent data quality of the intermediate products L1B and L1C. Therefore, besides the reflectivity, the radiometric, spectral, geometric, and general uniformities of the three official EnMAP data product levels (L1B, L1C, and L2A) are monitored based on the EnMAP Product Validation Plan (PVP). In-situ and scene-based scenarios are performed to validate the three official EnMAP product levels:

- L1B (radiometrically-corrected and spectrally-characterized radiance data) products are validated regarding absolute and relative radiometric uncertainty based on in-situ measurements, spatially-coherent artifacts (striping and dead pixel), signal-to-noise ratio (SNR), spectral parameters (e.g., center wavelength, bandwidth, and smile), and spatial parameters (keystone and modulation transfer function).
- L1C (geometrically corrected L1B) products are validated regarding geometric performance (absolute and relative spatial misregistration), detector co-registration, and band-to-band co-registration.

- L2A (atmospherically corrected L1C) products are validated regarding reflectance uncertainty for land and water surfaces, aerosol optical thickness, and columnar water vapor.

For several synchronous earth acquisitions from EMIT, PRISMA, DESIS, and Sentinel-2, L2A cross-validation scenarios are also performed and presented.

Results

This holistic validation strategy, based exclusively on earth observations and independent in-situ data, focuses on monitoring the impact of calibration efforts and instrument stability on the L2A land and water products. For this purpose, the validation analyses aggregate all generated valid matchups with independent in-situ data. In-depth results from the most critical and up-to-date validation scenarios are presented. All in-situ data matchups generated until then, general validations, and data quality improvements based on updates of the official EnMAP pre-processing will be integrated into the presented results. Land as well as water validation results are presented. The current status of the ongoing validation effort indicates that all L2A relevant parameters are well inside the mission requirements (see Figure 1) and within the range demanded by the user community. Cross-validation scenarios for PICS and other sites complement the respective validation scenarios and indicate the interoperability of the EnMAP L2A products. The presented results show that the product quality has significantly improved for several scenarios or at least is stable on a high product quality level since the launch, thanks to the continuous efforts of the DLR GS and the support of the independent product validation. All these complementary validation scenarios enable an adequate temporal resolution and globally homogeneously distributed validations of the official EnMAP products. The presented validation results indicate the importance and sensitivity to a well-balanced coverage of the relevant parameter range.

Outlook for the future

A single-site, single-pixel oriented validation does not cover the full range of relevant parameters satisfactory, and the significance is limited. Therefore, the independent product validation will hide towards a more global, full-swath-orientated monitoring approach. Cross-validations with other satellite systems, e.g., EMIT, PRISMA, and S2, but also airborne and drone-based campaigns from the international community, will play an essential role in the future. Additionally, validations and sites will be further extended with respect to improved balancing regarding surface and atmospheric conditions, altitude, and overall global distribution. Also, full uncertainty propagation and traceability are envisaged to be implemented in the validation chain. The comprehensive independent EnMAP validation is seen as an essential task regarding transferability, harmonization, and interoperability. Thus, future missions like CHIME and SBG will increase the efforts in this direction.

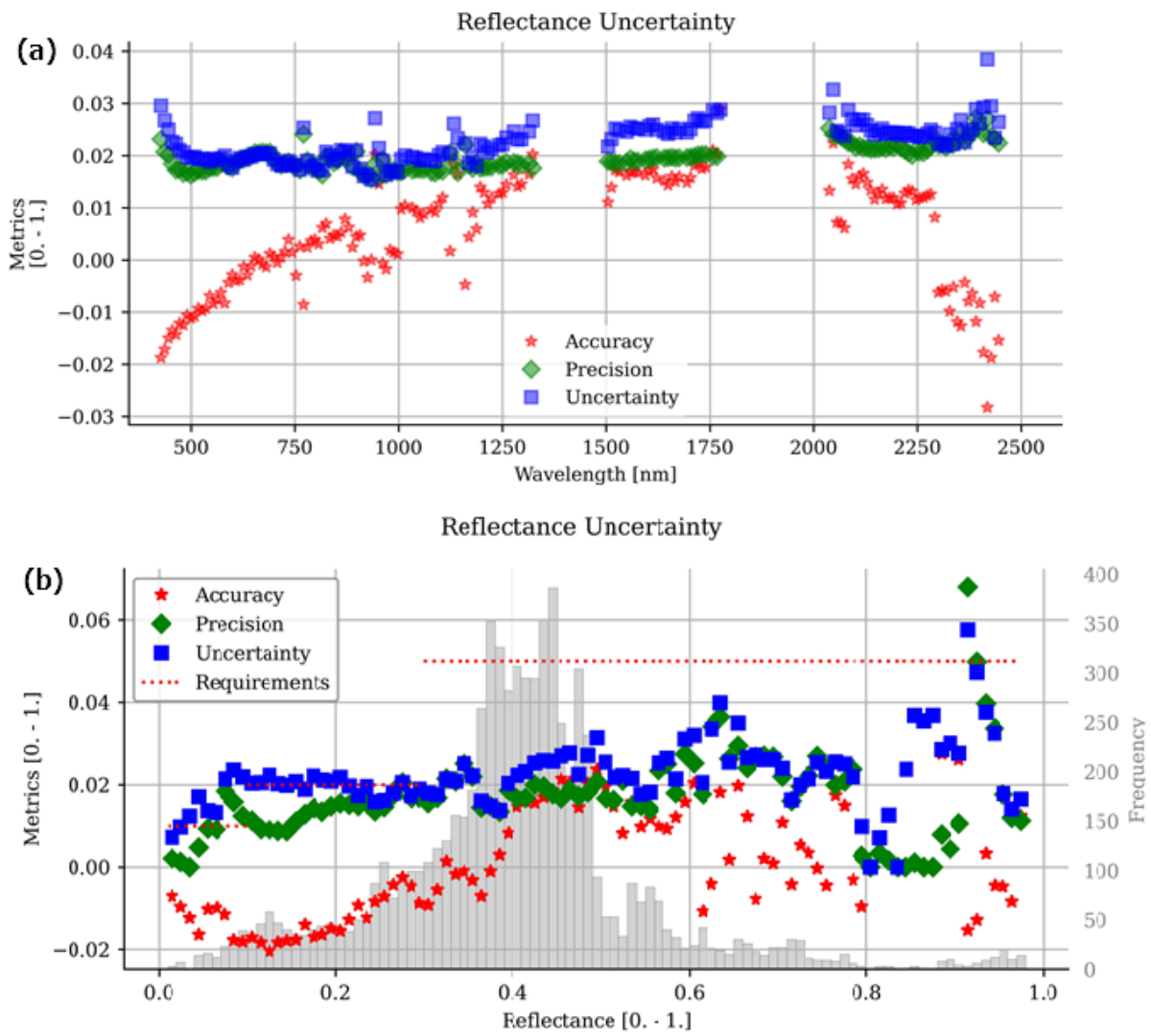


Figure 1 (a) Wavelength-dependent and (b) Level-dependent reflectance uncertainty plot based on 25 EnMAP in-situ matchups

**Them.Sess. 2-2: Hyperspectral
imaging of chlorophyll
fluorescence across scales -
PART I: retrieval and modeling
trends**

SIF spectrum retrieval in the framework of the ESA EE-8 FLEX mission

EARSeL Valencia 2024
Abstract
Corresponding Author:
sergio.cogliati@unimib.it

[Sergio Cogliati](#)¹, Pietro Chierichetti¹, Jorge Vicent², Neus Sabater³, Pekka Kolmonen³, Gwennaél Matot², Matthias Drusch⁴, Marc Bouvet⁴, Claudia Isola⁴, Roberto Colombo¹, José Moreno⁵

¹ UNIVERSITY OF MILANO-BICOCCA, ITALY;

² MAGELLIUM, FRANCE

³ FINNISH METEOROLOGICAL INSTITUTE, FINLAND

⁴ ESA-ESTEC, THE NETHERLANDS

⁵ UNIVERSITY OF VALENCIA, SPAIN

Keywords (5): Imaging Spectroscopy, Solar-Induced Fluorescence, FLEX, L2RM, Optimal Estimation

Challenge

The *FLUORescence Imaging Spectrometer* (FLORIS) aboard of the European Space Agency (ESA) Fluorescence Explorer (FLEX) mission is specifically designed to provide high-spectral resolution radiance observations in the 500-780 nm spectral range. The instrument design is primarily targeted to enable accurate and consistent retrieval of (i) Solar-Induced Fluorescence (SIF) spectrum comprehensive of the red and far-red peaks, (ii) canopy biophysical variables, and (iii) non-photochemical energy dissipation. In the framework of the FLEX preparatory activities, the Level-2 Retrieval Module (L2RM) study is devoted to design, implement, and test the L2 processor that is structured in four interconnected modules. The L2B "Fluorescence/Reflectance retrieval" module is explicitly dedicated to disentangling SIF and reflectance spectra after atmospheric characterization/correction performed from the previous L2A module.

Methodology

The L2B uses surface apparent reflectance spectrum (and uncertainty) provided from L2A to estimate the state vector (x). The latter contains free parameters of the forward operator used to model SIF and R spectra and to predict surface apparent reflectance spectrum in the range 670-780 nm. The inverse problem is solved based on Bayes' theorem about probability density and takes Gaussian distribution of the uncertainties as a basis. The approach used in this work refers to the probabilistic formalism known as *Optimal Estimation*. The method predicts apparent reflectance by iteratively optimizing the state vector x based on a cost function that incorporates goodness-of-fit and prior information criteria. Particularly, the inverse method employs data uncertainty (S_y) and a-priori parameters variance-covariance matrices (S_a). The first enables different wavebands to be weighed differently, the second helps to regularize the inverse problem providing covariance between parameters. The strength of a-priori is also balanced numerically to increase sensitivity to the information content of the spectral measurements. Finally, uncertainty from previous processing modules is taken as input and consistently propagated within the fluorescence retrieval. The inversion approach was tested by means of synthetic scenes produced from the FLEX End-2-End simulator (FLEX-E2E), to assess the retrieval performance on realistic synthetic data at the best of the current instrument engineering model.

Results

The analysis enables to assess the L2B retrieval accuracy in different conditions, considering several types of canopies, atmosphere conditions and instrument performance. The L2B retrieval accuracy assessment (Figure 1) is based on several requirements that compare retrieved SIF against the reference values generated from the FLEX-E2E. Specifically, SIF at the O₂ bands is considered because its contribution is larger in these windows even if they are also the most complex to model and correct from the L2A (atmospheric correction). SIF peaks maximum values are other characteristic wavelengths since they are important for the downstream scientific exploitation of FLEX to better characterize plant functioning. Finally, the spectrally integrated SIF (i.e., total SIF) represents the total fluorescence emission at all wavelengths that is also relevant for physiological modelling activities. The results show that SIF spectra retrieved from the synthetic image show meaningful behaviour and L2B correctly retrieves SIF spectra for the different types of vegetation with higher/lower SIF. The retrieval at the O₂ bands is more accurate compared to the emission peak and generally close to the mission requirement. Error in red SIF is generally lower compared to far-red, while total SIF shows a larger error inherited from the different wavelengths. Performances will be analysed also considering effects such as adjacency, stray-light and different instrument random noise configurations.

Outlook for the future

Several developments are envisaged to improve the retrieval performance. For example, the a-priori matrix (S_a) enables to restrict the solution domain to physically plausible spectra. It was built as a constant matrix regardless the land cover, from a comprehensive set of RT model simulations. However, SIF varies among different type of canopies and physiology, therefore S_a can be refined to properly account for different targets and conditions. Also, apparent reflectance uncertainty estimated during the atmospheric characterization is used to weight the different wavelengths. Typically, the uncertainty is larger within the O₂ bands because the instrument noise is higher, and because the atmospheric characterization is more complex. This implies that spectral bands most sensitive to SIF (O₂ bands) have a lower weight during numerical inversion. Numerical methods could be implemented to better balance the weight assigned to most critical wavelengths in the O₂ bands.

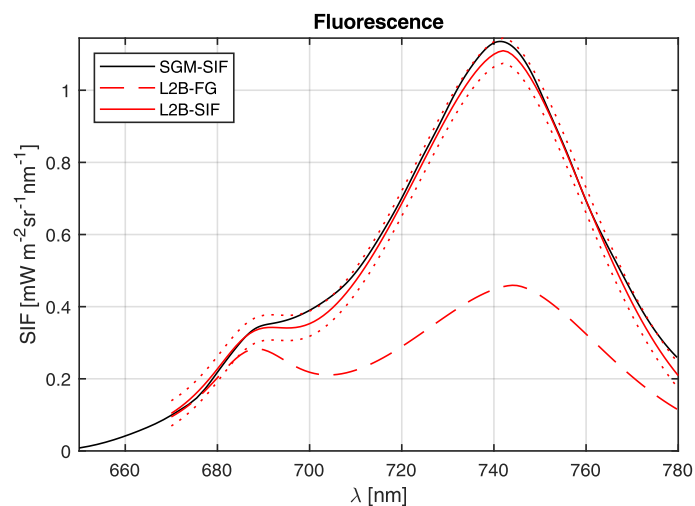


Figure 1: Example of SIF spectrum retrieval: reference from FLEX-E2E Scene Generator Module (black), first guess (red dashed), retrieved (red continuous) uncertainty (red dotted line).

Leveraging a large-scale radiative transfer simulation for an emulator based retrieval scheme of sun-induced fluorescence in HyPlant imagery

Jim Buffat¹, Miguel Pato², Stefan Auer², Kevin Alonso³, Emiliano Carmona², Stefan Maier², Rupert Müller², Patrick Rademske¹, Uwe Rascher¹, Hanno Scharr⁴

¹ Forschungszentrum Jülich GmbH, Institute of Bio- and Geosciences, IBG-2: Plant Sciences, Jülich, Germany

² German Aerospace Center (DLR), Earth Observation Center, Remote Sensing Technology Institute, Oberpfaffenhofen, Germany

³ RHEA Group c/o European Space Agency (ESA), Largo Galileo Galilei, Frascati, Italy

⁴ Forschungszentrum Jülich GmbH, Institute of Advanced Simulations, IAS-8: Data Analytics and Machine Learning, Jülich, Germany

Keywords (5): Earth Observation, Sun-induced Fluorescence, Hyperspectral, Neural Network, Machine Learning

Challenge (800 - 1000 characters incl. spaces)

The prediction of sun-induced fluorescence (SIF) from hyperspectral radiance has been identified as a corner stone to assess plants' photosynthetic efficiency remotely. It is widely accepted that remotely sensed SIF offers great potential for a variety of applications. To provide such estimates, top-of-canopy SIF products derived from passively sensed radiance measurements of various airborne and spaceborne sensors have been developed over the last decades. To date, however, physically based SIF retrieval schemes require a prohibitive use of computationally costly radiative transfer simulations especially when used in complex observational conditions such as in hilly terrain. In this contribution we report on our on-going work to develop a lightweight self-supervised neural network to retrieve SIF in the O₂-A absorption band of HyPlant acquisitions. We aim at a tight integration of a physical radiative transfer model with the network to ensure physically sound predictions by leveraging large scale simulation and emulation of HyPlant at-sensor radiance observations. We report on first results that we achieve on a dedicated data set.

Methodology (1200 – 1500 characters incl. spaces)

We formulate the SIF retrieval scheme as a feature based optimization performed by a neural network. A specifically designed neural network is trained to spectrally fit a physical model of the at-sensor radiance to observed data. The loss formulation for training involves the fitting residuals and additional regularizers guaranteeing physiological and physical constraints. We moreover take advantage of variability constraints in the architectural set up. Contrarily to other spectral fitting methods the physical model is, however, not implemented explicitly. Instead we make use of a fast and accurate emulator built from a large database of simulated HyPlant spectra mapping the simulation parameters to the hyperspectral at-sensor radiance (cf. Fig. 1). The presented approach is completely self-supervised, differently to supervised approaches where the network would be trained to directly predict a SIF label. A supervised approach for SIF prediction from DESIS data based on a similarly constructed data set was developed in parallel and has been submitted by Pato et al.

We model the radiative transfer around the O₂-A absorption band (740 - 780 nm) with a general-purpose simulation tool based on MODTRAN6. The simulation tool parameterizes surface properties, geometrical conditions and sensor characteristics affecting the at-sensor radiance with 13 parameters. Detailed analysis of the parameters' sensitivities with respect to the at-sensor fluorescence signal and a precise determination of observed parameter ranges allow us to realistically model HyPlant at-sensor radiance. We generated hyperspectral simulation databases (349 bands, spectral sampling interval of 0.11 nm) by extensively sampling the input parameter ranges.

Results (1200 – 1500 characters incl. spaces)

Our work explores a self-supervised neural network based SIF prediction scheme leveraging an emulator trained on a large-scale hyperspectral database. We show that the implementation of the emulator as a 4th degree polynomial yields a mean radiance error of less than 0.1 mW/m²/sr/nm across the O₂-A band which is less than 10% of a typical SIF at-sensor signal. We furthermore detail that the emulator yields highly realistic spectra by showing that the mean fitting residual of the neural network over the whole fitted spectrum is less than 1.5 mW/m²/sr/nm in a typical HyPlant flight line.

The proposed network was trained on a preliminary compilation of HyPlant acquisitions from 2018 - 2023 (30 acquisitions) and tested on a data set of HyPlant campaigns from 2018 and 2020 where suitable top-of-canopy SIF measurements exist that can be used as ground truth in a validation study. We find our approach to yield comparable results to the state-of-the-art Spectral Fitting Method for HyPlant (Cogliati et al. 2019) with significant ($p < 0.01$) correlation scores larger than 0.85 with respect to the top-of-canopy SIF measurements.

Furthermore we acquired additional HyPlant data over hilly terrain in 2022 and 2023 to be able to test the retrieval under conditions that are not suitable for operational state-of-the-art SIF retrieval schemes. In Fig. 2 we show an exemplary HyPlant acquisition and corresponding SIF predictions. Although we cannot conduct a validation study with ground measurements in these cases, we are able to assert that the resulting SIF predictions are not correlated to the topography as is the case with other methods. Further work will focus on establishing a better base line to validate the SIF prediction under these challenging conditions.

Outlook for the future (800 - 1000 characters incl. spaces)

The presented network was trained and tested on a particular compilation of HyPlant acquisitions. Our results indicate that the training leads to good performance with respect to ground measurements and suggested consistent performance in a variety of topographic and observational conditions. Further work will address specifically the consistency of our approach across larger HyPlant data sets and the potential benefit of larger training data sets for the generalization capability of the network.

We believe that the presented approach could be used as a blueprint for computationally efficient SIF retrieval for arbitrary hyperspectral sensors with suitable spatial and spectral resolution. If it can be shown that the network may be trained on a default data set once and then applied for prediction on new data without or only with short additional training times, the presented approach could be interesting for SIF prediction in air and spaceborne sensor missions with high data throughput where efficiency is a key requirement. Therefore, we will extend the validation of this approach to simulated data of the upcoming FLEX mission of ESA.

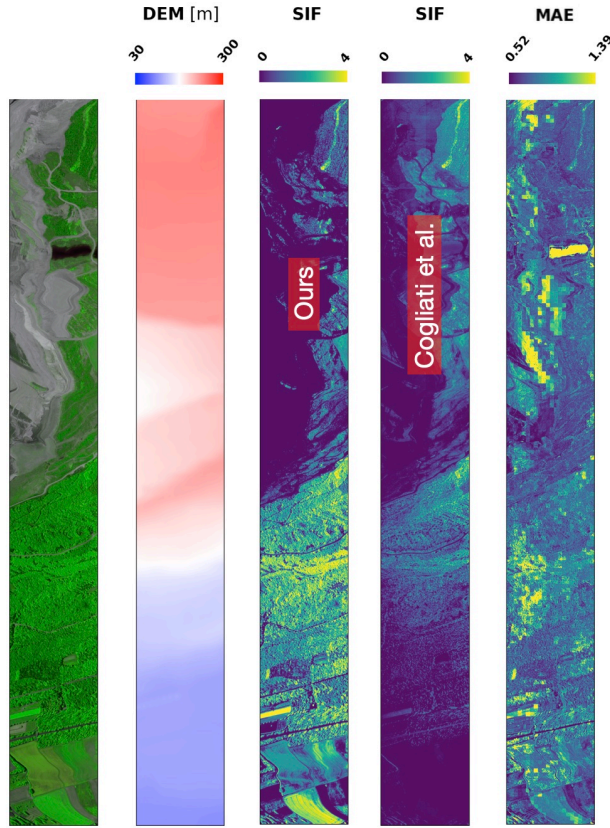


Figure 1: Comparison of SIF prediction of a HyPlant acquisition in hilly terrain (14/06/2022, 09:47 UTC, Jülich DE). Shown are a false color composite of the input data, a DEM warped to sensor geometry, the top-of-canopy SIF prediction following our approach, the top-of-canopy SIF prediction following the Spectral Fitting Method (Cogliati et al. 2019) and the mean absolute error (MAE) of our approach over the fitted HyPlant spectra (left to right). All SIF magnitudes are shown at 761 nm. SIF and MAE are given in units of $\text{mW}/\text{m}^2/\text{sr}/\text{nm}$.

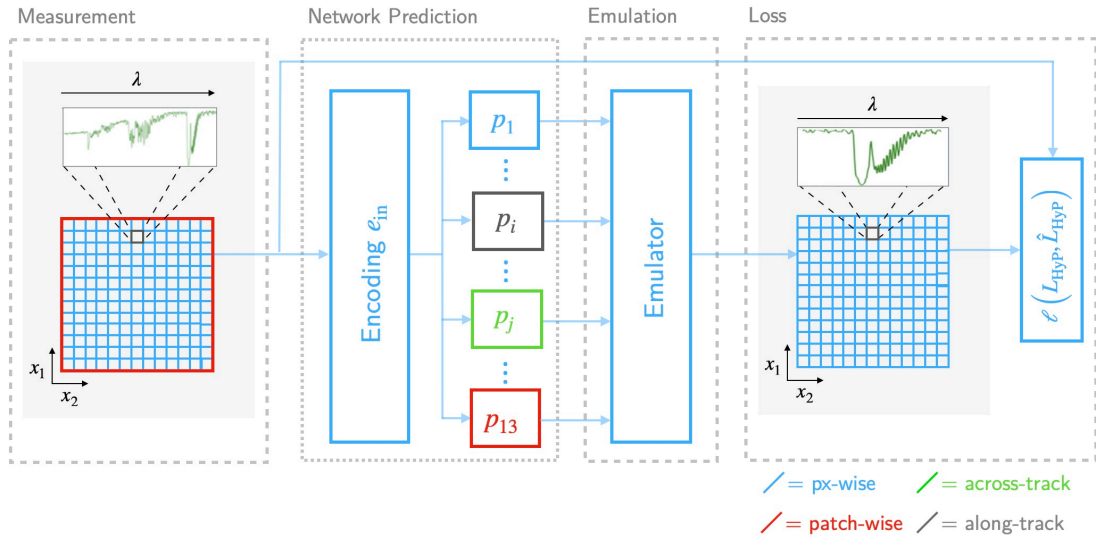


Figure 2: Sketch of the set-up used for training and prediction in this contribution. We provide patches of HyPlant acquisition in sensor geometry, encode it and pass the encoding to submodules p_k predicting physical values for all 13 parameters used in the simulation. Depending on the parameter we estimate a value for each pixel, for a single along-track or across-track position, or a single value for the whole patch. The estimated parameters are then passed to the emulator which provides us simulated HyPlant at-sensor radiance in the range 740 - 780 nm. The fluorescence per pixel is derived from the estimated parameterization.

MIDNIGHTS – Monitoring Instrument Detecting NIGHT Spectra: a low-cost system for validation and calibration of SIF retrievals

Troy Magney¹, Logan Brissette¹, Devin McHugh¹, Christopher YS Wong¹

¹ University of California, Davis, USA

Keywords (5): Solar-induced fluorescence, instrument development, calibration, plant ecophysiology, remote sensing

Challenge

Chlorophyll fluorescence measured at the leaf scale through pulse amplitude modulation (PAM) has provided valuable insight into photosynthesis. At the canopy- and satellite-scale, solar-induced fluorescence (SIF) provides a method to estimate the photosynthetic activity of plants across spatiotemporal scales. However, retrieving SIF signal remotely requires instruments with high spectral resolution, making it difficult and often expensive to measure canopy-level steady-state chlorophyll fluorescence under natural sunlight. Beyond this, careful consideration of what the SIF signal represents mechanistically must be considered as SIF is currently only measured during the day and therefore offers information on the plant status encompassing both dynamic and sustained processes. Recent advances have demonstrated the potential for inducing nighttime chlorophyll fluorescence via LED light sources at the canopy-scale, which can be retrieved as LED-induced chlorophyll fluorescence (LEDIF), potentially serving as a baseline indicator of plant health and photochemical capacity, independent of daytime conditions.

Methodology

We built a novel low-cost photodiode system that retrieves far-red chlorophyll fluorescence emission from a far-red photodiode induced by a blue light emitting diode (LED) light-source, for two hours at night, above the canopy (Monitoring Instrument Detecting NIGHT Spectra (MIDNIGHTS), Fig. 1). Our objective was to determine if an active remote sensing based nighttime photodiode method could track changes in canopy-scale LED-induced chlorophyll fluorescence (LEDIF) during an imposed drought in a controlled environment, and from a vineyard during the growing season. For comparison, far-red LEDIF (720 - 740 nm) was retrieved using both low-cost photodiodes (LEDIF_{photodiode}) and a hyperspectral instrument (LEDIF_{hyperspectral}) at night. For the controlled experiment, to link the LEDIF signal with physiological drought response, we tracked stomatal conductance (gsw) using a porometer as an indicator of plant water status, two leaf-level vegetation indices — photochemical reflectance index, PRI; normalized difference vegetation index, NDVI— to represent xanthophyll and chlorophyll pigment dynamics, respectively, and a pulse-amplitude modulation (PAM) device to measure photochemical and non-photochemical dynamics of photochemistry. For the vineyard study, we used blue LEDs to induce canopy chlorophyll fluorescence emissions and retrieved LEDIF using both LEDIF_{hyperspectral} and LEDIF_{photodiode} approaches, paired with Quantum sensors located 0.9 m above a grapevine canopy. In combination with eddy covariance estimates of GPP and a tower-based remote sensing system for SIF retrieval, our objectives are to a) explore how chlorophyll fluorescence spectra changes (red and far-red magnitude and R:FR), and b) evaluate the performance of the two LEDIF retrievals for tracking the phenology of GPP and SIF in a vineyard from late July to October.

Results

In the controlled environment study, our results demonstrate a similar performance between the photodiode and hyperspectral retrievals of LEDIF ($R^2=0.77$). Furthermore, LEDIF_{photodiode} closely tracked

drought responses with photochemical quenching ($R^2=0.69$), Fv/Fm ($R^2=0.59$), and leaf-level PRI ($R^2= 0.59$). From this study, we determined the low-cost LEDIF_{photodiode} approach has the potential to be a meaningful indicator of photosynthetic activity at spatial scales greater than an individual leaf and over time. Following these results, we deployed MIDNIGHTS at a vineyard site in Central California and found LEDIF retrieved by the hyperspectral sensor demonstrated strong correlations with daytime SIF and gross primary productivity (GPP) during mid to end of season phenology ($R^2 > 0.70$). We highlight that the photodiode sensors performed worse due to poor sensitivity of the small chlorophyll fluorescence signal (weaker signal-to-noise ratio). Therefore, we suggest further optimization with longer sensor integration times, more powerful blue LED light source albeit with careful consideration of optimal light intensity, or closer sensor to canopy distance. The hyperspectral LEDIF retrieval, which optimized signal-to-noise ratio, demonstrated its ability to track decreasing chlorophyll fluorescence which correlated with midday SIF and GPP. Beyond phenology, the spectral shape of Chl fluorescence at night highlights the red:far-red SIF ratio and its ability to track chlorophyll concentration over time. Thus, LEDIF offers a technique to monitor changes in chlorophyll content, and likely potential photosynthetic capacity uninhibited by instantaneous conditions such as PAR that would impact SIF dynamics.

Outlook for the future

Monitoring the baseline health status of plants is difficult because of their dynamic responses to the environment over the course of a day to sunlight, temperature, and water availability. Measuring plants at night may offers an alternative method to assess a plant's baseline health status. Here we use blue LED lights at night to induce the light re-emission of lights from leaves via a red-far-red chlorophyll fluorescence signal detected by a low-cost system. We found that this signal closely tracks the seasonal variation of photosynthesis and imposed stress. Because this signal was measured at night, unconfounded by daytime variation of sunlight, temperature, and water availability, our low-cost system offers an approach to assess a plants photosynthetic capacity and baseline health. This method could serve as a baseline indicator to be used for comparison with SIF measurements and standardized across field sites making continuous SIF measurements. Overall, LEDIF offers a technique to monitor night-time chlorophyll fluorescence emissions (and changes in its spectral shape with a hyperspectral sensor) to assess the phenology of canopy-scale photosynthetic potential.

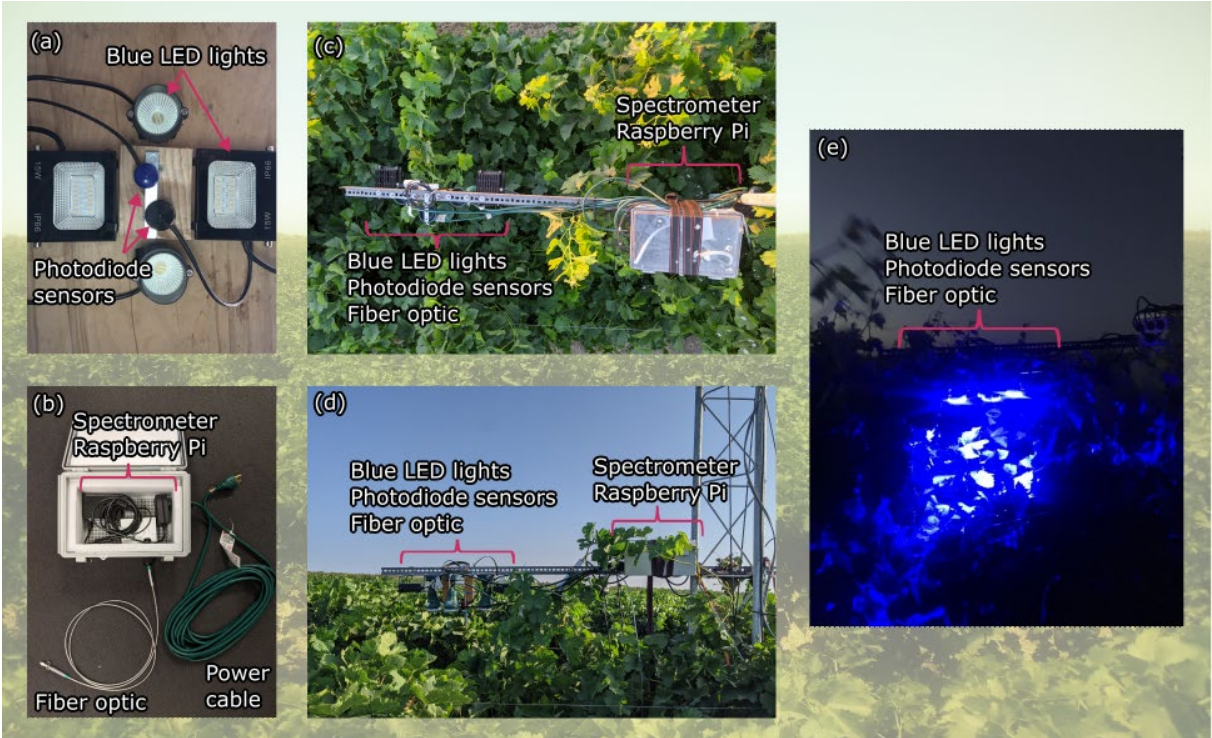


Figure 1. Pictures detailing the MIDNIGHTS (Monitoring Instrument Detecting NIGHT Spectra) LEDIF system. (a) shows the blue LED light and sensor system (note that this picture does not show the fiber optic, and an additional blue LED light was added prior to field deployment); (b) shows the weatherproof case enclosing the hyperspectral spectrometer, Raspberry Pi and extending fiber optic and power cable; (c) shows an overhead view; (d) shows a side view; and (e) shows a side view of the MIDNIGHTS system at night with the blue LEDs on.

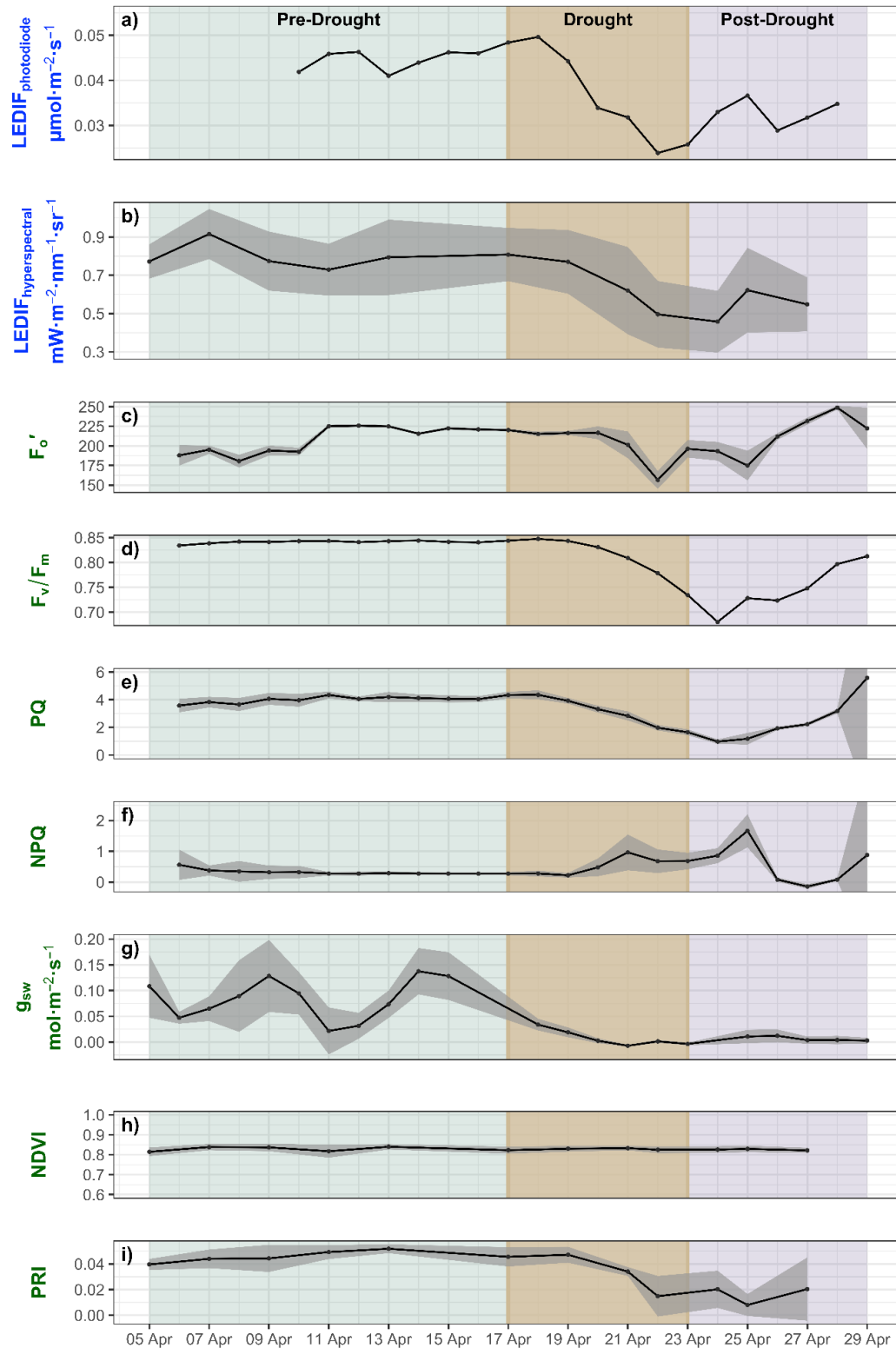


Figure 2. Distinct periods throughout the study are indicated by distinct colors: green indicates pre-drought, brown indicates experimentally imposed drought, and purple indicates post-drought. Blue text refers to canopy-level

measurements, green text refers to leaf-level measurements. Note that not all measurements have the same y-axis scale. (a) shows the continuous low-cost broadband photodiode sensor LEDIF data, and (b) shows the hyperspectral spectroradiometer LEDIF data. (c)-(f) shows time-series of leaf-level parameters collected from the MONI-PAM instrument. (g) shows the stomatal conductance at leaf level from the LI-600 porometer. (h)-(i) shows time-series of calculated leaf-level vegetation indices (NDVI and PRI). For canopy-level: grey shaded regions indicate the standard deviation between the four scans taken on each sampling day. For leaf-level: grey shaded regions indicate the standard deviation between the twelve leaves scanned on each sampling day.

Solar-induced Chlorophyll Fluorescence Efficiency Estimated with Radiative Transfer Modelling and Airborne Diurnal Measurements in Barley

EARSeL Valencia 2024

Abstract

Corresponding Author: j.bendig@fz-juelich.de

Juliane Bendig^{1,3,4}, Zbyněk Malenovský^{2,3}, Bastian Siegmann¹, Julie Krämer¹, Uwe Rascher¹

¹ RESEARCH CENTRE JUELICH, INSTITUTE FOR BIO&GEOSCIENCES (IBG-2), GERMANY

² UNIVERSITY OF BONN, INSTITUTE OF GEOGRAPHY, GERMANY

³ UNIVERSITY OF TASMANIA, SCHOOL OF GEOGRAPHY, PLANNING, AND SPATIAL SCIENCES, AUSTRALIA

⁴ CENTRE D'ETUDES SPATIALES DE LA BIOSPHERE, FRANCE

Keywords (5): SIF escape probability, discrete anisotropic radiative transfer, NIRv, FCVI, UAV, HyPlant

Challenge

Solar-induced chlorophyll fluorescence (SIF) has potential to become an effective remote sensing vegetation productivity and stress indicator. A challenge on the way to this goal are strong impacts by vegetation structure and changes in solar illumination geometry on its measurements. Therefore, standardisation approaches limiting these factors have been developed for SIF measured at 760 nm (F760). This work is testing the fluorescence correction capabilities of the vegetation index FCVI (Yang et al. 2020, *Remote Sens. Environ.*, 240) and the near infrared vegetation indices for hyperspectral data NIRv and NIRvH1/H2 (Zheng et al. 2021, *Remote Sens. Environ.*, 267). The first objective was to systematically assess the performance of both approaches in the discrete anisotropic radiative transfer model (DART). The second objective was to test their practical applicability for interpreting data from two technically different sensors - an imaging and a point-measuring spectrometers.

Methodology

A diurnal SIF dataset was collected in a barley phenotyping experiment in Germany on 29 June 2018 (50°37'25.30"N, 6°59'14.06"E, altitude 225 m). The experiment consisted of various genotypes, which were in late fruit development or early ripening stage, triggered by the 2018 summer heat wave in Europe. SIF data was acquired between 11:30 and 17:00 local time within six aircraft imaging spectrometer and four uncrewed aerial vehicle (UAV) point spectrometer flights. Measured leaf area index (LAI), leaf water and dry matter content, leaf chlorophyll a+b content (modelled), photosynthetically active radiation (PAR), and soil spectra were used to parameterise the canopy radiative transfer model DART. In the model, combinations of LAI, leaf angle distributions, leaf optical properties, including variations in joint photosystem I and II quantum efficiency (FQE), were simulated over realistic soil background. The performance of FCVI and NIRvH1/H2 F760 emission efficiency (ϵ_F) was evaluated against the modelled leaf F760 ϵ_F directly, and as the relative error, computed between leaf F760 leaf ϵ_F and FCVI and NIRvH1/H2 ϵ_F , respectively. FCVI and NIRvH1/H2 ϵ_F were also computed for the measured aerial data of selected experiment plots. For the cross-comparison, spatial matching of nine experiment barley plots, observed with the UAV spectrometer, was ensured by spatially aggregating the HyPlant imaging spectroscopy pixels.

Results

In the DART simulated data, top of canopy (TOC) F760 emissions increased with LAI from ~0 to 14 $\text{mWm}^{-2}\text{nm}^{-1}\text{sr}^{-1}$, while reaching $>20 \text{mWm}^{-2}\text{nm}^{-1}\text{sr}^{-1}$ on the leaf level. Slope and offset in the linear relationship

between leaf F760 and TOC F760 were driven by leaf angle, with planophile leaf angles exhibiting higher canopy F760 than spherical and erectophile leaf angle distributions. TOC F760 for a canopy with LAI ≥ 2 was 50% lower than leaf F760. Similarly, the apparent PAR of green vegetation is about 50% lower than total PAR for LAI < 2 . TOC FCVI ϵ_F had higher overall root mean square error (RMSE) ($1.83 \text{ nm}^{-1}10^{-5}$) than TOC NIRvH1 ϵ_F (RMSE $0.55 \text{ nm}^{-1}10^{-5}$), which was performing better than NIRv ϵ_F and NIRvH2 ϵ_F . The relative error was used to define cases, where applying normalisation approaches leads to a high uncertainty in ϵ_F . We found that FCVI < 0.28 produces up to 100% relative error, while for NIRvH1 the threshold is < 0.25 , with planophile canopies producing the highest errors. Both, FCVI and NIRvH1, were computed for the aerial data measured from UAV and by HyPlant, showing very high agreement between both approaches (R^2 0.93, RMSE $0.52 \text{ nm}^{-1}10^{-5}$). In the diurnal trend, FCVI and NIRvH1 revealed clearly higher F760 afternoon efficiency than in TOC F760.

Outlook for the future

FCVI is easy to compute and reliably corrects for solar irradiation and canopy structure when LAI > 2 . NIRvH1 (and NIRv, NIRvH2) are more robust for canopies with LAI < 2 and match leaf ϵ_F more closely, but its calculation requires more inputs. When applied to aerial imaging spectroscopy data and a point spectrometer, both approaches produced comparable results for barley varieties in late growth stages (LAI 1.8-9.5). This study investigated standardization of F760 only. In the future, we expect that robust F687 ϵ_F methods will also become available and can be compared to a direct retrieval of fluorescence quantum efficiency, obtained through downscaling approaches estimating emitted fluorescence from the photosystems.

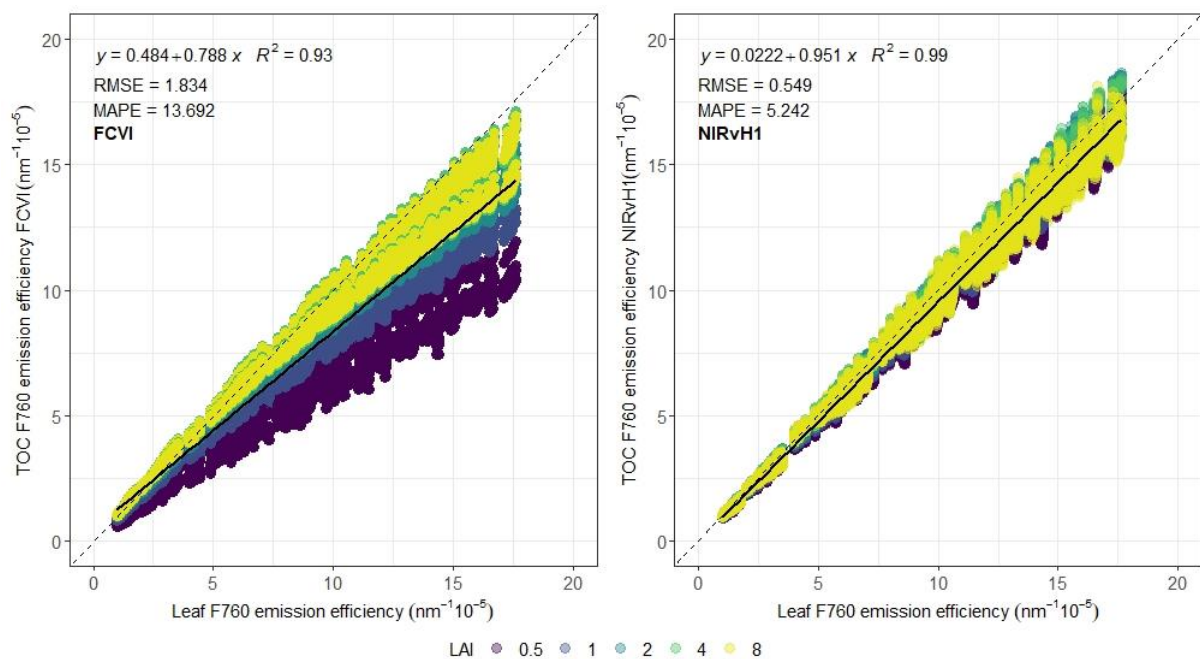


Figure 1 Comparison of DART modelled top of canopy (TOC) F760 efficiency calculated with FCVI or NIRvH1 against Leaf F60 emission efficiency, coloured by LAI 0.5-8. The dashed line indicates the 1:1 line, the black line is the combined regression line for all LAI, and R^2 indicates the coefficient of determination, root mean square error is RMSE and mean absolute percent error is MAPE respectively (Bendig et al, in prep.).

A novel approach to retrieve canopy evapotranspiration from hyperspectral reflectance and solar-induced fluorescence data

Bastian Siegmann^{1,2}, Egor Prikaziuk², Oscar Hartogensis³, Mary Rose Mangan³, Jim Buffat¹, Julie Krämer¹, Juan Quiros Vargas¹, Juliane Bendig¹, Patrick Rademske¹, Uwe Rascher¹ and Christiaan van der Tol²

¹ Forschungszentrum Jülich, Institute for Bio- and Geosciences, IBG-2: Plant Science, Germany

² University of Twente, Faculty of Geo-Information Science and Earth Observation (ITC), The Netherlands

³ Wageningen University and Research, Department of Environmental Sciences, The Netherlands

Keywords (5): Latent heat flux, solar-induced fluorescence, evapotranspiration, hyperspectral remote sensing, airborne data, SCOPE, machine-learning regression, emulation

Challenge (800 - 1000 characters incl. spaces)

The increase in extreme weather events has a strong impact on the exchange of water and energy in agricultural ecosystems. Evapotranspiration (ET), as a hydrological key variable, is an important component of the energy, water and carbon cycles and provides vital information to forecast and monitor drought events. ET retrieval methods can be divided into two main groups: i) surface energy balance residual and ii) meteorologically-based methods. Methods from the latter group can be combined with remote sensing (RS) observations to provide spatial ET estimates. Since RS-based solar-induced fluorescence (SIF) is a proxy of photosynthesis (PS) and due to the fact that transpiration and PS are coupled processes, different approaches have been developed that make use of SIF information to estimate ET. In this study, we want to explore the potential of the SCOPE model combined with a regression technique to improve ET estimates of an agricultural field from airborne reflectance and SIF data.

Methodology (1200 – 1500 characters incl. spaces)

A time-series consisting of seven airborne SIF and reflectance data sets of an alfalfa field in Spain was recorded by the HyPlant airborne imager from 15 to 27 July 2021. First, 3000 reflectance simulations were generated with the radiative transfer model (RTM) for incident radiation from the sun and the sky implemented as one module in SCOPE. Subsequently, a hybrid inversion scheme was applied that combines the SCOPE simulations with kernel-ridge regression (KRR) to retrieve leaf and canopy parameters from the airborne reflectance data. The inverted parameters for each pixel and meteorological data from a weather station (e.g., air pressure) were then used to run the full SCOPE model in forward mode to produce spatial estimates of ET expressed as latent heat from the reflectance data (LE_{SCOPE}). Second, all input variables of the SCOPE simulations from the previous step, extended by the corresponding simulation outputs SIF₇₆₀, and fraction of absorbed photosynthetically active radiation by chlorophyll (fAPAR_{chl}), were used to build a SCOPE emulator using again KRR to predict the target variable LE. Finally, this KRR model was applied to the airborne SIF and reflectance data, combined with the

meteorological observations, to produce another latent heat flux prediction including SIF and $fAPAR_{chl}$ (LE_{EMU}). Both LE estimates were finally compared to LE derived from instantaneous flux measurements of an eddy-covariance station derived at the time of the aircraft overflights (LE_{EC}).

Results (1200 – 1500 characters incl. spaces)

The inversion of the SCOPE model in the first step led to a good match between the spatial estimates of leaf area index (LAI) and leaf chlorophyll content (LCC) with field measurements of the same parameters (LAI: $R^2 = 0.86$, $RMSE = 0.62 \text{ m}^2 \text{ m}^{-2}$, LCC: $R^2 = 0.69$, $RMSE = 11.37 \mu\text{g cm}^{-2}$). Furthermore, the comparison of the averaged simulated and measured reflectance and SIF_{760} values within the footprints of the EC station provided a high level of agreement (reflectance.: $RMSE = 0.0222$, SIF_{760} : $RMSE = 0.26 \text{ mW m}^{-2} \text{ nm}^{-1} \text{ sr}^{-1}$), which was a prerequisite for including SIF_{760} in the prediction of LE as it was done in step 2. Figure 1 shows the scatterplots of the two spatial LE predictions from HyPlant compared to the LE reference data derived from the EC station. The LE_{SCOPE} model provides a high R^2 of 0.96, but the derived latent heat flux from the airborne data, especially for the later observations, shows a distinct underestimation compared to the LE_{EC} estimates. Although the LE_{EMU} model is characterized by a slightly lower R^2 , the slope of the regression line is distinctly higher, the RMSE is lower and the regression line shows a better agreement with the 1:1 line. Figure 2 shows a RGB composite of the investigated alfalfa field recorded on 22 July and the corresponding SIF_{760} and $fAPAR_{chl}$ maps as well as the LE_{EMU} map derived with the developed SCOPE emulator.

Outlook for the future (800 - 1000 characters incl. spaces)

The results of this study illustrate that additional RS-based information about SIF_{760} and $fAPAR_{chl}$ can help to improve spatial estimates of LE. This is especially important for the early detection of drought events and to develop adapted irrigation strategies in agriculture. In future research, the presented method will be transferred to other crops and different climatic regions to investigate the full potential of the developed emulator. We also plan to compare our results to spatial estimates produced with standard RS-based methods to predict LE. In addition, the development of a SIF-based LE product could be of great interest for ESA's Fluorescence EXplorer (FLEX) satellite mission, as ESA will only deliver products up to level 2C and encourages the scientific community to develop innovative level 3 and 4 products. Although further research is needed, we are convinced that the presented method has the potential to become such an innovative level 3 product derived from FLEX data.

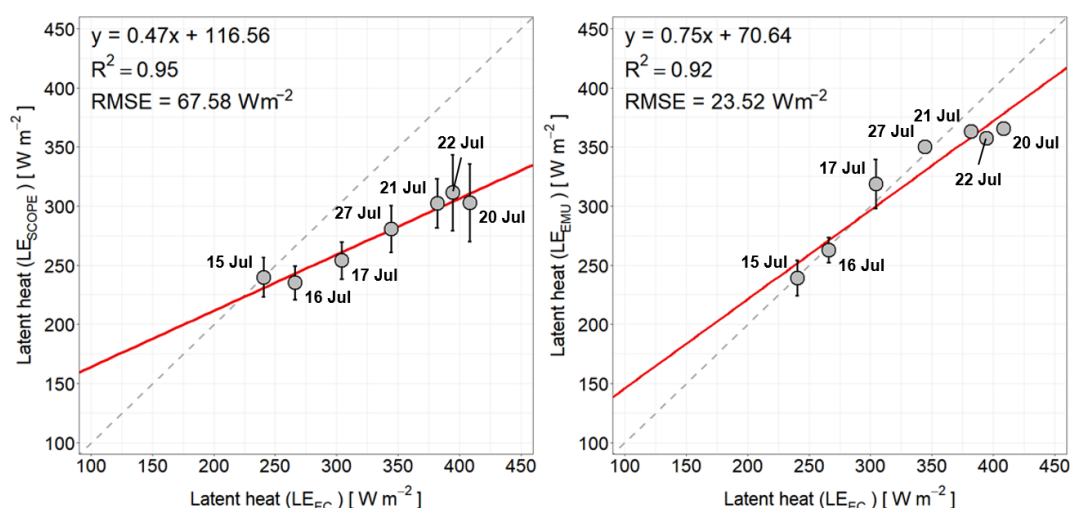


Figure 1 Scatterplot of latent heat derived from eddy-covariance measurements (LE_{EC}) (reference) in comparison to latent heat simulated with SCOPE (LE_{SCOPE}) (left) as well as derived from a SCOPE emulator extended by SIF_{760} and $fAPAR_{chl}$ as additional input parameters (LE_{EMU}) (right). The grey dots represent the LE_{EC} estimates and the corresponding averaged LE_{SCOPE} and LE_{EMU} estimates within the footprint of the eddy covariance measurement at the

time points of the airborne data acquisition. The red line illustrates the regression line, while the grey dashed line represents the 1:1 line.

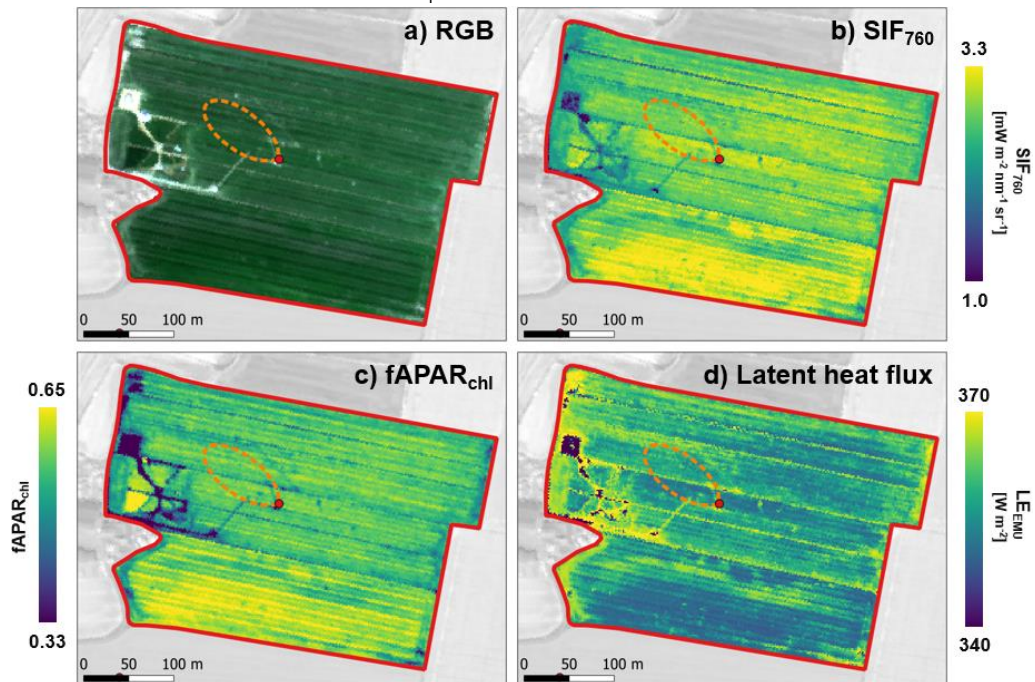


Figure 2 Maps of the investigated alfalfa field in the north-east of Spain recorded on 22 July 2021. RGB composite of the field (a), SIF₇₆₀ map (b), fAPAR_{chl} map (c) and LE map (d). The red dot shows the location of the EC station in the field and the area delimited by the dashed orange line represents the footprint of the EC measurement at the time of the airborne data acquisition.

Retrieving Sun-Induced Chlorophyll Fluorescence from water bodies using the FLEX mission.

EARSel Valencia 2024

Abstract

Corresponding Author: carolina.tenjo@uv.es

Carolina Tenjo¹, Shari Van Wittenberghe¹, Antonio Ruiz-Verdú¹, Jesús Delegido¹, José Moreno¹
(Style: Authors, presenting author underlined)

¹ Universitat de València
(Style: Affiliations;)

Keywords (5): Water, Fluorescence, FLEX, Level-2, Atmospheric Correction,

Challenge (800 - 1000 characters incl. spaces)

Recently, a new algorithm has been developed to retrieve Sun-Induced Chlorophyll Fluorescence (SICF) signal from water bodies using hyperspectral data (Tenjo, et al, 2021, Remote sensing 13), enhancing the accuracy of SICF compared to other methods such as the Fluorescence Line Height (FLH) method. This work analyses the feasibility of integrating the proposed algorithm into the future FLEX mission, given that the FLEX mission concept is specifically designed for retrieving SICF from terrestrial vegetation.

FLEX consists of a single platform with a hyperspectral FluORescence Imaging Spectrometer (FLORIS). FLORIS has two imaging pushbroom spectrometers, one, acquiring in the 500-780 nm spectral range at 2 nm spectral resolution (FLORIS Low Resolution spectrometer, FLORIS LR) and another acquiring at 0.1 nm in the O2A range and acquiring at 0.3 nm in the O2B range (FLORIS High Resolution spectrometer, FLORIS HR2 and FLORIS HR1 respectively). FLORIS has 300 m of spatial resolution and 150 km of swath covering the land and coastal areas over the Earth.

Methodology (1200 – 1500 characters incl. spaces)

To evaluate the potential of the FLEX mission to retrieve the Sun-Induced Chlorophyll Fluorescence (SICF) signal from aquatic environments, the following approach was taken: 1. Calculation of the Noise Equivalent Delta Radiance (NE Δ L) necessary for detecting SICF emission with a 10% margin of error. This calculation was based on the typical SICF emission of two different water types: (1) ocean and (2) inland/coastal waters, respectively with SICF peak radiance values of approximately 0.22 and 1.0 mW·m⁻²·sr⁻¹·nm⁻¹.

2. Assessment of the impact of instrumental noise on the retrieval of water leaving reflectance by generating two synthetic FLEX images, one corresponding to each water type. This simulation was performed using the FLEX end-to-end mission performance simulator. 3. Testing of a data processing workflow designed for SICF retrieval from the two simulated images assuming an ideal atmospheric correction. The methodology used for this stage adhered to the guidelines provided by Tenjo, et al. (2021, Remote Sensing 13). This approach is based on SICF estimation as the difference between water-leaving reflectance with SICF and water-leaving reflectance without SICF. Since the latter is unknown, it is estimated by normalizing water-leaving reflectance at 780 nm and subsequently performing a spline fitting, which involves estimating three anchor points within the SICF spectral range using machine learning techniques.

Results (1200 – 1500 characters incl. spaces)

The instrumental noises from FLORIS present certain limitations when attempting to perform water leaving reflectance retrieval from ocean waters. However, it provides sufficient signal for achieving reasonably accurate water leaving reflectance retrieval from typical inland and coastal waters. After implementing an ideal atmospheric correction, water leaving reflectance can be obtained with some residual noise. To enhance the accuracy and smoothness of water-leaving reflectance retrieval, advanced methods like the LOESS smoothing technique are employed.

Notably, the most pronounced errors in water-leaving reflectance retrieval are observed within the O2A spectral range. Fortunately, these errors do not significantly affect the application of the proposed SICF retrieval method. However, the residual noise, which amounts to approximately 0.5% at 780 nm, does have an impact on the retrieval process since the method requires water-leaving reflectance normalization at 780 nm. This noise is particularly problematic for Machine Learning methods, which are highly sensitive to such noise levels.

Among the various MLRAs explored, the Kernel Ridge Regression (KRR) method results as the least sensitive to noise, resulting in a SICF peak retrieval with a relative error of around 20% for coastal and inland water types and 50% for oceanic water types.

Outlook for the future (800 - 1000 characters incl. spaces)

Retrieval methods based on Machine Learning methods can significantly improve using more extensive and diverse water leaving reflectance databases. These databases can encompass a wider range of variables, including the content of other pigments. By incorporating a broader and more varied dataset, the models can be better trained, improving their performance and accuracy in the estimation of the three anchor points.

The improvement of this methodology involve addressing the computational aspects, such as optimizing algorithms and exploiting high-performance computing resources, to facilitate the generation of a more robust database and the training of machine learning methods on this expanded dataset. The results of this effort will be the more accurate and reliable retrievals. This represents a challenge for future research, promising advancements in the field of remote sensing and data interpretation.

Potential of the Fluorescence Explorer mission for inland and coastal water science and applications

Alexander Damm^{1,2}, Daniel Odermatt^{1,2}

¹ UNIVERSITY OF ZURICH, DEPARTMENT OF GEOGRAPHY, SWITZERLAND

² EAWAG, SWISS FEDERAL INSTITUTE OF AQUATIC SCIENCE & TECHNOLOGY, SURFACE WATERS – RESEARCH AND MANAGEMENT, SWITZERLAND

Keywords (5): Aquatic ecosystems, gap analysis, atmospheric correction, information retrieval, application development

Challenge

Inland and coastal waters are important ecosystems that offer a wide range of functions and services. Ongoing environmental change and human activities severely threaten these ecosystems. Detailed monitoring of aquatic ecosystems is a prerequisite to assess their state, to investigate their responses to climate change, and to define management and conservation strategies. Remote sensing (RS) based monitoring of inland water and coastal ecosystems is challenged by their complex optical properties and high spatio-temporal dynamics. In addition, no ecosystem-specific satellite mission exists yet, and monitoring relies on existing missions that meet observational needs only partly. The upcoming Fluorescence Explorer (FLEX) imaging spectroscopy mission comes with novel specifications that complement this application potential in a unique way. This contribution aims to conceptually evaluate the potential and complementarity of FLEX to advance aquatic science and applications.

Methodology

A gap analysis will be applied to confront observational needs against FLEX mission characteristics and to assess the capacity of FLEX to advance RS data pre-processing, information retrieval and application development for aquatic ecosystems. A particular focus will be on the evaluation of the spatial and temporal sampling design of FLEX considering the temporal dynamics and spatial extents of aquatic ecosystems. Further, radiometric and spectral characteristics of FLEX are reflected against the specific needs to measure particularly dark inland waters and river ecosystems, and against requirements for a reliable retrieval of biogeophysical data products. The state of the art of atmospheric correction of spectral water-leaving radiance and reflectance measurements will be investigated and possible contributions of FLEX for an advancement of atmospheric correction methods identified. Last, considering the FLEX mission's aim to measure terrestrial photosynthesis, the potential of FLEX measurements for aquatic applications including phytoplankton productivity and diversity are assessed.

Expected results

Various conceptual insights on the use of FLEX mission data for inland and coastal water research and applications are expected. The review of the FLEX spatial and temporal sampling capacity will allow statements on the fraction of global freshwater ecosystems that can potentially be measured, and on contributions to observe relatively slowly changing aquatic properties (e.g. surface water extent) and

relatively quickly changing properties such as water quality and biotic processes (e.g. sediment load, phytoplankton concentration, phytoplankton productivity). The investigation of radiometric (e.g. signal-to-noise ratio) and spectral characteristics (e.g. spectral sampling interval and band width) of FLEX data will enable insight on possibilities to retrieve inherent optical properties and water constituents depending on the optical complexity of waters (e.g. case 1 oceanic waters vs case 2 inland waters) and differences in their reflectance magnitude (e.g. sediment rich bright lakes vs. productive dark lakes). The feasibility of atmospheric correction of FLEX mission data over water surfaces or even its advancement will be discussed in the context of particular complications such as the presence of sun-glint or adjacency effects. A synthesis of above addressed FLEX data characteristics is expected to identify possible application fields of FLEX data, e.g. phytoplankton productivity estimates, harmful algae bloom detection or phytoplankton diversity assessment.

Outlook for the future

The satellite-based capacity to measure and monitor inland and coastal waters is less advanced than required, and there is no dedicated water mission particularly for freshwater ecosystems yet. The results of this gap analysis can guide FLEX mission preparation activities so that the data of this upcoming mission can also be used for the assessment and monitoring of these valuable ecosystems. The approach of this study has potential for an even more extensive gap analysis that confronts requirements for an adequate satellite-based monitoring of inland and coastal water ecosystems against existing observational capacity provided by non-optimized available and upcoming missions. Results of such an analysis could help consolidating sampling requirements and mission objectives for a dedicated space-based water mission.

**Them.Sess. 2-3: Thermal Infrared
(TIR) Remote Sensing Special
Session**

Evaluation of the Daytime corrected AVHRR Land Surface Temperature Time Series

[Philipp Reiners](#)¹, [Stefanie Holzwarth](#)¹, [Claudia Kuenzer](#)^{1,2}

¹ German Aerospace Center (DLR), German Remote Sensing Data Center (DFD), 82234 Wessling, Germany

² University of Wuerzburg, Institute of Geography and Geology, Chair of Remote Sensing, 97074 Würzburg, Germany

Keywords (5): Land Surface Temperature, AVHRR, Climate Change, Global Change, Global Warming

Challenge

For monitoring conditions repeatedly over large areas, satellite derived LST has become an indispensable tool. However, to make climate relevant statements and quantify the impact of land surface variables over long time, we need sensors that are available for more than 30 years. The AVHRR is the only sensor providing spatially and temporally continuous, daily measurements for 40 years. The TIMELINE project of the German Aerospace Center (DLR) aims at the generation of a homogeneous multi-decadal time series from AVHRR data (3 different AVHRR sensors on 16 platforms) over Europe and North Africa (Dech et al., 2021). However, different observation times of the AVHRR sensors affect the observed temperature and therefore the AVHRR LST time series (Reiners et al., 2021). In addition, the orbital drift effect, resulting in a slowly changing observation time during the lifetime of one sensor is influencing the time series. In this study, a new approach for correcting daytime effects in the AVHRR LST time series is presented. This approach is then validated by comparing observations from different AVHRR platforms of the same day and checking the corrected AVHRR LST time series against the CCI LST time series as well as against in situ air temperature observations.

Methodology

To correct the AVHRR LST time series for daytime effects, the LST derived from the AVHRR daytime overpasses is normalized to the observation time of 1 p.m. and the LST from the AVHRR night-time overpasses is normalized to the observation time of 3 a.m. . The normalization is performed via correction terms, which are derived individually for every pixel and time in the time series using information about the daily temperature cycle taken from SERVIRI geostationary LST data (Sismanidis et al., 2020).

For the validation it was assumed, that differences between same-day AVHRR observations only occur due to different daytimes and therefore should be minimized after the correction. To observe the effect of the correction these observations were correlated before and after the correction. Furthermore, the AVHRR LST time series was compared to the ESA CCI L3S daytime and night-time LST product for the years 1996-2018 for selected 1x1° tiles across Europe. After the correction no or minimal trends in the difference between these products should be visible, as the ESA CCI product has a stable observation time (Good et al., 2022). Finally, monthly anomalies of AVHRR LST were correlated with monthly anomalies of air temperature, taken from the EUSTACE station network across Europe (Rayner et al., 2020). Here, the correlation between the two anomalies, as well as the trend of the distance between these variables was analysed.

Results

For the analysis of same day observations in the TIMELINE LST time series more than 1 million data points have been compared for each tile. The analysis showed high improvements due to the daytime correction. Biases of up to 14 K (e.g. between NOAA-12 and NOAA-14) could be reduced to < 1 K for most of the 1x1° tiles. Correlation coefficients could be improved from 0.5 to > 0.9 and mean absolute differences could be improved from >16 K to < 3 K for most of the tiles.

The comparison between uncorrected daytime TIMELINE and CCI LST showed high drift effects for NOAA-14 between 1996 and 2002 and minor drift effects for NOAA-17 between 2008 and 2010 and NOAA-19 from 2016. Figure 1 shows that these trends were minimized after daytime correction for one example tile over Spain. The remaining trends were for most files < 0.3 K per decade meeting the threshold requirements for satellite-derived LST climate data records defined by the CEOS Land Product Validation Group. It has to be noticed, that the remaining trend can either be due to inconsistencies in the TIMELINE LST product or due to uncertainties within the CCI LST product. The high bias of TIMELINE LST towards CCI LST can be explained by the fact, that TIMELINE LST was normalized to 13h observation time, while CCI LST refers to 10.30h observation time.

The comparison of corrected TIMELINE LST and air temperature anomalies showed high correlations (> 0.8) for more than 100 stations across Europe. However, at most of the stations, as e.g. for SZEGET (Figure 2), LST showed higher trends than air temperature, which can be explained by different responses to climate change of these two variables.

Outlook for the future

The presented daytime correction approach visibly improved the consistency of the TIMELINE LST time series. The pixel-wise available information derived from the geostationary data allows an accurate and efficient daytime correction for the whole 40-year time series for large parts of Europe.

The comparison with CCI LST and air temperature data still showed low trends in the differences, which can be attributed to sensor transitions in the TIMELINE LST time series. These trends should be investigated to further improve this dataset. However, this dataset with its unique temporal coverage and resolution (40 years, daily +) enables numerous studies regarding land atmosphere interactions and climate and global change.

Resources

Dech S, Holzwarth S, Asam S, Andresen T, Bachmann M, Boettcher M, u. a. Potential and Challenges of Harmonizing 40 Years of AVHRR Data: The TIMELINE Experience. *Remote Sensing*. 10. September 2021;13(18):3618.

Good, E.J.; Aldred, F.M.; Ghent, D.J.; Veal, K.L.; Jimenez, C. An Analysis of the Stability and Trends in the LST_cci Land Surface Temperature Datasets Over Europe. *Earth Space Sci.* 2022, 9, e2022EA002317. <https://doi.org/10.1029/2022ea002317>

Rayner, N. A., R. Auchmann, J. Bessembinder, S., Brönnimann, Y. Brugnara, F. Capponi, L., Carrea, E. M. A. Dodd, D. Ghent, E. Good, J., L. Høyer, J. J. Kennedy, E. C. Kent, R. E., Killick, P. van der Linden, F., Lindgren, K. S., Madsen, C. J. Merchant, J. R. Mitchelson, C., P. Morice, P. Nielsen-Englyst, P. F. Ortiz, J., J. Remedios, G. van der Schrier, A. A., Squintu, A. Stephens, P. W. Thorne, R. T., Tonboe, T. Trent, K. L. Veal, A. M., Waterfall, K. Winfield, J. Winn & R. I., Woolway (2020) The EUSTACE Project: Delivering Global, Daily Information on Surface Air Temperature. *Bulletin of the American Meteorological Society*, 101, E1924-E1947.

Reiners P, Asam S, Frey C, Holzwarth S, Bachmann M, Sobrino J, u. a. Validation of AVHRR Land Surface Temperature with MODIS and In Situ LST—A TIMELINE Thematic Processor. *Remote Sensing*. 1. September 2021;13(17):3473.

Sismanidis P, Bechtel B, Keramitsoglou I, Götsche F, Kiranoudis CT, Satellite-derived quantification of the diurnal and annual dynamics of land surface temperature, *Remote Sensing of Environment*, Volume 265, 2021, 112642, <https://doi.org/10.1016/j.rse.2021.112642>.

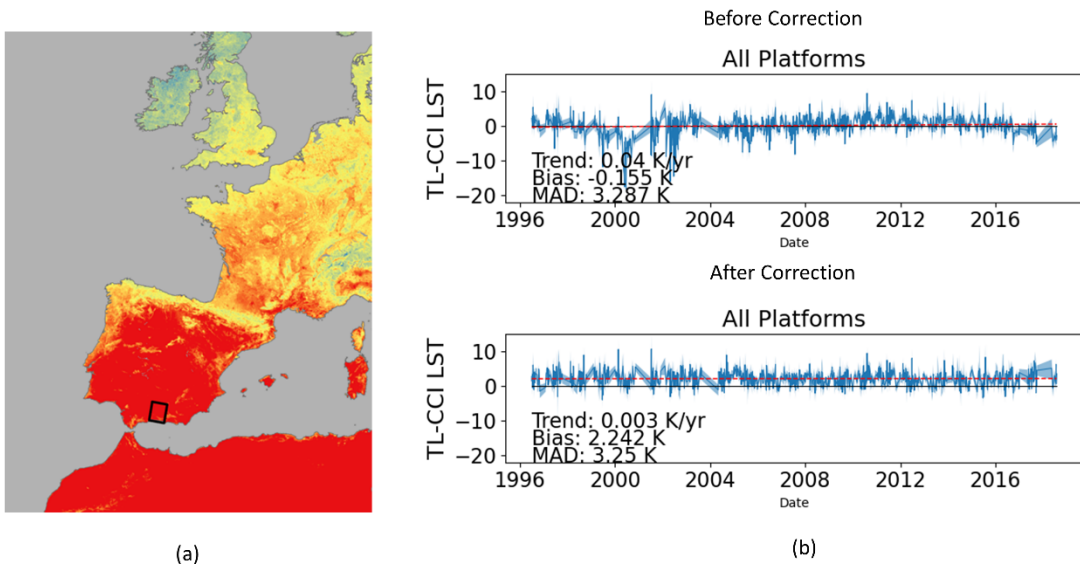


Figure 1 (a) Location of a 1x1° tile in Spain used for the comparison between TIMELINE and CCI LST (b) Difference between TIMELINE and CCI LST before and after the daytime correction

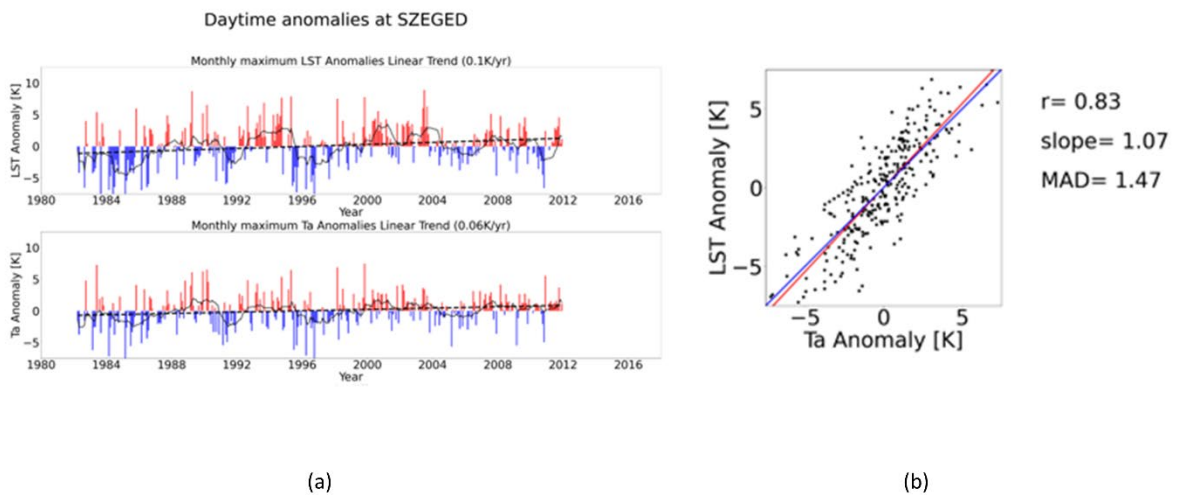


Figure 2 (a) Monthly anomalies of daytime corrected TIMELINE LST (up) and air temperature (bottom) at Szegeged station located in Hungary (b) Correlation between these variables at the same station

Comparing Forest Species Emissivity Using Airborne Thermal Infrared Hyperspectral data in a Mixed Temperate Forest

Hillary Korir, [Elnaz Neinavaz](#), Roshanak Darvishzadeh, Andrew K. Skidmore

¹ University of Twente, Department of Natural Resource, The Netherlands

² University of Twente, Department of Natural Resource, The Netherlands

³ University of Twente, Department of Natural Resource, The Netherlands

⁴ University of Twente, Department of Natural Resource, The Netherlands

Keywords (5): TIR, Airborne, Canopy emissivity, Hyperspectral, Mann-Whitney U test, Land cover

Challenge

The need to identify and remotely speciate different vegetation classes in mixed forest environments continues to be an important area for ecosystem conservation and management purposes. Such applications generally rely on the biochemical and biophysical properties found in the VNIR (0.3–1.0 μm) and SWIR (1.0–2.5 μm) regions. Nevertheless, foliar spectral behaviour in the TIR (8–14 μm) domain has significant interspecies variability that has been shown to correlate with the spectral features of key plant constituents. Different plant species have been successfully discriminated in the laboratory using leaf emissivity spectra. However, given the complexity of emissivity at the canopy level, species discrimination using canopy emissivity spectra obtained from airborne TIR remains unexplored. This study aims to compare the differences in the canopy emissivity spectra obtained from the airborne TIR hyperspectral data among and between various vegetation covers in a mixed temperate forest.

Methodology

The vegetation classes were investigated using airborne TIR hyperspectral images captured using AISA Owl thermal hyperspectral sensors during a flight campaign under clear skies in Bavaria Forest National Park in south-eastern Germany. Thermal infrared data pre-processing steps, including radiance calibration, radiometric and geometric correction and data masking, were performed prior to the separation of land surface temperature from canopy emissivity. Canopy emissivity spectral measurements were then extracted based on the locations of tree species as recorded during the EUFAR and BIOSPACE fieldwork projects. For analysis, the pairwise Mann-Whitney U test was used to assess whether different vegetation cover types (e.g., spruce, beech and fir) exhibit both inter and intra-species statistical differences by means of their canopy emissivity spectra. Furthermore, multiple Mann-Whitney U test comparing the emissivity spectra of species at each of the 102 spectral channels was done to determine the specific wavelengths in which species could be distinguished. Subsequently, the level of species separability in the hyperspectral space was quantified based on the Jeffries-Matusita and Bhattacharya distance measures.

Expected results

The research showed the presence of intra and interspecies canopy emissivity variation. The differences in canopy emissivity between beech and spruce ($U = 2541872$, $p\text{-value} = 0.001$) as well as between beech

and fir ($U = 774369$, $p\text{-value} = 0.003$) were statistically significant. While the differences in canopy emissivity between spruce and fir ($U = 617202$, $p\text{-value} = 0.672$) were not statistically significant. Comparing the spectral emissivity variability within species, the results of this study demonstrate that the spectral emissivity responses vary among beech and spruce tree species growing in different locations. The differences in canopy emissivity were statistically different for 4 out of 23 beech trees and 6 out of 20 spruce trees, which all had high leaf area index (LAI) values. As previously suggested, the differences in biophysical properties, specifically LAI, influenced spectral emissivity variability within species. Additionally, the MWU test specifically identified nine wavelength locations: 9.71 μm , 10.06 μm , 10.11 μm , 10.16 μm , 10.70 μm , 11.55 μm , 11.60 μm , 11.89 μm and 11.90 μm as able to distinguish at least one species. Finally, the spectral separability showed that the results showed that while the species are not entirely separable, the spectral pair of spruce and beech were more discriminable in the hyperspectral space than either pair of fir and spruce or spruce and beech.

Outlook for the future

Firstly, this study demonstrated that the AISA Owl TIR hyperspectral sensor is suitable for data acquisition from materials with prominent spectral features, such as gases and geologic samples, but is also feasible for acquiring information from materials with very subtle spectral signatures, such as vegetation. Nevertheless, future projects may need to consider other TIR sensors with finer specifications to obtain better spectral emissivity contrast. Secondly, this study predominantly used the Mann-Whiney U test because of the uneven sample size. However, its statistical power can be diminished with increasing uneven sample groups. Therefore, future projects may explore other statistical tests, such as the analysis of variance tests with quadratic discriminant analysis, to avoid the limitations of pairwise analysis. Finally, analysing other factors, such as vegetation dryness, tree age, and soil, that impact inter and intra-species spectral variation would improve this study.

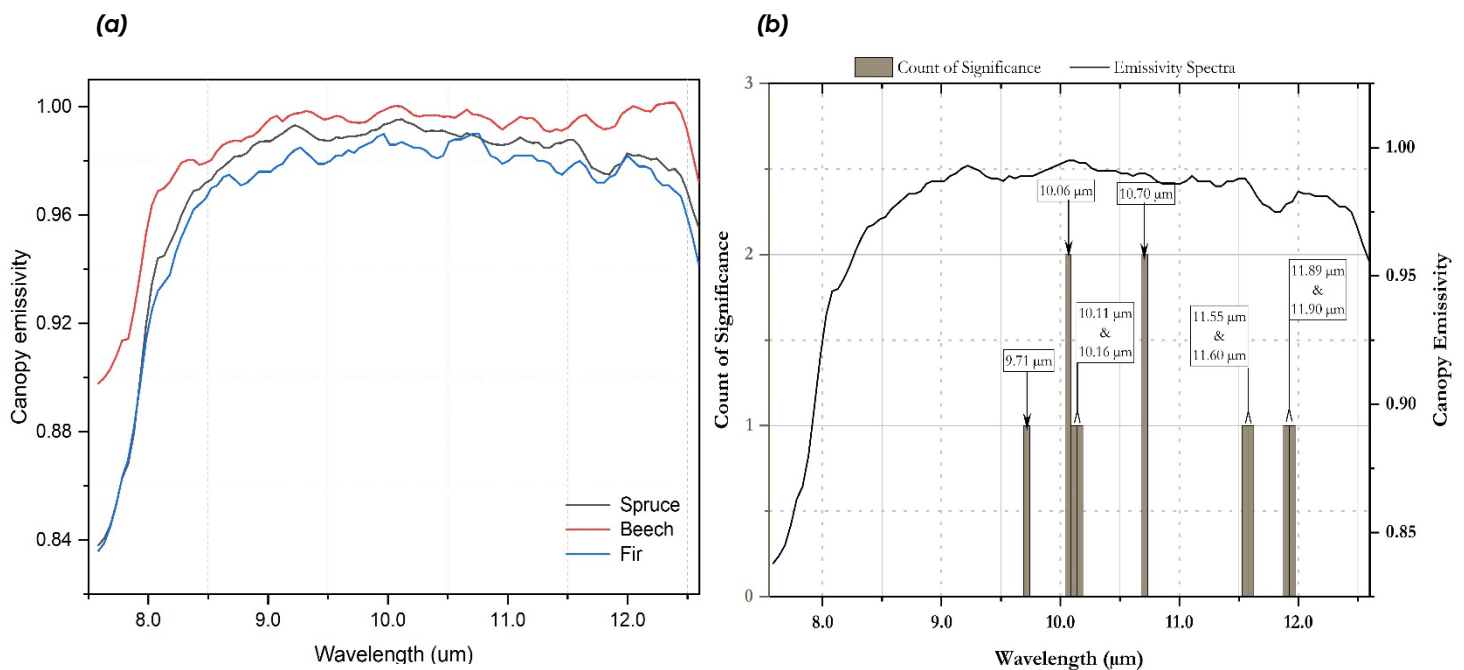


Figure (a) Canopy emissivity spectra plots for spruce, beech and fir against wavelengths. The colour black represents spruce, the colour red represents beech, and the colour blue represents fir; (b) Frequency plot of statistically significant differences between tree species: beech, spruce and fir. Prominent wavelength locations are identified and labelled. Alongside, a typical emissivity spectra is plotted to show the wavebands.

Hyperspectral Soil Property Mapping Using Thermal Infrared (LWIR) Imagery

EARSeL Valencia 2024

Abstract

Corresponding Author: Helge Daempfling
[hdaemp@gfz-potsdam.de]

Helge L. C. Daempfling^{1,2}, Robert Milewski¹, Sabine Chabrillat^{1,2}

¹ German Research Centre for Geosciences Potsdam, Section Remote Sensing and Geoinformatics, Germany

² Leibniz University Hannover, Institute of Soil Science, Germany

KEYWORDS (5): SOIL PROPERTIES, HYPERSPECTRAL, THERMAL (LWIR), LABORATORY, AIRBORNE

Challenge

To address food security and climate change challenges, the European Commission and the MOSES project advocate soil quality mapping and monitoring. Our soils, the largest terrestrial carbon reservoir, are vital to the health of our ecosystems. The use of advanced thermal hyperspectral sensors was investigated in order to evaluate the properties of topsoil. The objective of this work is to establish reference databases and validate airborne applications for soil property estimation using these sensors in a laboratory setting. As part of our study, we combined field measurements of bare soil pixels with lab measurements and chemical analysis of various soil samples. A workflow from on-site and lab measurements to airborne measurements was developed using samples from global study sites, including Greece and Italy. In the LWIR thermal infrared region, properties of soil such as quartz and feldspar can be detected that are not detectable in the VNIR and SWIR regions. With this approach, we are able to extend our existing VNIR and SWIR spectral analysis methods to thermal (LWIR) analysis of soils.

Methodology

Our study sites are located in Northern Greece (Western Macedonia) in the intensively agricultural used areas around the Amyntaio lignite mine. More than 250 soil samples were collected in several field campaigns 2018-2023 covering the highly variable soils of the region. In 2019 an airborne survey acquired a hyperspectral dataset with the HySpex (VNIR+SWIR), and Hyper-Cam (LWIR) hyperspectral imaging systems covering the study site. We established a workflow for on-site soil sampling, temperature, and emissivity measurements using an Agilent handheld FTIR system, and automated temperature loggers buried close to the soil surface. In the laboratory environment, we tested hyperspectral thermal measurements using pre heated samples and a heating plate setup in order to gain a strong SNR and reduce reflections effects from the surrounding. For these measurements we developed, tested and implemented a laboratory TES to create a soil emissivity reference data base that allows direct comparison and validation of airborne thermal measurements. In this workflow, we used the measured emissivity spectra to characterise the measurable properties of soils in the thermal region such as quartz and feldspar content, as well as SOC.

Expected Results and Outlook

We expect to create a sophisticated workflow for the processing of hyperspectral LWIR images including the test of different atmospheric correction methods and approaches for temperature-emissivity separation exploiting the high spectral resolution of the Hyper-Cam. Within this process we plan on

creating a thermal hyperspectral soil spectral library that serves as a basis for the post processing and analysis of airborne thermal hyperspectral images. By using this chemically validated hyperspectral soil database we plan to derive several important soil parameters from the hyperspectral thermal images and create parameter maps and particular exploit the LWIR spectral information to improve the estimation of coarse texture soils that lack distinct spectral absorption characteristics in the VNIR-SWIR (e.g., sand content, quartz and feldspar mineralogy). A further goal of this work is the validation of the soil products derived from recent relevant satellite sensors (e.g., EnMAP, ECOSTRESS), as well as the simulation of upcoming next generation of hyperspectral optical and thermal multispectral satellite missions (ESA CHIME and LSTM, NASA/JPL SBG) to evaluate their potential for quantitative soil properties mapping on larger scales.

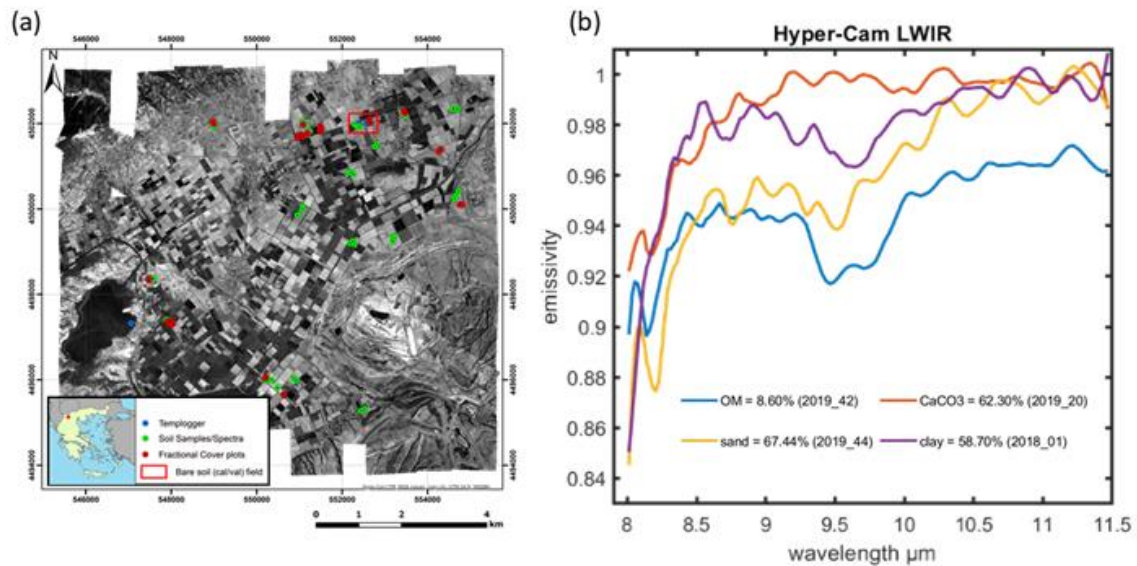


Figure (a) Hyper-Cam airborne imagery showing LWIR radiance mosaic and sample locations (b) Spectral emissivity of regional soil surfaces

A Comparative Analysis Of Airborne Hyperspectral And Thermal Infrared Data In The Assessment Of Peatland Drying: A Case Study Of Tuchola Forest, Poland

[Martyna Wietecha](#)^{1,2}, Dominik Kopeć^{1,2}, Justyna Wylazłowska², Agata Zakrzewska², Jan Niedzielko², Maciej Gąbka³, Mariusz Lamentowicz⁴, Stanisław Rosadziński³, Stefan Konczal⁵

¹ University of Łódź, Department of Biogeography, Paleoecology and Nature Conservation, Poland

² MGGP Aero, Poland

³ Adam Mickiewicz University, Department of Hydrobiology, Poland

⁴ Adam Mickiewicz University, Laboratory of Climate Change Ecology, Poland

⁵ Woźwoda Forest District, Poland

Keywords: Hyperspectral, Thermal Infrared, Vegetation

Challenge

Peatlands play a crucial role in preserving global biodiversity and climate regulation. Unfortunately, the area of wetlands in good ecological condition is dramatically decreasing (Hu et al. 2017, *Sci. Total Environ.* 586). Therefore, developing an effective, fast, and objective method for assessing the state of peatland ecosystems represents a crucial challenge in nature conservation. Currently, remote sensing (RS) is considered one of the most useful methods for assessing the condition of wetlands (Guo et al. 2017, *Sensors* 17). In this regard, in 2022 a peatlands condition assessment was carried out for two forest districts (Woźwoda and Tuchola, northern Poland), using RS methods. The study aimed to evaluate the current state of peatland vegetation and to identify changes that may indicate peatland drying. The research involved a comparative analysis of the informativeness and usefulness of hyperspectral and thermal infrared data for analyzing the peatlands drying.

Methodology

A multi-sensor aerial platform, enabling the simultaneous acquisition of hyperspectral (HS), thermal infrared (TIR), and airborne laser scanning (ALS) data was used in the study. The data was obtained on July 20, 2022. Additionally, thermal data was collected during the night of July 20-21, 2022. Based on TIR data and meteorological measurements, the Crop Water Stress Index (CWSI) was also calculated. Field reference information was collected for 100 polygons. It included details regarding visual assessments of

moss drying levels, vascular plant drying levels, peatland rehydration levels, and ground moisture measurements. The location, size, and botanical characteristics of the polygons were also determined. A multifactorial peatland drying index was also created, considering all symptoms of peatland drying. The initial phase of the analysis involved examining correlations between RS and field-collected data. Selected spectral indices (SI), daytime temperature (TIRd), nighttime temperature (TIRn), daily temperature amplitude (TIRdn), and CWSI were used as remote sensing input data for the analysis. The next step involved predicting peatland drying for the entire area of selected peatlands using machine learning methods. The use of various sets of input data for modeling a multifactorial peatland drying index was tested, including Minimum Noise Fraction (MNF) bands, SI, TIRd, TIRn, TIRdn, CWSI, and statistics computed from ALS data, related to the structure of vegetation. The final stage of the work involved an analysis of the informativeness of remote sensing data in the context of determining the peatland condition.

Expected results

The initial results of Spearman correlation ($p=0.05$) analysis demonstrate that both the information derived from hyperspectral and thermal data exhibit a significant correlation with the features determining peatland drying. Notably, thermal data exhibit a stronger correlation with specific features. Among the analyzed features determining peatland drying, the highest correlation with RS data is observed for moss drying levels (up to $r=0.84$ with CWSI) and multifactorial peatland drying index (up to $r=0.75$ with TIRdn). Among the analyzed hyperspectral indices, the CAI (Cellulose Absorption Index) displays the strongest correlation with moss drying levels ($r=0.80$), LCAI (Lignin Cellulose Absorption Index) with vascular plant drying levels ($r=0.54$), and mNDWI (Modified Normalized Difference Water Index) with peatland rehydration levels ($r=-0.61$) and ground moisture ($r=-0.66$). Regarding thermal data-derived information, the TIRd, TIRdn, and the CWSI exhibit the strongest correlation with the characteristics determining peatland drying. In the case of multifactorial peatland drying index modeling, the best results were obtained using the full dataset, including MNF bands, specified SI, TIRd, TIRn, TIRdn, and CWSI ($r^2=0.46$). The most significant factors for the model are TIRdn, TIRd, selected SI, MNF bands, and TIRn. The ALS-derived statistics turned out to be less significant in the modeling process.

Outlook for the future

Through the application of advanced technologies, such as hyperspectral and thermal remote sensing, along with the currently intensively evolving analytical methods such as machine learning, it is possible to obtain objective and standardized information about the condition of peatlands. The results of this study can be used to identify the most desiccated areas, which can help take actions related to their protection and restoration. Understanding which types of remote sensing data are the most informative for assessing the condition of peatlands will lead to better resource allocation and monitoring, resulting in a more effective peatland conservation strategy. Future research could focus on advanced data fusion, machine learning applications, long-term monitoring, exploring climate change impacts, and encouraging international collaboration to standardize peatland condition assessment practices.

A novel method to derive land surface temperature and spectral emissivity from airborne hyperspectral thermal infrared image data

Hu, T.¹, Schlerf, M.¹, Ronellenfisch¹, F., Skokovic, D.³, Llorens, R.³, Corbari, C.², Sobrino, J.³, Mancini, M.², Hoffmann¹, L., Mallick, K.¹

¹ Luxembourg Institute of Science and Technology, Luxembourg

² Politecnico di Milano, Italy

³ University of Valencia, Spain

Keywords (5): Earth Observation, Urban, Hyperspectral, Land Use, Copernicus

Challenge

A novel method to derive land surface temperature (LST) and spectral emissivity (LSE) from airborne hyperspectral thermal infrared data has been developed and validated using ground measurements. The novel method corrects for atmospheric effects and separates temperature and emissivity. It was tested data collected during a campaign in the Burana study area (Italy) in 2022.

Methodology

Airborne hyperspectral thermal infrared (TIR) images were acquired on 13-15 July 2022 with up to three overpasses per day. The sensor was flown at two survey heights of about 800 m and 3200 m above ground resulting in ground resolutions of 1 m and 4 m. Hyper-Cam LW is Fourier transformed infrared spectrometer with a focal plane array and a spectral range of 7.7-11.5 micrometers. Raw interferograms were converted via Fourier transformation and sensor calibration using the two internal blackbodies with known temperatures and emissivity into spectral radiances. Single image tiles were orthorectified and georeferenced using information from the onboard GPS and IMU units and then mosaicked into single flight lines and further into seamless mosaics.

To remove the atmospheric effects on the airborne observations, the MODerate resolution atmospheric TRANsmission (MODTRAN) atmospheric radiative transfer model was used driven by the European Centre for Medium-Range Weather Forecasts (ECMWF) ERA5 atmospheric profiles. The hourly ERA data with a spatial resolution of 0.25° was temporally interpolated to the flight overpass time. The atmospheric profile spatially closest to the centre of each image was used to depict the atmospheric condition of the entire image. The interpolated atmospheric profiles were then input into the MODTRAN model. Consequently, the three atmospheric parameters, i.e., transmittance, atmospheric upwelling and downwelling longwave radiations, were obtained and convolved to the bands of airborne data using the spectral response functions. The temperature and emissivity separation (TES) algorithm was adjusted to fit in with the hyperspectral airborne data. By inputting

the three atmospheric parameters into the TES algorithm, temperature and emissivity were retrieved simultaneously.

Expected results

Overall, the airborne LST agree well with the ground temperatures for water and relatively well for melon, grass, wheat, and lotus with little time gaps, but less well for soil and the crop measurements taken at longer time gaps. The average absolute error for water is about 0.8 K which is somewhat larger as in previous airborne validation studies and can be partly explained by the temporal gaps between the overpass and the ground measurement. Airborne spectral LSE compared reasonably well with in situ emissivity measurements for wheat and watermelon.

Outlook for the future

The method allows to map land surface emissivity in 64 spectral bands at very high spatial resolution (1-5 meter) and at flexible time, e.g., several times during a day and can serve as a valuable input to many applications such as irrigation management, crop stress detection, mapping of soil properties etc.

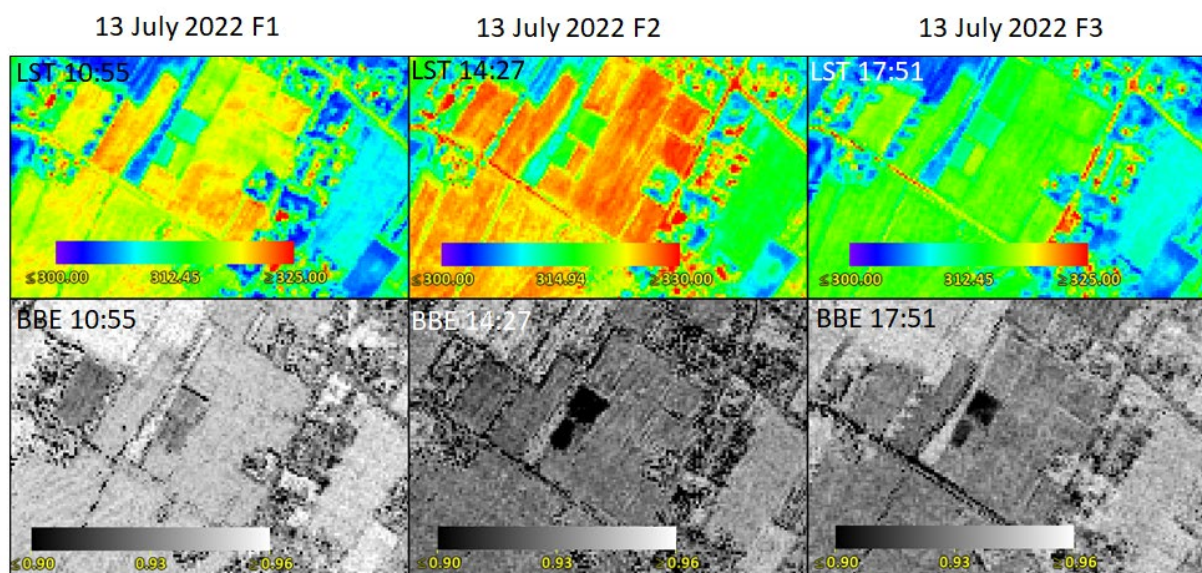


Figure Subsets of LST (top) and broadband land surface emissivity (LSE, bottom) in Concordia study site for morning (F1, 10:55), afternoon (F2, 14:27) and evening (F3, 17:51) overpasses depicting diurnal surface temperature dynamics and spatial differences in surface temperature and emissivity between different types of surfaces.

**Them.Sess. 2-4: EnMAP's first two
years in orbit- current status and
recent activities II**

EnMAP mission after 2 years in orbit: Advances from the scientific exploitation program

Sabine Chabrilat^{1,2}, Maximilian Brell¹, Karl Segl¹, Saskia Foerster¹, Robert Milewski¹, Saeid Asadzadeh¹, Kathrin Ward¹, Daniel Scheffler¹, Alexander Kokhanovsky¹, Stephane Guillaso¹, Arlena Brosinsky¹, Kathrin Koch¹, Tobias Hank³, Astrid Bracher⁴, Mariana Soppa⁴, Anke Schickling⁵, Michael Bock⁵

¹ German Research Centre for Geosciences Potsdam, remote Sensing and Geoinformatics, Germany

² Leibniz University Hannover, Institute of Soil Science, Germany

³ Ludwig Maximilian University, Munchen, Germany

⁴ Alfred-Wegener Institute Helmholtz Center for Polar and Marine Research, Bremerhaven, Germany

⁵ Space Agency, German Aerospace Center (DLR), Bonn, Germany

KEYWORDS (5): SPACEBORNE, HYPERSPECTRAL, ENMAP, SCIENCE EXPLOITATION AND APPLICATIONS

Challenge (800 - 1000 characters incl. spaces)

The Environmental Mapping and Analysis Program (EnMAP) is the first spaceborne German hyperspectral satellite mission, which started on 1st April 2022 and is in operational phase since November 2022. The primary goal of the EnMAP mission is to provide accurate and diagnostic information on the state and evolution of the Earth's ecosystems for research and applications in fields such as agriculture and forestry, geology and soils, urban areas, coastal and inland waters. The core themes of EnMAP are monitoring environmental changes, ecosystem responses to human activities, and management of natural resources such as soils and minerals. EnMAP started on 1st April 2022 and is in operational phase since November 2022, with strong expectations regarding data quality and impact on core scientific research exploitations. The challenges of the mission scientific preparatory and exploitation activities are manifold including demonstration of the science potential of the EnMAP mission, support of the user community and support of the project management with data quality, exploitation program, making a bridge with the EnMAP user community.

Methodology (1200 – 1500 characters incl. spaces)

EnMAP orbital sensor is based on a push-broom type sensor concept [2] and operates in a polar, sun-synchronous, low orbit around Earth at 652 km height. EnMAP's core parameters are a regional coverage at global scale (target mission), 30 m pixel size, tile size 30 km x 30 km, 242 spectral channels (currently 224 bands are delivered to the users), revisit of 27 days at nadir and 4 days with off-nadir tilting (+-30°). The EnMAP archives and requests for new observations can be accessed based on a free and open data policy through the EnMAP portal at <https://planning.enmap.org/>. The project management of the EnMAP mission is with the DLR Space Agency in Bonn, Germany. The sensor was built by OHB System AG and the Ground Segment is led by DLR in Oberpfaffenhofen.

The ENMAP Science Activities and exploitation program is led by the GFZ in Potsdam with the support of the EnMAP Science Advisory Group (EnSAG) and the EnMAP science project teams at GFZ Potsdam with partners from the Humboldt University Berlin, Ludwig-Maximilian University Munchen, and Alfred-Wegener Institute AWI in Germany. The mission science support program aims to support communication with the

wider EnMAP science community and to ensure scientific state-of-the-art data exploitation, to support and advise the mission project management on a) the scientific and technical issues in the field of mission performance, and b) in all areas related to science exploitation such as identifying potential new fields of research, encourage cooperation on an international level and promote and expand awareness of EnMAP data by scientific publications and presentations.

Results (1200 – 1500 characters incl. spaces)

In this presentation we will show an overview of most updated results of the EnMAP science exploitation program in terms of a) EnMAP products external Validation (data quality monitoring) and assessment of sensor performance, b) EnMAP science and applications with demonstration cases of new science fields of EnMAP data in the areas of soil research, critical raw materials identification, atmospheric and snow/ice research, ecological research and crop physiology, and water quality mapping and monitoring, c) further development of user training and user software as included in the QGIS EnMAP-Box Toolbox and in the HYPERedu online education program, and d) mission support activities resulting in provision of time-series and hot-spots monitoring in areas of interests through the background and foreground mission activities.

Outlook for the future (800 - 1000 characters incl. spaces)

The availability of spaceborne hyperspectral images is still limited and generating time-series is even more challenging. In the future, EnMAP is looking at further monitoring of our Earth's health, and expanding the research program to include operational Earth surface processes mapping and monitoring applications based on new and advanced state-of-the art algorithms including more radiative transfer modeling but also hybrid learning and new deep learning/artificial intelligence methodologies, advanced knowledge on the Earth's surface spectral signatures, extension of in-situ databases and standardised soil spectral libraries (SSLs) for improved calibration and validation of soil surface model, and better estimates of minerals composition. For this, synergies with concordant hyperspectral VNIR/SWIR missions such as PRISMA and EMIT to improve hyperspectral Earth coverage is essential toward demonstration of harmonisation of datasets and fused hyperspectral products. Furthermore, development of testbench datasets, standards, and protocols are further main long term objectives of the EnMAP science program.

Towards informed default-parametrizations of machine-learning algorithms for biophysical variable retrieval in the EnMAP-Box

Tobias Hank¹, Stefanie Steinhauser¹, Aaron Banze¹, Matthias Woche¹

¹ LUDWIG-MAXIMILIANS-UNIVERSITÄT Munich, Department of Geography, Germany

Keywords (5): Agriculture, Machine Learning, Biophysical Variables, EnMAP, EnMAP-Box

Challenge

Machine-Learning-Regression-Algorithms (MLRAs) have turned out to be an efficient solution for deriving biophysical and biochemical information from spectroscopic measurements. The rich data about vegetation status, growth and health that is stored within the reflectance spectra of ground-based, vehicle-operated, airborne or satellite-supported instruments can most effectively be accessed via well-trained non-linear and non-parametric models. The precise and targeted training of these models thereby is key for their successful implementation in practice, e.g. as part of agricultural management decision support systems. In this study, we make use of an extensive in-situ data set, consisting of field spectroscopy and corresponding biophysical/chemical variables from winter wheat fields in Southern Germany, to derive optimized default configurations for machine learning regression setups as components of a new hybrid retrieval workflow that will soon be released in the software EnMAP-Box.

Methodology

Only few years ago, hyperspectral data had been very scarce and studies had mostly been limited to local airborne experiments. Today, a new generation of EO satellites provides large amounts of hyperspectral data and has increased the spatial coverage of imaging spectroscopy that is available on the Globe by several orders of magnitude already within the first months of operation. While in former times large parts of the workload in scientific studies were concerned with acquiring and pre-processing airborne data, the satellite data now can be accessed free of charge and can be downloaded in fully pre-processed formats; ready to use.

The EnMAP mission has been supported by a dedicated science program. One major outcome of this framework is the free software EnMAP-Box, which is available as a plugin for the QGIS software. The tools of the EnMAP-Box cover a wide range of methods including simple parametric, non-linear and non-parametric, physically-based and even hybrid retrieval approaches that can be applied to retrieve agriculturally relevant information from hyperspectral data. Among the different algorithms that are part of the EnMAP-Box's agricultural applications, the hybrid approach, which combines physical reflectance modelling with machine learning, is the most promising for use with future hyperspectral data, because it enables the retrieval of quantitative information even for satellite acquisitions from remote areas that cannot be supported by in-situ measurements.

Expected results

The current implementation of the hybrid retrieval technique in the EnMAP-Box allows for deriving four variables (LAI, Cab, Cm, ALIA) via an artificial neural network (ANN) that can be trained on a synthetically compiled data base derived from the PROSAIL model family. A new implementation of this workflow will

soon allow training machine-learning regression models for the full range of the standard variables of the PROSAIL model family (Fig. 1). The workflow will further allow for selecting different machine-learning-algorithms, i.e. ANN, SVR, GPR, RFR etc. and different levels of dimensionality reduction via PCA. Users will further be able to optimize the training database via active learning. While this high degree of freedom allows users to specifically tailor the retrieval towards their specific data and needs, it comes at the price that users are forced to decide about large numbers of complex configurations. To assist with configuring their workflow, the tool will be initialized with a set of default configurations. As the hybrid inversion tool, i.e. the EnMAP Vegetation Processor, is intended to be used mainly for the derivation of information from agricultural crops, these default values should not be set at random, but should rather be optimized for their application on homogeneous crops. In a small study we used plot-based data from five consecutive growing seasons of winter wheat. The data has been sampled in the MNI test area north of Munich in Southern Germany.

Outlook for the future

From the study we expect answers to questions like: Which MLRA works best for which variable? Does it require scaling of the data and, if yes, which kind of scaling works best? Does it require reducing data dimensionality and, if yes, which number of features should be selected? Will internal active learning improve the results? Will integrating in-situ data in the AL process further improve the quality? Etc.

Based on the answers to those questions, default-configurations for the setup of the MLRA training will be derived. Users will still be able to configure individual trainings; however, the default configuration will assist their decisions by providing an informed starting point for successful variable retrievals. It is important to highlight that the default configuration will be optimized for applying the tool on homogeneous agricultural areas. The tool, however, can of course be applied to all surfaces that can be described via the turbid-medium assumption of the PROSAIL models.

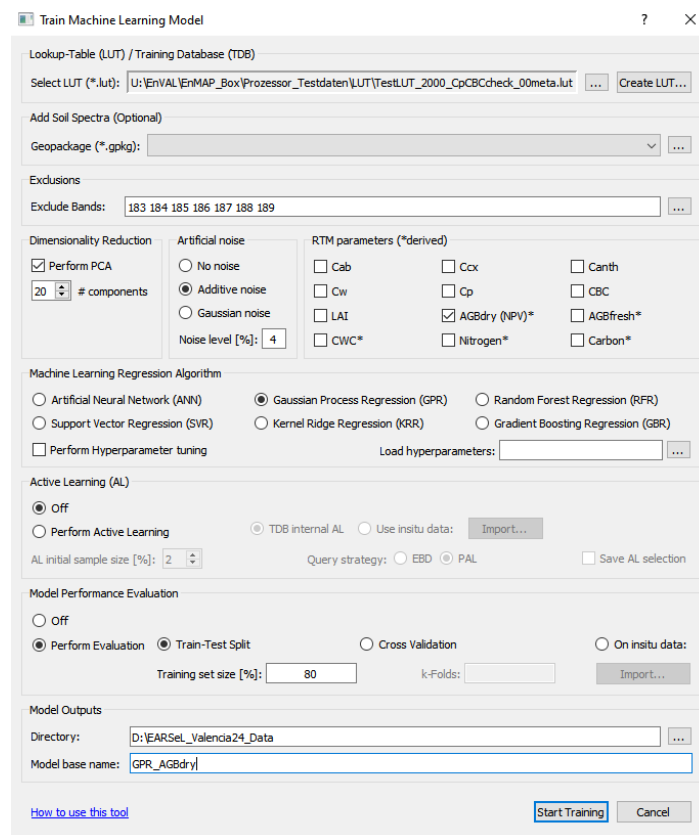


Figure 1 Graphical user interface of the new MLRA training in the EnMAP-Box showing the complexity of the configuration. Users will be assisted with configuring their workflow via informed default-settings that are optimized for retrieving biophysical and biochemical from homogeneous (agricultural) crops.

Towards a universal approach for retrieval of non-photosynthetic vegetation across ecosystems from EnMAP time series

[Akpona Okujeni](#)¹, Katja Kowalski¹, Neija Elvekjaer¹, Patrick Hostert¹

¹ Humboldt-Universität zu Berlin, Geography Department, Germany

Keywords (5): Imaging Spectroscopy, Hyperspectral Satellite, Spectral Unmixing, Vegetation, NPV

Challenge

Non-photosynthetic vegetation (NPV) serves as an essential indicator with wide-ranging applications in assessing ecosystem condition and vegetation vitality. In the realm of current and future spaceborne imaging spectroscopy missions, NPV is considered a key variable to be quantified globally with improved accuracy. The high spectral resolution of these missions has been recognized as a crucial factor for enhancing the differentiation between NPV and soil, a capability anticipated to address the limitations encountered in multispectral image analyses. Nevertheless, the task of quantifying NPV globally represents a significant challenge. Vegetation is highly diverse and dynamic through space and time, and no universal approach has been established so far for NPV retrieval from hyperspectral satellite time series across ecosystems.

Methodology

NPV is typically quantified as the fractional cover per pixel (in %) or as the biomass per unit area (e.g., in g/m²). A general advantage of fractional cover is its straightforward retrieval through spectral unmixing, which relies on a set of endmembers (EM) representing pure NPV spectra and the remaining components, typically green vegetation (GV) and soil. EMs are frequently derived from images, simplifying the retrieval process. The use of a triangular feature space, defined by the Normalized Difference Vegetation Index (NDVI) and the Cellulose Absorption Index (CAI), has been demonstrated to be a universally applicable concept for developing EM libraries from image data. Therein, pure NPV, GV, and soil spectra form the vertices and mixtures of these three components the respective feature space. Likewise, machine learning regression-based unmixing, using synthetically generated training information from such EM libraries, has proven to be a powerful approach for fractional cover mapping. In this study, we combined the NDVI/CAI feature space concept with regression-based unmixing for NPV fractional cover retrieval across various Mediterranean-type ecosystems in California using a 1-year hyperspectral time series acquired by the Environmental Mapping and Analysis Program (EnMAP).

Results

Our results revealed consistent multi-seasonal NDVI/CAI feature spaces for various ecosystems, including forests, shrublands, grasslands and croplands. While most ecosystems displayed a similar triangular shape, the density distribution indicated different abundances of NPV, GV, and soil related to the respective ecosystem characteristics and condition through the season. Identified EM represented typical green and non-photosynthetic spectra for different plant growth forms, crop types, as well as background

surfaces such as soils and rock outcrops. A generalized regression model based on the combined multi-ecosystem EM library resulted in reliable fractional cover maps illustrating the spatial patterns and seasonal variability of NPV cover across ecosystems. Qualitative assessment of maps based on field survey information confirmed the overall performance of the model to accurately estimate NPV fractional cover. By spectrally resampling the EnMAP time series to match the spectral band configuration of multispectral Landsat 8/9 and Sentinel-2 as well as future superspectral Landsat Next imagery, we demonstrated the benefit of spaceborne imaging spectroscopy for improved NPV retrieval, particularly at the low- and the high-end of the fraction range between 0 and 100%.

Outlook for the future

Our results demonstrate that the combination of the NDVI/CAI feature space with regression-based unmixing represents a universal approach applicable in diverse ecological settings over time, making it a valuable method for cross-ecosystem NPV fractional cover retrieval. The EnMAP time series utilized in this study represents a unique, high-quality hyperspectral data source, which proved superior to multispectral data. Future work will focus on extending this analysis beyond Mediterranean-type ecosystems in California, for example by including temperate and arid regions worldwide. In this regard, the NDVI/CAI feature space analysis will support the development of global EM libraries of NPV, GV, and soil, contributing to the idea of analysis ready spectral databases for ecosystem research. Moreover, the potential of machine learning will be further harnessed to develop generalized regression models for global retrieval of continuous time series of NPV fractional cover from EnMAP.

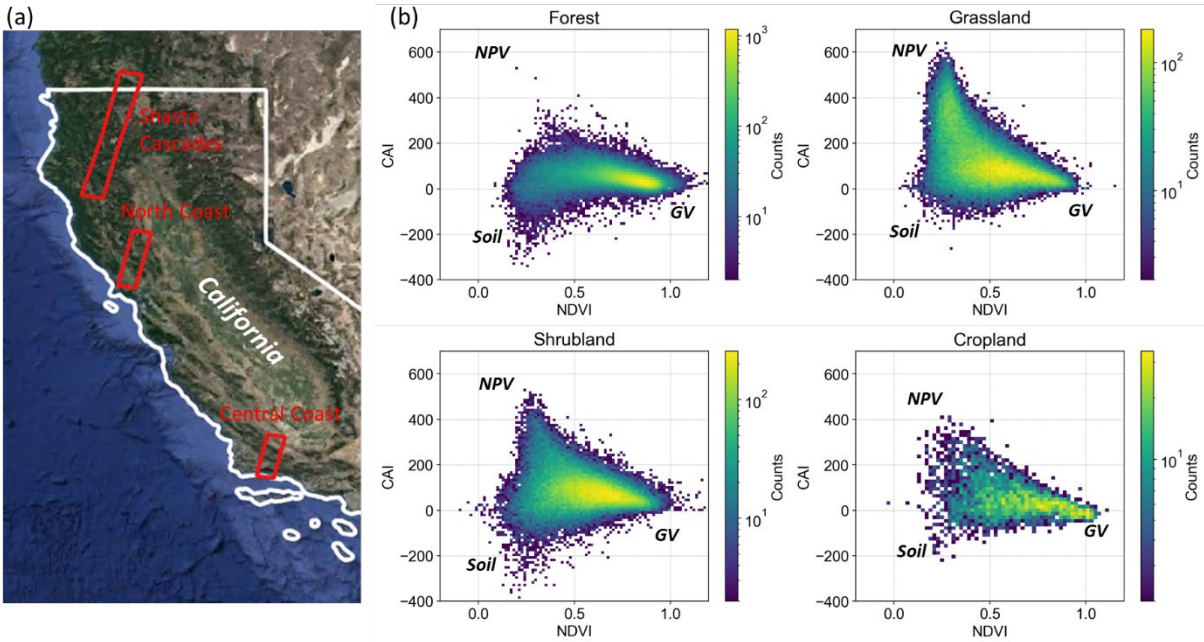


Figure (a) Footprints of the EnMAP time series acquired across various Mediterranean-type ecosystems in California and (b) corresponding multi-seasonal NDVI/CAI feature spaces.

EnMAP Hyperspectral Data for Mineral Exploration: Case Studies and Application Examples

EARSel Valencia 2024

Abstract

Corresponding Author: saeid@gfz-potsdam.de

[Saeid Asadzadeh](#)¹, Sabine Chabrilat^{1,2}

¹ Helmholtz Centre Potsdam, GFZ German Research Centre for Geosciences, 14473 Potsdam, Germany

² Leibniz University Hannover, Institute of soil science, 30419 Hannover, Germany

Keywords (5): EnMAP, Hyperspectral data, Mineral mapping, Alteration footprints, polynomial fitting.

Challenge

Mining new resources remains essential to meet the increasing demands for raw materials during green transitions and adhere to sustainability standards. Among the readily available methodologies that can significantly contribute to the discovery of new resources of base metals and critical raw materials is spaceborne remote sensing technology, including the newly available EnMAP imaging instrument with global data coverage. While airborne imaging systems have been in use for several decades, the application of this technology has fully matured for only a few specific mineral deposits, meaning that the capabilities (and limitations) of imaging spectroscopic techniques are fully understood through several case studies. For the majority of mineral deposits, however, the application is immature or at best semi-mature because only sporadic case studies are available, yielding inconclusive results. To bridge this gap, more case studies need to be developed using state-of-the-art remote sensing data, exemplified here by the EnMAP imagery.

Methodology

To demonstrate this, we conducted an analysis of EnMAP hyperspectral data across four distinct deposit types located in arid regions around the world. The target areas comprise a porphyry copper deposit in Iran (Dehaj), a Volcanogenic Massive Sulfide (VMS) deposit in Iran (Taknar), a Mississippi Valley Type (MVT) Pb-Zn mineralization in Yemen (Jabali), and a Rare Earth Element (REE)-bearing carbonatite in the USA (Mountain Pass). For each of these sites, the Level 2A orthorectified surface reflectance data of EnMAP was obtained/ordered and then processed by using the polynomial fitting technique. This simple yet effective approach involves fitting a polynomial to a continuum-removal spectrum to parametrize the diagnostic absorption features of target minerals, including wavelength minimum, depth, width, area, and asymmetry. This is accomplished by fitting a quadratic function to a local minimum and calculating the first derivative of the fitted function to yield the wavelength of minimum reflectance over a user-specified wavelength range. This minimum value is then used to calculate the remaining spectral parameters. By analyzing the resulting parameters, the type of mineral and its state, including relative abundance, compositional variations, and crystallinity is mapped over each study area.

Results

In the case of the porphyry copper deposit, the white mica composition map effectively unveiled the high-temperature core of the system, which had eluded detection during field studies and drilling due to intense hydrothermal activities. The presence of Al-rich white mica in this map highlighted the central high-temperature core of the system. White mica chemistry also proved invaluable in mapping the fluid migration pathways and deposition centers of the VMS-related ore, in addition to highlighting new concealed areas with potential for similar mineralization. For the MVT deposit in Yemen, a reduction in

carbonate contents (indicating dissolution of carbonates during hydrothermal evolution), a transition in mineralogy from calcite to dolomite, and the occurrences of highly crystalline kaolinite were observed to be associated with the known Pb-Zn mineralization. Over the carbonatite-hosted REE deposit, EnMAP successfully resolved the characteristic doublet absorption features of Nd embedded in bastnaesite ore in the 740 and 800 nm wavelengths, as well as the carbonate feature at 2340 nm using VNIR and SWIR bands, respectively.

Outlook for the future

Our study indicated that EnMAP outperforms previous generations of multi- and hyperspectral datasets in terms of remote sensing alteration mapping. The high-quality data offered by EnMAP can enable exploration geologists to identify, characterize, and map a rich number of spectrally active minerals over the earth's surface. This is thanks to EnMAP's higher number of bands, accurate calibration, and high signal-to-noise ratio (SNR). These capabilities can be effectively used to search for new mineral resources in arid to semi-arid regions across the globe. The demonstrated capability of EnMAP to directly detect rare earth elements (REEs), which was demonstrated for the first time in this study, can usher in a new era for remote sensing-based exploration of REEs. Despite the encouraging results, additional case studies should still be developed (and field-verified) to fully comprehend the potential and limitations of EnMAP data in each of these application domains.

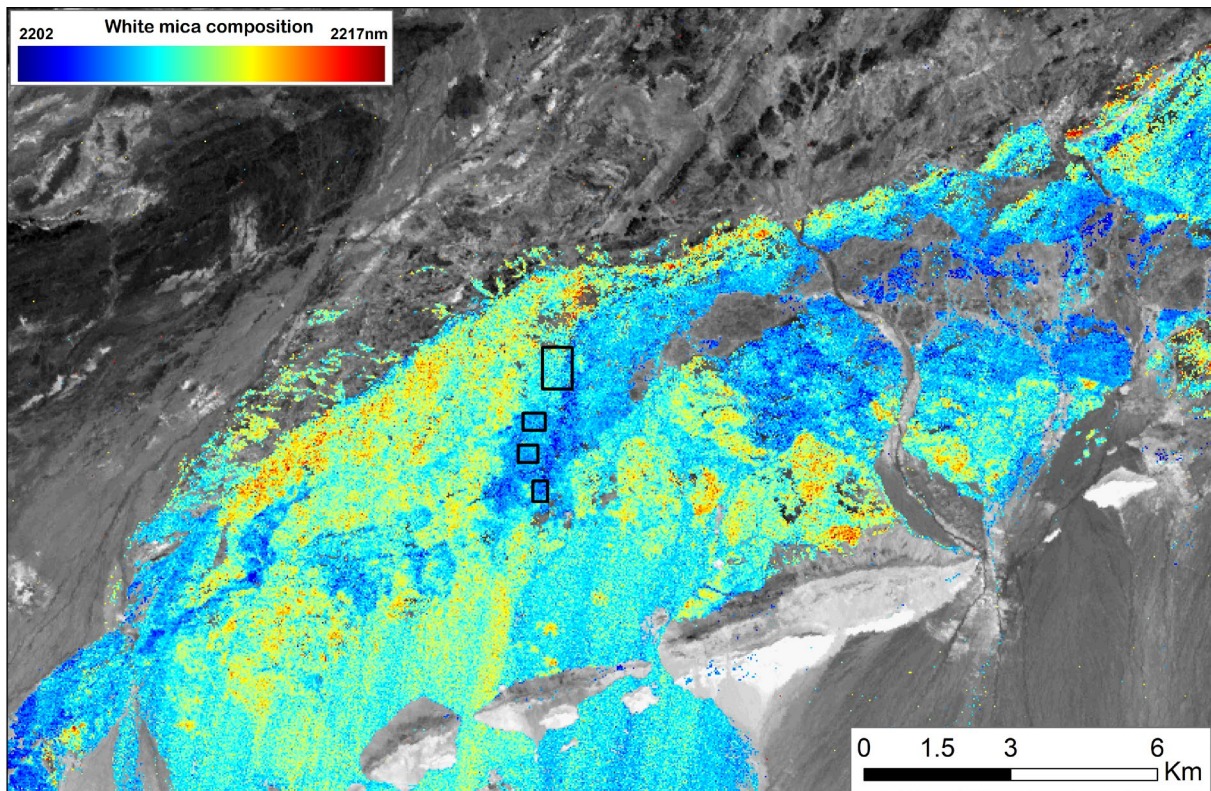


Figure The chemistry of white mica over the Taknar VMS deposit (Iran) revealed by EnMAP data. The parts with shorter wavelength highlight the Al-rich white mica, indicating the recharge zones and potential ore deposition centres.

A.

EARSel Valencia 2024
Abstract
Corresponding Author:
nejja.elvekjaer@hu-berlin.de

Advantages of EnMAP time series for plant life-form mapping and fuel type characterization in fire-prone Mediterranean ecosystems

NEIJA ELVEKJAER¹, V. DONG PHAM², P. HOSTERT¹, S. VAN DER LINDEN², A. JANZ¹, A. OKUJENI¹

¹ HUMBOLDT-UNIVERSITÄT ZU BERLIN, GERMANY

² UNIVERSITÄT GREIFSWALD, GERMANY

Keywords (5): Imaging Spectroscopy, Spectral Unmixing, Deep Learning, Vegetation, Fire risk

Challenge

Satellite-derived vegetation maps are crucial for monitoring fire-prone ecosystems. These maps provide essential information about various plant life-forms, including trees, shrubs, herbs, and non-vegetation surface types, which are important for defining fuel types and fuel models for fire risk analysis. However, fire-prone ecosystems are often complex, containing multiple plant life-forms within a single pixel. In previous research, Support Vector Regression-based unmixing techniques were employed to quantify plant life-forms using simulated Environmental Mapping and Analysis Program (EnMAP) data across diverse ecoregions in California. This work highlighted the benefit of hyperspectral over multispectral data for such mapping approaches, while noting limitations related to the use of simulated data and the lack of a time series that allow integration of spectral-temporal metrics. The launch of the EnMAP mission in 2022 marked a milestone in making hyperspectral time series available, enabling the incorporation of hyperspectral-temporal metrics to enhance the unmixing of plant life-forms.

Methodology

In this study, we apply a spectral unmixing workflow to a one-year hyperspectral EnMAP time series in California. Our study areas include both the arid central and the more humid northern regions of California. Specifically, two of the study areas span from the coastal areas to the inner Central Valley, while one study area covers the mountainous terrain in northern California. These three locations include diverse ecoregions, such as grasslands, shrublands, open-canopy woodlands and dense forests, all of which have been influenced by a complex history of wildfires.

To enhance the unmixing workflow, we integrate spectral-temporal metrics and employ a multi-class 1D-Convolutional Neural Network (CNN), generating plant life-form fraction maps for all study areas. The accuracy of these predicted fraction maps is assessed by comparing them to reference fractions obtained through high-resolution image interpretation and field data. Furthermore, we explore the connection between our fraction maps and fuel type classification systems by utilizing field data and extracting structural information from LIDAR (Light Detection and Ranging) technology. This comprehensive approach allows us to better understand the relationship between spectral information, vegetation fractions, and fuel types in a region, where on the one hand fires are prevalent and an important landscape factor and on the other hand monthly EnMAP time series exist.

Results

Our results demonstrate the successful application of EnMAP data for the mapping of plant life-forms within Mediterranean ecosystems. We found that by incorporating temporal metrics from hyperspectral

time series, our model exhibited improved robustness and accuracy in distinguishing between plant life-form classes. Thus, allowing to better differentiate between challenging classes and mitigate overestimations at lower fraction ranges. By combining fraction maps, structural information and field survey data we further provide a flexible and user-friendly framework for characterizing fuel types. Our results show the effectiveness of the unmixing approach for estimating plant life forms and acquiring essential information for fuel type mapping enabling efficient land management and wildfire risk assessment without the need for extensive field surveys.

Outlook for the future

In light of increasing fire hazards within Mediterranean ecosystems, there is a growing demand for updated fuel information to support comprehensive risk analysis. Our findings highlight the potential of hyperspectral timeseries data for vegetation and fuel type mapping. Furthermore, the synergistic use of timeseries of hyperspectral imagery with ancillary information on vegetation structure and state enables the prompt generation of fuel type maps. Depending on data availability, such maps can be readily expanded to encompass expansive areas that would otherwise be challenging to survey using conventional methods. Upcoming hyperspectral operational missions have the potential to automate the generation of wall-to-wall fuel type maps. This workflow is a step in this direction, taking advantage of the spectral and temporal resolution of hyperspectral satellite missions to enhance knowledge of vegetation fractions and fuel type distributions over larger areas.

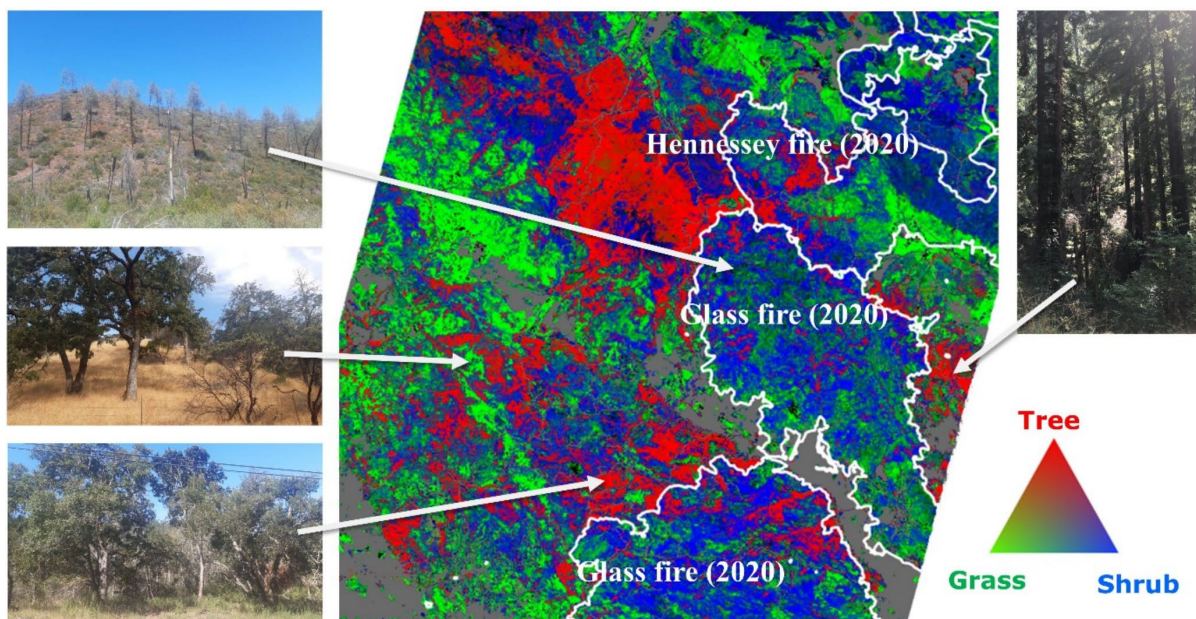


Figure Fraction map covering part of the Central Coast study site along with field photos showing different landscapes and fuel types. Fractions estimates reflect fire perimeters from 2020.

EnsAD: EnMAP Satellite-based Algae Detection for Copernicus and Downstream Services

Dagmar Müller¹, Bi Shun², Rüdiger Röttgers², Martin Hieronymi², Jorge García³, Katalin Blix⁵, Ana Ruescas^{1,3}, Julia Amorós³, Kerstin Stelzer¹, Carsten Brockmann¹, Eefke van der Lee⁴, Annika Grage⁴, Karin Heyer⁴, Johannes Timm⁴

¹ Brockmann Consult GmbH, Germany

² HEREON, Germany

³ University of Valencia, Spain

⁴ Federal Maritime and Hydrographic Agency BSH, Germany

⁵ UiT The Arctic University of Norway, Norway

Keywords (5): Phytoplankton optical types, Forward Inversion, EnMAP, Coastal and Inland, Water quality

Challenge

The EnsAD project aims at further developing the methods from preparatory studies for algae group recognition, at opening potential uses of hyperspectral satellite products for water quality assessment and preparing for operational use with the Copernicus mission CHIME and the NASA mission PACE. The developed method must be robust and flexible to address both coastal waters and inland waters and provide demonstration products for EnMAP data. National reporting and warning services concerning water quality and harmful algae blooms profit from the algae group detection e.g., of cyanobacteria. The complete processing chain will be designed to feed into ecosystem model assimilation starting from hyperspectral data via deriving an algae group product. The biogeochemical forecasts can be improved by adding satellite-based information on algae groups.

Methodology

Hyperspectral water leaving reflectance between 400 and 750nm are inverted into concentrations of six phytoplankton groups, concentration of non-algal particles (NAP) and CDOM absorption at 440nm. The inversion employs the full bio-geo-optical model in forward mode, which accounts for spectral specific absorption and scattering of the phytoplankton groups, the absorption and scattering of minerogenic and biogenic detritus, CDOM absorption and the optical properties of pure sea water. Water leaving reflectance is derived by the ratios of backscattering and total attenuation, handled differently for pure water and other particles. The minimisation of errors is based on the difference between the forward modelled reflectance spectrum and the input spectrum weighted by the uncertainty of the input spectrum. Additional free parameters of the inversion are the backscattering ratios of minerogenic and biogenic detritus and the slope of CDOM absorption. To minimise the calculation time, start values of the iterative process are estimated by a simple linear model of band ratios and line heights. The output of the inversion process can be chosen by the user, which can reach from the concentrations only or a full set of spectral absorption and backscattering spectra.

Validation is based on concentrations of water constituents and in-situ reflectance spectra convolved with the EnMAP spectral response functions.

Results

The inversion by iterative forward modelling has been validated with the GLORIA in-situ database (Figure 1). Total phytoplankton concentration from the inversion correlated very well with GLORIA in-situ chlorophyll concentration ($R^2=0.85$, median symmetry accuracy $\varepsilon=-27.1\%$). CDOM absorption is retrieved with good quality ($R^2=0.53$, $\varepsilon=6.0\%$). NAP is expected to compare to total suspended matter with a strong negative bias, but the correlation is still high ($R^2=0.66$, $\varepsilon=-74\%$).

First tests on the SpecWa insitu data, which includes information on four phytoplankton groups, show that the forward model needs further adjustment in phytoplankton specific scattering properties. Similar results have been obtained by investigating EnMAP L2A extracts of strong cyanobacteria blooms.

EnMAP L2A spectra over clear water can show a large contribution of spectral noise in the blue part of the spectrum, because the signal is very low and non-linear instrument response can become apparent. Using the shape of the spectrum directly in approaches which build on the second or fourth derivative of the spectrum would fail without further preparation of the input data. The iterative forward modelling inversion can handle these spectra well and derive realistic concentrations, because it builds entirely on fixed spectral shapes for phytoplankton absorption and scattering.

The procedure can work with any kind of hyperspectral data given within a minimum range of 440 to 710nm.

Outlook for the future

Our immediate plans involve adding several new components to the bio-optical model. The fluorescence of three important pigments (chlorophyll-a, phycoerythrin and phycocyanin) could account for some observed systematic deviations in the spectral shapes between forward model and original spectrum.

Currently, the inversion can be applied to extracted spectra only. The iterative process would be too slow to use it directly on a full satellite image. Observing the EnMAP extracts, we will employ a two-step approach in machine learning. In a first step, the spectrally noisy data will be smoothed based on the full iterative inversion approach. By transferring the noisy spectrum into the regime of smooth model spectra a backward propagation neural network can be trained, which derives the water properties. The model-based smoothing can also be interesting for all derivative-based algorithms. The neural network will allow the inversion of full satellite images at reasonable speed.

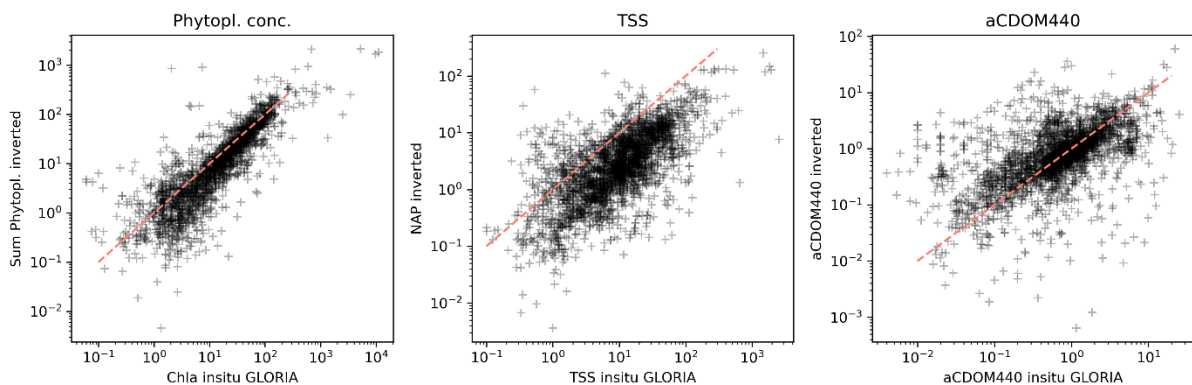


Figure 1 Inversion results of total phytoplankton concentration (Sum Phytopl, left), non-algal particle concentration (NAP, middle) and CDOM absorption (aCDOM440, right) against in-situ values from GLORIA dataset.

**Them.Sess. 2-5: Hyperspectral
imaging of chlorophyll
fluorescence across scales -
PART II: sampling strategies and
interpretation**

Measuring plant fluorescence across scales to understand the dynamics of photosynthesis and stress resilience – steps towards the development of novel vegetation products

EARSeL Valencia 2024

Abstract

Corresponding Author: u.rascher@fz-juelich.de

Uwe Rascher, Juliane Bendig, Jim Buffat, Antony Castro, Sofia Choza Farias, David Herrera, Ireneus Kleppert, Deepthi Konche, Caspar Kneer, Oliver Knopf, Julie Krämer, Vera Krieger, Onno Muller, Huaiyue Peng, Juan Quiros-Vargas, Saja Salattna, Theresa Sandmann, Bastian Siegmann

Forschungszentrum Jülich GmbH, Leo-Brandt-Str, Institute of Bio- and Geosciences, IBG-2: Plant Sciences, 52425 Jülich, Germany

Keywords (5): Solar-induced Fluorescence (SIF), vegetation, photosynthesis, dynamic plant traits, airborne imaging spectroscopy

Challenge (800 - 1000 characters incl. spaces)

Photosynthesis (measured as electron transport or CO₂ uptake rate) is greatly dependent on the ecology of the plant species, absorbed PAR, and other environmental factors such as drought or extreme temperatures. The regulation of photosynthesis happens mainly on the cell or leaf level. Solar-induced fluorescence (SIF) is a faint red light, which is emitted from the core of the photosynthetic machinery, and which is known to be related to the efficiency of photosynthetic electron transport. Nowadays SIF can be retrieved from leaf-level, ground-based, airborne and satellite platforms, but close relationships between efficiency of photosynthesis and SIF are only established on leaf-level. On larger scales other factors, such as changes in canopy structure influence the intensity of SIF. FLEX and other satellite instruments are on the step to providing high resolution maps of SIF, but our scientific knowledge on how to translate the intensity of the fluorescence signal to the regulatory properties of leaf photosynthesis are still sketchy.

Methodology (1200 – 1500 characters incl. spaces)

We aim to develop the mechanistic understanding how top-of-canopy SIF is related to leaf-level photosynthesis by combining established active fluorescence with novel passive fluorescence and hyperspectral reflectance measurements. We try to measure and understand the interplay of canopy structure, leaf display, SIF on the level of single leaves and the top-of-canopy signal by combining leaf-level measurements with a novel ground-based hyperspectral imaging systems (HyScreen), which demonstrate that the non-linear SIF-photosynthesis behaviour can be detected on the canopy scale and traced to the single leaf properties.

From this spatial scale we move up to the next level and use our high-performance airborne imaging spectrometer *HyPlant* in combination with a newly developed UAV-based SIF camera for larger scale SIF and reflectance measurements. These data are being used to test different down-scaling or normalization approaches to extract quantitative leaf-level proxies of SIF and their sensitivity to environmental stress. Using normalization approaches we could demonstrate the potential of SIF to detect early signs of drought stress or reduced soil water availability or the beneficial diversity effect in mixed cropping systems.

Expected results (1200 – 1500 characters incl. spaces)

In this presentation we will give an overview on our concept and nested measurement approach to understand the dynamics of canopy reflectance, SIF, and physiological regulation on the leaf level. We present approaches how to relate top-of- canopy SIF and reflectance information to the actual functional status of photosynthesis. We review our attempts to use active and passive reference targets to validate our SIF measurements on all spatial levels, which are the basis to quantitatively link SIF measurements to rates of photosynthesis. We will show quantitative data from various controlled field experiments, where we used controlled environmental stressors in combination with a detailed characterization of the functional response of the crops species, to quantitatively understand the mechanistic link between actual rates of photosynthetic electron transport and top-of-canopy measurements of fluorescence. We combine active and passive fluorescence technologies on various scales to develop data sets and forward models to develop a good scientific understanding on the quantitative relation between photosynthetic electron transport, non-photochemical energy dissipation and the dynamic changes in leaf and canopy reflectance and fluorescence emission.

Outlook for the future (800 - 1000 characters incl. spaces)

FLEX is currently scheduled to be launched in 2026 and the European Space Agency will deliver L1 2 data products, i.e. top-of-canopy radiance, reflectance and fluorescence emission. These data need to be translated to higher level data products, such as actual rates of photosynthetic carbon uptake rates or specific stress indices. The mechanistic knowledge, which we currently develop on the single plant, plot and field scale will build the basis for the formulation of higher-level data products of FLEX, which will be developed in the next years preparing the operation of the FLEX satellite mission.

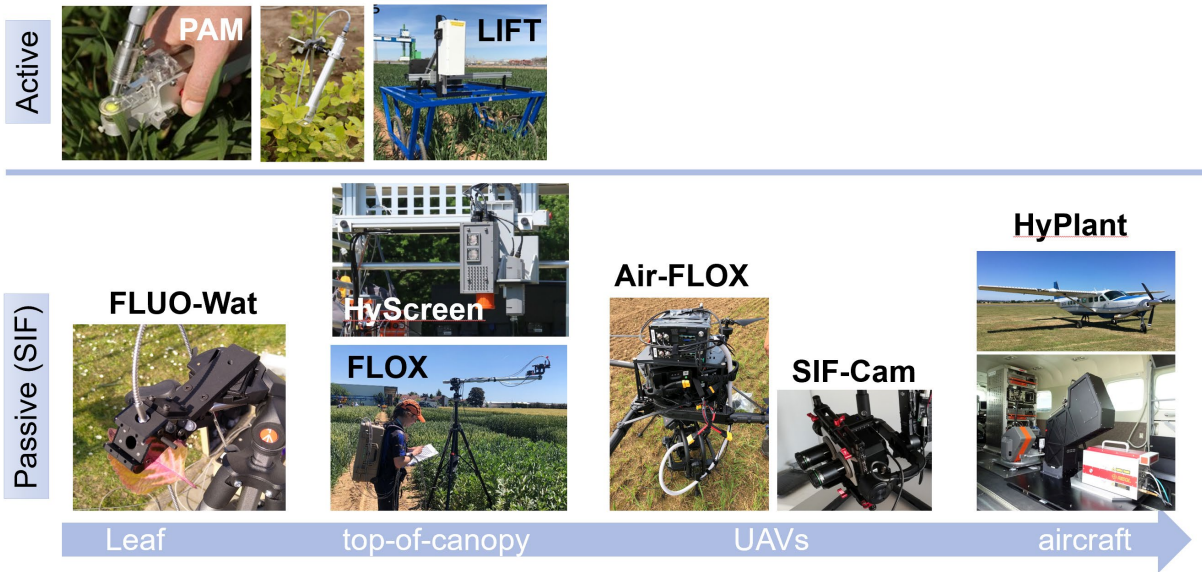


Figure Overview on the currently available instrumentation that is available to quantify fluorescence emission from the leaf to the aircraft level. Active methods (upper panels) deliver information rich data on the energy distribution within the photosystems; however, those systems are limited in their applicability as they require an active excitation of the photosynthetic machinery. Passive systems (lower panels) have become available in the past years complementing the active approaches. Passive, i.e., solar-induced, methods have the advantage to be applicable from larger distances, but we need to develop a better scientific understanding on how to quantitatively interpret the SIF signal.

Waking before the snow melts: Seasonal timing of fluorescence and photosynthetic yields at needle and canopy scales in evergreen needleleaf forests

Zoe Pierrat^{1,2}, Troy Magney³, Andrew Maguire¹, Logan Brissette³, Russell Doughty⁴, David R. Bowling⁵, Barry Logan⁶, Nicholas Parazoo¹, Jochen Stutz²

¹ University of California Los Angeles, Department of Atmospheric and Oceanic Sciences, USA

² Jet Propulsion Laboratory, California Institute of Technology, USA

³ University of California Davis, Department of Plant Sciences, USA

⁴ University of Oklahoma, College of Atmospheric and Geographic Sciences, USA

⁵ University of Utah, School of Biological Sciences, USA

⁶ Bowdoin College, Biology Department, USA

Keywords (5): Evergreen needleleaf forests, solar-induced fluorescence, phenology, photosynthesis, snow

Challenge

The seasonal timing and magnitude of photosynthesis in evergreen needleleaf forests (ENFs) has major implications for the carbon cycle and is increasingly sensitive to a changing climate system. An earlier onset of photosynthesis in the spring can lead to increased carbon uptake throughout the growing season. However, early depletion of water reserves can lead to early photosynthetic cessation and continued respiration during warm late-season periods - increasing carbon loss and dampening total carbon fixation over the photosynthetically active season. Despite this importance, determining the start and end of the growing season in ENFs is challenging due to a lack of field measurements and difficulty interpreting satellite data, which are impacted by snow, cloud cover, and the pervasive 'greenness' of these systems. Therefore, the goal of this study is to evaluate how we can best capture seasonal transitions in ENFs with remote sensing.

Methodology

To link physiological changes with remote sensing during transition seasons, we collected data at three different ENF sites across a broad latitudinal gradient (Alaska, Colorado, Saskatchewan). We collected continuous needle-scale measurements of fluorescence and photochemical yields using a MONI-PAM fluorometer. We compared these data with tower-based remote sensing of Solar Induced Chlorophyll Fluorescence and Gross Primary Productivity (GPP) across sites. To account for the impact of radiative effects on the SIF signal, we calculate intensity-normalized SIF (SIF_{relative}) and explain how this is an effective proxy for the yield of fluorescence. To account for snow on remote sensing observations, we derived a theoretical framework of the radiative transfer of light through snow for observations of SIF, SIF_{relative}, and common vegetation indices under snow-covered conditions. By linking photosynthesis and fluorescence measurements across multiple scales, we can evaluate the biological underpinnings of remote sensing observations.

Results

We show that needle-scale fluorescence (φ_F) and photochemical (φ_P) yields closely track one another across the seasonal cycle across multiple sites and years. Further, we find that needle-scale measurements can be scaled to the canopy with eddy-covariance GPP and SIF data. We observe close correspondence between needle-scale φ_F and φ_P and canopy scale $SIF_{relative}$ and GPP-derived light-use-efficiency of photosynthesis (LUE_P). Based on these results, we conclude that $SIF_{relative}$ is effective at tracking the seasonality of photosynthesis in ENF. These independent, temporally continuous datasets additionally confirm an increase in physiological activity prior to snowmelt across all three evergreen forests. This suggests that data-driven and process-based carbon cycle models which assume negligible physiological activity prior to snowmelt are inherently flawed, and emphasizes the need for remote sensing proxies that can capture photosynthetic activity even in the presence of snow. Ultimately, we probe the spectral biology of evergreen forests to advance our understanding of how climate change is impacting ENF photosynthesis.

Outlook for the future

In evergreen forests, patterns of temperature and precipitation are changing with climate change, and their collective influence determines the timing of the spring and fall transition seasons. By comparing measurements across scales, we develop a framework for future work linking underlying biology with remote sensing. Because $SIF_{relative}$ shows potential for overcoming challenges associated with disentangling the physiological from the physical effects on SIF (illumination and snow) at sites across a latitudinal gradient experiencing different environmental conditions, our results demonstrate its utility in future research. Finally, our results highlight the mechanistic underpinnings of what SIF data can (and cannot) tell us about seasonal transitions in ENF photosynthesis - an essential step towards improving monitoring of these ecosystems globally.

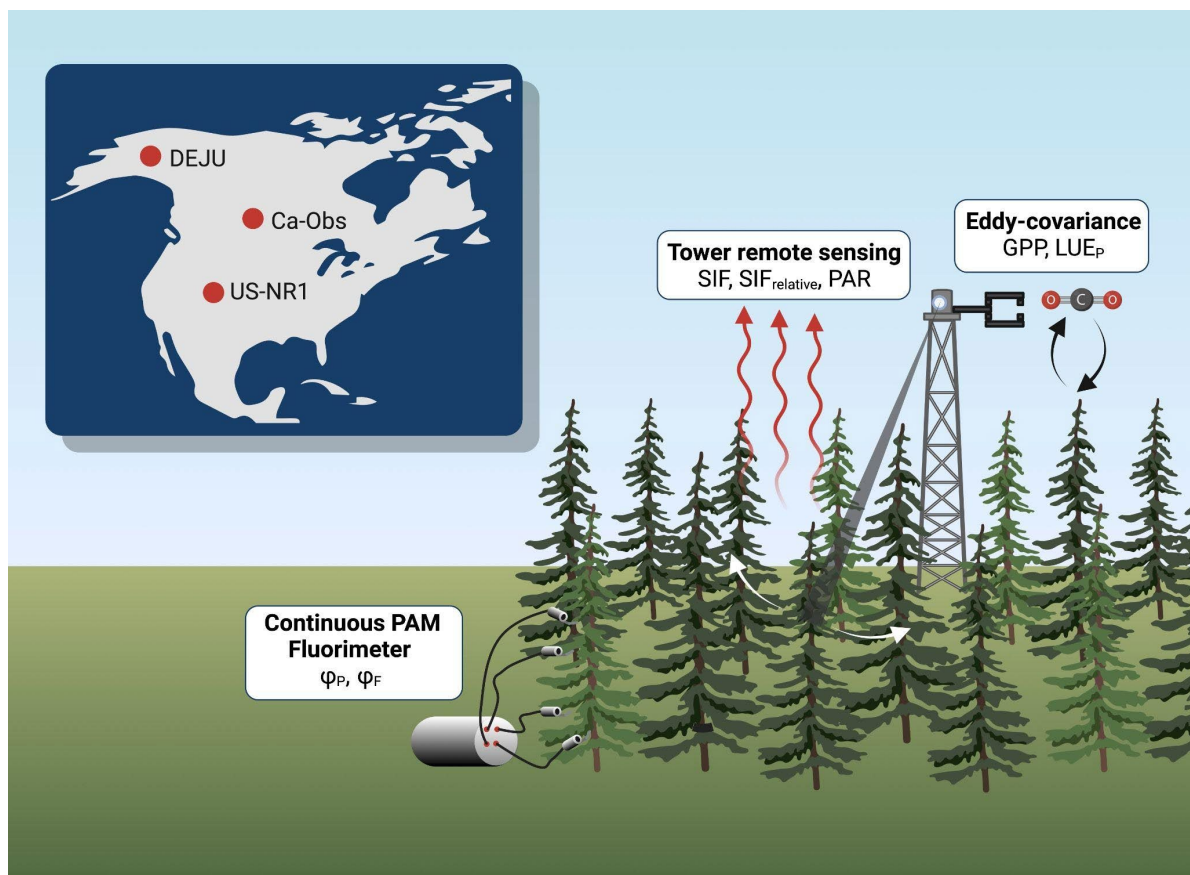


Figure 1 General overview of measurements and parameters derived from instruments at the study sites. Note that Ca-Obs did not have continuous PAM fluorimeter data available. An inset map shows the location of each study site.

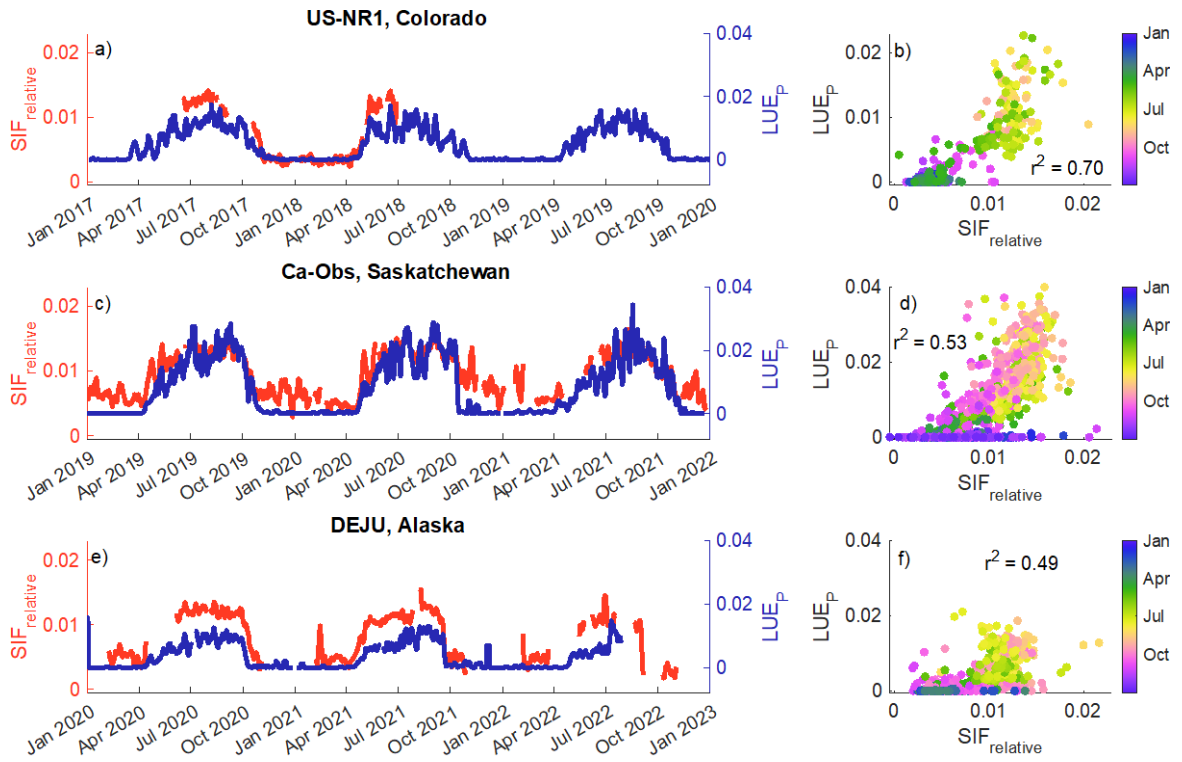


Figure 2 a, c, e: Time series of five-day moving average of tower-based SIF_{relative} (red) and LUE_P (blue) over three seasons at US-NR1 (a), Ca-Obs (c), and DEJU (e). Scatterplots of daily average LUE_P and SIF_{relative} at US-NR1 (b), Ca-Obs (d), and DEJU (f), colored by month.

New approaches for environmental sensing using a UAV-based Active Laser Fluorescence Imaging System

Lammert Kooistra¹, Hasib Mustafa², Chenglong Zhang¹, Harm Bartholomeus¹

¹ Wageningen University and Research, Laboratory of Geo-Information Science and Remote Sensing, Wageningen, The Netherlands

² University of Twente, Faculty of Engineering Technology, Enschede, The Netherlands

Keywords (5): Hyperspectral camera, prototype, soft robotics, temperature sensing

Challenge

One of the long standing challenges in EU's environmental policies is the low spatial and temporal resolution of available data for many regions. Although the existing electronic sensor technologies can address this problem to a certain extent, the cost of maintenance and the increase in e-waste becomes a major concern. The EU H2020 I-Seed project aims to mitigate this problem by introducing novel soft, miniaturized, biodegradable robots capable of sensing the key parameters at the top soil and air above soil using integrated fluorescing material in the robot.

By biomimicking the plant seeds, these miniaturized robots are made into artificial seed-like structure capable of performing similar actions as of the real seeds in terms of flying, dispersing and burrowing. These artificial seeds will be dispersed over the target area using Unmanned Aerial Vehicles (UAV), and later will be geo-localized using RGB imagery. The follow-up action will be the read-out of these artificial seeds (termed as 'I-Seed') acting as optical sensor by changing their fluorescence emission as per the sensing parameters of interest, such as temperature, humidity, and elemental mercury. Such optical read-out requires a lightweight active laser fluorescence observation system including a hyperspectral camera that can be deployed on UAVs.

This contribution presents the prototype of the Active Laser Fluorescence (ALF) Imaging System and the evaluation of the system from the lab to the field with focus on the I-Seed temperature sensors.

Methodology

The Active Laser Fluorescence (ALF) Imaging System prototype (Figure 1) consists of several modules, that serve various purposes for validation and read-out of the fluorescence signal from the I-Seed temperature sensor (Figure 1). The current design consists of following modules: 1) Excitation module; 2) Area-scan spectroscopy module; 3) Hyperspectral Imaging Module; 4) Triangulation module; 5) RGB Imaging module; 6) Verification module; and 7) Computation module. Starting point for the development of the ALF Imaging System prototype was to build it on Commercially Off-the-self (COTS) optical components. From the physical dimensions and the spatial positioning of the COTS elements, the casing and mounts were designed in CAD software.

The design of the UAV ALF Imaging System needs to meet several requirements. A critical step was the construction and miniaturization of the system to dimensions and weight which will allow it to be carried by a UAV platform. Initially we aimed for the DJI M300 UAV as carrying platform. This limits the payload weight to a maximum of 2.7 kgs. Moreover, the downwash airflow of the rotors of the UAV limits the minimum working distance to 4 m, below which the turbulent airflow is strong enough to move the seeds from their original landing position.

In this design, we employed an excitation module providing the required excitation power and wavelength for laser-induced fluorescence. This module consists of the 980 nm laser head, laser power supply and cylindrical lens for shaping the output laser beam from rectangular to line shape.

The detection of the fluorescence signal is based on the Hyperspectral Imaging Module which provides the localization and spectroscopic response of the I-Seed sensor. This module consists of objective lens, focusing lens, slit, collimating lens, grating, focusing lens and camera (Allied Vision).

Initial characterisation and evaluation of the prototype was done in a laboratory set-up. The influence of relevant factors (distance, excitation power, sensor orientation, uniformity sensor, % fluorescent, integration time spectrometer, sensor degradation) on the fluorescence signal was evaluated in sensitivity analysis experiments. After characterisation, the prototype was evaluated under field conditions.

Expected results

The fluorescence emission from the I-Seed temperature samples were measured at a distance of 4m for varying excitation intensities at an integration time of 3s and temperatures ranging from 5 to 40 C. With increasing sample temperature, the ratio of peaks changes, and therefore, can be utilized to sense temperature of the sample (Figure 2). Along with spectroscopy, imaging of the sample was carried out from a distance of 4m to assess the capabilities of localization from RGB imagery during laser excitation. This ensures the precise positioning of the samples in the ground during optical read-out, which may get shifted by wind or animals. In addition, results of the sensitivity analysis showed clear influence of sensor orientation and uniformity of the sensor, which need to be accounted for in field conditions.

Outlook for the future

In context of the I-Seed scenario, quantification of the emitted fluorescence signal strength from I-Seeds is important as it indicates the concentration or level of monitored environmental parameter. Several factors can affect the system's signal-to-noise ratio (SNR), and thereby, the actual development of the system has been started from a laboratory-based setup to achieve a complete understanding of the level of influence of these parameters for real-world field applications. We demonstrated the read-out of stable signal with good SNR up to a distance of 4m in controlled condition. Critical environmental conditions and sample behavior were assessed to evaluate their effect on signal read-out. Proof of principle for temperature read-out using both ratiometric and temporal approach have been realized. The lightweight prototype and the miniaturization for UAV deployment has been realized. Next steps are now focusing on evaluation of the prototype in a field situation.

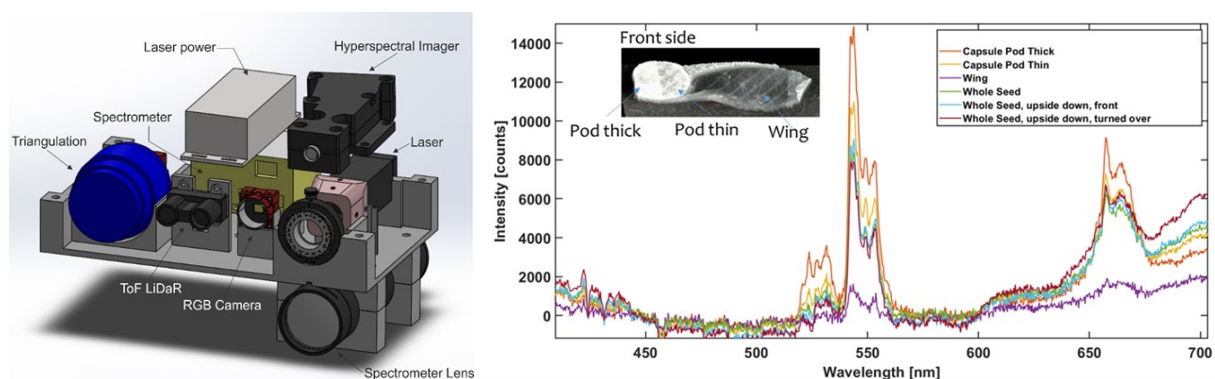


Figure 1: (left) Design and components for the Active Laser Fluorescence Imaging System and (b) Spectra of I-Seed Samara prototype at distance of 4 m, laser intensity of 2.6 W/cm² and an integration time of 500 msec. Inset shows photograph of the I-Seed Samara prototype with different parts labelled accordingly.

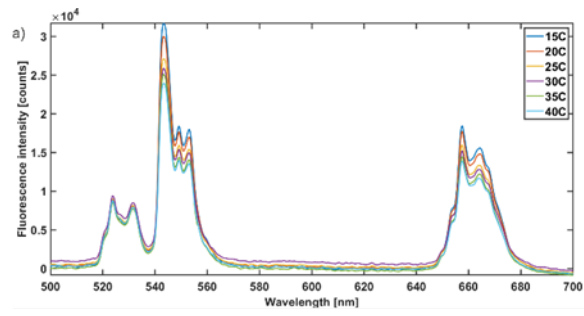


Figure 2: Change in spectra of fluorescing samples with varying sample temperature at a distance of 4 m for an excitation laser power of 2.8W.

Top of Canopy Fluorescence Quantum Efficiency from Hyperspectral Point-radiometer Systems

[Adrian Moncholi-Estornell](#)¹, Maria Pilar Cendrero-Mateo¹, José Moreno¹, Shari Van Wittenberghe¹

¹ University of Valencia, Image Processing Laboratory, Spain

Keywords (5): Field radiometry, Cal/Val, Hyperspectral, Spectral Unmixing, Fluorescence Quantum Efficiency

Challenge

Remote sensing of Solar-Induced Fluorescence (SIF) is challenged by the complex and dynamic nature of photosynthetic surfaces, which exhibit spatial and temporal variations in SIF emissions. These variations make it complex to compare SIF measurements across different scales in calibration and validation activities. Addressing this challenge requires the development of novel platforms, measurement protocols and algorithms to improve the quantification and interpretation of reflected radiance and SIF, while investigating the impact of spatial heterogeneity and structural and biophysical effects on SIF. Therefore, with the aim of interpreting fluorescence from hyperspectral measurements, as a first step to obtain estimates of photosynthesis (i.e., Fluorescence Quantum Efficiency FQE), it is key to prioritise the study of complex phenomena related to variations in PAR within the canopy and spectral unmixing analysis to disentangle the contribution of photosynthetic (i.e., sunlit and shaded) and non-photosynthetic surfaces to the measured TOC reflected radiance.

Methodology

To create a plant canopy experiment with varying levels of vegetation cover, we designed a field experiment based on a transect of potted plants placed in different densities and patterns, several designs were implemented to create vegetation transects with different levels of vegetation cover. A multisensor cable-suspended motorized platform called FluoCat was used to measure the transects. It is equipped with the Piccolo Doppio dual spectrometer system and a MAIAS2 multispectral camera. The MAIA reflectance images were used to obtain the reference total fractional vegetation cover and the reference sunlit fractional vegetation cover to validate the products derived from the Piccolo point spectroradiometer system. A linear spectral unmixing method was proposed to estimate the contribution of soil, sunlit, and shaded vegetation from the total reflectance spectrum measured at canopy level. By knowing the measured surface endmembers and combining them with a spectral fitting algorithm, we propose to unravel the abundance of each element. The weights used to combine the endmembers to fit the surface reflectance spectrum are understood as the abundance of each endmember. Later, the retrieved sunlit FVC was used to estimate the green APAR flux, and this was combined with the integral of the spectrally resolved fluorescence to calculate the FQE and compared with leaf level measurements.

Results

Comparing the reference and fitted reflectance spectra, our results show that the three endmembers (Sunlit and shaded vegetation, and soil) decomposition approach provides better results than using only two endmembers (total vegetation and soil). Regarding the differentiation between total fractional vegetation cover and FVCsunlit, both the two and three endmember approaches provided accurate

results when comparing Piccolo FVC_{total} and MAIA FVC_{total}, with an R-squared value of 0.88 and RMSE ranging from 0.11 to 0.13. However, only the 3-endmembers approach has the ability to discriminate between FVC_{total} and FVC_{sunlit}, resulting in an improved estimate of FVC_{sunlit} (RMSE=0.14) compared to using the 2-endmembers FVC_{total} to estimate the sunlit fraction (RMSE=0.21). The differentiation of these two parameters allows the separation of changes in the measured fluorescence driven by structural effects. Regarding the quantification of the real FQE, it is interesting to note that, with the exception of FVC_{sunlit} below 20%, similar FQE values were obtained throughout the experiment regardless of the fractional vegetation cover. The results indicated an overestimation of the retrieved values obtained by the Specfit method in cases of low FVC. FQE-TOC underestimated FQE at the leaf level. In 4 of the 11 transects analysed, the TOC measurements were statistically different from the leaf level measurements. However, despite the slight differences, the canopy and leaf level FQE values were in the same range and the variability along the experiment was similar.

Outlook for the future

For the future hyperspectral missions focused on the vegetation monitoring, further studies are needed to properly characterise and correct for the effects of canopy vertical structure in more heterogeneous areas, and to improve fluorescence retrieval to downscale TOC measurements to the photosynthetic surface level. In addition, improvement with more sophisticated spectral fitting algorithms for unmixing, with further characterisation of green (i.e., specific pigment absorption) and non-green (i.e., woody material and soil absorption libraries) end members, as well as atmospheric correction and thermal measurements should be incorporated into the proposed methodology to provide a robust estimate of photosynthetic activity.

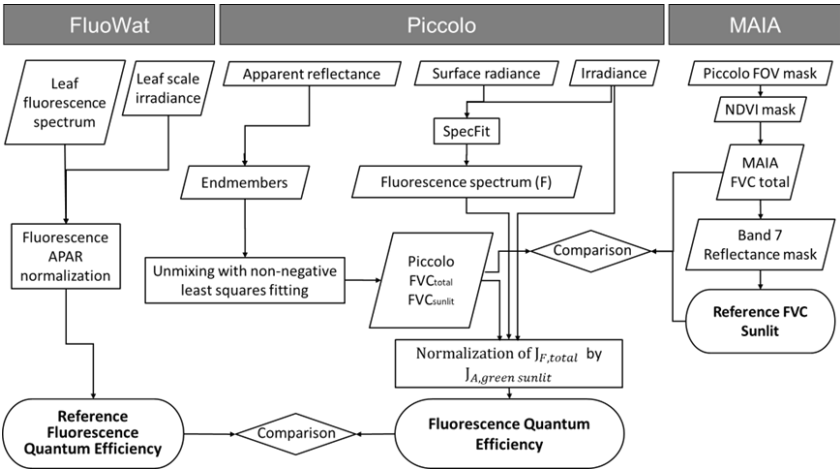


Figure 1. The methodology presented aims to derive the top-of-canopy fluorescence quantum efficiency (FQE) and then compare it to the leaf reference value. This methodology encompasses the processing sequences for various products derived from the FluoWat, Piccolo, and MAIA systems, as well as the processing steps required to obtain the essential variables for calculating the FQE. Adapted from (Moncholi-Estornell et al. 2023).

Defining The Spatial Heterogeneity Of FLEX Sun-Induced Chlorophyll Fluorescence From Hyperspectral HyPlant And Multispectral Sentinel-2 Data

[Nela Jantol](#)¹, Egor Prikaziuk², Marco Celesti³, Itzá Hernández-Sequeira⁴, Enrico Tomelleri⁵, Javier Pacheco-Labrador⁶, Shari Van Wittenberghe⁷, Filiberto Pla⁴, Subhajt Bandopadhyay⁸, Gerbrand Koren⁹, Bastian Siegmann¹⁰, Tarzan Legović¹, Hrvoje Kutnjak¹¹, M.Pilar Cendrero-Mateo⁷

¹Laboratory for Remote Sensing and GIS, Oikon - Institute of Applied Ecology, Croatia

²Faculty Geo-Information Science and Earth Observation, ITC, University of Twente, the Netherlands

³ HE Space for ESA - European Space Agency, European Space Research and Technology Centre (ESA-ESTEC), the Netherlands

⁴ Institute of New Imaging Technologies, University Jaume I, Castellón de la Plana, Spain

⁵ Faculty of Science and Technology, Free University of Bozen/Bolzano, Italy

⁶Max Planck Institute for Biogeochemistry, Germany

⁷ Laboratory of Earth Observation, Image Processing Laboratory, University of Valencia, C/ Catedrático Agustín Escardino, Spain

⁸ Department of Geography and Environmental Science, University of Southampton, UK

⁹Copernicus Institute of Sustainable Development, Utrecht University, Utrecht, the Netherlands

¹⁰ Institute of Bio- and Geosciences, Plant Sciences (IBG-2), Forschungszentrum Jülich, Germany

¹¹ Division of Plant Science, University of Zagreb Faculty of Agriculture, Croatia

KEYWORDS (5): SPATIAL HETEROGENEITY, SIF, HYPERSPECTRAL SENSOR, SENTINEL-2, FLEX

Challenge

The dynamic nature of Sun-Induced chlorophyll Fluorescence (SIF) makes it highly recommended to characterize its spatiotemporal heterogeneity before using it to monitor vegetation from space. SIF is the light emitted by plants within the spectral window of 650-800 nm and is characterized by having a peak in the red (685nm) and far-red (740nm) regions of the spectrum. The main challenge when characterizing SIF spatial heterogeneity is the lack of high spectral and spatial resolution satellite data needed to properly retrieve the functional-based (i.e. APAR and NPQ) and structural-based (i.e. LAI, fCover) traits driving SIF dynamic changes. However, what we do have available are high spatial resolution Sentinel-2 (20x20 m) based products (i.e., reflected radiance, vegetation indices, and biophysical traits). Within this context, we propose to use S2 imagery information to quantify the spatial heterogeneity of a FLEX pixel (300 x 300m).

Methodology

We used HyPlant airborne imagery acquired over an agricultural area in Braccagni (Italy) to emulate Sentinel-2-like top-of-the-canopy reflectance and SIF imagery at different spatial resolutions (i.e., 300, 20, and 5 m). In the context of the COST Action Optical synergies for spatiotemporal SENSing of Scalable ECOphysiological traits (SENSECO), in which this study was conducted, we proposed direct (i.e., spatial heterogeneity coefficient, standard deviation, normalized entropy, ensemble decision trees) and patch mosaic (i.e., local Moran's I) approaches to characterize the spatial heterogeneity of SIF collected at 760

and 687 nm and predictor variables. Vegetation indices (NDVI, near-infrared reflectance of terrestrial vegetation-NIRv, chlorophyll red-edge, EVI and MSI), biophysical traits (fAPAR, LAI, fCover, leaf chlorophyll content-LCC) and bands B6, B7, B8, B8A, B9 were used as predictors. For spatial heterogeneity coefficient approach, scene classifications maps were produced using supervised and unsupervised (k-means clustering) methods. We evaluated the potential of each approach to characterize SIF heterogeneity (SIF_{760,300} and SIF_{687,300}) by comparing the heterogeneity metrics calculated from the HyPlant SIF and Sentinel-2 predictors and calculating the square of Pearson's correlation coefficient (R^2).

Expected results

The application of different methods to describe the spatial heterogeneity of sun-induced fluorescence provided interesting insights, particularly for the use of standard deviation, the spatial heterogeneity coefficient and ensemble decision trees using machine learning algorithms. Among all methods, the structured related NIRv index explained SIF heterogeneity the best, compared to other vegetation indices (i.e., NDVI, ChIRE, EVI), biophysical traits (i.e., fAPAR, fCover, LCC, LAI) or S2 reflectance bands.

In general terms, the vegetation indices, biophysical traits, and Sentinel-2 bands related to vegetation structure (i.e., NIRv, fAPAR, fCover, LAI, B7 (red edge)) predicted SIF spatial heterogeneity the best. We decided to use fAPAR instead of fCover because they are highly correlated. Regarding the methods, ensemble decision trees was the best-performing approach ($R^2 > 0.8$ for SIF_{760,300} and $R^2 > 0.6$ for SIF_{687,300}). The standard deviation method, despite its simple implementation, casted $R^2 > 0.6$ for SIF_{760,300} and $R^2 > 0.1-0.4$ for SIF_{687,300} when NIRv, fCover, LAI and B7 were used as predictors, showing similar results to the spatial heterogeneity coefficient (using scene classification map produced with unsupervised classification) approach. Finally, the Local Moran's I and normalized entropy methods did not perform well for predicting SIF heterogeneity. It is worth noting that the spatial heterogeneity was better predicted for SIF_{760,300} than for SIF_{687,300}.

Outlook for the future

Based on the results of the current study, future work should include the application of the proposed methods to a larger dataset, such as other regions with different ecosystems (i.e., forest, grassland, boreal and/or tropical forest) to then determine which combination of method and vegetation indices or biophysical traits should be implemented in each ecosystem type. Additionally, if using spatial heterogeneity coefficient, determining the optimal number of clusters in unsupervised classification for producing maps over an area should be explored further. If our results are confirmed, our study would be a precursor for a SIF pixel heterogeneity product that could be implemented in the FLEX ground segment processing chain.

(1)

(2)

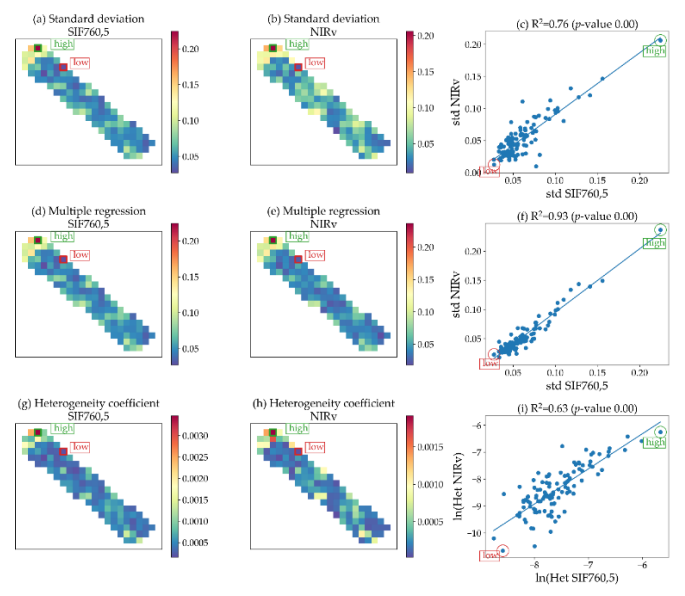
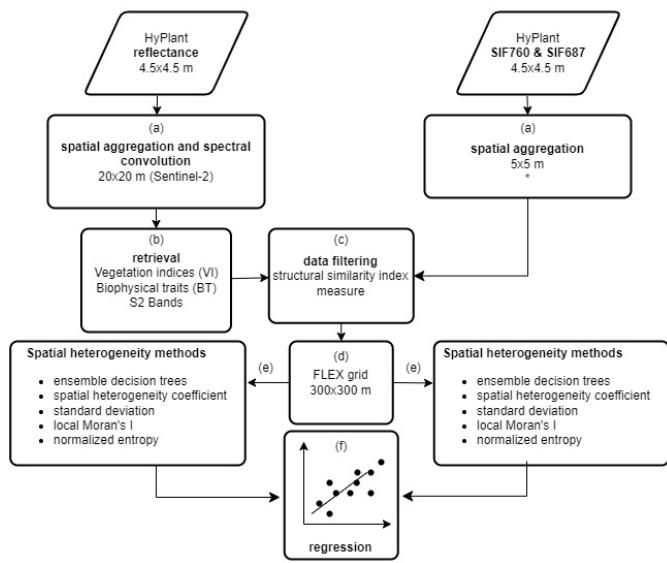


Figure (1) Workflow diagram. (2) Heterogeneity maps (300 × 300 m) for standard deviation, ensemble decision trees and spatial het-erogeneity coefficient approaches; (a,d,g) reference SIF760; (b,e,h) best predictor NIRv; (c,f,i) scatter plots with lowest (green circle) and highest (red circle) heterogeneity pixels highlighted.

Tracing changes in subsurface water storage through a novel satellite-based time-series of far-red solar-induced fluorescence emission efficiency

EARSel Valencia 2024

Abstract

Corresponding Author: d.herrera@fz-juelich.de

[David Herrera](#)¹, Uwe Rascher¹, Alexandre Belleflamme², Bastian Siegmann¹

¹ Forschungszentrum Jülich GmbH, IBG-2, Germany

² Forschungszentrum Jülich GmbH, IBG-3, Germany

Keywords (5): Earth Observation, SIF, Drought, PARFLOW, Tropomi

Challenge (800 - 1000 characters incl. spaces)

Satellite based measurements of solar-induced chlorophyll fluorescence (SIF) are globally available with a daily temporal resolution since 2018. The TROPISIF (Guanter et al., 2021. Earth System Science Data, Issue 11) and the Caltech SIF products (Köhler et al., 2018. Geophysical Research Letters, Issue 19) are based on observations of the ESA satellite Sentinel-5P and use similar data driven approaches to derive top-of-canopy (TOC) far-red SIF. However, TOC SIF information are affected by canopy structural effects and the illumination conditions at the time of data acquisition. For this reason, SIF satellite data needs to be downscaled to the leaf level and normalized for the amount of incoming photosynthetically active radiation (iPAR) to eventually calculate SIF emission efficiency (ϵ_f). ϵ_f in comparison to TOC SIF is more strongly linked to the photosynthetic activity of plants and thus has high potential to contribute to the improvement of satellite-based GPP estimations and the early detection of vegetation stress (e.g., drought stress). In this study, we explore the potential of SIF as an early indicator for drought stress by calculating and comparing a downscaled satellite-based SIF product to subsurface water storage data (sss) modelled by the PARFLOW/CLM hydrological model over the course of 6 years from 2018-2023 in Germany.

Methodology (1200 – 1500 characters incl. spaces)

To achieve this goal we combined daily observations of reflectance and SIF from Sentinel-5P (both part of the TROPISIF product) with daily information about iPAR from MODIS. To ensure that the SIF product can be used as an indicator for the dynamic physiological changes of vegetation canopies the SIF satellite data were day length corrected and filtered by the phase angle to correct for fluctuations caused by the sun-sensor geometry as proposed by Köhler et al. (2018. Remote Sensing of Environment, Volume 204). First, the Sentinel-5P reflectance product was used to calculate the NIRv ($\text{NIRv} = \text{NDVI} * R_{781}$) and subsequently this information was combined with the Sentinel-5P SIF product (SIF_{743corr}) and the PAR product of MODIS (MDC18C2) to calculate ϵ_f :

$$\epsilon_f = \frac{\pi * \text{SIF}_{743}}{\text{NIRv} * \text{iPAR}}$$

The generated ϵ_f time-series covering entire Germany in the spatial and the period 2018-2023 in the temporal domain was then compared to daily information about subsurface water storage (sss) derived with PARFLOW/CLM hydrological model simulations in the frame of the ADAPTER project (<https://adapter-projekt.org/>) (Belleflamme et al. 2023. Frontiers in Water, Volume 5). The sss and sss anomaly products for 10 different soil depths ranging from 2 cm to 3 m were gridded to the same spatial resolution as the ϵ_f satellite data (0.05°). To allow for a more nuanced look into the behaviour of ϵ_f compared to sss the data were classified into different biomes (agricultural areas, shrub- and grasslands, deciduous forests and coniferous forests).

Results (1200 – 1500 characters incl. spaces)

To combine PAR, SIF and reflectance data in a computationally efficient way Google Earth Engine (GEE) was used to produce the ϵ_f time-series covering the period 2018-2023. Seasonal dynamics in the ϵ_f time-series are not as pronounced as in the SIF743 time-series (Figure 1, left). A first comparison of ϵ_f of agricultural areas to sss at 30 cm (Fig. 1, A) shows similar spatial and temporal trends. Especially for longer periods of negative sss anomaly (Fig. 1, B) ϵ_f shows a good agreement to the two sss trends. This result is a first sign that ϵ_f has the potential to be used as an indicator for the early detection of drought stress. Additionally, the availability of sss products derived for different soil depths allows for a more detailed analysis how ϵ_f of the different biomes is changing as a reaction to the onset of drought events.

Outlook for the future (800 - 1000 characters incl. spaces)

While the initial goal of creating an ϵ_f time series was achieved. Its potential use for drought detection, now needs to be further evaluated. This evaluation can be conducted by calculating an ϵ_f anomaly product, which in combination with the sss products depth and the four different biomes will help in tracing reactions of ϵ_f to sss. Furthermore, the the ϵ_f and sss time-series needs to be harmonized and subdivided into smaller regions of interest (ROIs) representing specific parts of Germany (e.g. federal state level). In the temporal domain the focus of the analysis will be on specific periods of the time-series that are characterized by prolonged negative sss anomaly, which is an indicator for drought events. Once the data have been prepared, time-series correlation analyses will be conducted, such as cross correlation analysis, to estimate temporal lags of the ϵ_f data in comparison to the sss data. This future work will provide vital information if and under which conditions ϵ_f can be used to track changes in the sss anomaly time-series and thus help to investigate the potential of ϵ_f for the detection of drought stress in different biomes.

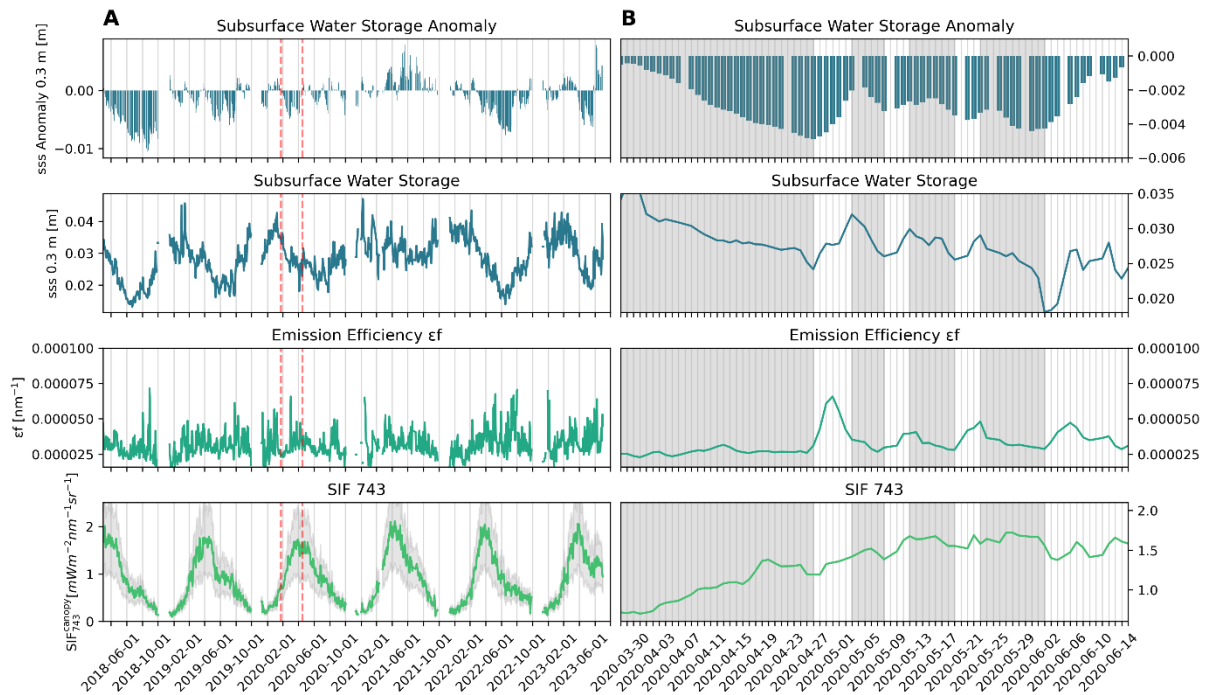


Figure 1 sss anomaly, sss, ϵ_f and SIF743 temporal trends of photosynthetically active vegetation composed of three day averages for agricultural areas in Germany from 2018-2023. While panel A shows the entire observation period, panel B focuses on a period characterized by high variations in sss anomaly from 25 March to 15 June 2020. The period is represented by vertical red lines in panel A. The grey coloured areas in panel B highlight possible drought onset events as observed in the sss temporal trend.

**Them.Sess. 2-6: Advances in
DESI data products and
applications**

Identifying and handling of errors caused by spectral ambiguities over water

Peter Gege¹, Milad Niroumand-Jadidi²

¹ German Aerospace Center (DLR), Remote Sensing Technology Institute, Münchner Str. 20, Oberpfaffenhofen, D-82234 Weßling, Germany

² Digital Society Center, Fondazione Bruno Kessler, Via Sommarive, 18 I-38123, Trento, Italy

KEYWORDS (5): REMOTE SENSING, WATER, HYPERSPECTRAL, DESIS, WASI

Challenge

All surface waters contain phytoplankton, coloured dissolved organic matter (CDOM) and non-algal particles. The diversity of type, chemical composition, size distribution, and in particular concentration introduces a fundamental numerical problem to data analysis: different combinations of water constituents can lead to similar reflectance spectra. These spectral ambiguities not only depend on the water constituents, but also on the sensor: less bands and increased noise reduce the measured spectral information and therefore increase the ambiguity problem. This problem is unfortunately not easily recognized during data processing, i.e. the concentration maps derived from a multispectral or hyperspectral image can appear plausible even when spectral ambiguities introduce severe errors.

Methodology

The Water Colour Simulator (WASI) software is available since 20 years for simulating spectral measurements in and above water, and for analysing such measurements by inverse modelling. Its module WASI-2D can process images from multispectral and hyperspectral sensors since 10 years. A new module, WASI-AI, has now been developed that combines physical modelling with Artificial Intelligence (AI) for image processing. Processing randomly selected pixels with two independent methods, inverse modelling and AI, makes it possible to determine the presence of ambiguities for each fit parameter: without ambiguities, the results are highly correlated, while the results become increasingly decorrelated the more severe the ambiguity problem is. Correlation plots of inverse modelling vs. AI results are therefore useful to identify ambiguity problems. WASI has been designed from the beginning for handling such problems by allowing the user to import site-specific optical properties to each model parameter, deciding for all model parameters if they shall be used as fit parameters or kept constant, defining image-specific initial values and ranges for each fit parameter, and giving the sensor bands different weights according to their information content and noise. The correlation plots now allow assessing the usefulness of each measure and optimizing image processing with respect to the ambiguity problem.

Results

A number of multispectral and hyperspectral satellite images has been processed with both inverse modelling and AI, allowing us to (1) identify fit parameters that are affected by spectral ambiguities and (2) finetune the inverse modelling to make the results more consistent. We present a statistic of the affected parameters and elaborate on the differences between multispectral and hyperspectral sensors

in terms of sensitivity to spectral ambiguities. We furthermore present the measures that have been turned out to be most effective for reducing the uncertainties caused by spectral ambiguities.

Our most ambitious goal was distinguishing from space different phytoplankton groups that occur as mixtures at low to moderate concentrations. Low concentration in combination with similar optical properties require a hyperspectral sensor and little noise. From all currently available spaceborne sensors with a spatial resolution suitable for inland waters, DESIS has the highest spectral resolution, therefore we used DESIS images from Lake Constance as test dataset. As expected, the spectral ambiguity problem is quite heavy for this task due to the similarity of the optical properties of phytoplankton groups. By applying the described methodology, we were able to improve the number of distinguishable groups from two to four for one scene, while for other scenes still just two groups could be differentiated, but with reduced uncertainty.

Outlook for the future

The described methodology has been implemented as a new module into the software WASI. Once the paper is published (it is currently in review), a new version of WASI will be released. WASI is a Windows program with graphical user interface and can be downloaded free of charge from <https://ioccg.org/resources/software/>.

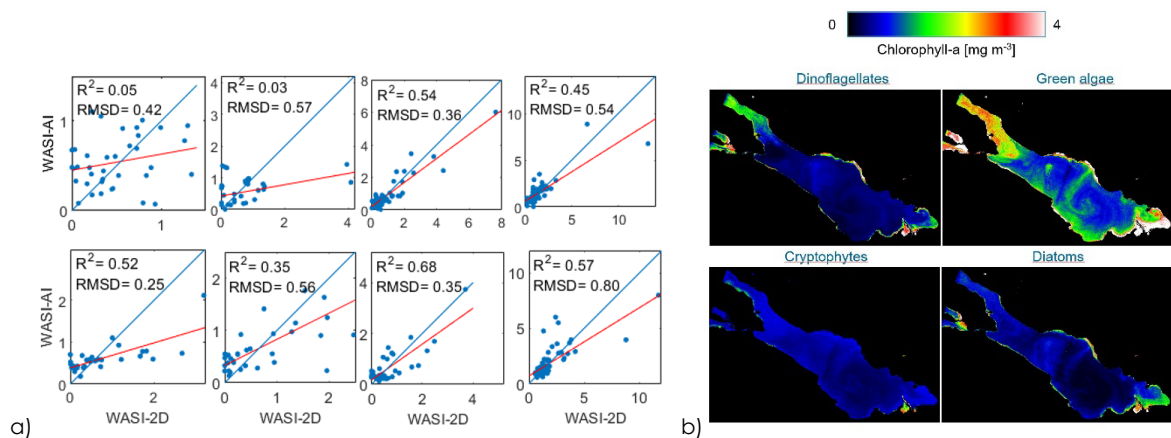


Figure (a) Correlation plot of physics-based inversion (WASI-2D) vs. statistics-based data analysis (WASI-AI). Upper row: all bands weighted equally; only 2 phytoplankton groups have $R^2 > 0.3$. Lower row: band-specific weighting applied; 4 phytoplankton groups have $R^2 > 0.3$. (b) Result of phytoplankton classification of DESIS image from Lake Constance from 14 Aug 2021.

Hyperspectral Imaging of the Earth with the DESIS instrument

EARSeL Valencia 2024

Abstract

Corresponding Author:

Emiliano.Carmona@dlr.de

Emiliano Carmona¹, Martin Bachmann², Daniele Cerra¹, Raquel de los Reyes¹, Daniele Dietrich², Uta Heiden¹, Uwe Knodt³, David Krutz⁴, Heath Lester⁵, Rupert Müller¹, Mirco Tegler⁶

¹ Remote Sensing Technology Institute, DLR, 82234 Weßling, Germany

² German Remote Sensing Data Center, DLR, 82234 Weßling, Germany

³ Institute of Space Systems, DLR, 28359 Bremen, Germany

⁴ Institute of Optical Sensor Systems, DLR, 12489 Berlin, Germany

⁵ Teledyne Brown Engineering (TBE), 300 Sparkman Drive, Huntsville, AL 35805, USA

⁶ German Remote Sensing Data Center, DLR, 17235 Neustrelitz, Germany

Keywords (5): Imaging spectroscopy, Earth Observation, Spaceborne, Applications, Land use

Challenge

In recent years, spaceborne imaging spectroscopy has made significant progress, evolving from a limited range of instruments and available data to a broad selection of missions, simultaneously acquiring quality data over large areas of the Earth. The spectral information provided by these missions is playing an increasingly important role in our understanding of the Earth's surface and its dynamic processes, in monitoring the environment and in managing the Earth's resources.

DEGIS, launched in June 2018, was the mission that inaugurated this new time, followed by the missions PRISMA (2019), HISUI (2019), EnMAP (2022) and EMIT (2022). DEGIS has been in operation for more than 5 years and has acquired by 6 November 2023, 279,146 images of the Earth. A large community of commercial and scientific users employ regularly DEGIS products on applications ranging from environmental monitoring and precision agriculture to coastal and marine studies.

Methodology

DEGIS is a pushbroom imaging spectrometer operating in the VNIR range (400 – 1000 nm) with a narrow (2.55 nm) spectral sampling. The mission is a collaboration between the German Aerospace Centre (DLR) and TBE. The instrument is installed on the International Space Station (ISS), more precisely on the MUSES platform. MUSES, built and operated by Teledyne Brown Engineering (TBE), provides DEGIS with communication, power, and pointing capabilities. The DEGIS instrument was built by DLR, which also provides the processing software. The spatial resolution is 30 m and the swath width is 30 km while the swath length varies, depending on the planned acquisitions. TBE provides the Ground Segment, which is responsible for operating and tasking DEGIS, archiving the received data and processing on demand the products that TBE commercial users tasked or ordered from the catalogue. DLR also has established a Ground Segment that obtains the DEGIS products from TBE archive and it archives and processes the DEGIS products for DLR scientific users.

Both commercial and scientific users obtain DEGIS products as tiles of 30 × 30 km, processed to different levels and with different processing options. Level 1B products (L1B) correspond to radiometric Top of Atmosphere (TOA) at sensor geometry radiances. Level 1C (L1C) are L1B products that are ortho-rectified. Finally, Level 2A (L2A) are ortho-rectified atmospherically corrected Bottom of Atmosphere (BOA) reflectances.

Results

The performance of DESIS is monitored by the DLR ground segment. Analysis of the calibration data shows that the spectral stability of the instrument is within 0.11 nm (RMSE). Moreover, the vicarious radiometric calibration of the instrument shows that the radiometric accuracy is in the range of 4% – 5% above 450 nm. The sensor shows, however, a higher variability below 500 nm which can reach 20%/year at lower wavelengths (below 420 nm). Regarding geometric performance, the automatic extraction of ground control points (GCPs) during LIC processing achieves an accuracy of ~20 m (RMSE) for both along and across-track directions. The accuracy in scenes where no GCPs can be extracted is reduced to ~300 m and ~500 m, respectively across and along the track.

DESI products are being used by a growing user community in a wide range of applications. The large number of DESIS products enables the development of applications that need to be trained on large volumes of data or data acquired under different observation conditions, as a result of the ISS orbit which is not polar. Since the start of operations, two DESIS user workshops have been held in 2021 and 2023, demonstrating the interest of the scientific community and the applications of DESIS data in different fields. DESIS data are used to obtain soil, vegetation or snow parameters, to classify forests and crops, to study inland and coastal water quality, as well as for more specific agricultural applications.

Outlook for the future

DESI has been in operation for more than 5 years, exceeding the initially planned lifetime of the mission. During this time, the mission has operated without major problems, producing one of the largest catalogues of remotely sensed hyperspectral data available today (see Figure). Some areas of the Earth have been acquired several tens of times, providing unique hyperspectral timeseries spanning several years.

Given the instrument's good status, DESIS is expected to continue operating in the coming years. DLR also plans an extension of the archive in the first half of 2024, offering direct download of L2A DESIS data. The large data volume already acquired, and to be acquired in the future, together with the narrow sampling distance, offers many possibilities for synergies and research opportunities when combined with data from other missions. All this makes DESIS one important element of the future of imaging spectroscopy in the coming years.

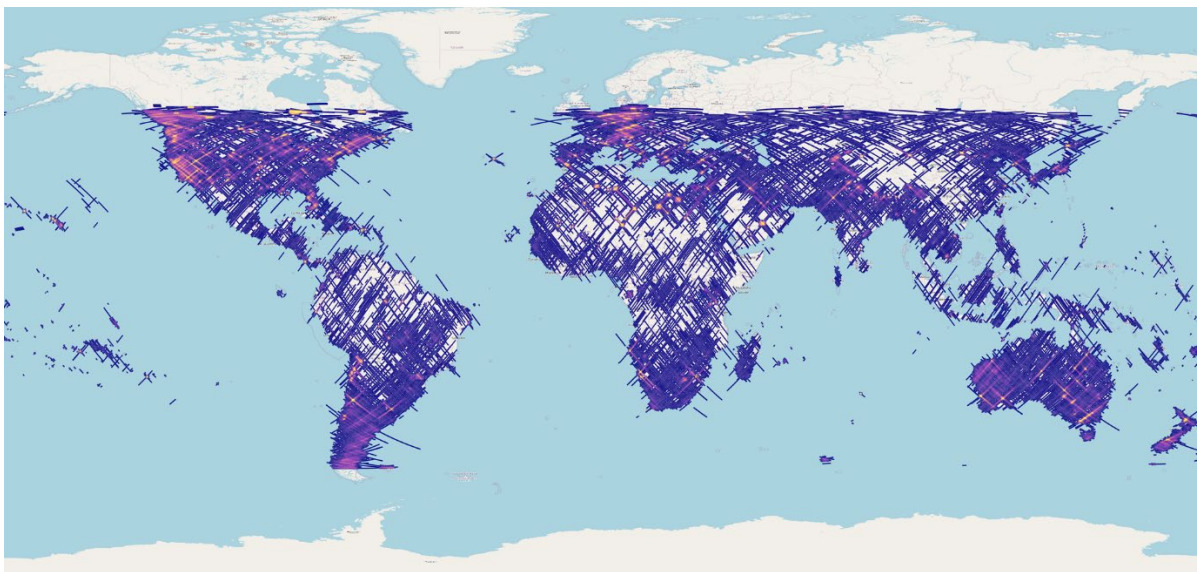


Figure Heatmap showing the number of DESIS scenes acquired until October 2023. The yellow and white hotspots correspond, respectively, to more than 35 and more than 100 products over these areas.

**[Formatting guidelines for
abstract submission]**

EARSeL Valencia 2024

Abstract

Corresponding Author: paul.karlshoefer@dlr.de

**Temporal Soil Composites from the
EnMAP and DESIS hyperspectral image
archive**

Paul Karlshöfer¹, Kevin Kühl¹, David Marshall¹, Martin Bachmann², Uta Heiden¹

¹ IMF-PBA, DLR, Münchener Straße 20, 82234 Weßling, Germany

² DFD-LAX, DLR, Münchener Straße 20, 82234 Weßling, Germany

Keywords (5): Temporal Composites, EnMAP, fractional vegetation cover, soil, moisture

Challenge (800 - 1000 characters incl. spaces)

Building temporal composites using the extensive archives of the multispectral workhorses Landsat and Sentinel-2 becomes increasingly important for environmental studies such as land cover classification, urban studies, and soil parameter retrievals. With the recent launches of spaceborne hyperspectral instruments such as DESIS, PRISMA, and EnMAP, the generation of hyperspectral temporal composites is enabled.

Image composites naturally require multiple observations of the same region. As of the present date, the frequent acquisition of multiple observations for scenes captured by the EnMAP (Environmental Mapping and Analysis Program) sensor remains uncommon. Nevertheless, our experience with DESIS data has demonstrated that even a small quantity (<10) of high-quality and mostly cloud-free scenes suffices for the creation of densely populated composites. In this study, we investigate the circumstances under which the hyperspectral image archives from EnMAP and DESIS can be utilised for the production of both general and specialised composites.

Methodology (1200 – 1500 characters incl. spaces)

Naturally, the generation of composites requires multiple scenes that overlap and become a temporal stack. This stack is initially probed for any inaccuracies in the geometric correction which are corrected, if necessary. Then, an algorithm iteratively eliminates outliers and converges eventually on a single spectrum, which will be chosen for the final composite, where the selected spectrum best represents the most dominant spectral class. Additionally, the method excludes hazy or cloudy pixels, which might not have been detected by the cloud mask, early in the selection process. For soil composites, a map representing fractional vegetation cover (FCover) which is computed from spectral unmixing (Marshall et al., 2021) guides the selection towards soil spectra. On a side track, the selection of soil pixels by spectral unmixing is compared to the use of spectral indices such as NDVI, PV+IR2 or NBR2.

Currently, the incorporation of soil moisture content into the process is an area of ongoing development. It remains to be determined whether synthetic spectra and/or sensor data, correlated with weather information, will be integrated. Once the moisture content is reliably calculated per pixel, the composite spectra ideally are corrected to reduce the amount of variance in that dimension throughout the composite.

Results (1200 – 1500 characters incl. spaces)

To date, solely initial composite have been derived through the utilisation of EnMAP data. Nonetheless, the aforementioned approach has demonstrated its efficacy when applied to DESIS data, as illustrated in the accompanying figure. For instance the current method has revealed a notable enhancement in the mitigation of cloud and haze-related distortions within the ultimate composite output.

Taking into consideration the comprehensive spectral coverage of EnMAP data, which includes not only the VNIR (400-1000 nm) range but also extends into the SWIR (1000-2500 nm) spectrum, this capability facilitates the determination of fractional vegetation cover and thereby supports a more discriminating quest for optimal soil pixel selection. Subsequently, these soil composites hold the potential for inferring soil attributes such as the moisture and organic carbon content. Furthermore, the additional information on FCover proves valuable for quantifying soil organic carbon without interference from the non-photosynthetic vegetation (NPV) component, which may be distributed over the soil surface.

Finally, a comparative analysis will be conducted to assess the composites derived from data obtained by the EnMAP and DESIS instruments.

Outlook for the future (800 - 1000 characters incl. spaces)

Indeed, the expanding repository of hyperspectral data inherently contributes to the facilitation and augmentation of soil composite generation. With the increasing volume of data, the precision in establishing the minimum prerequisites for generating these composites will be notably enhanced.

An essential aspect lies in the validation of the ultimate products. Given their composition spanning a significant time frame, the validation through in-situ measurements proves to be unfeasible. Nevertheless, it is possible to cross-check individual input scenes for a limited number of pixels with other hyperspectral or multispectral datasets, acquired through various means such as on-orbit, airborne, or ground-based measurements. This approach serves to validate the pixel selection process and provides the means of establishing a confidence interval for the derived results.

As for the generated products, they can be correlated with soil sample databases, such as the LUCAS topsoil database. The work on this is planned in the scope of a different project.

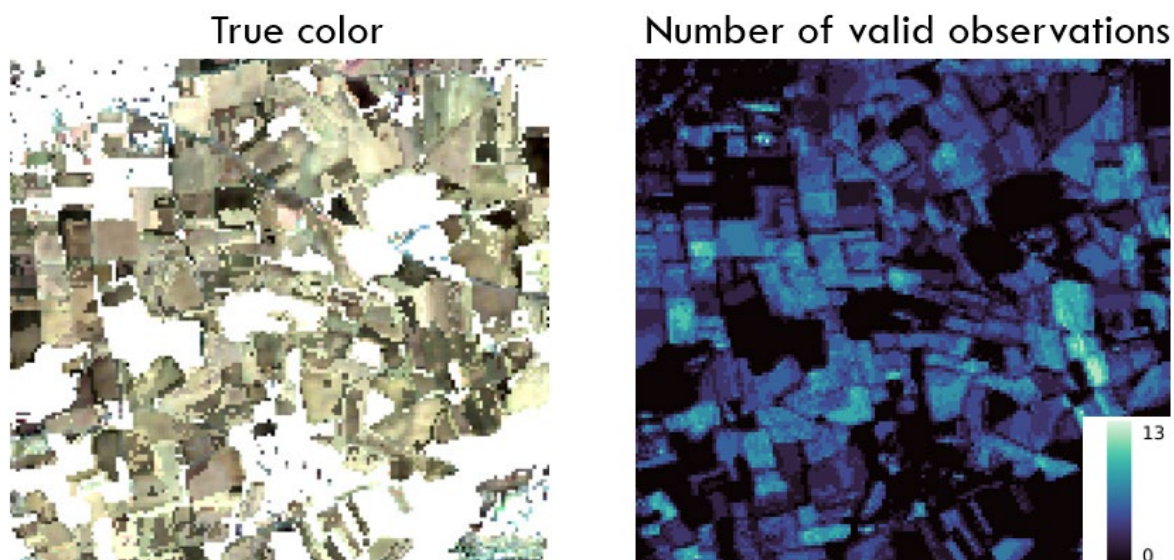


Figure Example for a densely populated DESIS soil composite in true colour (left) and in with the number of corresponding observations (right). Zoomed in northwest of Munich, Germany.

Towards a machine learning retrieval of solar-induced fluorescence from DESIS data

[Miguel Pato](#)¹, Jim Buffat², Kevin Alonso³, Stefan Auer¹, Emiliano Carmona¹, Stefan Maier¹, Rupert Müller¹, Patrick Rademske², Uwe Rascher², Hanno Scharr⁴

¹ German Aerospace Center (DLR), Earth Observation Center, Remote Sensing Technology Institute, Oberpfaffenhofen, Germany

² Forschungszentrum Jülich GmbH, Institute of Bio- and Geosciences, IBG-2: Plant Sciences, Jülich, Germany

³ RHEA Group c/o European Space Agency (ESA), Largo Galileo Galilei, Frascati, Italy

⁴ Forschungszentrum Jülich GmbH, Institute of Advanced Simulations, IAS-8: Data Analytics and Machine Learning, Jülich, Germany

Keywords (5): Earth observation, solar-induced fluorescence, DESIS, radiative transfer, machine learning

Challenge

One of the most important biophysical parameters to assess and monitor plant health is the solar-induced fluorescence (SIF) emitted during photosynthesis. Over the last decades, SIF retrieval with on-ground and airborne spectrometers (such as HyPlant) has successfully helped study fluorescence at high spatial resolution, but with limited spatial and temporal coverages. Using data from current and future spaceborne spectrometers has the potential to monitor fluorescence over extended regions with high temporal frequency. In this respect, the DESIS imaging spectrometer operating on the International Space Station can play a decisive role given its spectral (3.5 nm) and spatial (30 m) resolutions, spatial coverage and revisit times. In this contribution, we report on our on-going effort to develop a machine learning (ML) approach to SIF retrieval in the O₂-A absorption band tailored to the DESIS instrument.

Methodology

The starting point of our work consists in the simulation of at-sensor radiance spectra in the O₂-A band taking into account atmosphere, geometry, surface and sensor aspects in detail. The radiative transfer in the atmosphere is modelled using MODTRAN6 and considerable effort is put into simulating realistic spectra based on expert knowledge of the DESIS spectrometer. We developed a general-purpose simulation tool and used it to carry out a comprehensive sensitivity analysis in order to identify the key parameters for SIF retrieval in the O₂-A band as well as their ranges. An extensive set of databases of simulated at-sensor radiance spectra for DESIS was then generated encompassing a wide range of atmosphere conditions, observation geometries, surface parameters and sensor characteristics. The multi-dimensional input space consists of 12 dimensions and was sampled with different methods (uniform grid, random and Halton) so that the complex interplay between the input parameters is suitably captured. A sequence of databases of increasing complexity was prepared to aid the learning process, with the final databases containing over 10 million spectra. The realistic nature of these spectra was ensured through comparison to real data from DESIS and HyPlant in order to control any domain gap between simulation and data.

Results

Two applications of the simulated databases described above are explored in our work. First, we trained a forward simulator of at-sensor radiances using simple ML methods. Our results show that fourth-degree polynomials are both fast and accurate ML simulators. In fact, typical computation times are 10–20 μ s per spectrum (instead of minutes for the full simulation) and the at-sensor radiance errors amount to less than 0.1 $\text{mW}/\text{m}^2/\text{sr}/\text{nm}$ across the $\text{O}_2\text{-A}$ band (less than 10% of a typical SIF signal). The proposed ML simulator can be instrumental for SIF retrieval by enabling fast simulation of large datasets and by its integration in self-supervised inversion schemes (see submission by Buffat et al.). These applications are currently not feasible with a full-fledge simulation.

Second, we designed a multi-layer perceptron with residual links and trained it on the simulated data to retrieve SIF from DESIS in the $\text{O}_2\text{-A}$ band. The model predicts SIF pixelwise and its performance is validated with DESIS/HyPlant coincident datasets from 2020 and 2023. The figure below shows a SIF map retrieved by our model for part of a DESIS scene. The SIF estimates are fairly well correlated with the HyPlant retrieval based on a traditional method and show some dependency on surface reflectance. The results are still preliminary and more work is needed for a full validation of the method. However, our findings are promising for the final goal of retrieving SIF from DESIS data with a robust ML approach.

Outlook for the future

The DESIS imaging spectrometer has been continuously delivering high spectral resolution measurements from the International Space Station since 2018 and will likely continue to do so in the next years. Although not designed specifically for SIF retrieval, DESIS has suitable spectral properties for the task and a large catalogue of data from around the world. Our preliminary results suggest that an ML method trained on realistic simulations can in fact retrieve SIF from DESIS at-sensor radiance spectra around the $\text{O}_2\text{-A}$ band. If it turns out that such SIF retrieval can be made reliably on a routine basis, then the existing and future DESIS data will automatically enable the mapping of fluorescence from any land site in the globe at high spatial resolution, frequent revisit times and at different local times.

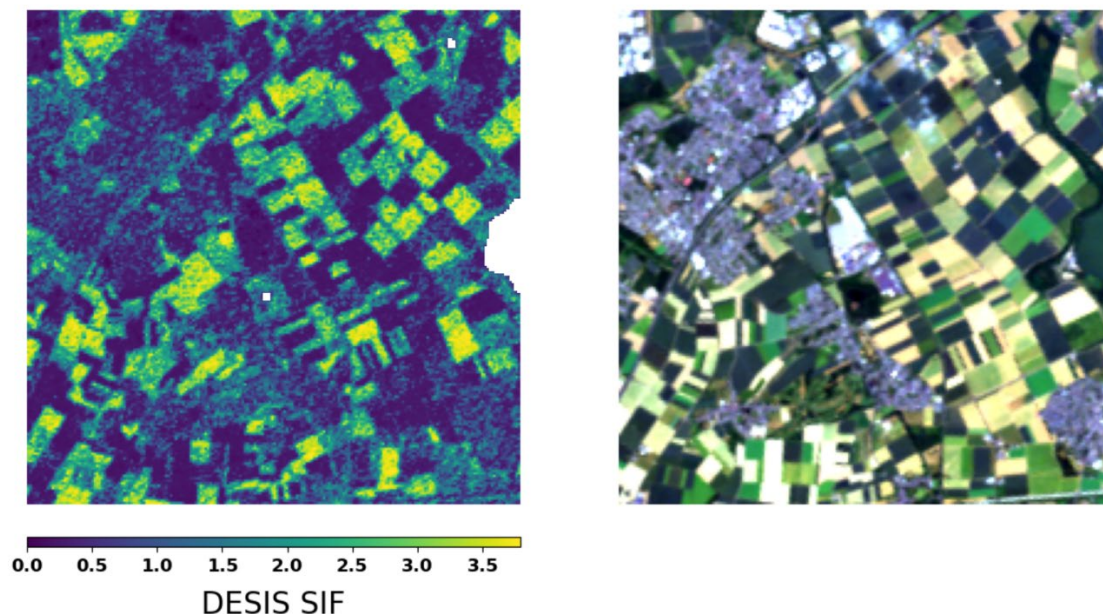


Figure DESIS SIF retrieval preliminary results. The left panel shows the SIF retrieved by the proposed ML model (in units of $\text{mW}/\text{m}^2/\text{sr}/\text{nm}$), while the right panel is the corresponding true color composite based on DESIS reflectances.

**Them.Sess. 2-7: Status and
applications of the PRISMA
mission at the turn of 5 years
in orbit**

HYPERSENSPECTRAL APPLICATIONS and INNOVATION: the “PRISMA SCIENZA” ASI program fostering the national downstream sector

EARSel Valencia 2024
Abstract
Corresponding Author: giorgio.licciardi@asi.it

Giorgio Licciardi, Maria Girolamo Daraio, Maria Elena Cianfanelli, Maria Libera Battagliere, Rocchina Guarini, Luigi D'Amato, Antonio Montuori, Alessandro Coletta

ASI – Italian Space Agency

Keywords (5): Earth Observation, Hyperspectral, downstream applications

Challenges in the Italian Space Economy

Space technologies and applications have the potential to benefit European society and economy, addressing major societal challenges while bolstering synergies between public and private sectors. Space technologies can stimulate economic growth and spawn new markets by fostering the development of innovative products and services tailored to meet user needs. However, the downstream space market poses unique challenges mainly due to its disjointed nature and by insufficient interactions between stakeholders. The Italian space industry, primarily comprised of Small Medium Enterprises (SMEs) (80%), encapsulates these issues, necessitating a robust ecosystem to streamline the space venture value chain. Italy holds a significant position in this regard, being among the few nations worldwide that offer a comprehensive production chain in the space sector, ranging from Research & Development (R&D) infrastructures, space technology manufacturing, to an extensive satellite constellation. This environment fosters the development of innovative products and services aimed at addressing traditional market needs through space-related technology.

ASI approach for data exploitation

In response to identified challenges, the Italian Space Agency established the Downstream and Application Services Unit (UDS) to enhance the competitiveness of national SMEs, industries, and academia. In this framework, UDS has launched a suite of initiatives in support of Italian industrial downstream sector, which encompass four main categories:

- Advocating for the utilization of Italian, European, and partner institutions' space infrastructures.
- Enhancing awareness and adoption of space-derived products and services within traditional market sectors.
- Addressing specific needs within Industrial, Scientific, and Public Administration sectors.
- Concentrating on specific thematic areas of interest for the Italian and European systems.

These categories translate into practical actions through project funding, networking activities, and in-depth analyses of stakeholders' needs. The Unit's initiatives act as a catalyst for innovation, fostering a robust and dynamic Italian space industry. Among these actions, the PRISMA SCIENZA program is an initiative leveraging the scientific data from PRISMA mission for the benefit of the Italian Communities, including universities, public research bodies, and industries. This program plays a pivotal role in supporting full data exploitation of the mission, simultaneously promoting the development of Italian expertise in the Hyperspectral (HS) remote sensing sector.

The PRISMA-SCIENZA Program

The PRISMA SCIENZA program aims to establish a skilled user group in the short term and promote the mission at both national and international level. In the long term, it will stimulate interest in application-

specific uses of products, which will support the complete data exploitation of the mission. More in detail, the main aims of the PRISMA SCIENZA call are:

- Gather comprehensive knowledge about the skills and scientific interests of the PRISMA mission user community. This understanding forms the bedrock of strategic decisions for future space missions.
- Inspire and engage the national community in the scientific use of PRISMA data and exploring its potential.
- Expand the array of possible applications of mission data. This broadens the reach of space technology, leading to innovative applications in diverse sectors.
- Promote the development of Italian know-how and strengthen existing skills in the HS remote sensing sector.

The program has funded the first 15 out of 23 proposals that met the call requirements. The proposals focus on various topics, spanning from air quality to precision agriculture, from water parameters monitoring to cultural heritage. It is also worth to note that most of the received proposals were from consortia composed by Universities, research centres, public bodies and SMEs. The projects have a duration of 2 years and started in the spring of 2022.

At conference time, some results of PRISMA SCIENZA projects will be presented in order to discuss, share and give evidence of main achievements carried out by national scientific and industrial community, for the exploitation of PRISMA data in support of diverse application fields and case studies.

Outlook for the future

Starting from the experience gained with the PRISMA SCIENZA initiative, ASI moved to a broader approach with the I4DP - Innovation for Downstream Preparation program. I4DP represent a "progressive" ASI roadmap in the downstream sector

- to supports the demonstrative development of new technologies, products, and services, incorporating various types of space data (EO, SATNAV, SATCOM) and other cutting-edge technologies such as Artificial Intelligence, Data analytics, and the Internet of Things;
- to allow the acceleration of scientific and technological development, through the implementation of demonstrators and pilot projects capable of using national systems dedicated to the management of geo-spatial data;
- to prepare new generation downstream services, useful for users engaged in the governance and monitoring of the territory and its resources, using entrepreneurial and scientific skills and enhancing the infrastructure investments made by ASI

The program is divided into 3 different actions (market, Public Administrations, Science), based on the different categories of users to which it will be directed (Public Administrations, Companies, Universities or Research Centers). While the I4DP Science action is devoted to support the development of innovative solutions by Universities and Research Centers, the I4DP-market and Public Administration actions are chiefly geared towards SMEs, but also encourages the participation of start-ups and scale-ups. Their primary objective is to foster the development of innovative services and products with high Technology Readiness Levels (TRLs), positioning them for commercial exploitation.

Conclusions

Being one of the few nations with a comprehensive space industry production chain, spanning both upstream and downstream sectors, Italy has a strategic advantage, serving as a liaison between the space industry and traditional markets, fostering mutually beneficial interactions. The above-mentioned initiative positioned Italy as a leading player in hyperspectral remote sensing technology.

The Characterization of Phosphate Waste Rock Piles using PRISMA Hyperspectral Images

Abdelhak EL MANSOUR¹, Ahmed LAAMRANI², Abdellatif EL GHALI¹, Rachid HAKKOU^{1,3}, Mostafa BENZAAZOUA¹

¹ Mohammed VI Polytechnic University, Geology and Sustainable Mining Institute (GSMI), Benguerir, Morocco

² Mohammed VI Polytechnic University, Center of Remote Sensing Application, Benguerir, Morocco

³ Imed-Lab, Faculty of Sciences and Technology, Cadi Ayyad University (UCA), Marrakech, Morocco

Keywords (5): Hyperspectral imaging, waste rock piles, phosphate mine, PRISMA

Challenge (800 - 1000 characters incl. spaces)

The exponentially growing production of phosphate ore, driven by surging demand across numerous industries, underscores the fundamental role of this naturally occurring mineral. Highly regarded for its exceptional properties, phosphate ore serves as an indispensable resource at the heart of a diverse array of applications. Its significance transcends individual sectors, and it resonates globally, highlighting its intrinsic relevance. However, as the phosphate mining industry expands to meet increasing demands, it confronts a challenge in the form of phosphate waste rock piles (PWRPs). These accumulations necessitate thorough characterization for their identification. To address this concern and move towards a sustainable future for phosphate mining, hyperspectral imaging (HSI) emerges as a promising tool. HSI enables the detection and analysis of various PWRPs characteristics, offering insights and innovative strategies that could redefine the industry's landscape.

Methodology (1200 – 1500 characters incl. spaces)

To characterize spatially and mineralogically the constituents of the PWRPs of the Benguerir phosphate mine, we used a PRISMA L2D cloud-free scene acquired on 12 February 2022. Simultaneously, we conducted a sampling campaign on Panel 2 of the Benguerir mine following a linear grid. With a 5 m step between samples, we collected 100 topsoil samples from the PWRPs over 625 m. Moreover, we crushed and ground the samples to 75 µm for X-ray diffraction (XRD) and X-ray fluorescence (XRF) analysis.

HSI was treated using the ARTMO toolbox in MATLAB and ENVI 7.5 (L3Harris technologies, USA). Before going through the processing, several bad bands were eliminated. Afterward, we obtained the smoothed spectra by interpolating the removed bands, applying spline interpolation, and smoothing using Python. The Principal Component Analysis (PCA) and Minimum Noise Fraction (MNF) were applied to reduce the spectral dimensions of the bands. Moreover, we tested three models for the supervised classification: the Spectral Angle Mapper (SAM), the Minimum Distance classification, and the maximum likelihood. This is done with different lithologies as input datasets, afterward, the three models were trained to map and extract spectral features of the PRISMA image.

Results (1200 – 1500 characters incl. spaces)

Preliminary results indicate that PWRPs are highly heterogeneous based on the reflectance spectra of the study area. According to the mineralogical results, the XRD characterization indicates the presence of different minerals that constitute the PWRPs including fluorapatite, quartz, dolomite, calcite, palygorskite, and montmorillonite. Furthermore, quartz, calcite, phosphate pellets, phosphatic clasts, and biofragments were detected in thin sections of PWRPs. The high heterogeneity of PWRPs is further supported by XRF results, which show that SiO₂ percentages had a large variance with a minimum value of 7% and a maximum value of 62.61%. P₂O₅ ranges from shallow values of approximately 1% to high values of over 23%. Significant variations were also seen in other major elements, such as MgO and CaO.

For the machine learning models, the Support Vector Machine and the maximum likelihood showed 3 and 4 mapped lithologies respectively. In contrast, the Minimum Distance (MD) algorithm showed encouraging results in detecting the minerals that constitute PWRPs, the MD classifier mapped all the lithologies used in the input data. It showed a high distinguishability of lithologies over phosphate waste rock piles, otherwise, the model still needs to be validated to check its accuracy.

Outlook for the future (800 - 1000 characters incl. spaces)

In our pursuit of a deeper comprehension of the composition of PWRPs, we are eager to harness the potential of spectroscopy. This analytical approach allows us to scrutinize the chemical, mineralogical, and hyperspectral attributes of PWRPs, thereby enabling us to gain a comprehensive understanding of their composition. By identifying regions rich in value-added elements, such as phosphorus (P), and pinpointing areas that necessitate restoration and reclamation, we can facilitate the transition towards more sustainable phosphate mining practices. Our integration of spectroscopy, in conjunction with the utilization of Unmanned Aerial Vehicles for data collection, promises to provide us with critical insights into the characteristics of PWRPs. This knowledge will be invaluable in addressing the challenges associated with phosphate resource exploitation, ultimately contributing to the growth and prosperity of the mining industry.

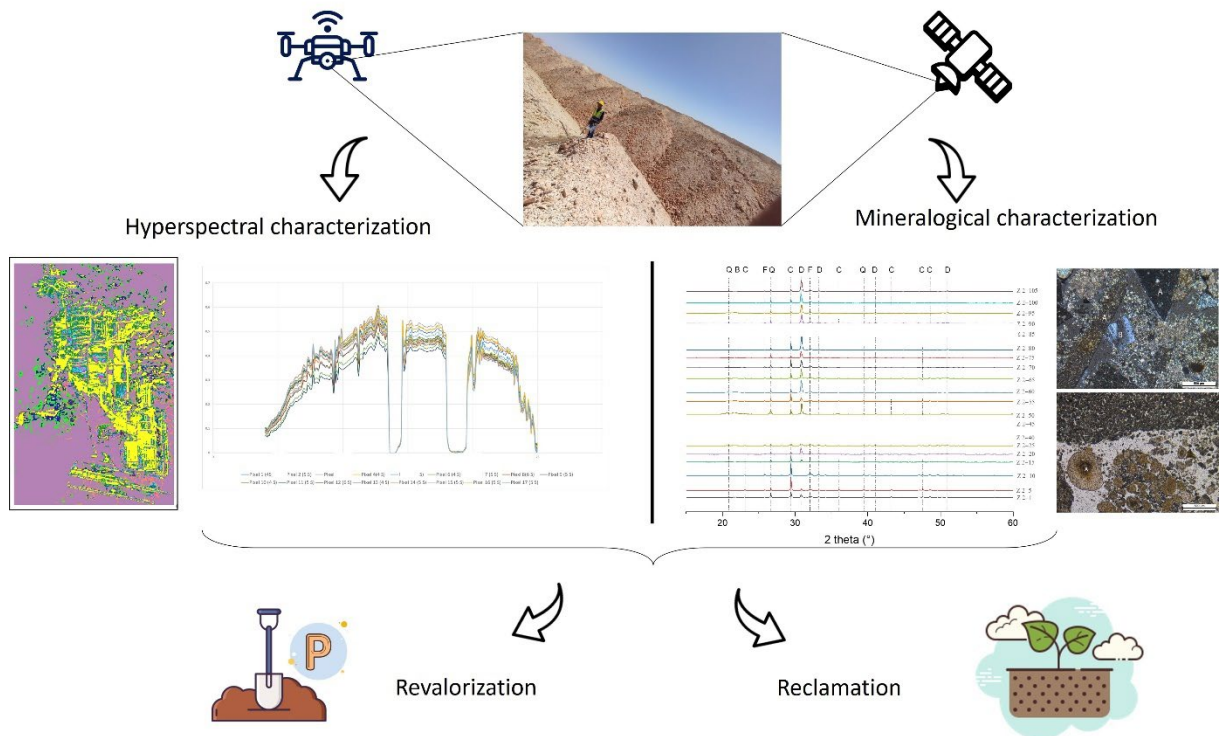


Figure The methodological approach adopted for the characterization of phosphate waste rock piles

Estimation of photosynthetic and non-photosynthetic vegetation structural traits in Mediterranean tree-grass ecosystem using *in situ* and PRISMA satellite hyperspectral data

M. Dolores Raya-Sereno¹, M. Pilar Martín¹, Rosario Gonzalez-Cascon², Vicente Burchard-Levine³, Daniel Pfitzer¹, Lucía Casillas¹, David Riaño¹, Javier Pacheco⁴, Héctor Nieto³

¹ ENVIRONMENTAL REMOTE SENSING AND SPECTROSCOPY LABORATORY, SPECLAB-CSIC, SPAIN

² NATIONAL INSTITUTE FOR AGRICULTURE AND FOOD RESEARCH AND TECHNOLOGY, INIA-CSIC, DEPARTMENT OF ENVIRONMENT, SPAIN

³ INSTITUTE OF AGRICULTURAL SCIENCES, ICA-CSIC, SPAIN

⁴ MAX PLANCK INSTITUTE FOR BIOGEOCHEMISTRY, HANS KNÖLL STRABE, GERMANY

Keywords (5): Field spectroscopy, PRISMA hyperspectral images, *in situ* data, tree-grass, non-photosynthetic vegetation

Challenge

Pastures and tree-grass ecosystems provide essential eco-services to rural and urban livelihoods. The sustainable management of pastures faces new challenges where the quality and quantity of pasture production (and therefore economic profitability) must be approached. Quantifying traits such as biomass or leaf area index (LAI) through remote sensing is relevant for monitoring seasonal, annual, and long-term vegetation changes. However, the distinction between photosynthetic and non-photosynthetic vegetation (PV and NPV) traits is complex because it relies on the narrow absorption band of lignin and cellulose in the short-wave infrared (SWIR) region. New medium-resolution hyperspectral satellite missions, such as PRISMA, offer new opportunities in this area. The research aims to investigate the ability of PRISMA images to estimate PV and NPV structural traits in Mediterranean tree-grass ecosystem using spectral indices and *in situ* data.

Methodology

In situ and satellite hyperspectral data from a tree-grass ecosystem located at Majadas de Tiétar long-term experimental station (39°56'26"N, 5°46'29"W) was used to calibrate empirical models to estimate aboveground biomass (ABG) and leaf area index (LAI) for the grass layer. 27 PRISMA Level 2D images were acquired from the study between 2020 and 2023 in different grassland phenophases: autumn regrowth (AR), biomass peak (BP), summer drought (SD), and grass decay (GD). To resolve the co-registration issues in PRISMA imagery, this study adapted an automated open-source Python code originally designed for airborne mosaics (https://github.com/hectornieto/airborne_tools). Atmospheric water absorption bands and noisy spectral bands were removed by comparison with ground-based spectra acquired in six sampling campaigns in nine permanent 25 × 25 m grass plots and nine tree crowns, using an ASD FieldSpec 3 spectroradiometer (Analytical Spectral Devices Inc., Boulder, Co, USA) covering a 400-2400 nm spectral range. Two diagonal NE-SW and NW-SE transects per plot were measured and averaged to be representative and comparable with 30 m pixel PRISMA images. A total of 175 valid spectral bands were used to calculate 50 spectral indices that were also calculated using ASD spectra. Regression analysis between *in situ* measurements of AGB and LAI for the total, PV and NPV fractions and spectral indices allowed us to derive the most accurate models to estimate grass traits using PRISMA images.

Results

The results of this study revealed that PRISMA and ASD reflectance factors were coherent in all spectral regions when a weighted average of the tree and grass field spectra was used considering the fractional cover of each vegetation strata in the image mixed pixels (Fig. 1a). Regarding the regression models to estimate structural traits, the newly Continuum Interpolated NPV Depth index (CINDI) obtained the best accuracy to retrieve NPV AGB ($R^2 = 0.45$) closely followed by the traditional Cellulose Absorption Index (CAI) calculated with ASD data ($R^2 = 0.43$) (Fig. 1b). The PRISMA indices showed lower relationships ($R^2 \leq 0.17$) in comparison with ASD indices (Fig. 1b), which might be related to a lower radiometric quality of PRISMA SWIR bands. The chlorophyll-based indices such as the Normalized Difference Red-Edge (NDRE), Normalized Green (NG), and Red-edge Chlorophyll calculated with ASD showed a significant correlation with PV LAI data ($R^2 \geq 0.61$). In this case, the correlation obtained with PRISMA indices was also lower, and The Optimized soil-adjusted Vegetation Index (OSAVI) and NG achieved the best performance ($R^2 \geq 0.46$). These results demonstrated that the improved spectral resolution from the new-generation of hyperspectral sensors is still insufficient for accurately estimating NPV structural traits, particularly in heterogeneous ecosystems where spatial resolution is also relevant.

Outlook for the future

Predicting structural traits from satellite imagery remains a challenge for the research community, especially in complex tree-grass ecosystems, where different land cover classes (grass, trees, shadows, and soil) co-exist at the medium-resolution satellite image pixels, and the presence of NPV is highly variable both in time and space. Future perspectives should focus on using laboratory and field spectroscopy to derive spectral libraries. This would allow a characterization of the different ecosystem components, especially the NPV, which is underrepresented in existing global datasets. Indeed, relatively few spectra from vegetation types at senescent stages are included in spectral libraries. Upgraded libraries might help to improve linear and non-linear unmixing analysis and the estimation of NPV cover and derived traits from the new and upcoming superspectral and hyperspectral satellite sensors.

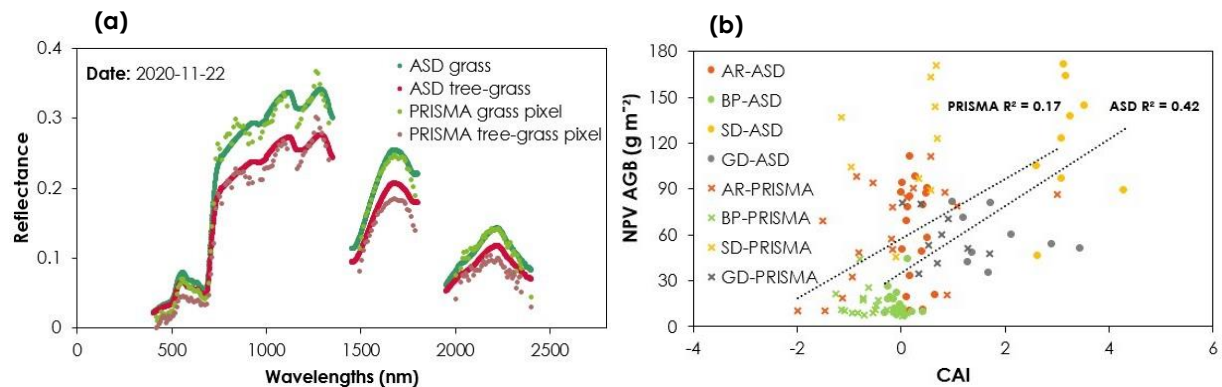


Figure 1 (a) Comparison of field spectra measured with ASD, where ASD grass=spectra acquired on the grass layer and ASD tree-grass=weighted average of spectra acquired over the grass layer (80%) and the tree crowns (20%). Noisy bands due to atmospheric absorption (ASD) and sensor issues (PRISMA) have been removed (b) Linear regression and coefficient of determination (R^2) between NPV AGB and CAI calculated from ASD (circles) and PRISMA (crosses). Different colours refer to the temporal classification of the samples in four phenophases (AR: autumn regrowth in orange, BP: biomass peak in green, SD: summer drought in yellow, GD: grass decay in grey).

EXPLOITATION OF THE PRISMA HYPERSENSPECTRAL PAYLOAD FOR VEGETATION, FUEL AND BURN SCAR MAPPING

Renato Aurigemma¹, Carlo De Michele², Salvatore Falanga Bolognesi², Barbara Hirn ³, Valerio Pisacane¹, Salvatore Schiano Lo Moriello¹, Fabiana Ravellino¹ and Fabrizio Ferrucci³.

¹Eurosoft s.r.l., via Nuova Nuova Poggioreale 60 L, Centro Polifunzionale bldg. 13, 80143 Naples, Italy.

²Ariospace s.r.l., via Nuova Nuova Poggioreale 60 L, Centro Polifunzionale bldg. 13, 80143 Naples, Italy.

³IES Consulting s.r.l., via di San Valentino 34, Rome, Italy

Keywords (5): Hyperspectral, PRISMA, Vegetation Classification, Forest fires, Burn scars.

Challenge (800 - 1000 characters incl. spaces)

In the management of wildfire activities within a specific area, accurately characterizing the geographic and temporal aspects of vegetation, particularly in terms of available fuel mass, is crucial. The current European-scale Fuel Map, distributed by Copernicus as part of the EFFIS service, is derived from moderate-resolution multispectral data and has a nominal scale of 1/500,000. However, for most fire-related activities, a more detailed fuel scale of approximately 1/50,000 or better is deemed necessary. This scale aligns with the 30-meter resolution data provided by the HYC sensor aboard PRISMA. The HYPERFUEL project, initiated in mid-2022 and scheduled for completion in mid-2024, aims to develop Fuel Maps based on PRISMA data with seasonal updates. The project also focuses on testing the reliability of frequent fuel updates by utilizing multispectral data with similar spatial resolution, such as Sentinel-2/MSI and/or Landsat-OLI, which offer near-weekly revisit rates.

Methodology (1200 – 1500 characters incl. spaces)

The recursive operational HYPERFUEL workflow starts from statistically significant vegetation classifications based on PRISMA. The hyperspectral vegetation landscape is obtained through a Machine Learning-based supervised classification approach to landcover/landuse classes, calibrated on Pseudo-Invariant Features (PIF) identified and inspected.

The subsequent hierarchical fuel classification is based on 85 fuel types split into six main categories and one 'non-fuel' category. Here we use data from PRISMA, including hyperspectral vegetation maps, burned area vectors, and Differenced Normalized Burn Ratios (dNBR), leveraging on three sets of recent, EO/non-EO derived ancillary data: vegetation canopy height, dry matter per hectare (Mg/ha), and fractional landcover density.

The vegetation depletion by fires is done by the end-to-end, unsupervised burn scar mapping 'MyME2' procedure based on the Permanent Reflectors and the automated combination of multi temporal and contextual spectral analyses; it was improved to work on hyperspectral data in four PRISMA stable wavelengths windows within the Red-Edge, NIR, SWIR1 and SWIR2 regions. For fire simulation purposes, severely burned areas are set 'non-burnable' until the next season.

Fuel maps are computed once per season on PRISMA hyperspectral data, first in multi temporal then in contextual mode. Biomass fuel availability and location are updated weekly-to-monthly by systematically subtracting devegetated areas, detected/contoured in Sentinel-2 data as a function of burn severity levels, from the PRISMA fuel landscape. The processing loop closes with the assessment of variational fuel quantities in the next PRISMA image.

Results (1200 – 1500 characters incl. spaces)

In total, we dealt with 24 vegetation classification scenarios associated to 6 types of classifiers and 4 training data selection strategies, considering a random cross-validation approach in which labelled samples are randomly split into training and validation sets. The assessment of output accuracies is based on the common statistical measures Overall Accuracy (OA) and Unweighted Kappa. We dissected the best model identified, which corresponded to Random Forest classifier (Kappa statistic = 0.817 and OA = 92.0% in cross-validation).

Fuel maps are computed once per season on PRISMA hyperspectral data, first in multi temporal then in contextual mode. Biomass fuel availability and location are updated weekly-to-monthly by systematically subtracting devegetated areas, detected/contoured in Sentinel-2 data as a function of burn severity levels, from the PRISMA fuel landscape. The processing loop closes with the assessment of variational fuel quantities in the next PRISMA image.

As part of the project, an IT platform is being created for the collection of input data, the generation and consultation of fuel maps via WEB. This platform will also allow access to data via domain standard interfaces such as WCS, WMS and WFS.

Outlook for the future (800 - 1000 characters incl. spaces)

The future evolution of the project activities will be dedicated to giving greater robustness to the process automation. The team will undertake to evaluate upgrades relating to future hyperspectral data sources, including "PRISMA 2" and data from the future IRIDE constellation where applicable.

Machine Learning-based supervised classification approach

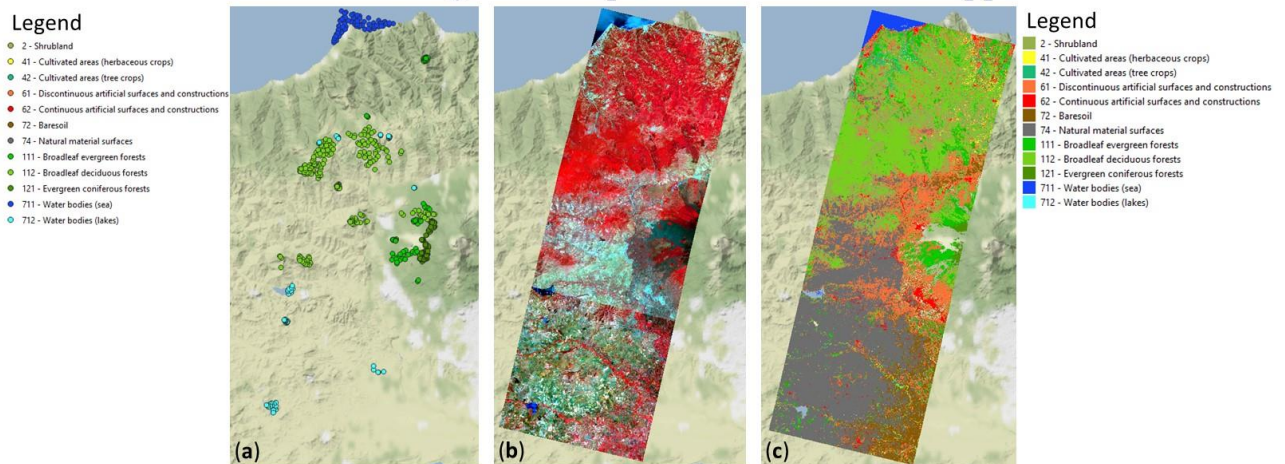
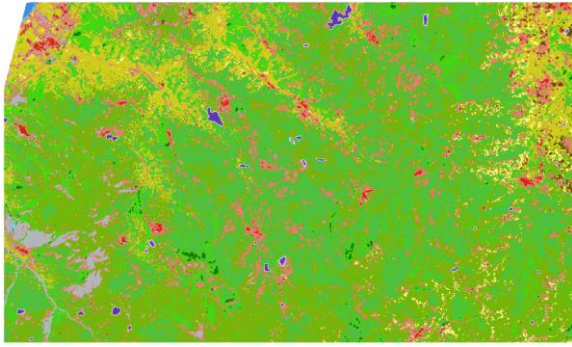
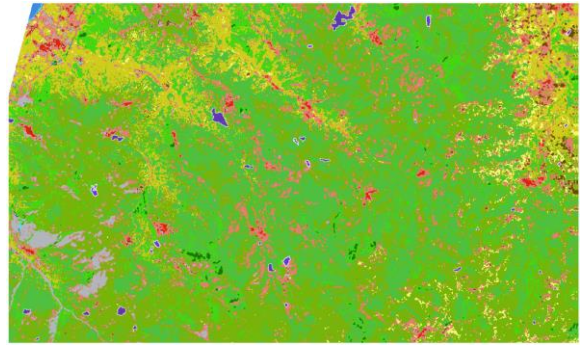


Figure 1 Machine Learning-based supervised classification approach: (a) ground truth samples acquired over the study area in the Sicily region (southern Italy) and spanning multiple parcels, (b) PRISMA Level 2D RGB=bands B55/B36/B26, (c) classification map obtained associated with the best model (Random Forest, OA=92%).



23 August 2022



21 September 2022

Figure 2 Example of Fuel Map with PRISMA updated near monthly by withdrawing burn scars marked 'non-fuel'.

Developing Algorithms for Estimating Functional Traits and Biodiversity Indices from PRISMA Imagery

Rossini Micol¹, Tagliabue Giulia¹, Gentili Rodolfo¹, Savinelli Beatrice¹, Vignali Luigi¹, Gao Jiawei¹, Picchi Valentina³, Antonella Calzone³, Colombo Roberto¹, Panigada Cinzia¹

¹ University of Milano - Bicocca, Department of Earth and Environmental Sciences, Milano, Italy

² CREA Research Centre for Engineering and Agro-Food Processing, Milano, Italy

Keywords: forest functional traits, machine learning, biodiversity, spectral diversity, PRISMA satellite

Challenge

Remote sensing data have been used with different degrees of success to monitor changes in forest biodiversity during the last few decades. The combination of remotely sensed and field-collected data, under the Spectral Variation Hypothesis, represents one of the most promising approaches to perform large scale biodiversity monitoring.

Here we investigate the potential of hyperspectral data collected by the PRISMA satellite of the Italian Space Agency in estimating key plant functional traits and capturing information on plant diversity in a mixed forest ecosystem.

In particular, we exploited PRISMA data to develop a machine learning retrieval workflow to map key forest traits. We combined trait maps within a multi-variate approach to estimate the forest functional diversity. We then compared functional, taxonomic and spectral diversity indices calculated on PRISMA images with field plant data, using different statistical approaches. The patterns in the plant diversity maps were discussed in relation to several factors, expected to drive biodiversity changes in the study areas.

Methodology

The study was performed in the Ticino Regional Park (Italy) a temperate mixed forest located along the Ticino river in the Po plain. The forest is mainly composed of oak-hornbeam mesophytic mixed forests, with a significant presence of invasive allochthonous species. In summer 2022, several images were collected over the Ticino Park with the PRISMA satellite. This satellite was designed by the Italian Space Agency (ASI) and it features a hyperspectral sensor with 240 spectral channels from 400 to 2500 nm and a ground spatial resolution of 30 m. Two intensive field campaigns were organized in June and September 2022 contemporary to the PRISMA overpasses. Data on species composition of the overstorey and understorey were collected in about 100 plots and biodiversity indices were computed. Also, based on their ecological importance in terms of plant functioning, Leaf Area Index (LAI), Leaf Chlorophyll Content (LCC), Leaf Nitrogen Content (LNC), Leaf Water Content (LWC) and Leaf Mass Area (LMA) were measured.

For the retrieval of the forest traits of interest, different machine learning regression algorithms were tested: Gaussian Processes Regression (GPR), Neural Networks (NN), Partial Least Squares Regression (PLSR), Random Forest Regression (RF) and Support Vector Regression (SVR).

Emerging methods based on remotely sensed data (i.e. PRISMA images) that aim at the estimation of α and β spectral diversity, were applied using the R package "biodivMapR". Information theory metrics

(e.g. Rao's Q) are also computed on a combination of leaf and canopy traits to characterise forest functional biodiversity.

Results

A positive and statistically significant correlation was found for all the investigated traits. Among the leaf level traits, the best results were obtained for LWC ($r^2=0.97$, nRMSE=4.7%) and LMA ($r^2=0.95$, nRMSE=5.6%), while slightly worse results were obtained for LCC and LNC ($r^2=0.44$, nRMSE=18.3% and $r^2=0.63$, nRMSE=14.2%, respectively). LAI was estimated accurately ($r^2=0.91$, nRMSE=8.3%). The best retrieval algorithm for each trait was then applied to PRISMA images. The resulting maps are shown in Figure 1.

In general, we observed high spatial heterogeneity of LCC, LNC and LAI and a relative homogeneity for LWC and LMA which show lower values in broadleaves compared to conifers, mainly present in the Northern part of the Park.

The plant trait maps were combined within a multi-variate approach to estimate the forest functional diversity and compared with the taxonomic and spectral diversity maps obtained from the "biodivMapR" package. Results show that diversity taxonomic and spectral indices patterns are similar in areas characterised by high diversity level. Moreover, the spatial distribution of trait diversity generally agrees with regard to the spatial patterns of the spectral diversity maps. This is related to the species gradient from South to North in the study area and the coinciding reduced trait variability towards the forest edges.

Outlook for the future

The results obtained in this study demonstrated that the retrieval of a broad set of leaf and canopy traits from hyperspectral satellites using machine learning retrieval schemes is feasible, paving the way for future operational algorithms for the routine mapping of vegetation traits from spaceborne sensors. Moreover, we showed that spaceborne hyperspectral remote sensing is a promising and cost-effective data source to enable plant biodiversity mapping. This is essential in perspective of the current and upcoming availability of new hyperspectral missions such as DLR's EnMAP, NASA's SBG and ESA's CHIME. Future studies should focus on extending the current approach to larger areas, and exploring the combination of data from other sensor types.

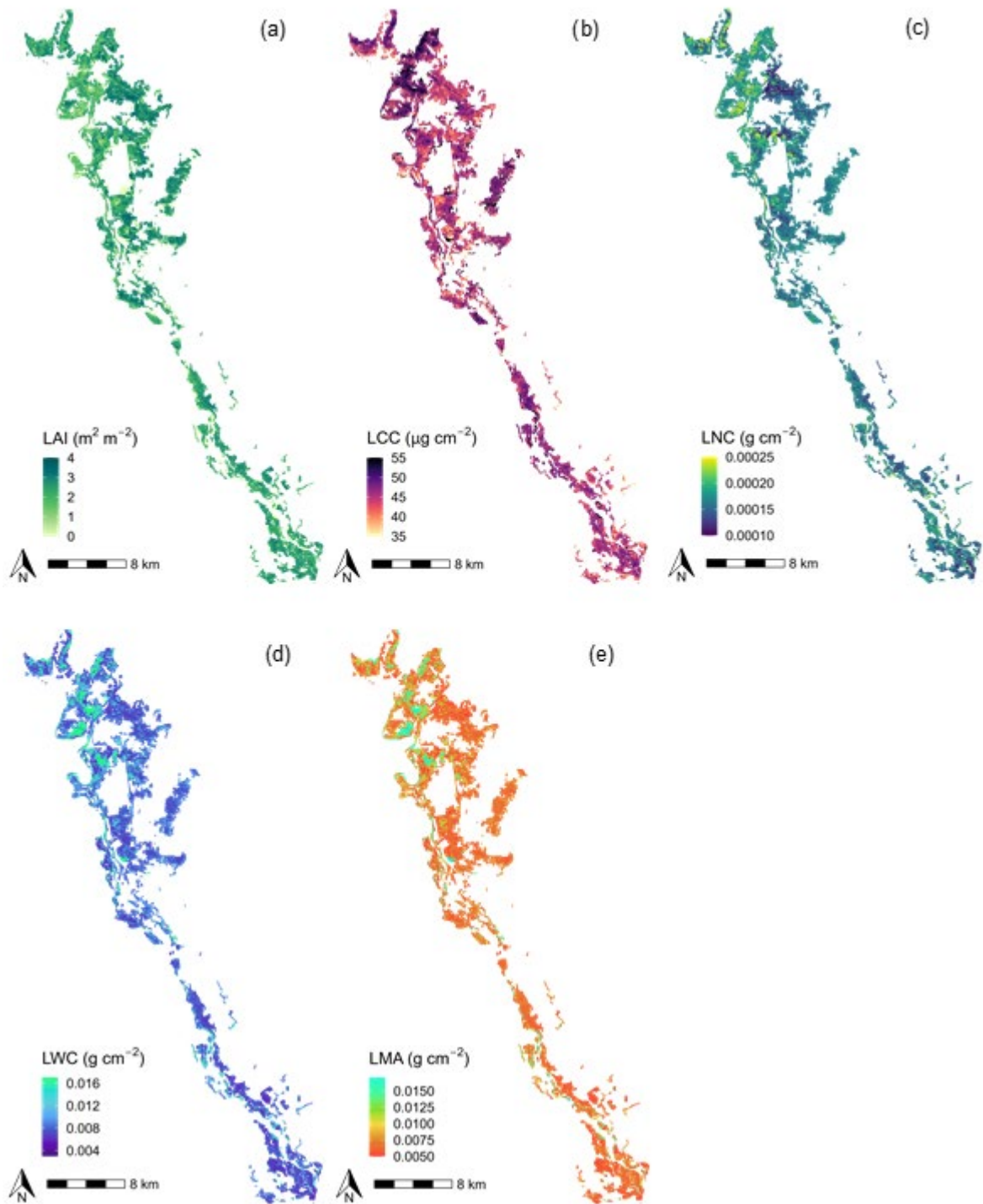


Figure 1. Leaf Area Index (LAI) (a), Leaf Chlorophyll Content (LCC) (b), Leaf Nitrogen Content (LNC) (c), Leaf Water Content (LWC) (d) and Leaf Mass Area (LMA) (e) maps of the Ticino Park in June 2022.

ACKNOWLEDGEMENTS

This work is carried out within Contract "PRIS4VEG" n. 2022-5-U.0 (CUP F43C22000000005), funded by ASI in the "PRISMA SCIENZA" program.

**Them.Sess. 2-8: Results from
the EMIT imaging
spectroscopy mission on the
International Space Station**

First Year of Observations and Key Results from NASA's EMIT Imaging Spectroscopy Mission

Robert O. Green, David R. Thompson, and EMIT Team

¹ JET PROPULSION LABORATORY CALIFORNIA INSTITUTE OF TECHNOLOGY

Keywords (5): Imaging Spectroscopy, Minerals, Greenhouse Gases, Earth System

Challenge

Historically, multi-spectral remote sensing observations under sample the available information in the radiance spectrum of the Earth and other planets. For example, multi-spectral measurements cannot accurately map the spectral signatures found in the hundreds of different minerals found on the Earth's surface. The same is true for the spectral signatures available in terrestrial and aquatic ecosystems, coastal and inland waters, and the complex signatures of snow and ice. Many important science questions and applications today require new, more quantitative products with uncertainties. High fidelity imaging spectroscopy from the visible to the short wavelength infrared (VSWIR) portion of the spectra provides a path forward. EMIT's mission science specifically requires the determination of the mineral composition of the Earth's arid land dust source regions to advance understanding of the direct radiative forcing across our planet from mineral dust aerosols. Additionally, this spectral range is especially relevant for measurement of methane and carbon dioxide point source emissions. The EMIT mission and imaging spectrometer are designed to address this challenge with next-generation imaging spectroscopy measurements along with state-of-the-art algorithms and products with uncertainties.

Methodology

The EMIT mission and instrument team has specified and developed a first-of-its-kind high throughput F/1.8 full VSWIR Dyson imaging spectrometer. The spectral range is 380 to 2500 nm with 7.5 nm spectral sampling. The signal-to-noise ratio is greater than 400 over much of the spectrum for the reference mineral observation conditions. EMIT has a spatial swath which is >70 km with nominally 60 m spatial sampling. Spectral cross-track non-uniformity is less than 5 percent. Instrumental measurement artifacts have been minimized. The EMIT instrument was designed, developed, and calibrated at the NASA Jet Propulsion Laboratory in 41 months. EMIT was launched to the International Space Station on the 14 of July 2022, with installation and first light observation soon afterward. With early on-orbit measurements, the EMIT team employed new methods for validation as well as for spectral, radiometric, spatial, and uniformity calibration and refinement. EMIT has now been measuring the Earth's arid and adjacent lands across six continents for more than a year. In that timeframe, more than 50,000 image cubes have been collected, calibrated to radiance, atmospherically corrected to surface reflectance, and used to generate the required mineral composition maps with corresponding uncertainties. These observations and products are being used to achieve the EMIT science objectives. EMIT measurements are relevant for measuring methane and carbon dioxide point source emissions. To support this a set of algorithms and products have been developed to detect, measure, and report GHG plumes below the ISS. To advance Earth science and applications for all, the EMIT measurements and products are available from the NASA Land Processes Distributed Active Archive Center (LP DAAC) for use by the Earth science and applications community (<https://lpdaac.usgs.gov/data/get-started-data/collection-overview/missions/emit-overview/>). All algorithms are available from the public GitHub (<https://github.com/emit-sds/>).

Expected results

With more than one year of imaging spectroscopy observations, EMIT has nominally sampled the arid and adjacent lands that are the primary source of mineral dust aerosols for the Earth system. The areas sampled are shown in Figure 1 below. The sampling has been sufficient to collect an effectively cloud-free base data set. These measurements are being processed to at-instrument radiance, surface reflectance, and dust source minerals. These products are being used to develop new dust source mineral maps. An example mineral map for North Africa and Arabia is shown in Figure 2. These data sets are described and can be located on the EMIT website and the VSWIR Imaging Spectroscopy Interface for Open Science (VISIONS) open data portal and discovery. The EMIT dust source mineral products are being validated and gridded to provide new constraints for advanced Earth System Models. These new inputs for the Earth System Models will be used to achieve the EMIT science objectives to constrain the sign and magnitude of mineral dust-related radiative forcing at regional and global scales and predict the increase or decrease of available dust sources under future climate scenarios. In concert with EMIT's GHG measurement capability more than 700 methane plumes have been mapped and are reported in the VISIONS open data portal (<https://earth.jpl.nasa.gov/emit/data/data-portal/Greenhouse-Gases/>). All EMIT measurements, products, and model results are archived at the LP DAAC.

Outlook for the future

The future is bright for state-of-the-art imaging spectroscopy observations of the Earth System that are needed today to answer important new science questions and pursue new applications with advanced spectroscopic measurements and products with traceable uncertainties. The EMIT mission and imaging spectroscopy observations, algorithms, and products are important steps in this direction. The EMIT team is working hard to share our experiences and results and support a broad set of future imaging spectroscopy missions for the Earth and through the solar system.



Figure 1 Current EMIT measured data set of >50,000 spectral image cubes. All can be view through the EMIT open data VISIONS portal with links to the products and the LP DAAC.

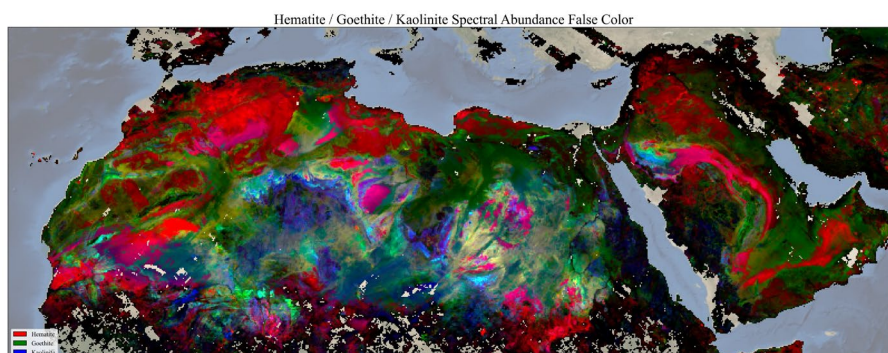


Figure2 Initial EMT mineral map for Hematite, Goethite, and Kaolinite across the mineral dust source regions of North Africa and Arabia.

On-orbit Calibration and Performance of NASA's EMIT Imaging Spectrometer

David R. Thompson, Robert O. Green, Philip Brodrick, K. Dana Chadwick, Red Willow Coleman, Regina Eckert, Andrew K. Thorpe, and the EMIT Team

Jet Propulsion Laboratory, California Institute of Technology

NASA's new orbital imaging spectrometer, the Earth Surface Mineral Dust Source Investigation (EMIT), was launched to the International Space Station in July 2023. EMIT is a Visible-Shortwave Infrared Imaging Spectrometer measuring the wavelength interval from 380-2500 nm at approximately 7.4 nm sampling. At the time of this writing EMIT has delivered over 60000 spectral radiance and reflectance images to public archives. Notably, EMIT carries no onboard calibration sources or mechanisms of any kind – not even a shutter. Instead, the Earth itself is used as a calibration target, dark target, wavelength standard, flat field, and geolocation reference. Its simple design emphasizes high radiometric stability, high spatial uniformity, and vicarious calibration. Here we describe the protocols and results of our initial on-orbit characterization and calibration process. This information was previously published in a recent manuscript (Thompson et al., public preprint in review, 2023) but presented to the EARSel audience for the first time.

First, we describe spectral calibration achieved by measuring the position of atmospheric absorption features. EMIT shows spatial uniformity of its wavelength calibration within 2% of a channel width. We demonstrate the capability to adjust focal plane array alignment on orbit with sub-micron precision, removing a slight tilt that developed after each of its two thermal cycles. Next, we describe the radiometric calibration process. We maintain radiometric calibration with a flat field update based on long temporal medians of many images to average over variability in scene content. This process successfully measures changes in FPA element gain drift at the level of 0.1% per month. Finally, vicarious calibration over playa surfaces is used to adjust radiometric calibration coefficients. These adjustments, combined with the EMIT atmosphere/surface inversion process, yields good alignment with held-out validation sites. Finally, we validate the predictions of the EMIT radiometric sensitivity model by direct measurements of signal to noise ratios over homogeneous targets. These approaches demonstrate that EMIT is exceeding performance requirements, with data quality sufficient for the next generation of global spectroscopic science investigations.

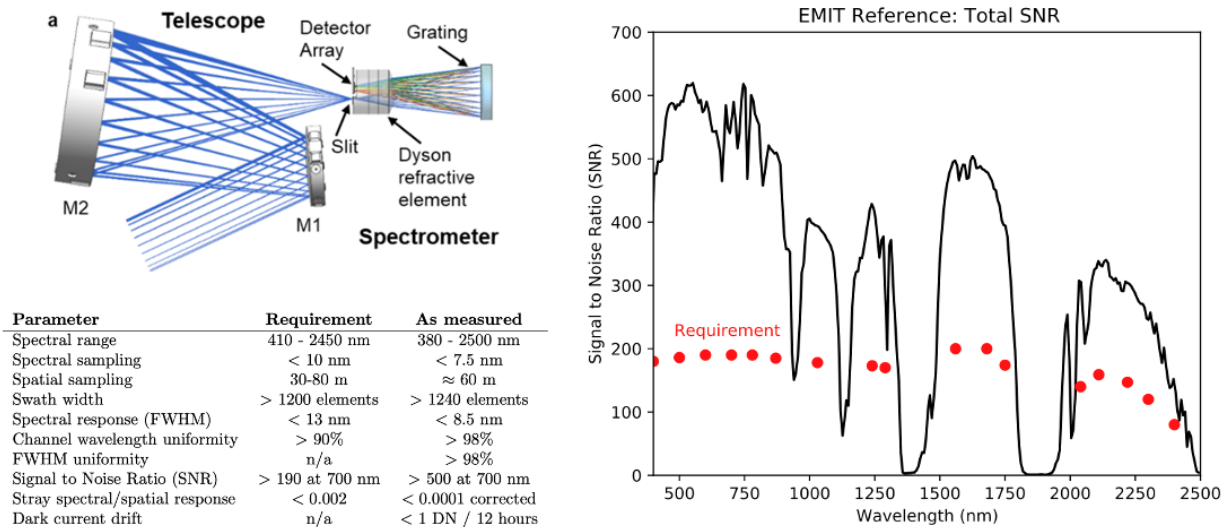


Figure: EMIT optical layout, performance specifications, and SNR curve (reference case of 20% reflectance at 45 degrees solar zenith angle).

Evaluating the accuracy of surface reflectance products from the EMIT imaging spectrometer

[Red Willow Coleman](#)¹, David R. Thompson¹, Philip G. Brodrick¹, Francisco Ochoa^{1,2}, Gregory S. Okin², Raymond Kokaly³, Gregg Swayze³, Todd Hoefen³, John M. Meyer³, Evan Cox³, Eyal Ben Dor⁴, Daniela Heller Pearlshien⁴, Robert O. Green¹ and the EMIT Science Team

¹ Jet Propulsion Laboratory, California Institute of Technology, Pasadena, CA, USA

² University of California Los Angeles, CA, USA

³ United States Geological Survey, CO, USA

⁴ Tel Aviv University, Israel

Keywords (5): Earth Observation, EMIT, Hyperspectral, Surface Reflectance, Validation

Challenge

The Earth surface Mineral dust source InvestIgation (EMIT) is an imaging spectrometer on the International Space Station that aims to measure the mineral composition of Earth's dust producing regions. The EMIT instrument is unique both in that it has no onboard calibration mechanism and is the first orbital mission to use optimal estimation, a novel atmospheric correction approach that uses at-sensor radiance to infer both surface reflectance and atmospheric state parameters. As such, validation of the EMIT surface reflectance product will confirm that these approaches are successful and can be operationalized for future imaging spectroscopy missions. We present a two-part systematic accuracy assessment of the EMIT surface reflectance product in this abstract.

Methodology/Results

First, we conducted multiple independent vicarious validation experiments that characterize EMIT reflectance performance for a representative range of scenes. We considered automated calibration facilities, manual measurement of traditional open playa validation sites, and several mixed vegetation wild land sites. We also assessed the surface reflectance repeatability and stability with measurements of Pseudoinvariant Calibration Sites (PICS) where no ground truth data are available. Temporally coincident observations showed discrepancies consistent with an EMIT reflectance product standard error of +/-1.0% of absolute reflectance for typical arid land regions at the core of the EMIT science objectives. This finding is broadly consistent with the first calibration studies conducted by the EMIT team [Thompson et al. 2023, preprint]. This discrepancy grows to +/- 2.7% for observations at different dates and solar angles, which we attribute to real changes in the Hemispherical Directional Reflectance Factor (HDRF).

Our second contribution is demonstrating an account of instrument and algorithm uncertainties that explains discrepancies for these comparisons. Analysis of pseudoinvariant sites and playa acquisitions across multiple months indicated that most variance can be explained entirely by differing spatial footprints and forward-propagated measurement uncertainty rather than systematic radiometric calibration error (**Figure 1**). A handful of outlier cases indicate challenging atmospheric conditions with phenomena outside the atmospheric model. Taken in concert, these findings demonstrate that a space-based imaging spectrometer can acquire high-quality spectra across a wide range of observing conditions.

Outlook for the future

EMIT's spectral accuracy and stability is enabling high-quality measurements of Earth surface processes to support a diverse set of scientific fields, including geology, terrestrial and aquatic ecology, and cryosphere science. Calibration and validation of the EMIT surface reflectance product will be an ongoing process to ensure that the instrument is spectrally stable and accurate throughout the life of the mission. For example, there are ongoing EMIT field campaigns across the western U.S. that will provide additional insight on the surface reflectance product's performance in heterogeneous vegetated observing conditions. In addition, spatiotemporally coincident observations between EMIT and other airborne (AVIRIS) and spaceborne (EnMAP, DESIS, HiSUI) imaging spectrometers could provide an interesting comparison of surface reflectance products from different instruments.

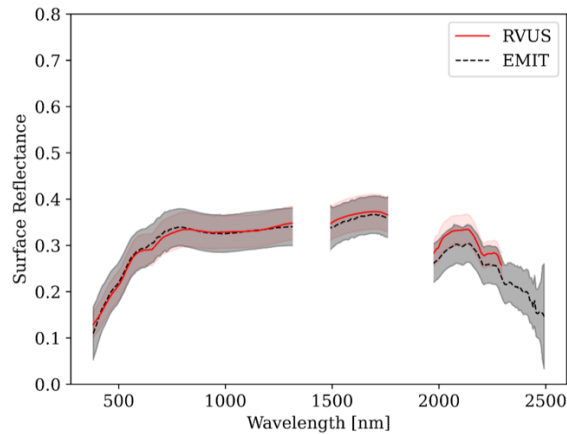


Figure 1: Comparison of RadCalNet bottom-of-atmosphere (BOA) reflectance at Railroad Valley Playa (RVUS, red line) to the surface reflectance of a spatiotemporally coincident EMIT overpass (black line) on 2023/06/12. The shaded regions demarcate a 2σ uncertainty.

Copyright 2023 California Institute of Technology. All rights reserved. US Government Support Acknowledged.

Mapping snow properties on a global scale - A first outlook to the SBG/CHIME era using observations from the EMIT imaging spectrometer

EARSel Valencia 2024

Abstract

Corresponding Author: urs.n.bohn@jpl.nasa.gov

Niklas Bohn¹, Edward H. Bair², Philip G. Brodrick¹, Nimrod Carmon¹, Jeff Dozier³, Robert O. Green¹, Thomas H. Painter⁴, David R. Thompson¹

¹Jet Propulsion Laboratory, California Institute of Technology, USA

²Leidos Inc., USA

³University of California, Santa Barbara, USA

⁴University of California, Los Angeles, USA

Keywords (5): EMIT, imaging spectroscopy, snow and ice, topography, SBG

Challenge

Snow plays a key role in Earth's radiation budget by having the highest albedo of all natural surfaces, and therefore, introducing potential cooling effects to Earth's climate. This cooling potential is a direct function of the amount of absorbed solar radiation. However, as snow warms and melts, its effective grain size increases and its reflectance decreases in the near-infrared where half of solar irradiance occurs. Likewise, small light-absorbing particles (LAP), such as mineral dust, black or brown carbon, and algae, lower the snow's visible albedo (the other half of the irradiance), leading to enhanced melting and the retreat of snow cover. Exposing the underlying darker surface contributes to climate warming and thus represents the large component of climate sensitivity to change. It is therefore of particular importance to monitor the spatial and temporal occurrence of LAP on a global scale. Such monitoring can be achieved by orbital imaging spectrometers but requires independently applicable retrieval algorithms that account for surface characteristics. A major challenge is posed by local topography, which significantly impacts shape and magnitude of snow albedo but is currently neglected in most existing inversion schemes.

Methodology

The upcoming orbital imaging spectroscopy missions SBG and CHIME will give approximately weekly combined observations of reflected solar radiation from almost all locations on Earth's land surface. The measurements will feature both spectral and spatial resolutions of ~10 nm and 30 m, respectively, enabling the detection and quantification of grain size and LAP by resolving their subtle absorption characteristics. As a first outlook to this new era of Earth observation, we present retrieval maps of snow surface parameters and associated uncertainties obtained from NASA's Earth Surface Mineral Dust Source Investigation (EMIT) imaging spectrometer, which is an Earth Venture mission installed on the International Space Station (ISS) with similar instrumentation to those of SBG and CHIME. We apply joint atmosphere and surface modeling to retrieve per-pixel values of snow grain size and LAP concentration. The approach is based on a coupled snow-atmosphere radiative transfer model and considers the effects of topography by optimizing for local illumination conditions. To a certain degree, this captures directional effects in the snow reflectance and makes it more independent from digital elevation models (DEM). However, the accuracy of inferring surface slope and aspect directly from measured radiances decreases with larger subpixel variability in the reflectance.

Results

The approach enables a detailed outline of retrieval sensitivity to local surface characteristics. Our results demonstrate reduced errors in estimated snow grain size of up to 200 μm when topographic characteristics are considered in the retrieval scheme. Likewise, the concentration of especially inorganic LAP can be over- or underestimated by up to 75 $\mu\text{g/g}$. On the other hand, correlation analysis shows that the retrieval of biological LAP is less affected by topography. We demonstrate that inaccurately quantified LAP concentration can propagate through to differences in estimated radiative forcing of up

to instantaneous 400 W/m^2 . Furthermore, we compare our results to digital elevation models and achieve good agreement between calculated and retrieved surface angles. Our findings confirm conclusions from previous studies that local topography impacts reflected radiance both in shape and magnitude, which enables a determination of slope and aspect from the measurement itself without needing external DEMs. Finally, we illustrate global patterns of snow surface parameters and their relationship to topographic features, surely limited to EMIT's target mask, which does not cover polar regions. However, we capture most of the low- to mid-latitude mountain snow cover, which shows the largest variability in surface slope and aspect.

Outlook for the future

Our topography-aware forward model couples atmosphere and surface radiative transfer to improve retrievals of snow properties on a global scale, particularly in mountainous terrain. The approach facilitates a physics-based model parameterization by directly optimizing atmospheric parameters and geobiophysical properties of the snow surface. However, further work is needed to increase accuracy and applicability of the algorithms. Mixed pixels must be considered and both ice and LAP optical properties need a more detailed investigation to account for local geographical characteristics. Nevertheless, our findings will be essential for the conception of retrieval algorithms for SBG and CHIME, as these missions provide the framework to develop and enhance processing schemes and retrieval algorithms on a global scale.

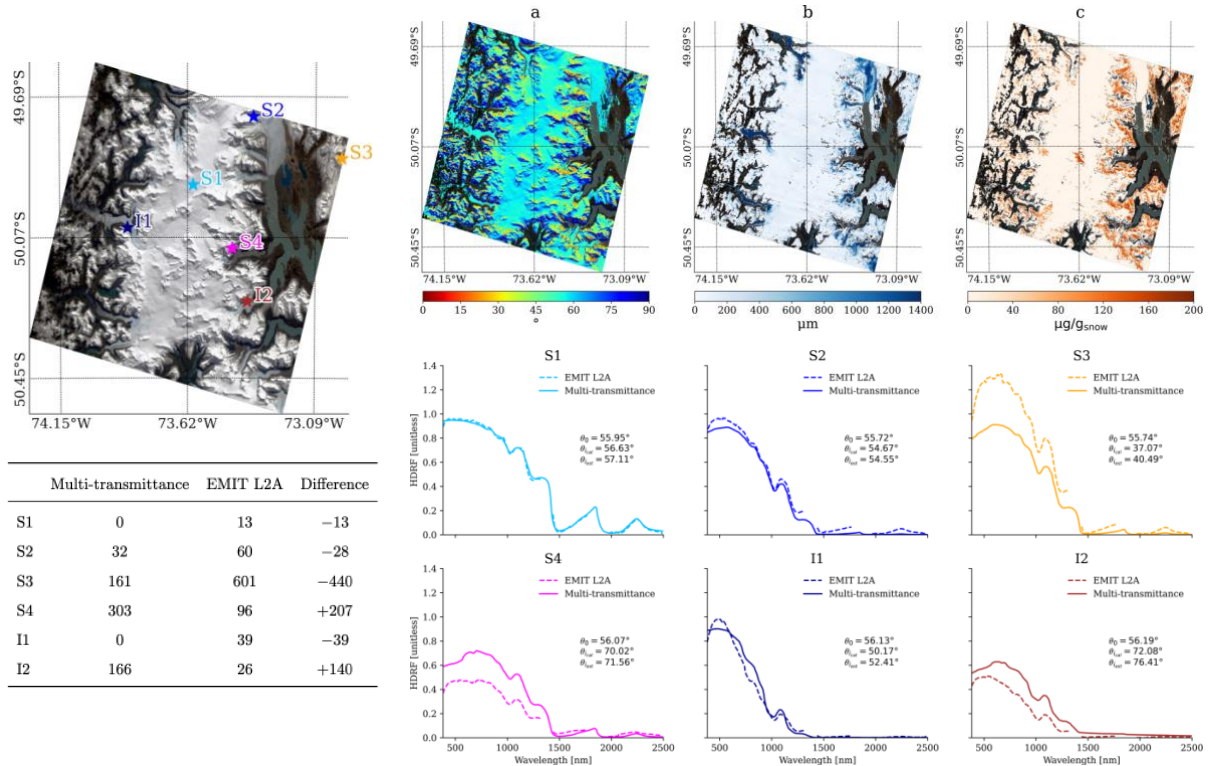


Figure 1. Retrieval maps, surface reflectance, and LAP radiative forcing from a selected EMIT image of the Patagonian Ice Sheet in Chile, South America. The true-color RGB indicates the locations of the six selected spectra. Retrieval maps show a) local solar zenith angle (SZ), b) snow grain size, and c) dust mass mixing ratio. Spectral plots compare our results (multi-transmittance) to official EMIT L2A products and indicate top-of-atmosphere, as well as retrieved and DEM-calculated SZ. The table highlights differences in estimated LAP radiative forcing in units of W/m^2 for the six cases.

EMIT Applications and Data Accessibility

K. Dana Chadwick¹, Robert O Green¹, David R Thompson¹, Philip G Brodrick¹, Kelly Luis¹, Niklas Bohn¹, Michael Bramble¹, Andrew Thorpe¹, Erik Bolch², Brianna Lind², Mahsa Jami², Aaron Friesz², Cole Krehbiel²

¹ Jet Propulsion Laboratory, California Institute of Technology, Pasadena, CA, USA

² Land Processes Distributed Active Archive Center, U.S. Geological Survey (USGS) Earth Resources Observation and Science (EROS) Center

Keywords (5): EMIT, Imaging Spectroscopy, Applications, Open Science

Challenge (800 - 1000 characters incl. spaces)

Since launch, the Earth surface Mineral dust source Investigation (EMIT) mission, a visible to shortwave infrared (VSWIR) imaging spectrometer, has collected billions of visible to shortwave infrared spectra across dust-producing regions of the Earth. These data are being used to determine surface mineral composition, as well as providing high quality reflectance data to support a variety of other uses. These data products, available through Land Processes Distributed Active Archive Center (LP DAAC), will support diverse research and applications beyond EMIT's original mission, benefiting society. The EMIT research and applications team and the LP DAAC are collaborating to maximize the applications potential of these data, as well as their accessibility. The challenge is to make the high data volume produced by the EMIT mission accessible to users from various research and applied science fields.

Methodology (1200 – 1500 characters incl. spaces)

The EMIT team has set a standard for openness, curiosity, and engagement by actively supporting and encouraging slack dialogues and consistently working in the open (via GitHub). With LP DAAC, the EMIT team co-developed a series of comprehensive tutorials for data products and partners with other missions (ECOSTRESS) and initiatives (the United States Greenhouse Gas Center) to develop community relevant resources. These tutorials are available to the public through video recordings and GitHub repositories, ensuring widescale accessibility and user-friendliness. As a first in the Earth observing community, the data processing pipeline for all EMIT products is completely open to the public and example workbooks and resources are available through the EMIT Resources repository hosted by the LP DAAC. We encourage the community to contribute their own examples and resources to the EMIT Resources repository and the VSWIR Imaging and Thermal Applications, Learning, and Science (VITALS) repository, also hosted by LP DAAC. The team has also nurtured a dynamic environment by hosting interns who've delved into various applications subject areas. This collective effort highlights EMIT's commitment to advancing applied science areas beyond methane monitoring and fostering innovation in diverse domains. As EMIT applications area advance, we continue to engage stakeholders domestically and internationally to advance uses of EMIT data to address local and global societal challenges.

Expected results (1200 – 1500 characters incl. spaces)

Improving data accessibility, tutorial development, and fostering interagency collaboration can unlock a multitude of expanded applications for EMIT data across various domains. For instance, VSWIR data has been used to assess water availability and snow pack condition across the western United States, and

EMIT is currently being explored to augment these studies. EMIT data can detect zones of hydrothermal alteration on volcanoes, serving as an indicator of debris flow risk. It aids in monitoring harmful algal blooms, coral health, and benthic cover, informing scientific investigations aimed at preserving vital freshwater and coastal ecosystems. EMIT's data collection covers agricultural regions across the globe, where it can provide essential information on crop types, health, crop residues, and soil mineralogy, contributing to the optimization of agricultural production. VSWIR spectrometers have aided in acid mine cleanup efforts, an area which the EMIT team is exploring. Finally, EMIT data facilitates assessing fire risk through canopy water content, and vegetation fractional cover. Broader data acquisition by EMIT as it enters its extended mission holds promise for expanding beyond its primary mission focus on mineralogy and providing insights across a range of disciplines. By improving data accessibility, tutorial resources, and fostering collaboration, EMIT data can be harnessed to address a wide range of critical issues, benefiting both society and the environment.

Outlook for the future (800 - 1000 characters incl. spaces)

As EMIT enters its extended mission, it will begin to acquire data across additional regions of the Earth's surface, expanding the potential users and use cases for these measurements. The EMIT team remains committed to providing high quality data using transparent algorithms as our dataset grows and we seek to expand the products that are provided for end users. Both the development of tutorials and open-source algorithms provide ample starting points for students, academics, researchers, and more to begin working with EMIT data and analysing it for their own purposes. As we look towards the growing constellation of orbital VSWIR imaging spectrometers, developing these resources, and cultivating experienced end users will enable these data to provide insight for decision-making across many domains.

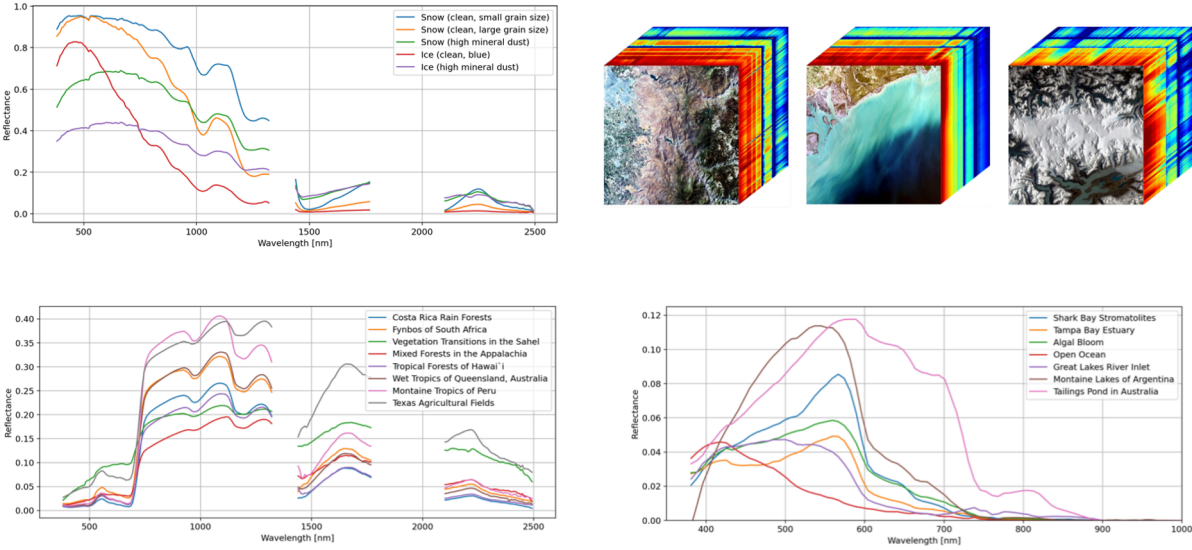


Figure 1. Examples of EMIT spectra collected over different types of surfaces including vegetation, water, and snow and ice. The image cubes in the top right depict a red-green-blue image of a data cube with the third dimension showing the intensity of reflectance data from the visible to shortwave infrared around the edges of the cubes.

Global Mineral Products From EMIT: From Radiance To Earth System Model

Philip G. Brodrick¹, Robert O. Green¹, David R. Thompson¹, and the EMIT Science Team

¹ Jet Propulsion Laboratory, California Institute of Technology, United States of America

Keywords (5): EMIT, geology, ESM

Challenge

Global imaging spectroscopy promises to transform the way in which we characterize the Earth's surface, leading us from an era of coarse land-cover categorization toward a more quantitative measurement of subpixel constituent distributions. At the same time, a lack of knowledge of dust source mineral composition drives a major portion of uncertainty for global dust related radiative forcing. From its vantage point on the International Space Station, the Earth Surface Mineral Dust Source Investigation (EMIT) imaging spectrometer has measured reflected solar radiation from 380 to 2500 nm with 285 contiguous spectral channels, at an approximate 60 meter ground resolution and an approximately 80 km wide swath near the equator. These products, processed through to geology and mosaiced together, can provide direct input into Earth System Model simulations to better constrain the sign of global dust related radiative forcing.

Methodology

EMIT radiance data are first processed to model the surface reflectance and atmospheric state simultaneously through Optimal Estimation, which couples together radiative transfer, instrument characteristics, and prior knowledge of surface characteristics together in a Bayesian optimization framework. This process facilitates estimating the most likely solution state along with the corresponding uncertainty. We then exercise the EMIT Science Data System, which utilizes a linear feature-matching algorithm called Tetracorder to compare a wide range of mineral spectra from the USGS spectral library and map the presence of the most likely library constituent. We then utilize quantitative x-ray diffraction results to translate the detected minerals to abundances of each of 10 key minerals for Earth System Models: kaolinite, calcite, dolomite, hematite, goethite, gypsum, chlorite, illite, vermiculite, and montmorillonite. In order to determine the total amount of soil present in each pixel, we also utilize a monte carlo based spectral unmixing analysis to map mixtures of photosynthetic vegetation, non-photosynthetic vegetation, and soil in arid regions spanning the globe. Masks for standing surface liquid water, snow and ice, clouds and cloud shadows, and urban materials are also generated and applied in order to constrain the results to relevant regions. For each of these products, we propagate the uncertainty estimated from the surface reflectance retrieval in order to provide estimated uncertainty around the biogeophysical property retrievals. Finally, we mosaic these results together into a cohesive, global mosaic that can be used as input into an Earth System Model.

Expected results

Here we show EMIT products at each stage (radiance all the way through global mineralogy). We describe the performance and remaining challenges in mapping these different constituents, followed by an analysis of the intersection of these parameters and their geographic distributions. We also investigate the spatially-explicit uncertainty in each of these products - propagated forward from surface reflectance and augmented by additional model uncertainty. All EMIT data products are

available through the Land Processes Distributed Active Archive Center (LP DAAC), and all code is available through github under a centralized organization (emit-sds). We discuss how and where to find these data and code, as well as additional tools for exploring early data products and understanding where future acquisitions will be collected.

Please upload 1-2 figures or graphical abstract (min 300 dpi. jpeg/png)

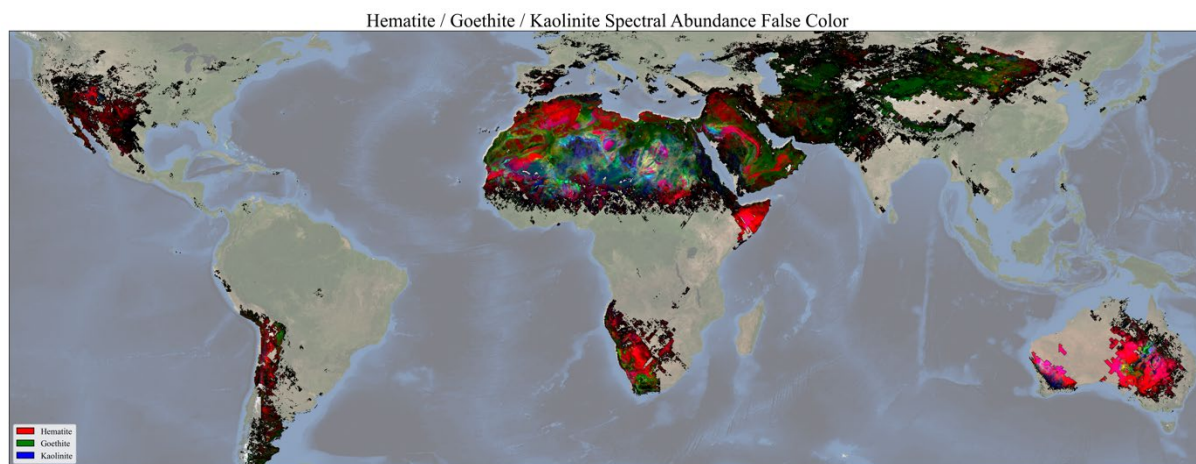


Figure Distribution of mineral spectral abundance of three of the EMIT 10 minerals.

**Them.Sess. 2-9: Discovering
the world's aquatic
ecosystems through
spaceborne spectroscopy:
status and prospects**

GALENE: a future hyperspectral satellite mission for observing coastal and inland aquatic ecosystems and wetlands

Malik Chami¹, Astrid Bracher², Xavier Briottet³, Maycira Costa⁴, Alexander Damm-Reiser⁵, Arnold Dekker⁶, Peter Gege⁷, Shungu Garaba⁸, Claudia Giardino⁹, Els Knaeps¹⁰, Tiit Kutser¹¹, Richard Lucas¹², Daniel Odermatt¹³, Gerard Otter¹⁴, Nima Pahlevan¹⁵, Nicole Pinnel¹⁶, Sindy Sterckx¹⁷, Kevin Turpie¹⁸

¹ Sorbonne Université, Laboratoire Lagrange Observatoire Côte d'Azur, France

² Alfred Wegener Institute, Germany

³ ONERA, France

⁴ University of Victoria, Canada

⁵ University of Zurich, Switzerland

⁶ CSIRO, Australia

⁷ German Aerospace Center (DLR), Germany

⁸ University of Oldenburg, Germany

⁹ National Research Council (CNR), Italy

¹⁰ VITO, Belgium

¹¹ University of Tartu, Estonia

¹² Aberystwyth University, UK

¹³ Eawag, Switzerland

¹⁴ TNO, The Netherlands

¹⁵ NASA, USA

¹⁶ *German Aerospace Center (DLR), Germany*

¹⁷ *VITO, Belgium*

¹⁸ *University of Maryland, Baltimore County, USA*

Keywords (5): Remote Sensing, Aquatic Ecosystems, Hyperspectral, Coastal, Inland waters

Challenge

Coastal and inland aquatic ecosystems are of fundamental interest to society and economy, given their tight link to urbanization, economic value creation, and ecosystemic services delivery. They play a significant role in the carbon cycle, and they comprise critical habitats for biodiversity. Aquatic ecosystems are continuously impacted by natural processes and human activities. Many of these impacts become more frequent and severe, particularly with increasing population and climate change. Hence, there is a need (i) to generate reliable, robust and timely evidence of how these environments are changing, (ii) to understand processes causing these changes and their societal, health, and economic consequences, and (iii) to identify steps towards conservation, restoration and sustainable use of water and dependent ecosystems, and resources.

Methodology

Systematic, high-quality and global observations, such as those provided by satellite remote sensing techniques, are key to understand complex aquatic systems. While multitudes of remote sensing missions have been specifically designed for studying ocean biology and biogeochemistry as well as for evaluating terrestrial environments, remote sensing missions dedicated to studying critical coastal and

inland aquatic ecosystems at global scale are non-existent. Thus, these ecosystems remain among the most understudied habitats on the Earth's surface. Current and forthcoming missions are either not suited to provide a global coverage (e.g., PRISMA, EnMAP) or to obtain reliable data over dark waters (e.g., carbon-rich lakes) due to inadequate radiometric sensitivity (e.g., Sentinel-2/MSI). They also fall short of requirements for characterizing biodiversity variables such as benthic habitat structure and phytoplankton assemblages due to their inadequate spatial and spectral resolution, respectively (e.g., Sentinel-2/MSI, Sentinel-3/OLCI). Similar limitations exist for wetland ecosystems, which compromises their management and protection.

Results

A future satellite mission named Global Assessment of Limnological, Estuarine and Neritic Ecosystems (GALENE) has been proposed to ESA to respond to current and future challenges linked to aquatic ecosystems. The mission concept consists of a synergy of three innovative instruments, namely a hyperspectral sensor, a panchromatic camera and a polarimeter. GALENE will then provide optimized measurements of these environments by enabling an adaptive spectral, spatial, multidirectional and polarimetric sampling of properties and processes in water columns, benthic habitats and associated wetlands.

Outlook for the future

GALENE will substantially contribute to solving global water challenges, including water pollution and ensuring clean drinking water supply for all and protecting coastal areas and populations. The GALENE science objectives and the main innovative features will be presented.

A PERSPECTIVE ON THE RELEVANCE OF THE CHIME MISSION FOR MONITORING INLAND AND COASTAL WATERS

Marco Celesti¹, Kevin Alonso², Valentina Boccia³, Laurent Despoisse⁴, Alice Fabbretto^{5,6}, Diego Fernandez-Prieto³, Antonio Gabriele⁴, Ferran Gascon³, Nafiseh Ghasemi⁴, Claudia Giardino⁵, Giuseppe Ottavianelli³, Andrea Pellegrino⁵, Helene Strese⁴, Heidrun Weber⁴, Jens Nieke⁴

¹ HE Space for ESA - European Space Agency, European Space Research and Technology Centre (ESA-ESTEC), Noordwijk, The Netherlands

² RHEA for ESA - European Space Agency, European Space Research Institute (ESA-ESRIN), Frascati, Italy

³ European Space Agency, European Space Research Institute (ESA-ESRIN), Frascati, Italy

⁴ European Space Agency, European Space Research and Technology Centre (ESA-ESTEC), The Netherlands

⁵ Institute for Electromagnetic Sensing of the Environment, National Research Council (CNR-IREA), Milano, Italy

⁶ Department of Remote Sensing, Tartu University, Tartu Observatory, Tartu, Estonia

Keywords (5): Earth Observation, Imaging Spectroscopy, Copernicus, Inland waters, Coastal waters, CHIME

The Copernicus Hyperspectral Imaging Mission for the Environment (CHIME) will provide routine hyperspectral Earth observations over the land and coastal zones through the Copernicus Programme in support of EU- and related policies for the management of natural resources, assets, and benefits. This unique visible-to-shortwave infrared spectroscopy based observational capability will provide unique and major contributions in fulfilling user requirements in the domains of raw materials and sustainable agricultural management with a focus on soil productivity, sustainable raw materials development and sustainable use of nutrients and water, food security, and biodiversity.

Despite being optimised for operational monitoring of terrestrial ecosystems, CHIME Level-1 and Level-2 products will be relevant for a broad range of user communities. In particular, the water quality user community will benefit from CHIME routine hyperspectral observation of all inland water bodies and all coastal waters (including those surrounding islands greater than 100 km²) (Figure 1). CHIME measurements will cover the spectral range from 400 to 2500 nanometres with a ~8.4 nm spectral sampling interval and a ~10 nm full width at half maximum. CHIME will allow the operational provision of innovative high spatial resolution (up to 30 m) water products and services beyond the current capabilities offered by multispectral observatories, including retrieval of phytoplankton pigments (e.g. to detect potentially harmful algal blooms), retrieval of total suspended matter with its organic and inorganic fractions (e.g. as a tracer of mass transport, coastal erosion), improved submerged habitats classification (e.g. of corals, macrophytes, seagrass, in support to ecosystems assessment in fragile environment). Moreover, the continuous spectral information in the VSWIR will be useful to identify

and classify patches of floating materials and debris (e.g., plastic, sargassum seaweed, oil spills). With two operational units in orbit, CHIME will provide an 11-day revisit time over the entire acquisition mask, with opportunities for a shorter coverage time at high latitudes considering partial overlaps between orbits. This will allow unprecedented routine monitoring and operational services beyond the capacity of the current scientific imaging spectroscopy missions (e.g., PRISMA from ASI, EnMAP and DESIS from DLR, EMIT from NASA/JPL).

As a baseline, a state-of-the-art, water-specific atmospheric correction algorithm is being developed within the CHIME Level-2 operational processor on top of the land atmospheric correction. This will be applied to all inland water bodies and coastal waters within the CHIME acquisition mask (specific mask still under definition), providing the user community with a solid baseline to develop high quality, high spatial resolution downstream water products and services.

In this contribution, the potential and the limitations of CHIME measurements for inland and coastal waters monitoring and management will be discussed, including a preliminary quantitative assessment based on top-of-atmosphere radiances from the PRISMA mission. Moreover, a summary of the main activities carried out during CHIME Phase A/B1 and B2, as well as the ongoing and planned activities for Phase C/D/E will be summarised.

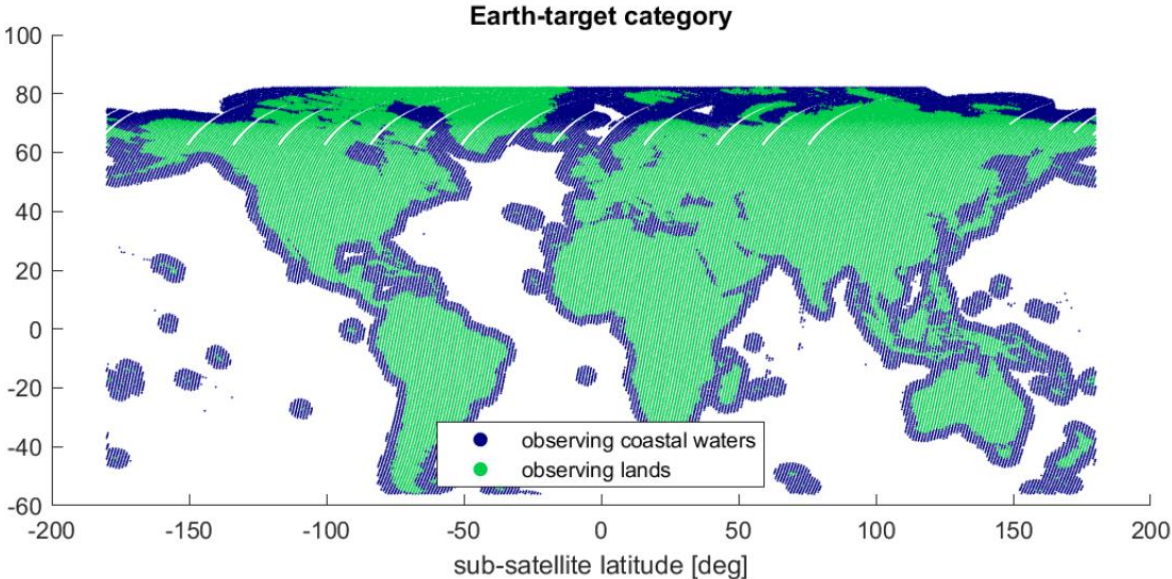


Figure 1 CHIME acquisition mask

Hyperspectral EnMAP Data Processing for aquatic science and applications

EARSel Valencia 2024
Abstract
Corresponding Author:
nicole.pinnel@dlr.de

Nicole Pinnel¹, Max Langheinrich², Thomas Heege³, Mariana A. Soppa⁴, Peter Gege², Raquel de los Reyes², Astrid Bracher^{4,5}, Emiliano Carmona²

¹ German Aerospace Center (DLR), Remote Sensing Data Center, D-82234 Weßling, Germany

² German Aerospace Center (DLR), Remote Sensing Technology Institute, D-82234 Weßling, Germany

³ EOMAP GmbH, Earth Observation and Environmental Solutions GmbH, D-82229 Seefeld, Germany

⁴ Alfred-Wegener-Institute, Helmholtz Center for Polar and Marine Research, D-27570 Bremerhaven, Germany

⁵ University Bremen (UB), Institute of Environmental Physics, D-28359 Bremen, Germany

Keywords (5): Earth Observation, Hyperspectral, Spaceborne Mission, EnMAP, Aquatic Ecosystems

Challenge

EnMAP, the Environmental Mapping Analysis Program, is a German satellite mission that was successfully launched in April 2022. EnMAP is an optical (VNIR/SWIR) remote sensing mission with high spatial (30 m GSD) and spectral (FWHM ~6-12 nm) resolution. Although primarily designed for terrestrial applications, EnMAP exhibits substantial potential for aquatic studies due to its hyperspectral capabilities.

In comparison to other sensors, EnMAP ground segment processing is pioneering by providing separate processing chains for land and water, allowing for specialized data processing for each application. It also includes a sunglint avoidance algorithm using EnMAP's tilting capability for mitigating the impact of sunglint-contaminated pixels in specific geographical constellations. This research focuses on how EnMAP can be used for studying aquatic ecosystems, with emphasis on EnMAP water processing and applications in aquatic research.

Methodology

The EnMAP satellite is equipped with a VNIR-SWIR push-broom hyperspectral imager that covers a spectral range from 420 to 2450 nm and comprises 224 contiguous spectral bands. EnMAP follows a sun-synchronous orbit with a standard revisit period of 27 days, which can be reduced to less than four days through its off-nadir pointing capabilities. The EnMAP ground segment, managed by the German Aerospace Center (DLR), oversees the satellite control, data reception, storage, and processing.

Users have access to three different product levels: L1B, L1C, and L2A. What stand out is its separate processing chains for land and water pixels within the L2A processing. Besides the standard processing using land atmospheric correction algorithms (PACO), the aquatic processing is done using the Modular Inversion and Processing System (MIP) developed by EOMAP GmbH, offering two types of water reflectance data: subsurface irradiance reflectance and normalized water leaving reflectance.

To enhance the acquisition of glint-free data, a sunglint mitigation strategy has been implemented by selecting optimal image acquisition geometries on user requests. All EnMAP products are processed on-demand using the most up-to-date processor versions and undergo rigorous radiometric and spectral calibration. The ground segment conducts regular assessments of EnMAP products to ensure mission requirements, whereby these products are additionally subject to independent validation by the science team.

Expected results

EnMAP's specific water-related data products play a significant role in advancing aquatic research, offering a substantial advantage, especially for researchers who were previously dependent on terrestrial sensors that required custom atmospheric corrections and thus when working in aquatic environments limiting their ability to fully exploit the potential of the data.

EnMAP's global coverage, which extends to high latitudes ($\pm 74^\circ$) and incorporates off-nadir capabilities, also facilitates observations in remote and challenging areas, including polar regions. The hyperspectral data is particularly advantageous for coastal and inland waters, allowing detailed examination of optical components within the water column and on the seafloor. The advanced spectral resolution in the visible, near-infrared, and shortwave-infrared enables the improved assessment of e.g. phytoplankton functional types and dissolved organic carbon levels. In optical shallow and clear waters, it further allows improved monitoring and differentiating of benthic substrate types and derive bathymetry. The detailed quantification of these constituents can contribute significantly to our understanding of various processes such as carbon cycling, nutrient availability, and preservation of threatened ecosystems like coral reefs, seagrass meadows, and mangrove forests.

This paper will discuss in detail the advantages of the EnMAP processing chain and will present various applications that make use of EnMAP's hyperspectral water reflectance data.

Outlook for the future

Delivering accurate water reflectance data is crucial for improving our knowledge of coastal and inland water environments. Achieving such accuracy is a complex task because of the difficulties related to correcting for atmospheric effects, the complex properties of water and aerosols, and the added complications when dealing with areas close to land, ice, or human-made structures. Optimized processing can help obtaining valuable data over aquatic ecosystems to make terrestrial Earth observing sensors significantly more useful for aquatic ecosystem monitoring. EnMAP provides a unique opportunity to gain a deeper understanding of aquatic ecosystems and the influence of human activities on aquatic environments, and thus be a pathfinder for future operational hyperspectral missions.

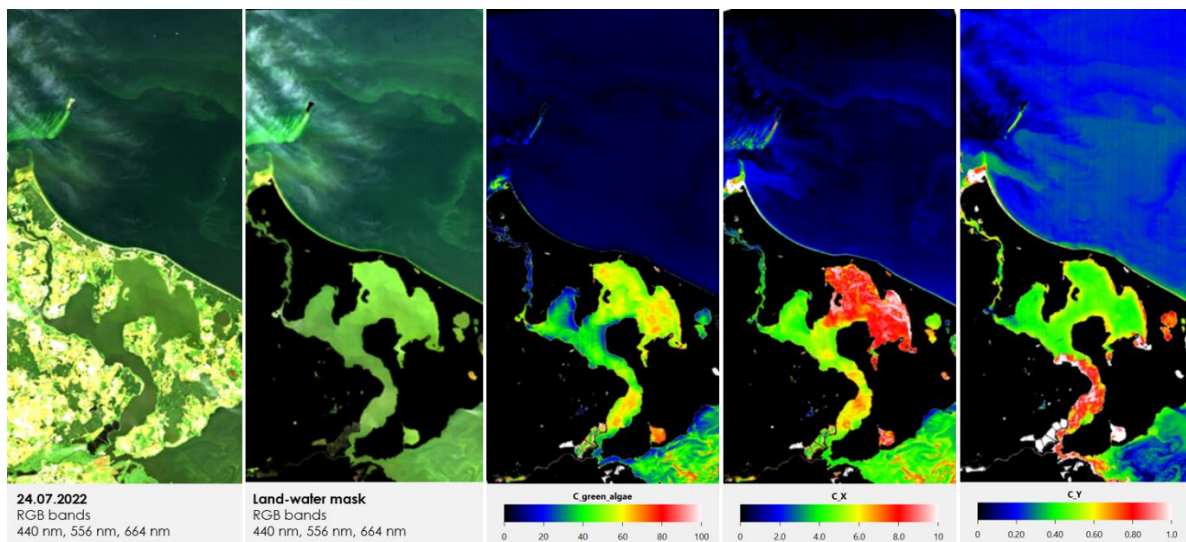


Figure EnMAP scene acquired on July 24th, 2022 over the northern Stettiner Haff and Baltic Sea in Germany. The thematic maps (inversion by WASI-2D) show the concentrations of green algae (CHL in $\mu\text{g/l}$), suspended matter (TSM in mg/l), and CDOM absorption (in m^{-1}).

Aquatic observations by the EMIT imaging spectrometer onboard the International Space Station

EARSel Valencia 2024

Abstract

Corresponding Author: Kelly Luis

[Kelly Luis](#)¹, David R. Thompson¹, Robert O. Green¹, U. Niklas Bohn¹, Philip G. Brodrick¹, K. Dana Chadwick, Regina Eckert and the EMIT Team

¹ JET PROPULSION LABORATORY, CALIFORNIA INSTITUTE OF TECHNOLOGY

Keywords (2): Imaging Spectroscopy, Aquatic, EMIT

Challenge

NASA's Earth Surface Mineral Dust Source Investigation (EMIT) imaging spectrometer onboard the International Space Station (ISS) has been operating for over one year, acquiring over 60,000 different scenes globally, and delivering the associated radiance and reflectance data to the Land Processes Distributed Active Archive Center (LPDAAC). It has demonstrated several features that are valuable for observations of aquatic targets, including high spatial uniformity and high radiometric precision (signal to noise ratio (SNR)). With a spatial resolution of 60 meters and 40 bands in the visible wavelengths (400-700 nm) at ~7.5 nm spectral resolution, the design of EMIT is advantageous for remote sensing of inland and coastal aquatic waters, ecologically and economically valuable ecosystems subject to wide ranging biological and biogeochemical fluxes. This presentation explores the value of the EMIT imaging spectrometer across aquatic ecosystems.

Methodology

Publicly available EMIT radiance and reflectance products and associated code provide the aquatic remote sensing community an opportunity to refine aquatic atmospheric correction approaches and to develop aquatic spectroscopic algorithms and data products. The EMIT Level 1b radiance and geolocation data product provides at-sensor calibrated radiance measurements and coincident observation data including viewing and solar geometries, timing, topographic, and additional observational information. The EMIT Level 2a reflectance, uncertainty, and masks data product provides surface reflectance, associated uncertainty estimates, and a reflectance mask file. The surface reflectance retrieval algorithm is based on a Bayesian Maximum A Posteriori (MAP) inversion, which has been demonstrated in multiple coastal aquatic imaging spectroscopy field campaigns. The uncertainty estimates are on a per-pixel, per-band basis. The mask file includes cloud, cirrus, dilated, land, spacecraft masks and two data quality bands are retrieved from the L2a surface reflectance for aerosol optical depth and water vapor. Associated code for generating these data products is available on Github. In addition, EMIT data products are cloud accessible via NASA Earthdata Cloud, and LPDAAC has developed python modules and tutorials for processing EMIT datasets.

Expected results

We present representative spectra of different inland and coastal water types. The enhanced spatial and spectral resolution of EMIT enables retrievals of key biological and biogeochemical parameters as well as information on aquatic habitat composition. EMIT has retrieved surface reflectance spectra indicative of phytoplankton blooms, sediment plumes, and an array of lake, riverine, estuarine processes. Through

leveraging EMIT's spectroscopic information, surface reflectance can be used to reveal new perspectives on aquatic biological and biogeochemical processes. For aquatic habitat composition, EMIT coverage over coastal ecosystems such as coral reefs, kelp beds, wetlands, and mangroves provides critical shallow benthic and surface habitat composition information. We will also present initial analyses of apparent and inherent optical properties, such as diffuse attenuation coefficients and total absorption and backscattering coefficients. These initial analyses will be complemented by the retrieval of water quality parameters such as turbidity and chlorophyll. We will close with a discussion of future planned algorithmic advances, including glint modeling and shallow water remote sensing methods for retrieving bathymetry and benthic community structure, to facilitate aquatic studies based on EMIT data.

Outlook for the future

EMIT's current target mask focuses mainly on arid terrestrial regions. Following a mission review in 2024, it is likely that EMIT's target mask can be extended to accelerate aquatic science and applications objectives. The extension of the target mask will facilitate synergistic activities with upcoming ocean color missions such as Plankton, Aerosol, Cloud, and ocean Ecosystem (PACE) and Geostationary Littoral Imaging and Monitoring Radiometer (GLIMR). Cross platform biological and biogeochemical algorithm development will enable spaceborne spectroscopy studies in dynamic inland and coastal aquatic ecosystems. With upcoming spaceborne spectrometer launches to look forward to, EMIT provides the aquatic remote sensing community and user groups with critical precursor data today to prepare for the unprecedented amount of aquatic spectroscopy data ahead.

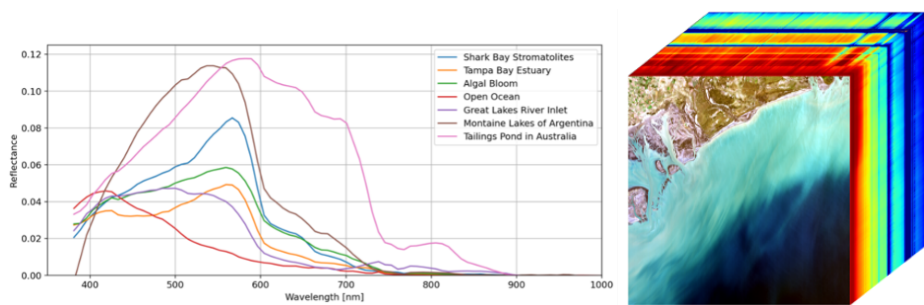


Figure 1: EMIT data cube and representative reflectance spectra from different water types around the world. All examples are single pixels, unsmoothed.

Title**NASA's Plankton, Aerosol, Cloud, ocean Ecosystem (PACE) mission: Ushering a new era in ocean colour measurements**

Antonio Mannino¹, Jeremy Werdell¹, PACE Project and partners²
(Style: Authors, presenting author underlined)

¹ NASA Goddard Space Flight Center, Ocean Ecology Lab, USA

² USA and Netherlands

Keywords (5): Earth Observation, Hyperspectral, Ocean Colour, PACE, Phytoplankton

Challenge (800 - 1000 characters incl. spaces)

With the [Plankton, Aerosol, Cloud, ocean Ecosystem mission](#) (PACE), NASA embarks upon a new era of unprecedented global ocean and atmospheric satellite observations of the Earth. PACE's primary instrument, the Ocean Color Instrument (OCI) consists of two spectrometers that continuously span ~320-600 nm and 580-895 nm, with an additional seven discrete shortwave infrared bands (from 0.94 to 2.26 microns) enabling unprecedented spectral resolution and radiometric sensitivity to quantify properties of ocean colour, aerosols and clouds with 1-2-day global coverage. OCI will be complemented by two multi-angle polarimeters, SPEXone and HARP2 for advanced characterization of aerosol and cloud properties. SPEXone provides five viewing angles and hyperspectral radiance from 385-770 nm, HARP2 offers hyperangular (10-60 viewing angles) observations in four multi-spectral bands. Our challenge is to employ the vast spectral content from OCI (~292 bands) to derive phytoplankton community composition.

Methodology (1200 – 1500 characters incl. spaces)

The PACE project will produce a suite of high-quality ocean colour data products derived from OCI's Top-of-Atmosphere (TOA) radiance including hyperspectral ocean remote sensing reflectance (R_{rs}) at 5 nm spectral resolution and sampling at 1.25 or 2.5 nm between 350-895 nm. OCI's exceptional signal-to-noise ratio (SNR) in the UV-Vis enables utilization of the 5 nm spectral bands for downstream derived products culminating in the retrieval of phytoplankton community composition (PCC). Multiple algorithms are currently being evaluated and implemented to quantify PCC. These algorithms employ hyperspectral R_{rs}, phytoplankton absorption and/or diagnostic pigments as their primary inputs. PCC data products yield information of abundances or biomass proportions of taxonomic groups (diatoms, dinoflagellates, cyanobacteria, etc.) or size-based groups (pico-, nano-, micro-plankton). Fundamental to the success of PCC data product quality are the source data used to develop and evaluate the algorithms. In preparation for PACE, a rigorous data quality control has been implemented for SeaBASS (NASA's field measurement data archive) and NOMAD (NASA's algorithm development database) to support algorithm development and evaluation and data product validation. At this time, PCC algorithms will be implemented on a provisional basis PCC. Once performance is verified, PCC algorithms will be processed and distributed as standard data products.

Results (1200 – 1500 characters incl. spaces)

PACE will be launching in late January to February 2024 timeframe. Hence, there are no data products from the PACE mission at this time but will become available when this conference convenes. This presentation will share early mission hyperspectral Rrs and other preliminary data products including PCC and inherent optical properties (IOPs). Performance of the Ocean Color Instrument from pre-launch characterization and commissioning will be presented. The end-of-life systematic uncertainties for OCI are estimated at <0.5% (TOA radiances referenced to typical ocean radiances) and <0.6% for the portion of the spectrum (580-600 nm) that overlaps across the two spectrometers.

Outlook for the future (800 - 1000 characters incl. spaces)

Thus, PACE will be capable of performing radiometric and polarimetric ocean and atmosphere surveys, returning a range of biogeophysical data from which properties of the ocean and atmosphere can be produced to add to other critical climate and Earth system variables. With advanced global remote sensing capabilities, PACE will provide high quality observations that contribute to an extended time series of satellite data records on ocean ecosystems, including coastal and inland waters, and atmospheric properties of aerosols and clouds. Global measurements from PACE will enable advanced understanding of delicate ocean ecosystems, understanding of vulnerable coastal regions, quantification of the atmosphere-ocean carbon cycling, unparalleled characterization of ecosystem change and function including PCC, improved characterization of cloud and aerosol properties, air and water quality, and cross-disciplinary studies of atmospheric, terrestrial, and aquatic processes and interactions.

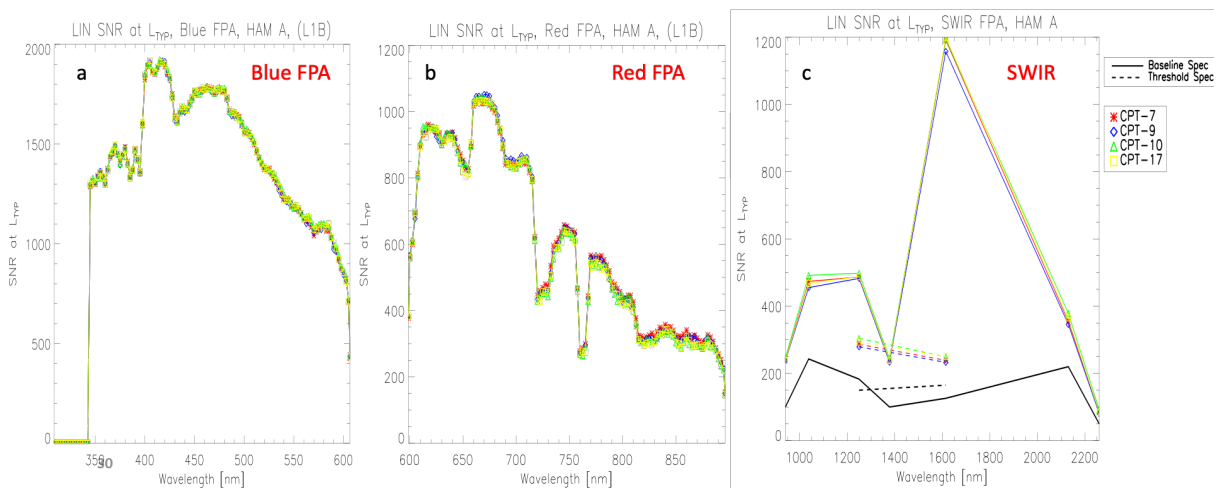


Figure (a) Signal-to-Noise ratio for 5 nm spectral bands at ocean typical radiances of the Blue focal plane assembly (FPA), (b) the Red FPA, and (c) short-wave infrared (SWIR) bands.

Title

NASA's Geostationary Littoral Imaging and Monitoring Radiometer (GLIMR)

Antonio Mannino¹, Joseph Salisbury², GLIMR Team³

¹ NASA Goddard Space Flight Center, Ocean Ecology Lab, USA

² University of New Hampshire, USA

³ various institutions, USA

Keywords (5): Earth Observation, Hyperspectral, Ocean Colour, GLIMR, Diurnal

Challenge (800 - 1000 characters incl. spaces)

With its vantage point from geostationary orbit, NASA's Geostationary Littoral Imaging and Monitoring Radiometer (GLIMR) will be the first hyperspectral ocean colour sensor in the Western Hemisphere to study ocean processes at the diurnal timescales required to observe the dynamic ecological, biogeochemical and physical processes within coastal and ocean waters. GLIMR is uniquely designed to capture the temporal and spatial evolution of phytoplankton blooms, which grow and dissipate on scales of hours to days, monitor phytoplankton growth rates and shifts in community composition, resolve coastal features, fronts, eddies and upwelling areas, and monitor biogeochemical fluxes and land-ocean exchanges at sub-diurnal to multi-day scales. At the heart of the GLIMR instrument is a spectrometer with a nadir ground sample distance of 300 m, spectral range between 340-1040nm, and capability to scan the Gulf of Mexico every 70 minutes (six times per day) at a high SNR performance. Launch is planned for no earlier than 2027.

Methodology (1200 – 1500 characters incl. spaces)

GLIMR will acquire hyperspectral radiances at 250+ channels between 340-1040 nm at spectral resolution of ~2 nm to 20 nm from UV to NIR, respectively, for production of a suite of standard and advanced ocean colour data products. GLIMR's primary science region include the Gulf of Mexico to be scanned six times per day as well as the Amazon River and Orinoco River plume extents, United States East and West coastal ocean regions, Hawaii region, Caribbean Sea surrounding Puerto Rico and vast areas of the South Pacific, each will each be scanned two or more times per day. The combined spectral, spatial and temporal capabilities of GLIMR provide novel means to study coastal ocean processes and for societal applications such as identifying and tracking harmful algal blooms and oil spills. The aim of this presentation is to introduce the GLIMR mission and discuss how the science team will apply GLIMR's ocean colour observations to quantify land-ocean exchanges of sediments, organic matter, and other materials between and within coastal ecosystems. GLIMR will improve quantification of primary productivity and carbon fluxes within coastal aquatic ecosystems and across the nearshore-to-ocean seascapes.

Results (1200 – 1500 characters incl. spaces)

GLIMR will be launching in the 2027-2028 timeframe. Hence, there are no data products from GLIMR mission at this time. This presentation will describe the science aims, algorithms and data products planned, and an overview of expected instrument performance including top-of-atmosphere radiance uncertainties, signal-to-noise ratio, spectral and spatial registration as well as uncertainties in water-leaving reflectance.

Outlook for the future (800 - 1000 characters incl. spaces)

GLIMR is poised to revolutionize our understanding of phytoplankton physiology and community changes, ocean productivity, land-estuary-ocean exchanges and dynamics of carbon and sediments, biology-physics interactions at sub-mesoscale, detection and prediction of harmful algal bloom evolution, oil spill thickness, extent and prediction, and much more. For instance, GLIMR's multiple observations per day enables the use of ocean colour to follow water masses (at sub-tidal temporal scale) to quantify surface currents and at adequate spatial resolution (~300 to 600 m). Because "fast" observations are not enabled by polar-orbiting satellites, GLIMR, as well as current and past GOCI sensors, will enable us to move beyond studying the effects of the process, and into the study of the processes themselves.

**Them.Sess. 2-10:
Hyperspectral Remote
Sensing of Forest Traits I**

Influence of surface anisotropy on trait-based functional diversity metrics

Marius Vöggtli¹, Isabelle S. Helfenstein¹, Meredith C. Schuman^{1,2}, Michael E. Schaepman¹, Mathias Kneubühler¹, Alexander Damm^{1,3}

¹ Department of Geography, University of Zurich, Zurich, Switzerland

² Department of Chemistry, University of Zurich, Zurich, Switzerland

³ Eawag, Swiss Federal Institute of Aquatic Science & Technology, Surface Waters – Research and Management, Dübendorf, Switzerland

Keywords (5): Data processing, anisotropy, APEX, temperate forests, functional diversity

Challenge

Recent studies have successfully assessed plant biodiversity via functional diversity (FD) metrics derived from remote sensing-based plant trait estimates. However, we lack an understanding of how data processing steps influence biodiversity estimates and conclusions drawn from such data products. Among other effects, high spatial resolution surface reflectance data used to derive plant traits and FD metrics are influenced by surface anisotropy originating from geometric-optical and volumetric scattering mechanisms. The extent to which surface anisotropy influences FD metrics is largely unknown.

Since there is a need for processing and analysis workflows that enable reliable and comparable results, we investigate the influence of anisotropy uncorrected and corrected data on FD metrics. We take advantage of overlapping, near-simultaneous imagery over a forested mountain that has been well characterized in terms of biodiversity and determine the influence of processing on FD metrics.

Methodology

We present a data experiment to quantify the effect of surface anisotropy on FD estimates in temperate forest ecosystems. The retrieval of FD relies on a well-established method that combines spectral index-based plant trait information to calculate the FD metrics richness (FRic) and divergence (FDiv).

We use three APEX imaging spectroscopy flight lines (FLn) from 7 July 2016 over the *Laegern* forest in northern Switzerland with different observation angles. The data have a spatial resolution of 2 m and spectrally cover 400 to 2500 nm in 284 bands. All FLn have a common overlap area of roughly 2 km x 1 km. The data were processed using a standard approach (ATCOR-4 based atmospheric correction considering a digital elevation model) and optionally with a semi-empirical anisotropy correction (BREFCOR).

In the overlap area, three physiological plant traits are estimated from spectral indices: water content using the Normalized Difference Water Index (NDWI), chlorophyll content using the Red-Edge Chlorophyll Index (Clre), and carotenoid content using the Chlorophyll Carotenoid Index (CCI). Then, FRic and FDiv values are calculated within a disk-shaped moving window with a radius of 30 pixels (60 m).

Finally, to investigate the influence of anisotropy effects on the estimated plant traits and the calculated FD measures, the results obtained from standard reflectance data are compared with those obtained from reflectance data with an additional semi-empirical anisotropy correction.

Results

Preliminary results show apparent differences in FRic values in three different FLn representing the same area. In particular, in FLn 1, distinctly larger FRic values than in the other two can be observed. FLn 2 and 3 show much smaller but more similar FRic values.

Applying an anisotropy correction (Figure 1, right) leads to a more equal FRic with lower variation across flight lines compared with the results without correction (Figure 1, left). The reduction is clearly visible between FLn 2 and 3, where the median FRic values are closer after, compared to before, an anisotropy correction (difference of 0.006 vs. 0.015). Although the difference between FLn 1 and the other two is reduced, it remains large, indicating an effect other than anisotropy as a leading cause.

FDiv (Figure 2) appears to be more robust than FRic. On the one hand, there is much less variation in FDiv between FLn compared to FRic. On the other hand, anisotropy correction does not appear to have a noticeable influence on FDiv values.

Our results suggest that surface anisotropy influences FRic estimates via the underlying anisotropy sensitivity of underlying trait values, while FDiv seems not to be affected. Our results also suggest that a semi-empirical anisotropy correction can reduce anisotropy effects and therefore reduce FRic differences across observation angles. This emphasizes the importance of pre-processing on data products, especially when integrating different sensors and scales.

Outlook for the future

In further analyses building on the presented approach and preliminary results, various aspects can be addressed. This includes focusing on potential causes for observed differences in traits and FD between FLn, e.g., by analyzing processing parameters and illumination and observation geometries.

In previous studies, shadow masks were applied to minimize the influence of shade effects. However, the extent to which shade caused by geometric-optical scattering influences the results is yet to be determined. Separating shaded and sunlit pixels will provide insights into this. Furthermore, we aim to investigate the influence of scale by varying the window size for calculating FRic and FDiv.

Understanding the influence of anisotropy on FD metrics from remotely sensed data should facilitate the quantitative comparison of datasets. Analyzing multi-temporal data available at *Laegern* could thus deliver further insights into the role of anisotropy on the resulting data products.

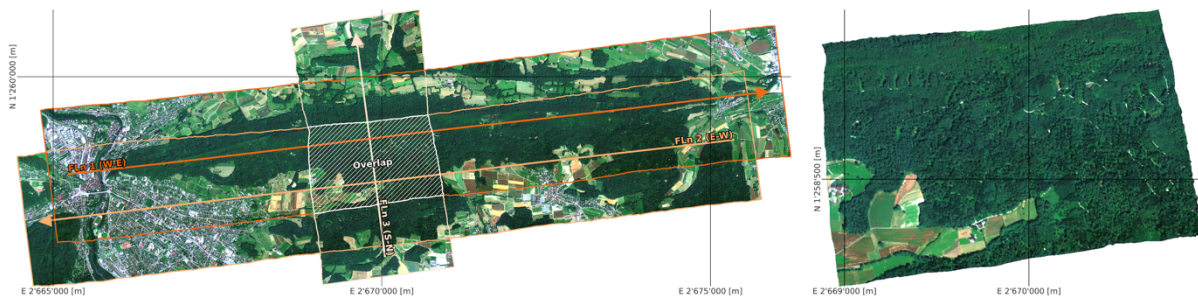


Figure 1 Left: Overview of the three flight lines covering the *Laegern* forest study site. N/E/S/W mean cardinal directions of the flight lines' headings. Right: RGB visualization of flight line 1 clipped to the overlapping region.

Functional richness (FRic) and functional divergence (FDiv) from NDWI, CCI, Clre

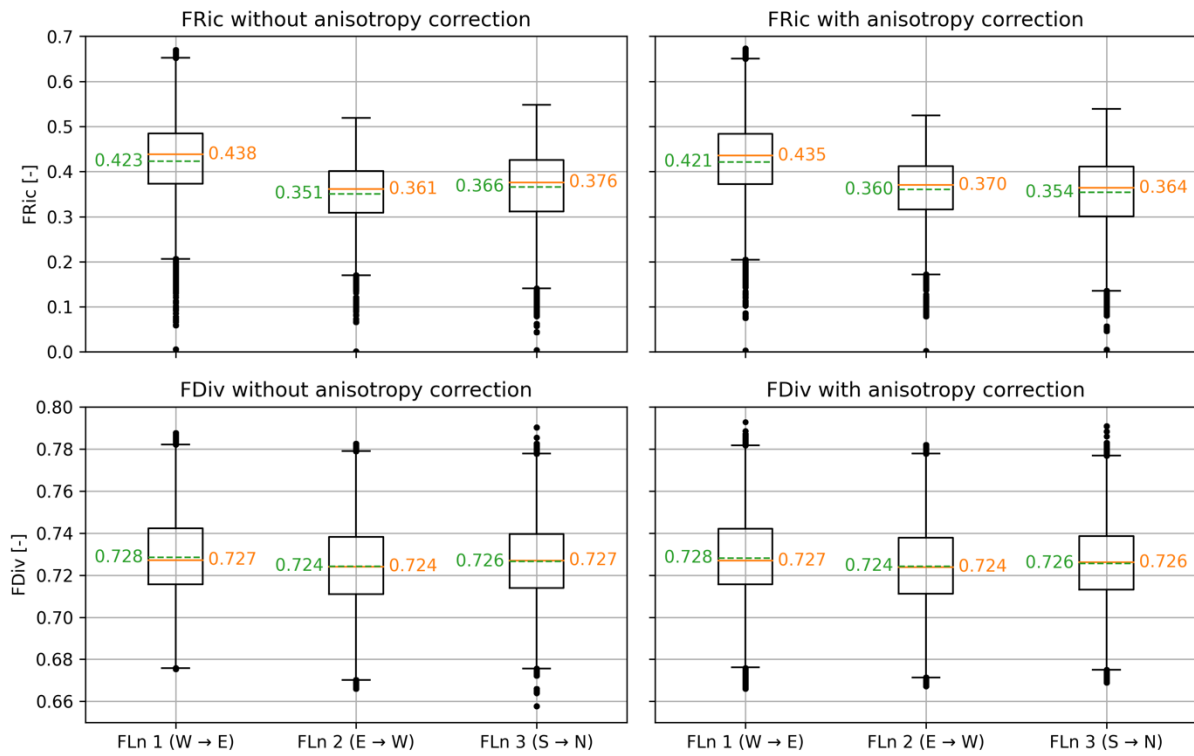


Figure 2 Boxplots for functional richness (FRic) and functional divergence (FDiv) in three flight lines calculated based on reflectance data without anisotropy correction (left) and with anisotropy correction (right). The green dashed line and green numbers show mean values, and the orange line and orange numbers show median values. N/E/S/W mean cardinal directions of the flight lines' headings.

Exploring the spectral variation hypothesis for α - and β -diversity: A comparison of open vegetation and forests

Christine I. B. Wallis^{1,2}, Anna L. Crofts¹, Mark Vellend¹
(Style: Authors, presenting author underlined)

¹ University of Sherbrooke, Department of biology, Canada

² Technische Universität Berlin, Geoinformation in Environmental Planning, Germany

Keywords (5): Plant diversity, imaging spectroscopy,

Challenge (800 - 1000 characters incl. spaces)

Airborne hyperspectral imaging holds great promise for estimating plant diversity and composition, given its unprecedented combination of aerial coverage, spatial resolution, and spectral detail. Recently, there has been renewed attention toward the spectral variation hypothesis (SVH), which predicts that higher spectral variation is correlated with greater variation in plant diversity. To date, local and regional tests of the SVH have shown highly variable results, from very strong plant-spectral diversity relationships to low or even negative associations. While several studies have highlighted methodological challenges involved with the SVH, comparing these studies is difficult since the link between spectral variation and plant diversity appears to depend also on ecological context. One major research gap is that the hypothesis has rarely been tested in different vegetation types across the taxonomic, functional, and phylogenetic dimensions of diversity.

Methodology (1200 – 1500 characters incl. spaces)

As part of the Canadian Airborne Biodiversity Observatory (CABO), we surveyed hyperspectral and vegetation data in plots across five sites (three open vegetation sites, two forest sites), with the plots at forested sites arranged along an elevational gradient. Airborne hyperspectral surveys were conducted alongside the plant inventories in 2018, 2019 and 2020 using two comparable pushbroom imagers collecting spectral information over 288 spectral bands, covering the visible and near-infrared (NIR) regions. At open vegetation sites, the plant community was surveyed in 3 m x 3 m square plots, and for forest sites, the tree community was surveyed in 15 m radius circular plots (as seen from above). We employed generalized additive models to test the relationship between plant and spectral α -diversity. β -diversity was assessed using distance-based and ordination-based approaches (Mantel test and Procrustes analyses, respectively). We hypothesized that the functional dimension of diversity would exhibit stronger links to spectral diversity, at both the α - and β -levels, because spectra are a direct expression of foliar and canopy chemical and structural characteristics. We also proposed that species turnover along the elevational gradient at the forested sites would enhance spectral-plant relationships, particularly for β -diversity. We thus aimed to help refine the spectral variation hypothesis and compare its applicability in open vegetation and forests.

Expected results (1200 – 1500 characters incl. spaces)

Generalized additive models revealed that spectral diversity was a better predictor of functional α -diversity than of taxonomic or phylogenetic α -diversity in both vegetation types. Mantel tests and Procrustes analyses revealed weak to moderate associations between spectral and plant β -diversity and composition in open vegetation, and moderate associations in forests. The better fit in forests appeared to be influenced by the presence of an elevational gradient and associated species turnover (from deciduous to coniferous trees); we observed weaker relationships when examining only a subset of this gradient. So far, interactions between environmental gradients, species turnover and the SVH have been overlooked in the literature and may underlie the high variability in the strength of associations between plant and spectral diversity reported to date. Finally, we found that different wavelength bands contributed to spectral α -diversity in open vegetation vs. forests, suggesting different spectral features are important for different vegetation types. In conclusion, spectral diversity is a potentially powerful tool for biodiversity assessment, but it requires a context-specific approach.

Outlook for the future (800 - 1000 characters incl. spaces)

Our findings suggest that spectral diversity is particularly effective for modelling functional α -diversity across diverse vegetation types. However, it is important to note that its applicability to modelling plant composition and β -diversity may depend on the specific ecological context. Future studies could benefit from a more in-depth exploration of the SVH along various environmental gradients, incorporating a wider range of functional traits and spectral wavelength bands (e.g., short-wave infrared bands) but also spectral feature selection. This would provide a more comprehensive understanding of the drivers of spectral diversity across various vegetation types, but particularly in open vegetation ecosystems where non-biological spectral noise and multiple environmental gradients may pose a significant challenge. Based on our findings we thus recommend a nuanced and context-specific approach to using hyperspectral imaging for biodiversity assessments and conservation planning.

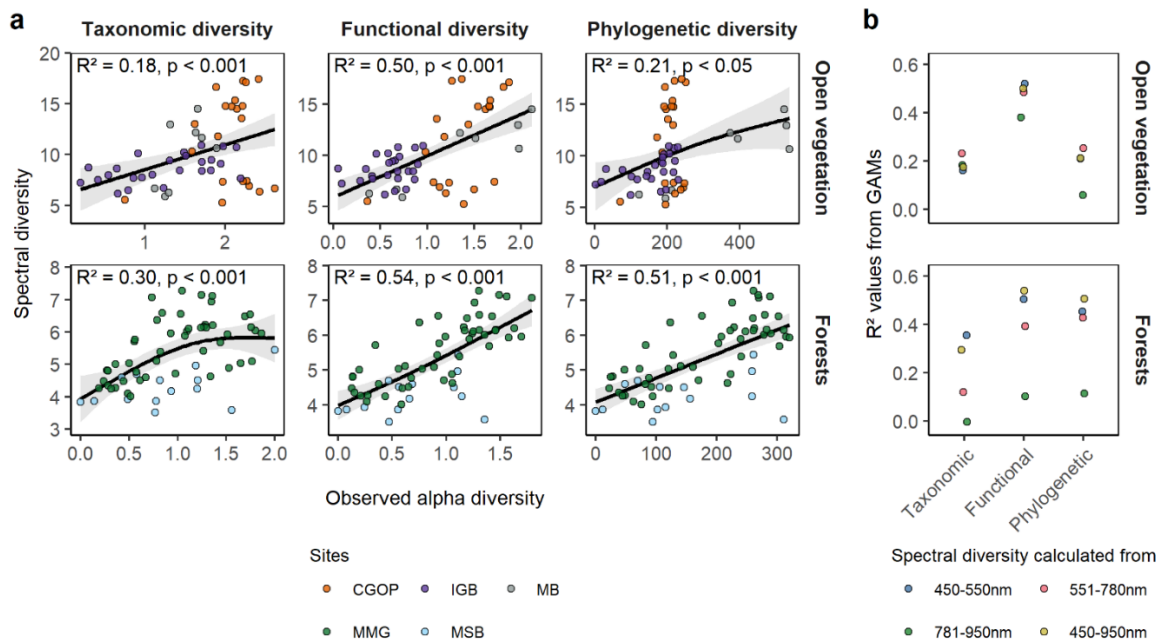


Figure 1 Model fits derived from generalized additive models of spectral diversity and plant α -diversity with spectral diversity calculated from (a) all wavelength bands and (b) specific spectral regions. We used Shannon diversity, functional dispersion, and the mean pairwise phylogenetic distance for taxonomic, functional, and phylogenetic diversity, respectively. Points in a) represent raw data values, and the solid black line indicates the smooth GAM function (allowed basis functions range between 1-4) with its standard error (shaded area).

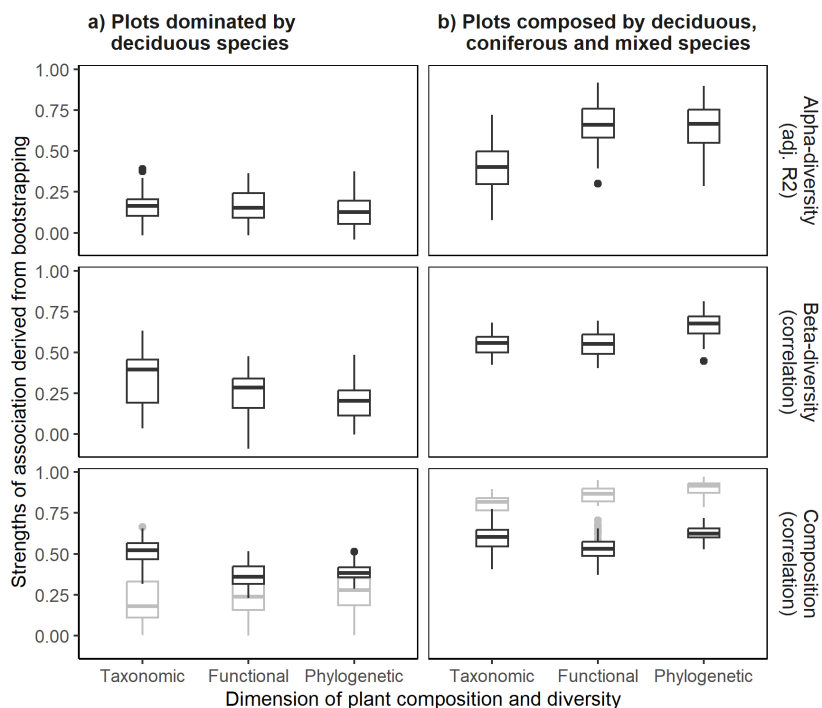


Figure 2 Strengths of association for α - and β -diversity with plots sampled over different portions of the tree composition gradient. Simulating a shorter gradient, a) shows the results for plots dominated by deciduous species (>75% crown coverage) and b) shows the results for plots that were equally sampled over the three strata deciduous-dominated (>75% of crown coverage), coniferous-dominated (>75% of crown coverage) and mixed species (25-75% of deciduous/coniferous crown coverage). All results were bootstrapped with 50 iterations using a random sample of 21 plots from the defined sites in each iteration. Boxplots show the median strength of association and interquartile ranges from bootstrapping. For the adjusted R^2 and correlation coefficient values, we applied generalized additive regression models, Mantel tests, and Procrustes analyses. For Procrustes analyses, test results using only one component are shown in grey.

Upscaling Drought Disturbance Monitoring in the Amazon Forests by Combining Terrestrial Laser Scanning and Field Spectroscopy

EARSeL Valencia 2024

Abstract

Corresponding Author:

wouter.vandenbroeck@ugent.be

Wouter A. J. Van den Broeck¹, Zane T. Cooper¹, Wout Cherlet¹, Patrick Meir², Antonio Carlos Lola da Costa³, Kim Calders¹

¹ Ghent University, CAVElab, Belgium

² University of Edinburgh, UK

³ Universidade Federal de Para & Museu Paraense Emilio Goeldi, Brazil

Keywords (5): virtual forests, terrestrial laser scanning, field spectroscopy, radiative transfer modelling, forest drought monitoring

Challenge

With increasing frequency and intensity of extreme drought events in Amazon forests due to climate change, understanding their impact on the ecosystem is crucial. One critical challenge lies in how drought disturbance will alter the 3D forest structure and composition locally, and how we can monitor these forest changes globally. Addressing this challenge, we present new unique data for the Caxiuanã throughfall exclusion field experiment in eastern Amazonia - the longest running drought experiment in the tropics. Our data consists of two complementary sources: terrestrial laser scanning (TLS) and field spectroscopy. TLS is increasingly recognized as a pivotal technology for forest monitoring, offering highly detailed measurements of 3D vegetation structure. On the other hand, spectroscopy can provide the spectral signature of the main biophysical components of the forest scene. We show that the fusion of both enables the creation of realistic virtual forests, which can serve as input for (optical) radiative transfer models (RTM), allowing for the upscaling of forest monitoring.

Methodology

The study site consists of two 1 ha research plots established in 2001 in the Caxiuanã National Forest, a tropical lowland rainforest in the state of Para, northeast of Brazil (1°43' S, 51°27' W). The first plot is a control plot without any manipulation. The second plot is the throughfall exclusion (TFE) experiment, where plastic panels at 1-2m above the ground cover the entirety of the area, thereby excluding 50% of canopy rain throughfall. For both plots, we collected TLS and field spectroscopy measurements in October 2023 (dry season). Plots were scanned using a RIEGL VZ400i in a 10x10 grid with both an upright and tilt scan at each position (600kHz). Individual scans are subsequently co-registered in RISCAN-PRO to form a single complete point cloud. Reflectance spectra (350 nm – 2500 nm) of leaves, bark and soil were collected using an ASD FieldSpec 4 Hi-Res radiospectrometer. For 51 individual trees, nine top of canopy leaves were sampled and measured (2x per leaf), and 4 bark reflectance measurements at ca. 2m above ground level were taken. For 29 individuals, leaf measurements were repeated pre-dawn and at midday to check for any diurnal spectral variation. Soil measurements were taken at patches lit by direct sunlight. Spectra were averaged to derive a single reflectance curve for each individual and component.

Expected results

Figure 1 shows the steps for conversion of a segmented TLS point cloud into a virtual forest for radiative transfer modelling. First, the different components (soil, stem and branches, leaves) in the 3D point cloud

are semantically segmented and the individual trees processed into some volumetric representation. The different components can then be spectrally parameterized, allowing for the creation of a structurally and radiometrically realistic digital replica of the forest: a 'digital twin forest'. These digital twins can be used as input for (optical) radiative transfer modelling. RTMs enhance our ability to monitor and understand the coupling between emitted, reflected or scattered electromagnetic (EM) waves and a 3D scene, and therefore are a powerful tool to establish the physically-based link between in situ structure and how it is monitored with satellite remote sensing. Explicit digital forest twins will be constructed according to the abovementioned processing pipeline for both the Caxiuana control and drought plot. This will then allow for running RTM models such as DART (<https://dart.omp.eu/#/>) and Eradiate (<https://www.eradiate.eu/site/>) to simulate and compare remote sensing products, and increase our understanding of the impact of drought on 3D forest structure as seen from space.

Outlook for the future

A next step is to move from 'static' 3D digital twins to 'dynamic' 4D digital twins, to incorporate the temporal dimension. For Caxiuana, both plots have been scanned before in the years 2015 and 2018. Co-registering these data opens avenues for unexplored research into the impact of drought on Amazon forests. Furthermore, ongoing and future work within the context of the SPACETWIN project (<https://spacetwin.ugent.be/>) focuses on enhancing our understanding on forest disturbances and recovery from space. The project will focus on the impact of drought, but also fire logging and insect disturbances across a range of tropical and temperate forest ecosystems. SPACETWIN aims to integrate realistic TLS-derived digital twins of forest structure with spectroscopic measurements as RTM input to build an emulator for optical, lidar and radar satellite data that will allow for near real-time interpretation of disturbances.

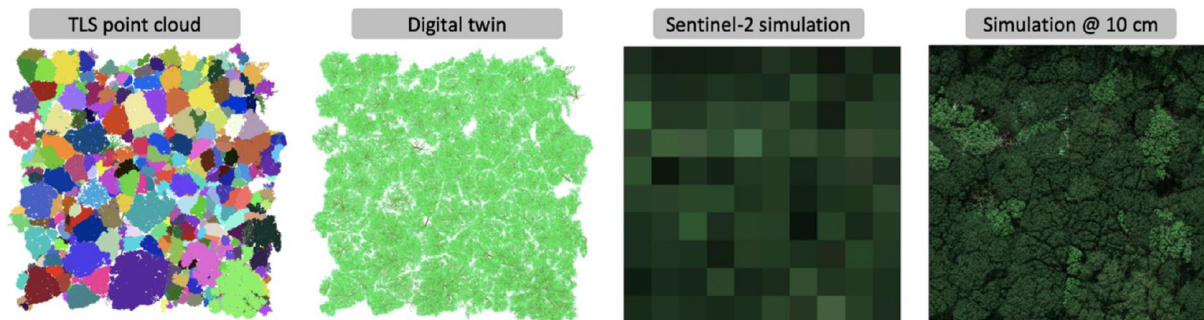


Figure 1 Conversion of a segmented point cloud from terrestrial laser scanning into a virtual forest for radiative transfer modelling: example of 1 ha Wytham Woods (Calders et al., 2018). From left to right: view from above of the 3D point cloud segmented into single trees; digital twin (digital terrain model not shown here); simulated Sentinel-2 satellite image over this scene with associated spectral signatures using the librat RTM for a 10 m spatial resolution image (real Sentinel-2 spatial resolution); & RTM simulation using a 10 cm ground sampling distance.

Acknowledgements

This research was funded by the European Union (ERC-2021-STG Grant agreement No. 101039795). Views and opinions expressed are however those of the author(s) only and do not necessarily reflect those of the European Union or the European Research Council Executive Agency. Neither the European Union nor the granting authority can be held responsible for them.

Challenges of hyperspectral high-throughput phenotyping for drought tolerance in conifer seedlings

EARSel Valencia 2024

Abstract

Corresponding Author:

[eva.neuwirthova@natur.cuni.cz]

Eva Neuwirthová^{1,2}, Jaroslav Čepel¹, Jiří Chuchlík¹, Zuzana Lhotáková², Jan Stejskal¹, Miroslav Píkl³, Daniel Provazník¹, Jana Albrechtová², Milan Lstibůrek¹

¹Department of Genetics and Physiology of Forest Trees, Faculty of Forestry and Wood Sciences, Czech University of Life Sciences Prague, Czech Republic.

²Department of Experimental Plant Biology, Faculty of Science, Charles University, Czech Republic

³Global Change Research Centre, Academy of Science of the Czech Republic, Bělidla 4a, 60300 Brno, Czech Republic

Keywords (5): Phenotyping unit, Fluorescence, Hyperspectral imaging, Segmentation, Machine learning algorithm

Challenge

Optical properties of foliage, (reflectance, and fluorescence) offer non-destructive insights into plant physiology. High throughput phenotyping (HTP) include several imaging approaches allowing to evaluate leaf biophysical properties based on its optical properties.

HTP at the plant level is mostly used for economically important crops, model organisms or seedlings of deciduous trees, but little attention has been paid to conifers at the individual or leaf level, due to the difficulties resulting from thin needle-like foliage.

Getting the information from the images depends on segmentation the object of the interest from the background. Segmentation can be challenging for parts of the plants with small projection area such as conifer needles. The aim is to compare unsupervised (thresholding) and supervised (machine learning) segmentation of hyperspectral images with fluorescence and thermal image data to identify three populations of Scots pine seedlings under drought treatment.

Methodology

Two-year-old Scots pine seedlings from three populations underwent a joint greenhouse experiment spanning from February 21st to August 5th, 2022. 405 individuals were subjected to 84 days of drought treatment, followed by 36 days of rewatering.

Throughout a 164-days, leaf physiological traits were measured in the phenotyping unit at multiple time points. The facility was equipped with imaging sensors for RGB, thermal, fluorescence, and hyperspectral scanning. Physiological attributes were analysed: steady-state and maximum quantum yield response of photosystem II (QY_Lss, QY_max), non-photochemical quenching at steady state (NPQ_Lss), needle relative chlorophyll content (Rel_ChI), and needle temperature difference from the ambient air temperature (Delta_T). To explore variations among the treated populations in leaf functional traits, we employed linear mixed models (LMM). Hyperspectral imaging (HSI) of reflectance were captured using two cameras, a) VNIR range (350-900 nm) and b) the SWIR range (900-1700 nm), with spatial resolutions of 1920 × 1000 and 640 × 512 px, respectively. Unsupervised segmentations were employed for thermal and fluorescence sensor data; however, these methods proved inadequate for segmentation of HSI. To segment seedlings from HSI, we will utilise convolutional neural network algorithms, YOLO on a training dataset. Differences in reflectance between treatments and populations will be compared with the results from fluorescence and thermal sensors.

Results

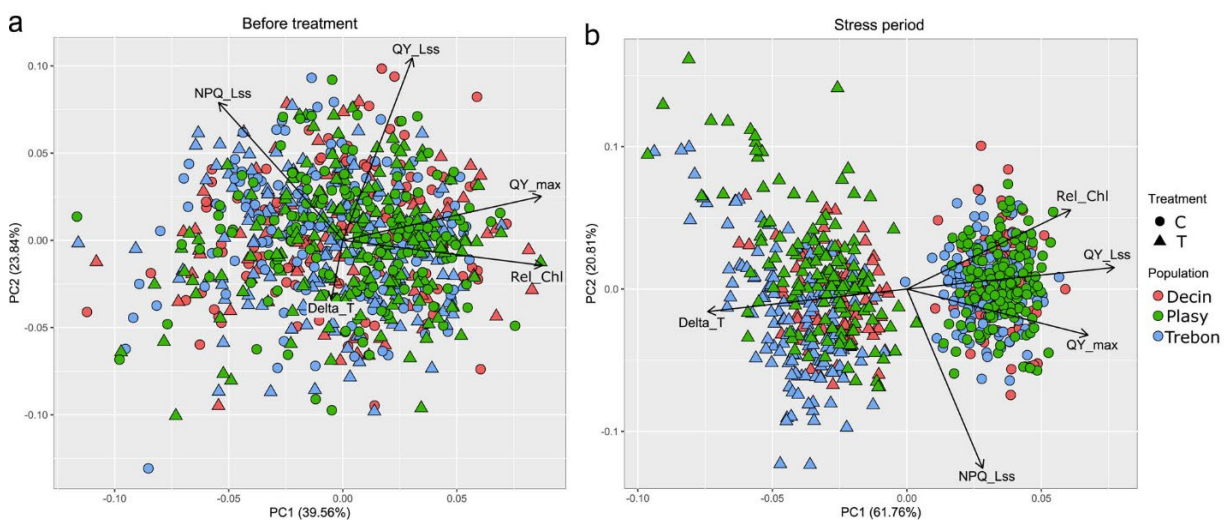
Utilizing LMM we detected significant variations among three populations of Scots pine seedlings in functional physiological traits, including NPQ_Lss, Rel_ChI, and Delta_T, before the irrigation reduction and during the stress period; QY_Lss, QY_max differed among populations only during the stress period. Despite significant differences observed in individual parameters analyzed separately by LMM, this variability may not be sufficient for a clear separation of populations, as demonstrated by Principal component analysis (PCA) of all five physiological parameters at two time points. Prior to the reduction in irrigation, the score distribution of individual populations appeared to be homogeneous, like the control group of plants during the dry period. Contrastingly, the stressed plants showed a more homogenous distribution of population scores. This trend in population differentiation was mainly driven by relative chlorophyll content (Rel_ChI) from HTP. The study involves an ongoing analysis of the separation of treatments and populations using LMM and PCA on hyperspectral data. Hyperspectral data will be segmented using both unsupervised and supervised methods. The primary objective is to assess the compatibility of these data with our physiological functional traits, with the goal of identifying the optimal optical sensor and physiological traits that can serve as the most effective markers for distinguishing among three populations of the Scots pine seedlings.

Outlook for the future

The selection based on seedlings' functional physiological traits shows promise for early-age screening in nurseries. Evaluating the quality of plant material helps foresters in plant breeding and plant selection, especially in the context of the increasing problems of drought caused by climate change throughout Europe. Early-age detection of drought-tolerant individuals allows for the identification of individuals highly adapted to specific target environments. Conifers are important woody plants for the sustainability of forest ecosystems but pose a challenge in terms of obtaining and processing optical properties due to the low projection area of the needles. Machine learning methods can help overcome this problem, whether it is due to the limited projection area of individual plant parts or the low spatial resolution of the camera. The novelty of this study lies in testing algorithms for reliable segmentation of hyperspectral images of conifer seedlings at the individual level.

Figure (a) PCA of the five functional parameters before the treatment
(b) PCA of the five functional parameters in the stress period.

Points refer to individual seedlings (n=810), shapes correspond to the C = control, T= drought-treated; colours correspond to the progeny of three Scots pine locally adapted populations: D = Decin, P = Plasy, T = Trebon.



Acknowledgements: We thank Dr. Klára Panzarová and PSI (Photon System Instruments) s.r.o. for providing the phenotyping unit and data acquisition.

**Them.Sess. 2-11: Technical
discussions on imaging
spectroscopy**

Hyperspectral Point Cloud Geometric and Atmospheric Processing in Complex Terrain

EARSeL Valencia 2024

Abstract

Corresponding Author: daniel@rese-apps.com

Daniel Schläpfer¹, Simon Alexander Trim^{1,2}

¹ ReSe Applications LLC, Switzerland

² University of Zurich, Switzerland

Keywords (5): Processing Chain, Hyperspectral, Geometric Correction, Atmospheric Correction, Point Clouds

Challenge

Drone based hyperspectral imaging (HSI) systems provide the opportunity to map complex terrain structures such as vertical mine faces, buildings or forest borders at high spectral and spatial resolutions. Indeed, the data acquisition may be done at oblique observation geometries in order to get a better view of vertical structures. Hardware systems are in development which provide laser scanning data in combination with HSI sensors. HSI data of terrain with vertical and overhang surfaces require to fundamentally change currently existing HSI imagery processing approaches. So far, raster representations of digital elevation data in surface models (DSM) or terrain models (DTM) were the basis for both geometric and atmospheric corrections. For true 3-dimensional processing, the point cloud structure is more appropriate. This paper tries outlines a novel concepts for geometric correction, atmospheric compensation and reflectance retrieval based on point cloud data structures.

Methodology

The workflow presented in this contribution is optimized for HSI data which are taken simultaneously to LIDAR scanning. The goal is to have a fully automatic processing chain which creates georeferenced HSI reflectance data in complex terrain. For efficiency reasons, the geometric information is kept in point cloud format while the HSI imagery is stored as raw sensor frame-based data cubes. The two data entities are to be linked such that radiometric corrections can be applied to the HSI data based on the geometric information from the point cloud and the related surface mesh.

The preprocessing of HSI data is typically split into three parts:

- [1] Raw data processing: this includes the data calibration, point cloud filtering and mesh generation
- [2] Geometric processing: ray tracing of the HSI data observation geometry onto the surface mesh and surface normal generation
- [3] Reflectance retrieval: correction of radiometric effects of the atmospheric transmittance, aerosol scattering, adjacency effects, terrain irradiance and BRDF variations.

We focus in this paper on [2] and [3]. The geometric and radiometric processes are coupled into one streamlined processing system which allows to retrieve accurate reflectances within a few hours after data acquisition.

Results

Based on the above requirements, a processing system is developed and tested. It is applied to sample data taken within the m4mining (EU Horizon) project and is evaluated based on extensive field measurements of reflectance properties of mineralogically interesting targets.

For the geometric processing, we rely on state-of-the-art ray tracing technologies such that each HSI spectrum can be linked to a valid 3D position in absolute x/y/z coordinates. The retrieved results are to be filtered appropriately to avoid backward intersections and secondary intersection problems. Specifically, the process is designed such that all observation angles including fully horizontal and even slightly upward observations are supported.

For the reflectance retrieval, the surface normal vectors as well as the neighbourhood data structure from the mesh generation is used for an optimal illumination correction. In a 2nd step, the terrain information is inverted to raw geometry in order to retrieve local dependencies and to apply spatial filters for the calculation of terrain and adjacency influences on each pixel. This workflow is also suitable for retrieving reflectance values in shaded areas based on iterative aerosol scattering estimates.

Applying these processes to the HSI data delivers hyperspectral point cloud outputs. Figure 1 shows results on a tree structure based on current technology.

Outlook

A new 3D point cloud-based hyperspectral processing workflow has been defined. The system will be further optimized on the basis of data acquisitions in open pit mines. The evaluation will specifically focus on the retrieval of accurate reflectance spectra in shaded areas and from oblique viewing angles. Other than displayed in Figure 1, the 3-dimensional structures can be fully mapped by the new processing system in conjunction with an integrated hardware system.

The irradiance calculation for such situations is very challenging and requires to put up a model for the calculation of the hemispherical irradiance variation in the true 3D world. It is expected that working solutions will be implemented in the course of the ongoing m4mining EU horizon project and operationally usable tools will be made available to the public upon completion of the development project.

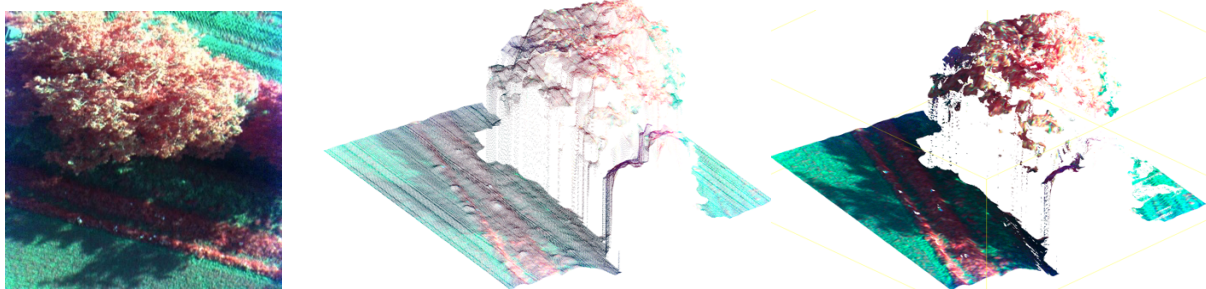


Figure 1: 3-dimensional hyperspectral point cloud display of a tree structure in false color display, using standard DSM data. Left, original HSI image, middle: hyperspectral point cloud, right: meshed surface of valid HSI data points.

A small hyperspectral satellite mission targeting big image quality

Stefan Livens¹, Dirk Nuyts¹

¹ VITO Remote Sensing, Belgium

KEYWORDS: HYPERSPECTRAL SATELLITE MISSION, , IMAGE QUALITY, IN ORBIT DEMONSTRATOR, PUSHFRAME IMAGING, IMAGING EXPERIMENTS

Challenge

Satellite missions carrying Imaging spectrometers have long been rare and their use was very limited due to their small imaging capacities. Recently, more imaging capacity is being realized, with missions like PRISMA and EnMAP fuelling larger interest to address remote sensing applications using spaceborne hyperspectral data.

Some future missions intend to further increase both imaging quality and capacity. Meanwhile, breakthrough technological developments (e.g. thin-film hyperspectral detectors) allow to build very small hyperspectral missions (e.g. 6U CubeSats). Commercial NewSpace companies are now building hyperspectral constellations to realize dramatic improvements in coverage and revisit times.

To valorising this abundance of data requires the image quality to be sufficient to address many applications. The small size imposes trade-offs on platform stability, data downlink limitations, light gathering, etc.. The next challenge is to pair cost-efficiency with an improved image quality, which is the goal of the development of the CSIMBA instrument and IPERLITE mission

Methodology

The CSIMBA instrument is based on a frame imager combining a 3076x4096 pixel CMOS detector with directly deposited thin film narrow bands interference filters. 192 different filters are each laid out over 12 adjacent lines, together covering a 470nm to 900nm spectral range with 5nm spectral resolution. On the remaining sensor area, 2 areas for panchromatic imaging are placed. The imager is combined with a compact wide swath TMA telescope with focal length= 135mm, and F/4.5 . Using typical satellite forward motion, it can perform push-frame acquisitions which combine image capture with high resolution in both spectral and spatial domains. The mission will operate from a 500km altitude to provide a 80km swath and a 20m GSD..

The satellite speed imposes not only short integration times, and to capture all spectral bands at all locations requires a sustained frame rate of at least 30 fps (corresponding to 1 acquisition after moving over 12 image lines). We however set a much more ambitious target: a frame rate of 360 fps. This allows to acquire a new image after moving over a single line. As there are 12 lines per spectral band, 12 independent acquisitions can be made. The results can be summed up per pixel, which implements a digital equivalent to Time Delay Integration (TDI). The read out electronics and onboard computing capabilities have been designed to handle this fast readout and the accumulation of up to 12 stage of Digital TDI. The read-out also supports additional acquisition and processing modes. We defined modes that use a combination of panchromatic and hyperspectral imaging, and a mode which implements high dynamic range (HDR) imaging by combining acquisitions with 2 different integration times.

Expected results

The optical system has been manufactured and characterised in the lab. The measured MTF is 0,55 at @550nm and > 0.44 over the full range, exceeding the requirements of > 0,41 @550nm and >0.38 full range.

The spectral characteristics of the imager have been characterised, confirming the spectral range and bandwidth. To estimate the signal to noise ratio (SNR), we have made simulations using the characteristics of the sensor and spectral filters to compute imager outputs for any given input radiance signal.

The results for a standard reference input radiance of $100 \text{ W}\cdot\text{m}^{-2}\cdot\text{sr}^{-1}\cdot\mu\text{m}^{-1}$ (a realistic value in space) show a fairly large variation in SNR over the spectrum. For imaging without TDI, the average SNR= 35 (varying between 14 and 92). By switching to imaging mode with 12 stages of digital TDI, the SNR improves with a factor $\text{SQRT}(12)$: average SNR = 120 (varying between 48 and 320). This illustrates the major advantage achieved by implementing the digital TDI imaging mode.

The mission offers a downlink of 18,75GB per day, which corresponds with an area of about 17500 km² of full spectral imaging at 20m GSD.

Outlook for the future

The launch of the mission is foreseen in 2025. During the commissioning phase, advanced geometric and radiometric vicarious calibration will be carried out, as well as verification of the MTF and spectral performance. For the radiometry dedicated acquisitions over stable desert sites and lunar acquisitions are planned, including concurrent acquisitions with other missions to facilitate cross-calibration.

The default imaging mode uses 12 stage TDI. Alternative imaging modes will also be explored, including high dynamic range imaging and a low light imaging mode combining longer integration times with spatial binning. Panchromatic imaging will be explored in experiments on multi-angular imaging and super-resolution. The combination of hyperspectral and panchromatic imaging will be used, e.g. to aid deblurring, improve SNR or improve geometry.

Acquisitions over selected application sites will be carried out to demonstrate the capability and benefits of the mission. Thus it can contribute to innovation and quality improvements for small hyperspectral satellite missions.

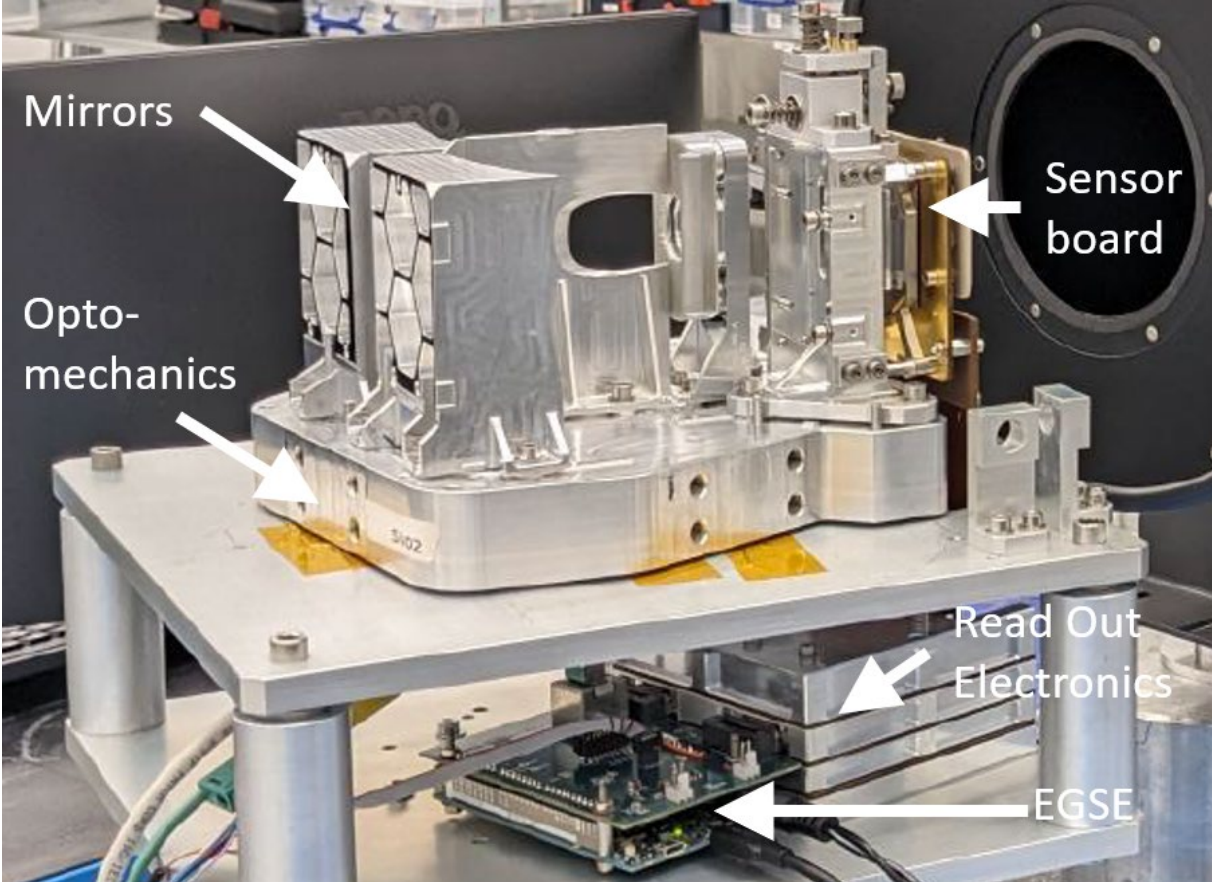


Figure CSIMBA instrument with indication of different subsystems

Not as dirty as they look: flawed spectral measurements of bright surfaces

Edward Bair¹, Dar Roberts², David R. Thompson³, Brenton A. Wilder⁴, Niklas Bohn³, Miguel Román¹, Christopher J. Crawford⁵, Jeff Dozier²

¹ Leidos Inc., USA

² University of California, Santa Barbara, USA

³ Jet Propulsion Laboratory, California Institute of Technology, USA

⁴ Boise State University, USA

⁵ US Geological Survey, USA

Keywords (5): atmospheric correction, snow, hooking, bright targets, light-absorbing particles

Challenge (800 - 1000 characters incl. spaces)

Planned and recently launched spaceborne imaging spectrometers (e.g., PRISMA, EnMAP, EMIT, CHIME, SBG) increase the quality and resolution of global imagery, but standard surface reflectance products struggle over bright surfaces such as snow and playas. For example, a common artifact in surface reflectance products for both for airborne and spaceborne imaging spectrometers (multi- and hyperspectral), is a “hook” in the shortest wavelengths, whereby the surface reflectance appears to decrease in the shorter visible wavelengths, below 600 nm. Over snow, this decrease in apparent reflected radiation is often mistaken for the presence of light-absorbing particles (LAP) (e.g., soot or dust).

Likewise, ground validation for bright targets is challenging. A review of sites worldwide where the bihemispherical reflectance (albedo) of snow is measured shows flaws where darker objects are within a downlooking radiometer’s field of view, thereby erroneously decreasing the calculated broadband albedo. Further complicating retrievals for snow is that its surface is rarely flat, but sloped, and marked by features such as sastrugi or ablation hollows that reduce its apparent reflectance.

Methodology (1200 – 1500 characters incl. spaces)

Shortwave hooking was documented in multiple standard reflectance products for airborne and spaceborne sensors, both in simple terrain such as lakes covered with an optically thick snowpack and in rugged terrain such as steep mountain slopes on a variety of aspects. Radiative transfer and Mie theory models were used to estimate downwelling and upwelling radiation from snow and for mixed pixels. Bright and dark surface albedos that contribute to the path radiance term, i.e., reflected radiation from the atmosphere above target, were used in a radiative transfer model. Topographic corrections were applied to examine the effect of topography and compare with uncorrected retrievals.

Sites worldwide were examined and documented. At the CRREL-UCSB Energy Site (CUES, <https://snow.ucsb.edu>), a remotely-controlled and self-levelling boom was built in 2015 to keep downlooking radiometers ~1 m above the snow surface. An automated terrestrial laser scanner was installed to map the snow surface at hourly and finer timesteps. Corrections were applied to the snow surface in conjunction with an analytical model to simulate multiple reflection events such as photon trapping.

Results (1200 – 1500 characters incl. spaces)

Because ice is so transparent, its complex refractive index has not been reliably measured at 200-400 nm. Differences in optical constants in the published literature lead to modelled values with some hooking or no hooking in this region for clean snow. This source of uncertainty is minor .

Other sources of uncertainty are more substantial and can be separated into atmospheric and surface modelling issues. For bright surfaces, the atmospheric modelling error is the common assumption of too dark of an albedo (e.g. 0.25) for areas adjacent to the target. Incorporating a too-low value in the atmospheric correction causes an underestimation of the path radiance, resulting in a hooking error, which can slope down or up in the visible wavelengths. This error can also be caused by simplified assumptions about the surface, i.e., not accounting for topography, which leads to an incorrectly modelled proportion of blue-shifted downwelling solar radiation. These hooking errors are pernicious in that they alter the spectral shape, a far more difficult condition to correct for than consistent changes in spectral magnitude.

Another surface modelling error is not accounting for surface roughness at the centimetre scale. This can cause an apparent broadband albedo (i.e., rough surface) that diverges from the intrinsic albedo (i.e., smooth surface) by 5-6%. In case of instruments with lower spectral resolution, darkening from surface roughness can be easily confused with darkening from LAP, but imaging spectrometers can distinguish the darkening sources.

Outlook for the future (800 - 1000 characters incl. spaces)

End users of future sensors—such as Landsat Next, CHIME, or SBG—will be able to perform their own atmospheric correction, but the majority will use standard surface reflectance products. Currently, these surface reflectance products (e.g., Landsat 8/9) are providing inaccurate spectral shapes over bright targets, leading to overestimates of LAP and their radiative forcing on Earth's climate. Our goal is to raise awareness and reduce these errors to improve the quality of research. For example, such errors may be partly responsible for our poor agreement between modelled and remotely sensed estimates of pollutants. Rectifying this situation is imperative to gain a better understanding of the effects of global pollution on planetary albedo.

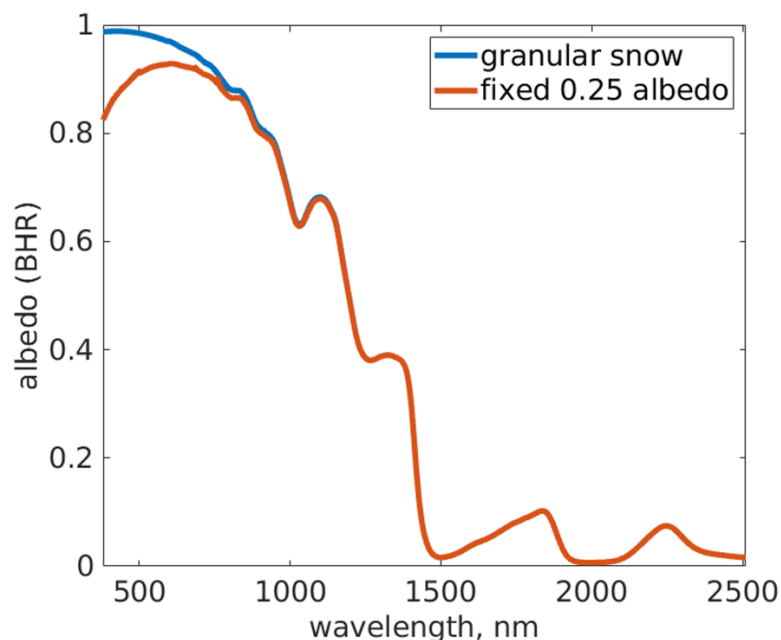


Figure Modelled spectral bihemispherical reflectance of clean snow using two different surface albedos for areas adjacent to the target. The fixed 0.25 albedo is commonly used and shows the shortwave hooking that is easily misattributed to light-absorbing particles such as soot. The granular snow albedo varies with wavelength and looks similar to the blue curve, which is the expected shape.

Creating Temporal Hyperspectral Regional Endmember Bundles (THREBs): Automatic imaged based EM extraction and library reduction to derive regional fractional vegetation cover

[Kevin Kühl](#)¹, David Marshall Ingram¹, Uta Heiden¹, Martin Bachmann¹

¹ German Aerospace Center (DLR), Earth Observation Center (EOC), Weßling, Germany

Keywords: Hyperspectral, Fractional Vegetation Cover, Unmixing, THREB, EnMAP

Challenge

With the increasing availability of hyperspectral images (HSI) through missions like PRISMA, DESIS, and EnMAP, as well as the upcoming CHIME mission, the opportunities for large scale analyses are now being realized. Simultaneously, the establishment of operational processing chains is becoming increasingly important. With that in mind, the Earth Observation Centre at DLR has developed an fCover processor which extracts and classifies endmembers from HSI and, following a spectral unmixing step, generates soil and vegetation cover maps. To generate homogeneous fCover maps over large areas it is necessary to overcome challenges like generalized EM libraries, incoherent unmixing, and unintentional use of false EMs that can occur in single scene processing. The methodology presented here alters the established fCover processor by exploring the potential of processing multiple scenes, thereby creating temporal hyperspectral regional endmember bundles (THREBs) and generating coherent region-wide fractional vegetation cover maps in an automated fashion.

Methodology

To create THREBs and fCover maps, the following methods were used. First, from each HSI within a predefined region, EMs are extracted using the SSEE method (D.M. Rogge et al. 2007 Remote Sens 3, no 110). After the extraction of the pure spectra, the EMs are labelled using a well-trained Random Forest classifier and stored in a preliminary THREB. These steps are performed for multiple scenes in a defined region. To ensure maximum spectral variability, the preliminary THREB is pruned regarding scene-specific features of individual but consecutive HSIs using the AMUSES approach (Degerick, et al. 2017, Remote Sens 9, no 6). This method adds a spectral separability measure to the workflow of MUSIC-PA to decrease internal redundancy by a) selecting EMs that best represent the spectral variability by using the HySime algorithm b) calculating the Euclidean distance between estimated image subspace and EM spectrum and c) choosing spectra with the lowest projection error between the image and EMs. After sorting all library spectra by their distance to the HSI, only a fraction of the highest ranking spectra are retained based on predefined thresholds. The eligible spectra are assessed one by one using a spectral separability measure by combining the Jeffries Matusita distance and Spectral Angle (JMSA). Only if a signature is sufficiently dissimilar from an already chosen spectra, will it be included in the THREB. The final THREB is the resulting pruned EM library from all HSIs and is used as input to the linear spectral unmixing using the μ MESMA approach. As a result, Fractional Cover Maps with subpixel abundances of photosynthetically active vegetation (PV), non-photosynthetically active vegetation (NPV) and Bare Soil based on a regional THREB are generated.

Results

In a first comparison EnMAP scenes around Munich (29.6.23 & 25.09.23) and scenes from Camarena Spain between April and October 2022 were processed and unmixed by a) using EM extracted from single scenes and b) creating and using THREBs. Single scene processing reveals good results overall. However, even with small temporal or spatial differences between acquisitions, fCover abundances can differ substantially by $\pm 5\%PV$, $\pm 11\%NPV$, $\pm 8\%BS$ for two or more consecutive observations (25.09.23). Using THREBs showed a significant improvement concerning unmixing coherence of fCover abundances and RMSE values (by 0-18%). By combining region specific EMs (SSEE) in one preliminary THREB, reducing the preliminary THREB scene specific (AMUSES), and then unmixing all HSI of one region one by one (μ MESMA) with THREBs, the results improve compared to single scene processing. Additionally, ground truth data acquired near Munich in Oct 2023 confirm the assumption that THREBs increase the quality of large-scale analyses.

Outlook for the future

In the next step, Germany will be defined as a region by taking all available EnMAP scenes from 2022 and 2023 into account. THREBs will be compiled (annually and at 3-month intervals) as well as the corresponding fractional vegetation cover maps. These results will be compared to the outcomes of single scene processing to evaluate strengths and weaknesses and to further improve the proposed method. In this process, additional constraints can be explored and adjusted. In the second half of 2023, ground truth data were collected with simultaneous EnMAP overflights for validation. These measurements from an ASD field spectrometer and RGB cellphone images will be further integrated and used as a starting point for fCover/THREB evaluation. Through the development of expanding/evolving THREBs, the SSEE and machine learning steps in the fCover processor could be skipped and HSIs from existing (EnMAP) and future mission (CHIME) could be unmixed directly from a set of well characterized and consistent THREBs.

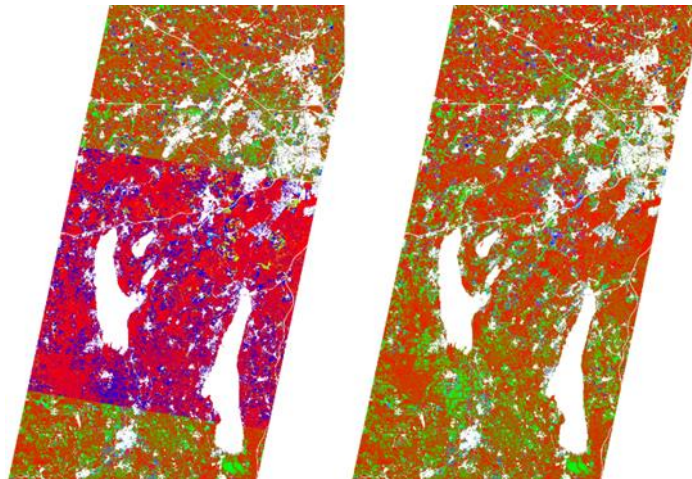


Figure (a) Single scene EM extraction and unmixing(left)and THREB unmixing (right). EnMAP 29.06.2023 south of Munich

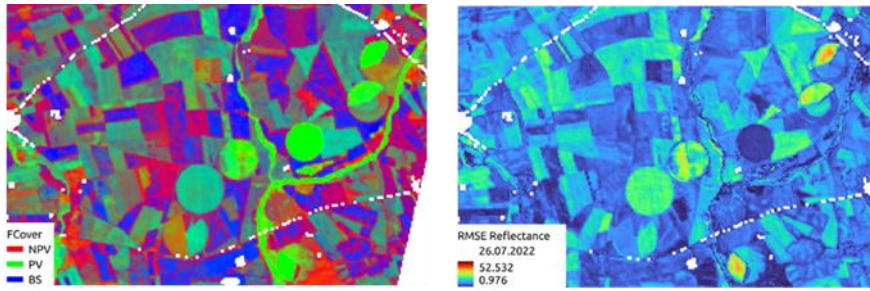


Figure (b) fCover sub-pixel abundance map(left) and corresponding RMSE values in Reflectance (right). Unmixing based on a THREB. EnMAP, Camarena, Spain 26.07.2022.

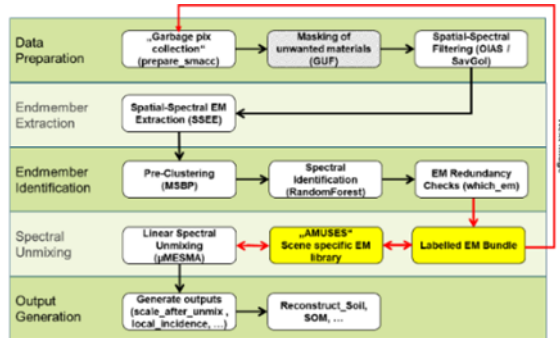


Figure (c) Overview of the adjusted fCover processing chain.

What's new in the EnMAP-Box? Visualization and analysis of EnMAP data for everyone.

Abstract for presentation in special Session:
"EnMAP's first two years in orbit- current,
status and recent activities."

Corresponding Author:
benjamin.jakimow@geo.hu-berlin.de

Benjamin Jakimow¹, Andreas Janz¹, Fabian Thiel², Leon-Friedrich Thomas³, Patrick Hostert,
Sebastian van der Linden²

¹ Humboldt-Universität zu Berlin, Germany

² University of Greifswald, Germany

³ University of Helsinki, Department of Agricultural Sciences, Finland

Keywords (5): Earth Observation, EnMAP, Open Source, Hyperspectral

Challenge (800 - 1000 characters incl. spaces)

Imaging spectroscopy (IS) data from missions like EnMAP, PRISMA and the upcoming CHIME and SBG programs holds immense potential for environmental monitoring, agriculture, and mineral exploration. However, harnessing the potential of IS has been challenging for many users due to the limitations of traditional GIS and remote sensing software, including high costs, restricted access, or insufficient flexibility to incorporate data from different sensors data formats.

With an increasing availability of IS from different sensors, users more than ever require solutions that support them to visualize and analyse raster images from IS instruments that may contain hundreds of bands and high band-correlations. Furthermore, appropriate tools and methods are needed to combine remote sensing data with data from other sources, e.g., field data, in a meaningful way.

The transition to open and free source software, open data policies and attempts for community wide standardization of data product addresses these challenges, promoting easy access to IS data and suitable software for a wide user community to display, explore and evaluate IS data in subsequent analyses.

Methodology (1200 – 1500 characters incl. spaces)

The EnMAP-Box is a python plugin that complements the popular free and open source geoinformation system QGIS with functionality for the visualization and analysis of IS Earth Observation data, especially from EnMAP, DESIS or PRISMA, and multispectral missions such as Landsat and Sentinel-2.

The EnMAP-Box (Fig. 1) combines functionality know from classic GIS software, like the wide support of raster and vector data formats, with capabilities know from remote sensing software, like recognition of wavelength information to select band-combinations. In particular, the EnMAP-Box adds more than 150 algorithms to the QGIS Processing Framework. These algorithms can be used in the QGIS model builder to create larger workflows. They can be run from the GUI, from Python or from the command line. The algorithms allow to easily use IS data as delivered by different data providers, to modify metadata, and to process and analyse raster and vector data to yield final products like classification maps and estimations of continuous biophysical variables.

The EnMAP-Box provides easy access to various state-of-the-art methods from machine learning, to process and evaluate processing results in accordance with state-of-the-art scientific practice. Using QGIS vector workflows, the EnMAP-Box offers comprehensive tools to collect and modify spectral libraries, providing maximum flexibility in defining profiles and profile metadata and ensuring data integrity. Various

research applications use the EnMAP-Box as a platform to provide easy access to context-specific applications, e.g., the EnMAP preprocessing tools (EnPT), the EnMAP Geological Mapper for Mineral Classification (EnGeoMAP) or an Interactive Visualization of Vegetation Reflectance Models (IVVRM).

Results (1200 – 1500 characters incl. spaces)

The EnMAP-Box has been successfully used in a variety of applications, ranging from land cover classification and vegetation health assessment to mineral mapping and environmental change detection. The use in and the feedback from different research environments was streamlined during software design and provided new capabilities for data visualization, management, and processing. The adoption and further development of visualization and process improvement concepts from various GIS and remote sensing software facilitates the use of the EnMAP-Box and IS data for a broad user community.

Since the first public EnMAP-Box release in the QGIS Plugin Repository in 2019, the EnMAP-Box has been downloaded more than 35.000 times. As now, more than 500 scientific publications and conference contributions mention the EnMAP-Box, which is used by researchers and in remote sensing education by different universities, by land managers, public authorities, and private companies. Following the release of the first operationally collected EnMAP data since End of 2022 and the accompanying need to use the data, demand for the EnMAP-Box significantly increased.

Outlook for the future (800 - 1000 characters incl. spaces)

For the next EnMAP-Box development phase (2024-2026) we will continuously adapt to changes in QGIS and the raster data delivered by EO data providers. Furthermore, it is planned to improve in several core capabilities: The use of EnMAP-Box processing algorithms in server / cloud processing environments will be made easier to facilitate the roll-out of workflows from Desktop to cloud environments. Using the CUDA framework, the EnMAP-Box will be enhanced with processing algorithms to perform semantic segmentation workflows (see Leon-Friedrich Thomas "Deep Learning based Semantic Segmentation Add-on for EnMAP-Box", this workshop). As the increasing availability of IS time series will allow more and more to analyse temporal aspects, the EnMAP-Box will be enhanced with capabilities for time series analysis. Also, the data visualization capabilities of the EnMAP-Box will be complemented by 3D capabilities to better explore the spectral-temporal feature space provided by field spectrometry and operational IS missions.

Figure 1 EnMAP-Box GUI with (a) data sources and different (b) data views like GIS maps (c + d) and spectral libraries (e), and the (f) raster layer styling panel for a quick selection of band combinations based on wavelength properties.

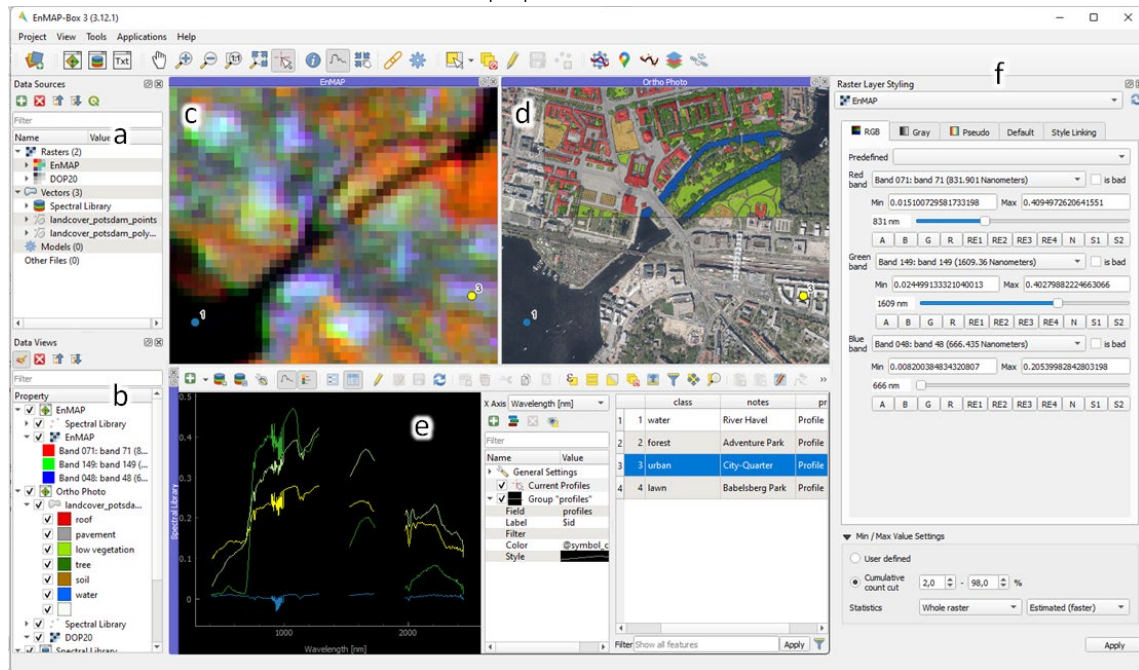
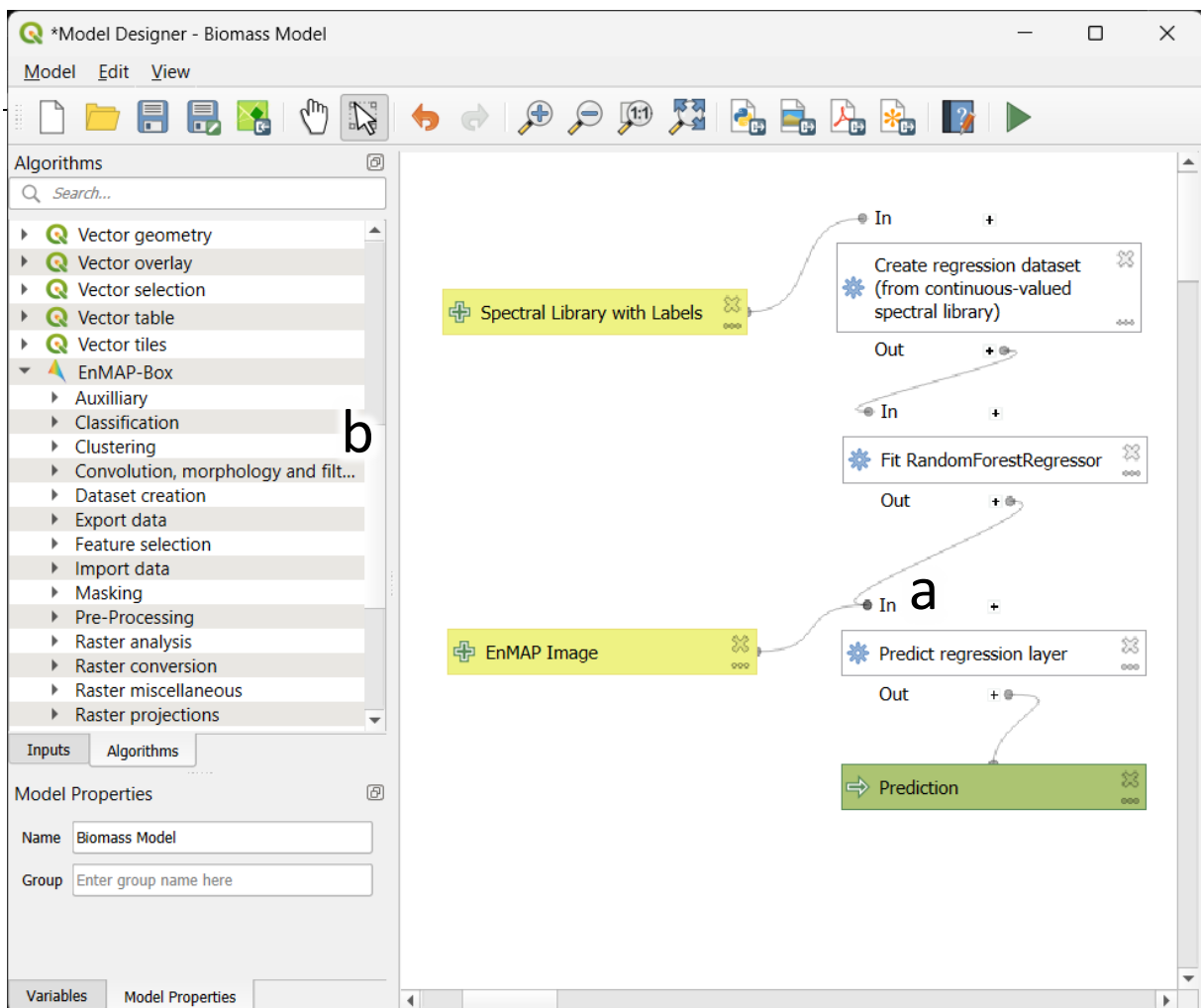


Figure 2 The QGIS Model Builder allows to create workflows (a) that built on the processing algorithms provided by (b) QGIS, EnMAP-Box and other QGIS plugins.



Poster Day 2: Poster session

PRISMA-Learn Project - Advanced Machine Learning Techniques for Data Fusion and Analysis of Images from the PRISMA Mission

EARSeL Valencia 2024

Abstract

Corresponding Author:

ignacio.gaston.masari@edu.unige.it

Luca Bergamasco⁴, Francesca Bovolo⁴, Lorenzo Bruzzone², Jia Chen³, Fabio Dell'Acqua³, Paolo Gamba³, [Ignacio Masari](#)¹, Gabriele Moser¹, Martina Pastorino¹, Sebastiano B. Serpico¹, Abhishek Singh², Giulio Weikmann²

¹ University of Genoa, Italy

² University of Trento, Italy

³ University of Pavia, Italy

⁴ Bruno Kessler Foundation, Italy

Keywords (5): Deep Learning, Change Detection, Land Cover Classification, Spectral Unmixing, Multiresolution Fusion.

Challenge

PRISMA-Learn is a project funded by ASI (ASI-UNIGE 2022-12-U.0 Contract) whose goal is to develop advanced machine learning techniques capitalizing on PRISMA's spectral and multi-resolution data and integration with other missions. The project consists in several activities that use innovative methodologies rooted in machine learning, pattern recognition, probabilistic graphical models and recent advances in deep learning, focusing on urban and agricultural applications. This project is divided into five different technical work-packages (WP). WP2101 deals with supervised classification by fusion of hyperspectral and panchromatic channels. WP2102 addresses the problem of heterogeneous Change Detection (CD) with domains of very different dimensionalities. WP3101 faces the challenge of unmixing in urban areas with coarse resolution hyperspectral images. WP5101 conducts CD with the aim to distinguish different kinds of change at ground. WP7101 addresses crop type classification leveraging on the detailed profile of the spectral signature of different crops.

Methodology

WP2101: The proposed technique is based on deep learning, with CNN-type architectures, and probabilistic graphical models, through the definition of a CRF model approximating the behaviour of the ideal fully connected CRF in a computationally tractable manner.

WP2102: The proposed unsupervised method integrates deep image-to-image translation with spectral clustering concepts to apply the heterogeneous CD method. A technique from the manifold learning field is used in pre-processing to reduce the dimensionality of one of the images to approximately match the other domain.

WP3101: Two deep learning nonlinear unmixing techniques: the Multitasks Autoencoder Hyperspectral Unmixing Model – MAHUM (Chen et al., 2023, IEEE TGRS, vol. 61) and a framework to use urban auxiliary data to enhance the information of hyperspectral images (Chen et al., 2023, WHISPERS).

WP5101: a Sparse Convolutional Autoencoder (CAE) learns the endmembers using an l_{21} regularization, non-negative weights, and sum-to-one constraints. The CAE operates on the difference image obtained from bi-temporal hyperspectral images to extract the abundance maps. A State-of-the-Art CD approach is applied to the difference image to obtain a binary change map. The abundance maps are used to separate changed pixels into different kinds of change classes.

WP7101: a 3D Contractive-Expansive-Contractive deep convolutional network (3D-CEC) is proposed to dynamically adjust the importance of different features at different scales.

Expected results

WP2101: The proposed supervised method generates a classification map at the spatial resolution of the panchromatic channel, while exploiting the richness of the spectral information provided by the hyperspectral channels. Experimental results related to a urban area will be presented at the workshop.

WP2102: the proposed method was tested on a real-world scenario with a couple of images from the recent PRISMA and COSMO-SkyMed missions of the Italian Space Agency.

WP3101: After different autoencoder unmixing methods are selected based on superpixel segmentation results, graph networks are used to retrieve similar blocks in the image and explore additional information in the images. Results on a PRISMA dataset about the city of Pavia, Italy, will be shown.

WP5101: the proposed method was tested using a couple of multitemporal PRISMA images acquired in Austria to detect various agricultural changes.

WP7101: the proposed architecture showed promising results on crops of 14 different cultivation types in the Austrian territory, using data from a single PRISMA hyperspectral acquisition. In particular, a stratified approach aimed to separate training and testing samples to obtain a dataset with greater spatial uncorrelation has been adopted.

Outlook for the future

The methods described above will be further optimized during the last months of the PRISMA-Learn project which is expected to end in June 2024. This final period will be also important for a more accurate validation of the results and performances



Figure 1 Qualitative comparison of the classification retrieved by the architecture presented in WP7101 on a stratified random sampling approach: (a) reference dataset; (b) classification map.

Integrating spaceborne hyperspectral data interpretation into mineral mapping workflows

Alice Burrell¹, Olivia Rhind¹, Alfred Baines¹, Richard Chiles¹, Mark Broadley¹

¹ CGG U.K. Services Ltd., CGG Crompton Way, Crawley, Surrey, United Kingdom RH10 9QN

Keywords (5): Mineral Mapping, Hyperspectral, Spectral Analysis, PRISMA, EnMAP

Abstract: The utilization of hyperspectral data in geological contexts, particularly for mineral exploration, has been a longstanding practice. This technique has found extensive application in the exploration workflows owing to its capacity for efficient and effective identification of key minerals. Minerals exhibit diagnostic absorption and reflection patterns at varying wavelengths, creating distinct spectral signatures. This emphasizes the indispensable role of hyperspectral data analysis in the realm of mineral exploration. The progression of hyperspectral remote sensing technologies has played a pivotal role in the proliferation of spaceborne hyperspectral sensors. This has expanded the accessibility of remote and previously hard-to-reach terrains, therefore improving hyperspectral-focused commercial applications. With expert analysis and geological contextualization, integrating spaceborne hyperspectral data could revolutionize mineral exploration.

CGG Satellite Mapping has carried out remote sensing studies over multiple mining districts to identify potential targets for further exploration. A multi-sensor, multi-scale methodology enables the analysis of spaceborne hyperspectral data in conjunction with existing mineral interpretation results. This led to additional insights into specific areas and demonstrated how hyperspectral data can add value to existing interpretations. Throughout projects, hyperspectral sensors PRISMA, EnMAP, and EMIT were integrated with Sentinel-2 and ASTER alongside commercial datasets including hyperspectral ZY1-02D and SWIR data from WorldView-3 multispectral satellite. Various Digital Elevation Models (DEMs) of increasing spatial resolution are also used to aid interpretation. Geological interpretation of project areas was based on true colour composites and false colour RGB composites developed from the multispectral layers alongside interpretation of DEM derivative layers. Hyperspectral data was processed to enhance the outputs from interpretation of these layers.

Following extensive pre-processing, the hyperspectral datasets were further processed to generate enhanced classifications and abundance maps over features of interest identified during previous interpretation steps. An assessment into the depth of a feature through spectral feature fitting and multispectral feature fitting was carried out. To further improve this, CGG have incorporated an additional examination of spectral absorption characteristics associated to specific mineral groups within their mineral mapping process, with pixel-wise automation of the process. Attention was given to analysing the position of absorption minima and the asymmetry in relation to the composition of minerals within individual pixels. The outputs of these processes are then utilized by spectral geologists alongside geological interpretation derived from multispectral and DEM derivatives.

Spectral geologists develop detailed mineral maps incorporating hyperspectral data outputs to understand more about each project AOI. The incorporation of hyperspectral data for mineral mapping on projects has allowed our spectral geologist to understand more about features such as families of intrusive dikes with distinct alteration haloes. Spectral analysis of specific endmembers of interest identified in these regions during the processing and analysis stage allowed differentiation between alteration mineral components. The integration of hyperspectral outputs into the specialist mapping and structural reinterpretation workflow improved the interpretation process and ensured identification of high-priority targets for further study.

Above and Beyond: UAV-borne hyperspectral mapping approaches at a legacy mine and tailings site within the M4Mining project

Friederike M. Koerting¹, Justus Constantin Hildebrand¹, Ekaterina Savinova², Steven Micklethwaite², Peter D. Erskine², David Lindblom³, Matthew Greenwood⁴, Dominic Brown⁴

¹ *NORSK ELEKTRO OPTIKK AS, HYSPEX, NORWAY*

² *THE UNIVERSITY OF QUEENSLAND, SUSTAINABLE MINERALS INSTITUTE, AUSTRALIA*

³ *PREDIKTERA AB, SWEDEN*

⁴ *GEOLOGICAL SURVEY QUEENSLAND, AUSTRALIA*

Keywords (5): hyperspectral, mine waste, UAV, critical minerals, mining

Challenge

The availability of diverse raw materials, including Al, Au, Co, REE, and Co, is critical for key economic sectors, paving the way for sustainable energy transition and technological advancement. Although recycling and alternative technologies are expected to reduce the reliance on primary raw materials, immediate access to essential metals and minerals still relies on mining fresh resources. The growing demand for these resources comes with inevitable consequences for mining, mineral processing, and environmental impact. Failing to address these raw material demands and mining ramifications could slow down global progress toward a cleaner energy future. Moreover, concerns regarding mine waste highlight the necessity for implementing sustainable solutions. The M4Mining project aims to champion sustainable mining practices through integrated remote sensing data to aid in the monitoring of these masses. Its overarching mission is to develop comprehensive remote sensing solutions for mining and tailings sites. The project development includes real-time mapping, a multi-sensor hyperspectral UAV-borne infrastructure, establishing best practices, resolving resolution gaps between satellite and UAV-based data and mine-scale to deposit-scale, real-time mapping approaches and effective data analytical techniques and user-friendly interfaces to present results to operators.

Methodology

To achieve this objective, several case study sites were chosen for field testing in Europe and Australia. The M4Mining partners completed their first field survey in North-Western Queensland at the Mary Kathleen legacy mine site in September 2023. The former Uranium (U) open pit mine was active until 1982 and rehabilitated in 1985. The area was monitored via UAV-borne hyperspectral (HySpex, Figure 1) and satellite-borne hyperspectral (EnMap) instruments to assess the site's rehabilitation. The Sustainable Minerals Institute (as part of the University of Queensland), the Geological Survey of Queensland and HySpex visited the open pit, adjacent tailings site and evaporation pond in September 2023 to collect hyperspectral drone imagery of the area, including a sampling campaign for future validation and to aid interpretation of the integrated drone and satellite data. Sampling spots were marked using chalk spray for efficient discrimination in the hyperspectral UAV data (Figure 3). The sampling spot locations were measured using a Leica Zeno GG04 plus smart antenna to obtain high-accuracy positions. In addition, we used a handheld field spectrometer, collecting data in the wavelength range of 500-2500nm, to characterise the spectral characteristics of the sample sites, taking 3-10 spectra across the highly heterogeneous areas. The surface of the sample area (uppermost 1-3cm) was split for analyses in the laboratory by geochemical and hyperspectral means. As a result, a unique spectral library will be

created of the collected samples to account for spectral endmembers for endmember-based analysis using mineral matching methods.

Results

Over the course of a 5-day survey, key locations of the covered Tailings Storage Facility (TSF) and evaporation pond were scanned with the hyperspectral drone, as well as the Southern half of the open pit (Figure 3). These data underwent preliminary analysis using various standard hyperspectral classification approaches (e.g., feature modelling, data-driven means, and indices) and the results are being evaluated based on accuracy, scalability, real-time availability, processing power, and value to mining industry professionals. The final resulting insights will be evaluated with a user perspective in mind, making the readability of the data products a key factor in determining the usefulness of a classification approach for onsite geologists and decision-makers.

Outlook for the future

This drone-based survey, the sampling campaign and the resulting mapping product comparison will lead the M4Mining project one step closer to advancing sustainable mining practices via the use of integrated remote sensing data, closing resolution gaps, and empowering decision-makers. The project's aspirations directly align with the EU's raw material security and environmental sustainability objectives. Leveraging advanced remote sensing, the project aims to contribute towards more sustainable monitoring approaches in areas of active and legacy mining.



Figure 1 HySpex hyperspectral imager mounted on a drone platform.

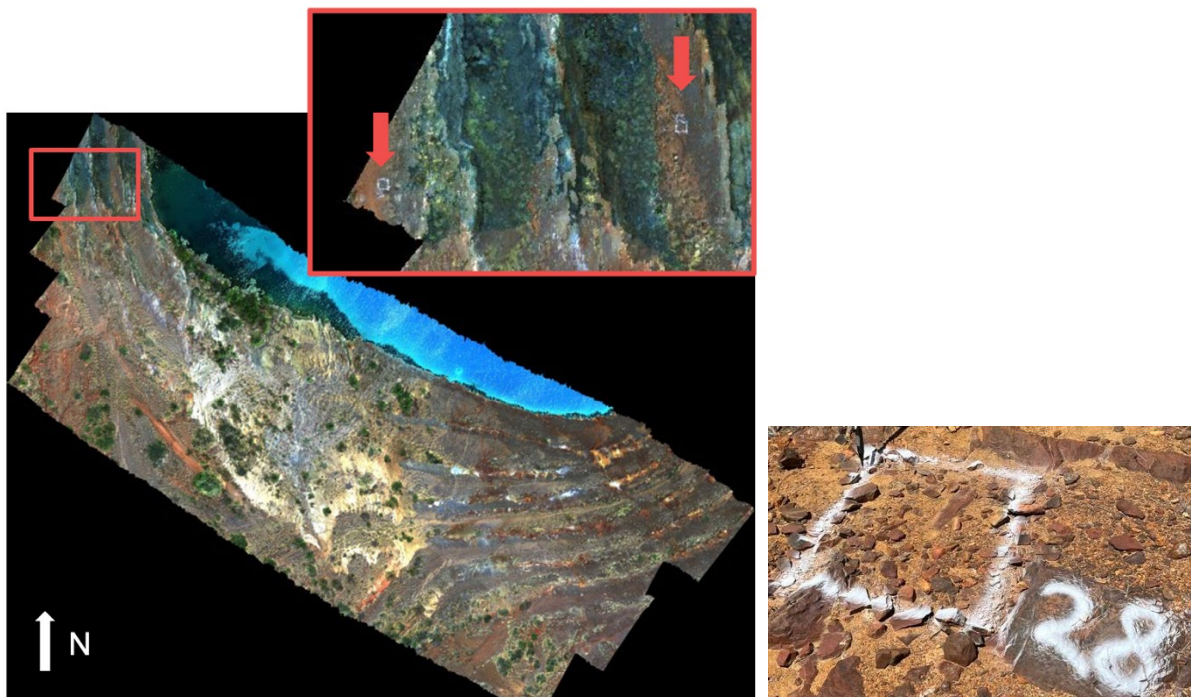


Figure 2 Left: UAV-based hyperspectral mosaic, showing the location of sampling points. Right: Sampling point 28, outlined square of ca. 50x50cm, marked with white chalk spray.

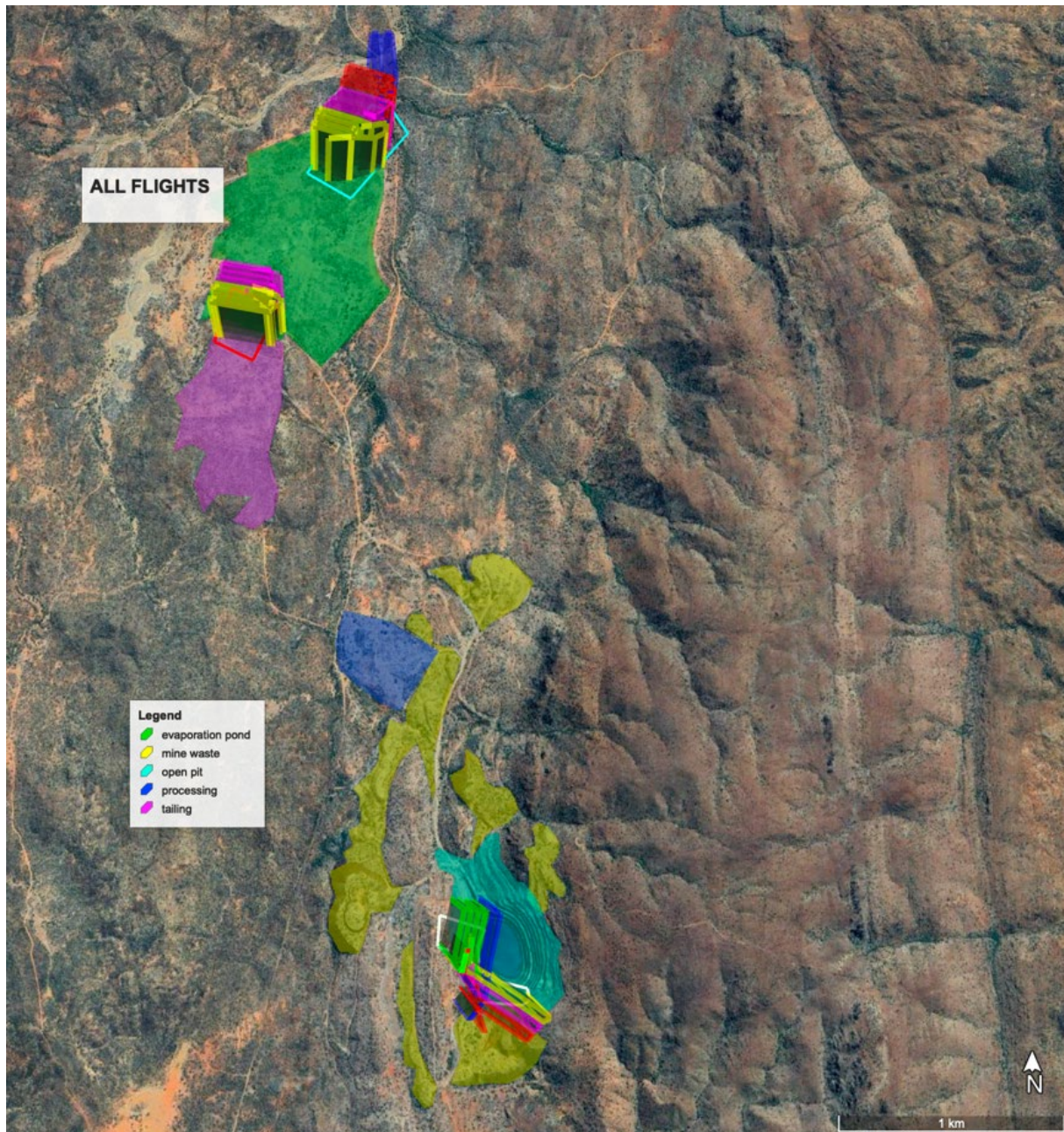


Figure 3 Overview of the Mary Kathleen mine. The map shows different facilities of the legacy mine site, as well as the UAV- flights covering subsets of those sites. Included are UAV flights from September 2023, covering parts of the TSFy (red polygon), evaporation pond (turquoise polygon) and open pit site (white polygons). Source: Google Earth, "Mary Kathleen", 20°43'53.61"S, 140° 0'23.79"E, date: 9/20/2022, accessed 9/16/2023

Impact of Surface Humidity on the Spectral Signature of Industrial and Mining Minerals – Implications for their Detection by Hyperspectral Imaging

EARSel Valencia 2024

Abstract

Corresponding Author: rodolphe.marion@cea.frErica Uccellatori^{1,2}, Stéphane Jacquemoud¹, [Rodolphe Marion](mailto:rodolphe.marion@cea.fr)²¹ Université Paris Cité, Institut de physique du globe de Paris, CNRS, 75005 Paris, France² CEA/DAM/DIF, F-91297 Arpajon, France**Keywords (5):** Mineral Detection, Soil Moisture Content, MARMIT Model, Airborne Hyperspectral Images

Challenge (800 - 1000 characters incl. spaces) 913

Airborne and spaceborne imaging spectroscopy has long been exploited to monitor land surfaces and provide information on their physical and chemical properties. Applications include monitoring vegetation, water, geology and soils. The reflectance of dry soils is a mixture of the spectral signature of their constituent elements. As the soil becomes wet, the reflectance decreases over all the solar spectrum, additional water absorption bands appear in the near infrared (NIR, 750-1300 nm) and shortwave infrared (SWIR, 1300-2500 nm), and the diagnostic absorption features of the minerals of interest tends to disappear. We then need to define adapted criteria to detect these minerals. The aim of this study is to examine the impact of soil moisture on the spectral signature of minerals related to industrial and mining activities, and to analyse the implications for their detection by hyperspectral imagery.

Methodology (1200 – 1500 characters incl. spaces) 1298

A laboratory experiment was set up to measure the reflectance spectra of 16 soil samples taken from industrial sites (bauxite, alumina, bauxaline, gypsum, calcite, etc.) at different moisture levels (Figure 1). The soils were fully saturated, then gradually dried. At each moisture level, we simultaneously measured their water content (by weighing) and acquired their reflectance spectra in the solar domain (using an ASD FieldSpec 3 Hi-Res spectroradiometer). These measurements were used to better understand the impact of water on soil spectral signatures. Firstly, the MARMIT model, which simulates soil reflectance spectra at different surface moisture levels, was calibrated on these data. The model has three input parameters (water layer thickness L , wet soil fraction ϵ , and particle volume fraction δ), and a calibration relation must be established for each soil. Secondly, criteria related to the shape of the absorption bands (position, amplitude, area) of minerals of interest were defined in order to study qualitatively and quantitatively the effect of moisture on absorption bands and their detectability. Finally, two hyperspectral images acquired on industrial sites (HySpex image on Gardanne and APEX image on Thann) were used to validate the approach on operational use cases.

Results (1200 – 1500 characters incl. spaces) 1278

Three criteria classically used to detect minerals were tested, both on laboratory measurements and on reflectance spectra simulated with the MARMIT model. 1) The wavelength position of the main mineral absorption bands (895 nm for bauxite and bauxaline, 1524 nm, 1551 nm, and 2270 nm for bauxite and alumina, 980 nm for red gypsum, 1750 nm, 2178 nm, and 2217 nm for white and red gypsum, 2340 nm for calcite). 2) A spectral index called the CIBR (Continuum Interpolated Band Ratio), based on reflectance measured at three wavelengths. 3) The area bounded by the reflectance curve and the straight line connecting the two edges of the absorption band, calculated when determining the convex envelope. If we consider the Thann2 soil sample, we observe the following behaviour (Figure 2): as the amount of water in the sample increases, the wavelength position of the red gypsum absorption band shifts towards

longer wavelengths, the CIBR increases, and the area decreases. The results obtained on reflectance spectra simulated by the MARMIT model are less conclusive, due to the difficulty of using the model in direct mode. The airborne images clearly show the absorption bands of the minerals of interest for areas with different humidity levels. Their analysis is in progress.

Outlook for the future (800 - 1000 characters incl. spaces) 917

The aim of this work was to extract information on soil mineralogical composition independently of its water content. Indeed, the presence of water tends to mask the absorption bands of minerals. The spectral deformations generated by the addition of water affect reflectance at all wavelengths in the solar domain, inducing shifts, broadenings and sometimes disappearances of absorption bands, making this task particularly challenging. These effects can vary from one mineral to another, depending on whether the spectra are acquired in the laboratory or from an airborne or spaceborne platform. Unlike remote sensing of vegetation, radiative transfer models that simulate soil reflectance spectra as a function of soil composition are still at their infancy, due to the complexity of the phenomena involved. Both theoretical and experimental work is still needed to understand how light interacts with a bare soil.

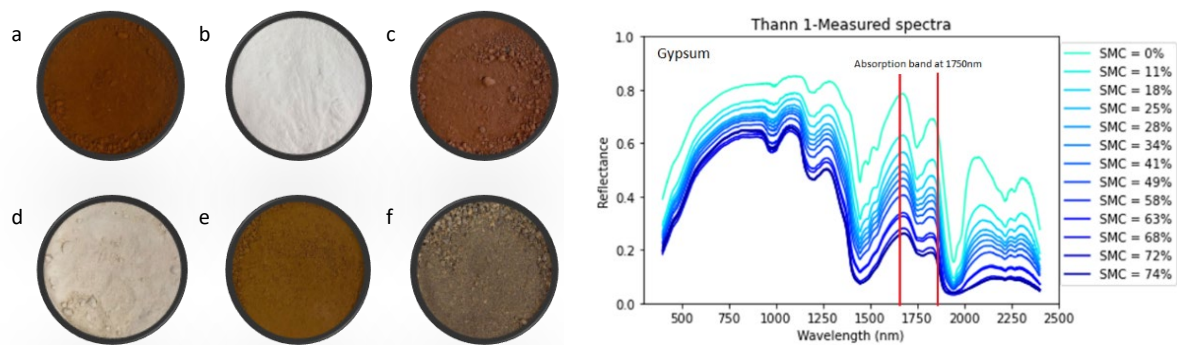


Figure 1. (Left) Soil samples collected in Gardanne (a-c) and Thann (d-f). (Right) Reflectance of the Thann-1 sample at different soil moisture contents (the absorption band at 1750 nm is typical of gypsum).

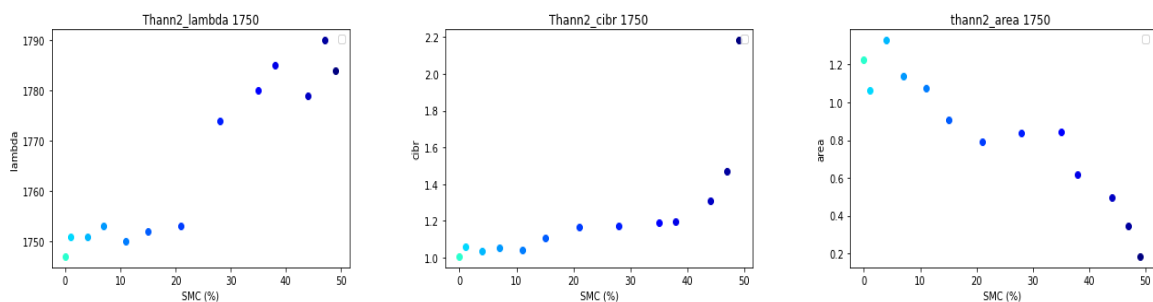


Figure 2. Variation of three factors calculated on the Thann-2 sample as a function of soil moisture content. (Left) Wavelength position of the red gypsum absorption band at 1750 nm. (Middle) Continuum Interpolated Band Ratio. (Right) Area bounded by the reflectance curve and the straight line connecting the two edges of the absorption band.

Spatial and spectral analysis of fairy circles in Namibia on landscape scale using satellite image processing and machine learning analysis

Klil Noy¹, Micha Silver¹, Ondrej Pesek^{1,2}, Hezi Yetzhak³, Eugene Morris⁴, Arnon Karnieli¹

¹ The Remote Sensing Laboratory, French Associates Institute for Agriculture and Biotechnology of Drylands, the Jacob Blaustein Institutes for Desert Research, Ben-Gurion University of the Negev, Sede Boker Campus, Israel.

² Department of Geomatics, Faculty of Civil Engineering, Czech Technical University in Prague, 166 29 Prague, Czech Republic

³ Department of Solar Energy and Environmental Physics, the Jacob Blaustein Institutes for Desert Research, Ben-Gurion University of the Negev, Sede Boker Campus, Israel

⁴ Gobabeb Namib Research institute, Walvis bay, Namibia

Keywords (5): Remote sensing, CNN model, spectral indices, texture variables, spatial autocorrelation

Challenge (800 - 1000 characters incl. spaces)

Fairy circles are a unique phenomenon in southwestern Africa and western Australia. These fairy circles are characterized by circular patches of bare soil or sand, 4–10 m in diameter, without trees, bushes, grasses, or even biocrusts that typically cover the area between the circles (matrix). The mysterious fairy circles have been studied for decades on a local scale in an attempt to explain their formation. However, the current project aimed at studying their spatial and spectral characteristics on a **landscape scale** in Namibia. The specific objectives of this research are (1) Processing satellite observations to explore the spatial and spectral distributions of the fairy circle phenomenon by applying statistical analysis and deep machine learning algorithms. (2) Analyzing the fairy circles geometric attributes to retrieve their spatial patterns regarding topographic features nearby.

Methodology (1200 – 1500 characters incl. spaces)

The research was conducted at the Giribes Plain, near the village of Sefontein, Namibia. Field and laboratory analyses were conducted and included grain size, mineralogical, and spectroscopic analyses. To fulfill the research goal, i.e., exploring the spatial distribution of the fairy circle phenomenon at a landscape scale using machine learning algorithms, the fairy circles were classified within 25 km² by processing 15 input layers through a convolutional neural network (CNN) model. The layers include four WorldView2 spectral bands (0.5m after pan sharpening), derived vegetation, biocrusts and mineral indices, and textural characteristics. 1600 fairy circles were manually labeled across the diverse transection in order to get the fully classified study area. The fairy circles geometry was extracted, and the spatial autocorrelation was performed using Getis ord G* Hot Spot and Local Indicators of Spatial Autocorrelation (LISA) of the Moran's I statistic. A Digital Surface Model (DSM) dataset at a 2.5-m resolution (315 km², including the entire valley and the surrounding mountain ridges) was used to extract the streams and watersheds and locate the study area's drainage points.

Expected results (1200 – 1500 characters incl. spaces)

By labeling 1600 fairy circles and using the CNN model, 14536 fairy circles were mapped with 0.97% accuracy and a binary cross-entropy loss function value of only 0.01. Field measurements and laboratory analysis justified the need to use the spectral indices for the model. Using the sphericity index over 14536 fairy circles, a Unique pattern of elongated fairy circles was found. The hotspot analysis, conducted over the sphericity index values, shows that most cold spots are located along the main

stream in the center of the valley, mainly on the eastern side of the stream. In contrast, the hotspots of the sphericity index are mainly located at the edges of the study area, next to the mountain ridges. Furthermore, a concentration of hotspot points is observed on the southwestern side of the study area. This result suggests that more fairy circles, in general, and more elongated fairy circles, in particular, are located in the southwest compared to the northern reach of the stream, as well as in the upstream areas of the alluvial fans. Seven watersheds that drain the periodic floodwater to the valley from the surrounding mountains were delineated by pinpointing seven drainage points in the study area. The largest (51 km²) is located on the western side, notably larger than all others (about 1 to 8 km²). Based on the DSM data, the longest axis of each fairy circle was detected and overlaid on the topographic map, showing the connectivity patterns of the elongated FCs.

Outlook for the future (800 - 1000 characters incl. spaces)

On a landscape scale, spatial and spectral analyses became possible only with valuable remote sensing retrievals, as well as with the application of deep statistical analysis and the use of machine learning algorithms. Using earth observation, an overview of fairy circles or other geometric features can be detected and analyzed on a landscape scale over different locations worldwide. The topographic impact may also give a comprehensive view of the phenomenon when observed on a landscape scale.

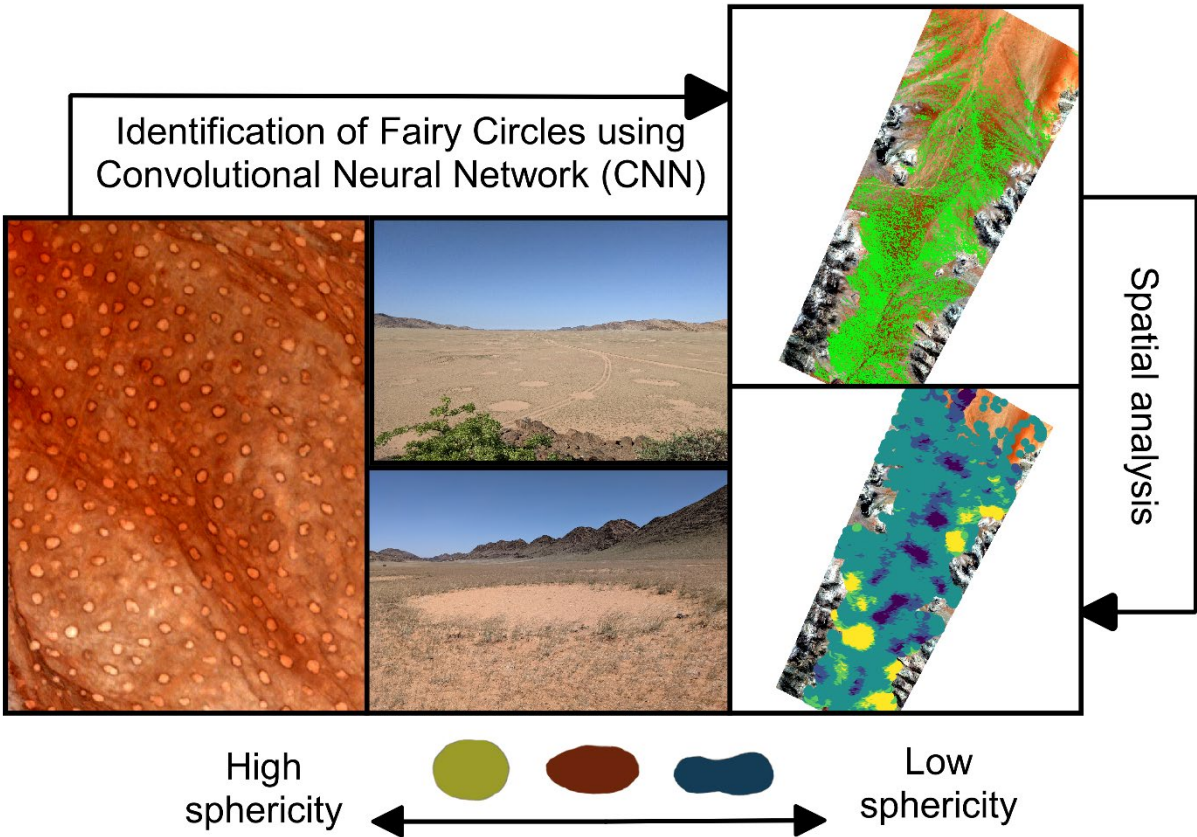


Figure1: (a) A section of a WorldView2 image showing the fairy circles (FC) in part of the Giribes Plain. (b) Ground-level photo of several FCs within a matrix. (c) Ground-level photo of a single FC. (d) Location of the 14536 FCs in the entire area resulting from the CNN model. (e) Hotspot analysis of the sphericity index.

Advancements in NIR Reflectance measurements of small leaves and pine needles

Nicolas Venjean¹

¹ Spectral Evolution Inc., USA

KEYWORDS (5): NIR, VEGETATION, HYPERSPECTRAL, SPECTROMETER, REFLECTANCE

Challenge

Capturing reflectance data of small vegetation samples such as pine needles, blades of grass, and tiny leaves can be challenging. The very small field of view needed for the measurement, as well as the required high sensitivity of the spectrometer can be obstacles to obtaining quality data.

As a trade-off, researchers have taken the habit of measuring the combined spectrum of many small samples bunched together. However, the resulting spectrum represents an average of the spectral features of all samples, not necessarily the individual trait of each sample.

This study presents a novel approach in capturing the individual spectrum of a single small sample. This study analyses the results obtained with an innovative small-leaf adapter coupled with a UV-Vis-NIR spectrometer with high sensitivity and high spectral evolution. The data was measured over the spectral range of 350 to 2500nm.

Methodology

A small-leaf holder was developed for compatibility with Spectral Evolution's leaf-clip reflectance probe. The holder sits in the field of view of the fiber optic cable connecting the leaf-clip to the spectroradiometer. The holder was 3D printed out of low-reflectance plastic, and a v-shape groove was implemented to minimize specular reflection. The NaturaSpec UV-Vis-NIR spectroradiometer from Spectral Evolution was chosen for measurements over the spectral range of 350 to 2500 nm. The detectors of the NaturaSpec have twice the amounts of sampling channels than other spectroradiometers available on the market. This results in an improvement of sensitivity and signal-to-noise by a factor of up to 40 in the NIR range.

3 types of small vegetation samples were measured with this method: individual blades of grass, small leaves and individual pine needles. 5 measurements were taken for each sample with the NaturaSpec spectroradiometer and small sample holder. Each measurement was the result of the average of 60 successive measurements of the same sample.

The DARWin spectral data acquisition and visualization software (Spectral Evolution) was used to control the instruments, visualize, and export the spectral data.

Results

Since the vegetation samples that are considered for the study are very small, (Fig 1) they do not completely fill the field of view of the fiber optic. Therefore, the spectral data captured with the leaf-clip reflectance probe and holder is an average of the spectral signature of the small vegetation sample and the plastic of the holder. The reflectance levels of the samples were low and sometimes hard to distinguish from the spectrum of the plastic of the holder. To extract the spectral signature of the vegetation only, the measurements were first done without a sample in the holder. The corresponding spectral signature of the plastic was then used as calibration for subsequent measurements.

The reflectance data of small samples measured with this new technique present a more precise curve (less noise) (fig 2. Reflectance of small leaf with new method) than the data gathered with the traditional method of bunching samples together. The signal-to-noise ratio especially in the UV-Vis range and upper NIR range is especially improved over measurements with lower resolution spectroradiometers.

All small samples analysed with this new method showed great improvement in the quality of the spectral data over the traditional method. Measurements also showed a good level of repeatability, as long as the vegetation sample was well centered in the field of view of the fiber optic.

Outlook for the future

The small-sample holder used in conjunction with a high-sensitivity spectrometer is a promising method to capture the spectral data of individual small samples of vegetation. Even though the samples do not fill the field of view of the fiber optic completely, the subtraction of the spectrum of the background can be obtained by using a low reflectance material for the sample holder.

The data acquire with this new method shows much improvement of the quality of the spectral data over traditional methods. The design of adapter could be easily modified to fit specific sample shapes or sizes.

Further studies will focus on how to minimize the effects of stray light and specular reflection. Markings on the adapter will be implemented to aid in centering the small samples in the field of view of the fiber optic.



Figure 1 example of small leaf sample

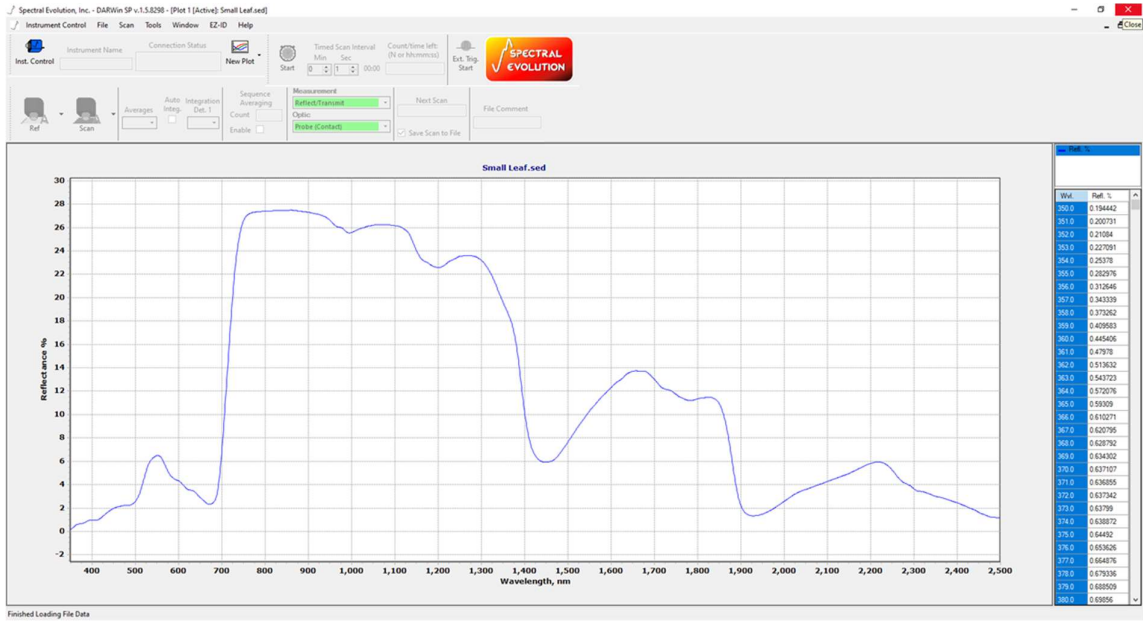


Figure 2 example of spectral data of small leaf captured with new method

Characterization of multi-angular response of vegetated surfaces in the optical domain and use of BRDF models

EARSel Valencia 2024
Abstract
Corresponding Author:
pietro.chierichetti@unimib.it

Pietro Chierichetti¹, Sergio Cogliati¹, Dirk Schuettemeyer², Jan Hanuš³, Marco Celesti⁴, Cinzia Panigada¹, Micol Rossini¹, Giulia Tagliabue¹, Luigi Vignali¹, Roberto Colombo¹

¹ UNIVERSITY OF MILANO-BICOCCA, MILAN, ITALY;

² EUROPEAN SPACE AGENCY, EUROPEAN SPACE RESEARCH AND TECHNOLOGY CENTRE, KEPLERLAAN 1, 2201 NORDWIJK, THE NETHERLANDS;

³ GLOBAL CHANGE RESEARCH INSTITUTE – CZECHGLOBE, CZECH ACADEMY OF SCIENCES, BĚLIDLA 986/4A, 60300 BRNO, CZECH REPUBLIC;

⁴ THE SPACE FOR ESA-EUROPEAN SPACE AGENCY, EUROPEAN SPACE RESEARCH AND TECHNOLOGY CENTRE (ESA-ESTEC), KEPLERLAAN 1, 2201 AZ NOORDWIJK, THE NETHERLAND

Keywords (5): Earth Observation, Hyperspectral, Copernicus, BRDF, Anisotropy

Challenge

The new generation of earth observation satellite missions (i.e., *Sentinel-2 Next Generation, Land Surface Thermal Mission*) will provide observations with a higher temporal resolution. To achieve this goal, they will need to increase also the field of view of the instruments aboard the satellite thus obtaining a larger swath on the ground. For this reason, it is important to understand how the canopy anisotropic effects may influence the observations, especially for off-nadir acquisitions. The activity was funded as part of the ESA SwathSense project, aimed at collecting multi-angle observations in the optical (VNIR) domains to measure the anisotropic behaviour of agricultural crops vegetation in order to assess the impact in the context of future ESA/Copernicus Sentinel-2 Next-Generation (S2NG) missions. The main goals of this work are: i) characterization of anisotropy of the alfalfa canopy from field and airborne data; ii) modelling reflectance by means of Kernel Driven Models.

Methodology

The spectral measurements were carried out between July 17th and 29th, 2021, in an agricultural area near Lleida (Spain). Optical field data were acquired with the field spectrometer Spectral Evolution SR-3500 along four different azimuthal planes: the solar principal plane (SPP), the plane perpendicular to the SPP, the plane that overlap the orbits (12° North) planned for the S2NG satellites, and the plane perpendicular to the latter (perpendicular S2), between [0° - ±45°] zenith angles. Airborne data were acquired with the VNIR Sensor CASI-1500, mounted on the FLIS (CheczGlobe), along the same azimuthal plane of the ground acquisitions. For each set of measurements, which correspond to the S2 configuration, seven images were acquired, one for each flight line, in each azimuth, thus resulting in a set of 21 remote sensing images that capture the scene with different viewing geometries. The field and airborne data were collected at solar noon and during the afternoon, to observe how the canopy anisotropy changes in relation to the different solar azimuth and zenith angles. The data collected during the campaign allowed the characterization of the anisotropy of natural surfaces. The analyses were carried out on both field data and airborne data in two spectral bands: RED (681 nm) and NIR (852 nm). The analysis of the BRDF was further extended by fitting the field data from 19/07 with a Kernel-driven semi-empirical model.

Results

The comparison between the field and airborne data shows that, in general, the latter have slightly lower values for the red wavelengths. Conversely, the behaviour is reversed in the NIR, and the airborne data show overestimated values compared to the field data. Overall, the relationship between the two sets of data is excellent (R^2 ranging from 0.90-0.98) considering the perpendicular S2 orbit azimuthal plane and the SPP plane (in both configurations), both in the red and near-infrared. The relationship between the data becomes more critical in the perpendicular SPP azimuthal plane. This is likely due to the lower variability of reflectance values, which results in a greater impact of instrumental noise in the experimental data or any outliers. In general, the differences observed between field and airborne data are mainly attributed to errors in the atmospheric correction.

Multi-angular reflectance was modelled with kernel-driven approach, the results show that the model provide the better performances. Especially, the best results (best fit) are obtained when the hot spot in the SPP is considered. In this case, the parameters estimated from the fit can be used to estimate the reflectance trend (multi-angle) of other azimuthal planes, even for those planes where the hotspot is not present. This result suggests the need to estimate the weight coefficients on reflectance trends in the azimuthal plane characterized by greater variability, that is, where the hotspot is present.

Outlook for the future

This work addressed challenges related to the measurement and analysis of vegetation anisotropy for optical remote sensing applications. The activity allowed to quantify the variation of reflectance at different wavelengths (in absolute terms and through the ANIF index) over the course of a day and for different days during the growth of agricultural crops. In the future we intend to further develop this work studying the multi-angular response over different canopies and also studying the anisotropic behaviour of Sun Induced Fluorescence (SIF) over agricultural crops. A field campaign has already been made in summer 2023, and few data have already been processed, but further analysis is planned in order to characterize the anisotropic response of SIF. Furthermore, we want to extend the study related to the characterisation of the anisotropy by means of the semi-empirical models both on reflectance and SIF.

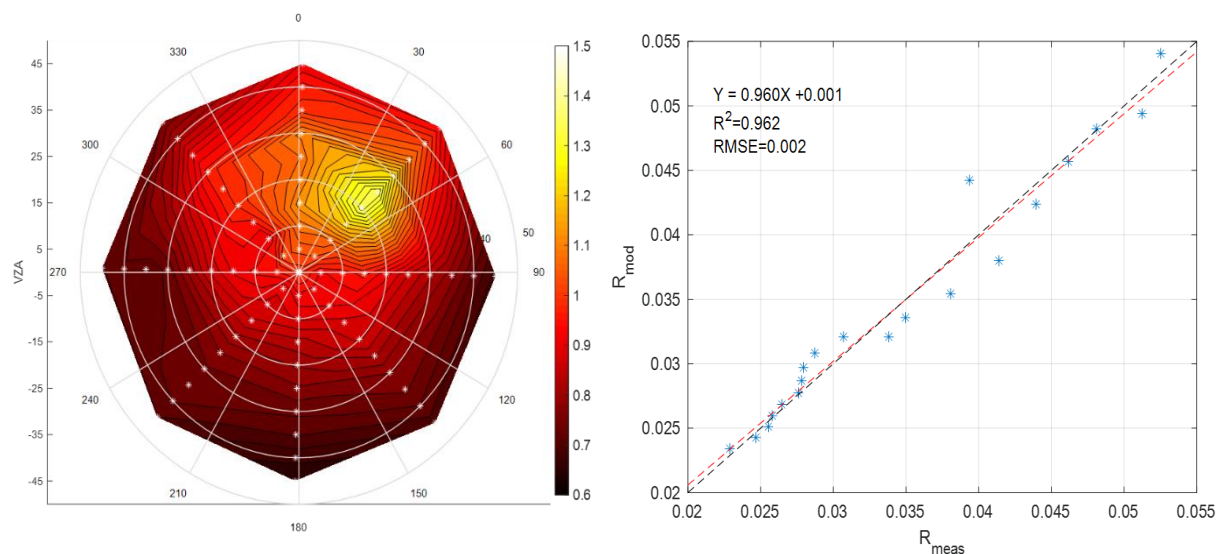


Figure (a) example of hemispherical reflectance of alfalfa (ANIF). The azimuthal angles are relative to sun position (sun position at 0°), white dots represent measurements at different angles; (b) example of the fit of field data with the Kernel-Driven model.

[Formatting guidelines for abstract submission]

EARSel Valencia 2024
Abstract
Corresponding Author:
[\[sofia.vanmoorsel@geo.uzh.ch\]](mailto:sofia.vanmoorsel@geo.uzh.ch)

Hyperspectral Leaf Spectroscopy Reveals the Response of Beech (*Fagus Sylvatica*) Seedlings from Across the Species' Range to Simulated Drought

Dave Kurath¹, Jolanda Klaver^{1,2}, Tis Voortman¹, Meredith C. Schuman^{1,3}, Sofia J. van Moorsel¹
(Style: Authors, presenting author underlined)

¹ University of Zurich, Department of Geography, Switzerland

² University of Zurich, Department of Evolutionary Biology and Environmental Studies, Switzerland

³ University of Zurich, Department of Chemistry, Switzerland

(Style: Affiliations;)

Keywords (5): Hyperspectral, *Fagus sylvatica*, Vegetation spectra, Radiative transfer model, Drought

Challenge (800 - 1000 characters incl. spaces)

Intraspecific diversity is the basis for adaptation to a changing climate, but how genotypic contributions and plasticity contribute to intraspecific trait diversity is still largely unknown. Beech (*Fagus sylvatica* L.) is common in Europe and ecologically, commercially, and culturally important. However, it is a drought-sensitive tree species and particularly vulnerable in the seedling and young growth phase. Climate change, including droughts and heatwaves, is likely to change the distribution of beech in Europe and lead to local population declines. Although there is significant research on beech drought responses, the use of spectroscopy to assess the physiological responses of beech seedlings is largely unexplored. We addressed this challenge using a common garden experiment. Specifically, we assessed the response of these seedlings to a simulated drought and furthermore asked whether and how beech tree seedlings can acclimate to drought via phenotypic plasticity within one season.

Methodology (1200 – 1500 characters incl. spaces)

To this aim, we conducted a common garden experiment with 184 2-year-old beech seedlings originating from 16 populations (provenances) across the species range in Europe with a focus on southern and eastern portions of the range (Fig. 1a), and with a known population genetic structure. We exposed half of the potted seedlings to two experimentally induced drought periods (i.e., rain-free days) in June and July 2023 (two weeks each). The two drought periods were intermitted by a recovery period. To exclude the rain, the pots were covered with pond film. The effect of the rain exclusion treatments was tracked using soil moisture sensors placed in a subset of the pots. To assess plant responses to drought, we measured seedling growth rates and leaf traits such as chlorophyll content and stomatal conductance. Using an ASD FieldSpec 4 spectrometer, we derived additional physiological, biochemical, and structural traits based on spectral indices. These include the Photochemical Reflection Index (PRI), which correlates with the efficiency of photosynthesis, the Normalized Difference Water Index (NDWI) and the Red-edge chlorophyll index (CIRE). Furthermore, we used an inversion of the validated PROSPECT-D radiative transfer model to derive plant parameters such as leaf pigmentation or leaf water content. This allowed us to capture a multitude of relevant physiological drought stress responses across beech tree genotypes.

Results (1200 – 1500 characters incl. spaces)

For both drought periods, the soil moisture sensors showed lower soil moisture for the drought treatment compared to the sensors placed in pots of the control group, indicating that rain exclusion had resulted in a strong drought effect. We could not detect differences in growth (length and stem diameter increments) between drought-treated and control seedlings, which may be an artefact of keeping these two-year-old seedlings in pots. However, the mean stomatal conductance in the drought treatment was significantly lower than in the control (235.3 mmol/m²s and 367.5 mmol/m²s, respectively, during the first drought).

Leaf spectroscopy proved to be a valuable tool in assessing the drought response of the studied seedlings with the spectra showing a clear signal of drought stress (Fig. 1b). The different provenances show a similar response to the induced drought treatment but that, depending on the leaf spectral index, genotype was also a significant determinant of drought stress (Fig. 1c). The constituents derived from the inverse PROSPECT-D model yielded detailed information on beech seedling physiology under drought stress (Fig. 2). Finally, we found that taller trees exhibited a stronger drought response. Taller trees faced more water scarcity because of their greater biomass. They had a greater demand for water and at the same time had less water available because their extensive root systems allowed less water storage in soil.

Outlook for the future (800 - 1000 characters incl. spaces)

Overall, our project contributes to understanding how intensified summer droughts influence plant physiological and morphological traits especially in *Fagus sylvatica*. Changes in frequency and intensity of summer droughts will be one of the fundamental determinants in future forestry and agriculture. Spectroscopy could provide a useful tool to efficiently map drought responses in beech populations. More research will be needed to close the gap between leaf level, canopy level and whole-ecosystem remote sensing methodologies. This will allow to upscale the methodology and assess drought responses over larger nurseries or mature forests. Knowledge about intraspecific diversity in the species' drought stress response will aid foresters in management and restoration approaches, and support efforts to help beech persist.

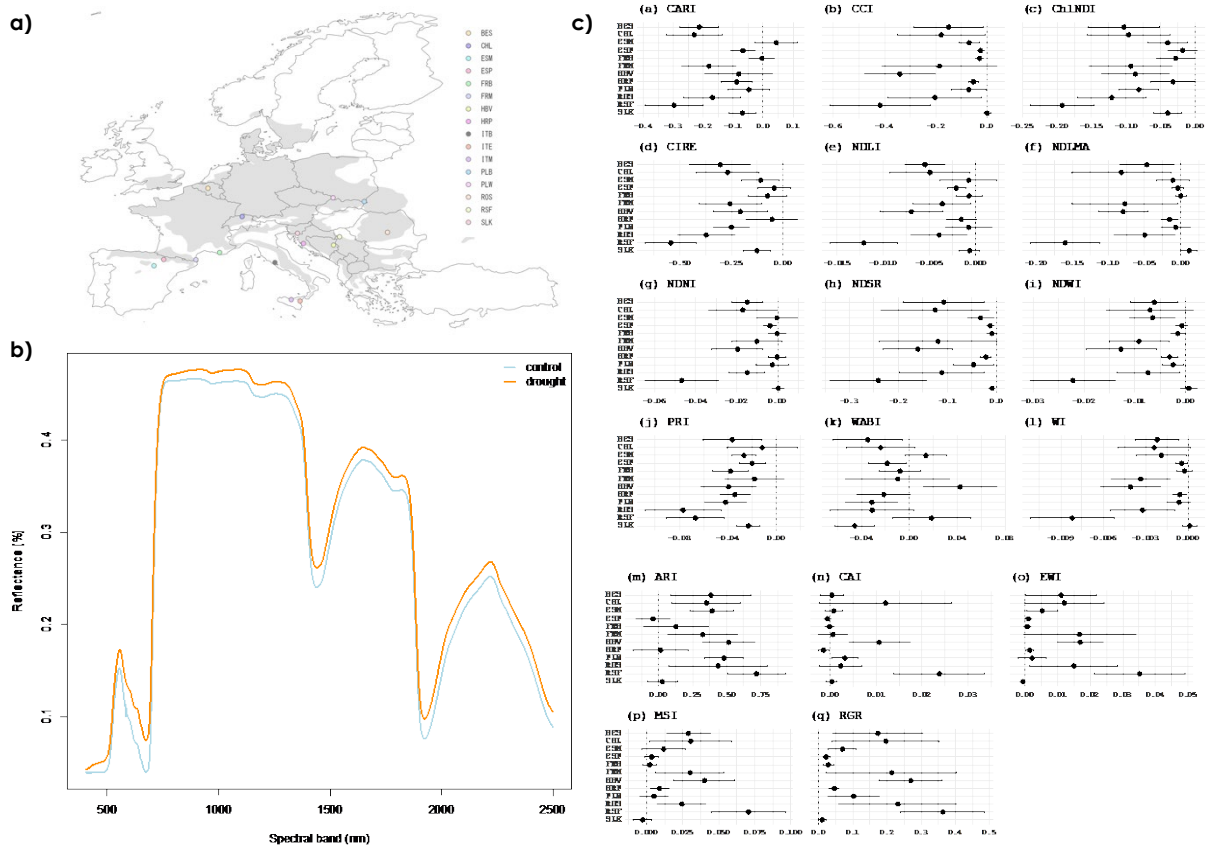


Figure 1. **a)** Overview of the provenances used in the experiment. The shaded area represents the species range of *F. sylvatica* across Europe. Provenances are named by the country code (e.g., BE corresponds to Belgium) and the first letter of the specific site. **b)** Mean spectra of beech seedlings in the control treatment (blue line) and drought treatment (orange line) during the June drought. **c)** Log response ratios (LRR) of 17 indices derived from spectral data from 12 provenances. If values are positive, this indicates that the drought treatment increased the value of a given index (panels m-q), if values are negative, the drought negatively impacted this index (panels a-l). Note that WABI (water balance index), had both significant positive and negative LRR (panel k).

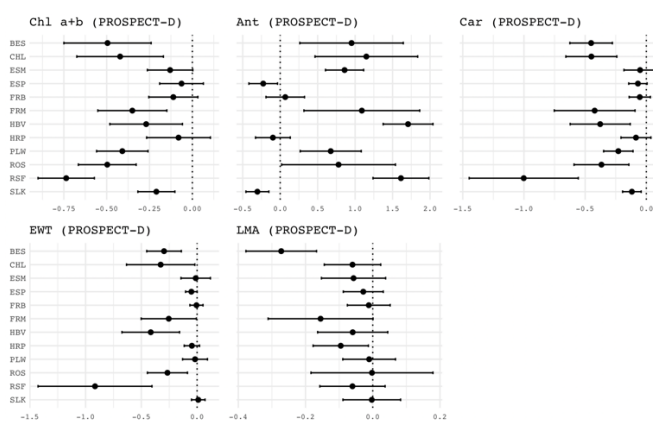


Figure 2. LRR based on the output of inverse PROSPECT-D modelling.

Linking Tower Remote Sensing with Ecosystem Fluxes - Opportunities, Challenges, and Recommendations for a Path Forward

Zoe Pierrat¹, Troy Magney², Loren Albert³, Xi Yang⁴, Anam Khan⁵, Benjamin Runkle⁶, Mallory Barnes⁷, Matt Dannenberg⁸, John Gamon⁹, Miriam Johnston⁸, Tommaso Julitta¹⁰, Charles Southwick³, Christopher Still³, William Woodgate¹¹,

¹ Jet Propulsion Laboratory, California Institute of Technology, USA

² University of California, Davis, USA

³ Oregon State University, USA

⁴ University of Virginia, USA

⁵ University of Wisconsin, USA

⁶ University of Arkansas, Fayetteville, USA

⁷ Indiana University, Bloomington, USA

⁸ University of Iowa, Iowa City, USA

⁹ University of Nebraska, Lincoln, USA

¹⁰ JB Hyperspectral Devices, Germany

¹¹ University of Queensland, Brisbane, Australia

Keywords (5): Tower based remote sensing, solar-induced fluorescence, hyperspectral, thermal, lidar

Challenge

Our ability to anticipate and plan for future changes to the climate system depends on a mechanistic understanding of water, energy, and carbon fluxes in terrestrial ecosystems. A global understanding of these fluxes is made possible by scaling up the insights gleaned from site-level research. However, tower flux measurements are limited in their spatial extent, provide area-averaged estimates across the tower footprint, and are subject to uncertainties associated with data processing. Remote sensing offers a means for upscaling eddy-covariance (EC) data and identifying biological processes that drive the observed fluxes. Unlike the EC flux community (FLUXNET, AmeriFlux), the diversity of sensor types, instrument designs, and scientific communities involved in proximal remote sensing presents standardization challenges and limits the ability to create an informatics framework that would allow a coherent data system ready for widespread use.

Methodology

Five different types of proximal remote sensing data are useful for addressing ecological questions when combined with flux data: light detection and ranging (LiDAR), spectral reflectance, solar-induced chlorophyll fluorescence (SIF), thermal radiance, and microwave backscatter (Figure 1). Our primary motivation is to describe the specific utility of these remote sensing types for advancing our understanding of flux data. We provide a technical overview of how tower-mounted remote sensing data can be used to advance flux science specifically within the flux tower footprint. In this overview, we highlight the questions that can be answered by combining different proximal remote sensing data types with flux data, outline where current co-located flux and remote sensing data exists, and provide practical recommendations for data collection. The recommendations provided in this synthesis came from community solicited comments and a workshop called 'Linking Optical and Energy Fluxes' hosted in July 2023 at the Mountain Research Station in Colorado. Over 40 attendees from around the world working on tower based remote sensing and fluxes set out to achieve 3 primary goals: 1) Build awareness of the existing synergies, challenges, and opportunities between remote sensing and flux science; 2) Foster new cross-disciplinary connections to identify and address knowledge gaps and uncertainties associated with

both flux and remote sensing data; and 3) Increase the accessibility, usability, and standardization of remote sensing data so that it can be used to inform flux data, following the FAIR principles.

Results

Lidar, thermal, spectral reflectance, SIF, and microwave data can provide unique and complimentary insights into ecosystem fluxes. For example, lidar can be combined with SIF and spectral reflectance data to infer canopy structural traits, plant stress detection, and carbon-use efficiency; SIF data can be used in tandem with spectral reflectance data for inferring light-use efficiency and thermal data to estimate water-use efficiency; and microwave backscatter data can be used with thermal data to approximate plant water use. Taken together, a synergy of these data with eddy covariance derived fluxes can help inform plant phenology, plant carbon uptake, carbon accumulation, evapotranspiration, and the temperature dependence of photosynthesis. To make these connections, however, specific attention needs to be paid to calibrations, data processing, spatial and temporal aggregation, and retrievals. Beyond this, choice of instrumentation and viewing geometry should be guided by the characteristics of the EC flux footprint at a given site. Although EC footprints are orders of magnitude larger than those of remote sensing observations, the optical footprint should be representative of the EC footprint depending on the heterogeneity of the site and other factors such as meteorological conditions. Users are faced with several choices in instrument configuration such as bi-hemispherical vs. hemispherical-conical, nadir vs. off-nadir, and stationary vs. scanning; while trade-offs are inevitable in these decisions, each can be leveraged to improve compatibility between optical and EC footprints. With these considerations, we can collectively build a robust, standardized data sharing protocol for tower-based remote sensing data.

Outlook for the future

Proximal remote sensing tools can help to quantify energy fluxes (carbon and water) and assess vegetation conditions at scales enabling mechanistic interpretation of acquired signal. The combination of these tools can help overcome some of the limitations and uncertainties of current carbon and water accounting methods. Embedding high spatial and temporal resolution proximal remote sensing systems into flux science will constrain uncertainties associated with spatially limited measurements, model development and evaluation, defining dynamic baselines for carbon projects, identifying spatially distinct landscape units, and maximizing the information content of current data networks. Development of robust, standardized proximal remote sensing system is needed, and transdisciplinary partnerships across remote sensing, ecosystem science and flux communities can help. Given the results and feedback from this workshop we are working towards a standardized database of tower-based remote sensing to enable validation and calibration of satellite data and terrestrial biosphere models.

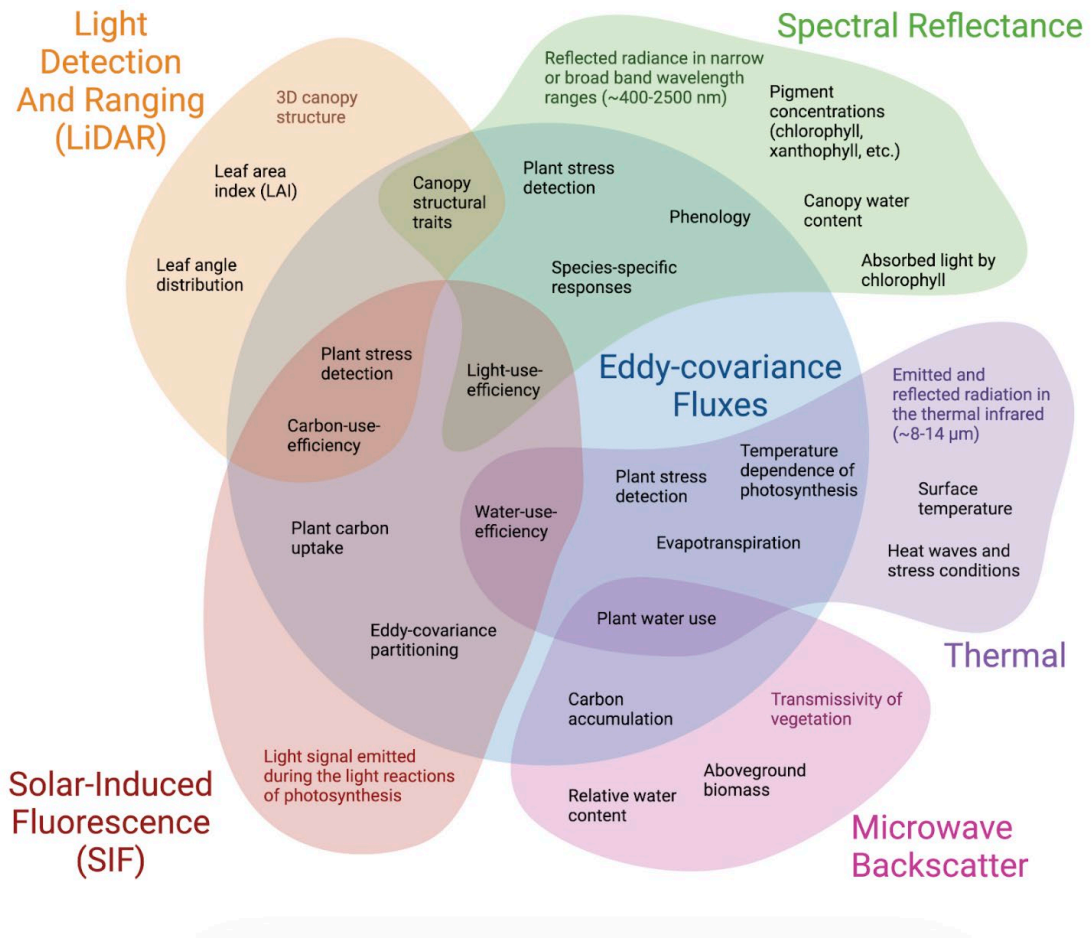


Figure 1. Synergies among different types of remote sensing measurements within the flux tower footprint.

Modeling forest canopy spectral transmittance using photon recollision probability

EARSeL Valencia 2024

Abstract

Corresponding Author: jaarne.hovi@aalto.fi

[Aarne Hovi](#)¹, [Růžena Janoutová](#)²

¹Aalto University, Finland

²Global Change Research Institute of the Czech Academy of Sciences

Keywords: in situ spectroscopy, forest, ecology, habitat, radiative transfer

Challenge

Understanding how forest canopies modulate the spectral properties of solar radiation, i.e., the spectral transmittance characteristics of forest canopies, is important both ecologically as well as for the interpretation of remote sensing data. Models of radiation transfer are a key tool in creating this understanding and developing physically based methods for interpreting hyperspectral remote sensing data. However, empirical evaluations of the models' performance in simulating forest canopy spectral transmittance have rarely been performed. This is partly because empirical measurements of canopy spectral transmittance are rare. Here we utilized a unique in situ data set to evaluate an approach for simulating forest canopy spectral transmittance based on photon recollision probability theory (p -theory).

Methodology

In situ measurements of forest canopy spectral transmittance were performed in clear-sky conditions in 21 study plots located in four study sites in Finland, Estonia, and in the Czech Republic. The sites were Hyytiälä (61°51'N, 24°18'E), Järvelja (58°17'N, 27°19'E), Bílý Kříž (49°30'E, 18°32'N), and Lanžhot (48°41'N, 16°57'E), representing boreal conifer-dominated, hemi-boreal mixed, temperate broadleaved, and temperate coniferous mountain forests, respectively. Canopy transmittance is defined here as the downward spectral irradiance below the canopy divided by that on top of the canopy, and it was measured using ASD FieldSpec3 and 4 spectrometers accompanied with cosine receptors. We employed a p -theory based model for simulating the canopy spectral transmittance. The model has spectral (spectra of forest floor, foliage, and woody elements) and spectrally invariant (canopy gap fractions, plant area index) parameters. We parameterized the model based on in situ hemispherical photographs giving canopy gap fraction and plant area index, and measurements of canopy element and forest floor spectral properties. We evaluated the performance of the model by comparing the simulated mean canopy spectral transmittance in each study plot against the in-situ measurements.

Results

Preliminary results of the experiment indicate qualitatively good performance of the p -theory in simulating the wavelength-dependence of canopy transmittance, i.e., the 'shape' of the canopy transmittance spectra: only slight overestimation of transmittance in the near- and shortwave-infrared region for broadleaved forests is observed. However, accurate parameterization of canopy gap fractions is important for correctly simulating the overall level of transmittance. Here we utilized hemispherical photographs and a binarization algorithm for deriving the canopy gap fractions. Sensitivity analyses performed with the model demonstrate the importance of woody elements and canopy clumping in affecting near-infrared scattering, and thus the observed canopy transmittance. Particularly the woody elements are important to include, in order to prevent significant overestimation of canopy scattering.

On the other hand, assuming direct solar radiation only, i.e., ignoring the diffuse component of the incoming irradiance had only minor effect on the simulated canopy transmittance in clear-sky conditions. Work on providing quantitative evaluation metrics (RMSE, bias) and assessing the model in simulating small-scale spatial variability is ongoing. We also plan to compare the results against a 3D radiative transfer model.

Outlook for the future

This work demonstrates the utility of in situ spectroscopy in characterizing habitat quality under forest canopies and quantifies the performance of p -theory in replicating these in situ measurements. Modeling canopy spectral transmittance can complement empirical observations and benefit ecophysiological research on how the vegetation on the forest floor respond to environmental conditions. Because canopy transmittance is a sub-component of forest reflectance models, the work also advances interpretation of hyperspectral remote sensing data based on these models. The p -theory is promising for applications where good computational performance is necessary, e.g., when modeling the diurnal variation of canopy spectral transmittance. Further comparison against a 3D radiative transfer model can reveal important insights on the spatial variability of canopy transmittance.

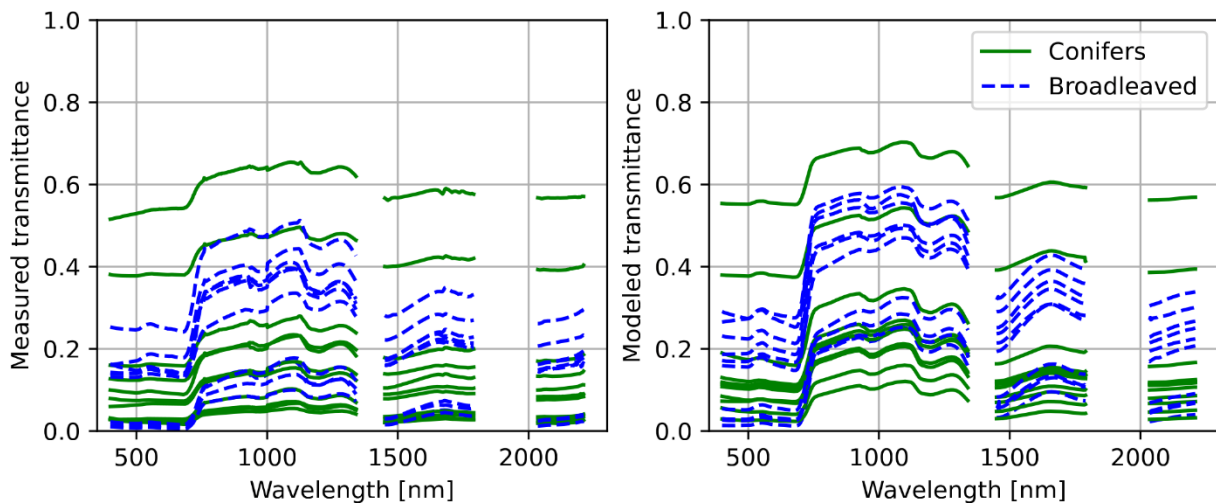


Figure 1. (a) Measured mean canopy transmittance spectra for each study plot and (b) corresponding spectra modelled based on p -theory. Wavelength regions that were noisy in the in-situ canopy transmittance or model input data have been masked out.

Sini-Selina Salko¹, Aarne Hovi¹, Iuliia Burdun¹, Jussi Juola¹, Miina Rautiainen¹

¹ Aalto University, Finland

Keywords: spectral measurements, peatland, vegetation, Sphagnum, plant functional type

Challenge

Northern peatlands store up to 25% of global soil organic carbon and host many endangered species; however, they are facing degradation due to climate change and draining. In northern peatlands, vegetation indicates the ecohydrology and health of the ecosystem. An understanding of the spectral characteristics of the vegetation in these peatlands will enable satellite-based monitoring of their status. To support the interpretation of new and forthcoming hyperspectral satellite missions, we need laboratory and in situ spectral measurements and a comprehensive understanding of the spectral characteristics of peatlands created based on them. In this study, we collected and analyzed an extensive spectral library of vascular and non-vascular vegetation in different arctic, boreal and hemiboreal peatlands ranging from southern Estonia (57°N) to northernmost Finland (69°N). A special focus was on Sphagnum mosses, which are a dominant feature in northern peatlands.

Methodology

First, after snow melt in 2022, we collected 90 samples of Sphagnum mosses representing 10 common species (Fig. 1a). The mosses were obtained from peatlands in Southern Finland and grew in habitats representing different nutrient levels. We measured their nadir-view reflectance spectra (350-2500 nm) in a laboratory setting with an ASD FieldSpec-4 spectrometer and a laboratory light source. All samples were measured in different stages of desiccation (as fresh, after 24 hours, after 48 hours, and after 1 week), so that we were able to analyze systematically how the spectra of different species change as the samples dry. Next, we conducted an extensive field campaign during two growing seasons (2022, 2023) in pristine peatlands in Estonia and Finland. We measured the nadir-view reflectance spectra of 450 vegetation plots (Fig. 1b). The vegetation plots represented different nutrient and moisture levels and hosted a large range of different types of vascular plants and peatland mosses. In addition to the spectral measurements, we also estimated cover fractions of different plant functional types from photographs of the plots and measured the moisture level of the plots. The data set was used to examine how the spectral signature of a plot is affected by the plant functional types present in its vegetation communities. To our knowledge, this is the largest spectral library of peatland vegetation collected to-date.

Results

Results from the laboratory study showed that Sphagnum moss species had, to different extents, species-specific spectral features. They were also visually distinct from the reflectance properties of vascular plants and lichens. Furthermore, the spectral responses that Sphagnum species exhibited during desiccation were characteristic of their habitats. The spectral regions that were strongly associated with the moisture content were within the shortwave infrared region. The spectral library of the Sphagnum mosses has been published as an open data set (doi: 10.17632/wm5fcxdmzd.1) and is thus already available for the remote sensing community to use.

Results from the field campaigns in Estonia and Finland, on the other hand, are not yet ready, because the measurements were only recently completed, and we are currently analyzing the data. Our preliminary results show that there is significant variation in the reflectance spectra of the different peatlands and their vegetation communities. In the conference, we will present a more comprehensive interpretation of how fractional covers of different plant functional types are connected to the spectral properties of vegetation from hemiboreal to arctic peatlands.

Outlook for the future

The spectral properties of vegetation in peatlands have been poorly understood until now. Our study creates a fundamental understanding of how surface vegetation (i.e., vascular plant and moss species) diversity and spectral variation are connected in northern peatlands. It also provides to-date the world's largest spectral libraries of northern peatland vegetation as open data. We anticipate that our analyses on the connections between plant diversity and in situ and laboratory spectra will support the development of operational methods for remote monitoring of peatland vegetation using data from the new and forthcoming hyperspectral satellite missions (e.g., EnMAP, PRISMA or CHIME). Finally, we expect that our spectral library will have future scientific uses in e.g., radiative forcing calculations (climate modeling) and biodiversity assessments.

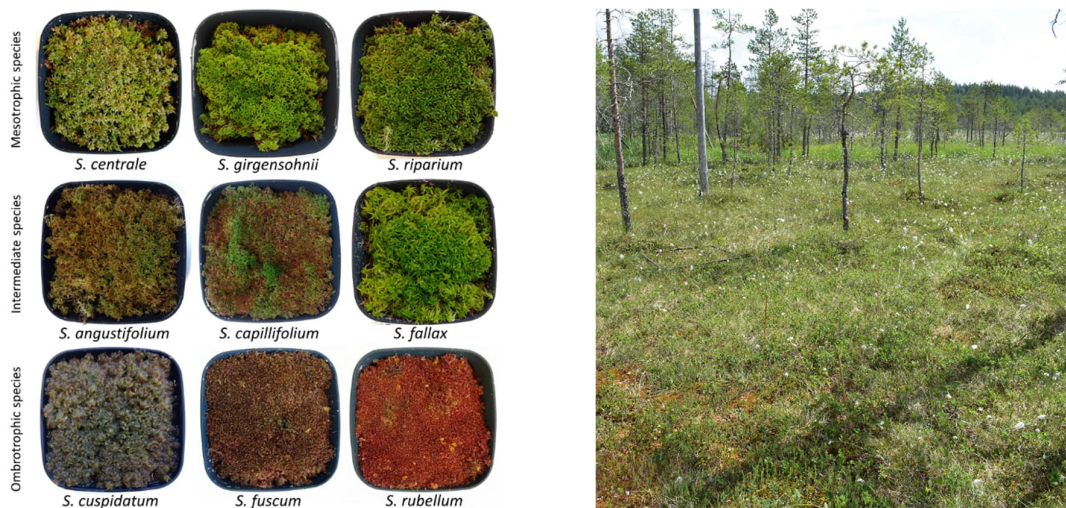


Figure 1. (a) Sphagnum moss species that were measured in the first part of the study. (Image credit: Salko et al. 2023. Ecology and Evolution. 2023;13:e10197, [CC BY 4.0 License](https://creativecommons.org/licenses/by/4.0/)). (b) Example of a field measurement site in the second part of the study,

abstract

EARSeL Valencia 2024
Abstract
Corresponding Author:
juliajoswigji@gmail.com

Remotely sensing intraspecific variation in European Beech (*Fagus sylvatica*) and its relation to drought

Julia S. Joswig¹, Meredith C. Schuman^{2,3}, Anna K. Schweiger⁴, Hannes Feilhauer¹

¹ RSC4Earth, Leipzig University, Leipzig, Germany

² Remote Sensing Laboratories, Department of Geography, University of Zurich, Zurich, Switzerland

³ Department of Chemistry, University of Zurich, Zurich, Switzerland

⁴ Department of Land Resources and Environmental Sciences, Montana State University, USA

Keywords (5): Intraspecific Variation, AVIRIS-NG, Drought, Traits, *Fagus sylvatica*

Challenge

Plant diversity is of vital importance for human well-being and at the same time rapidly decreasing at a pace exacerbated by global change. Intraspecific trait variation influences plant community structure and ecosystem functions and its loss may be an early indicator of biodiversity loss (Des Roches et al. 2018).

European beech (*Fagus sylvatica*), a dominant tree species of Central Europe, shows variable sensitivity to drought (Leuschner 2020). Increasing drought frequency and severity has led to diebacks observed across large parts of its range. In Germany and Switzerland, these occur in a patchy manner, where neighboring beech trees have very different outcomes (Frei et al. 2018, Gonzalez et al. 2021, Pfenninger et al. 2021, Weigel et al. 2023).

In this study, we aim to assess functional diversity of European beech from imaging spectroscopy data. Specifically, we analyze to which extent patterns of trait variation within beech forests are related to the probability of drought in these areas. Further, we examine the importance of past local drought events, long-term climate and soil factors for trait variation in beech.

Methodology

We are using airborne imaging spectroscopy data acquired over beech-dominated forests during the 2021 AVIRIS-NG campaign across six countries representing the edges and center of European beech distribution. Further, beech-dominated forests will be extracted using leaf type data provided by Copernicus.

We will derive foliar traits of these beech forests using radiative transfer model (RTM) inversion (Kattenborn et al. 2017). We will develop a scaling method that allows comparing the intraspecific trait variation observed to the expected per-location variation by leveraging existing information about the distribution of genetic variation across the range of European beech (Stefanini et al. 2023). We will then compare trait variation per forest with (1) average climatic conditions, and (2) exposure to drought during the past decades. Specifically, we will build linear ridge regression models to explain intraspecific trait variation and average trait expression per forest with climatic factors from WorldClim, soil factors from SoilGrids (Hengl et al. 2014), and drought events derived from Bioclim by CHELSA (Karger et al. 2017, Karger et al. 2018). Finally, we will assess the independent and joint effects of these factors for

explaining intraspecific trait variation as well as average trait expression per forest using hierarchical partitioning.

Results

We expect to see trait patterns change with climate and drought exposure, but less so with soil conditions. For example, we expect that stands in dryer habitats show lower values for stress-related traits, e.g., lower leaf mass per area (LMA), as well as lower values of leaf area index (LAI). Drought exposure may be related to average soil texture, however, we expect soil factors to independently explain average plant traits related to the leaf nutrient status, including chlorophyll content, or stress, such as LMA.

Moreover, we expect functional (intraspecific) diversity to be correlated with environmental conditions and drought exposure. In particular, we expect stress-related traits to vary less in dryer habitats compared to wetter habitats even when accounting for baseline differences in genetic diversity. Because beech grows across a wide range of soils characteristics, we might see trait variation increases with soil diversity potentially independent of climate.

We expect that increased drought probability will generally correlate with dryer habitats and thus lower intraspecific trait diversity. We furthermore expect the bias in trait diversity (central tendency) to vary systematically across the range, with more extreme values toward range extremes.

Outlook for the future

This study may improve our understanding of intraspecific trait variation across different climate, drought history and soil conditions. Accounting for baseline genetic variability will indicate locations where there is evidence for specific environmentally dependent plasticity or targeted selection. We aim to identify conditions and locations where the risk of beech tree die-offs are increased, and determine to what extent our predictions align with currently accepted knowledge for this species.

Finally, management decisions are usually taken locally, thus scaling down biogeographical processes becomes more important. This study will improve our understanding of the relative contributions of genetic variation, climate, soil and drought exposure at local (forest) scales.

We expect that our study will improve understanding of drought-related risks for a dominant tree species of central Europe and provide a better basis for management decisions.

References:

Des Roches, S., Post, D.M., Turley, N.E. *et al.* The ecological importance of intraspecific variation. *Nat Ecol Evol* **2**, 57–64 (2018). <https://doi.org/10.1038/s41559-017-0402-5>

Frej, E.R., Gossner, M.M., Vitasse, Y., Queloz, V., Dubach, V., Gessler, A., Ginzler, C., Hagedorn, F., Meusburger, K., Moor, M., Samblás Vives, E., Rigling, A., Uitentuis, I., von Arx, G. and Wohlgemuth, T. (2022), European beech dieback after premature leaf senescence during the 2018 drought in northern Switzerland. *Plant Biol J*, 24: 1132-1145. <https://doi.org/10.1111/plb.13467>

González de Andrés, E., Rosas, T., Camarero, J. J., & Martínez-Vilalta, J. (2021). The intraspecific variation of functional traits modulates drought resilience of European beech and pubescent oak. *Journal of Ecology*, 109, 3652–3669. <https://doi.org/10.1111/1365-2745.13743>

Hengl, I. et al. SoilGrids1km—global soil information based on automated mapping. *PLoS ONE* **9**, e105992 (2014).

Kattenborn, T., Fassnacht, F.E., Pierce, S., Lopatin, J., Grime, J.P. and Schmidtlein, S. (2017), Linking plant strategies and plant traits derived by radiative transfer modelling. *J Veg Sci*, 28: 717-727.
<https://doi.org/10.1111/jvs.12525>

Karger, D.N., Conrad, O., Böhner, J., Kawohl, T., Kreft, H., Soria-Auza, R.W., Zimmermann, N.E., Linder, P., Kessler, M. (2017). Climatologies at high resolution for the Earth land surface areas. *Scientific Data*. 4 170122. <https://doi.org/10.1038/sdata.2017.122>

Karger D.N., Conrad, O., Böhner, J., Kawohl, T., Kreft, H., Soria-Auza, R.W., Zimmermann, N.E., Linder, H.P., Kessler, M.. (2018) Data from: Climatologies at high resolution for the earth's land surface areas. *Dryad Digital Repository*.<http://dx.doi.org/doi:10.5061/dryad.kd1d4>

Leuschner C., Drought response of European beech (*Fagus sylvatica* L.)—A review, *Perspectives in Plant Ecology, Evolution and Systematics*, Volume 47 (2020) 125576, ISSN 1433-8319, <https://doi.org/10.1016/j.ppees.2020.125576>.

Pfenninger M., Reuss F, Kiebler A, Schönnenbeck P, Caliendo C, Gerber S, Cocchiararo B, Reuter S, Blüthgen N, Mody K, et al. 2021. Genomic basis for drought resistance in European beech forests threatened by climate change. *eLife* 10: e65532.

Stefanini, C., Csilléry, K., Ulaszewski, B. et al. A novel synthesis of two decades of microsatellite studies on European beech reveals decreasing genetic diversity from glacial refugia. *Tree Genetics & Genomes* **19**, 3 (2023). <https://doi.org/10.1007/s11295-022-01577-4>

Weigel, R., Bat-Enerel, B., Dulamsuren, C., Muffler, L., Weithmann, G., & Leuschner, C. (2023). Summer drought exposure, stand structure, and soil properties jointly control the growth of European beech along a steep precipitation gradient in northern Germany. *Global Change Biology*, 29, 763–779. <https://doi.org/10.1111/gcb.16506>

Mapping forest canopy water content using hyperspectral imagery

Laura Recuero¹, Margarita Huesca ², Roshanak Darvishzadeh ², Andrew K. Skidmore ^{2,3}, Tawanda W. Gara ⁴

¹ Universidad Politécnica de Madrid, Departamento de Economía Agraria, Estadística y Gestión de Empresas, Spain

² University of Twente, Faculty of Geo-Information Science and Earth Observation (ITC), Department of Natural Resources, The Netherlands.

³ Macquarie University, Department of Environmental Science, Australia

⁴ California State Polytechnic University Humboldt, Department of Environmental Science and Management, USA

Keywords (5): Earth Observation, Temperate Forest, Hyperspectral, Water Content, Partial Least Squares Regression.

Challenge

Forests face a growing threat from climate change, resulting in worldwide tree die-offs over recent decades. Leaf water content is crucial for assessing forest health, affecting physiological processes like photosynthesis or transpiration. Thus, developing spatial methods to assess canopy water content provides key insights into the forest's current state and potential changes from abiotic or biotic factors. The main challenge is its spatial variability due to factors like soil and atmospheric conditions. Remote sensing techniques, particularly hyperspectral data, offer a non-destructive alternative to labor-intensive and location-limited ground measurements. While these methods are often applied to various vegetation types, such as crops and grasslands, there's limited research in forests. Therefore, the primary goal of this study is to evaluate canopy water content in a mixed-temperate forest using airborne hyperspectral imagery and two empirical methods.

Methodology

The study area is Bavarian Forest National Park (BFNP), located in the southeast of Germany. The airborne hyperspectral data from Fenix sensor was acquired in July 2017 coincident with a field campaign. Its spatial resolution is about 3 m and covers 623 narrow spectral bands (380- 2500 nm). Measurements of Leaf Area Index (LAI) and Leaf Water content (LWC) were gathered across 30 plots of approximately 900 m² of various forest types: 10 broadleaf, 11 needleleaf, and 9 mixed stands. From this field information, the Equivalent Water Thickness metric was calculated at canopy level (EWT_{canopy}) and used to estimate this metric from hyperspectral data with two empirical methods, narrowband vegetation indices (NVIs) and the partial least squares regression (PLSR). Hyperspectral data were pre-processed and the mean spectral reflectance was calculated for each plot using a 9 × 9 pixel window to extract representative samples. The equations of five broadband vegetation indices were used to calculate the NVIs using all paired waveband combinations. Their relationships with EWT_{canopy} were explored in terms of Pearson correlation identifying the most sensitive regions. The specific band combination for each NVI that resulted in the highest correlation was used to generate a linear regression model. These results were compared with those obtained using different spectral regions as input in the PLSR model. All models were validated with the leave-one-out method.

Expected results

The NVIs approach showed that the most sensitive bands for canopy water estimation range between 1000 and 1370 nm. Particularly, Ratio-based NVIs (i.e. Normalized Difference Water Index ($NDWI_{narrow}$), and Water Index (WI_{narrow})) presented the best performance with a lower cross-validated root mean squared error ($RMSE_{cv}$) and a higher coefficient of determination (R^2_{cv}), followed by the $slope_{narrow}$ and the soil-based NVIs (i.e. Soil Adjusted Vegetation Index ($SAVI2_{narrow}$) and Transformed Soil Adjusted Vegetation Index ($TSAVI_{narrow}$)). Particularly, WI_{narrow} showed the best results with an $RMSE_{cv}$ of 0.0102 g/cm² and an R^2_{cv} of 0.6124. Regarding forest types, the highest errors in terms of the normalized $RMSE_{cv}$ were found in broadleaf stands whereas the mixed and needleleaf stands showed similar accuracies with slightly lower errors in needleleaf stands. PLSR results showed that the lowest $RMSE_{cv}$ of 0.0108 g/cm² was found when using the 16 most sensitive spectral bands obtaining an R^2_{cv} of 0.6516. Higher errors and lower R^2_{cv} were obtained when using the other spectral subsets with more spectral bands and when using the entire spectrum. The best performance of the PLSR model yields an increment of 6.40% in terms of R^2_{cv} , compared to the best results derived from the NVIs but did not lead to a reduction in $RMSE_{cv}$. A spatially continuous map was generated using the PLSR model which showed spatial coherence among forest types.

Outlook for the future

This study demonstrates the utility of hyperspectral data for estimating spatially continuous canopy water content in temperate forests. The strong performance of the WI_{narrow} and the PLSR model using only 16 spectral bands, suggests the possibility of upscaling EWT_{canopy} from hyperspectral to multispectral data, allowing vegetation water content monitoring using time series from satellites such as Sentinel-2 or Landsat. In addition, this approach can reduce the need for extensive field data enabling water content estimation over time with a lower cost. Moreover, the spatiotemporal analysis of EWT_{canopy} with satellite data contributes to monitor forest health, providing near-real-time information about forest's condition helping the forest managers in making decisions on forest conservation.

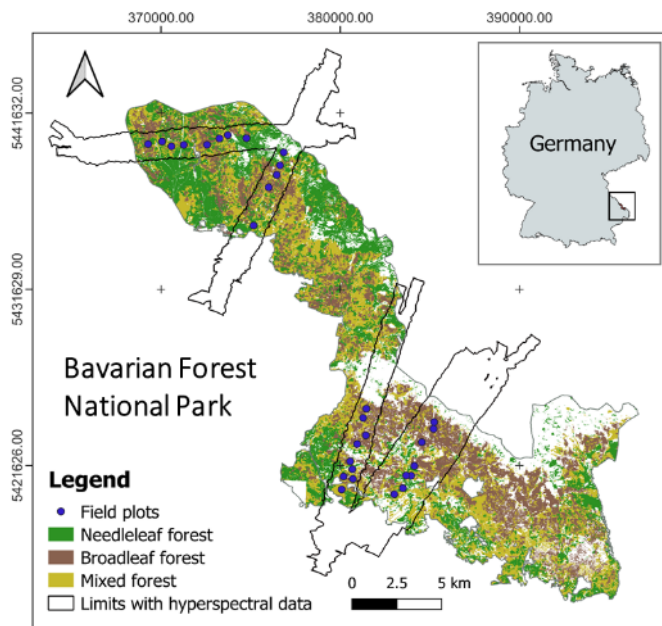


Figure The location of the Bavarian Forest National Park (BFNP) in Germany, the boundaries with Fenix hyperspectral data (black lines) and field plots (blue dots).

Dealing with variability in vegetation functional trait retrievals: case study of floodplain forests in Lanžhot, Czech Republic

EARSeL Valencia 2024

Abstract

Corresponding Author:

[lucie.kupkova@natur.cuni.cz]

Adenan Yandra Nofrizal¹, Lucie Kupková¹, Petr Lukeš³ Marian Švik^{3,4}, Lucie Červená¹, Zuzana Lhotáková², Eva Neuwirthová², Jana Albrechtová²,

¹ CHARLES UNIVERSITY, FACULTY OF SCIENCE, DEPARTMENT OF APPLIED GEOINFORMATICS AND CARTOGRAPHY, CZECH REPUBLIC

² CHARLES UNIVERSITY, FACULTY OF SCIENCE, DEPARTMENT OF PLANT EXPERIMENTAL BIOLOGY, CZECH REPUBLIC

³ GLOBAL CHANGE RESEARCH INSTITUTE OF THE CZECH ACADEMY OF SCIENCES, CZECH REPUBLIC

⁴ MASARYK UNIVERSITY, FACULTY OF SCIENCE, DEPARTMENT OF GEOGRAPHY, CZECH REPUBLIC

Keywords (5): vegetation functional traits, floodplain forest, chlorophyll content, radiative transfer modelling, statistical modelling

Challenge (800 - 1000 characters incl. spaces)

Vegetation traits are widely used indicators of the physiological status of vegetation. The retrieval of traits that vary within the canopy and within the stand/spatial level is a challenge that has not been wholly addressed yet. In the case of within-canopy variability, the challenging questions are: How does the retrieval performance of leaf-level traits differ for sun-exposed vs. shaded canopy positions? We hypothesize that the differences between the retrieval performance for sun-exposed and shaded traits will be smaller in spring and larger in summer and fall. In the case of spatial variability, our question is how the spectra/traits change from the leaf level to the individual tree level (0.5 m CASI data) and to mixed spectral information of several crowns (20 m Sentinel-2 data). In the context of our study site, where stands of rich structure and areas of monocultures are present, we assume that higher uncertainty in trait retrievals will be observed in stands of rich structure.

Methodology (1200 – 1500 characters incl. spaces)

Three types of data at different spatial scales were used: 1) measurements of leaf samples for the leaf level taken at different positions in the canopy; 2) CASI VHR hyperspectral data for the individual tree level, 3) Sentinel-2 data of mixed spectral information for the forest stand level. We worked with 405 leaf samples collected in the study area of the Lanžhot floodplain forest from 14 trees of the following species: Austrian Oak (2 trees), English oak (2 trees), European hornbeam (4 trees), Narrow-leaved ash (4 trees) and Small-leaved linden (2 trees). Tree samples were collected in seven consecutive campaigns on April 24-25, 2019, July 18-24, 2019, September 4-11, 2019, October 17-24, 2019, May 11, 2020, July 23-26, 2020, October 22, 2020. Various trait retrieval methods were used in order to compare their performance: 1) RTM models PROSPECT4 for the leaf level and inversion of PROSAIL to estimate canopy level traits. 2) further PLSR and for leaf level and 3) Random Forest for leaf level and neural networks (NN) in Machine Learning Regression Algorithms (MLRA) in ARTMO for the canopy scale. To determine the accuracy of the traits retrieval, the coefficient of determination (R^2) and normalized root-mean-square error (NRMSE) were used.

Preliminary results (1200 – 1500 characters incl. spaces)

The vegetation functional traits were retrieved for all the levels – leaf, crown (CASI) and stand (Sentinel-2). We estimated chlorophyll content (Cab), dry matter (Cm) and water content (Cw) for the leaf level and Cab and leaf area index (LAI) for the canopy/stands scale. As the first step, traits from both canopy positions were used for model training and validation. For the accuracy validation at the leaf scale (Figure 1), the best estimation was found for Cab using RF, for Cm using PLSR and for Cw using PLSR. However, RTM also brought good accuracies. The fit of estimated to measured values was quite consistent across the season (see colour curves in Figure 1). As Table 1 shows, on the canopy scale in general all models performed rather good (except of PLSR in campaign 2) in case of Cab traits estimations. Better estimations were in general achieved for Sentinel-2 and best performing method was RTM followed by PLSR for Sentinel-2 and by ML (NN) for CASI. While for LAI slightly better estimations were gained for CASI and the best performing method was PLSR. Comparing the variability of CASI and Sentinel-2 traits, the results for individual methods and campaigns are not unambiguous when we evaluate the overall area. In the next steps we will compare the variability of rich structure stands and areas of monocultures. We will also examine how the retrieval accuracy differs between sun and shade canopy position. The results will be presented on the conference.

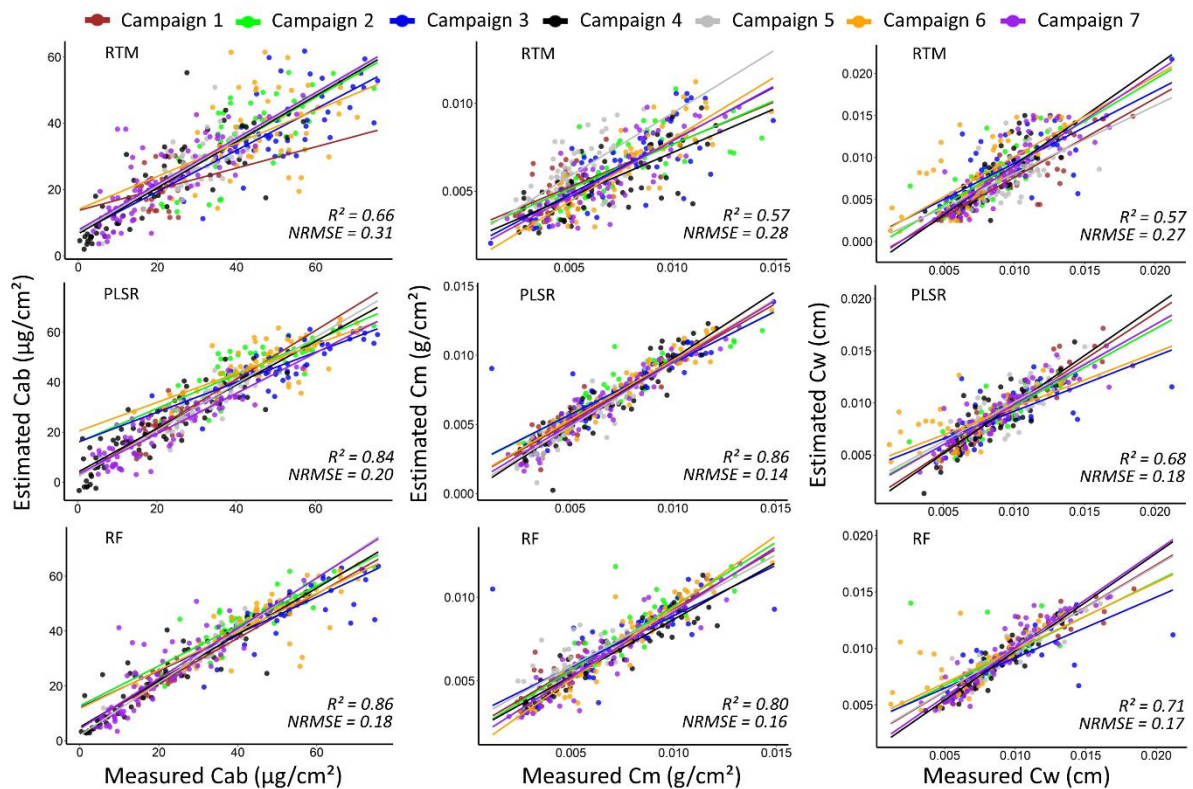


Figure 1. Estimations for the leaf scale using RTM, PLSR and RF. Leaf traits from both canopy positions – sun exposed and shaded were used for model training and validation.

	Cab						LAI					
	RTM		ML (NN)		PLSR		RTM		ML (NN)		PLSR	
	R2	NR MSE	R2	NR MSE	R2	NR MSE	R2	NR MSE	R2	NRM SE	R2	NRM SE
CASI Airborne												
Campaign 1	0.95	0.06	0.87	0.1	0.82	0.14	0.9	0.09	0.95	0.06	0.8	0.13
Campaign 2	0.82	0.14	0.67	0.16	0.49	0.26	0.87	0.1	0.77	0.28	0.86	0.11
Campaign 3	0.53	0.1	0.62	0.2	0.76	0.06	0.49	0.09	0.71	0.33	0.74	0.15
Campaign 4	0.68	0.34	0.65	0.39	0.56	0.39	0.61	0.2	0.56	0.29	0.9	0.08
Campaign 6	0.81	0.13	0.86	0.11	0.68	0.18	0.92	0.08	0.74	0.13	0.94	0.07
Sentinel 2												
Campaign 1	0.92	0.07	0.88	0.09	0.76	0.15	0.95	0.06	0.2	0.49	0.86	0.12
Campaign 2	0.88	0.1	0.81	0.15	0.87	0.11	0.89	0.09	0.73	0.14	0.83	0.12
Campaign 3	0.82	0.12	0.69	0.16	0.83	0.13	0.86	0.11	0.93	0.07	0.9	0.09
Campaign 4	0.58	0.34	0.72	0.29	0.87	0.21	0.31	0.12	0.75	0.14	0.58	0.2
Campaign 6	0.9	0.11	0.73	0.17	0.74	0.17	0.65	0.08	0.53	0.24	0.75	0.16

Table 1. Estimations for the canopy scale for CASI and Sentinel-2 using RTM, ML (NN) and PLSR

Outlook for the future (800 - 1000 characters incl. spaces)

In this study, the assessment of the physiological status of the vegetation is based on Cab, Cm and Cw for the leaf and Cab and LAI for canopy scale. Other traits could also be evaluated in the follow-up activities. At the leaf level, for example, these may include Carotenoids (Car), Brown pigment content (Cbrown) and Mesophyll structure (N). At the canopy scale, leaf mass per area (LMA) and specific leaf area (SLA) can also be considered. We propose to combine hyperspectral and Lidar data to improve the accuracy of 3D plant trait retrievals. Future work can also focus on predicting the variability of plant functional traits over large areas, using new spaceborne hyperspectral missions (e.g. PRISMA and EnMAP) can be used. Improvements can also be achieved by combining RTM with the other machine learning or deep learning techniques. Precise estimation of leaf-level traits from remote sensing can be used to predict ecosystem responses to environmental and climatic factors.

Identification of a biodiversity indicator species in the hyperspectral signature of boreal forests

EARSeL Valencia 2024

Abstract

Corresponding Author: eelis.halme@vtt.fi

Eelis Halme¹, Olli Ihalainen¹, Matti Möttöus¹

¹ VTT Technical Research Centre of Finland, Finland

Keywords: Earth observation, spectral libraries, reflectance model, common aspen, *Populus tremula* L.

Challenge

Biologically diverse boreal forests with structures similar to old-growth patches are under strong pressure from forest management and climate change. Such forest areas are identified and protected under national and European agendas. Identifying them remotely is possible by mapping indicator overstorey species characteristic of forest sites with high ecological value. Hyperspectral remote sensing, also known as imaging spectroscopy, has demonstrated capacity in tree species mapping and the reflectance differences between the tree species are documented in the lab-measured spectral libraries available online. However, the spectral libraries provide data for individual elements of the vegetation canopy, such as leaves and bark, while in the actual hyperspectral image of a forest canopy these signals are convoluted with the effects of canopy structure and illumination geometry. Thus, mapping of species is generally done empirically, by supervised or non-supervised classification of hyperspectral imagery. As this cannot be the preferred approach for automatic detection of ecologically important forest habitats for large areas, we tested how a physically-based forest reflectance model can upscale the spectral signals of the canopy elements of an important indicator overstorey species in European boreal forest, common aspen (*Populus tremula* L.), to allow its detection in air- and spaceborne hyperspectral data.

Methodology

We used a sophisticated forest reflectance model FRT (Forest Reflectance and Transmittance), well suited for the task and validated using measurements and model intercomparison. The simulations of forest spectral reflectance used the spectral reflectance and transmittance properties of the foliage and bark of tree species measured in Finland and Estonia and were performed considering the actual distributions of forest variables (incl. species composition, tree height, stand density) determined from country-wide sampling of forest plots. Forest floor was assumed to compose of typical vegetation and other material of the modelled forest sites and its reflectance constructed from the samples available in online spectral libraries. Forest reflectance was simulated at the level of a stand, assumed to correspond to the pixel size of a high-resolution hyperspectral satellite sensor (e.g. EnMAP or CHIME). The simulated stands included ones consisting only of the indicator species (i.e. aspen) as well as varying mixtures of aspen with the species occurring naturally in same stands, typically silver birch (*Betula pendula* Roth) and Norway spruce (*Picea abies* (L.) Karst.). The separability of the different species based on their spectra was first tested at leaf level and then for the simulated stand level spectra using standard classifiers. Next, we tested the theory of spectral invariants to retrieve the mean reflectance factor of the leaf in the simulated stand spectrum and compared it with the spectral library-derived spectrum of aspen. Finally, we applied the best-working algorithm to hyperspectral data acquired over Southern Finland with known presence of aspen trees in mixed stands.

Expected results

The greatest probability of confusing the species studied here based on their spectra was for the broadleaves. The leaf level spectra of aspen and silver birch – the most common broadleaf species in the boreal region – were best separable in the visible to red edge spectral regions (Figure 1 and 2) and a narrow SWIR band at approx. 1900 nm in the shortwave infrared – but the latter is masked by atmospheric absorption. They were easily separable at the level of the leaf and pure stands, although having different leaf angle distributions. As the share of aspen leaves in the simulated stands decreases, so does the spectral separability. The theory of spectral invariants allowed to separate the two broadleaf species at the level of a stand.

Outlook for the future

Recent studies have shown that the spectral properties of tree leaves at peak growing season may remain constant over large geographic area, indicating the possibility of the use of spectral libraries for mapping biodiversity hotspots. Also, physical methods allow to scale leaf reflectance to that of a canopy and vice versa in a computationally efficient manner. Thus, approaches based on forest reflectance models or other mathematical tools will allow to use the spectral differences quantified for leaves in robust large-scale species mapping. Further work is still needed in quantifying the effects of spatial and temporal variation in leaf spectra and canopy structure on the species identification.

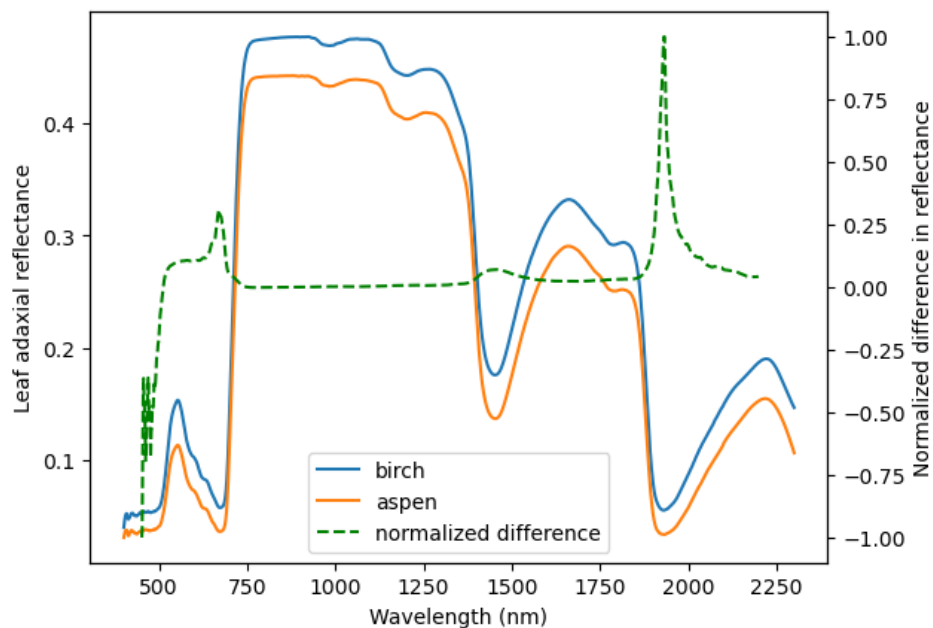


Figure 1 Aspen and birch adaxial reflectance from a spectral library (doi: [10.17632/nvgjcn5nsx.1](https://doi.org/10.17632/nvgjcn5nsx.1)) averaged from measurements of 57 canopy top-layer leaves for each species, and their normalized difference.

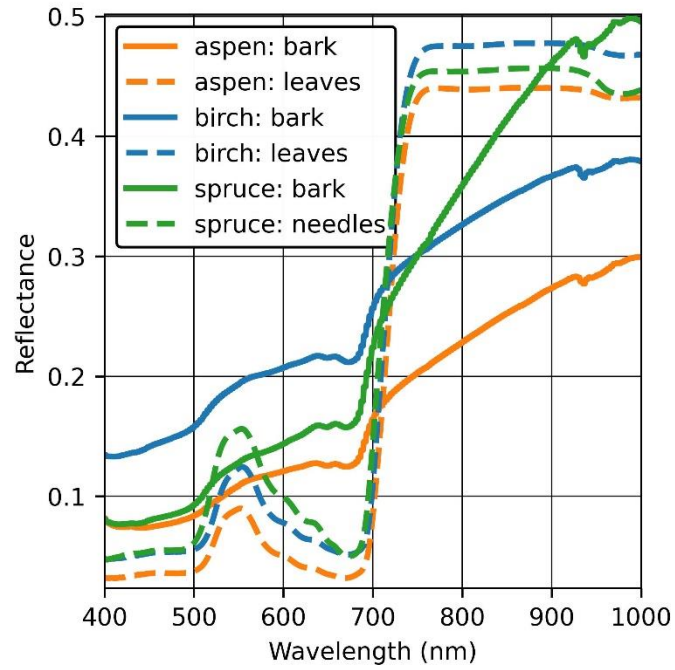


Figure 2 Examples of reflectance spectra of aspen and birch leaves (adaxial) and spruce needles of sample trees from Järvelja, Estonia (doi: [10.17632/t5f554s7cn.1](https://doi.org/10.17632/t5f554s7cn.1)). In addition, stem bark reflectance spectra of the same tree species are presented (doi: [10.17632/pwfxgzz5fj.2](https://doi.org/10.17632/pwfxgzz5fj.2)).

The PANDA-WATER project: PRISMA Products and Applications for inland and coastal WATER

EARSeL Valencia 2024

Abstract

Corresponding Author: federica.braga@cnr.it

[Federica Braga](#)¹, Mariano Bresciani², Alessia Tricomi³, Vittorio Brando¹, Alice Fabbretto²⁻⁴, Claudia Giardino², Paolo Villa², Andrea Pellegrino², Salvatore Mangano², Gian Marco Scarpa¹, Maria Laura Zoffoli¹, Giorgia Manfè¹, Marco Bellacicco¹, Federico Falcini¹, Jaime Pitarch¹, Luis Gonzales Vilas¹, Roberta Bruno³, Maria Libera Battagliere⁵, Giorgio Licciardi⁵, Maria Girolamo Daraio⁵

¹ National Research Council, Institute of Marine Sciences, Italy

² National Research Council, Institute for Electromagnetic Sensing of the Environment, Italy

³ e-GEOS S.P.A., Italy

⁴ Tartu University, Department of Remote Sensing, Estonia

⁵ Italian Space Agency, Downstream & Applications Unit, Italy

Keywords (5): PRISMA, Imaging Spectroscopy, Water Quality, Aquatic Ecosystems, Validation

Challenge

Started in September 2022, the PANDA-WATER project is part of the ASI's programme "PRISMA-SCIENZA". PANDA-WATER aims to assess PRISMA suitability for addressing challenges in aquatic sciences and ecosystem monitoring, exploiting its radiometric sensitivity, spatial and spectral resolutions. The overall objective of PANDA-WATER is to provide a set of innovative satellite products, derived from imaging spectrometry, that enables the retrieval of parameters of interest for coastal and inland water applications. The novelty of PANDA-WATER stems from the application of state-of-the-art algorithms that exploit the hyperspectral PRISMA data, thus resulting in enhanced observational capabilities respect to current Copernicus missions. This work provides an overview of the scientific context of the project, the methodology and the ongoing activities, with an outlook towards the contribution to upcoming hyperspectral missions (i.e., Copernicus CHIME, NASA's PACE and SBG, ASI's PSG).

Methodology

The capabilities of PRISMA imaging spectrometry, combined with innovative analysis techniques, are exploited to improve existing products and to develop innovative products for inland and coastal ecosystems. These products focus on: optically active water constituents; particle size distribution; water depth and benthic substrate; natural or artificial floating materials; cyanobacteria and harmful algal blooms. To ensure the radiometric adequacy of PRISMA for aquatic applications, preprocessing of the data is performed prior developing and testing the algorithms. Preprocessing includes the evaluation of environmental noise equivalent reflectance, sun-glint and cloud masking and the accuracy assessment of atmospherically corrected reflectance. Surface reflectance and water quality products are validated using matchup data from radiometers installed on stationary platforms and targeted in situ campaigns, also allowing algorithm parametrization and development. Moreover, to address the need for higher spatial resolution in inland and transitional waters, a novel pansharpener approach has been developed. Water quality products are obtained using different approaches: e.g. bio-optical modelling inversion techniques to characterize the benthic substrate and water depth in optically shallow waters and machine learning models to detect phycocyanin concentration or to map floating materials.

Results

In this section, some preliminary results of the PANDA-WATER project are presented and discussed. Figure 1 shows the qualitative comparison of water reflectance derived from PRISMA (L2C standard atmospheric correction processor and ACOLITE atmospheric correction tool) and measured in situ for the Venetian Lagoon and Lake Trasimeno. Depending on the water conditions and related optical complexity, satellite and in situ reflectance spectra vary in terms of the shape and magnitude. Both L2C and ACOLITE performed adequately in inland waters, but ACOLITE showed better results compared to L2C in coastal waters. In Figure 2a, the benthic substrate map for the Venetian Lagoon, obtained with the BOMBER bio-optical modelling inversion, shows the distribution coverage of the two major groups of submerged aquatic vegetation (seagrasses and macroalgae) and the bare substrate. In situ surveys and thematic maps of submerged vegetation coverage confirmed the accuracy of the derived map and its ability to discriminate between benthic cover classes. The phycocyanin concentration map, generated for the Lake Trasimeno, was obtained with the Mixture Density Network machine learning algorithm (Figure 2b). Although in situ data for validation was unavailable, the results appear qualitatively consistent with the characteristics of the site. Further analysis is required for testing algorithms and models and assessing uncertainties.

Outlook for the future

PRISMA is a pre-operational mission that is included in the "roadmap" of hyperspectral missions and plays a strategic role in the future of hyperspectral operational mission within Sentinel missions of Copernicus European Program. Demonstrating the capabilities of PRISMA for observing coastal, transitional and inland waters, the PANDA-WATER project may contribute to the perspective of a fully operational hyperspectral mission. The optical complexity of inland and coastal waters, which usually shows a fast rate of change and a patchy distribution of water components, makes crucial the synergetic exploitation of multi- and hyperspectral satellite missions. This will improve the temporal observational capabilities of a single mission addressing challenges in aquatic sciences and meeting end-user needs and requirements for ecosystem management and monitoring.

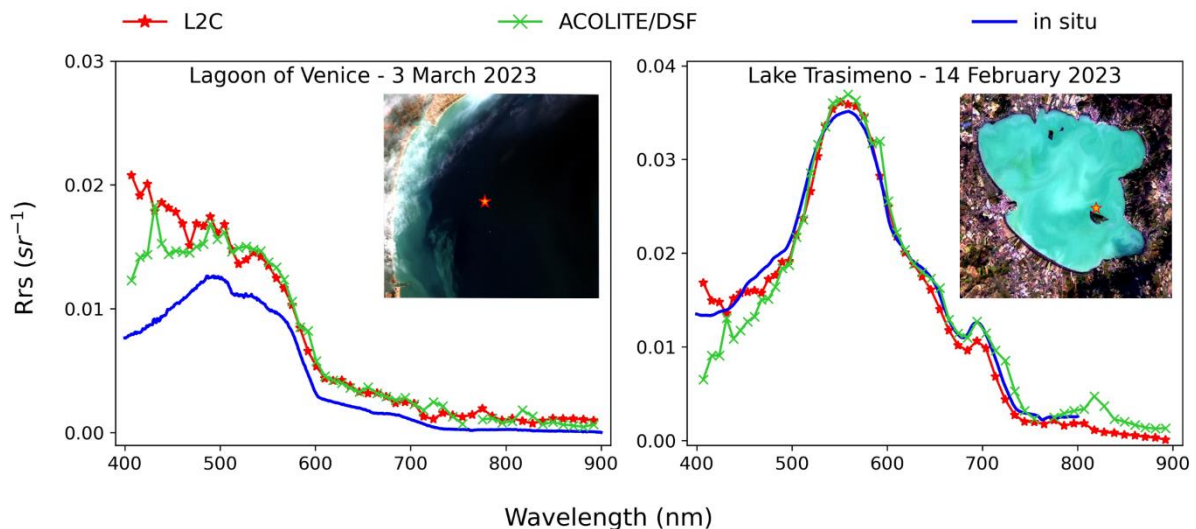


Figure 1 Qualitative comparison of remote sensing reflectance (R_{rs}) for the Venetian Lagoon (left) and Lake Trasimeno (right). In situ R_{rs} obtained from autonomous radiometer systems (blue); PRISMA R_{rs} processed using: Level 2 standard atmospheric correction processor (L2C) (red); ACOLITE atmospheric correction tool with the dark spectrum fitting (DSF) algorithm (ACOLITE/DSF) (green).

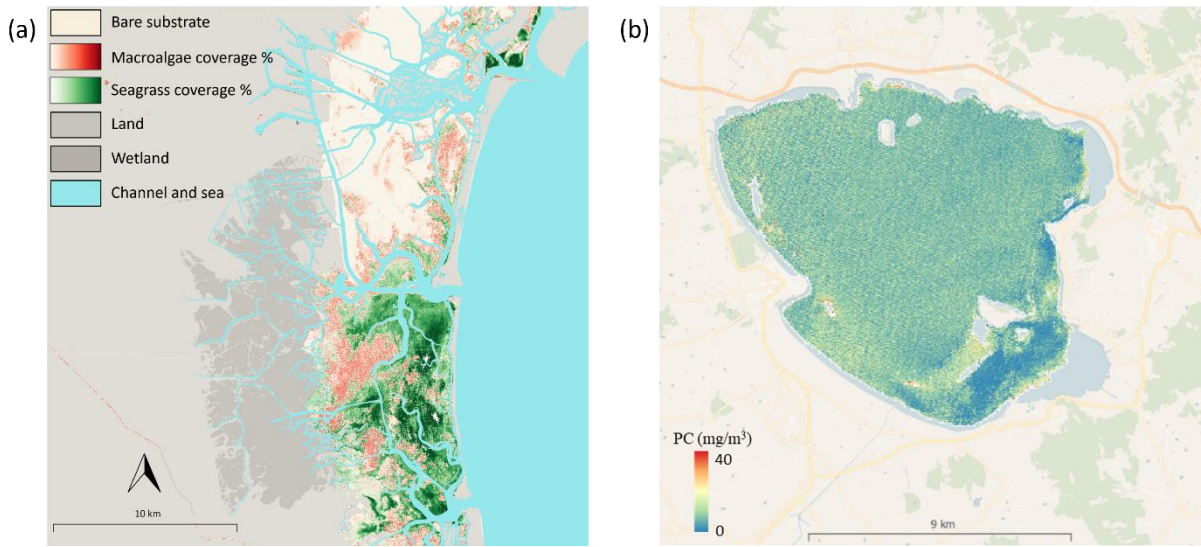


Figure 2 (a) Benthic substrate coverage characterization for the Venetian Lagoon (PRISMA data acquired on 11th September 2023); (b) Phycocyanin concentration map for Lake Trasimeno (PRISMA data acquired on 20th July 2022).

Chlorophyll-b Detection Over Concentrated Harmful Algal Blooms Using Hyperspectral PRISMA Imagery

Maria Laura Zoffoli¹, Pierre Gernez², Michaël Retho³, Soazig Manach³, Federica Braga⁴

¹ Consiglio Nazionale delle Ricerche, Istituto di Scienze Marine (CNR-ISMAR), 00133, Rome, Italy

² Nantes Université, Institut des Substances et Organismes de la Mer, ISOMer, UR 2160, F-44000 Nantes, FRANCE

³ Ifremer, LITTORAL, F-56100, Lorient, France

⁴ Consiglio Nazionale delle Ricerche, Istituto di Scienze Marine (CNR-ISMAR), 30122, Venice, Italy

Keywords: phytoplankton blooms, *Lepidodinium chlorophorum*, line height algorithm, HAB

Challenge

Intense harmful algal bloom (HAB) events in coastal waters are expected to increase in frequency in the coming decades. On the French Atlantic coast, blooms of *Lepidodinium chlorophorum* (LEPI) are observed almost every year during the summer months. Even though LEPI does not produce toxic substances, it is considered as a HAB specie because the large cell accumulation during blooms can lead to anoxic conditions, resulting in the massive mortality of fish and molluscs, ecosystem imbalances, and impacts on human health. LEPI is a green dinoflagellate that lacks some of the diagnostic pigments of most dinoflagellate species, such as Perinidin or Chlorophyll-c. However, it does contain Violaxanthin and Chlorophyll-b (Chl-b), which is specific of green algae. The unique pigmentary profile of LEPI can pose challenges for detection algorithms. In this study, we explored the capabilities of hyperspectral PRISMA data to detect the presence of Chl-b during a concentrated bloom of LEPI in France.

Methodology

Within the scope of the PANDA-Water project, we utilized a PRISMA image acquired on 30/07/2022 from the French Atlantic coast during a phytoplankton bloom dominated by LEPI. The image was corrected from atmospheric effects using ACOLITE to obtain remote sensing reflectance (Rrs). Pixel samples were then extracted over the most concentrated areas of the bloom, and their average computed. The standardized PRISMA spectrum showed a good agreement with Rrs in situ measurements obtained during a LEPI bloom in the same region (Fig. 1A). Notably, this Rrs spectrum exhibited a distinct absorption band at approximately 650 nm, indicative of Chl-b. To detect the presence of Chl-b, we introduced the CbLH algorithm, which is based on the line height (LH) computed from the bands at 628, 646 and 665 nm. This algorithm establishes a baseline through linear interpolation between 628 and 665 nm and uses the distance between the interpolated value and the measured value at 646 nm as a proxy of Chl-b concentration (Fig. 1B). The CbLH algorithm was applied to the PRISMA imagery of the LEPI bloom, and to another PRISMA image captured during a concentrated bloom on 24/07/2022, dominated by *Lingulodinium polyedra* (LINGU), a HAB-forming species lacking Chl-b and serving as control. The Chlorophyll-a (Chl-a) algorithm (Smith et al., 2018, Remote Sens. Environ., 215) was also applied to both images for the detection of the whole area occupied by each bloom.

Results

Both HAB blooms occurred on the French Atlantic coast, with a 6-day gap between them, and the LEPI bloom situated to the north of the LINGU bloom. In situ water samples collected for phytoplankton identification during these events confirmed that LEPI dominated on 30/7, while LINGU dominated on 24/7. In intense events, Chl-a concentration reached approximately 200 mg m^{-3} , common during massive summer blooms (Fig. 2a and c).

The CbLH algorithm, applied to PRISMA data, effectively detected the presence of Chl-b during the LEPI bloom (Fig. 2b). PRISMA's medium spatial (30m pixel) and hyperspectral resolution enabled the identification of narrow spectral features. While this method serves as a proxy of Chl-b and has not been calibrated to quantify its concentration, it is a reliable indicator of the pigment presence, and by extension, the presence of LEPI and relative LEPI cell abundances within the bloom. The bloom in this event was distributed in two patches: a northern one displaying an increasing gradient in cell concentration from the Vilaine river to deep waters, and a southern patch that was more compact and concentrated. The variation in cell concentration within the patch likely responds to coastal water circulation and the influence of strong tides. As expected, when applied to the LINGU bloom, the CbLH algorithm did not reveal the presence of Chl-b confirming the absence of LEPI on the 24/7 and suggesting that our algorithm performs well (Fig. 2d).

Outlook for the future

The results of this study have a two-fold aim: firstly, to enhance the monitoring of HAB events and their responsible species, and secondly, to showcase the potential of hyperspectral data for this application. It underscores the significance of incorporating a greater number of spectral bands in the red region that can contribute to species identification. Future efforts will concentrate on assessing the effect of sediments on the spectral features and the influence of mixed-species blooms where LEPI co-dominated with other species. This will help determine the algorithm applicability under varying environmental conditions that usually are found in the dynamic coastal waters. Additionally, it is worthwhile to explore the application of the CbLH algorithm in cyanobacteria-dominated blooms (also lacking Chl-b) as a control case.

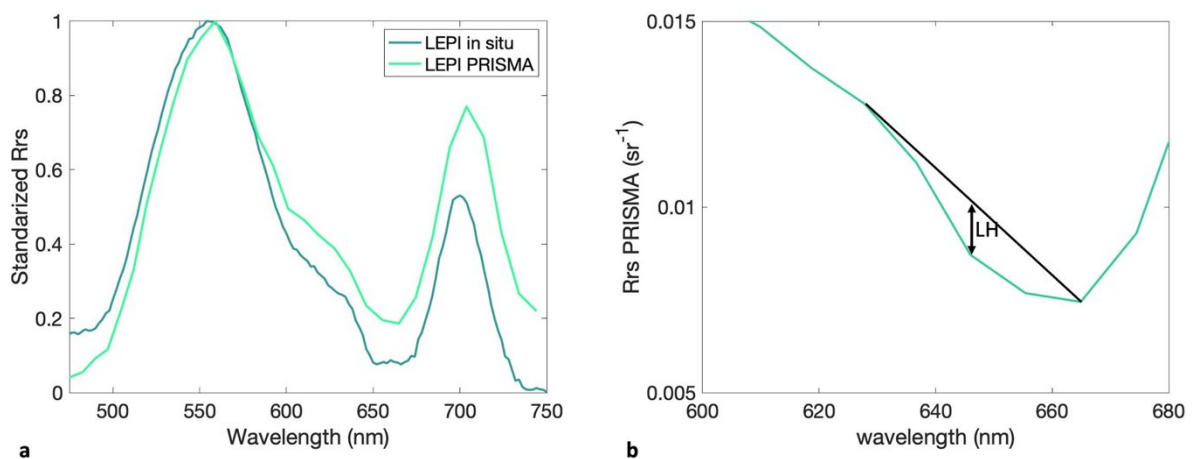


Figure 1 (a) standardized hyperspectral Rrs spectra of LEPI bloom acquired by PRISMA and in situ and (b) representation of the line height (LH) Chl-b measurements where the CbLH algorithm relies on.

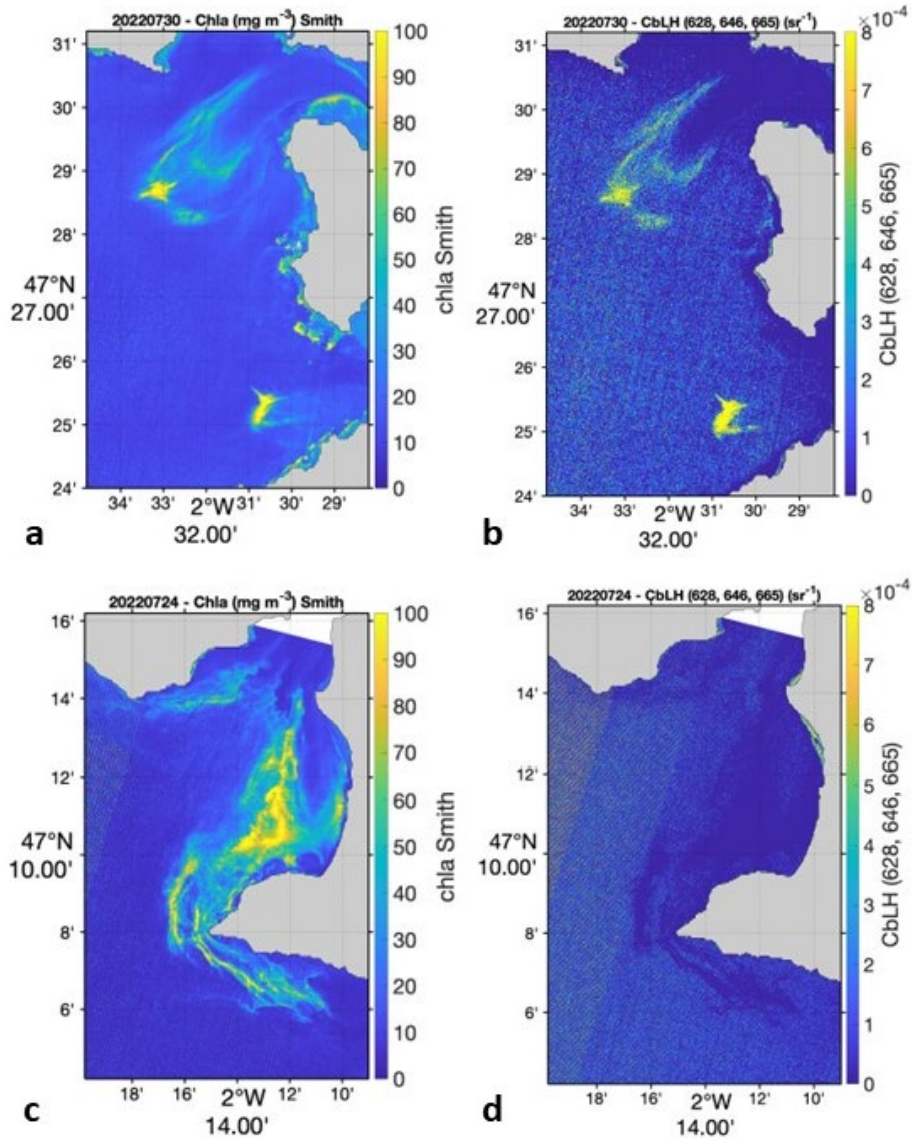


Figure 2 Chlorophylls maps derived from PRISMA images (a) Chl-a during the LEPI bloom; (b) Chl-b using the CbLH the LEPI during bloom; (c) Chl-a during the LINGU bloom; and (d) Chl-b using the CbLH during the LINGU bloom

PRISMA Prototype Algorithms for estimating environmental damage and land degradation vulnerability: the SAPP4VU project

EARSeL Valencia 2024
Abstract

Corresponding Author:
stefano.pignatti@imaa.cnr.it

Stefano Pignatti¹, Maria Francesca Carfora², Rosa Coluzzi¹, Italia De Feis², Vito Imbrenda¹, Giovanni Laneve³, Maria Lanfredi¹, Saham Mirzaei¹, Angelo Palombo¹, Simone Pascucci¹, Francesco Rossi¹⁻³, Federico Santini¹, Tiziana Simoniello¹, Vanguri Rajesh³

¹ Institute of Methodologies for Environmental Analysis (IMAA)- Italian National Research Council (CNR), C. da S.Loja, 85050 Tito Scalo, Italy

² Istituto per le Applicazioni del Calcolo "Mauro Picone" –(IAC)- Italian National Research Council (CNR), Via Pietro Castellino 111, 80131 – Napoli, Italy

³ Scuola Ingegneria Aeronautica (SIA), University of Rome "La Sapienza", Via Eudossiana 18, 00184 Roma, Italy

Keywords (5): PRISMA, land degradation, Land Use, vegetation,

Challenge

The project "Development of PRISMA Prototype Algorithms for estimating environmental damage and Vulnerability to land degradation" (SAPP4VU), funded by ASI, aims at developing processing methods and algorithms for the full exploitation of PRISMA data to assess the vulnerability of ecosystems related to slow dynamic phenomena (e.g. Land Degradation) as well as to extreme events (e.g. fires, floods, extreme weather events). This is to foster sustainable and climate-smart farming strategies.

We selected a study area (Metaponto plain, South Italy) having both healthy and degraded condition to evaluate the PRISMA capability in ecological equilibrium assessment. For ecosystem damages and post-damage recovery, different study sites were selected across the Italian peninsula.

In this context, the SAPP4VU main objectives are to develop and optimize techniques and algorithms for new product development from PRISMA data to monitor ecosystems exposed to anthropogenic and meteo-climatic forcing.

Methodology

The technical part of the project can be divided into blocks: PRISMA pre-processing, Algorithms & variable estimation, Realization of prototype products, and Validation Plan. At this stage of the project, the two initial blocks are approaching the final results and are pertaining to this communication.

The first block involves a preliminary methodological activity aimed at optimizing the PRISMA data processing chain which includes a review of the quality of PRISMA data based on the state of the art correction methods of image denoising/de-stripping algorithms for radiance processing level and the algorithm improvement for cloud masking and atmospheric correction (i.e. including DEM and adjacency effects) comprising the evaluation of the usefulness of applying a BRDF correction.

The second block regards the ecosystem spatial description and the vegetation parameter retrievals. The former is developed by optimizing a) clustering techniques and b) machine learning and deep learning classification techniques to identify the spatial pattern of the main agro-forestry cover classes (i.e. ecosystems description). The optimum band selection (among 188 indices) was done by Random

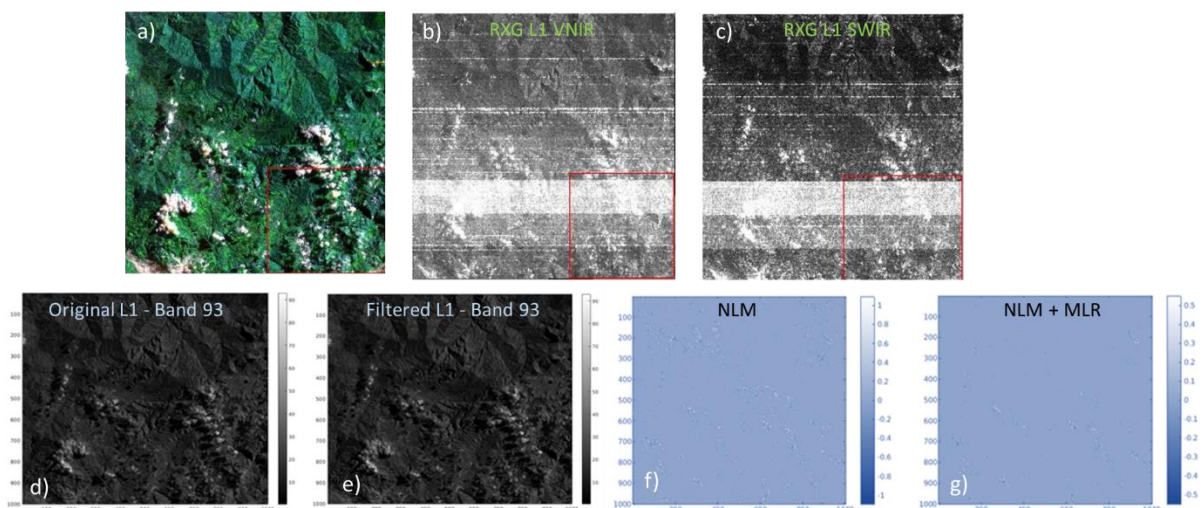
Forest algorithm and a hybrid approach (the combination of RTM and MLR techniques) was used to retrieve the biophysical variables.

At present four PRISMA images have been acquired in the 2023 summer/autumn season.

Results

Results related to the first processing block include the implementation of techniques for de-stripping, noise characterization and reduction in a dedicated Python pipeline. Specifically, along with the well-known Variational Stationary Noise Remover (VNSR) and Non-Local Means (NLM) algorithms, that have been tailored for PRISMA images, a robust procedure for the identification of both photon and thermal noise has been developed and tested on images of different sites and seasons. For cloud detection, the PRISMA L1 cloud mask product has been considered as a starting point to be improved by using some specific machine learning algorithms, already applied for this task on different sensors by some of the authors. Preliminary results show room for a better identification of cloudy pixels with this methodology.

For the second block related to the ecosystem spatial description and the vegetation parameter retrievals, a set of different vegetation indices (188) was evaluated. As direct methods may not always capture the full complexity of vegetation indices, which can vary based on plant species, growth stage, and environmental conditions, we used the spectral signatures of various tree species and training a random forest classification algorithm to determine which indices are most essential for distinguishing between species. As a result, we were able to identify a set of 85 indices out of 188 evaluated that are more performing in forest species detection.



Examples of noise detection on PRISMA L1 bands: First row, RGB image (a), identification of stripes with an RX global algorithm on a VNIR (b) and SWIR band; Second row, an original (d) and filtered (e) L1 band (B93 -1240nm) and its relative noise estimated with Non Local Means (NLM) alone (f) and coupled with multiple linear regressions (MLR) (g) for the Pignola site (Southern Italy).

Outlook for the future

On the base on the ongoing acquisition phase on the test areas that involves PRISMA and hopefully EnMAP in the future, the further steps will include the development of procedures to: a) derive and integrate LST time series at a scale suitable to PRISMA resolution; b) address the critical need for higher spatial resolution in hyperspectral data analysis, focusing on enhancing PRISMA satellite images from 30 meters to 10 meters by integrating them with Sentinel-2 data; c) the setup of a clustering procedure of the retrieved biophysical PRISMA parameters normalized by land cover; and d) apply a Random Forest procedure trained with the clusters previously identified to detect anomalies in vegetation cover following an extreme weather event, pest attack, pollution, etc.

Quantify Non-Photosynthetic Vegetation (NPV) fraction in the Kenyan Grasslands through Unmixing Hyperspectral Remote Sensing Data

Rodolfo Ceriani^{1,2}, Francesco Fava², Katayoun Fakhherifard⁵, Giulia Tagliabue³, Micol Rossini³, Sonja Leitner⁴, Cinzia Panigada³, Vincent Odongo⁴, Valentina Vaglia², Paul Mutuo⁴, Kelvin Kinuthia⁴, Monica Pepe⁵

¹ DISAA, Department of Agricultural and Environmental Sciences, University of Milan, Milan, Italy, rodolfo.ceriani@unimi.it

² ESP, Department of Environmental Science and Policy, University of Milan, Milan, Italy, francesco.fava@unimi.it

³ DISAT, Department of Earth and Environmental Sciences, University of Milan-Bicocca, Milan, Italy, giulia.tagliabue@unimib.it, micol.rossini@unimib.it, cinzia.panigada@unimib.it

⁴ Mazingira Centre for Environmental Research and Education, International Livestock Research Institute (ILRI), Nairobi, Kenya, s.leitner@cgiar.org

⁵ IREA, National Research Council, Milano, Italy, pepe.m@irea.cnr.it

Keywords (5): Earth Observation, Grasslands, Hyperspectral, Non-photosynthetic Vegetation, PRISMA

Challenge

Non-photosynthetic vegetation (NPV), because of its key role in water, nutrient, and carbon cycling, is an essential variable to monitor in agroecosystems. Despite its importance, the literature about NPV quantification from satellite in rangeland systems, where NPV plays an important role for animal nutrition, is still limited.

New generation hyperspectral satellites, such as PRISMA (PRecursore IperSpettrale della Missione Applicativa), offer unprecedented research opportunities in fields that were previously only investigated by proximal and aerial sensing. Hyperspectral sensors provide high spectral resolution, and particularly in the shortwave infrared, where the spectral features of carbon-based constituents of plants are distinctive, thus allowing for better characterization of NPV.

The goal of this study is to demonstrate a quantitative method for mapping NPV in semi-natural grasslands using PRISMA hyperspectral imagery, allowing us to better understand the distribution and abundance of non-living vegetation.

Methodology

The study site is Kenya's Kapiti Research Station and Wildlife Conservancy area (Fig. 1). A PRISMA scene was acquired on January 19th, 2023. The bottom of atmosphere reflectance standard product (L2D) was pre-processed to obtain a more accurate geocoding by applying AROSICS python package.

A field campaign was conducted on the week of January 18th-22nd, 2023, measuring ground reference spectra for validation of PRISMA reflectance, and of the NPV prediction model. A total of 26 (Fig. 1) plots were established across 4 main areas: for each plot, the reflectance was acquired with a full-range (0.35 to 2.5 μ m) portable spectrometer together with nadir digital images of the sensor field of view. The digital images were processed to estimate the NPV and soil cover fractions. This enabled us to

create a dataset containing the NPV and bare soil fractional cover, together with the corresponding reflectance resampled to align with PRISMA spectral bands.

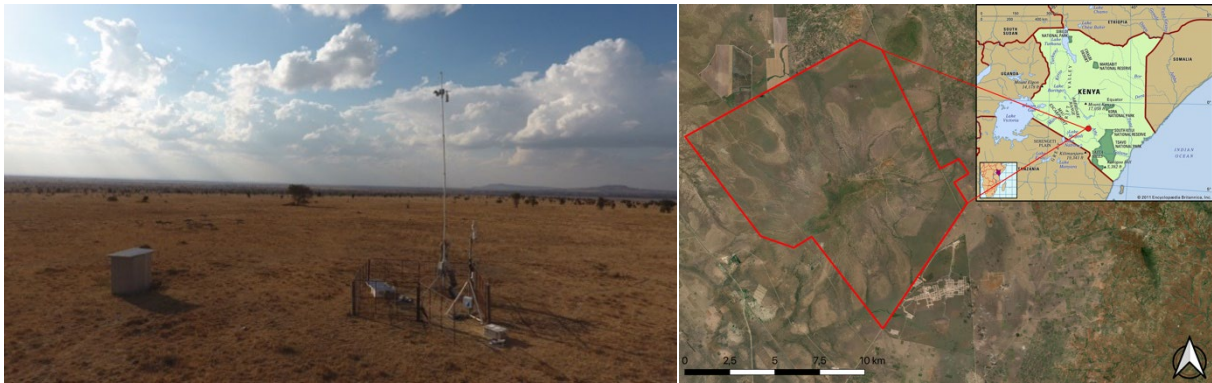


Figure 1 Kapiti research station during the dry season (on the left). The 4 study areas where the 26 plots were sampled during the field campaign (on the right).

An NPV prediction model, originally developed to quantify NPV of intensive crops, was adapted and tested for this study. The model was trained using a USGS spectral library, containing nearly 900 in-situ surface reflectance spectra collected from different farmlands in North America. The Gaussian Exponential Optimization (EGO) of selected absorption bands was first applied to the spectra in the USGS spectral library. Then, a machine learning algorithm (i.e., Random Forest - RF) was used to find a non-linear regression between the absorption bands characteristics (band depth, width, center, and asymmetry) extracted by EGO and the corresponding NPV percentages.

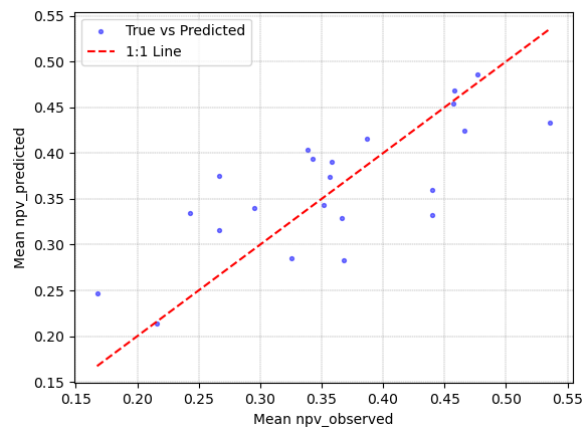


Figure 2 Statistical analysis on NPV abundance observed and predicted by the RF model, calibrated with nadiral images and spectral signatures (R^2 : 0.73, MSE: 0.017, RPD: 1.93).

Results

Statistical analyses revealed that the model could be adapted for use in rangeland (Fig. 2). Despite the vast differences in vegetation and soil chemistry between intensive crops and semi-natural grasslands, the model's training on a large spectral library proved to be robust enough. This model based on key-feature absorption bands represents a new methodology that could be used for NPV mapping in grassland domain.

Based on good performances on spectral libraries the RF model was applied to the PRISMA image, to generate a map of NPV fraction for the study area (Fig. 3). The resulting map was generated from the PRISMA scene acquired on January 19th, co-occurrent with the field campaign (Fig. 4).

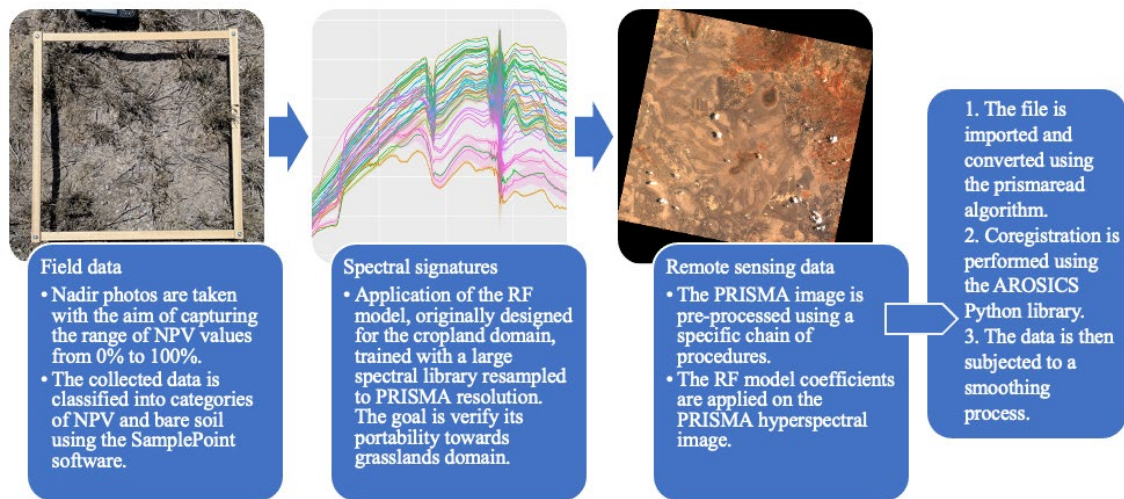


Figure 3 Workflow used for obtaining NPV quantification map from PRISMA image, pre-processed to correct some geocode and spectral noises problems.

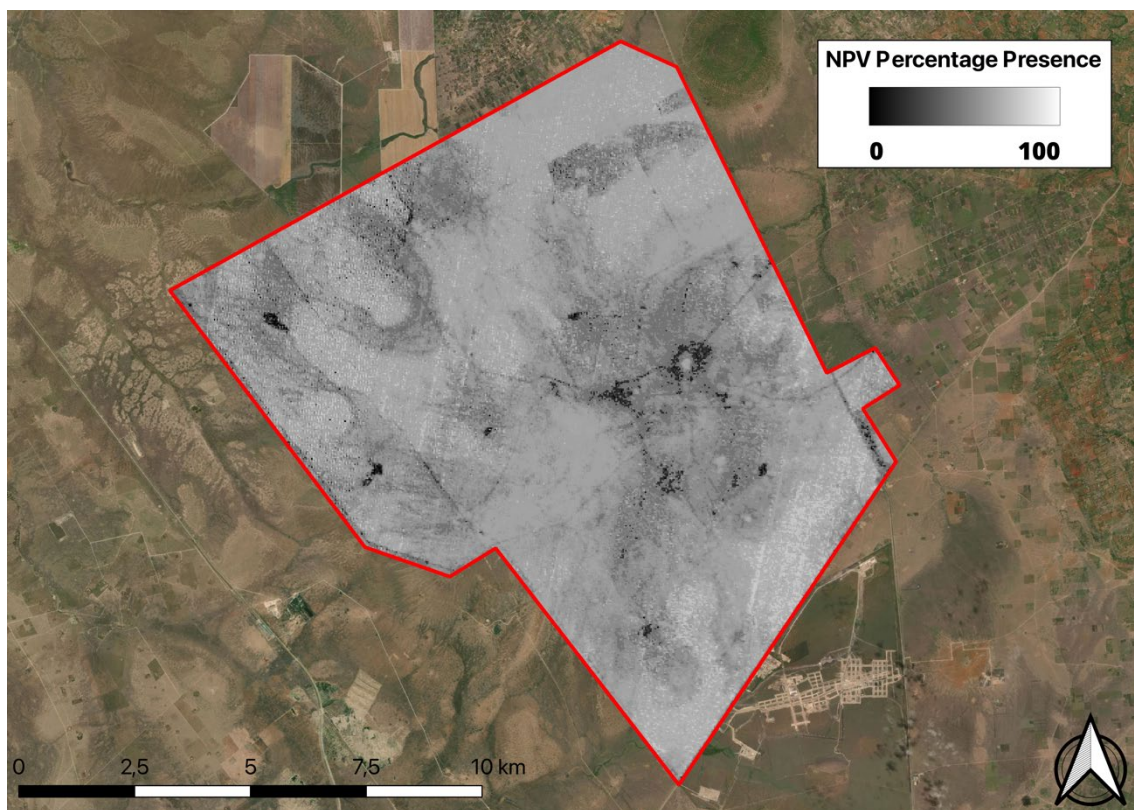


Figure 4 NPV quantification map generated for the study area, applying the RF model on the PRISMA image.

Outlook for the future

The results are highly promising as the model demonstrates adaptability and versatility and the NPV map shows realistic spatial patterns, based on our knowledge of the territory and vegetation characteristics during the study period. This shows the potential of PRISMA hyperspectral data to map NPV on semi-natural ecosystems characterized by high spatial heterogeneity. Quantifying NPV fraction is crucial for assessing and monitoring the health of arid and semi-arid rangelands, understanding vegetation dynamics, and supporting improved grazing management.

The next planned steps for the study include the accuracy assessment of the map using independent ground data collected during PRISMA acquisition, the testing of the algorithm at different times to capture temporal variability and the evaluation of a similar modelling approach for retrieving dry biomass.

Explorative Analysis for Assessing Wheat Yield and Grain Protein Content with Machine Learning and PRISMA Hyperspectral Data

EARSel Valencia 2024
Abstract
Corresponding Author:
ranghetti.m@irea.cnt.it

Marina Ranghetti^{2,1}, Mirco Boschetti¹, Francesco Nutini¹, Micol Rossini², Gabriele Candiani¹

¹ IREA, National Research Council, via Corti 12, 20133 Milano, Italy

² Remote Sensing Of Environmental Dynamics Lab., Dip. Scienze dell'ambiente e del territorio, Università Milano-Bicocca, 20126 Milano, Italy

Keywords (5): Yield, Grain Protein Content, PRISMA, Machine Learning, Remote Sensing

Challenge

Estimating yield and Grain Protein Content (GPC) is of crucial importance in modern agriculture. Within the framework of the Sustainable Development Goal 2 outlined in Agenda 2030, which aims to end hunger, achieve food security and promote sustainable agriculture, accurate yield and GPC prediction is essential for effective resource allocation and ensuring food availability. In recent years, remote sensing and machine learning (ML) techniques have emerged as powerful tools for their estimation. Spaceborne hyperspectral data may open new opportunities for the development of new methodologies. In this context, this work aims to explore the potential of ML techniques to estimate wheat yield and GPC from hyperspectral spaceborne data. Specifically, we want to assess the robustness of the ML combined with dimensionality reduction techniques, the impact of the crop phenological phase and the capabilities to estimate, prior the end of season, these parameters in a real farming condition.

Methodology

The test site is located North-East of Italy. From 2020 to 2022, close to the harvesting period, in-situ campaigns were carried out in different durum and soft wheat fields to quantify yield and GPC for a total of 101 and 90 samples, respectively. The EO dataset consists of 13 images acquired by the PRISMA hyperspectral imaging satellite. Each PRISMA image underwent preprocessing operations to obtain a co-registered and smoothed reflectance spectra product. The assessment of yield and GPC was performed for each year and available PRISMA date, separately, using Machine Learning Regression Algorithms (MLRA), which require a set of input-output pairs as training database. Two types of inputs were used to train the algorithms: i) PRISMA reflectance spectra (SP), or ii) a set of crop traits (TR), which include chlorophyll content (CCC), nitrogen content (CNC) and leaf area index (LAI) estimated from PRISMA spectra using a hybrid approach. The output corresponds to yield, GPC and their product (YGPC). The training phase was performed using two ML regression algorithms: Partial Least Square Regression (PLSR) and Gaussian Process Regression (GPR). The MLRAs were run by applying the Principal Component Analysis (PCA) as dimensionality reductions to the inputs. The performance of all model combinations (2 ML algorithms×3 crop traits×2 input sources×13 PRISMA dates) was assessed through a k-fold cross-validation technique and the best model configuration was assessed.

Results

Results showed that the performances of the tested MLRA combinations markedly differed depending on the analysed dates and parameters. Table 1 provides a summary of the best results obtained for the tested configuration of MLRA, input and output variable. Generally, the tested algorithms allowed to obtain quite accurate estimation of yield and YGPC, with best nRMSE ranging from 13% to 17%, in specific dates of the three investigated years. GPC estimation proved to be more challenging with nRMSE ranging in the best case from 22% to 24% and no significant correlation between estimated and measured GPC

values in 2020. The good correlation value obtained in 2021 is spoiled by outliers. Among the two ML algorithms tested in this study, considering yield and YGPC results, PLSR generally performed better than GPR. According to the results, the best image acquisition period for the estimation of the considered parameters corresponds to the early grain filling phenological phase. During that phase, good performances were obtained for all the investigated variables, except for GPC model, thus, YGPC resulted as a good candidate for future estimation of grain nitrogen uptake which is considered a proxy of grain quality. Finally, the comparison between models generated with different sources of input showed that direct use of reflectance information from of hyperspectral data provided slightly better results than using crop traits estimations as input.

Table 1. Best model performance (R2 and nRMSE) for yield, GPC and YGPC estimated according to the year of the dataset (2000, 2021 and 2022), ML (PLSR, GPR) and input (SP - spectral data and TR - crop traits).

Year	ML input	Yield				GPC				YGPC			
		PRISMA date	ML	R2	nRMSE	PRISMA date	ML	R2	nRMSE	PRISMA date	ML	R2	nRMSE
2020	TR	23/05/2020	PLSR	0.49	15%	07/04/2020	GPR	0	24%	23/05/2020	PLSR	0.47	16%
	SP	23/05/2020	PLSR	0.58	13%	23/05/2020	GPR	0.11	22%	23/05/2020	PLSR	0.49	15%
2021	TR	24/04/2021	PLSR	0.48	17%	23/05/2021	GPR	0.34	25%	24/04/2021	PLSR	0.32	18%
	SP	04/06/2021	PLSR	0.46	17%	23/05/2021	GPR	0.52	20%	21/06/2021	PLSR	0.47	16%
2022	TR	12/05/2022	GPR	0.31	19%	12/05/2022	PLSR	0.06	30%	12/05/2022	PLSR	0.06	28%
	SP	12/05/2022	PLSR	0.46	17%	12/05/2022	PLSR	0.44	24%	12/05/2022	PLSR	0.65	17%

Outlook for the future (800 - 1000 characters incl. spaces)

This work explored machine learning methods for the estimation of yield, GPC and YGPC considering as input reflectance or crop traits estimations from hyperspectral data. In general, the proposed method showed good performance for the estimation of yield and YGPC during early grain filling period, while the estimation of GPC proved to be more challenging. Future and ongoing activities involve generation and validation of ML models by means of a multi-year wheat dataset, also exploiting the field data collected during 2023, which includes around 40 samples of both yield and GPC. The new multi-year dataset (from 2020 to 2023) has been created only using the PRISMA images closest to early grain filling period. It is essential to analyse the performance of various machine learning algorithms during both the training and validation phases. Figure 1 displays preliminary validation results for a yield multi-year model created through the training of a Random Forest with fine-tuned parameters.

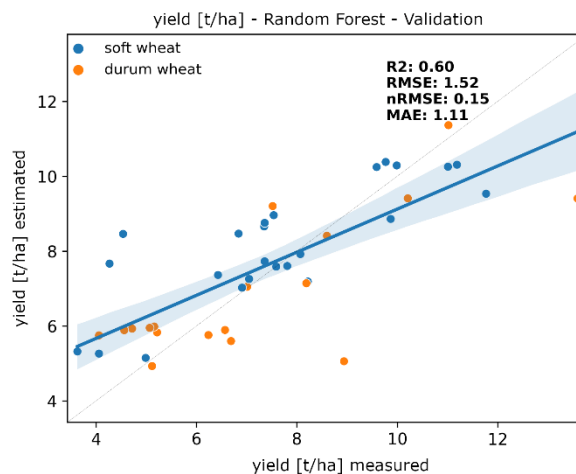


Figure 1. yield validation scatterplot using random forest algorithm.

Acknowledgements

This work is carried out within the framework of the Project "EO4NUTRI - Earth Observation for estimating and predicting crop nutrients" in response to EXPRO+ ESA AO/1-11144/22/1-EF FOR AGRICULTURE SCIENCE PRECURSORS and with the contribution of the DIITET project "DIT.AD022.207 – STRIVE - La Scienza per le TRansizioni Industriale, Verde, Energetica (FOE 2022)", sub task activity "Agro-Sensing – "2.0".

Early- Season Crop Mapping Using PRISMA image and Machine and Deep Learning Techniques

EARSeL Valencia 2024

Abstract

Corresponding Author: [sahammirzaei@cnr.it]

Saham Mirzaei¹, Stefano Pignatti¹, Maria Francesca Carfora², Francesco Rossi¹⁻³, Simone Pascucci¹, Federico Santini¹, Angelo Palombo¹

¹ Institute of Methodologies for Environmental Analysis (IMAA)- Italian National Research Council (CNR), C. DA S.LOJA, 85050 Tito Scalo, Italy

² Istituto per le Applicazioni del Calcolo "Mauro Picone" –(IAC)- Italian National Research Council (CNR), Via Pietro Castellino 111, 80131 – Napoli, Italy

³ Scuola Ingegneria Aeronautica (SIA), University of Rome "LA SAPIENZA", Via Eudossiana 18, 00184 Roma, Italy

Keywords: Crop Mapping, Machine Learning, Deep Learning, PRISMA

Challenge

Early-season crop mapping could be useful for estimating the under-cultivation area and yield which are vital information for marketing and decision-making for food security. Most of the developed post-season crop mapping methods are based on time-series analysis of the multispectral images of all growing season data. Hence, early-season crop mapping still is an interesting topic for research studies. Hyperspectral data provided by point spectroscopy and airborne sensors have successfully been used for crop mapping in the different growing stages even with one-shot measurement. Moving from proximal/airborne levels to spaceborne level is a hard task, because of the lower signal/noise ratio, spectral mixing and atmosphere attenuation. The present study, developed within the SAPP4VU and PRISM4VEG projects, supported by the Italian Space Agency (ASI), aims to consider the capability of PRISMA images for early-season crop mapping using machine and deep learning techniques.

Methodology

This study was done in two farms: the Maccarese in central Italy (latitude 41°52'18"N, longitude 12°14'05"E, altitude 8 m a.s.l., annual precipitation 812.9 mm) and the Jolanda in north-east Italy (latitude 44°52'59" N, longitude 11°58'48" E, altitude 1 m a.s.l., annual precipitation 691 mm). Wheat, barley, herbage, hybrid grain (i.e. triticale), fava beans, pea and thistle weed to identify non-cultivated fields, were considered. Support Vector Machine (SVM) and 3-Dimensional Convolutional Neural Networks (3D-CNN) techniques have been used for classifying the images. For SVM, radial basis function (RBF) kernels with optimized C and gamma coefficients were used. The 3D-CNN was trained by an initial learning rate of 0.001 for 20 epochs, a 256 batch size, momentum 0.9, learning rate factor 0.01, and Adam optimization. PRISMA images acquired on 2021/04/01, 2021/05/17, 2022/04/12, 2023/02/02, and 2023/03/21 in the Maccarese site and 2021/04/24, 2022/04/30, 2022/05/12, 2023/03/04, and 2023/05/24 in Jolanda site have been used. PRISMA L2D images were co-registered with the closest Sentinel-2 image to assure the co-registration (of about 0.5pixel of RMS) and smoothed by Savitzky-Golay filter (frame size of 7, 3rd degree polynomial). The dimensions of images (150 bands after band removal) were reduced by the Principal Component Analysis (PCA) approach and then PCs were normalized. The pixels of each image are randomly divided into training (70 %) and test sets (30 %).

Results

An optimum of 13 PCs were selected for the PRISMA image dimension reduction. An optimum spatial window size of 7 pixels was selected for 3D-CNN, based on Overall Accuracy (OA). The optimum coefficients for SVM were $C=1.27$ and $\gamma=1$. The 3D-CNN method (OA = 88 %) produces a better result than the SVM method (OA = 77 %) for classifying the abovementioned 7 species. Better accuracy of the 3D-CNN method could be related to taking advantage of the spatial information besides spectral data, while the SVM method is only based on spectral data, and considers each pixel as independent data. Among the species, barley showed the lowest user accuracy (SVM = 71 % and 3D-CNN = 84 %). The reason could be related to the similarity between the spectral signature and the growing calendar of barley and wheat species which leads to higher commission errors. The thistle weed showed the highest user accuracy (SVM = 80 % and 3D-CNN = 91 %). Classification errors in field edge pixels are higher than in central pixels, which is related to spectral mixing with neighbour fields with no similar cultivation; it is also related to the presence of trees/brushes surroundings the cultivated fields. A negative 30-meter buffer (1 pixel) in the edge of fields results in 1 %, and 3 % improvement in the overall accuracy of classification by 3D-CNN and SVM, respectively.

Outlook for the future

PRISMA images are not available regularly with fine temporal resolution. The date of image acquisition is important because the spectral signature of the plant changes during the growing season as biophysical parameters change. To fill this gap, the images of the available hyperspectral satellites like EnMAP and EMIT, and the upcoming missions like CHIME and PRISMA-2 will be analysed. Moreover, the combination of PRISMA images and other fine-temporal resolution satellite data like Sentinel-2 which has the capability to derive the phenological metrics should be considered for future research. As regards the tested algorithms, the efficiency of the 3D-CNN on 30 meters-resolution images is limited by the presence of small-size fields. Future work should explore the usefulness of sharpening techniques to overcome the spatial resolution problem.

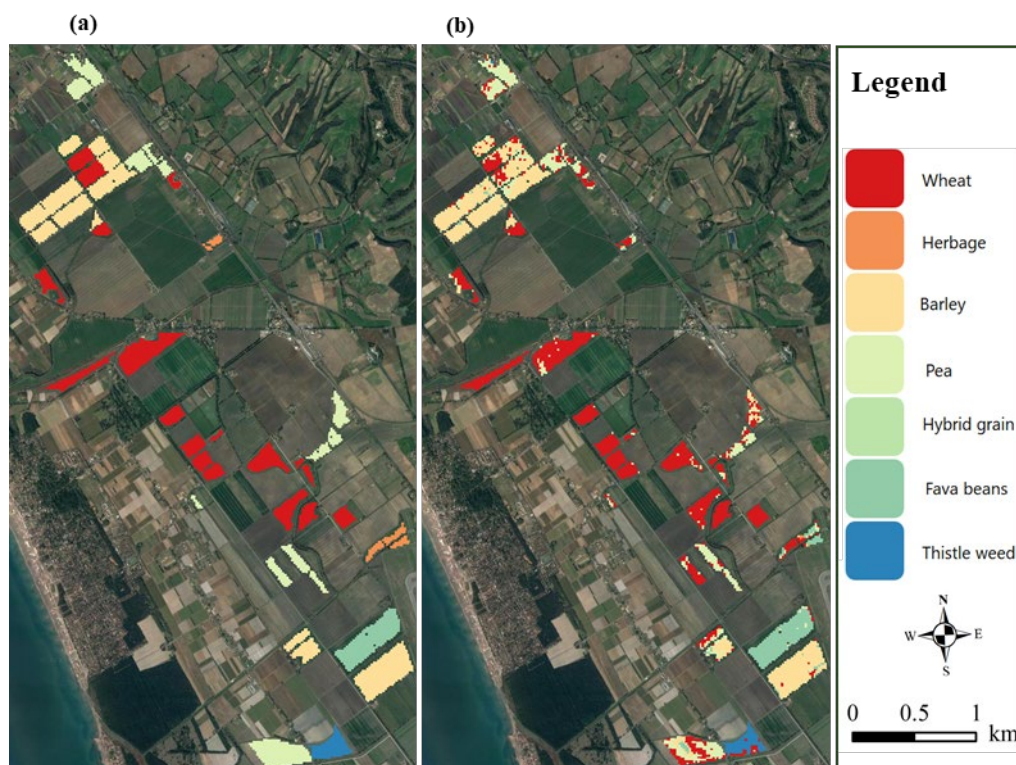


Figure 1. (a) Ground truth map and (b) produced map by Support Vector Machine (SVM) for winter-2021 season cultivation of Maccarese site.



Figure 2. (a) Ground truth map and (b) produced map by 3-Dimensional Convolutional Neural Networks (3D-CNN) method for winter-2022 season cultivation of Jolanda site.

Radiometric evaluation of the updated version of the hyperspectral PRISMA products

Andrea Pellegrino^{1,2}, Alice Fabbretto^{1,3}, Mariano Bresciani¹, Federica Braga⁴, Vittorio Ernesto Brando⁵, Salvatore Mangano¹, Claudia Giardino¹

¹ Institute for Electromagnetic Sensing of the Environment, National Research Council (CNR-IREA), Milano, Italy

² University of Sapienza, Department of Engineering, Roma, Italy

³ Tartu University, Department of Remote Sensing, Tartu, Estonia

⁴ Institute of Marine Sciences, National Research Council (CNR-ISMAR), Venice, Italy

⁵ Institute of Marine Sciences, National Research Council (CNR-ISMAR), Rome, Italy

Keywords (5): Earth Observation, Inland water, Hyperspectral, Radiance, Reflectance

Challenge

In remote sensing, validation is a fundamental process, which provides a quantitative assessment of suitability of satellite observations for the intended use of the data and applications, and their compliance with mission requirements. Therefore, also Imaging spectroscopy missions take a great advantage from calibration/validation approaches that help to track the uncertainties associated with instrument noise, algorithms performance to first generate reflectance and then downstream products, as well as to verify the calibration of satellites in orbit. In this study, it is provided an assessment of hyperspectral PRISMA products, by using in-situ reference measurements. Particularly, focusing on evaluating the differences of radiance data (L1) before and after the most recent calibration update of PRISMA instrument. Furthermore, the differences in the downstream reflectance products (L2) have been evaluated for completeness. L1 will be analysed over the PRISCAV project study areas, while the L2 intercomparison is extended to few more lakes.

Methodology

The evaluation of the two versions of the PRISMA L1 products was carried out in terms of radiance at TOA according to the degree of agreement obtained between the satellite observations and in-situ measurements. The analysis was performed over the inland water sites defined in the PRISCAV project (Garda and Trasimeno lakes). In-situ reflectance data were obtained from autonomous radiometers mounted on fixed platforms, that carry out continuous hyperspectral measurements (i.e. WISPstation and HYPSTAR). To obtain radiance data comparable with L1, the in-situ reflectance measurements were propagated to the TOA by using the radiative transfer 6S code. PRISMA L1 products, both versions, were spectrally evaluated through the calculation of residuals between satellite and simulated in-situ radiances. For the evaluation of PRISMA L2 products, an analytical comparison was performed with reference in-situ data. The latter were also extracted from autonomous radiometers, by also adding three more lakes for which global AERONET-OC multispectral data were available. The evaluation was performed by means of a statistical analysis considering the common Coefficient of determination (R^2) and the Root Mean Square Error (RMSE). In order to perform the statistical analysis, the hyperspectral in-

situ data were spectrally resampled according to PRISMA band setting, while in the case of multispectral data, the PRISMA bands closest to the corresponding bands of in-situ measurements were selected.

Results

The residuals calculated for the PRISMA L1 in terms of radiance, shown in Figure 1, illustrated that in the case of Lake Garda (clear deep water) the new version of the L1 fits better, while for Lake Trasimeno (turbid shallow water) the old version fits better and there is for both versions a greater standard deviation.

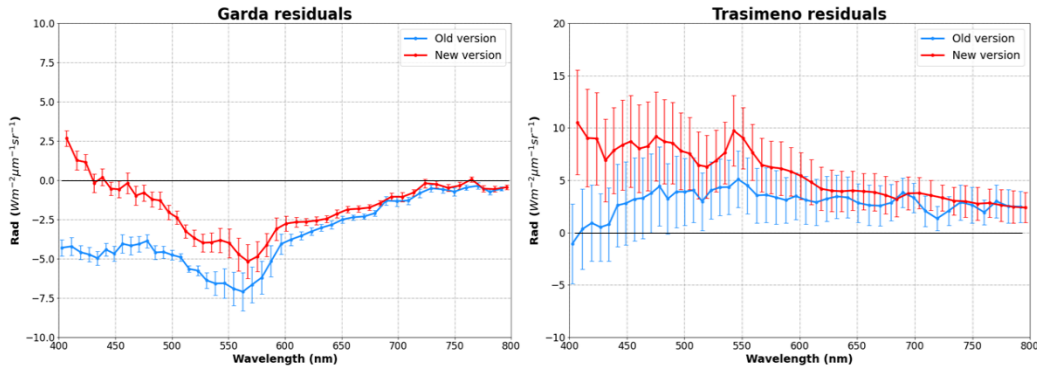


Figure 1- Residuals (Rad, $Wm^{-2}\mu m^{-1}sr^{-1}$ units) of TOA radiances between PRISMA and simulated in-situ data for the two different versions (v3.9-2 old version and v4.1-0 new version). Five images over Lake Garda and five over Lake Trasimeno are considered in the comparison. The bars show the standard deviation.

For the L2 analysis, performed in terms of Reflectance remote sensing (Rrs), in addition to Garda and Trasimeno lakes of the PRISCAV project, the following three lakes (presented in Pellegrino et al., 2023, Remote Sensing, 15) were considered: Vänern (oligotrophic state with high CDOM concentration), Erie (affected by the presence of phytoplankton blooms) and Okeechobee (characterised by humic-rich waters). In this case, scatterplots were generated for all bands common to PRISMA and in-situ observations. Figure 2 shows examples for the 443 nm, 560 nm and 667 nm bands. Overall, the best accordance for L2 products from the two different versions and in-situ measurements occurs in the green and in the red regions, while the blue region shows lower correlation. Furthermore, the disagreement is generally represented as an overestimation of PRISMA Rrs spectrum compared to the in-situ measurement. Statistically based, a lower RMSE (of about $0.002 sr^{-1}$) was obtained in the case of L2 derived from the old version L1 than that obtained from the L2 derived from the new version; while the R^2 value remained almost unchanged (highest value reached for the case of the 560 nm band, about 0.7).

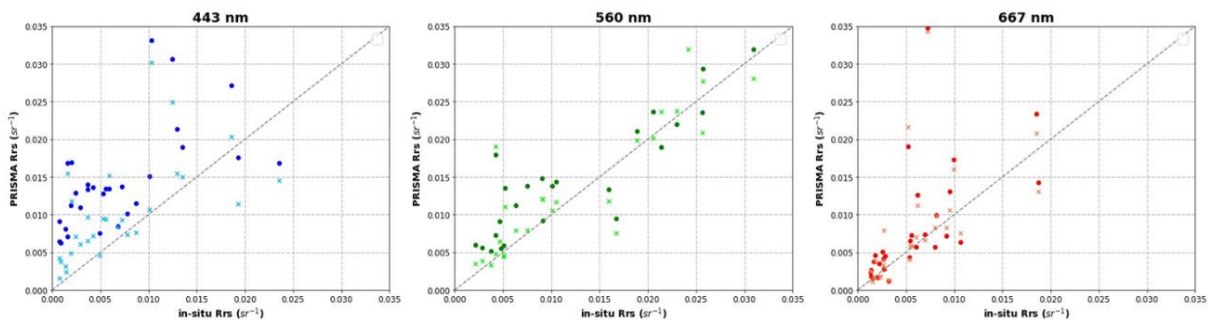


Figure 2-The scatterplots show the PRISMA Rrs (sr^{-1}) on the y-axis and the in-situ Rrs (sr^{-1}) on the x-axis at three wavelengths. In total, 25 images are used for analysis. The comparison between satellite and in-situ observations is considered within a ± 1 h time window. The darker dots represent PRISMA L2 products from the new version of the L1 and the lighter crosses represent PRISMA L2 products from the old version of the L1. The dotted line represents the 1:1 line.

Outlook for the future

Assessing uncertainties in hyperspectral data products is a challenging task and validation activities are crucial and need to be performed periodically over the lifetime of a satellite mission. This allows to obtain satellite products that are increasingly accurate and representative of the actual state of an observed aquatic site, so that they can be used to support water management activities. In particular, having a good characterisation of the state of a lake also makes it possible to perform studies of the current environmental crisis, since lakes are considered sentinels of climate change, as they respond sensitively and rapidly to climatic and hydrological changes in catchment areas. This work will be extended by considering coastal water sites, to evaluate in sites with different optical water characteristics how the accuracy of satellite products varies; this activity could also provide valuable information in view of the future hyperspectral missions such as PRISMA-2G and CHIME.

Assessing PRISMA imagery for soil organic matter prediction in a complex forested area: An ensemble machine learning approach

Francisco M. Canero, Victor Rodriguez-Galiano
(Style: Authors, *presenting author underlined*)

UNIVERSITY OF SEVILLA, DEPARTMENT OF PHYSICAL GEOGRAPHY, SPAIN

KEYWORDS (5): PRISMA, HYPERSPECTRAL, MEDITERRANEAN, SIERRA DE LAS NIEVES, ENSEMBLE LEARNING

Challenge

Soil mapping could be benefited from different remotely sensed data sources, including novel satellite hyperspectral missions such as PRISMA, EnMAP or DESIS, and forthcoming CHIME or SGB. These missions will provide unprecedented data recording vis-NIR and SWIR spectra for large areas of the earth. Although soil imaging spectroscopy has proven reliable to predict soil properties in bare soil, few research has evaluated the use of hyperspectral remote sensing in other land covers. Other approaches such as deriving narrow-band indices could relate soil properties with overlying vegetation spectra. Hence, these images might improve soil mapping frameworks together with innovative modelling approaches such as ensemble learning and Feature Selection methods. This study aimed at assessing hyperspectral data from PRISMA for soil organic matter (SOM) prediction and mapping in Sierra de las Nieves, a complex forested Mediterranean area in southern Spain.

Methodology

Ninety-two soil samples were taken from Sierra de las Nieves (SN), southern Spain. In this study, a L2D PRISMA image captured over SN on 17 February 2022 was used, removing noisy and atmospheric water-absorption bands. A predictive dataset was constructed combining 194 raw PRISMA bands, 58 narrow-band indices derived from the Vegetation Indices Toolbox of EnMAP-Box, and 13 terrain features derived from Digital Elevation Model of Spanish Geographical Service. A two-step modelling framework was built based on an ensemble learner built with Random Forest, using four base learners (Random Forest, Support Vector Machine, Extreme Gradient Boosting trees and Neural Networks), followed by a wrapper-based sequential Feature Selection method. A hyperparameter tuning was performed for each base learner and for the ensemble model. Interpretation of results were driven by three methods: i) a bivariate correlation analysis between SOM and each feature, ii) the results of Feature Selection, and iii) Accumulated Local Effect, an explainable machine learning method. A 4-fold cross validation was performed to get the performance measures, both in hyperparameter tuning and Feature Selection procedures. Two performance measures were used in this study, R^2 and root mean squared error (RMSE).

Results

The best results were achieved using the ensemble learner alone, achieving a R^2 of 0.193 and RMSE of 5.93, while ensemble with Feature Selection got a R^2 of 0.07 and a RMSE of 6.349. The RMSE results of the base learners ranged from 6.24 (Neural Network) to 7.92 (eXtreme Gradient Boosting). The NIR bands of PRISMA showed the higher correlations with SOM, achieving values higher than 0.3. The two narrow-band indices with the highest correlation with SOM were CRI and CRI2 (0.41 and 0.42, whereas Channel Network Base Level was the terrain feature with higher correlation (0.31). The model with Feature Selection only selected a feature, which could explain its lower performance compared with the ensemble alone (with all features). The feature selected was 1099 nm band, a NIR feature for which the Accumulated Local

Effect (ALE) showed a positive relation, that is, lower reflectance values were related with lower SOM values, while higher SOM values were associated with higher reflectance in 1099 nm band. Mapping results depicted higher SOM values concentrated in areas with higher altitude and forested areas of the study area, and lower values outside the protected area, where the main land cover is associated with agricultural areas.

Outlook for the future

Those results underpinned that SOM modelling is suitable using hyperspectral data derived from PRISMA imagery, achieving acceptable results considering the variability of SOM target data and the high number of features. The spatial patterns were coherent with land cover distribution in the study area, relating higher values with forested covers such as trees, shrublands and grasslands, and lower values with agricultural areas. The NIR band selected suggested that PRISMA can represent indirectly this feature through spectral signal, therefore further research evaluating hyperspectral data in other geographical areas should be carried. The results of ensemble modelling showed the improved performance of ensemble with all features, being useful in avoiding the limitations of each base learner. However, novel methods should be assessed and included in the ensemble, such as other learners or Feature Selection methods

Figures

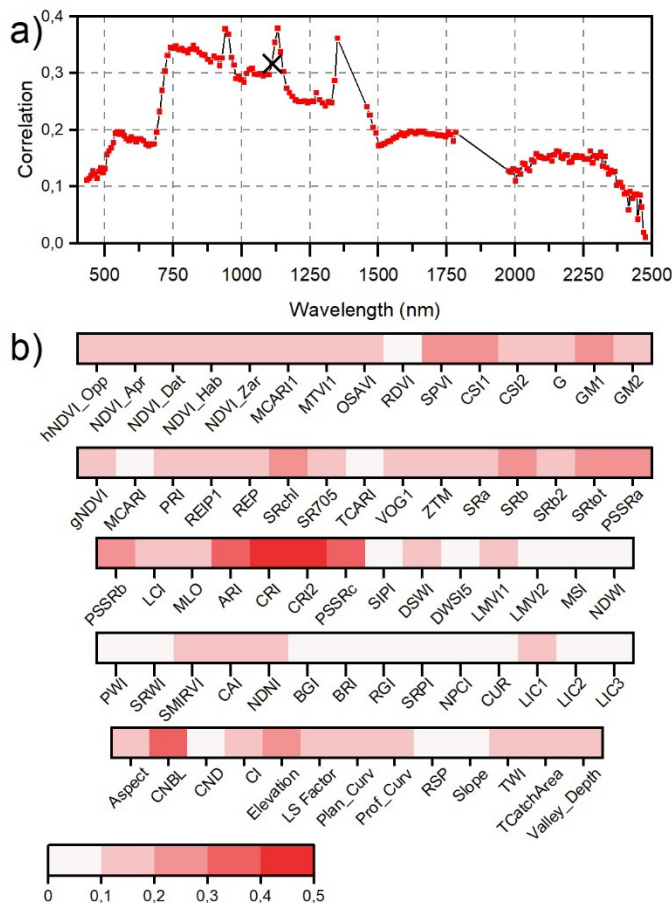


Fig. Pairwise absolute correlation a) between SOM and PRISMA bands (above) and b) narrowband indices and terrain features with SOM (lower). Each dot in a) denotes individual band. Crosses indicate which features were selected by ensemble model using hyperspectral dataset.

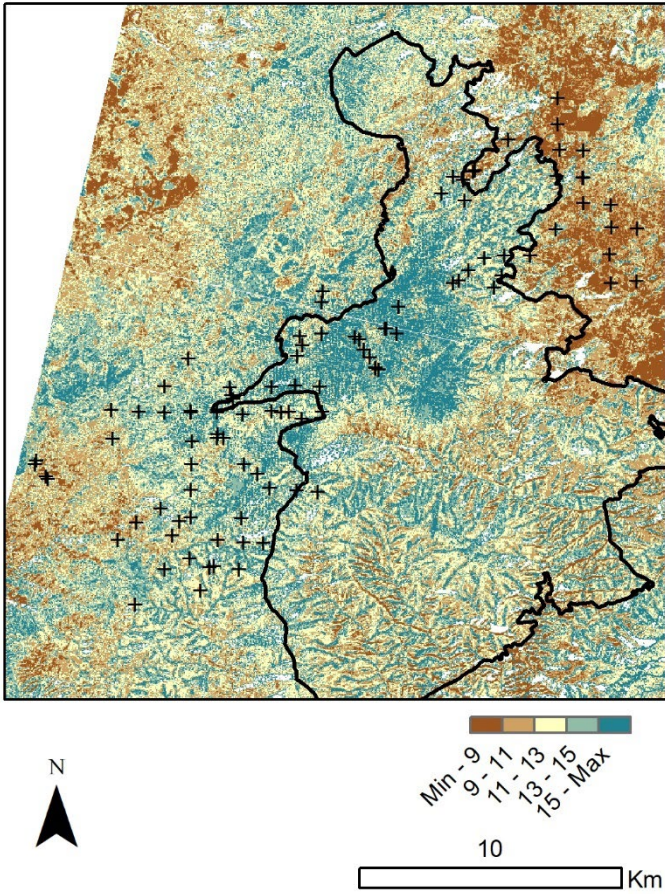


Fig. Spatial prediction of SOM using the ensemble model alone.

Characterization of Spectral Response Function of High-Resolution Chlorophyll Fluorescence Spectrometer Using the Slanted-Edge Method

Óscar Gutiérrez de la Cámara¹, Félix Muñoz¹, Jorge Alonso², Marcos Jiménez¹, Tomas Belenguer^{3, 4}

¹ National Institute of Aerospace Technology (INTA), Earth and Atmosphere Observation Department, Spain

² National Institute of Aerospace Technology (INTA), Flight Physics Department, Spain

³ National Institute of Aerospace Technology (INTA), Space Optics Department, Spain

⁴ Complutense University of Madrid (UCM), Optics Department, Spain

Keywords: hyperspectral, Edge, spectrometer, stray light, SRF

Challenge

The estimation of solar-induced chlorophyll fluorescence (SIF) through remote sensing spectrometers demands high spectral resolution and advanced retrieval methods ¹. While the Spectral Response Function (SRF) holds the potential to enhance measurement accuracy, its characterization may require experimental assemblies with significantly heightened spectral resolution. Various methodologies have been explored, including the use of large calibration facilities ² and the deployment of monochromators with well-documented spectral responses ³.

This research aims to develop a novel approach: the creation of a spectral slanted-edge pattern using a monochromator. This pattern is captured by a hyperspectral pushbroom imager. By adapting the ISO 12233:2023 ⁴ algorithms originally designed for assessing the spatial response of cameras, we can measure the SRF. This method offers a straightforward setup and eliminates the need for comprehensive knowledge of the monochromator's response characteristics.

Methodology

The methodology was implemented specifically on Headwall Hyperspec® high-resolution chlorophyll fluorescence (CFL) spectrometer. It consists of 2160 spectral bands, stepped 0.05 nanometers within 670 to 780 nm. The pushbroom imaging technique involves the sequential acquisition of spectral and spatial information by continuously scanning a stationary scene.

Sensor records two-dimensional images through the accumulation of one-dimensional across-track readings over time (along-track).

The experimental setup involves a Czerny-Turner monochromator. A turntable-mounted grating provides temporal spectral modulation. A collimator-projector system targets the beam to the input of CFL focused onto a single across-track pixel. By synchronizing the spectral modulation of the monochromator with the acquisition time of the sensor, parameters can be adjusted to induce a spectral slope of 1 to 5 degrees for the slanted edge of the image made with along-track pixels by rows and spectral bands by columns.

A region of interest was chosen, and the image's edge was processed using ISO 12233:2023 algorithms. This processing was correlated with the line spread function, representing the SRF of the across-track pixel and the spectral band where the peak was observed. This iterative process was applied to several across

pixels in the field of view (FOV) and along the spectral range, resulting in the assembly of a comprehensive SRF dataset from the CFL's array detector.

Results

An example of the results obtained from ISO12233 processed data is presented in Figure 1. The slanted edge was focused on across-track pixel number 800 in order to be processed and to generate the normalized super-sampled edge spread function (ESF). It was derived to obtain the relative SRF, represented by black 'x' points. A series of dots shows an ideal Gaussian response function, centered at 1079.3, with a Full Width at Half Maximum (FWHM) of 2.9 spectral bands. When multiplied by the spectral band step, this results in a measurement of 0.15 nanometers, which aligns with the manufacturer's specifications of 0.1 to 0.2 nm for FWHM.

There is a significant interest in characterizing the stray light effect on these sensors. It can be interpreted as the deviation from ideal behaviour. In Figure 1, this effect is observed on both the dark (left) and the bright (right) sides of edge. An interesting observation is that on dark side, the dispersion and result values are lower than on the bright side, possibly due to inherent signal noise.

In Figure 2 FWHM of the SRF, obtained at various angles within CFL's field of view (FOV), are shown. The circles on the graph denote mean values derived from all sampled bands, while the error bars represent the standard deviation of these samples.

The results provide a comprehensive sample of the SRF associated with numerous pixels in the CFL sensor's detector array. Estimations of the FWHM for other elements are based on this sample.

Outlook for the future

As next step, our primary objective is to improve the validation method in order to refine the available results. The high spectral resolution of CFL introduces uncertainty in its characterization.

The fundamental principles of this method can be applied to a broad range of spectroradiometers. These instruments should capture spectra at specific intervals and synchronize them with the monochromator's spectral scan. Furthermore, the monochromator's output should provide sufficient spectral width. The ASD FieldSpec3 spectrometer, known for its well-documented and characterized features, emerges as a promising candidate for implementing and validating this method.

Additionally, by measuring the spatial response function associated with each detector element and integrating it with the SRF, a spatial-spectral response function can be derived. This function will comprehensively characterize the CFL's response and will be used within the data processing chain once the methodology is validated.

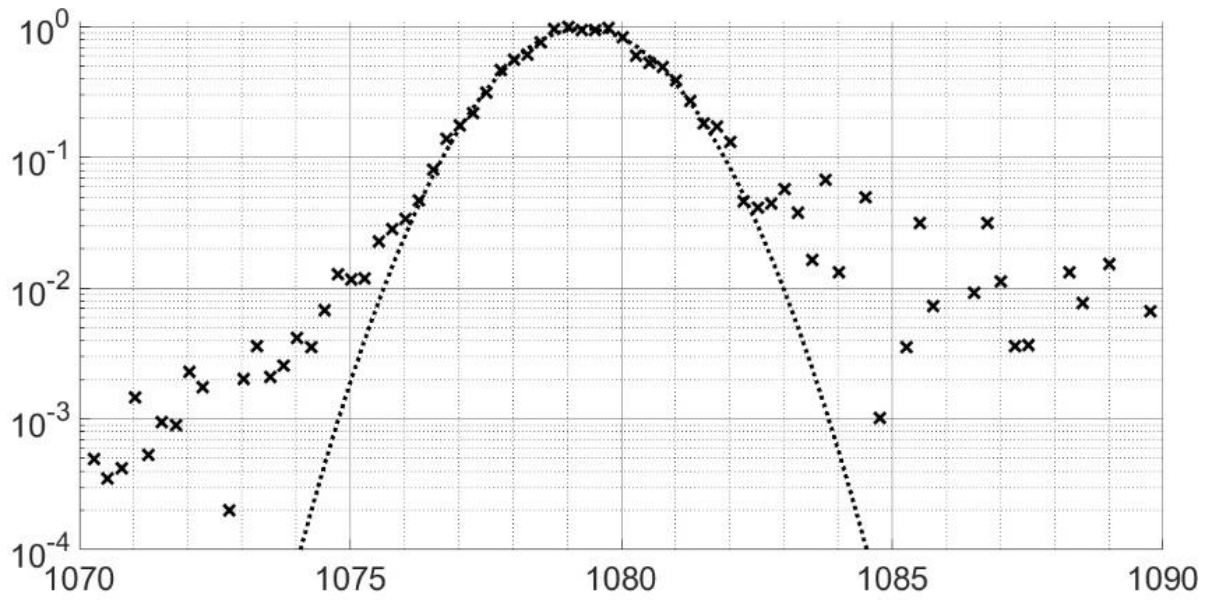


Figure 1 SRF plot obtained for a single CFL pixel at across-track number 800 (nadir), around spectral band number 1080. The y-axis represents the normalized response value, and the x-axis represents the spectral band number.

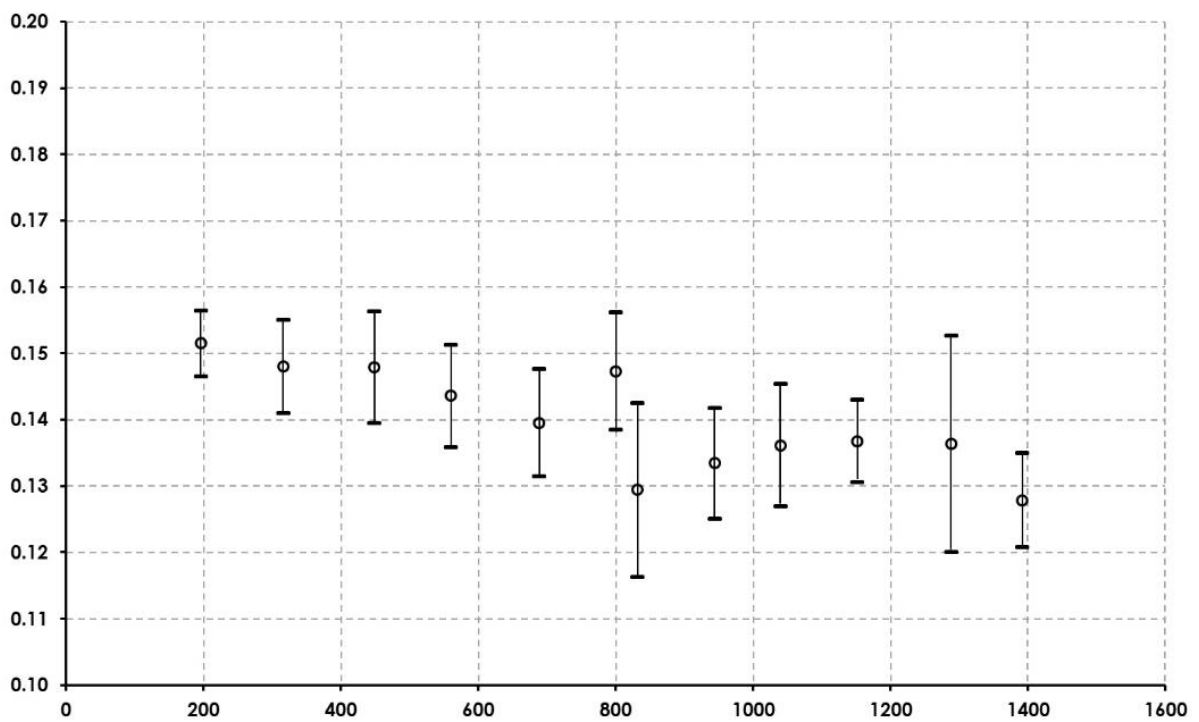


Figure 2 The data represents the Full Width at Half Maximum (FWHM) in nanometers of the Spectral Response Function (SRF) associated with several across-track pixels along its field of view, calculated as the mean of all the sampled spectral bands. The x-axis represents the spatial across-track pixel number out of 1600 columns in the CFL array, and the y-axis represents the FWHM value.

References

- [1] Sentinel-5p Innovation – Solar Induced Chlorophyll Fluorescence [Internet]. Available from: <https://s5p-troposif.noveltis.fr/>.
- [2] Paynter I, Cook B, Corp L, Nagol J, McCorkel J. Characterization of FIREFLY, an Imaging Spectrometer Designed for Remote Sensing of Solar Induced Fluorescence. *Sensors* [Internet]. 2020 Sep 1; 20(17):1–40. Available from: <https://doi.org/10.3390/s20174682>
- [3] Scharr H, Rademske P, Alonso L, Cogliati S, Rascher U. Spatio-spectral deconvolution for high resolution spectral imaging with an application to the estimation of sun-induced fluorescence. *Remote Sens Environ*. 2021 Dec 15;267:112718. Available from: <https://doi.org/10.1016/j.rse.2021.112718>
- [4] Photography ISO/TC 42. ISO 12233:2023 Photography — Electronic still picture imaging — Resolution and spatial frequency responses [Internet]. Available from: <https://www.iso.org/standard/79169.html>

Non-linear research directions to address the spatial scaling issue of solar-induced chlorophyll fluorescence (SIF) imagery

EARSeL Valencia 2024

Abstract

Corresponding Author: Juan Quiros-Vargas
j.quiros@fz-juelich.de

Juan Quiros-Vargas¹, Gregory Duveiller², Bastian Siegmann¹, Uwe Rascher¹

¹ Institute of Bio- and Geosciences, Plant Sciences (IBG-2), Forschungszentrum Jülich GmbH, Jülich, Germany, 52428

² Max Planck Institute for Biogeochemistry, Department of Biogeochemical Integration, Jena, Germany, 07745

Keywords: solar-induced chlorophyll fluorescence (SIF), SIF spatial downscaling, fractal geometry, semi-empirical downscaling, spatial resolution

Challenge

Solar-induced chlorophyll fluorescence (SIF) is a low intensity red glow emitted by vegetation from the core of the photosynthetic machinery, and which is closely related to the physiological status of plants. As a consequence, SIF data is sensible to the initial functional processes triggered by plants when exposed to stress conditions. This characteristic sensibility of SIF to evolving plant stress makes it a promising remotely sensed biophysical variable for early stress detection. Nevertheless, SIF-based early stress detection demands high resolution information at both spatial and temporal scales. When considering satellite scale, the latter represents a major challenge, since the high temporal resolution requirements (daily to sub-daily for an effective early stress detection) typically translates into coarse spatial resolution data. Consequently, the spatial downscaling (understood as an increase of the spatial resolution) of SIF satellite information is nowadays of utmost importance within the SIF research community, targeting the improvement in the amount and quality of information in SIF imagery. Currently, the SIF downscaling research is generally focused on the use of linear relations between SIF and explanatory variables like the land surface temperature and vegetation indices, derived from higher spatial resolution remote sensing data. Yet, besides the abovementioned efforts, more flexible SIF-downscaling approaches have to be investigated trying to meet the dynamism of SIF in diverse ecosystems. Therefore, in this study we aim to emphasize two ideas to address the non-linear spatial downscaling of SIF, namely: fractal theory downscaling and semi-empirical downscaling from process-based frameworks.

Results

- Fractal-based downscaled: in Quiros-Vargas et al. (2022; DOI: 10.1007/978-3-030-26050-7_120-1) the fractal theory is proposed as a potential direction to address the SIF-spatial downscaling. Such theory states that natural phenomena can be described as a repetition of patterns (fractal geometry) across spatiotemporal scales. The presence of a fractal geometry can be recognized through different mathematical approaches, e.g. based on power laws, as addressed by Quiros-Vargas et al.; where the authors found that the total SIF of vegetation objects within a 60 ha soybean field followed a power law distribution across spatial scales (1.5, 5, 10 and 15 m pixel⁻¹), indicating the presence of a fractal geometry.

- Semi-empirical downscaling: in Duveiller & Cescatti (2016, DOI: 10.1016/j.rse.2016.04.027) and Duveiller et al. (2020, DOI: 10.5194/essd-12-1101-2020) another approach for the spatial downscaling of SIF is proposed. The authors propose the spatial resolution of SIF products by connecting fine spatial resolution explanatory variables to the coarse SIF variable through the calibration of a non-linear physically-sound model over a spatial moving window. In the cases of these papers, the model was a light-use efficiency model, where stress was characterized based on downregulating factors linked to water availability and thermal conditions, respectively estimated by the normalized difference water index and land surface temperature. This same approach could be extended to include a new modelling formulation that connects to the modulation of the SIF-GPP relationship based on estimation of non-photochemical quenching (NPQ), possibly approximated by LST or the photochemical reflection index (PRI).

Outlook for the future

Updated information will be presented at the conference, towards overcoming the limitations and challenges reported in Quiros et al. 2022 (DOI: 10.1007/978-3-030-26050-7_120-1; concerning the fractal geometry-based research direction), and Duveiller & Cescatti (2016; DOI: 10.1016/j.rse.2016.04.027) and Duveiller et al. (2020; DOI: 10.5194/essd-12-1101-2020; concerning the semi-empirical downscaling research direction) will be presented and discussed at the conference. With the updated results (which are in preparation by the time of submission of this abstract), we aim to provide a more complete version of the ideas firstly proposed in the above-mentioned references, by answering questions that remained open in those studies. For instance, progresses in the fractal geometry-based research direction proposed will be focused on the improvements in the image segmentation step, which precedes the power laws estimation.

Uncertainty Assessment in Sun-Induced Chlorophyll Fluorescence Retrieval for FLEX Calibration and Validation Campaigns

Juanjo Peón¹, Marcos Jiménez¹, M^aPilar Cendrero-Mateo², Adrián Moncholí², Javier Gorroño³, Shari Van Wittenberghe², José Moreno²

¹ National Institute of Aerospace Technology (INTA), Department of Earth Observation and Atmosphere, Spain

² University of Valencia, Imaging Processing Laboratory (IPL), Spain

³ Universitat Politècnica de València, Research Institute of Water and Environmental Engineering (IIAMA), Spain

Keywords (5): FLEX-S3, sun-induced chlorophyll fluorescence, uncertainty, FloX, Monte Carlo

Challenge

The upcoming European Space Agency's (ESA) Fluorescence EXplorer-Sentinel 3 (FLEX-S3) will be the first mission to quantify photosynthetic activity by mapping vegetation fluorescence. According to the FLEX mission requirements, a Sun-Induced Chlorophyll Fluorescence (SIF) uncertainty of 10% should be met to provide reliable estimates of photosynthetic efficiency, i.e., uncertainties of less than 30%. Similarly, the SIF ground truth measurements should also meet the mission requirements, therefore the uncertainties associated with 1) instrument performance and calibration, 2) retrieval algorithm assumptions, and 3) site-dependent spatial/temporal variability need to be characterized and propagated for a fair comparison.

As part of the L3L4FLEX project, a ground and airborne campaign was carried out in July 2020 at the Las Tiesas experimental site, Barrax, Spain. During this field campaign, airborne, cable-suspended, and in-situ (i.e., FloX system) SIF measurements were performed at different locations, including homogeneous and heterogeneous areas. With the aim of advancing the end-to-end uncertainty estimation in FLEX validation campaigns, this work estimated the uncertainty introduced in the fluorescence product by the retrieval algorithm assumptions using a Monte Carlo (MC) approach.

Methodology

A FloX system (JB-Hyperspectral Devices, Düsseldorf, Germany) was placed in a two-meter tower above a homogeneous *Festuca* spp. field for continuous measurements. The FloX measurement protocol consisted of simultaneous radiance (L) and irradiance (E) measurements every 30 seconds. SIF was retrieved using the improved Fraunhofer line depth (iFLD) [1], spectral fitting method (SFM) [2], and spectral fitting algorithm (SpecFit) [3]. Uncertainty estimation included instrument performance using, as a first estimate, the indoor L and E repeatability measurements over an integrating sphere on the day before the campaign. These uncertainties were combined with the outdoor L and E reproducibility and fed into a MC simulation, the spectral autocorrelation of the FloX fluo bands and the correlation between E and L was also considered. The MC method was applied to the SpecFit algorithm to allow a direct comparison with the FLEX L2 products.

Results

FloX-Fluo SIF estimates over a *Festuca* spp. field on July 21 using the iFLD, SFM and SpecFit algorithms are shown in Figure 1a, for the O₂B (687 nm, R: red) and O₂A (760 nm, FR: far red) absorption features. SIF values obtained using the three algorithms showed an increasing trend throughout the morning, however iFLD

algorithm provided higher and noisier SIF values than the SFM and SpecFit methods for both O₂ absorption features. The results using the SFM and SpecFit algorithms were similar, with a Pearson correlation coefficient of 0.97-0.92 and a mean absolute error of 0.04-0.05 mW m⁻² sr⁻¹ nm⁻¹ for the O₂A and O₂B absorption features respectively. While the iFLD and SFM algorithms only estimate the SIF in the O₂ absorption features, the SpecFit algorithm allows the retrieval of the full SIF spectrum, as shown in Figure 1b. The global uncertainty in E and L considering the indoors repeatability and outdoors reproducibility was less than 1% at a 95% confidence level. SIF retrieval uncertainty over a Festuca spp. field obtained using a Monte Carlo simulation with a sample size of 1000, was about 3% and 8% at a 95% confidence level for the O₂A and O₂B absorption features respectively.

Outlook for the future

The result presented in this study, represent one of the key elements in the roadmap of the Spanish Cal/Val FLEX-S3 campaigns implementation. The following steps are intended to provide a complete SIF and reflectance uncertainty estimate for both ground and airborne instruments. We will progressively analyze and incorporate the different sources of uncertainty for the instrumentation, the retrieval and the spatial/temporal variability, for the purpose to obtain an integrated value of reflectance and SIF over a 300x300m FLEX-S3 pixel area.

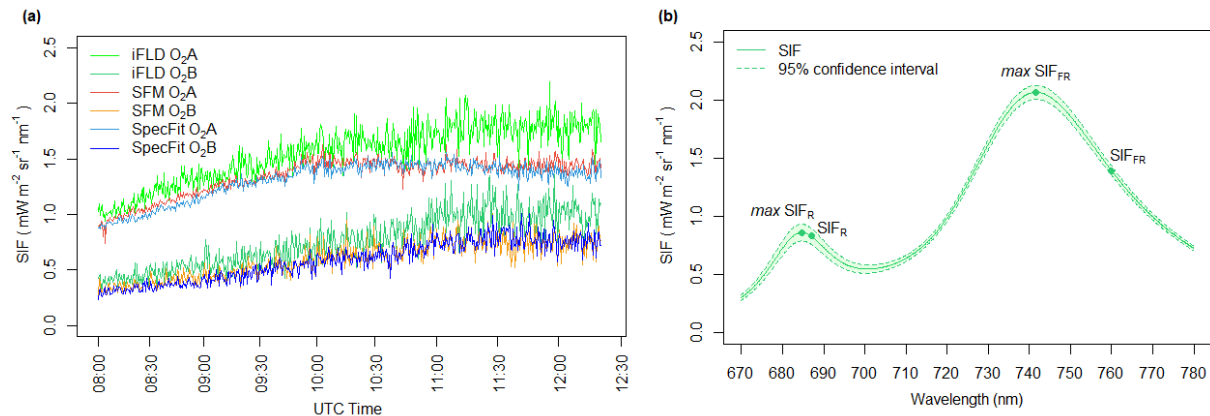


Figure 1 (a) FLoX-Fluo SIF estimates at O₂A and O₂B over a Festuca spp. field on July 21, 2020 using the iFLD, SFM and SpecFit algorithms and (b) FLoX-Fluo SIF estimates over a Festuca spp. field on July 21, 2020 at 11:00 UTC obtained using SpecFit and uncertainty.

References

- [1] Alonso, L., et al. IEEE Geosci. Remote. Sens. 2008, 5:4, 620-624. DOI: 10.1109/LGRS.2008.2001180.
- [2] Meroni, M., et al. Remote Sens. Environ. 2010, 114:2, 363-374. DOI: 10.1016/j.rse.2009.09.010.
- [3] Cogliati, S., et al. Remote Sens. 2019, 11, 1840. DOI: 10.3390/rs11161840.

Title**End-to-end simulations to optimize hyperspectral mission requirements for 7 scientific applications**

Briottet X.¹, Adeline K.¹, Bajjouk T.², Carrère V.³, Chami M.⁴, Constans Y.¹, Derimian Y.⁷, Dupiau A.¹⁻⁵, Dumont M.⁶, Doz S.¹, Fabre S.¹, Foucher P. Y.¹, Herbin H.⁷, Jacquemoud S.⁵, Lang M.⁸, Le Bris A.⁹, Litvinov P.¹⁶, Loyer S.¹⁰, Marion R.¹¹, Minghelli A.¹², Miraglio T.¹, Sheeren D.⁸, Szymanski B.¹³, Romand F.¹⁵, Desjardins C.¹⁴, Rodat D.¹⁴, Cheul B.¹⁴

- ¹ Université de Toulouse, ONERA DOTA, Toulouse, France, xavier.briottet@onera.fr, karine.adeline@onera.fr, sophie.fabre@onera.fr, yohann.constans@onera.fr, stephanie.doz@onera.fr, pierre-yves.foucher@onera.fr, thomas.miraglio@onera.fr
- ² Ifremer, DYNECO, LEBCO, Plouzané, France, touria.bajjouk@ifremer.fr
- ³ Nantes Université, Laboratoire de Planétologie et Géosciences, Nantes, France, veronique.carrere@univ-nantes.fr
- ⁴ Université Côte d'Azur, Observatoire de la Côte d'Azur, CNRS, Sorbonne Université (UFR918), Laboratoire Lagrange, Nice, France, malik.chami@upmc.fr
- ⁵ Université Paris Cité, Institut de Physique du Globe de Paris, CNRS, Paris, France, jacquemoud@ipggp.fr
- ⁶ Université Grenoble Alpes, Université de Toulouse, Météo-France, CNRS, CNRM, Centre d'Etudes de la Neige, Grenoble, France, marie.dumont@meteo.fr
- ⁷ Université de Lille, CNRS, LOA, Villeneuve d'Ascq, France, herve.herbin@univ-lille.fr; yevgeny.derimian@univ-lille.fr
- ⁸ Université de Toulouse, INRAE, UMR DYNAFOR, Castanet Tolosane, France, david.sheeren@ensat.fr
- ⁹ University Gustave Eiffel, LASTIG, ENSG, IGN, Saint-Mandé, France, arnaud.le-bris@ign.fr
- ¹⁰ SHOM, Brest, France, sophie.loyer@shom.fr
- ¹¹ CEA/DAM/DIF, Arpajon, France, rodolphe.marion@cea.fr
- ¹² Université de Toulon, CNRS, SeaTech, LIS, Toulon, France, audrey.minghelli@univ-tln.fr
- ¹³ DGA, Paris, France, benjamin.szymanski@intradef.gouv.fr
- ¹⁴ CNES, Toulouse, France, camille.desjardins@cnes.fr, damien.rodatt@cnes.fr
- ¹⁵ ACRI-ST, Sophia-Antipolis, France, frederic.romand@acri-st.fr
- ¹⁶ GRASP SAS, Villeneuve d'Ascq, France, pavel.litvinov@grasp-sas.com

Keywords (5): New Mission, Hyperspectral, Applications, End-to-End Simulation

Challenge (800 - 1000 characters incl. spaces)

CNES is currently carrying out a Phase A study to assess the feasibility of a future hyperspectral imaging sensor (10 m spatial resolution) combined with a panchromatic camera (2.5 m spatial resolution). CNES asked a French Mission Advisory Group (MAG) on hyperspectral, representing a broad French scientific community to provide recommendations for various user applications taking into account the instrument's cost, and compactness constraints with a specific focus on the ShortWave InfraRed (SWIR) spectral range. Based on an end-to-end simulator taking into account several combinations of Signal-to-Noise-ratio (SNR), radiometric calibration accuracy and spectral sampling strategy, this work aims to study the impact of instrument design on performances for a large variety of hyperspectral end-user themes: geoscience, forestry, coastal and inland waters, urban areas, industrial plumes, cryosphere and atmosphere.

Methodology (1200 – 1500 characters incl. spaces)

The methodology is based on an end-to-end simulator capable of simulating Top-of-Atmosphere radiance from reflectance spectra measured in the laboratory/field or from airborne hyperspectral images. These product levels are then used to retrieve surface reflectance after performing atmospheric corrections where errors in the knowledge of water vapor content and aerosols abundance are introduced. The sensor is modelled with 24 realistic instrumental parameters (6 spectral strategies with

different spectral samplings and spectral resolutions in the SWIR, 2 radiometric calibration performances and 2 SNR). Several applications are evaluated by estimating the following parameters using up-to-date processing's techniques: geosciences (mineralogy and soil moisture content estimation), forestry (tree species classification, leaf functional trait estimation), coastal and inland waters (bathymetry, water column estimation, shallow water bottom and coastal habitat classification), urban areas (land use classification), industrial plumes (factory smoke, methane and carbon dioxide estimation), cryosphere (specific surface area and equivalent black carbon concentration) and atmosphere (aerosols, gas). 648 simulations were thus evaluated enabling us to select the best compromise in terms of spectral configuration, radiometric calibration and SNR.

Results (1200 – 1500 characters incl. spaces)

Applications whose methods are based on the use of the global spectral signature depend little on the spectral sampling. It has been shown that a 16/20 nm spectral sampling in the SWIR domain can meet the needs of most of the applications tested. However, the MAG recommended a 10 nm spectral sampling in the SWIR for applications requiring well-localized absorption bands, such as mineralogy, industrial plumes or atmospheric gases. Furthermore, a slight loss of performances was observed as radiometric calibration performance decreased, with a few exceptions in bathymetry and cryosphere where performance was improved. Finally, even with the lower SNR level, most of the applications evaluated were fulfilled, with the exception of bathymetry and shallow water classification due to low reflectance levels, and carbon dioxide and methane estimation, the latter requiring the highest SNR levels.

Outlook for the future (800 - 1000 characters incl. spaces)

On the basis of these results, CNES is currently evaluating the best compromise for designing the future hyperspectral sensor (BIODIVERSITY) to meet the objectives of the prioritized applications. Certain perspectives linked to the end-to-end simulator have been already identified: i) on the sensor by updating the sensor characteristics in the frame of the project progress; ii) on atmospheric corrections by estimating the atmospheric parameters directly from the image, whose quality depends on sensor performance. These developments will have a direct impact on the quality of the results for each application. Some applications, such as soil moisture content estimation and snow characterization, used reflectance spectra as input and will be investigated on images. The BIODIVERSITY sensor also features a panchromatic band, so these applications will also be evaluated on fused hyperspectral and panchromatic images. Finally, a number of applications that were missing in this work, like crop trait characterisation, pollution monitoring and plastic detection, will be investigated in the near future.

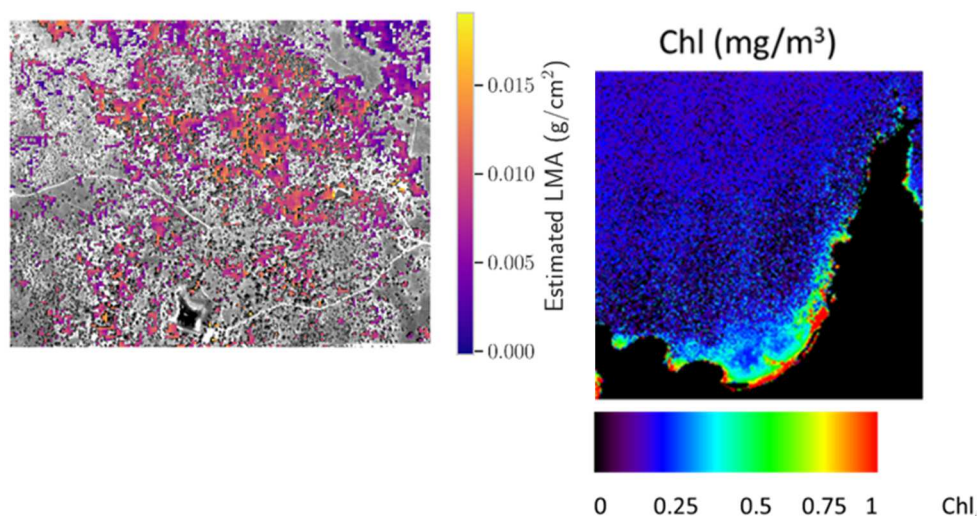


Figure (Left) Leaf Mass per Area (LMA) map of California Black Oak (*Quercus kelloggii*) at the Tonzi site, CA, USA and (Right) chlorophyll map at the Porquerolles site, France. Results were obtained with optimistic noise, 10 nm spectral sampling and bandwidth, and target calibration.

[Formatting guidelines for abstract submission]

EARSeL Valencia 2024
Abstract
Corresponding Author:
[\[stefano.pignatti@imaa.cnr.it\]](mailto:stefano.pignatti@imaa.cnr.it)

Agricultural Soil Properties Mapping From PRISMA And EnMap Data: Exploiting Multitemporal Bare Soil Approaches

Francesco Rossi⁴, Luca Marrone¹, Khalil Misbah¹⁻⁵, Saham Mirzae², Alessia Tricomi⁶, Raffaele Casa¹, [Stefano Pignatti](mailto:stefano.pignatti@imaa.cnr.it)² and Giovanni Laneve³

¹UNIVERSITY OF TUSCIA, DAFNE, VITERBO, ITALY

²CNR-IMAA, ROME, ITALY

³SIA, UNIVERSITY OF SAPIENZA, ROME, ITALY

⁴UNIVERSITY OF SAPIENZA, DIAEE, ROME, ITALY

⁵COLLEGE OF AGRICULTURE AND ENVIRONMENTAL SCIENCES, UM6P, BENGUERIR, MAROCCO

⁶E-GEOS, ROMA, ITALY

Keywords (5): Topsoil, Soil Carbon, Hyperspectral, PRISMA, EnMAP

Challenge (800 - 1000 characters incl. spaces)

Understanding the properties of agricultural soils is essential for optimising food production and the overall efficiency of agricultural systems. To obtain key information on soil characteristics, remote sensing techniques are increasingly employed. By analysing the distinct "spectral signature" of materials, it is possible to estimate these characteristics in a quantitative manner accurately (Ben-Dor et al. 1995, Soil Sci Soc Am J 59:364–372).

The Italian PRISMA and the German EnMAP hyperspectral satellite missions are expected to greatly contribute to the improved knowledge of agricultural soil properties spatial variability and mapping.

In this study, multiple bare soil PRISMA and EnMAP hyperspectral images acquired over agricultural fields in Northern Italy were used to retrieve Soil Organic Matter (SOM), CaCO₃, and texture topsoil properties using Machine Learning Regression Algorithms and were validated using an adapted field measurement scheme for soil sampling and analysis.

Methodology (1200 – 1500 characters incl. spaces)

The study site is located in the Jolanda di Savoia farm (Lat. 44.87°N, Lon. 11.97°E) (Italy). Soils are characterised by a significant variability, with the presence of buried paleo-channels dating back to the past presence of marshland, in which land reclamation was carried out since the end of 1800s.

Between 2019 and 2023, respectively 15 PRISMA and 6 EnMAP images were acquired. Concurrently, topsoil samples were collected on 32 agricultural fields, according to Elementary Sampling Units (ESU) of 30 by 30 m, followed by laboratory analyses of SOM, CaCO₃, texture and pH.

To select only bare soil signals, excluding the presence of photosynthetic or non-photosynthetic vegetation, various processes were employed. These included the combined utilization of spectral indices such as the Normalized Difference Vegetation Index (NDVI) and the non-photosynthetic vegetation index (nCai). Two different spectral libraries were assembled, using respectively PRISMA and EnMap bare soil reflectance acquired on different dates, associated with the corresponding soil properties. The optimal

samples were selected from the soil libraries, employing several criteria, such as prioritizing those exhibiting the lowest soil moisture levels.

The dataset underwent different preprocessing techniques to reduce the impact of noisy bands. Different machine learning regression algorithms were then trained on these libraries using a K-fold cross-validation approach.

Results (1200 – 1500 characters incl. spaces)

Different methodologies of spectra extraction from the different acquisition dates available for PRISMA and EnMAP were tested, along with different preprocessing approaches and machine learning algorithms, in various combinations. The results showed that selecting dates from a multitemporal soil reflectance set, based on soil moisture and applying spectral pre-treatments, can generally improve the accuracy of predictions, though the best pre-treatment varied depending on the soil properties and sensor. The multi-date approach needs further refinement as the indexes used do not consistently select the driest soil for both datasets.

Partial Least Squares Regression (PLSR) was found to be a highly consistent and successful algorithm for prediction. For Clay, the best results were achieved using the PRISMA sensor, Relevance Vector Machine algorithm, and Derivative of first-order preprocessing technique, resulting in an R2 of 0.82 and Root Mean Square Error (RME) of 6.72%. For Silt, the EnMap sensor, PLSR algorithm, and Derivative of first-order preprocessing technique yielded an R2 of 0.81 and RME of 5.49%. For SOM, the PRISMA sensor and PLSR algorithm provided the best results, with a R2 of 0.77 and RME of 1.84%. Lastly, for CaCO₃, the best results were obtained by PRISMA using a Standard Normal Variate preprocessing technique applied to absorbance smoothed with Savitzky-Golay filter of the first, yielding an R2 of 0.58 and RME of 2.60%.

Outlook for the future (800 - 1000 characters incl. spaces)

These preliminary tests have yielded promising results, as PRISMA and EnMAP time series were both able to retrieve most soil parameters with comparable accuracy, considering the smaller number of EnMAP acquisitions available than for PRISMA. Repeated bare soil acquisitions from both sensors could be valuable and synergic for agricultural soils mapping, though further testing could help identify the strengths and weaknesses of each multitemporal data extraction approach. Overall, this offers a constructive step towards improving our ability to understand soil characteristics and improve agricultural and environmental practices.

Forthcoming investigations should focus on the development of more general methodologies. In this context, good opportunities arise from the use of open lab-based soil spectrum libraries (OSSL) in methodologies such as Spiking or reinforced learning, as well as the integration of data from proximate sensors through the application of data fusion techniques.

Please upload 1-2 figures or a graphical abstract (min 300 dpi. jpeg/png)

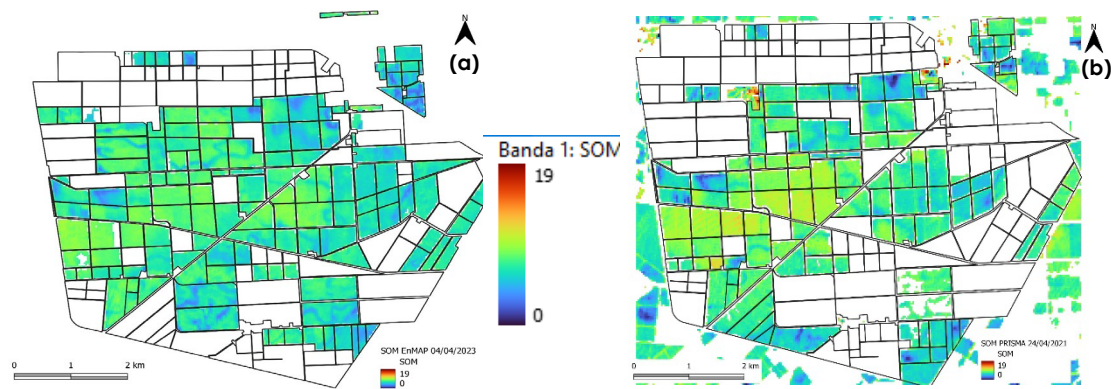


Figure Example of Machine learning Soil Organic Matter regression applied respectively on (a) EnMap (b) PRISMA.

Them.Sess. 3-1: Hyperspectral Remote Sensing of Forest Traits II

Leaf Spectroscopy of Defence Traits in Temperate Forests

Rui Xie¹, Roshanak Darvishzadeh¹, Andrew Skidmore^{1,2}, Freek van der Meer¹

¹ University of Twente, Faculty of Geo-information Science and Earth Observation, The Netherlands

² Macquarie University, Department of Environmental Science, Australia

Keywords: Leaf Spectroscopy, Total Phenolics, Temperate Forests, Continuum Removal, PLSR

Challenge (800 - 1000 characters incl. spaces)

Total phenolics are an important group of secondary metabolites universally distributed in vascular plants and play an essential role in the defence of plants against biotic and abiotic stressors (also known as "defence traits"). Accurate quantification of total phenolics is key for understanding the phytochemical diversity and plant response to environmental changes. Leaf spectroscopy offers a great opportunity for predicting foliar traits in a non-destructive and cost-effective way. However, previous studies using spectroscopy have been mainly limited to leaf primary biochemical traits, with few focus on plant defence traits. In particular, it remains to be explored how total phenolics vary among temperate tree species and whether they can be assessed using the leaf spectral signature.

Methodology (1200 – 1500 characters incl. spaces)

The objective of this study is to use leaf spectroscopy to examine the retrieval and absorption features of an ecologically important biochemical (i.e., total phenolics) in temperate forests. To achieve this, the leaf samples over four dominant species (i.e., English oak, European beech, Norway spruce and Scots pine) were collected during fieldwork in 2021 summer from two European temperate forests. Leaf reflectance was measured using ASD FieldSpec3 equipped with an integrating sphere, after which the concentrations of total phenolics were determined using the standard Folin–Ciocalteu method in the laboratory.

Continuum removal was applied to the leaf reflectance spectra in order to enhance the assessment of the subtle absorption features relevant to total phenolics in four temperate species. Further, we performed the Partial Least Square Regression (PLSR) to estimate the content of total phenolics from continuum-removed reflectance. Predictive models were built using the SWIR region of the spectrum (1000–2200 nm). Model performance was assessed using coefficient of determination (R^2) and normalised root-mean-square error (NRMSE%). The contribution bands were evaluated by computing the variable importance projection (VIP) and PLSR standard coefficients, respectively.

Results (1200 – 1500 characters incl. spaces)

The chemical analysis demonstrated significant differences in the concentration of total phenolics across four temperate species ($p < 0.05$), indicating a potential of total phenolics for species discrimination. We observed the concentrations of total phenolics are generally higher in broadleaf species (i.e., English oak and European beech) than in coniferous species (i.e., Norway spruce and Scots pine). The spectral analysis revealed persistent and distinct phenolic absorption features near 1666 nm in the continuum-removed spectra of English oak, Norway spruce and European beech. While the reflectance of Scots pine needles showed a weaker absorption feature near 1653 nm, shorter ward of phenolic features of other species.

Our modelling results show that the total phenolics can be accurately estimated using PLSR with R^2 of 0.79 and NRMSE of 9.95% (Fig. 1a). As shown in Fig. 1b, the identified informative bands are well corresponded between PLSR standard coefficients and VIP measures. Specifically, the spectral bands that are significant for predicting total phenolics are situated in 1400–1500, 1640–1680, 1700–1730 and 2090–2180 nm, matched with known features that are characteristic of phenolic compounds.

Outlook for the future (800 - 1000 characters incl. spaces)

Our study extended our understanding of absorption features of total phenolics in temperate tree species as well as demonstrated the potential of spectroscopy to accurately predict phenolic compounds across temperate forests at the leaf level. The findings of this study paved the way for mapping and monitoring phenolic compounds in temperate forests at the canopy or landscape level using the next generation of air- and spaceborne spectroscopy imaging, such as DESIS, PRISMA and EnMAP. In addition, it is important to understand the impact of changing environmental conditions on the variation of phenolic compounds. In future studies, we will also investigate the retrieval of specific phenolic compounds that play influential roles in ecosystem functioning in other vegetation types or biomes to promote the characterization of vegetation properties.

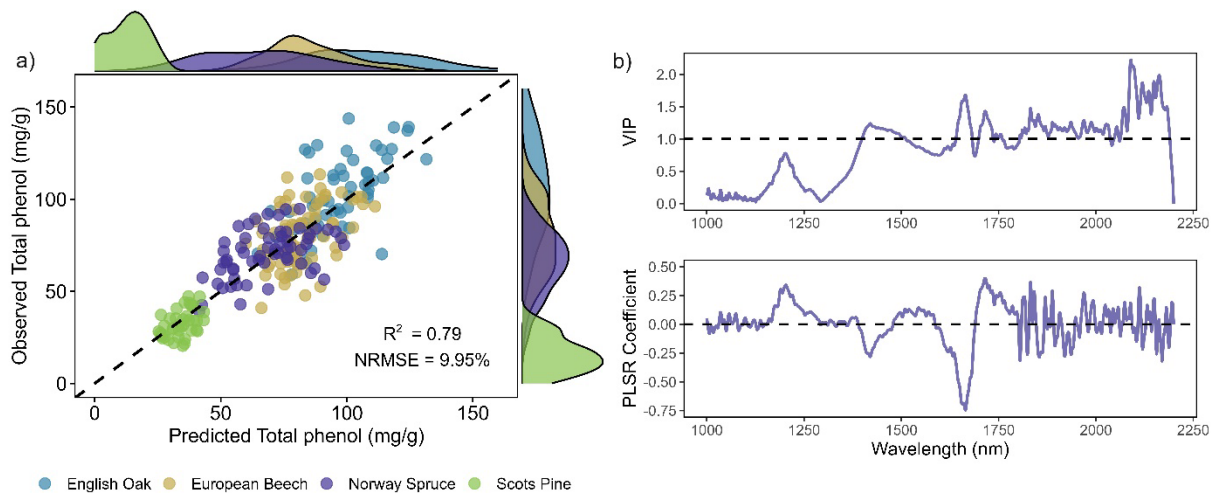


Figure 1 a) Observed versus predicted total phenolics and b) Variable importance projection (VIP, top panel) and PLSR coefficients (bottom panel) for total phenolics predicted using the PLSR model. Marginal plots show kernel density distribution for observed and predicted total phenolics.

Mapping Phyllosphere and Soil Fungal Function Using AVRIS-NG Hyperspectral Data

EARSeL Valencia 2024

Abstract

Corresponding Author:

[\[a.siegenthaler@utwente.nl\]](mailto:a.siegenthaler@utwente.nl)

A. Siegenthaler¹, H. Abdullah¹, A.K. Skidmore¹, Y. Duan¹, M.S.D. Rousseau¹

¹ Faculty of Geo-Information Science and Earth Observation (ITC), University of Twente, P.O. Box 217, 7500 AE Enschede, The Netherlands.

KEYWORDS (5): AVRIS-NG, eDNA, FOREST, FUNGI, TROPHIC MODES

Challenge

Microbial communities play a crucial role in forest ecosystems, where they are fundamental to the health, structure, and sustainability of the forest. Developments in molecular research allow for the evaluation of these understudied communities but are generally too costly and labour intensive for large-scale assessments. In temperate forests, the collection of samples from the top canopy (phyllosphere) especially poses challenges due to the accessibility of the crown of tall (30+ meter) trees, greatly limiting the spatial and temporal density of existing sample points. Advances in hyperspectral sensors offers a solution for bridging these data gaps, enabling the extrapolation of environmental DNA (eDNA)-based microbial profiles across extensive regions.

Methodology

To demonstrate the utilisation of hyperspectral airborne data to predict and map microbial functions of temperate European forests, we modelled the spatial distribution of fungal trophic groups in the soil and top-canopy using AVRIS-NG hyperspectral airborne data collected from the Bavarian Forest National Park in Germany. Putative functional profiles were created from eDNA (genetic material obtained from environmental samples [e.g. canopy, soil] without capturing the organisms themselves) samples from soil and top-canopy leaf material. The public data base “Funguild” was used to concatenate eDNA taxonomic data to functional profiles, allowing linking microbial profiles to ecosystem functions. The fungal functional profiles were used as training and validation data for the models (using PLSR and gaussian processing algorithms), which were consecutive inverted for prediction and mapping.

Results

Our results show for the first time that microbial function in the soil and canopy can accurately predicted for temperate European forests when combining eDNA point profiles with AVRIS-NG hyperspectral airborne data. The findings demonstrate that fungal trophic groups show substantial variation in their spatial distribution across a forest landscape. Furthermore, top canopy functions were predicted with higher reliability than soil microbial functions, presumably due to the stronger link between the phyllosphere and host-tree attributes (chemical, compositional, and functional characteristics) that can be sensed remotely using spectral reflectance.

Outlook for the future (800 - 1000 characters incl. spaces)

This study demonstrates a clear example of how spaceborne next generation hyperspectral data could be used to effectively predict putative microbial functions, providing maps and models with high relevance for forest ecology and management. The findings of this study highlight a significant breakthrough in utilizing airborne or spaceborne next-generation hyperspectral data to effectively predict putative microbial functions, and this research offers valuable insights and tools essential for the sustainable management of forests. Looking ahead, novel next-generation remote sensing platforms, such as the imminent launch of the CHIME satellite, holds the promise of revolutionizing the utilisation and upscaling of environmental DNA (eDNA) point-based information, offering innovative solutions for addressing ecological challenges on a global scale.

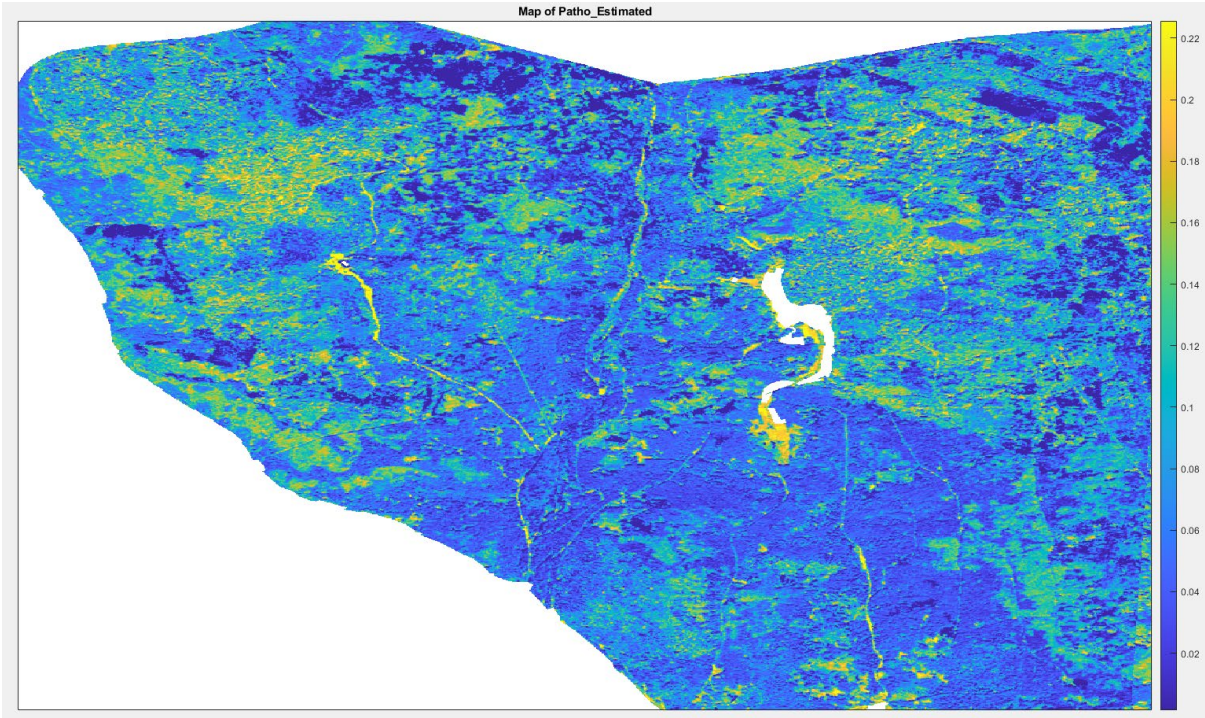


Figure Detail of map showing estimated relative abundance of Pathotrophic fungi in the phyllosphere of Bavaria National Park, Germany. Colour gradient represents the estimated proportion of DNA reads belonging to Pathotrophic fungi in the top-canopy phyllosphere.

Title: Retrieving leaf lignocellulose of conifer species using PROSPECT-PRO model

EARSel Valencia 2024
Abstract
Corresponding autor:
Alejandra Torres-Rodriguez
a.torresrodriguez@twente.nl

Alejandra Torres-Rodriguez^{1*}, Roshanak Darvishzadeh¹, Andrew K. Skidmore¹, Tiejun Wang¹,

¹Department of Natural Resources, Faculty of Geo-Information Science and Earth Observation (ITC), University of Twente, P.O. box 217, 7500 AE, Enschede, The Netherlands.

Keywords (5): Leaf traits, PROSPECT-PRO, Lignocellulosic Biomass, Hyperspectral, conifers

Challenge

Lignocellulosic biomass in leaves provides structural support to the plant, facilitating water transport, and protecting it from biotic threats and various stress factors. Lignocellulose makes up for most portion of the dry weight in tree species. Previously, subdividing leaf mass per area (LMA) into its components, including lignocellulose, using radiative transfer models has been a challenge. However, a recent recalibration of the PROSPECT model, now known as PROSPECT-PRO, has made this possible. Yet the model applicability needs to be explored for coniferous tree species. Therefore, this study aimed to evaluate the ability of PROSPECT-PRO to retrieve leaf lignocellulose for Norway spruce and Scots pine tree species in Germany and the Netherlands. To achieve this, we conducted hyperspectral measurements of fresh leaves and, utilized the spectral range from 800 to 2400 nm and the selection of optimal spectral bands in model inversion for retrieval of lignocellulose.

Methodology

We collected a dataset of 80 leaf samples from the upper canopy of Norway spruce ($n = 50$) and Scots pine ($n = 30$). Shortly after, the reflectance and transmittance spectra were measured with ASD FieldSpec-3 with an integrating sphere. Lignocellulose laboratory measurements were conducted through ethanol extraction with a 'high-throughput mini Soxhlet,' while nitrogen-bearing compounds were indirectly determined from total elemental nitrogen measurements with a CHN/O Elemental analyser. Water content was calculated as the difference between the fresh and dry weights of the total sample mass using an ADC AM350. A look-up table (LUT) approach was employed based on the field measurements.

The model was inverted through the wavelength region of 800 to 2400 nm. Additionally, the model was also inverted on a spectral subset by selecting optimal spectral bands for lignocellulose. These bands were determined as optimal using an adaptation of the forward feature selection method: iteratively inverting the model, each time adding a spectral band segment of 10 nm bandwidth, starting with the segment with the lowest error (RMSE) (Figure 1) and, selecting the non-continuous spectral subset that yielded the highest accuracy in terms of coefficient of determination (R^2).

Results

The PROSPECT-PRO model inversion successfully retrieved leaf lignocellulose with moderately reasonable accuracy, using both the 800 to 2400 nm spectral range and the selected optimal spectral bands (Figure 2). In the first case, the retrieval accuracy for leaf lignocellulose of Scots pine was $R^2 = 0.58$, RMSE = 0.0049, NRMSE = 0.28, and for Norway spruce was $R^2 = 0.61$, RMSE = 0.0029, NRMSE = 0.17. The inversion, by selecting the optimal spectral bands, resulted in a slight improvement with the following accuracy: Scots pine was $R^2 = 0.60$, RMSE = 0.0035, NRMSE = 0.20 and for Norway spruce is $R^2 = 0.67$, RMSE = 0.0019, NRMSE = 0.11. The resulting optimal bands for leaf lignocellulose retrieval were found between

1230 and 1370 nm for both tree species (Figure 1), closely coinciding with absorption peaks corresponding to lignin and cellulose.

Outlook for the future

This study marks meaningful progress in the retrieval of leaf lignocellulose with the PROSPECT-PRO model, particularly for coniferous tree species. While the performance metrics revealed the model's effectiveness, they also revealed a moderate level of accuracy. The coefficient of determination results (R^2) reveal there is still some unexplained variance in leaf lignocellulose. Notably, hemicellulose was not considered in the absorption peak calibration of the model, in contrast to lignin and cellulose. By incorporating lignocellulose, the model's performance could be potentially enhanced. Furthermore, it is important to acknowledge that the proportions of leaf lignocellulose (including their individual constituents) can vary across different plant species. Enhancing the model's accuracy in leaf lignocellulose retrieval may be achievable by incorporating a wider variety of plant species and biomes during the model calibration. Moreover, consistent with prior studies, our findings emphasize the importance of considering near-infrared bands (NIR) to enhance the estimation of dry matter components, benefiting from their minimal water interference.

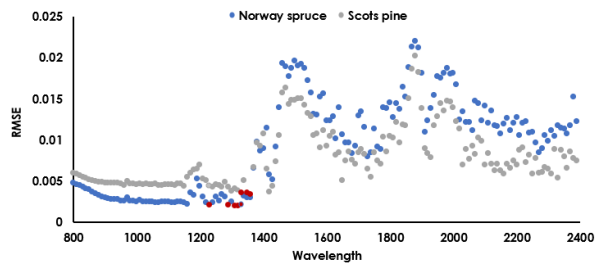


Figure 1. RMSE values resulting from the retrieval of lignocellulose using PROSPECT-PRO for each spectral band segment (10 nm width). In red, are the spectral segments that were determined as optimal for leaf lignocellulose retrieval.

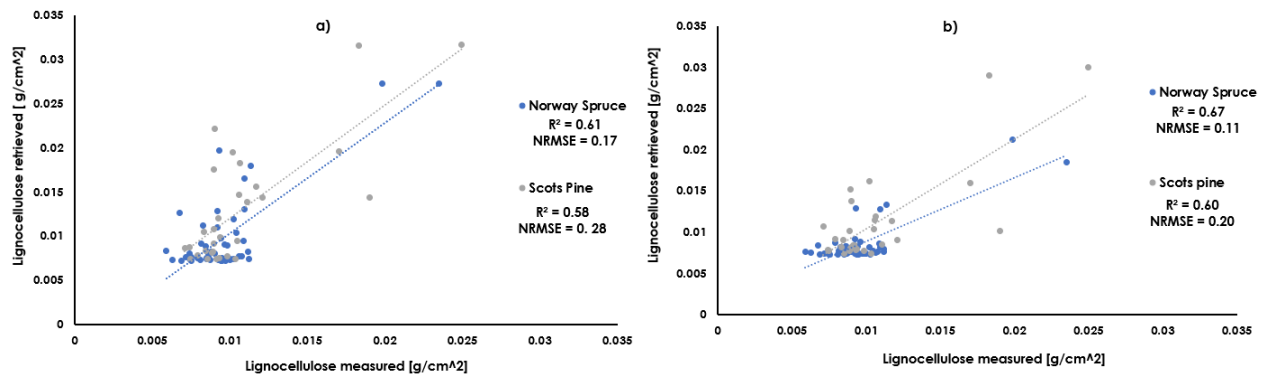


Figure 2. Measured and retrieved lignocellulose using PROSPECT-PRO inversion considering: (a) wavelengths ranging from 800 to 2400 nm and, (b) optimal spectral bands selected for lignocellulose.

Quantifying Canopy Nitrogen Content in a Soil-Acidified Temperate Forest Using Image Spectroscopy

EARSeL Valencia 2024

Abstract

Corresponding Author:

h.j.abdullah-1@utwente.nl

Haidi Abdullah^{*1}, Andrew K. Skidmore¹, Andjin Siegenthaler¹, Roshanak Darvishzadeh¹, Elnaz Neinavaz¹, Alejandra Torres-Rodriguez¹, Yiwei Duan¹.

¹ Faculty of Geo-Information Science and Earth Observation (ITC), University of Twente, P.O. Box 217, 7500 AE Enschede, The Netherlands.

Keywords (5): Canopy Nitrogen Content, Image Spectroscopy, PRISMA, Soil Acidification, PLSR

Challenge

The challenge of monitoring the impact of soil acidification on forest health is a critical ecological concern, particularly in the context of increasing nitrogen deposition, which results in decreased soil pH levels. Soil acidification, often stemming from excess nitrogen deposition from sources such as industrial emissions and agricultural runoff, has far-reaching consequences on forest ecosystems. It disrupts the delicate natural nutrient balance within these ecosystems, directly influencing nutrient availability to the forest's resident trees. The interplay of soil acidification and nitrogen deposition creates a multifaceted problem for forest management and conservation. When soil pH levels drop, it can lead to leaching of essential nutrients, like calcium and magnesium, which are vital for the health of both the soil and the trees. This nutrient imbalance negatively affects the growth and vitality of the forest ecosystem, making it imperative to monitor and mitigate these changes effectively. Traditionally, monitoring the impact of soil acidification on forest health has been a challenging task. To address this, scientists and environmental researchers have been exploring advanced technologies, one of which is the use of hyperspectral satellites like PRISMA. These newly launched satellites have the potential to revolutionize our ability to assess the effects of soil acidification on forest ecosystems.

Hyperspectral satellites like PRISMA offer a promising tool to monitor the impact of soil acidification by measuring canopy nitrogen content as a proxy for forest health. These satellites are equipped with advanced sensors capable of capturing a wide range of spectral information. Measuring canopy nitrogen content provides insights into the forest's ability to take up nutrients from the soil, which can be severely hampered by soil acidification. By monitoring these changes over time, researchers can gain a better understanding of how soil acidification impacts forest health, tree growth, and overall ecosystem resilience. This information is invaluable for developing targeted strategies to mitigate the negative consequences of soil acidification and nitrogen deposition on forests.

In conclusion, the challenges posed by soil acidification and nitrogen deposition on forest health are pressing environmental issues. The disruption of the natural nutrient balance within forest ecosystems can have profound effects on their vitality. Fortunately, recent advancements in satellite technology, particularly the launch of hyperspectral satellites like PRISMA, provide a promising avenue for monitoring these impacts by measuring canopy nitrogen content. This innovative approach enables us to better understand and address the complex ecological challenges posed by soil acidification and its consequences on forest ecosystems.

Methodology (1200 – 1500 characters incl. spaces)

In this study, our primary focus was to examine the influence of stressed forests, which have experienced nitrogen deposition and soil acidification, on the nitrogen content within the forest ecosystem. We employed hyperspectral data obtained from the PRISMA satellite, combined with on-site field measurements of nitrogen content. To accomplish this, a dedicated field campaign was carried out in 2021 to gather data on leaf nitrogen content within two distinct stressed forests in the central Netherlands, specifically Hoge Veluwe and Veluwezoom. To collect leaf samples, we followed a meticulous procedure. An average of 2–3 branches was selected from each tree. The chosen branches were all from the upper sections of the trees, where they were exposed to ample sunlight. The heights of the trees ranged from approximately 25 to 30 meters. Our method involved using a crossbow to shoot an arrow equipped with a fishing line, which was then attached to a branch with sunlit leaves. The fishing line served as a conduit for a rope, which we maneuvered over the targeted branch. Once the rope was in place, the branch was gently pulled until it separated from the tree. The needles were promptly collected from the fallen branches and placed in labeled plastic zip-lock bags. These bags were further protected by wet pulp paper and transported to the laboratory in a portable cooling box filled with frozen ice packs to ensure the samples remained cool. To assess foliar nitrogen levels, the collected needles were subjected to a 72-hour drying process within an oven set at 60°C. Subsequently, the dried needles were finely ground using a mortar and pestle until they achieved a soft, powdery consistency. The resulting material was then sifted through a 0.25 mm mesh screen. Following this, 2 mg of the powdered leaves were carefully transferred into small aluminium capsules for nitrogen content measurements, which were conducted using an organic elemental analyzer (FLASH 2000). In the final stage of our analysis, we utilized a Partial Least Square Regression (PLSR) model to estimate the canopy's nitrogen content. PLSR is a regression method that takes into consideration both the variance of the explanatory and dependent variables. It establishes a linear relationship between a set of dependent (Y) variables, in this case, canopy nitrogen content, and a set of predictor (X) variables, represented by the spectral reflectance data obtained in this study.

Expected results (1200 – 1500 characters incl. spaces)

The study's outcomes demonstrate that hyperspectral data derived from the PRISMA satellite can reliably estimate forest canopy nitrogen content, yielding a root mean square error (RMSE_{cv}) of 20.25 and a cross-validated coefficient of determination (R²_{CV}) of 0.60.

Furthermore, our investigations uncover significant variations within these two forests, characterized by patches exhibiting notably low soil pH levels (pH < 3). These acidic patches have a discernible impact, leading to a significant ($p \leq 0.05$) reduction in canopy nitrogen content, especially in coniferous stands when compared to deciduous stands. In addition, our in-situ measurements of both soil and leaf nitrogen content provide compelling evidence of variations between these two forest types (coniferous and deciduous). There's a substantial difference in nitrogen content and soil pH levels, with coniferous forests displaying lower values.

Moreover, the comparative analysis of these two national parks, Veluwezoom and Hoge Veluwe, reveals distinct differences. Veluwezoom, in particular, stands out as being more acidic and possessing lower canopy nitrogen content in contrast to Hoge Veluwe.

Outlook for the future (800 - 1000 characters incl. spaces)

This research offers a compelling illustration of the practical application of cutting-edge spaceborne hyperspectral technology in predicting canopy nitrogen content within a stressed, acidified temperate forest environment. By harnessing this advanced technology, the study has successfully generated maps and predictive models with substantial implications for both the field of forest ecology and forest management strategies. This contribution is of paramount significance not only for the scientific community but also for policymakers and forest management authorities.

The utilization of spaceborne next-generation hyperspectral data for canopy nitrogen content prediction represents a breakthrough in the field of ecological assessment. Such predictions are indispensable for understanding the health and vitality of forest ecosystems and informing appropriate management

practices. Looking ahead, the promise of revolutionizing remote sensing capabilities looms on the horizon with the impending launch of the CHIME satellite. This innovative satellite technology is poised to significantly enhance the acquisition and analysis of spectral data from Earth's surface, offering novel solutions for addressing ecological challenges on a global scale. With CHIME and similar advancements, we can anticipate unprecedented progress in our ability to monitor, understand, and conserve forests and other ecosystems, ultimately contributing to the preservation of our planet's environmental health.

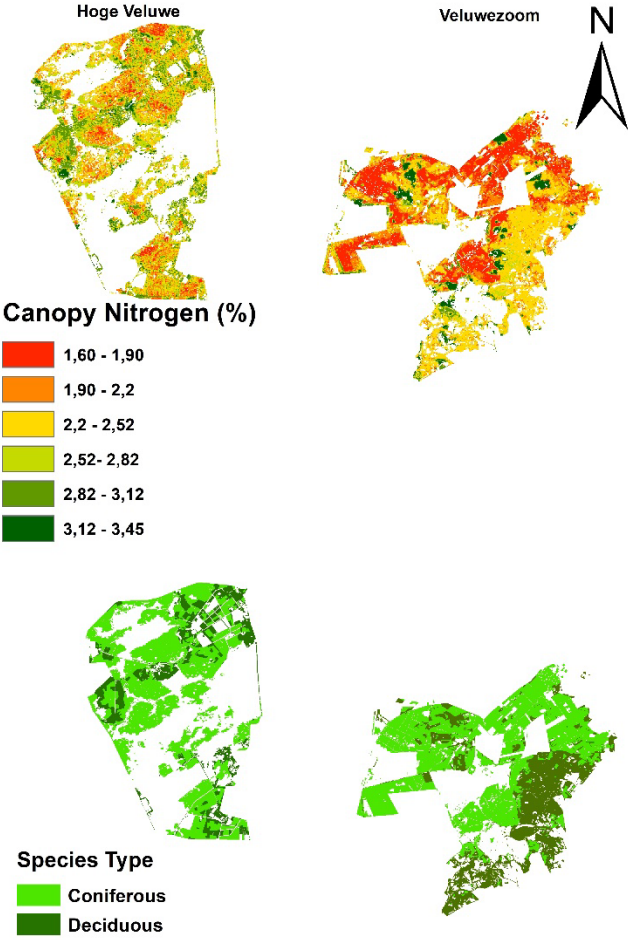


Figure Estimated maps of canopy nitrogen content using the PLSR model (top) and species distribution maps for the two national parks (bottom).

Mapping Leaf Pigment Contents of a Tall Eucalyptus Forest from Drone Imaging Spectroscopy Data Using the DART Model and Machine Learning

Zbyněk Malenovský^{1,2}, Krishna Lamsal², Růžena Janoutová³, Timothy Devereux^{4,5}, William Woodgate^{4,6}, Leonard Hambrecht², Emiliano Cimoli², Arko Lucieer², Lucie Homolová³, Omar Regaieg¹, Yingjie Wang⁷, Jean-Philippe Gastellu-Etchegorry⁷

¹ University of Bonn, Department of Geography, Germany

² University of Tasmania, School of Geography, Planning, and Spatial Sciences, Australia

³ The Czech Academy of Sciences, Global Change Research Institute, Czechia

⁴ University of Queensland, School the Environment, Australia

⁵ CSIRO, Space and Astronomy, Australia

⁶ CSIRO, Land and Water, Australia

⁷ CNES-CNRS-IRD-INRAE-UT3, Centre d'Etudes Spatiales de la Biosphère, France

Keywords: DART-Lux, Fluspect-Cx, Random Forest, chlorophyll a+b, carotenoids, anthocyanin

Challenge

The study objective is mapping of biochemical plant functional traits of individual trees, suitable for functional diversity and phenotyping assessments. Leaf chlorophylls a+b (Cab), total carotenoids' (Ccar), and anthocyanin (Cant) contents of sunlit parts of tall eucalyptus crowns were estimated by combining: (1) full three-dimensional (3D) reconstruction of a heterogeneous forest stand of Australian eucalypts from terrestrial laser scans (TLS) of the individual trees, (2) Discrete Anisotropic Radiative Transfer (DART) bidirectional Monte Carlo path tracing simulating the forest drone-based hyperspectral images, (3) complementary drone VNIR imaging spectroscopy data, and (4) Random Forest regressions, trained on reflectance images simulated for the study site by coupled Fluspect-Cx and DART models and applied per-pixel on the drone hyperspectral imagery (see Figure 1).

Methodology

The study was conducted at the Terrestrial Ecosystem Network (TERN) SuperSite Tumbarumba (southeastern Australia; -35.6565°N , 148.1517°E), which is an open multi-aged temperate, tall, and wet sclerophyll forest containing 402 trees of alpine ash (*Eucalyptus delegatensis*) and mountain gum (*Eucalyptus dalrympleana*) species in a 1 ha monitoring plot. State-of-the-art TLS and computer technology allowed us to reconstruct in 3D the 1 ha site containing individual leaves, trunks, and branches of all trees and understorey (grasses, herbs, and shrubs). Our 3D reconstruction method comprises three steps: (1) leaf-wood segmentation of a TLS point cloud, (2) reconstruction of woody parts, and (3) biologically realistic distribution of foliage within a tree crown. An uncrewed aerial system (UAS/ drone), carrying a Micro-Hyperspec spectrometer (Headwall Photonics, Inc., USA), was deployed at the site on 18 September 2019. It acquired images of 80 VNIR spectral bands (bandwidth of 5 nm and pixel size of 5 cm), processed into hemispherical-directional reflectance factor (HDRF). Coupled Fluspect-Cx and DART models were set to simulate 2268 UAS-matching hyperspectral images of the study site. DART reflectance signatures of sunlit crown pixels were extracted together with the Fluspect-Cx inputs and used for training and validating Random Forest (RF) non-linear regressions. RFs were consequently applied per sunlit crown pixel of UAS image to retrieve the actual Cab, Ccar, and Cant estimates.

Results

The reconstructed 3D trees and understorey were used to build the virtual 1 ha forest scene and, consequently, to simulate a hyperspectral image of the Tumbarumba site in the DART model. Comparison of the mean top-of-canopy (TOC) reflectance signatures generated by DART and extracted from the UAS image (Figure 1) revealed a close match in all simulated wavelengths (490 – 800 nm), which allowed us to continue with the Fluspect-Cx/DART generation of TOC reflectance factors for varying Cab, Ccar, and Cant inputs. RF algorithms, trained over the resulting reflectance look-up table, enabled Cab, Ccar, and Cant estimates from UAS image, resulting in plausible quantitative ranges and spatial patterns. RF training indicated a high importance of spectral bands around 680 nm for Cab and 490 – 550 nm for Ccar and Cant estimations. Statistical analyses showed overall low Cab and Ccar contents of sunlit crowns (max. around 9 and 5 $\mu\text{g}\cdot\text{cm}^{-2}$, respectively), while Cant was relatively high (max. close to 9 $\mu\text{g}\cdot\text{cm}^{-2}$). High Cant is typical for the early eucalypt growth phase when it protects young leaves against a potential high solar irradiation damage, corresponding to the springtime leaf flushes observed during the flight campaign. Histogram comparison of UAS-retrieved values against laboratory measurements indicated a good agreement for Cant but an underestimation for Cab and Ccar, which might be attributed to an insufficient number of TOC leaf samples collected during the tree sampling.

Outlook for the future

This study demonstrated a close agreement between DART-simulated and drone-acquired hyperspectral reflectance images in the case of spatially and structurally highly heterogeneous eucalyptus forest environment. This permitted radiative transfer-based inversions of biochemical functional traits of individual forest crowns from a very high spatial resolution (5 cm) hyperspectral nadir image. The achieved Cab, Ccar, and Cant maps are intended to be used for a validation purpose, specifically for a cross-comparison with the same map products retrieved at the coarser spatial resolution of 20 m from the Sentinel-2 MSI data acquired over the Tumbarumba site at the same time. The maps might also serve as inputs in the multi-scale assessment of forest functional diversity using a scalable kernel-based trait probability density approach, conducted at the spatial scale of individual tree crown parts.

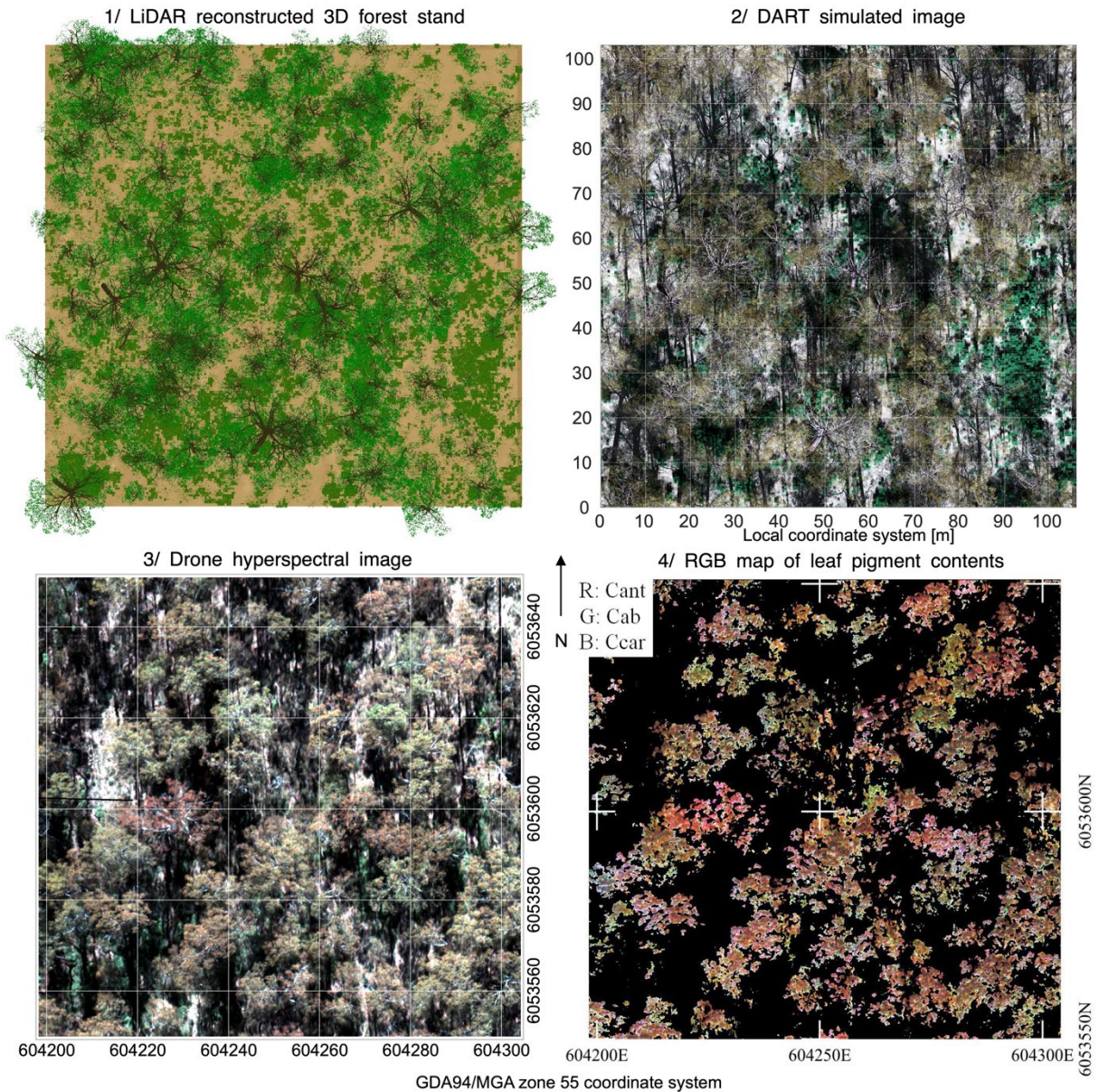


Figure 1: Graphical abstract illustrating outputs of main methodological steps: (1) creation of a 3D virtual eucalyptus forest stand from terrestrial laser scans (TLS), (2) drone hyperspectral image of the forest stand simulated in the Discrete Anisotropic Radiative Transfer (DART) model, (3) drone-acquired VNIR hyperspectral image (pixel size ~ 5 cm), and (4) RGB false colour composite of leaf pigment content maps (Red ~ Anthocyanin [Cant], Green ~ Chlorophyll a+b [Cab], and Blue ~ Carotenoids [Ccar]), retrieved per-pixel from the drone VNIR image by Random Forest regressions trained and validated over the Fluspect-Cx/DART-simulated reflectance look-up tables.

Plant trait estimation in a forest ecosystem from hyperspectral satellites through machine learning and hybrid approaches

Cinzia Panigada¹, Giulia Tagliabue¹, Jochem Verrelst², Jose Luis Garcia Soria², Gabriele Candiani³, Mirco Boschetti³, Miguel Morata², Rodolfo Gentili¹, Beatrice Savinelli¹, Luigi Vignali¹, Luca Gallia¹, Valentina Picchi⁴, Antonella Calzone⁴, Roberto Colombo¹, Rossini Micol¹

¹ University of Milano - Bicocca, Department of Earth and Environmental Sciences, Italy

² University of Valencia - Image Processing Laboratory - Laboratory for Earth Observation, Spain

³ Institute for Electromagnetic Sensing of the Environment, National Research Council, Italy

⁴ CREA Research Centre for Engineering and Agro-Food Processing, Italy

Keywords: Leaf nitrogen content, Leaf chlorophyll content, machine learning, hybrid models, CHIME, PRISMA

Challenge

Plant leaf and canopy traits play an important role in forest ecosystem monitoring. Their mapping is still challenging, although the recently launched and upcoming hyperspectral satellites, featuring contiguous visible-to-shortwave infrared spectral data, open opportunities for the accurate retrieval of multiple plant traits by new-generation models.

In the framework of the ESA project CHEES - Chime End to End mission performance Simulator, hybrid models have been already tested and validated for the retrieval of crop traits from synthetic hyperspectral spaceborne data; however, their exportability to real images has not been tested in natural forest ecosystems, where pure machine learning approaches are more used. In this contribution, these hybrid approaches and pure machine learning models are tested and validated on a unique dataset of PRISMA images and ground data collected in a forest ecosystem focusing on CHIME vegetation priority variables at leaf (i.e. leaf chlorophyll content (LCC), leaf nitrogen content (LNC), leaf water content (LWC) and leaf mass per area (LMA)) and canopy level (i.e. leaf area index (LAI), CCC, CNC, CWC).

Methodology

Two different approaches were investigated, machine learning regression algorithms (MLRAs) and hybrid approaches based on radiative transfer models coupled with MLRAs. The MLRAs tested were the Gaussian Processes Regression (GPR), Neural Networks (NN), Partial Least Squares Regression (PLSR), Random Forest Regression (RF) and Support Vector Regression (SVR).

MLRAs results were compared with results obtained by a hybrid retrieval workflow developed in the frame of CHEES project that couples simulation from radiative transfer models - RTMs (i.e. SCOPE 2.1 and PROSAIL) with MLRAs approaches. The algorithms were tested and validated for the first time on real PRISMA images acquired on a forested area, a mixed mesophytic oak forest (Ticino Regional Park, Northern Italy, 45.4286° N, 8.8342° E).

Two hyperspectral PRISMA mosaics (4 tiles each) were collected at different vegetative stage (June and September 2022) in order to capture plant trait variations from early summer to early fall. PRISMA images are the satellite products nowadays available that most closely resemble CHIME in terms of spectral range, number of band, and FWHM. Field activities were conducted in 50 forest stands contemporary to PRISMA acquisition to collect the plants traits useful to calibrate and validate the retrieval models.

Algorithm performances were evaluated in terms of standard goodness-of-fit statistics against the field dataset collected (i.e. r^2 and nRMSE).

Results

MLRAs performed well in leaf and canopy traits retrieval with high predictive capacity for all the models tested when PCA analyse was performed to reduce data dimensionality. Models were trained using the first 15 PRISMA synthetic bands and ground data collected in the field and were cross-validated through k-fold technique. The best performance for each plant traits was obtained with different models: LAI was best estimated by SVM ($r^2=0.91$, nRMSE= 8.99 %), LMA by KRR ($r^2=0.95$, nRMSE= 5.62 %), LCC by SVM ($r^2=0.44$, nRMSE= 18.27 %) and LNC by GPR ($r^2=0.63$, nRMSE= 14.15 %). However, GPR was the most robust model giving good performances for most of the traits, LAI, LMA and LNC, while performing poorly only with LCC (Figure 1). The general good performances of ML algorithms at leaf level showed that the information content of the PRISMA reflectance spectra is good enough to capture the slightly small differences linked to the variation of the leaf traits. Furthermore, ML algorithms are able to disentangle the effect on the spectra of LAI from leaf level traits giving good results at both, leaf and canopy level. Hybrid approaches developed in the frame of CHEES failed on the retrieval of traits at leaf level, while showed a good predictive power in the estimation of LAI ($r^2=0.79$, nRMSE= 12.5) and canopy plant traits, such as CCC ($r^2=0.74$, nRMSE=24.2). We noticed that better results were achieved when the algorithm optimization was conducted through active learning techniques using PRISMA spectra, otherwise, retrieval showed a significant plant trait overestimation.

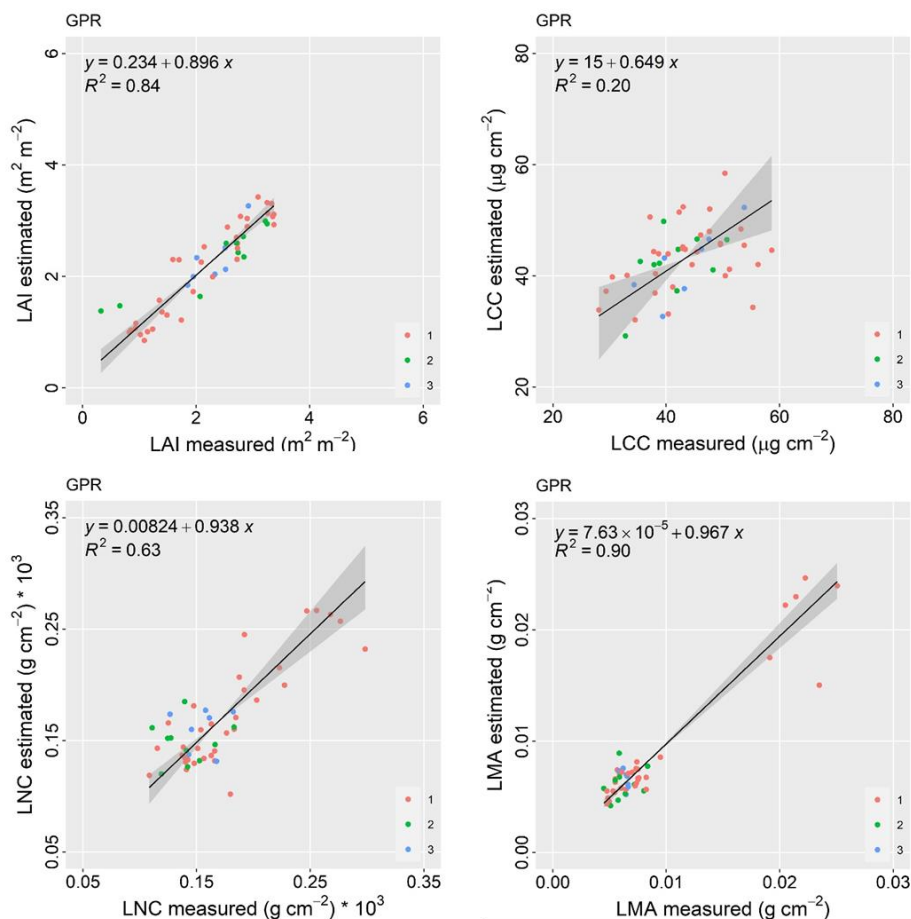


Figure 1. MLRAs performances. GPR shows high performances in most of the plant trait retrieval. Only in case of LCC, SVR shows higher performances.

Outlook for the future

MLRSs algorithm showed satisfactory performances in plant trait retrieval in forest ecosystem both at leaf and canopy level except for the LCC. MLRSs main drawback is that their robustness depend on the number, quality, and representativeness of the field datasets used for their calibration and validation. Collecting a good field dataset in forest ecosystems is time consuming and the variability needed to ensure statistical models exportability is hard to sample. This is why hybrid approaches are under investigation for operational satellite processors. Hybrid approaches imply the simulation through RTMs of larger dataset that easily resemble the high plant trait variability shown in nature. The poor performances at leaf level may be due to the RTM models that do not capture the slight differences in the spectra due to variations in leaf traits, or to difficulties to disentangle the LAI and leaf trait effects on the canopy spectra. Simulations by means of more complex RTMs, such as the 2D INFORM and the 3D DART models may be integrated in the algorithm to improve the exportability on natural ecosystems.

Acknowledgements

This work is carried out within Contract "PRIS4VEG" n. 2022-5-U.0 (CUP F43C22000000005), funded by ASI in the "PRISMA SCIENZA" program. Some hybrid algorithms were developed in the frame of the project CHEES - Chime End to End Mission Performance Simulator, funded by ESA (Contract reference 4000137752/22/NL/NA).

Them.Sess. 3-2: Exploring the synergies between imaging spectrometer missions and between multispectral data and imaging spectrometer data for advancing applications

Synergetic use of multispectral and hyperspectral imagery data for inland water applications

Alice Fabbretto^{1,2}, Andrea Pellegrino¹, Mariano Bresciani¹, Claudia Giardino¹, Federica Braga³, Krista Alikas², Nicola Ghirardi¹, Diana Vaičiūtė⁴

¹ National Research Council, Institute for Electromagnetic Sensing of the Environment, Italy

² University of Tartu, Department of Remote Sensing, Estonia

³ National Research Council, Institute of Marine Sciences, Italy

⁴ University of Klaipeda, Marine Science and Technology Centre, Lithuania

Keywords (5): PRISMA, EnMAP, MSI, water quality products, chlorophyll-a

Challenge

In the current era, as the world is dealing with an unprecedented environmental crisis in which inland and coastal water ecosystems face severe impacts, the application of spaceborne imaging spectroscopy has emerged as a powerful tool to enhance remote sensing capabilities in spatio-temporal environmental monitoring. This technology allows the acquisition of a continuous spectrum, enabling algorithms to retrieve a wider range of properties and achieve superior performance under different conditions and water types (Dierssen et al., 2021, *Environmental Science*, 9). The aim of this study is to present, by means of a couple of examples, the possible applications resulting from the synergetic use of imagery data collected by multispectral (Sentinel-2 MSI) and hyperspectral (PRISMA and EnMap) satellite sensors for mapping aquatic ecosystems in the context of various research activities and user-driven initiatives.

Methodology

The satellite data used in this analysis are those provided by the well-established multispectral sensor Sentinel-2 MSI operated by ESA and the two hyperspectral sensors PRISMA and EnMAP, respectively managed by ASI and DLR. After a comprehensive radiometric evaluation of the hyperspectral data, water quality products were generated for two aquatic ecosystems: the highly productive turbid water of the Curonian Lagoon and the shallow turbid water of Lake Trasimeno. In accordance with the state-of-the-art of retrieval algorithms of water constituents' (Odermatt et al., 2012, *Remote Sens. of Env.*, 118), two methods were tested: an adaptive semi-empirical algorithm built on band-ratio approach and the inversion of the bio-optical model implemented in BOMBER. The BOMBER model was run to generate the maps in terms of chlorophyll-a (chl-a) for Lake Trasimeno, whose intrinsic optical properties are well-known. Instead, given the evident spectral features of the reflectance data of the Curonian Lagoon, a semi-empirical algorithm was used. This algorithm exploited the presence of narrow, contiguous spectral bands that allowed for a better identification of local minima and maxima reflectance depending on chl-a concentration. To assess the agreement of the estimated water quality parameters obtained from PRISMA, EnMAP and MSI, a comparison was carried out with the in situ collected measurements, considering the following metrics: Coeff. of determination (R^2); Mean Absolute Error (MAE).

Results

In this section, a pair of examples will be shown where synchronous in situ, hyperspectral and multispectral satellite data were available. Figure 1 shows chl-a maps obtained with the semi-empirical model applied to PRISMA and MSI images over the Curonian Lagoon. The maps show how highest chl-a concentrations occur in the southernmost part of the lagoon, reaching values of around 120 mg/m³ in some areas as where the Nemunas River flows into the lagoon. Both products show good agreement with the in situ measurements, with a slight improvement by the PRISMA product ($R^2 = 0.87$, MAE = 9.73) compared to the MSI product ($R^2 = 0.85$, MAE = 10.25).

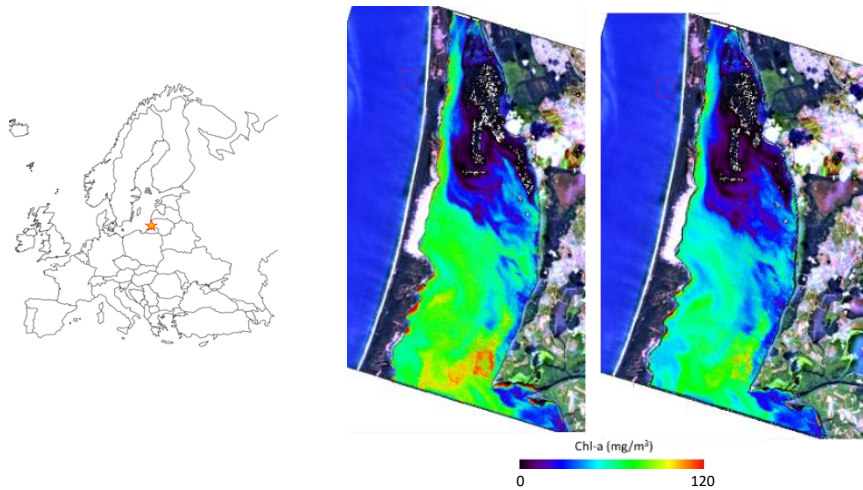


Figure 1: Chlorophyll-a maps generated by running the semi-empirical model in the Curonian Lagoon (Lithuania). The map derived from the PRISMA image is shown on the left of the figure and the map derived from the MSI image is shown on the right. The two images were acquired on 25/07/2021.

Figure 2 shows the chl-a maps produced by the bio-optical model BOMBER applied to EnMAP and MSI images of Lake Trasimeno. An average chl-a concentration of around 40 mg/m³ was observed in the lake, with higher values - up to 60 mg/m³ - found in the southernmost and westernmost parts of the lake. The map was cropped at the presence of emergent macrophytes in the southeastern bay. Chl-a derived products show good statistical agreement with the in situ measurements, with slightly different performance between the sensors: the product derived by the EnMAP image resulted in MAE = 3.01, the one derived by the MSI resulted in MAE = 3.51.

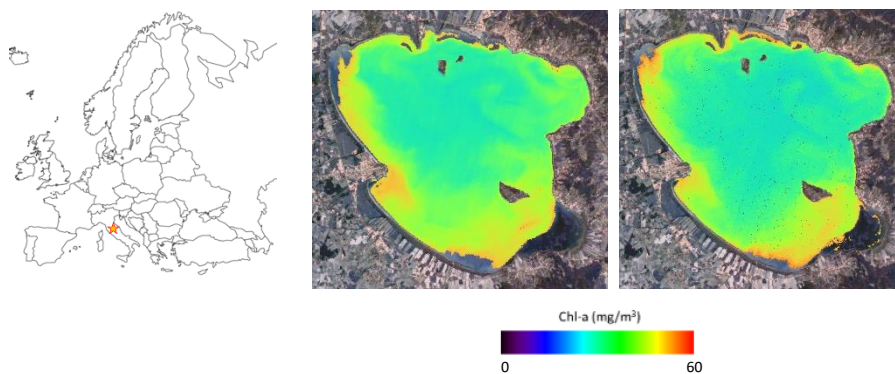


Figure 2: Chlorophyll-a maps generated by running the BOMBER model in Lake Trasimeno (Italy). The map derived from the EnMAP image is shown on the left of the figure and the map derived from the MSI image is shown on the right. The two images were acquired on 05/10/2022.

Outlook for the future

Multisource data integration plays a key role in remote sensing to understand and mitigate the growing influence of climate change and anthropogenic pressure on water ecosystems. The results of the study have highlighted the scientific potential of integrating satellite multispectral and hyperspectral data for mapping chl-a, a proxy of phytoplankton biomass and a key indicator of water quality. Hyperspectral data show the advantage of running bio-optical model inversion on contiguous bands of the entire spectral range to exploit multiple narrow bands for the identification of spectral features at a fine spectral scale. This allows for slightly more accurate water quality products that are representative of the state of the observed target. Despite the need of more in-depth analysis, when PRISMA and EnMAP data are used in synergy with in situ measurements and multispectral data, they could offer a relevant support also in view of the future hyperspectral missions (e.g., CHIME and PRISMA-2G) for improving water management activities.

CHIME Hypersense Campaign Data Harmonisation and Quality Assessment via Uncertainty Analysis

EARSeL Valencia 2024
Abstract
Corresponding Author:
[mike.werfeli@geo.uzh.ch]

[Mike Werfeli](#)¹, Daria Larcher¹, Andreas Hueni¹, Kimberly Mason¹, Cinzia Panigada², Giulia Tagliabue^{2,3}, Raquel De Los Reyes⁴, Jens Nieke⁵, Michael Rast⁶ and Marco Celesti⁵

¹ Remote Sensing Laboratories, University of Zurich, Department of Geography, Zurich, Switzerland

² University of Milano Bicocca, Milano, Italy

³ Jet Propulsion Laboratory, California Institute of Technology, Pasadena, United States of America

⁴ Deutsches Zentrum für Luft- und Raumfahrt DLR, Germany

⁵ European Space Agency ESA ESTEC, Noordwijk, The Netherlands

⁶ International Space Science Institute (ISSI), Bern, Switzerland

Keywords (5): CHIME, Calibration/Validation, imaging spectroscopy, uncertainty, point spread function

Challenge

In 2021, the Remote Sensing Laboratories (RSL) at the University of Zurich (UZH) successfully carried out an airborne imaging campaign on behalf of the European Space Agency (ESA) to support the upcoming Copernicus Hyperspectral Imaging Mission for the Environment (CHIME). The data recorded in this campaign are used to create a test bed and development environment for processing (e.g. up- and down scaling, Calibration / Validation (CAL/VAL)) and higher-level product algorithms of the upcoming CHIME space-based Earth observation (EO) mission. Therefore, six areas of interest (AOI) of the entire catalogue were selected for an in-depth data quality analysis. The Earth observation data (bottom of atmosphere reflectance) of the selected AOIs, imaged by space-based (PRISMA and DESIS) and airborne (AVIRIS-NG) imaging spectroradiometers and measured by field spectroradiometers collecting spectral ground control point (SGCP) data, were collected within a time window of ± 1 day.

Methodology

First, the different EO data sets were harmonised by reprojecting the images to the same Sentinel – 2 reference image. Data analysis of the EO data was performed with an updated version of the RSL in-house CAL/VAL tool, which is relying on the spectral information system SPECCHIO for a centralised database approach. Thereby, two spatially co-located reflectance spectra are compared, computing the spectral difference (SD), the spectral ratio (SR) and the measurement agreement.

Sensor related uncertainties estimated by the sensor operators were enriched with a geolocation uncertainty and propagated to SD and SR following the Guide to the Expression of Uncertainty in Measurement. To combine the sensor related uncertainty with geolocation uncertainty, spatially co-located pixel data were deconvolved based on the sensor specific point spread function (PSF), to estimate the pure spectral reflectance of the area covered by the nominal ground sampling distance. The geolocation uncertainty was estimated via a Monte Carlo approach, randomly moving the PSF within ± 1 pixel distance in across and along track direction and statistically summarising the deconvolved spectra. In addition, the measurement agreement between two measurements was computed, describing the similarity of two measurements statistically.

Finally, the space-based and airborne EO data were compiled to a Multi Scale Data Set (MSDS), where each sensor was compared to a virtual reference sensor. This reference sensor was modelled with the mean of all co-located spectral reflectance measurements available in the MSDS, weighted by their respective uncertainties.

Results

Running the CAL/VAL analysis on the EO data, reveals not only the quality of the recorded data but also the characteristics of the CAL/VAL target selected by the field teams (Figure 1 a and b). Figure 1 a and

b show the reflectance spectra resulting after deconvolving the spectrum based on the sensor specific PSF, moving around the SGCP location. In Figure 1a the SGCP is located in a homogeneous CAL/VAL target, showing little variation in the sampled spectra, thus resulting in a small radiometric uncertainty due to geolocation uncertainty. The SGCP in Figure 1b on the other hand is showing a suboptimal SGCP location. This SGC location is found at a more heterogenous target site, where bright and dark pixels are influencing the measurement at the SGCP. This variation results in a large geolocation uncertainty, which adds to the total uncertainty, increasing the final propagated measurement uncertainty. The greater large geolocation uncertainty has also an influence on the measurement agreement between two sensors. In figure 2 a and b the measurement agreement of the two respective SGCP locations are shown at different coverage factors ($k = 1$ until $k = 3$). Generally, the higher the coverage factor, the higher the agreement between the measurements compared, because the significance level increases and thus the probability to reject the similarity decreases. Also, the greater the single propagated uncertainties are, the better the measurements do agree, given that the probability for them to agree is bigger.

Outlook for the future

Here we present a method which shows how to do a CAL/VAL analysis on the example of a MSDS, containing space-based, airborne spectroscopy data, as well as field measurements. Applying a common geo- and orthorectification, and atmospheric correction facilitates a thorough sensor intercomparison as well as data quality assessment and reporting. The methodology applied in this data analysis highlights the importance of the target selection for CAL/VAL activities for airborne and space-based EO missions. A careful selection of a CAL/VAL site and thorough planning of data acquisition reduce the introduction of uncertainties related to heterogeneity within a potential site or a too small sized site, not covering a recorded pixel. In addition, we show how the estimation and propagation of uncertainties contributes to a well-founded and traceable data quality description.

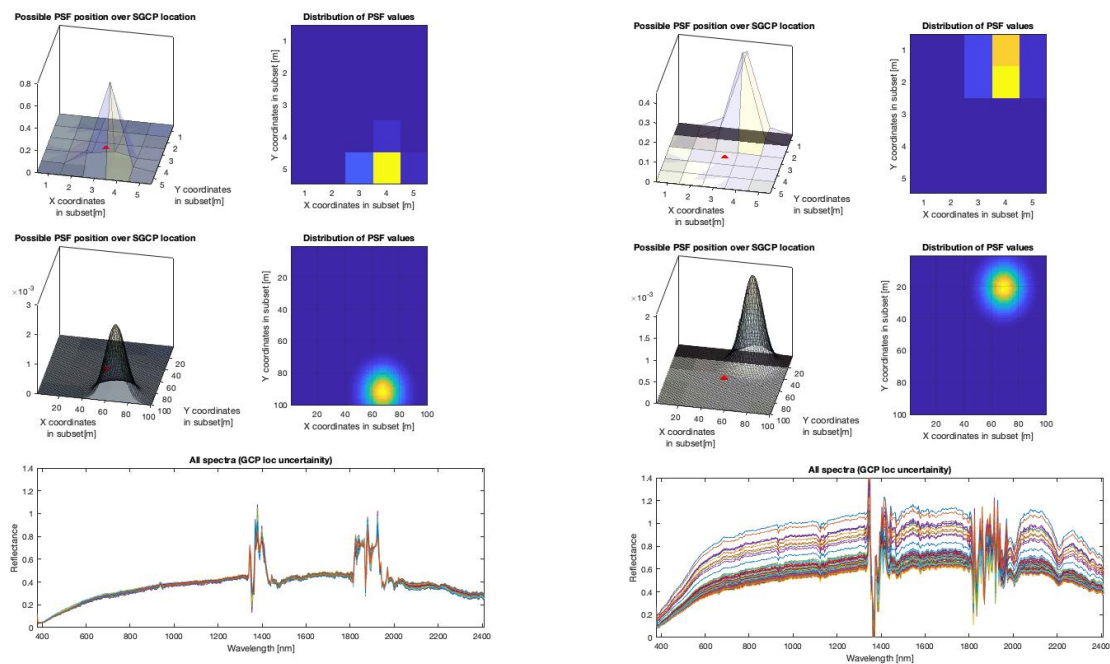


Figure 1 (a) example of an optimal CAL/VAL reference target and (b) example of a suboptimal CAL/VAL reference target

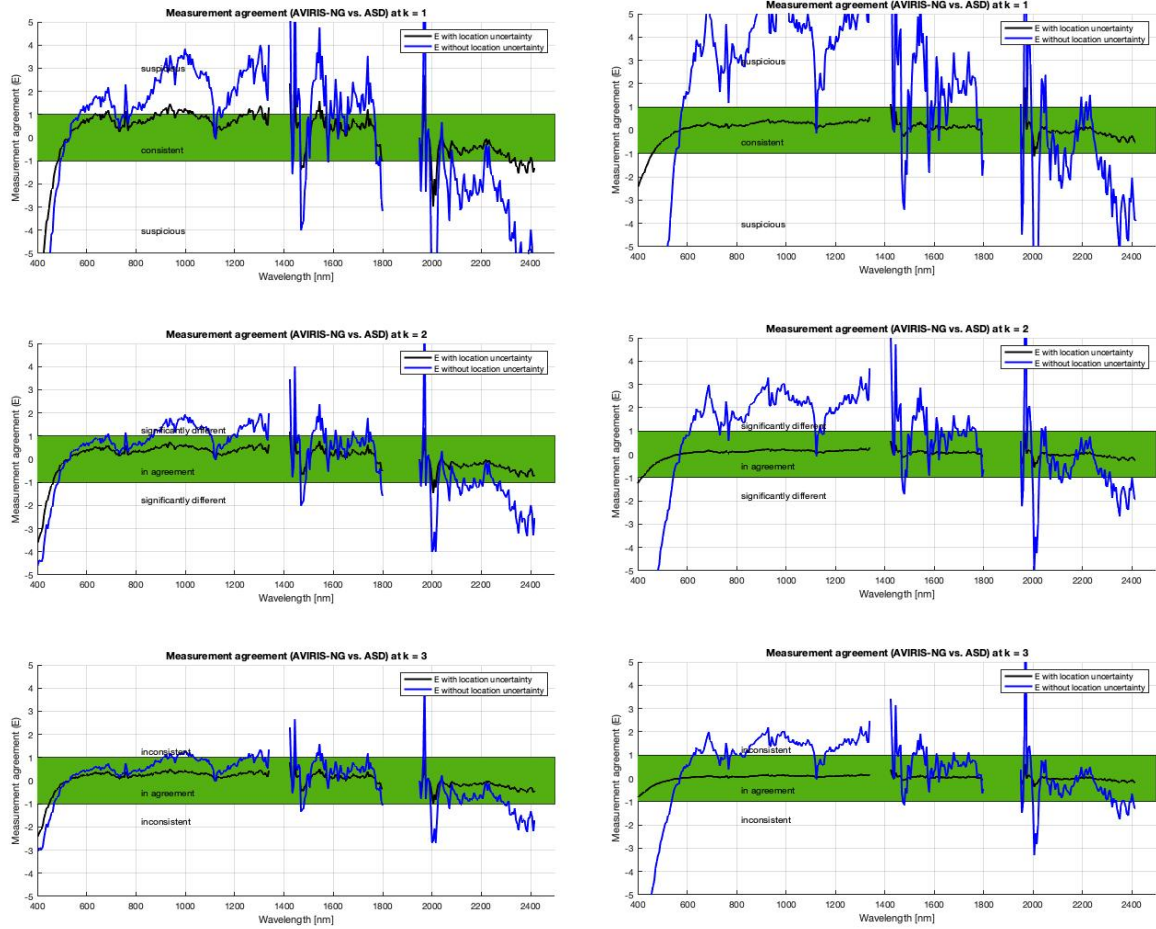


Figure 2 (a) Measurement agreement of an optimal CAL/VAL reference target and (b) measurement agreement of a suboptimal CAL/VAL reference target

**[Formatting guidelines for
abstract submission]**

EARSel Valencia 2024

Abstract

Corresponding Author:

[kopkane.d@czechglobe.cz]

**Fusion of airborne remote sensing data
for description of thermal heat island**

Daniel Kopkáně¹, Jan Novotný, Miroslav Píkl¹, Jan Hanuš¹, Lucie Homolová¹, František Zemek¹

¹ Global Change Research Institute CAS, Department of Remote Sensing, Czech Republic

KEYWORDS URBAN HEAT ISLAND, THERMAL, HYPERSPECTRAL, LIDAR

Challenge

Airborne surveys can be used to assess urban thermal regimes and heat islands because their high spatial and spectral resolution is particularly well suited to resolving highly heterogeneous systems (in terms of variation in size and spectral properties of objects) such as urban environments. CzechGlobe operates an airborne platform that enables complex synthesis of data from hyperspectral sensors in the visible, near and short-wave infrared and thermal parts of the electromagnetic spectrum. Combined with airborne laser scanning (LiDAR) data, it is then possible to produce an accurate classification of buildings, trees, paved and unpaved areas with surface temperature assignment, which can be further processed into specific maps to describe the Heat Island phenomenon.

Methodology

Airborne data for Brno municipality in the Czech Republic were processed into standardized products: land surface temperature, land surface emissivity, LIDAR point cloud, VNIR/SWIR reflectance. Over the data products we perform surface classification into buildings, trees, grass, pavements/roads and water. The separation allows the influence of different classes to be considered separately, e.g. roofs are typically the hottest surfaces but only have an indirect effect on pedestrians on the street through downwelling radiation.

The estimation of perceived temperature is divided into two steps. The first is to derive a proxy air temperature from the temperature of the trees (Figure 1c). The main assumption of this step is that the leaf temperature is close to air temperature (in case of sunlit leaves, the leaf temperature increases by a few degrees, e.g. +4K). Proper classification and filtering of suitable thermal pixels i.e., sufficiently large trees, that are corrected for the proportion of sunlit and shaded tree pixels by NIR radiation and tree height derived from LiDAR, should provide the distribution of air temperature across a vast urban landscape. The second step is to further process the air and surface temperature data into expected thermal comfort at a particular location (Figure 1d). It determines the expected perceived temperature based on urban structure, sky view factor, downwelling radiation, pavement and turf surface temperatures, and proxy air temperature.

Expected results

The results derived from the airborne image data can provide a complex view of an urban landscape, including classification of urban structures, reflectance and thermal properties (Figure 1). The interpolated proxy air temperature, corrected for insolation and tree height, shows a typical accuracy of better than 1 K from the value obtained by rigorous ground measurements. In the case of the calculated expected perceived temperature, the values show a reasonable degree of correlation with ground measurements, with a typical accuracy of about 3 K.

Outlook for the future

The processed data make it possible to highlight the heat island phenomenon of the city, both in terms of higher air temperature compared to the surrounding landscape, and by describing the heat load on the inhabitants, with detail down to the level of individual streets. Such results can be used to produce walkability maps expressing the heat stress. This can be used by local authorities to make informed decisions about local hotspots.

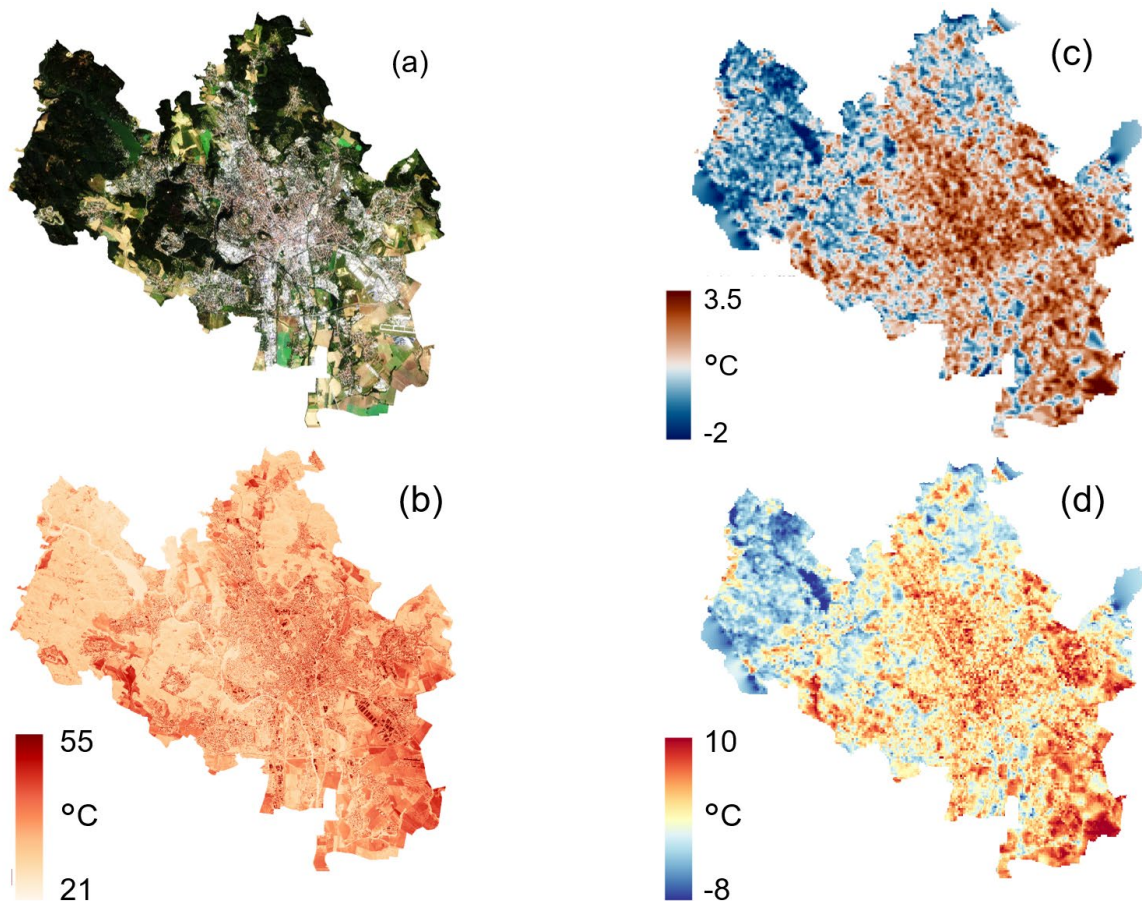


Figure 1 Airborne products for Brno (31. 8. 2019 around noon): a) true color, b) land surface temperature, LST, c) proxy of air temperature gradient*, d) estimated perceived temperature gradient*. *) gradient means difference between actual value and mean value of flight line

Towards consistent EnMAP, Landsat, and Sentinel-2 Analysis Ready Data cubes for multisensor monitoring applications

[Akpona Okujeni](#)¹, [Andreas Janz](#)¹, [Neija Elvekjaer](#)¹, [Katja Kowalski](#)¹, [Benjamin Jakimow](#)¹, [Sebastian van der Linden](#)², [Patrick Hostert](#)¹

¹ Humboldt-Universität zu Berlin, Germany

² University of Greifswald, Germany

Keywords (5): Hyperspectral, EnMAP, Analysis-Ready-Data, Multisensor

Challenge

Harmonized Landsat and Sentinel-2 Analysis Ready Data (ARD) cubes have significantly enhanced environmental monitoring applications based on multispectral time series. ARD cubes comprise consistently pre-processed Level 2 reflectance data and associated quality layer products, organized in a unified spatial tiling system for immediate and efficient application-oriented analysis. Recent missions like EnMAP or PRISMA add hyperspectral time series to existing multispectral archives, expanding the possibilities for more detailed ecosystem monitoring. To effectively utilize these novel datasets and explore their synergies, strategies for integrating satellite hyperspectral data into existing multispectral ARD cubes are essential. Furthermore, there is currently no solution available for creating best available pixel composites or spectral-temporal metrics from hyperspectral time series, even though such higher-level ARD products are operational in the multispectral image processing domain.

Methodology

We have developed a Python-based pipeline for seamlessly integrating EnMAP data into ARD cubes. Our workflow makes use of EnMAP Level 2A reflectance data and associated quality layer products provided through the EnMAP Data Access Portal. Products are automatically downloaded, unpacked, and saved on disk. All products are then re-projected into a target coordinate system and pixel grid, followed by spatial reorganization of the data into a systematic tiling system. The underlying target coordinate system, pixel grid, and tiling system are either defined by the user or by pre-existing data cubes. Further flexible options in this process include solutions for ad-hoc band subsetting based on lists of bad bands or wavelengths, band interpolation and smoothing, or masking of spectral images based on quality layers (e.g., cloud masks). Virtual mosaics of predefined band combinations enable a fast visualization of the EnMAP data cube. In scenarios where time series of EnMAP data are available, our pipeline also supports the creation of best available pixel composites for a user-defined temporal window and target date, along with statistical spectral-temporal metrics for all observations within a user-defined time period.

Results

We successfully obtained a 1-year time series of Level 2A EnMAP data for three study sites located in California. This dataset comprised between one and four acquisitions per month and study site, and was provided in spatially inconsistently overlapping image files. We further developed a combined Landsat and Sentinel-2 ARD cube based on all available images with a cloud coverage of up to 75% for the same period. This data cube was generated using the Framework for Operational Radiometric Correction for Environmental monitoring (FORCE) and was organized in 30x30 km tiles with the state-wide NAD83 /

California Albers coordinate system. The integration of our EnMAP time series into the multispectral data cube significantly streamlined the effective visualization and utilization of EnMAP time series, whether used independently or in conjunction with Landsat and Sentinel-2 data. Our application of the best available pixel compositing technique has demonstrated its effectiveness in generating cloud-free EnMAP mosaics, especially for data takes acquired from at least two neighbouring orbits within narrow observation windows. Furthermore, spectral-temporal metrics calculated from the entire year's spectral observations have proven to be a valuable input for mapping plant-life forms across the diverse ecosystems encompassed within the study sites.

Outlook for the future

Our pipeline provides a first framework towards consistent ARD cubes for multisensor monitoring applications using EnMAP, Landsat, and Sentinel-2 time series. We primarily focussed on challenges related to spatial harmonization among datasets, our next efforts will focus on the spectral component. Future work will promote integrating additional time series data obtained from missions such as PRISMA, enhancing the temporal density of satellite-based hyperspectral time series. The core algorithms will be implemented in the EnMAP-Box and all functionalities will be accessible through the EnMAP-Box API. Our developments represent a significant step towards advancing the integration of multisensor data from hyperspectral and multispectral satellite sensors for comprehensive environmental monitoring applications. It further paves the way towards future operational hyperspectral missions that will provide dense time series in a wall-to-wall fashion, such as CHIME or SBG.

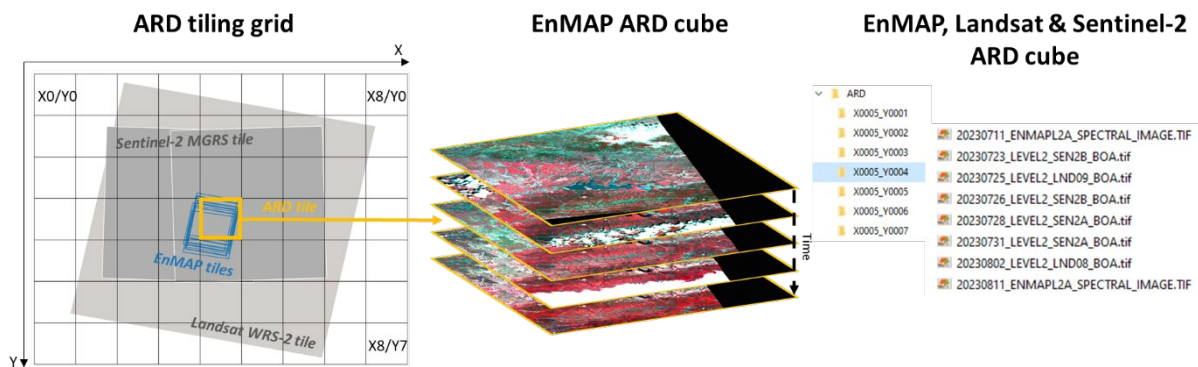


Figure Concept for creating consistent EnMAP, Landsat, and Sentinel-2 analysis-ready data cubes for multisensor applications

Mapping The Colors Of Flowering Phenology With Imaging Spectroscopy

[Yoseline Angel](#)^{1,2}, Dhruva Kathuria^{1,3}, Evan Lang^{1,4}, K. Dana Chadwick⁵, Philip G. Brodrick⁵, Alexey Shiklomanov¹

¹ NASA Goddard Space Flight Center, Earth Sciences Division, USA

² University of Maryland – College Park, ESSIC, USA

³ Morgan State University, GESTAR II, USA

⁴ Science Systems and Applications, Inc., USA

⁵ California Institute of Technology, Jet Propulsion Laboratory, USA

KEYWORDS: FLOWERING, IMAGING SPECTROSCOPY, PHENOLOGY, GAUSSIAN MIXTURE, FLOWERING NARROWBAND INDEX

Challenge

Flowering phenology shifts are widely reported as an effect of climate change. Modeling such landscape dynamics (e.g., phenophases, spatial distribution) could reveal hints on ecological processes such as understanding phenotypic pollinator selections based on flower color signaling and monitoring floral adaptations to environmental changes. Flowers absorb light along the ultraviolet (~300nm) to shortwave infrared wavelengths (< 800 nm), depending on the chemical structures of their pigments. Despite their ecological importance and unique spectra, there is a relative dearth of literature on the remote sensing of flowers. Imaging spectroscopy can measure the light reflected, absorbed, and transmitted by flower pigments across different spatio-temporal scales. However, quantifying flower coloration and its relative contribution to canopy spectral signal and monitoring such spatio-temporal phenology dynamics by integrating remote sensing with field-based ecology remains unexplored.

Methodology

Our research investigates novel methods to account for the weighted contributions of flowers, leaves, and soil to typical hyperspectral scenes crucial to (a) characterize the spectral variability within a pixel, (b) map flowering areas, and (c) reveal specific phenophases across species. Weekly time series imagery from the airborne imaging spectrometer AVIRIS-NG (427 spaced 5nm bands from 0.38 to 2.51 μ m and 5m spatial resolution) and field spectra were collected as part of the NASA SBG High-Frequency Time Series (SHIFT) campaign carried out in Santa Barbara, CA —acknowledged as one of the most biodiverse ecoregions in North America— during the spring of 2022. A diversity of native shrub and flowering species were observed in the study site. AVIRIS-NG imagery was atmospherically corrected via optimal estimation as implemented in the ISOFIT library, and field spectra from leaves, flowers, and soil within flowering sampled plots were spectrally resampled to match the AVIRIS-NG response. The processed data were input to 1) characterize the subpixel spectral variability using spectral mixture residual decomposition techniques to account for the relative contributions of common landscape elements (e.g., leaves, soil, and shades) and rare, targeted elements like flowers; 2) map flowering areas and provide uncertainty assessment metrics using the unsupervised Gaussian mixture model; 3) develop a flowering narrow-band index to study specific flowering phenophases across species.

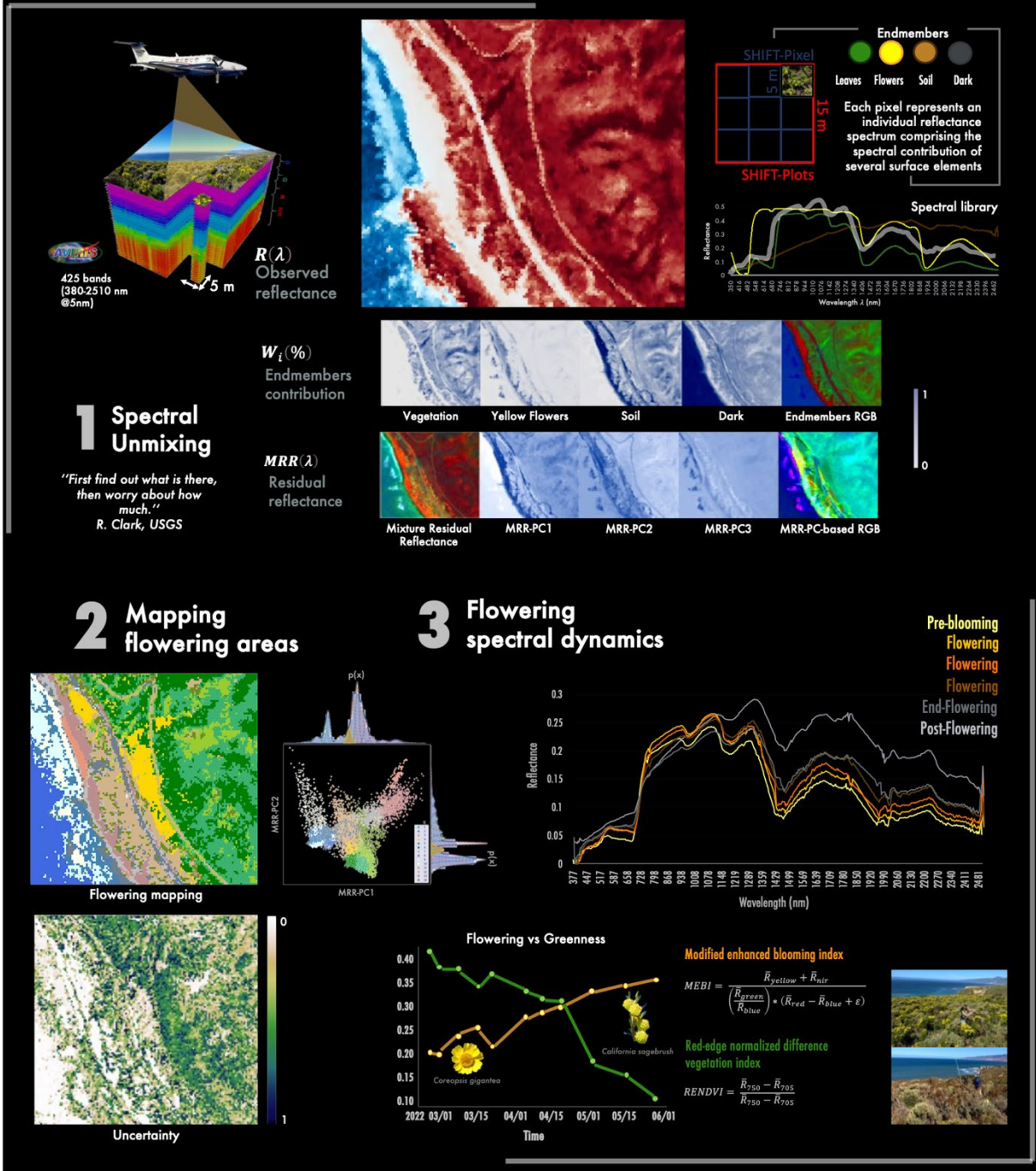
Results

Field spectra from flowers and leaves showed spectral differences at leaf-petal and canopy scales. High reflectance from flower spectra between green and red edge wavelengths (500 nm-700 nm) contrasts the leaves' spectral features due to the scarce chlorophyll content in yellow flowers. Such spectral differences become more subtle as leaves turn yellow across the season. Linear spectral unmixing allowed the computation of the weighted contribution of four major low-variance endmembers (leaves, flowers, soil, dark signal) and high-variance residual signal—mixture residual reflectance (MRR). A lower dimension feature space comprising the top three MRR principal components (MRR-PC) included 97% of the subtle spectral differences, enriching the spectral separability in this domain and allowing (a) identifying flowering clusters using the unsupervised Gaussian mixture model; (b) retrieving pixel-wise uncertainty of the results; (c) achieving an 80% certainty level average for the flowering clusters. Mapping flowering areas across the season, from pre- to post-flowering, let us identify gradient variations in spectral features within the visible and shortwave infrared ranges linked to flowering pigments and water content changes, respectively. Time series of the Modified Enhanced Blooming Index (MEBI) and the Red-Edge Normalized Difference Vegetation Index (RENDVI) reveal specific flowering and emergence/senesce sequence phenophases of the main flowering species in the study site.

Outlook for the future

Because of the remoteness and harshness of some environments, the most reasonable way to monitor blooming events is using remote sensing, and developing methods for mapping and tracking flowers is not just a gap to fill but a necessity. Overall, our approach for mapping flowering events from modeling spectro-temporal dynamics opens opportunities for exploiting data products from the new generation of spaceborne imaging spectrometers (e.g., SBG, EMIT, EnMAP, CHIME, PRISMA) to monitor floral cycles across large scales over floristic biodiverse hotspots. Further work will push our methodological framework to estimate sub-pixel flower fractions for diverse floral scenarios with multiple flower colors at broader spatial scales and provide insight for advancing physical-based models that parameterize primary flower pigment contents (e.g., carotenoids, betalains, and anthocyanins) for a quantitative understanding of flower coloration and its relative contribution to canopy spectral signals.

Mapping the colors of flowering phenology with imaging spectroscopy



Graphical abstract. Results demonstrate the mapping of yellow flowers using AVIRIS-NG surface reflectance data (top left). In-situ reflectance spectra of five yellow flower species over the entire VSWIR range (top right). Model outputs by step: (1) Unmixing spectral mixture residual results. (2) Principal component analysis based on MRR and Gaussian mixture model results (i.e., occurrence probabilities and uncertainties maps). Class X (yellow) from the GMM aligns spatially with regions known (from fieldwork) to contain yellow flowers (indicated with dashed orange lines). (3) Multitemporal average reflectance profiles from flowering areas show gradient dynamics from pre-blooming to post-flowering along the green, yellow, and short-wave infrared spectral region. Two vegetation indexes, the MEBI (yellow) and RENDVI (green), reveal flowering and greenness phenophases, respectively, of the two predominant species (e.g., *C. gigantea* and *A. californica*) in the clustered areas.

Species-Level Fractional Savannah Woody Vegetation Mapping with Drone and EnMap Hyperspectral Data

[Christina Karakizi](#)¹, Akpona Okujeni², Vasileios Tsironis³, Athina Psalta³, Konstantinos Karantzas³, Patrick Hostert², Elias Symeonakis¹

¹ Department of Natural Sciences, Manchester Metropolitan University, Manchester, M1 5GD, UK

² Geography Department, Humboldt-Universität zu Berlin, Unter den Linden 6, 10099 Berlin, Germany

³ Remote Sensing Laboratory, National Technical University of Athens, 15780 Zographos, Greece

Keywords (5): Satellite Data, Land Degradation, Neural Network, Regression, Bush Encroachment

Challenge

In order to meet the UN Sustainable Development Goal for Land Degradation Neutrality (LDN) by 2030 it is imperative to accomplish an assessment of the state of savannahs as early and as accurately as possible. Monitoring the species composition of vegetation is also essential for land degradation assessments, while respective spatially distributed species composition maps are still unavailable. UAV technologies employing hyperspectral (HS) cameras are increasingly employed for mapping different woody species, but their high cost has so far impeded their use for continuous monitoring. The recent launch of the EnMap HS satellite sensor could significantly improve our ability to distinguish between different savannah woody species at larger scales. This work targets the accurate mapping of the fractional cover of different woody species on a South African (SA) savannah region, based on EnMap HS data in combination with very high resolution multispectral drone data.

Methodology

Field data related with representative encroaching woody species of concern were acquired during field campaigns over a savannah region in Kalahari, SA during the summer dry season of 2023. In particular, field campaigns included the annotation of savannah vegetation types using GPS measurements and geo-tagged images, as well as the acquisition of drone data at 2cm spatial resolution, with a DJI Mavic 3M multispectral camera. The field annotations were combined with the drone data applying a U-NET semantic segmentation architecture for producing a labeled map including 3 woody species classes: i. Grewia-family, ii. Melfera-family, iii. Vachellia-family and 3 non-woody species categories: iv: Grasses, v: Soil, vi: Shadow. The classified map from the drone mosaic was then used for generating fractional woody cover (FWC) samples per woody species class at the EnMap spatial resolution, i.e., 30m. An EnMap image captured on the same period, including the field-campaigns' study area was requested and acquired via the EnMap IPS portal. Spatial registration status between the two datasets was assessed and validated as satisfactory. The Regression Toolbox of the EnMAP-Box was used as a python plugin for QGIS, in order to perform several regression experiments towards producing species-level FWC maps from the EnMap data, while also assessing various random sampling schemes and regression algorithms.

Expected results

The proposed methodology was designed and implemented to produce fractional cover maps for three representative woody species families in Kalahari savannah of SA at 30-m spatial resolution over an EnMap scene area. Important remarks were drawn by benchmarking different random sampling schemes and various regressors, available for use via the EnMap-box plug-in. The contribution of multi-temporal information on an intermediate, between the two main datasets, spatial resolution was also assessed, by employing as regression features, Sentinel-2 10-m data of multiple dates. Model cross validation and thorough visual assessments of the FWC maps beyond the training areas, demonstrated the suitability of our approach and EnMap data for accurately mapping FWC at the species level. Figure 1 presents some preliminary results of the proposed methodology using EnMap data and the Random Forest regression algorithm. On the left (Figure 1a) part of the U-Net classified map into 5 categories is presented. On the right (Figure 1b) part of the FWC map for the Melifera-family predicted on a larger extent of the EnMap scene is shown. The *Senegalia Melifera* thorn bush group is considered by the locals to be one of the most encroaching and undesirable species, as it can form rapidly impenetrable thickets and is not palatable to most animals.

Outlook for the future

Savannahs in Africa contain millions of pastoralists whose livelihoods are threatened by woody encroachment. The present work aims towards the direction of providing much needed information on the accurate mapping and evolution of the spatial distribution of specific woody species to intergovernmental and governmental policy makers and local stakeholders that will use it as baseline data for the development of sustainable management strategies and for assessing the effects of management decisions. The developed pipeline assesses the capabilities of the new-generation imaging spectrometer EnMAP in monitoring and mapping of savannah woody vegetation at the species level. Results and validation raise significant expectations for the expansion of such methodologies towards operational monitoring and mapping over extended areas for supporting decision making and planning.

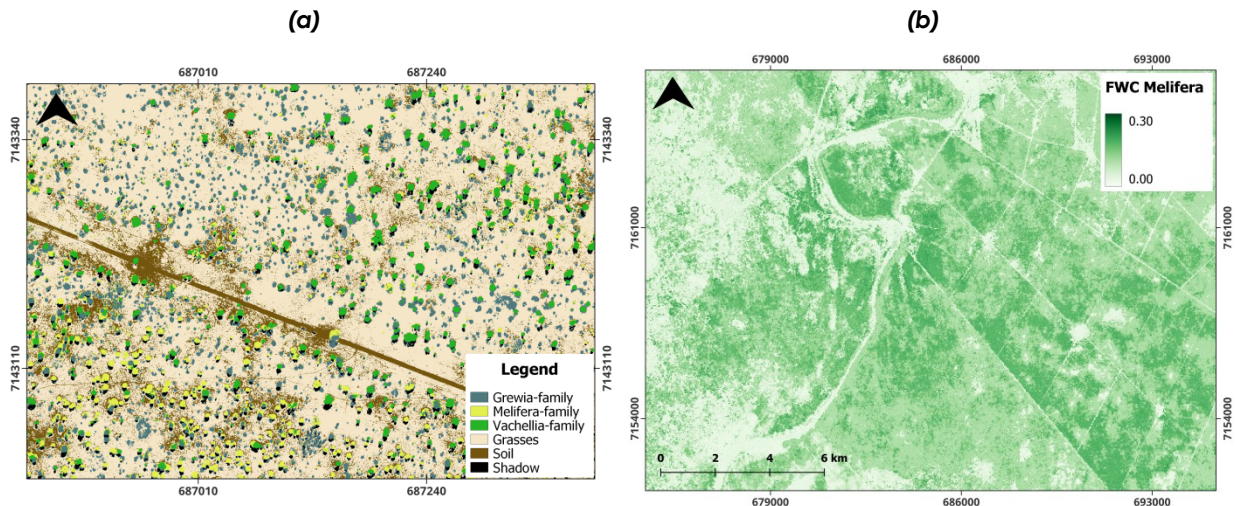


Figure 1: (a) Part of the 5-class map produced with U-Net and a drone mosaic and (b) part of the FWC map for the Melifera-family predicted on a larger extent of the EnMap scene.

Them.Sess. 3-3: Imaging spectroscopy for diverse ecosystem applications

Urban Tree Species Mapping – Development and Application of the Method using Hyperspectral and LiDAR Data Fusion

Jan Niedzielko¹, Dominik Kopeć^{1,2}, Justyna Wylazłowska¹, Jakub Charyton¹, Dominik Żmuda¹

¹ MGGP Aero, Poland

² University of Lodz, Department of Biogeography, Paleoecology and Nature Conservation, Poland

Keywords: Urban, Hyperspectral, Tree species, LiDAR, Classification

Challenge

The challenge was to develop a method of mapping tree species in an urban environment on a scale of the whole city. The urban greenery management required the information about the trees that would be reliable, continuous, at known error levels and up to date. Traditional field inventory methods are very expensive and time consuming. Datasets are often of varying standards, with unknown errors and missing data. Usually urban databases cover a little part of the city or sparse parts. Managers demanded information about the whole area, standardised, quality assessed and easy-to-use.

Having the knowledge of scientific use cases of airborne tree species inventories using LiDAR and Hyperspectral imagery, our goal was to develop an operational method of inventorying trees with taxa recognition. With the size of a tree and classification accuracy as the limitations of the method, it was necessary to define the border parameters and accuracy assessment framework as the integral part of the approach.

Methodology

The method was developed and demonstrated in the city of Warsaw. With over 1.7 million inhabitants and an area of 517 km sq. it is the largest city in Poland. We acquired Hyperspectral and LiDAR data simultaneously using a multisensor platform. During the flight campaign the extensive fieldwork was performed. About 15 000 reference trees were identified in the field, with precise location and taxa. The measurements were distributed throughout the whole city and designed to collect the sample of all main species that were previously known to grow in the city.

The method is divided into two stages: tree crown segmentation and species classification. The first stage starts from manually assisted treetop detection. Then the watershed segmentation is used to delineate tree crowns on the canopy height model. The second stage is the supervised classification using the machine learning algorithm CATBOOST. The process of feature extraction from raw HS imagery and point clouds produce a raster dataset that is the input to the classification process. Reference polygons are the result of the intersection of field measured points and tree crown segments. Usually the half of stratified random selected reference polygons is used for training and the other half for validation. Single tree is the unit of confusion matrix construction. The taxa class is assigned to segments through majority voting. In the iterative process of merging the taxa classes and refining the reference data, we define the final classification legend. It is a compromise between the detail level of the legend and accuracy of individual classes.

Results

In Warsaw we classified 60 classes with an overall accuracy of 0,809. We developed the strategies of combining the detailed taxa classes into broader classes that can be distinguished using ML techniques. Instead of categorising them into broader taxonomic groups such as genera, we use:

- aggregating similar species into groups of species (e.g. class 'Quercus robur, Quercus petraea' and class 'Quercus rubra, Quercus palustris')
- allocating cultivars with ornamental leaves a distinct grouping (e.g. class 'Acer platanoides' and class 'Acer platanoides purple cv')
- Keep even single species of high F1 accuracy as a separate class when combining other species to the genus class (e.g. class 'Tilia tomentosa' and class 'Tilia others')
- Combine species or even genera with similar morphologies and functions if it improves classification accuracy (e.g. class 'Thuja, Chamaecyparis, Juniperus, Platycladus')

Then we applied the method to 4 different cities. The maps of tree species were delivered to Rzeszów, Jasło, Sopot and Złotów, with the area of 129, 37, 17 and 12 km sq, respectively (Fig. 1). According to different sizes and species, we classified from 35 to 43 classes, with overall accuracy from 0.75 to 0.82. Obtaining results on five different datasets also allowed us to assess the expected accuracies for individual taxa.

Outlook for the future (800 - 1000 characters incl. spaces)

There are elements of the approach that can be altered with different state-of-the-art methods that should be checked for their accuracy and efficiency. Also the different parts of the workflow could be considered combining into fewer and more complex processes.

The classification approach could be switched to object-based, then numerous new features extracted from the whole segments could be used in the process. Also the raster feature dataset can be enriched with textural metrics. Alternative methods of dimensionality reduction could be tested. Finally, the whole process could be performed at once using the semantic segmentation DL approach. We would then benefit also from model transferability, as we don't need to collect extensive reference data for training and validating the model.

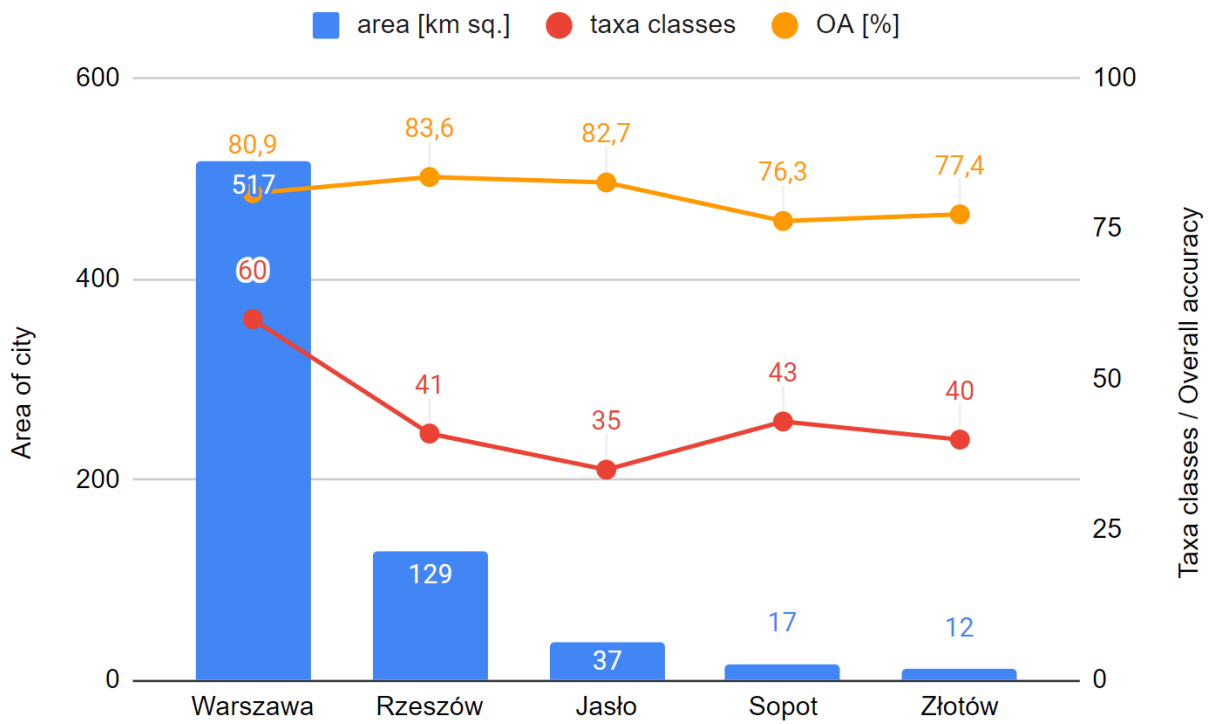


Figure 1 Area, number of classes and overall accuracy of tree species maps of 5 cities

Application hyperspectral data to assess the condition and identification of high mountain vegetation along the trails

Marlena Kycko¹, Bogdan Zagajewski¹, Tomasz Zwijacz-Kozica², Marcin Kluczek¹

¹ University of Warsaw, Faculty of Geography and Regional Studies, Department of Geoinformatics, Cartography and Remote Sensing, Poland

² Tatra National Park, Poland

Keywords: trampled vegetation, Hypex, alpine grassland, protected area, vegetation indices

Challenge

Analyzing and monitoring trampled vegetation helps in understanding species diversity, their resilience, and their susceptibility to human activity. This information aids in preserving and managing biodiversity in these fragile ecosystems. In high mountain environments, primary stress factors for plants include excessive light, limited water access, variable weather conditions, and trampling due to increased tourist activity. High intensity of these stress factors can lead to irreversible cellular changes, sometimes resulting in the death of plant cells. Recent field studies conducted in specific areas such as Kasprowy Wierch, Beskid, and Czerwone Wierchy (Kycko et al., 2014, 2017, 2018, 2019) have identified significant spectral ranges that statistically differentiate between the conditions of studied species affected by trampling and also reveal disparities among various species. Studies have been conducted in a non-invasive manner using remote sensing and fluorescence techniques.

Methodology

A methodology was developed using remote sensing vegetation indices and fluorescence parameters that illustrate the state of the photosynthetic apparatus and the dynamics of photosynthesis. Statistical methods allowed for relating conclusions and methodologies developed from field data to the scope of remote sensing information aerial acquisition. For this purpose, HySpex hyperspectral imagery acquired in 2019 and 2020. The processing and analysis of both images allowed the assessment of high mountain grassland vegetation's status during a specific period with resolutions of 2 meters. This analysis also involved identifying various vegetation types in the high mountain environment and available habitats and trampled areas. The classification of high mountain vegetation habitats in the Tatra National Park was accomplished using RF classifiers. The evaluation of alpine grassland conditions was conducted in zones adjacent to the tourist trail. Remote sensing indices were employed to describe: general condition - ARVI, NDVI (Figure 1b); chlorophyll content and condition - RARSa, GI; the amount of light used in photosynthesis - SIPI, PRI; nitrogen quantity - NDNI; dry matter in plants - PSRI, CAI; water content in vegetation - WBI, NDWI, along with crucial spectral ranges selected during field studies, illustrating the chlorophyll content in plants and other photosynthetically active pigments (653-654, 664-679, 687-690 nm), the quantity of water and building elements (139-1529, 1801-1878, 2055-2145, 2348-2358, 2410-2453 nm, Figure 1a).

Expected results

The research showed statistically significant differences in indicator values depending on the buffers used at varying distances from the trail. It also observed changes in the compactness of the plant cover along

the trail. Vegetation condition within 5 meters from the trails was assessed as good, but trampling significantly decreases vegetation condition and the density of its cover. Identification of trampled areas was carried out with overall accuracy of 91%, Kappa 0.85 (Figure 1c).

Outlook for the future

Studying trampled mountain vegetation assists in formulating conservation strategies. It helps in identifying areas vulnerable to damage and allows for the implementation of protective measures, such as setting up restricted zones or creating awareness among visitors about the impact of their activities. Monitoring these areas provides insights into the intensity and extent of human impact on these ecologically sensitive regions. In particular, the use of hyperspectral data allows remote analysis of precise vegetation parameters, identification of trampled areas. Additionally, remote sensing analysis and variables can improve species distribution models for alpine plant species in the context of biodiversity and species occurrence research.

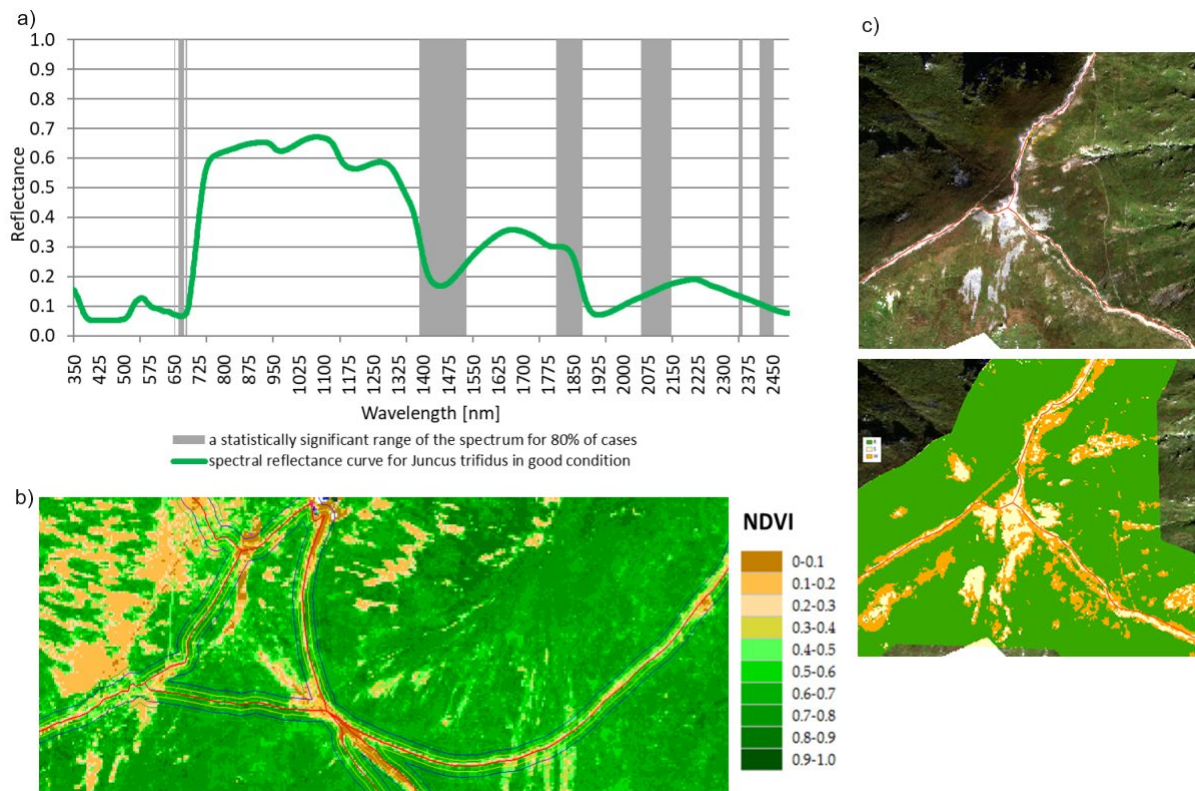


Figure 1 (a) spectral curves with statistically significant ranges, (b) NDVI calculated on HySpex data and (c) identification trampled areas

Biodiversity from imaging spectroscopy in contrasting tundra and fynbos biomes

EARSel Valencia 2024

Abstract

Corresponding Author:

[\[ptownsend@wisc.edu\]](mailto:ptownsend@wisc.edu)

[Philip A. Townsend](#)¹, Kyle R. Kovach¹, Henry A. Frye¹, Ting Zheng¹, Ryan P. Pavlick², Fabian D. Schneider², John A. Silander, Jr.³, Jeannine Cavender-Bares⁴, Simcellile Chenge⁵, Jasper A. Slingsby⁵,

¹ University of Wisconsin-Madison, Department of Forest & Wildlife Ecology, United States of America

² California Institute of Technology, Jet Propulsion Laboratory, United States of America

³ University of Connecticut, United States of America

⁴ University of Minnesota, United States of America

⁵ University of Cape Town, Department of Biological Sciences, South Africa

Keywords: Functional traits, biodiversity, fynbos, tundra, imaging spectroscopy

Challenge

NASA has recently completed two large-scale airborne imaging spectroscopy efforts: ABoVE (the Arctic-Boreal Vulnerability Experiment) and BioSCape (the Biodiversity Survey of the Cape). ABoVE focused on boreal forests and tundra of northern Canada and Alaska, while BioSCape addressed ecosystems of the Western Cape of South Africa, where natural vegetation is dominated by fynbos shrublands, one of the most species-diverse biomes on Earth. Both regions face significant threats from the effects of climate change and human activities, including invasive species, modified fire regimes and biodiversity loss. Imaging spectroscopy collections for ABoVE and BioSCape were motivated in part by the need for baseline data to understand the direction and pace of changes to these ecosystems. In both biomes, biodiversity loss is a major concern, although the shape of biodiversity differs. Tundra ecosystems are species poor but have high levels of functional diversity among the species present. Fynbos is exceptionally species rich, with high functional is a high diversity of plant physiognomic types present on a landscape. Imaging spectroscopy has emerged as a potentially powerful tool to quantify diversity, especially functional diversity, but the challenge remains on how to use spectroscopic data to meaningfully quantify diversity as observed on the ground. In both tundra and fynbos, the quantification of diversity using remote sensing is challenged by high fine scale heterogeneity resulting from the dominance of shrubs and graminoids smaller than pixel resolution of the imagery.

Methodology

We use imaging spectroscopy from AVIRIS-NG/AVIRIS-3 and leaf-level spectroscopy from field campaigns to quantify functional diversity in tundra and fynbos ecosystems. Leaf level spectra are tied to laboratory measurements of functional traits (e.g., leaf mass per area, pigments, nitrogen concentration, nonstructural carbohydrates, defensive compounds, and many more) to estimate traits for species present on hundreds of plots in both biomes. Upscaling via community weighted means is used to link species-level traits to image spectra and then map

foliar functional traits and functional diversity from AVIRIS-NG imagery. We then use multivariate analyses to quantify within- and between- species functional variation in each biome.

Expected results

Tundra and fynbos ecosystems exhibit comparable levels of functional trait variation across the traits we derived from spectroscopic data, although we expect that broad climatological differences between tundra and fynbos environments will result in differing overall trait spaces. In tundra ecosystems, there are high levels of within-taxa variation and considerable overlap in trait space among taxonomic groups, indicating that individual species can fill multiple functional roles depending on landscape context. The currently defined plant functional types for the tundra encompass broad functional niches, suggesting that the high variability within species in tundra systems may necessitate rethinking the classification of tundra functional types. We have just recently completed collection of data from the fynbos, but based on the literature we expect significant trait variation in the fynbos but with high functional redundancy among diverse species, which may complicate the use of imaging spectroscopy to quantify species diversity spatially across the fynbos, given both the small grain size of plants in fynbos and high rate of species turnover across sites.

Outlook for the future

Airborne imaging efforts such as ABoVE and BioSCape and associated field measurements are essential to prototype the use of future global-scale spaceborne imaging spectrometers to quantify diversity and ecosystem function. However, future missions with ~30m pixel resolution will be challenged to quantify diversity in ecosystems such as tundra and fynbos which have high levels of fine-grained species or functional diversity. Our work provides a baseline to assess diversity in these systems and assess the extent to which imaging spectroscopy can characterize the diversity in these systems.

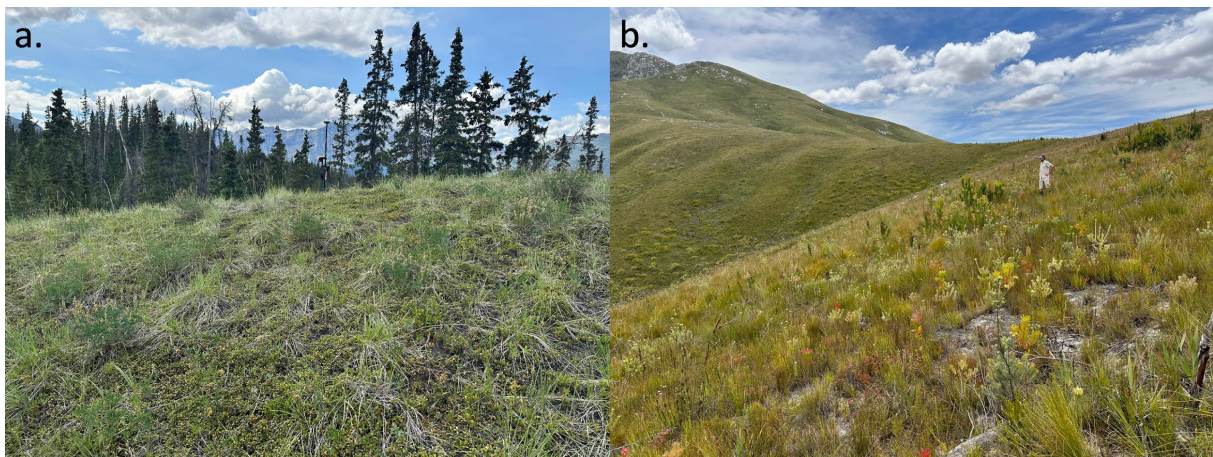


Figure 1. Illustration of contrasting diversity at the fine scale between low-species diversity/high functional diversity tundra (a) and high species-diversity fynbos (b).

Advancing The Monitoring Of Species Composition And Biomass In Grasslands Through Hyperspectral Satellites

Christine I. B. Wallis¹, Ann-Kathrin Holtgrave¹, Michael Förster¹, Birgit Kleinschmit¹

¹ Technische Universität Berlin, Geoinformation in Environmental Planning, Germany

Keywords (5): image spectroscopy, grassland quality, EnMAP, PRISMA, DESIS

Challenge (800 - 1000 characters incl. spaces)

Efficiently assessing grassland quality and understanding its dynamic response to land management practices is pivotal in contemporary ecological research. Traditional field-based monitoring is resource-intensive, prompting the exploration of remote sensing as a surrogate for comprehensive surveys. Leveraging image spectroscopy offers a valuable means to estimate grassland conditions and assess management impacts at varying scales. Hyperspectral data can be used to examine a wide range of vegetation characteristics such as leaf traits at the leaf or community level as well as the underlying species composition or related biomass. Particularly hyperspectral satellites like EnMAP, PRISMA, and DESIS, are promising for establishing a grassland monitoring system. However, these rather new satellite sensors have rarely been applied in grassland ecosystems and a direct comparison of the sensors is lacking in the grassland literature.

Methodology (1200 – 1500 characters incl. spaces)

In this study, we utilized data from the Biodiversity Exploratories Information System (BExIS) database including species plant abundance and plant biomass data collected from 150 grassland plots in Germany's three Biodiversity Exploratories between May and June in 2020 and 2023. Augmented by scenes from the satellites PRISMA, DESIS, and EnMAP (see Figure 1) our analysis integrates species composition and related biomass with hyperspectral imaging data. Procrustes Randomization test was used to examine the association between plant taxonomic and spectral composition across plots. We used the ordination solutions of the standardized two data matrices (spectral reflectance and Hellinger-transformed species abundance matrix per plot) for spectral and taxonomic composition, respectively. To address plot-wise univariate biomass values we use partial-least squares regression and variable importance in prediction (VIP) values to identify the most important wavelength band regions. The spectral reflectance data has been smoothed using a Savitzky-Golay-Filter and standardized using brightness normalization and continuum removal (band depth) using a segment hull, respectively. All analyses have been accomplished for each sensor separately and partly for multiple dates of record within the months April, May, and June if available.

Results (1200 – 1500 characters incl. spaces)

The acquired satellite data covers a total of 66 out of the 150 field plots within two of three grassland exploratories. Due to the temporal and spatial matching of field data and satellite scenes, the coverage of plots by each sensor varied from 16 to 32 plots. Our preliminary results highlight the critical role of the timing of data collection in spring concerning the plant-spectral composition relationship, influenced by grassland phenology and the initiation of land use management practices (primarily mowing) in June. Consequently, associations between spectral and plant composition varied across sensors and, notably, across different dates of record. We anticipate that these variations will be even more significant when modelling biomass. Regarding the comparison of the sensors used, we hypothesize that the inclusion of short-wave infrared data in EnMAP and PRISMA may offer benefits compared to sensors like DESIS, which cover only the visible and near-infrared regions. The VIP values from our PLSR analysis will aid in identifying these critical wavelength bands, which can guide future hyperspectral satellite missions and data collection strategies. However, we believe that the precise alignment of field surveys with the date of satellite record is of paramount importance.

Outlook for the future (800 - 1000 characters incl. spaces)

We propose that the monitoring of grassland ecosystems using satellite data can be effectively enhanced by additional UAV-based hyperspectral surveys. The rapid technical advancements in drone technology can support high-resolution grassland monitoring and be used to calibrate and validate the satellite image analysis. This becomes crucial when satellite records and field surveys do not align in time, allowing us to scale metrics from the field to UAV-based models and, ultimately, to hyperspectral satellite data. In addition to our focus on species composition and biomass, we also emphasize the importance of foliar leaf traits. These traits, when examined at the community level, enhance our understanding of nutrient gradients in grasslands and management intensity and should therefore be addressed in future studies using hyperspectral satellites.

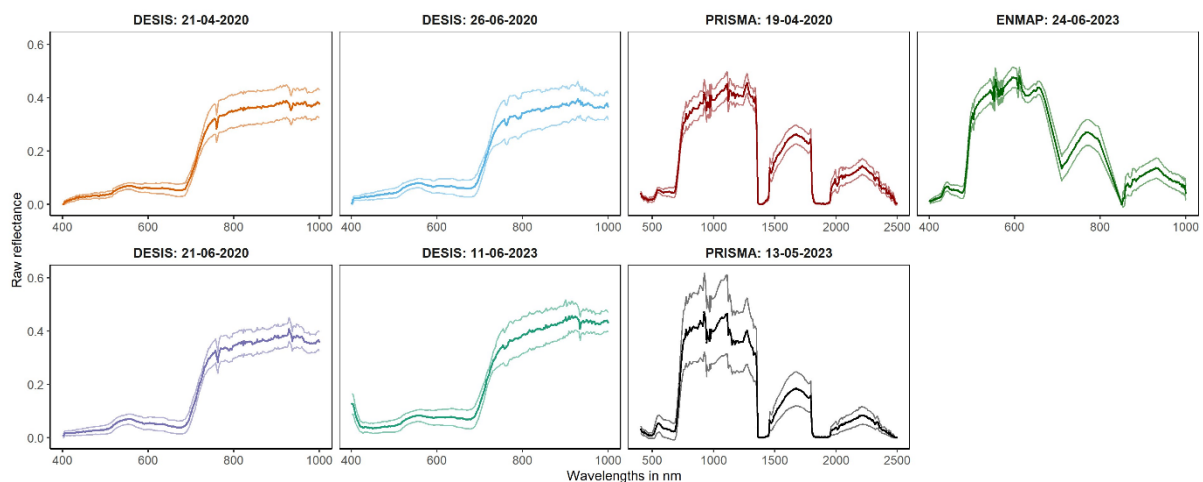


Figure 1: Raw reflectance and standard deviation for grassland plots of multiple hyperspectral sensors at different dates.

Biodiversity Survey of the Cape (BioSCape): A NASA campaign to understand Earth's biodiversity through the lens of spectroscopy

Philip G. Brodrick¹, Anabelle W. Cardoso^{2,3}, Adam M. Wilson², Erin Hester⁴, Jasper Slingsby³,
Cherie Forbes^{2,3}

¹ Jet Propulsion Laboratory, California Institute of Technology, Machine Learning and Instrument Autonomy Group, United States of America

² University at Buffalo, United States of America

³ University of Cape Town, South Africa

⁴ University of California, Merced, United States of America

Keywords (5): biodiversity, multi-sensor fusion, AVIRIS-NG, HyTES, LVIS

Challenge

Biodiversity loss jeopardizes human wellbeing and sustainable development, and addressing this is the target of all global conservation and many human development goals. Tracking progress towards these goals requires spatially explicit biodiversity and environmental data, monitored over the long term, but made available in near-real-time. Satellite remote sensing shows great promise to help achieve this, but has been limited in what it can detect due to issues of spatial or spectral resolution. Ultraviolet/visible to shortwave infrared (UVSWIR) and thermal infrared (TIR) data from imaging spectrometers and laser altimeter (lidar) data are now being collected via satellite. These novel data sets have the potential to provide information on the composition, structure, and function of ecosystems at scale, but their ability to measure, monitor, and explain the patterns of biodiversity and its drivers across diverse ecosystems both locally and globally is yet to be established.

Methodology

BioSCape's primary objective is to understand the structure, function, and composition of the study region's ecosystems, and to learn about how and why they are changing in time and space. The campaign will collect remote sensing and field data to study biodiversity to better conserve nature and its contributions to people. BioSCape is organized around three major research themes aimed at understanding:

- 1) Shifting community composition;
- 2) Ecosystem disturbance, resilience, and recovery; and
- 3) Ecosystem function and its contribution to people.

By integrating airborne and field-based measurements, BioSCape will explore and expand the capacity of such integrated datasets to produce accurate and scalable conclusions and help biodiversity conservation reach its potential efficacy. BioSCape's airborne sensors will

collect UVSWIR and TIR imaging spectroscopy and lidar data over terrestrial and aquatic targets using four NASA instruments: Airborne Visible Infrared Imaging Spectrometer-Next Generation (AVIRIS-NG), Portable Remote Imaging Spectrometer (PRISM), Hyperspectral Thermal Emission Spectrometer (HyTES), and Land-Vegetation and Ice Sensor (LVIS). The resulting dataset will be unprecedented in its instrument combination and level of detail, with nearly complete coverage of the electromagnetic spectrum at high resolution and coincident full-waveform lidar acquisitions.

Expected results

Tracking progress towards these goals requires spatially explicit biodiversity and environmental data, monitored over the long term, but made available in near-real-time. The fundamental BioSCape has to overcome is one of scale; ecosystems express biodiversity across multiple simultaneous lengthscales, and observations from different heights and with different sensors will be able to resolve different aspects of the systems in question. Here, we showcase early results highlighting the relative information yield between contemporaneous field, airborne, and satellite measurements. We highlight the research questions of the many individual principle investigators, along with the early results from airborne instrumentation. As part of NASA's effort to facilitate Open Science, all collected data will be delivered to one of the Distributed Archive and Analysis Centers, with no period of exclusive data access. During the campaign, data quality was assessed on a daily basis using quicklooks and a publicly available data viewer (Figure 1). We will present considerations for data management that have been deployed to lower the barrier of entry for scientists new to one of the instruments, and to provide near analysis ready data.



Figure 1 Example of the near real-time data platform built for field teams to view airborne data as it is collected and to aid in flight decisions.

Outlook for the future

BioSCape, as an integrated remote sensing field campaign, is designed to improve biodiversity conservation in South Africa by measuring biodiversity and creating relevant data products to improve biodiversity and ecosystem assessments and better inform environmental decision-making and policy. South Africa's established pathway from science to application and its diverse threats to biodiversity make the region a microcosm of global challenges and opportunities and the perfect place for a field campaign like BioSCape. Scientists and applications leaders will work together to make maximum use of the suite of field, airborne, and satellite data collected in both the short and long term. BioSCape will prepare the scientific community for the next generation of earth observation and push the boundaries of what is possible in remote sensing of biodiversity.

Ordination analysis with multitemporal EnMAP data to map patterns of species composition in peatland vegetation

[Christina Hellmann](#)¹, Bernd Bobertz¹, Hannes Feilhauer², Manuel Reese³, Marcel Schwieder⁴, Björn Waske³, Sebastian van der Linden¹

¹ University of Greifswald, Institute of Geology and Geography, partner in the Greifswald Mire Centre, Germany

² Leipzig University, Remote Sensing Centre for Earth System Research (RSC4Earth), Germany

³ Osnabrück University, Institute of Computer Science, Germany

⁴ Thünen Institute, Department of Farm Economics, Germany

Keywords (5): peatlands, monitoring, floristic gradients, *Phragmites australis*, *Phalaris arundinacea*

Challenge

Drained peatlands are carbon sources contributing 4% to global greenhouse gas emissions. To mitigate carbon emissions, they need to be rewetted. Concepts are required to monitor the success of rewetting. In the scope of the project ReWetSpec – Developing Hyperspectral Indicators for Fen Re-wetting, we monitor rewetting success with EnMAP data. EnMAP images offer high spectral resolution for relatively large areas, ideally on multiple dates per year. The high spectral resolution and range promise a high information content regarding vegetation composition and state. Peatlands are a mix of vegetation types; from wet meadows with small-scale vegetation patterns to rather homogenous wetland vegetation intermixed with different water fractions. Thus, mapping patterns of species composition in peatlands is challenging. Multitemporal data are promising when phenological stages of species are unique. Separate data sets may indicate different gradients, depending on the dominant plant species.

Methodology

The study area 'Polder Rustow Randow' is located in the river valley Teterower Peene, Mecklenburg-Western Pomerania, Germany. The ~370 ha area was rewetted from 2000 onwards. We recorded all species with their respective cover fractions from 66 squared plots (4x4m) on a 60m raster, twice, once in June and once in September 2023. Further, the cover fractions of green vegetation, NPV, soil and water were estimated. A spectral library using an ASD FieldSpec 4 FR was created for the vegetation plots. Field survey also included multi- and hyperspectral UAV acquisitions. We used two EnMAP scenes from June and August 2023 for the analyses.

We mapped gradual changes in peatland species composition with a multitemporal ordination analysis. First, gradients in species composition were assessed based on the vegetation field data from both dates and ordination analysis. The distribution of the plots in the ordination space was used to attribute spatial gradients. Axis scores for the plots were then used as target variables in regression models with field spectra (resampled to EnMAP resolution) and EnMAP image spectra. The UAV data served as an intermediate level to check representativeness of EnMAP pixels with regard to the field plots. We used cross-validation for validation. The model was then applied to the EnMAP data. For the training and application of the regression models, we tested single-date analysis with both acquisition dates as well as a combination of the two acquisitions.

Results

Results from the field survey showed that *Phalaris arundinacea* was dominant in areas with high water level fluctuations, and *Phragmites australis* close to open water. *Carex acutiformis*, *C. riparia* and *C. acuta* were dominant where water level show only minor changes. The *Agrostis stolonifera*-*Eleocharis palustris* community was often found in mechanically disturbed areas, e.g., by wildlife, and variable water levels. Under wetter and less disturbed conditions, the *Iris pseudacorus*-*Carex pseudocyperus* community was found.

The vegetation distribution is mainly driven by a water level gradient: from high stagnant water levels to high water level fluctuations with temporally ponded water, and moist conditions with almost no ponded water. Further, we expect to find a gradient along nutrient availability. We hope to find some of the described gradients in the EnMAP data (results pending).

The two EnMAP images are to a different extent influenced by water absorption, because meteorological conditions were different: June was dry, while August and September were wet, with water levels often above the surface. We expect that these differences lead to variations in the regression analysis of the two dates. We hope to get a better understanding on the relation between water and vegetation condition in space and time. Further, we want to test an improvement in mapping patterns of species composition by the combination of the two EnMAP images.

Outlook for the future

In future analyses, with dense EnMAP time series data, we want to compare the ordination analysis with regression based unmixing for quantitative species mapping from peatland specific indices. Further, inter- and intra-annual variations can be tested. The multi-temporal findings are then combined with dense time series of Landsat-Sentinel data to explore a potential spatial extrapolation.

Due to new upcoming hyperspectral missions, such as SBG and Chime, it will be important to test the transferability of ordination gradient analysis and regression based unmixing on hyperspectral data from different sensors (such as PRISMA at the moment). In the future, the combination of different data sets in analysis ready data cubes appears to be an interesting approach to decrease temporal and spatial gaps.

With our findings, we hope to make valuable contributions to a large-scale monitoring workflow to assess the upcoming rewetting efforts.

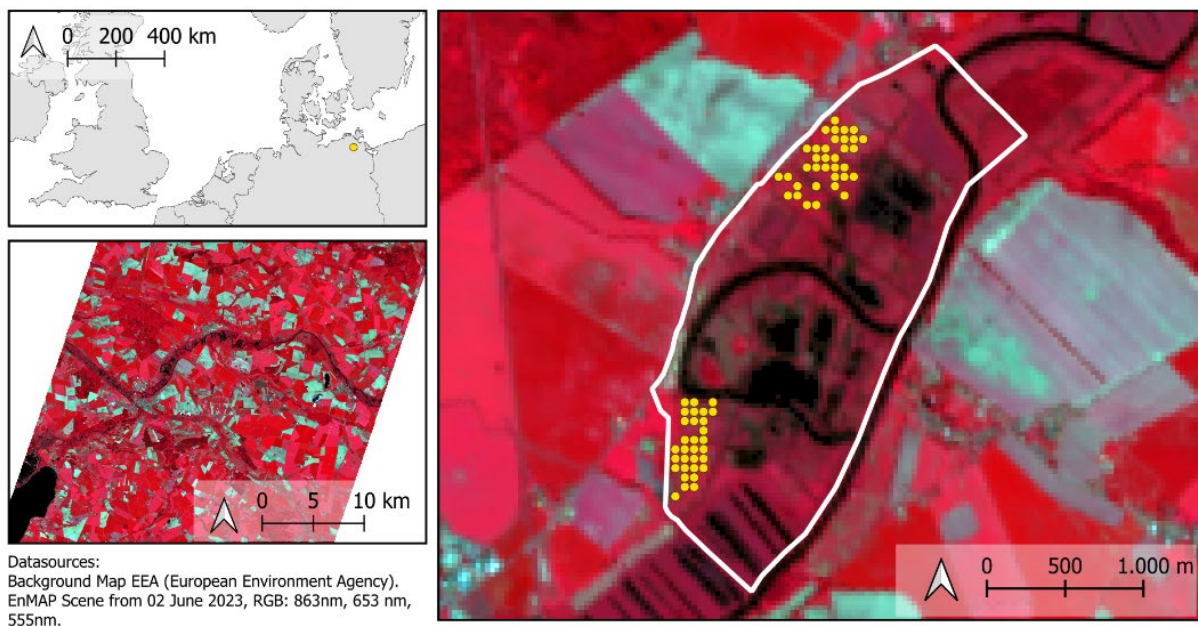


Figure: Overview of the study area in north-eastern Germany (top left), in the river valley Teterower Peene (bottom left) and the core study area, the 'Polder Rustow Randow' (right).

**Them.Sess. 3-4: Validation of
L2A products: content and
format for a global joint effort
to validate atmospheric
correction products**

Measurements and Simulations of Irradiance Fields

Andreas Hueni¹, Helena Kuehnle^{1,2}

¹ University of Zurich, RSL, Switzerland

² ETH Zurich, D-PHYS, Exoplanets and Habitability Group, Switzerland

Keywords (5): Field Spectroradiometry, Irradiance, Radiative Transfer Modelling

Challenge

Field spectroradiometry is a common way to capture in situ spectral surface reflectance data to be used in airborne or satellite-based instrument calibration and validation (CAL/VAL). The desired quantity is the surface reflectance, which, however, cannot be directly measured. Instead, it is estimated by first measuring the target reflected radiance as well as the irradiance and then computing the target reflectance factor by normalising the target radiance with the radiance reflected by a Lambertian 100% reflective surface.

Any error in the irradiance measurement will directly impact the estimated reflectance factor. It is thus of interest to investigate the quality of the irradiance data by employing radiative transfer models. This will also enable a cross-check of the irradiance assumptions taken both in atmospheric correction procedures and in at-sensor radiance simulations for instrument CAL/VAL in the radiance domain.

Methodology

The challenge of checking the quality of irradiance (E) measurements has been tackled in two stages: a) a post-analysis of a decade of spectral ground control point (SGCP) data acquired during airborne campaigns, and b) dedicated field measurements taken during the 2023 BioSCape campaign.

SGCP data were collected following the RSL standard protocol. Data were taken in radiance mode, bracketing 30 target scans with 5 pre/post Spectralon panel scans.

The analysis of the SGCP data involved clustering of all pre/post reference panel measurements and the extraction of metadata for the radiative transfer modelling (UTC, spatial position and elevation). The simulation of E at the bottom of atmosphere was carried out in LibRadtran, choosing the midlatitude summer standard atmosphere, and configuring the aerosol optical thickness (AOT) by selecting AOT values from the CAMS global reanalysis (EAC4) data, interpolated over time to match the acquisition time. A generic vegetation reflectance spectrum was chosen as background.

Based on the findings of , specialised field equipment was assembled to further investigate the distribution of direct and diffuse components of the irradiance field. The instrumentation includes a) an SVC spectroradiometer with an E integrating sphere, calibrated at WRC Davos, b) an MFR-7 Shadowband Radiometer modified to accommodate an ASD cosine receptor, thus providing spectral direct and diffuse E data, c) a Microtops device to estimate atmospheric properties.

Results

Results of the first part of the investigation showed that the simulation of the irradiance E was highly dependent on the choice of the background assumed for the scene (Fig. 1). It must be noted that

Libradtran is a 1D model and thus any specified background stretches into infinity, i.e. the adjacency effect is given by the chosen background. The implications on the modelled diffuse E (Fig. 2) are caused by two effects: a) the actual background near the location of the Spectralon panel may differ from the chosen standard background, and b) the chosen background is finite in reality and thus not representative of the true adjacent surface elements, which are rarely homogenous, nor are they on a level plain. As the diffuse component of E is heavily influenced by the interaction of background and aerosol scattering, effects are largest in the UV/Blue while diminishing towards the SWIR.

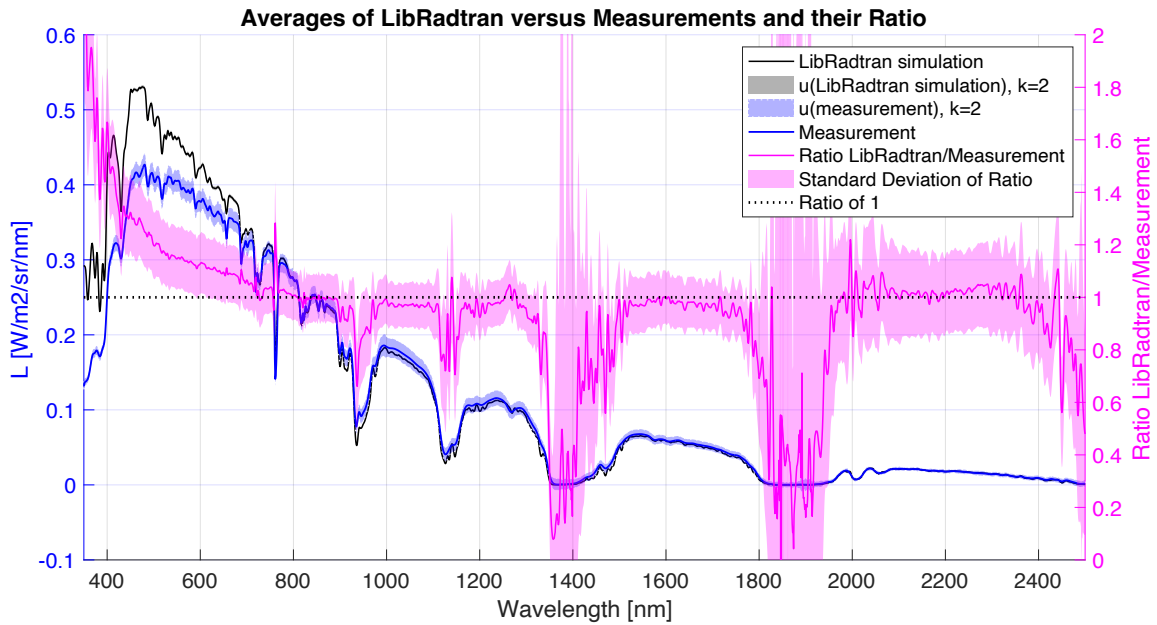
The instruments outlined above are able to characterise the incoming light field in a much more robust way. The irradiance integrating sphere of the SVC exhibits a near-perfect cosine response and its calibration versus a primary standard FEL lamp at WRC allows a dramatic reduction of the uncertainty of its measurement due to a shortened traceability chain. The diurnal character of the field data allows as well to cross-calibrate the ASD cosine receptor to the SVC sphere, thus compensating the non-ideal response of ASD diffuser and extending the traceability to the shadowband measurements.

Outlook for the future

Sensitivity assessments of the Libradtran model in relation to the defined background have shown a distinct and significant impact on the diffuse irradiance. It is thus of importance to close the gap between measurements and simulations through activities that help to better define the diffuse part of the incoming radiation. Of importance will be the employment of 3D radiative transfer models like DART or Eradiate, to accurately model the effects of adjacency. This takes the topographic into account and can thus replicates the adjacency effects on the measurements more accurately. By the same token, a sensitivity analysis of the spatial scale of adjacency effects will be required to define spatial buffers to be considered in adjacency effect simulation and correction.

Diurnal multi-instrument irradiance timeseries acquired in various natural settings characterised by other teams within the BioSCape campaign are expected to allow such detailed simulations of the irradiance fields.

Albedo 1.0 as Background



Generic Vegetation as Background

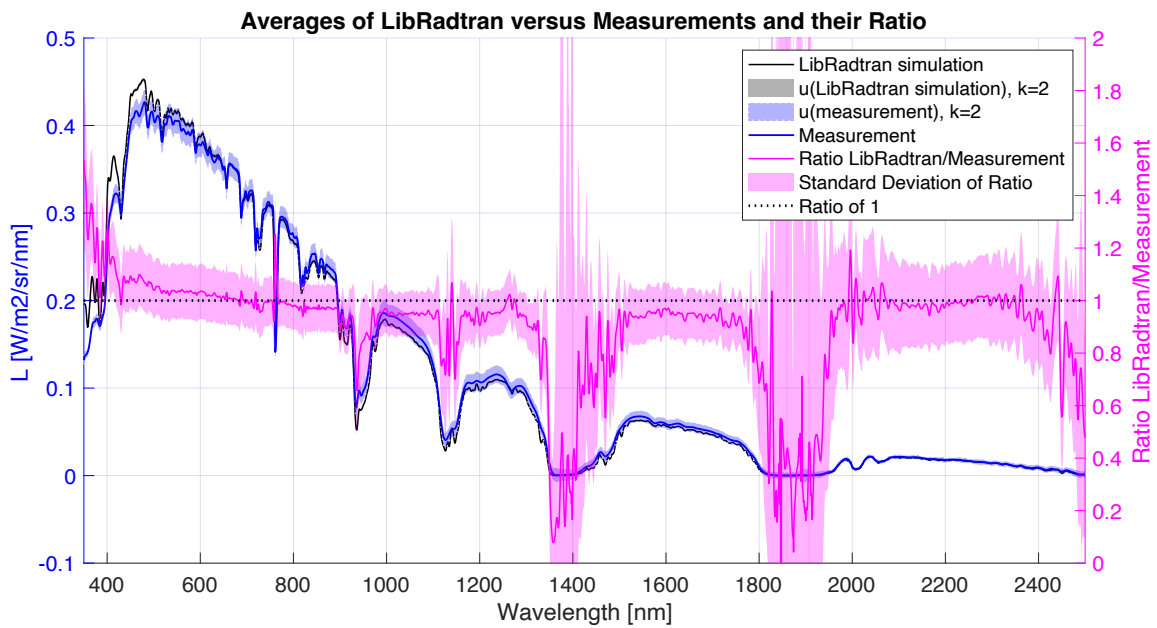


Figure 1 The effects of the choice of background on the comparison of average simulated irradiance and measured irradiance: albedo of 1.0 (top) versus a generic vegetation (bottom). Differences are most pronounced in the UV/Blue part of the spectrum due to multiple scattering effects between surface and atmosphere.

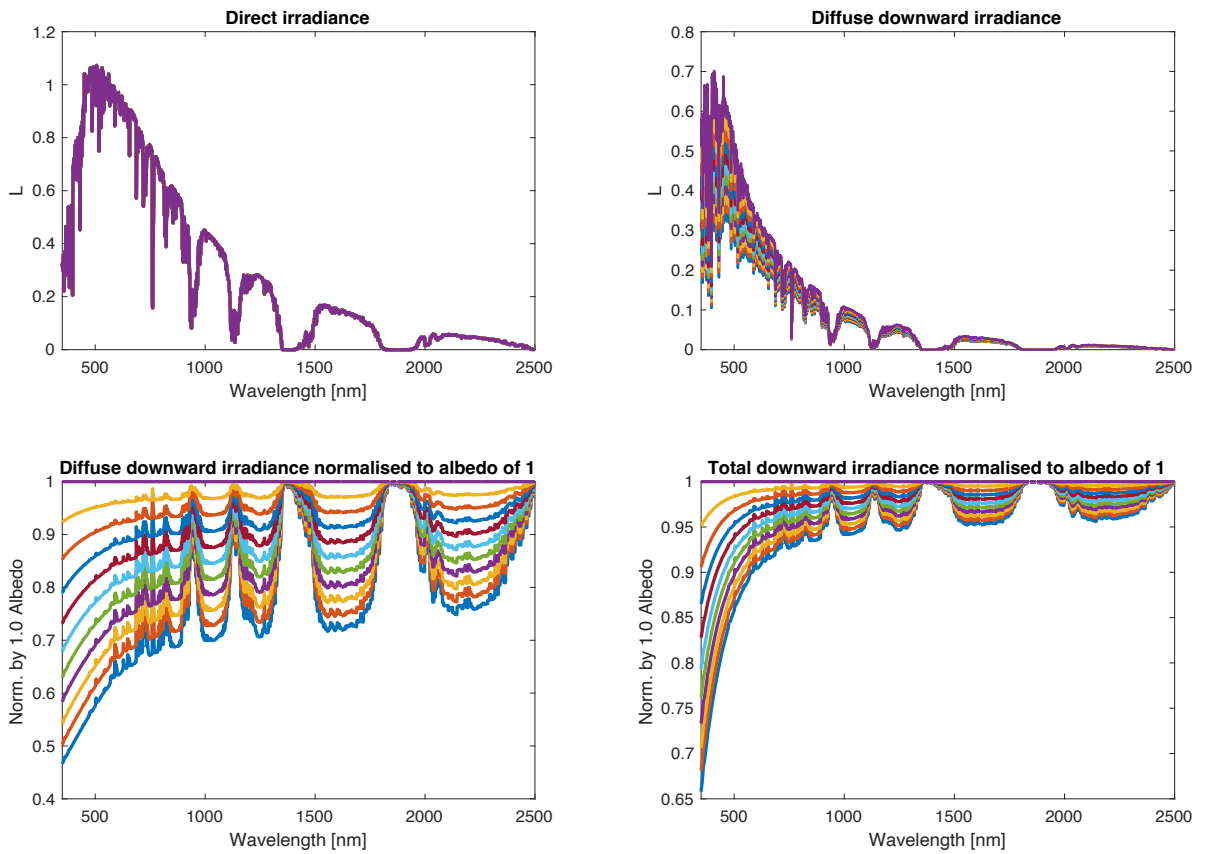


Figure 2 Results of a sensitivity study of irradiance on the defined background. Surface albedos between 0.0 and 1.0 at 0.1 step size lead to variations in the diffuse irradiance (top-right), while the direct irradiance (top-right) remains constant. Normalised results show that the diffuse irradiance changes up to 50% in the UV due to the background albedo, while the total irradiance is influenced up to 35% in the UV for an albedo of 0.0

Uncertainties in Field Spectroscopy Measurements: Impact of Different Distances of the Fibre Optic Tip of a Field Spectroradiometer to the Reference Panel on Reflectance Factors

Carmen Meiller¹, Andreas Hueni¹, Reinhard Furrer², Bernhard Schmid¹, Maria J. Santos¹

¹ University of Zurich, Department of Geography, Remote Sensing Laboratories, Switzerland

² University of Zurich, Department of Mathematics, Applied Statistics, Switzerland

Keywords: Field Spectroscopy, Uncertainty, CAL/VAL, Ground Truth, Traceability

Challenge

Field spectroscopy measurements are often used as so-called “*Ground Truth*” measurements for the calibration and/or validation of airborne or space-based sensors. Having a complete and traceable uncertainty assessment of a spectroscopic measurement is crucial to understand the quality of a data set, especially if it is used to calibrate or validate other sensors. To our knowledge, no complete uncertainty budget exists for reflectance factors calculated from field spectroscopy measurements. However, the latter are not as easy to obtain as one might think, as an operator and other environmental conditions can introduce a wide variety of biases that will influence the collected data. To contribute partly to the ambitious goal of a complete uncertainty budget for field spectroscopy measurements, an experiment was carried out to examine the influence of the distance between the fibre optic tip of a field spectroradiometer and the reference panel on acquired measurements.

Methodology

For the experiment, two setups (control and experiment) were installed, each consisting of a tripod with a reference panel mounted on top and an appliance holding a field spectroradiometer. For the control setup, the fibre optic tip of the spectroradiometer was held at a height of 15 cm (default distance) above the panel. For the experiment, the fibre optic tip was fixed in a pistol grip and could be moved between distances of 2 and 50 cm. Measurements were obtained simultaneously, always providing a control and an experimental measurement at a specific distance between 2 and 50 cm.

The data sets obtained from the different distances needed correction for several factors; first, a cross-calibration between the instruments was carried out, then a correction for the pistol grip, and finally a correction for the change of solar irradiance over time was done.

Thereafter, a model that can correct for different distances to the panel was derived from the data set by fitting spline functions per wavelength and distance.

To show the influence of different distances of the fibre optic tip to the panel on a field spectroscopy measurement, two additional data sets were collected. Reference panel measurements were obtained at 2 cm and at 15 cm, followed by a vegetation measurement. Next, the correction model was applied to the two data sets and the reflectance factors were calculated. Along with the correction model and the applied model, the accompanying uncertainties were propagated.

Results

Two results can be derived from the data analysis: a) the correction model itself (Fig. 1) and b) the correction model applied to the example data. The latter is visualised by a plot showing the relative difference between the three data sets (2 cm corrected and uncorrected and 15 cm corrected) and the uncorrected data at 15 cm (Fig. 2).

The correction model visualises that the ultraviolet (UV) and the violet part show a different trend than the remaining wavelengths. They show a decrease in correction factors from 2 cm to the default distance (factors: $1.03 - 1$), while the opposite occurs for blue to SWIR (increase from 2 cm to 15 cm (factors: $0.965 - 1$)). This means that radiances must be increased for wavelengths from 350 to about 450 nm and reduced for the remaining wavelengths to correct data from 2 cm up to the default distance to the panel. From 15 cm and greater distances, the correction factors appear to flatten out (values need to be multiplied by one).

In the difference plot we can make a similar observation: the uncorrected 2-cm measurement has a main deviation from the uncorrected 15-cm measurement at shorter wavelengths of -3.4 % maximum (UV). At 478 nm the deviation becomes positive and reaches 2.3 % until the end of the spectral range (2500 nm). The corrected 2-cm measurement, however, fluctuates between -1 and 1 % over the entire wavelength range. This shows that there are differences in radiance due to different distances and that we can correct for them.

Outlook for the future

Obtaining a complete uncertainty budget for field spectroscopy measurements is an important goal that must be achieved to reliably validate other sensors. This study covered only one small part of many components that make up the entire uncertainty of field spectroscopy measurements. However, it became evident that even such an apparently minor setup choice can have a non-negligible influence on the measurements obtained.

To achieve the potentially utopian goal of a complete uncertainty budget, further experiments need to be conducted and their contribution to the uncertainty be analysed and added to the budget.

It is also important to make the community aware of all the potential influences an operator may have that may distort the data collected. Therefore, this study helps to raise awareness about the collection of field spectroscopy data.

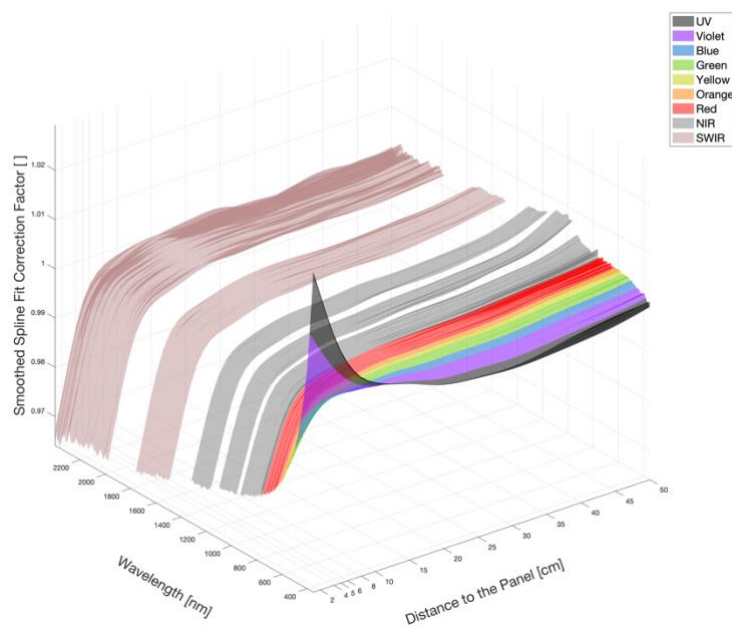


Figure 1 The correction model to correct for different distances to the panel per wavelength.

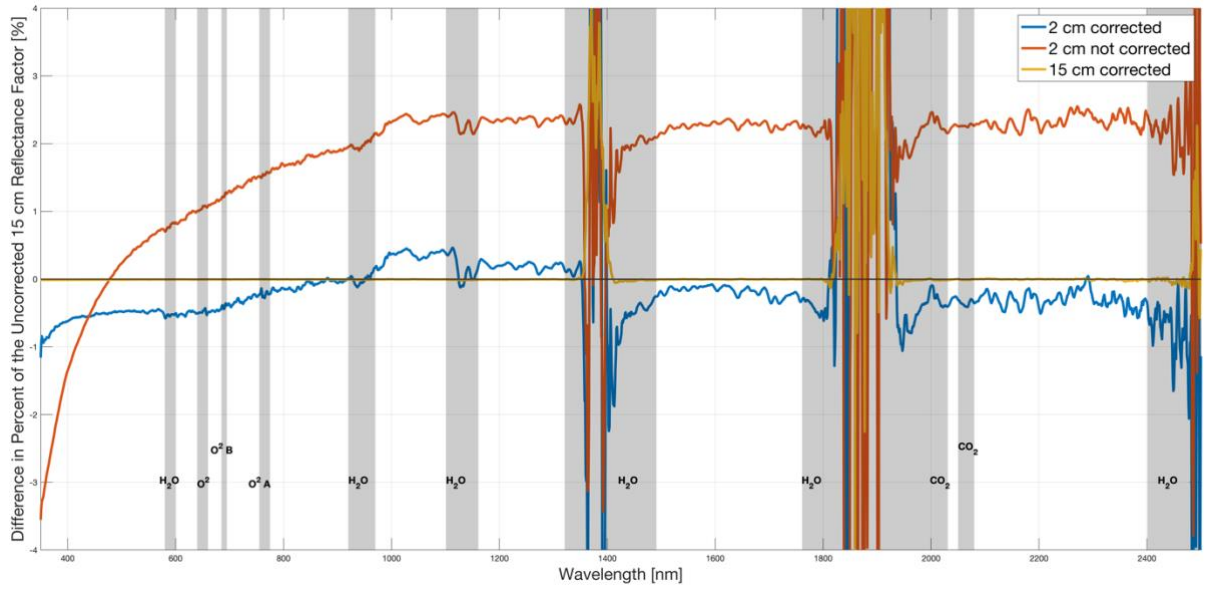


Figure 2 Difference between the uncorrected measurement at 15 cm and the corrected as well as uncorrected measurement at 2 cm in percent of the uncorrected measurement of 15 cm.

Developing an strategy to transfer TRUTHS radiometric accuracy to surface reflectance measurements

EARSel Valencia 2024

Abstract

Corresponding Author: jagorvie@upv.es

Javier Gorroño¹, Luis Guanter¹, Montserrat Piñol², Nigel Fox³ and Thorsten Fehr²
(Style: Authors, presenting author underlined)

¹ Universitat Politècnica de València, Research Institute of Water and Environmental Engineering (IIAMA), Spain

² European Space Research and Technology Centre (ESTEC) European Space Agency, Noordwijk, AZ, The Netherlands

³ National Physical Laboratory, Hampton Road, Teddington TW11 0LW, UK

Keywords (5): TRUTHS, surface reflectance, RadCalNet, BRDF, radiometry

Challenge (800 - 1000 characters incl. spaces)

The development of satellites missions such as TRUTHS (Traceable Radiometry Underpinning Terrestrial and Helio-Studies) and CLARREO (Climate Absolute Radiance and Refractivity Observatory) will be able to provide highly accurate and trusted SI-traceable climate records in the coming years.

In parallel, these accurate observations can be fundamental to improve the calibration of other sensors either in-flight or in-situ. In these calibration scenarios, the reference sensor will not limit the uncertainty of an inter-calibration process and thus facilitates a 'reference-calibration'. Thus, any extra effort related to the study and correction of errors of the calibration transfer process will result in a maximised calibration transfer.

The study here presented is focused on the development of a strategy to transfer the TRUTHS observations to instrumented sites or ad-hoc campaigns. The main challenge to transfer this accurate radiometric calibration is dependent on the angular and temporal match. The proposed methodology is capable of reproducing angular errors from nadir and from other angular reference. We will also focus on how these angular effects are interrelated with other aspects such as the orbit manouvres and atmospheric auxiliary information.

Methodology (1200 – 1500 characters incl. spaces)

The study of angular effects from TRUTHS observations over instrumented sites starts by producing a set of orbit files over different target sites. These files contain the information related to overpass time and angular configuration. The observation angle has been extended to the maximum angle that can be reached through manouvres.

This angular information can be coupled with a site surface bidirectional reflectance factor (BRDF). The default BRDF is extracted from MODIS MCD43A1 products. Further auxiliary information (e.g. height, aerosol content...) is ingested into Libradtran radiative transfer to reproduce the expected TOA reflectance as measured by the TRUTHS mission.

The setup can be configured to reproduce the TOA measurements in both nadir and for the specific overpass angular configuration but also considering different solar angles due to temporal mismatch between the TRUTHS overpass and the insitu measurement.

The methodology is applied to several instrumented sites that include RadCalNet or HyperNet sites. For these set of sites, not only the performance over one site but the multi-site performance is evaluated. Furthermore, the setup can be applied to any other site or ad-hoc campaign where reference measurements could be of interest.

Expected results (1200 – 1500 characters incl. spaces)

Figure 1 exemplifies the modelled viewing error at both a blue and near-infrared region of the spectrum. These results indicate how for several cases, no angular correction can result in errors over the 1% level.

Depending on the site, measurements can include a full BRDF measurements, a set of angles measurements or just nadir observations. For each one of the cases, a different approach will be needed. If an angular compensation is implemented, it is not only important a surface BRDF model but also the atmospheric parameterisation. For example,

Figure 1 reports the non-nadir errors at two aerosol optical thickness values (0.1 and 0.4). The results in the blue region show large changes in the angular correction for each aerosol level.

Figure 2 illustrates errors in TOA reflectance as a function of time delays between in-situ acquisitions and TRUTHS overpasses. In this timespan, the solar angle changes, thus producing a change that must be compensated and/or minimised. These errors can be highly significant in the near-infrared region with up to 1% for just 10 minutes mismatch.

Outlook for the future (800 - 1000 characters incl. spaces)

These first results are helpful in defining a strategy on how TRUTHS measurements can be used to improve the calibration of in-situ stations and ad-hoc campaign.

On the one hand, the access to an accurate surface BRDF and atmospheric modelling for these instrumented sites is crucial to minimise observation mismatch effects. The use of strategic pointing through manoeuvres can be used to accumulate observation and minimise its combined effect but cannot be applied as a systematic process for each site.

On the other hand, these first results indicate that a temporal difference of just 10 minutes might dominate the uncertainty budget with errors up to 1%. Thus, in order to maximise the benefit of TRUTHS measurements it might be needed to be below this target value.

Next steps are expected to consider a more case-by-case study together with a more detailed understanding of the combined effect between 1) different errors 2) different overpasses and 3) different sites.

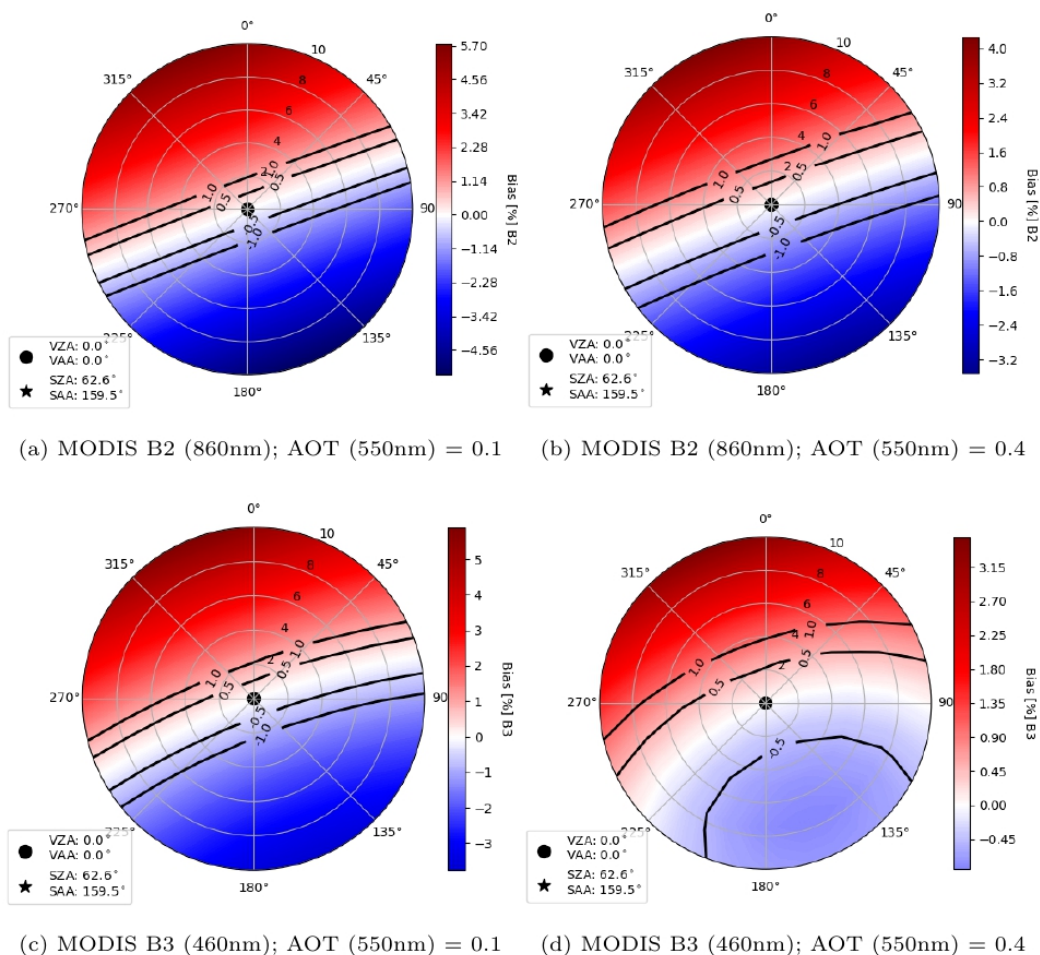


Figure 1 TRUTHS viewing error modeled for inclinations up to 10 degrees for MODIS bands B3 (460nm) and B2 (860nm) with two different aerosol optical thickness (AOT) scenarios at 550nm (0.1 and 0.4).

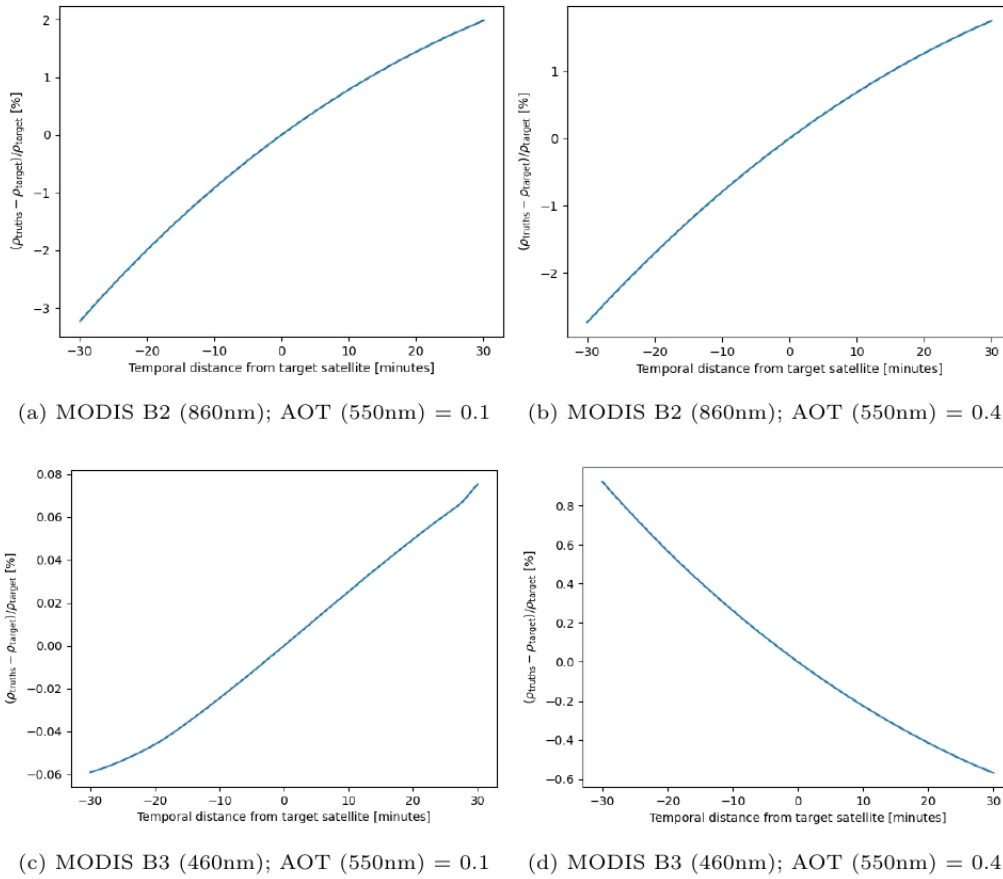


Figure 2 TRUTHS intercalibration error due to sun angle change in overpass differences up to 30 minutes and for MODIS bands B3 (460nm) and B2 (860nm) with two different aerosol optical thickness (AOT) scenarios at 550nm (0.1 and 0.4).

Validation of EnMAP Level-2A bottom-of-atmosphere reflectance produced with the EnMAP Processing Tool (EnPT)

EARSeL Valencia 2024
Abstract
Corresponding Author:
danschef@gfz-potsdam.de

Daniel Scheffler¹, Maximilian Brell¹, Mariana A. Soppa², Leonardo Alvarado², Astrid Bracher^{2,3}, Karl Segl¹, Sabine Chabrillat^{1,4}

¹ Helmholtz Centre Potsdam GFZ German Research Centre for Geosciences, Telegrafenberg, 14473 Potsdam, Germany

² Alfred Wegener Institute, AWI, Helmholtz Centre for Polar and Marine Research, Am Handelshafen 12, 27570 Bremerhaven, Germany

³ Institute of Environmental Physics, University of Bremen, Otto-Hahn-Allee 1, 28359 Bremen, Germany

⁴ Leibniz University Hannover, Institute of soil science, Herrenhäuser Str. 2, 30419 Hannover, Germany

Keywords: Validation, EnMAP, EnPT, Hyperspectral, Earth Observation

Challenge

The EnMAP Processing Tool (EnPT) is an alternative “do-it-yourself” pre-processing chain developed at the German Research Centre for Geosciences (GFZ) to generate orthorectified Level-2A bottom-of-atmosphere (BOA) reflectance from EnMAP Level-1B top-of-atmosphere (TOA) radiance (sensor geometry). Opposed to the official EnMAP processing chain provided by the EnMAP ground segment (GS), EnPT offers the users different workflow and algorithm options, and is freely available as open-source software that can be used as a standalone Python package, from the command line, or via a graphical user interface (GUI) implemented in the EnMAP-Box QGIS plugin. EnPT offers advanced co-registration and alignment to a user-specified spatial reference and provides free choice between three atmospheric correction approaches: SICOR and ISOFIT for land surfaces and ACwater/Polymer for water surfaces. Here, we present the results of a comprehensive validation of the EnPT output Level-2A reflectance concerning relative and absolute geometric accuracy and surface reflectance derived at different atmospheric and surface characteristics globally distributed. Cross-validation performances compared to the official EnMAP Level-2A product are presented.

Methodology

For validation of the EnPT Level-2A outputs, multiple EnMAP acquisitions are selected at sites already used to validate the official EnMAP Level-2A product by the independent EnMAP product validation efforts. These sites contain representative validation spots ideally suited for product validation due to their surface characteristics or availability of in-situ data. The EnMAP datasets are downloaded in Level-1B (TOA radiance) via the official EnMAP data access portal and then passed as input to the EnPT processing chain. The processing is executed with different sets of input parameters to consider all possible EnPT outputs in the validation. The produced orthorectified EnMAP Level-2A BOA reflectance (or normalized water leaving reflectance in case of ACwater) is then passed to EnVAL, a product validation software for EnMAP data developed at the GFZ. The validation of the geometric accuracy includes an assessment of the co-registration accuracy (1) between the two EnMAP detectors, the VNIR and the SWIR, and (2) between EnMAP and a selected spatial reference dataset. Co-registration performance metrics are computed based on the AROSICS algorithm, an automated approach for detecting and correcting

spatial misregistrations developed at the GFZ. For water surfaces, the produced EnMAP Level-2A normalized water-leaving reflectance is validated by the team of Alfred Wegener Institute (AWI). The spectral quality validation compares the EnMAP BOA reflectance and the normalized water-leaving reflectance with co-located in-situ spectral measurements.

Results

The results of the geometry validation include spatial distribution maps of the detected misregistration patterns and scatter plots indicating the registration errors in the x- and y- directions. Specific performance metrics such as RMSE or mean and standard deviation of absolute shifts are directly compared with the validation performances of the official EnMAP Level-2A product and the EnMAP mission quality requirements. The spectral validation results include plots of (1) EnMAP Level-2A BOA reflectance as produced by EnPT via the SICOR or ISOFIT atmospheric correction approaches for land surfaces and (2) normalized water-leaving reflectance spectra from ACwater/Polymer for water surfaces. Additional in-situ spectra and corresponding residuals enable an absolute assessment of the spectral quality of the EnPT Level-2A output depending on the different atmospheric correction approaches. Regarding the cross-validation between the EnPT Level-2A product and the official one from the ground segment, spectra are directly compared area-wide to assess the agreement between both processing chains.

Outlook for the future

EnPT is an actively maintained Python software, which is continuously updated and improved with state-of-the-art software concerning future developments and user feedback. Furthermore, the quality of the EnMAP L1B products may change over time depending on the processor version. Thus, continuous monitoring of the produced EnPT EnMAP Level-2A products is needed, which reflects quality changes in the output of EnPT over time or after algorithmic changes in the EnMAP ground segment pipeline. Future works could also consider the cross-validation of EnMAP Level-2A products generated with EnPT and other hyperspectral sensors, such as PRISMA, EMIT or DESIS.

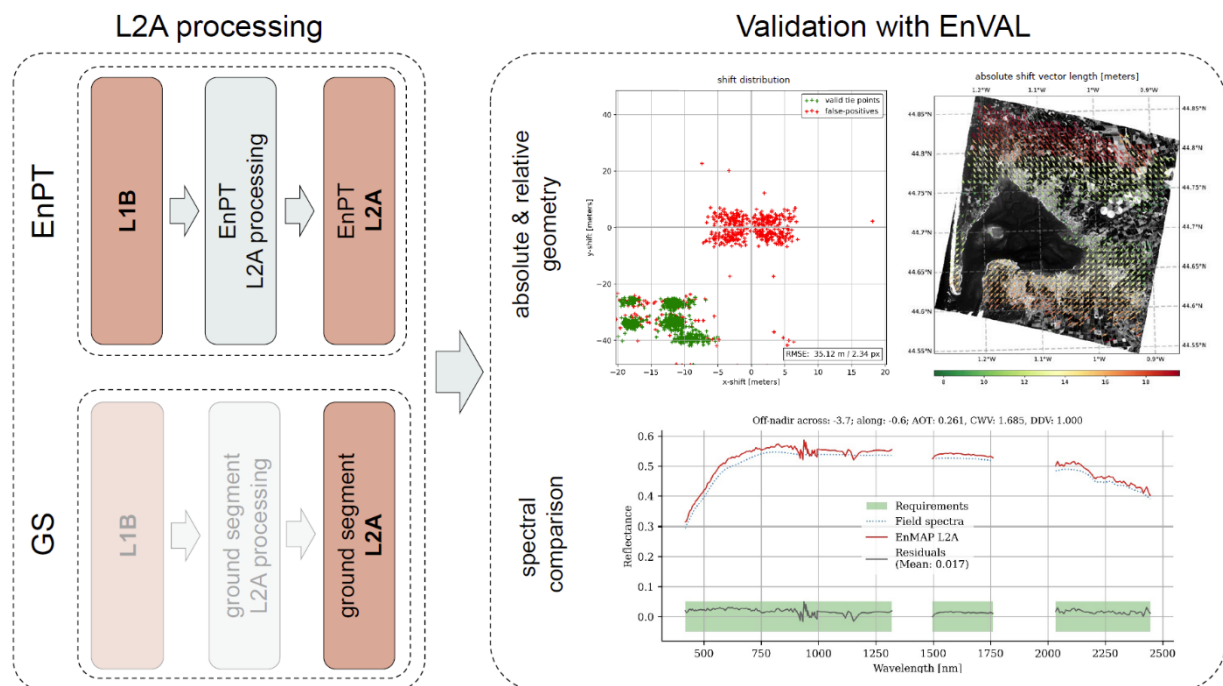


Figure 1 Exemplary results of the geometric and spectral validation of the EnPT Level-2A product including cross-validation with the L2A product of the ground segment

Next-Generation Imaging Spectroscopy Calibration Methods for SBG-VSWIR

[Regina Eckert](#)¹, David R. Thompson¹, Diana Blaney¹, Carl Bruce¹, Lori Moore¹, Byron Van Gorp¹, Zachary Small¹, Peter Sullivan¹, Hong Tang¹, Robert O. Green¹

¹ Jet Propulsion Laboratory, California Institute Of Technology, United States

Keywords: calibration, in-flight calibration, laboratory calibration, validation, nonlinearity calibration

Challenge

Current and planned global imaging spectrometer missions, such as PRISMA, DESIS, EnMAP, EMIT, CHIME, and SBG-VSWIR, require high-quality calibration to deliver the best possible spectra across the Earth. While intensive ground calibration provides holistic instrument characterization, small instrument shifts during launch and detector drift over time mean that in-flight calibration is needed to ensure consistent, high-quality results. In-flight calibration can involve instrument shutters, on-board sources, calibration panels, star trackers, or complex maneuvers to calibrate against the moon or sun. However, these methods add weight and complexity to the instrument design, and may involve increased uncertainty in the calibration over time as, for example, on-board sources or calibration panels degrade. For the SBG-VSWIR instrument, we therefore plan to use in-flight Earth-based calibration sources alongside laboratory calibration to ensure high-quality delivery of radiance spectra globally.

Methodology

NASA's Surface Biology and Geology (SBG) mission forms a core part of the upcoming Earth System observatory, and includes visible to shortwave infrared (VSWIR) and thermal infrared (TIR) instruments. SBG-VSWIR is planned to be a Dyson push-broom VSWIR spectrometer that will measure spectra with 10 nm spectral sampling at 30 m spatial sampling every 16 days globally. SBG-VSWIR plans to use the Earth as a calibration source for many key calibration aspects, as shown in Figure 1. For example, dark frames will be obtained from the unilluminated side of the Earth during every orbit, while the instrument flatfield will be updated from aggregated frames over time. Atmospheric features will be used to update the spectral calibration, while the radiometric calibration will be updated via in situ measurements of Earth surface, such as from the RadCalNet network. We have evaluated this plan using data from the EMIT instrument, to show the expected efficacy of the Earth-based calibration.

SBG-VSWIR additionally plans to use next generation laboratory calibration methods, including nonlinearity calibration measurements tested on the Mapping Imaging Spectrometer for Europa (MISE) instrument, which has a higher nonlinearity than expected on SBG-VSWIR. Four nonlinearity calibration measurements were compared with MISE, including a ramped spectral source, integration time sweep, controlled source changes, and a novel dual source method, which will be adapted for SBG-VSWIR characterization.

Results

Earth-based calibration methods have been extensively tested with NASA's EMIT instrument. Dark frames obtained over the unilluminated side of the Earth had a low drift over time, suggesting that this method is robust for dark collection. The EMIT flatfield has been fine-tuned on a frame-by-frame basis by taking the median of the previous 400 frames, which results in a statistically uniform input. This method has suppressed a consistent cosmetic striping effect from the pushbroom instrument. Repeated overflights of the Railroad Valley calibration site have shown a less than 1% radiometric error for EMIT, validating the Earth-based spectral and radiometric calibration updates. EMIT has shown high-quality spectra can be achieved with Earth-based calibration, and provides a strong template for SBG-VSWIR in-flight calibration plans.

Additional calibration of instrument characteristics such as detector nonlinearity are also planned for SBG-VSWIR to ensure high-quality spectra across the sensor dynamic range. Recent calibration of the MISE instrument has allowed a detailed comparison of different nonlinearity calibration measurements of an assembled spectrometer, as seen in Figure 2. Studies such as these will inform the laboratory calibration of SBG-VSWIR to complement the in-flight calibration updates.

Outlook for the future

Current methods of in-flight calibration have been shown to work with the EMIT instrument, providing high-quality spectra over a range of surface types. SBG-VSWIR will adapt these methods for truly global imaging. Improved laboratory measurements of nonlinearity will provide further spectrometer improvements. Investigation into polarization characterization is on-going for SBG-VSWIR. Polarization effects, while expected to be small, could have an effect over targets with low reflectance, such as aquatic areas, where the atmospheric path radiance has a large influence on the measured radiance at the sensor. Additionally, we are investigating how all stages of the calibration pipeline can be fine-tuned using in-flight, Earth-based data, which will ensure the calibration is as up-to-date and accurate as possible over the lifetime of the mission.

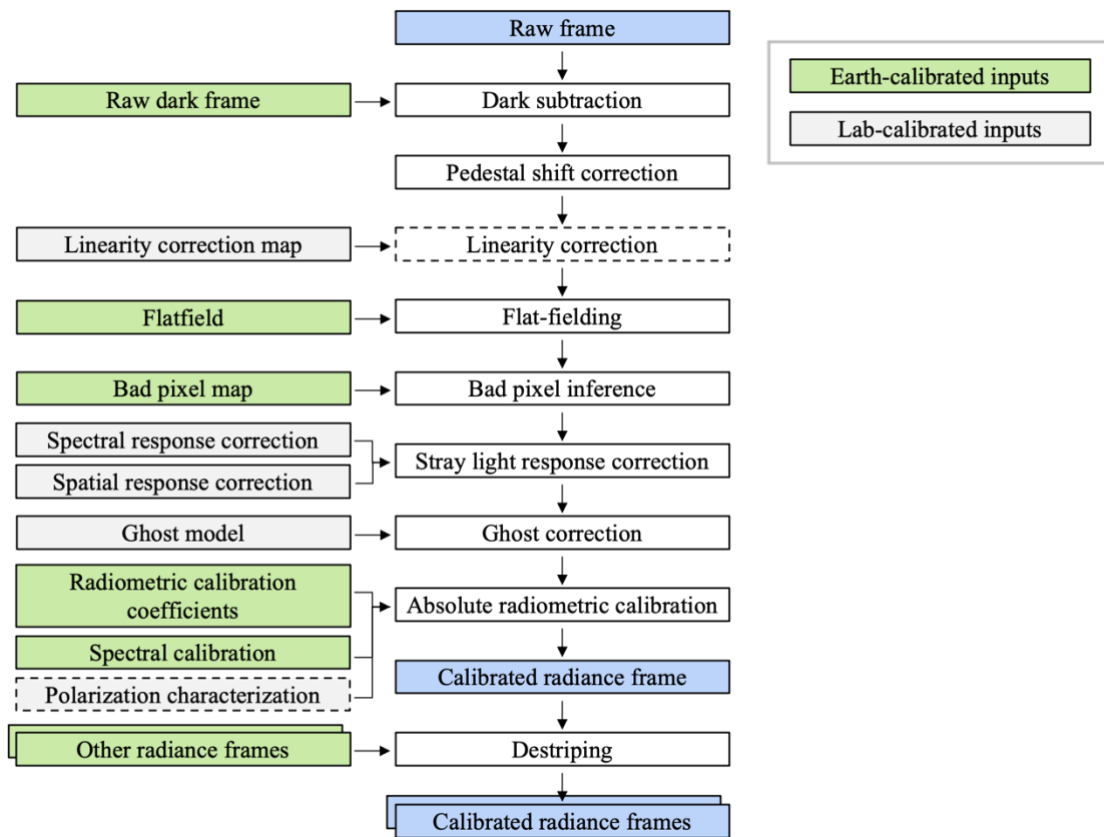


Figure 1: SBG- VSWIR calibration pipeline

Linearity mapping from input to output DN, divided by input DN (MISE spectrometer)

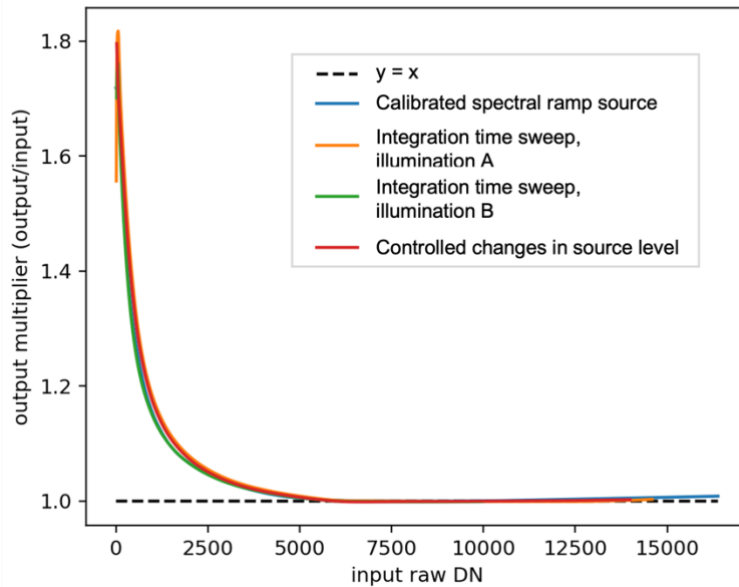


Figure 2: Different methods of laboratory nonlinearity calibration were compared for the Mapping Imaging Spectrometer for Europa (MISE). These methods can be used for nonlinearity characterization of future imaging spectrometers.

Evaluating the EnMAP L2A normalized water leaving reflectance product over two years of mission

EARSeL Valencia 2024

Abstract

Corresponding Author: msoppa@awi.de

*Mariana A. Soppa*¹, Maximillian Brell², Sabine Chabrilat^{2,3}, Leonardo Alvarado¹, Peter Gege⁴, Stefan Plattner⁴, Ian Somlai-Schweiger⁴, Thomas Schroeder⁵, Vittorio Brandò⁶, Simone Colella⁶, Mariano Bresciani⁷, Claudia Giardino⁷, Quinten Vanhellemont⁸, François Steinmetz⁹, Daniel Scheffler², Maximillian Langheinrich¹⁰, Emiliano Carmona¹⁰, Martin Bachmann¹⁰, Miguel Pato¹⁰, Laura La Porta¹¹, Sebastian Fischer¹¹, Astrid Bracher^{1,12}

¹ Alfred Wegener Institute, Helmholtz Center for Polar and Marine Research, Bremerhaven, Germany

² Helmholtz Center Potsdam, GFZ German Research Center for Geosciences, Potsdam, Germany

³ Leibniz University Hannover, Institute of soil science, Herrenhäuser Str. 2, 30419 Hannover, Germany

⁴ German Aerospace Center (DLR), Remote Sensing Technology Institute, Weßling, Germany

⁵ Commonwealth Scientific and Industrial Research Organisation (CSIRO) Environment, Brisbane, Australia

⁶ Consiglio Nazionale delle Ricerche, Istituto di Scienze Marine (CNR-ISMAR), Rome, Italy

⁷ Consiglio Nazionale delle Ricerche, Istituto per il Rilevamento Elettromagnetico dell'Ambiente (CNRI-REA), Milan, Italy

⁸ Royal Belgian Institute of Natural Sciences, Operational Directorate Natural Environments, Brussels, Belgium

⁹ HYGEOS, Lillie, France

¹⁰ Earth Observation Center (EOC), German Aerospace Center (DLR), Weßling, Germany

¹¹ Space Agency, German Aerospace Center (DLR), Bonn, Germany

¹² Institute of Environmental Physics, University of Bremen, Otto-Hahn-Allee 1, 28359 Bremen, Germany

Keywords (5): Hyperspectral, Validation, Atmospheric Correction, inland water, coastal water

Challenge

The Environmental Mapping and Analysis Program (EnMAP), launched in April 2022 provides valuable data with 30 x 30 m spatial resolution and 244 spectral bands and this data is expected to improve our knowledge of inland and coastal waters. However, the atmospheric correction of satellite data obtained over water poses a significant challenge in aquatic remote sensing. Notably, the water leaving radiance in the visible spectrum constitutes usually not more than 10% of the total radiance at top of atmosphere. The remaining 90% of the signal primarily comprises atmospheric radiance and surface reflection, necessitating robust removal to mitigate significant uncertainties in the water products. To address this, we assess the quality and compare the EnMAP water reflectance products generated by three atmospheric correction processors: (i) Modular Inversion Program (MIP) used by the EnMAP ground segment (GS), (ii) Polymer and (iii) Acolite. This evaluation aims to understand and address these challenges for enhanced accuracy in EnMAP water reflectance products.

Methodology

We evaluate the EnMAP normalized water leaving reflectance products derived from three atmospheric correction methods covering EnMAP acquisitions from the commissioning phase validation activities in July-October 2022 and the current operational phase. The L2A atmospheric correction implemented in the operational processing chain of the ground segment is the physics-based Modular Inversion and Processing System (MIP, EOMAP GmbH). We also assessed the quality of two more AC methods: Polymer and Acolite. The EnMAP-Polymer reflectance products were generated using the EnMAP Processing Tool (EnPT) and choosing the Polymer (HYGEOS) atmospheric correction. Polymer is a spectral matching algorithm in which atmospheric and oceanic signals are obtained simultaneously using the fully available VNIR spectrum. Acolite is a stand-alone software based on the Dark Spectrum Fitting (DSF) algorithm, and it was downloaded from <https://github.com/acolite/acolite>. Hyperspectral in situ measurements from international partners, projects, and extensive field campaigns have been used to validate the EnMAP L2A water product at six core sites spanning inland, coastal, and open ocean waters. These are Aqua Alta Oceanographic Tower (Italy), Lake Constance (Germany), Lake Trasimeno (Italy), Lampedusa (Italy), Lucinda Jetty Coastal Observatory (Australia), and Oostende (Belgium). The quality control of the match-ups follows the validation protocol and match-up statistics recommended by EUMETSAT.

Results

The EnMAP-MIP normalized water reflectance product from the EnMAP GS meets the accuracy requirements of the mission and is of the same magnitude and shape as the spectral variability of the in situ measurements (Figure b). The mission requirements for uncertainty (RMSE) of the normalized water leaving and subsurface reflectance for water applications, not considering strong atmospheric absorption regions and for Aerosol Optical Thickness (AOT) ≤ 0.4 , are as follows: 0.04 for $400 \text{ nm} < \lambda \leq 450 \text{ nm}$, 0.02 for $450 \text{ nm} < \lambda \leq 650 \text{ nm}$, and 0.01 for $650 \text{ nm} < \lambda \leq 800 \text{ nm}$. For AOT values larger than 0.4, the corresponding RMSE values are increased by 0.01. Based on the current results, we found improved performance of EnMAP-MIP reflectance products compared to those derived using Polymer and Acolite atmospheric correction algorithms. Nevertheless, spectral noise at shorter wavelengths is observed in the Level 2 product regardless of the atmospheric correction method applied at our study sites. This issue is being investigated by the EnMAP Ground Segment.

Outlook for the future

As the mission progresses and the number of match-ups increases, we aim to expand our assessment by incorporating the evaluation of atmospheric correction processors across various Optical Water Types (OWTs). This investigation seeks to understand how the inherent variability in aquatic properties influences the performance of different atmospheric correction processors and EnMAP normalized water leaving reflectance data. Additionally, we will extend the quality monitoring of the EnMAP water products by cross-comparing the products to other satellite missions such as DESIS, PRISMA, EMIT, and S2-MSI.

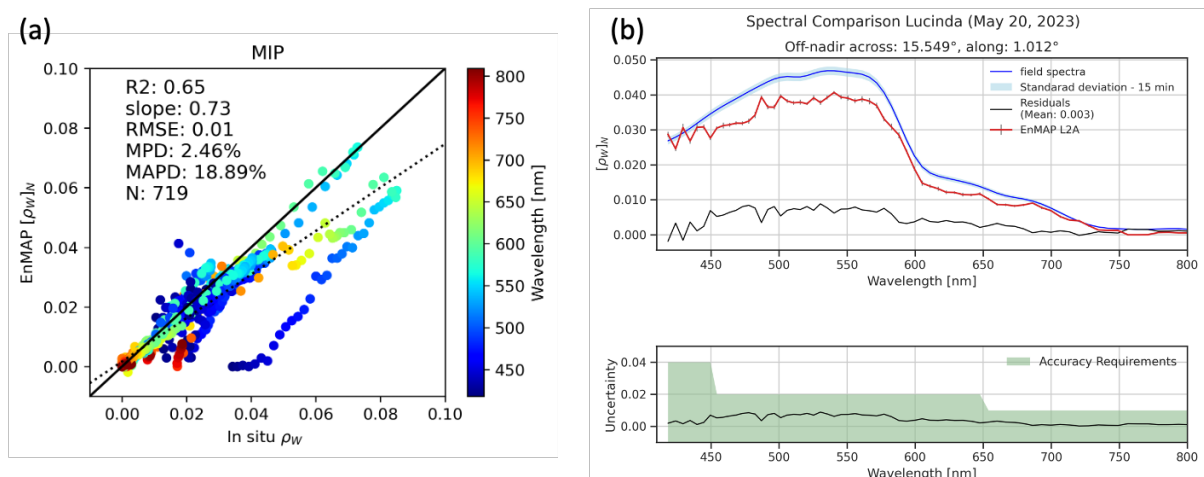


Figure (a) Scatterplot of EnMAP-MIP match-ups at all sites (v01.03.01), the solid black line is the 1:1 line, and the dotted line is the regression fit, and (b) example of a match-up between EnMAP (v01.04.00) and hyperspectral in situ measurements at Lucinda Jetty Coastal Observatory (Thomas Schroeder, CSIRO).

Them.Sess. 3-5: Hyperspectral remote sensing of vegetation health

How many bands - how narrow? A comparison of three different sensors for disease severity mapping

Miriam Machwitz¹, Christian Bossung¹, Mario Gilcher², Gilles Rock², Franz Ronellenfitsch¹, Adriano Gama¹, Daniel Molitor¹, Kristina Heilemann¹, Mareike Schultz³

¹ Luxembourg Institute of Science and Technology LIST, Remote sensing and natural resources modelling, 4422 Belvaux, Luxembourg

² Luxense Geodata, 4, rue Albert Simon, 5315 Contern, Luxembourg

³ Insitute Viti Vinicole, Ministère de l'Agriculture, 8, rue Nic Kieffer 5551 Remich, Luxembourg

Keywords (5): Unmanned Aerial Vehicles, vegetation, comparison hyperspectral-multispectral, plant disease

Challenge

Plant diseases are often correlated with leaf pigment contents, making the latter a reliable proxy for mapping disease symptoms. Hyperspectral data is considered the gold standard for modeling leaf pigment contents through hybrid RTM inversion. However, many of these bands exhibit autocorrelation, and the full range may not be necessary to accurately estimate leaf pigment content. Consequently, several studies explore the significance of different bands and artificially reduce dimensions.

Simulated multi-spectral sensors are based on hyperspectral data, but differences extend beyond the number of bands and bandwidth. Distinct companies employ various materials and engineering approaches, resulting in more theoretical outcomes from such studies. In addition to quality, there is significant variation in the workload required to obtain results. Hyperspectral data acquired with line scanning sensors may offer less geometric accuracy and necessitate the integration of additional data, unlike multispectral sensors. To comprehensively address these aspects, a genuine comparison provides more insight than a simulation of different sensors.

Methodology

We conducted a comparative analysis of data accuracy derived from three distinct sensors for the purpose of mapping Esca, a relevant disease in viticulture that manifests on individual plants. We examined four defined disease symptom classes: "no symptoms," "mild," "medium," and "severe symptom levels." The sensors were flown on the same day and include a hyperspectral sensor, the Headwall Nano VISNIR, as well as two multispectral sensors with varying bandwidths: the Micasense multispectral sensor and the Phantom P4 multispectral sensor. Our ultimate objective is to accurately map Esca disease symptoms.

To achieve this goal, we executed different processing steps and compared them in terms of accuracy and time efficiency. Preprocessing played a pivotal role in our analysis, considering the intricate structures of viticulture and the sporadic nature of the disease's occurrence on individual plants, which demand a high degree of geometric precision and the integration of various data sources. Additionally, we calculated and compared simple vegetation indices. Beyond vegetation indices, we estimated the concentration of leaf pigments, such as chlorophyll and carotenoids, using a hybrid Radiative Transfer Model (RTM) inversion approach with the ARTMO toolbox.

Expected results

Processing multispectral data proves to be significantly more efficient and requires minimal manual intervention to generate a valuable dataset. The preprocessing for the two multispectral sensors takes few hours to days with minimal interaction. In contrast, hyperspectral data demands approximately two weeks of processing, alongside continuous manual interactions and quality checks. Additionally, aligning the hyperspectral data with another dataset to attain 3D information on the vine requires substantial manual effort. However, even with this effort, the geometric accuracy for distinguishing vine from the background did not reach the level achieved by the multispectral data. Notably, a discernible difference of 10-30% was observed, whereas the two multispectral datasets demonstrated comparable geometric accuracy.

Even if the ROIs (region of interest) for the hyperspectral data were influenced by unwanted background vegetation, both the boxplots for Vegetation Indices (VIs) and leaf pigments exhibited narrower distributions and superior differentiation among the four symptom classes (Figure 1). Both multispectral sensors did not show sufficient results to differentiate between symptom classes.

For a year like to observed one (2023) with green background vegetation, the differentiation between vine and interspace became very challenging for the hyperspectral analysis since the 3D vine mask is purely based on an additional sensor. For years with dry background (2021), spectral information can support the elimination of background vegetation and the results of the hyperspectral based pigment modelling show even much higher accuracy and better differentiation between symptom classes (Figure 2). Unfortunately, for the 2021, no multi-spectral data was available, but a similar result to 2023 like show in Figure 1 can be expected.

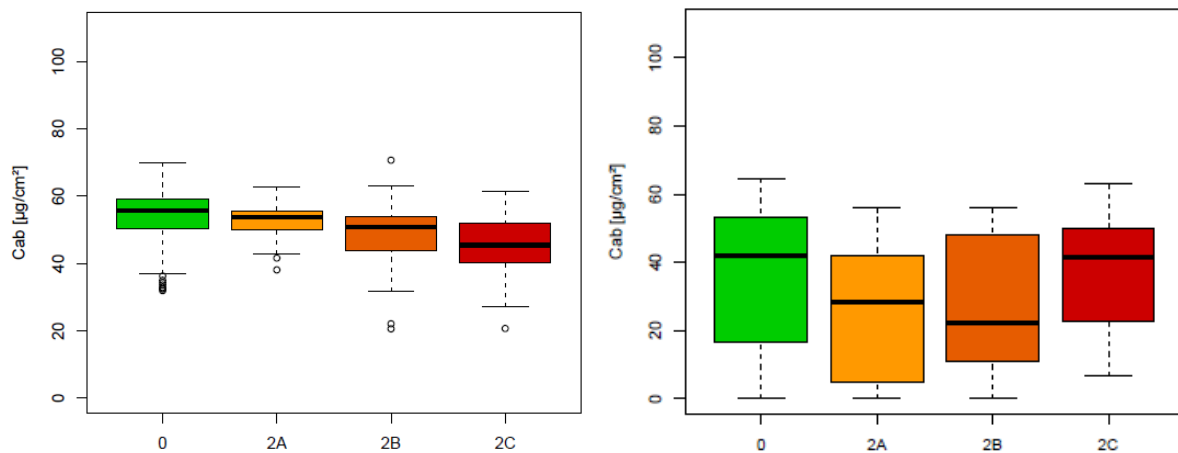


Figure 1: Differentiation between symptom classes based on chlorophyll content estimation with hyperspectral (left) and multispectral (right) data (green=no symptoms, yellow= mild symptoms, orange medium symptoms, red=severe symptoms) for the year 2023

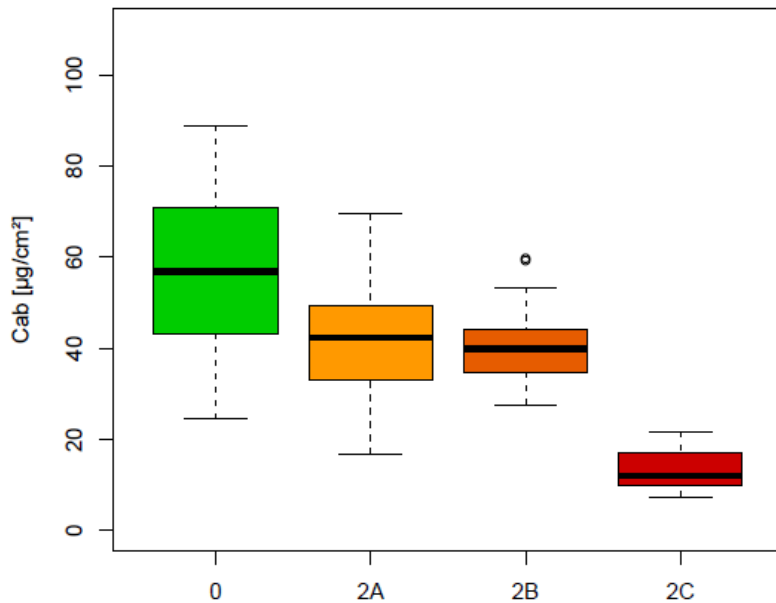


Figure 2: Differentiation between symptom classes based on chlorophyll content estimation with hyperspectral data for 2021 (green=no symptoms, yellow= mild symptoms, orange medium symptoms, red=severe symptoms)

Outlook for the future

We can summarize, that hyperspectral data is the preferred data source to receive accurate pigment content and disease severity estimations. However, for UAV platforms and complex canopy structures, multispectral data can achieve better accuracy with respect to geometric accuracy and 3D background masking. Especially for certain conditions like similar background vegetation in humid years, this might be a significant advantage. Still, the pigment modelling of the hyperspectral data overperformed the multispectral data. However, different meteorological conditions leading to different vegetation status and the performance of sensors is influence be these effects. Thus, this result is a case study and cannot be generalised. Facing climate change and extreme variations between years makes a comparison of sensors even more complex and multi-year analyses are needed.

Utilization of Deep Learning and Hyperspectral Imaging for Water-Deficient Potato Plant Identification

Janez Lapajne¹, Andrej Vončina², Uroš Žibrat³

¹ AGRICULTURAL INSTITUTE OF SLOVENIA, PLANT PROTECTION DEPARTMENT,
HACQUETOVA ULICA 17, LJUBLJANA, 1000 LJUBLJANA, SLOVENIA

Keywords (5): Hyperspectral imaging, Deep learning, Potato plant, Water-deficiency

Challenge

Potatoes are vital for global food security and sustainable development, but their growth is hindered by various stress factors, especially drought and heat. To mitigate these challenges, the use of hyperspectral imaging (HSI) and deep learning models is gaining prominence. HSI facilitates non-invasive monitoring, capturing plant variations in spectral and spatial features across different wavelengths, while deep learning models help classify and assess stress levels. Despite their potential, challenges like the "curse of dimensionality" and overfitting due to a high number of spectral bands persist. Current studies demonstrate the effectiveness of deep learning models in detecting stressors like virus infection, biotrophic phase of blight, and water stress in potatoes. However, these models remain underutilized, particularly in exploring the SWIR part of the spectrum. Addressing these gaps could significantly improve the understanding and management of stress factors, enhancing potato crop resilience and yield.

Methodology

An experiment was conducted at the Agricultural Institute of Slovenia from April to August 2022, focusing on two potato cultivars, KIS Krka (drought-resistant) and KIS Savinja (drought-sensitive). Controlled greenhouse conditions were maintained with specific temperature (21°C/15°C), humidity (60%), and photoperiod (14 hours). Tensiometers were used to monitor soil moisture, ensuring a specific range for well-watered and water-deficient plants. Hyperspectral imaging was conducted weekly over a 5-week period, starting after two weeks the plants were seeded, utilizing VNIR and SWIR spectral regions (dual-sensor setup). The imaging setup involved controlled lighting, a calibrated reflectance panel and Hypsux pushbroom cameras positioned 3 meters above the plants. In order to identify water-deficient plants, we employed a Convolutional Neural Network (CNN) integrated with an attention mechanism to dynamically recalibrate hyperspectral band channels. This approach assigns greater significance to informative spectral bands, while reducing the emphasis on irrelevant or noisy bands, effectively emphasizing spectral bands crucial for feature representation and the classification process. To evaluate the model, various datasets were created employing different data distributions and splitting methods. This enabled the assessment of their influence on the classification outcome. Classification metrics, including AUC-ROC, F1 score, precision, and recall, were assessed with the 95% confidence intervals, calculated using bootstrapping techniques.

Expected results

The attention-based deep neural network's performance yielded varying results for the two potato varieties. KIS Krka demonstrated better performance, achieving an overall AUC-ROC of 0.74, with the first imaging session showing the most difficulty. Subsequent sessions produced AUC-ROCs ranging from 0.71 to 0.87. In contrast, KIS Savinja yielded inferior results, with an average AUC-ROC of 0.64, reaching its highest performance with an AUC-ROC of 0.79 in imaging session two, while demonstrating the weakest

classification in session five (AUC-ROC of 0.52). However, the model effectively classified samples during the initial imaging sessions, achieving an AUC-ROC of 0.67. Precision and recall closely mirrored the F1 scores, indicating the absence of overfitting for both varieties. In subsequent assessments based on biased datasets the model produced artificially inflated results in almost all settings. KIS Krka achieving an AUC-ROC of 0.87 (17.6% increase) and KIS Savinja attaining an AUC-ROC of 0.76 (18.9% increase). However, the F1 scores for KIS Savinja fluctuated notably, dropping to 0.44 in imaging 3. Informative spectral bands varied across datasets and varieties, with certain ranges standing out prominently. Notably, the VNIR segment highlighted ranges of 475 – 580 nm, 660 – 730 nm, and 940 – 970 nm, while the SWIR segment emphasized ranges of 1420 – 1510 nm, 1875 – 2040 nm, and 2350 – 2480 nm.

Outlook for the future

The paper introduces a novel attention-based deep learning framework for detecting water-deficient potato plants using dual-sensor hyperspectral imaging. Results reveal the challenge of distinguishing between treatments due to similar spectral signatures, emphasizing the importance of spectral-spatial information. Spectral analyses highlight the role of chlorophyll and water content in the VNIR and SWIR ranges, aiding in physiological assessment. Deep learning models demonstrate improved classification performance when considering dataset biases. The study's findings have significant implications for precision agriculture and potato breeding, enabling optimized resource allocation and accelerated selection of drought-tolerant cultivars. The research also contributes to the development of remote sensing applications for targeted water management and pest prevention in changing climatic conditions.

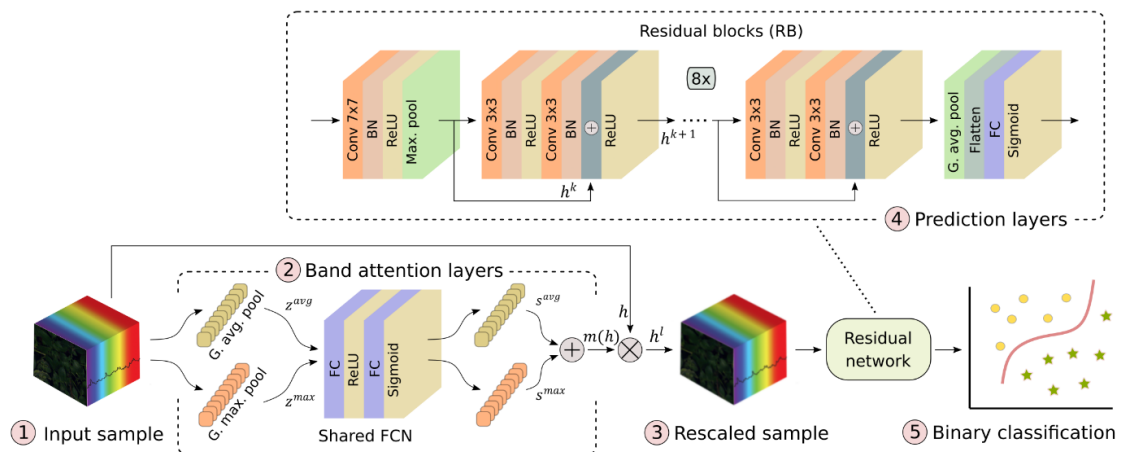


Figure 1 Architecture of attention deep learning model. Conv – convolution, BN – batch normalization, ReLU – rectified linear unit, G. max. pool. – global maximum pooling, G. avg. pool. – global average pooling, FC – fully connected.

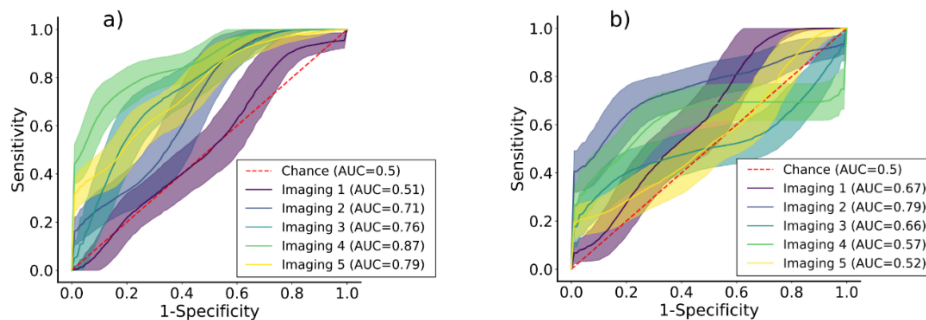


Figure 2 ROC curves for varieties a) KIS Krka and b) KIS Savinja. The legend includes mean values of AUCs corresponding to imaging sessions.

Understanding the effects of bacterial leaf blight disease on rice spectral signature

Ziyi Wang¹, Roshanak Darvishzadeh¹, Nancy Castilla², Alice Laborte², Andy Nelson¹

¹ Department of Natural Resources, Faculty of Geo-Information Science and Earth Observation (ITC), University of Twente, Enschede, Netherlands

² International Rice Research Institute, Los Baños, Philippines

Keywords (3): Canopy hyperspectral, Rice disease, Bacterial leaf blight

Challenge (800 - 1000 characters incl. spaces)

Rice is one of the main staple food for nearly half of the global population, rice production is closely associated with global food security. Rice bacterial leaf blight (BLB) caused by *Xanthomonas oryzae* pv *oryzae* is considered one of the most widely occurring diseases in tropical and temperate rice-growing areas, causing yield losses of around 2.72% globally. To prevent damage and yield loss caused by BLB infection, it is imperative to detect BLB-infected rice timely. Hyperspectral data containing thousands of narrow bands shows great potential to detect BLB in a rapid and accurate manner. Previous studies have revealed several spectral changes at the canopy scale but only focused on post-heading growth phases, which limits the use of hyperspectral data for early disease detection. To address this knowledge gap, this study aims to examine the feasibility of detecting BLB infection from canopy reflectance spectra at the pre-heading stage.

Methodology (1200 – 1500 characters incl. spaces)

A field experiment was conducted at the rice stem elongation phase at the Zeigler Experiment Station at the International Rice Research Institute (IRRI), Los Baños, Philippines. A highly susceptible rice variety (IR24), was grown in the wet season of 2023 when conditions are favourable to BLB. Rice leaves were inoculated at the tillering phase by cutting leaf tips and dipping in the suspension with the BLB pathogen. In non-inoculated plants, leaves were cut and dipped in distilled water only. Canopy hyperspectral reflectance and crop biophysical and biochemical parameters (e.g. SPAD, Leaf area index (LAI), canopy height, fresh biomass, dry biomass, canopy water content) were measured in inoculated (n=45) and non-inoculated (n=45) plots. The spectral reflectance of rice canopies was then pre-processed by removing the noisy bands and averaging. Linear discriminate analysis was conducted on each spectral wavelength to examine the separability of spectral bands, and 5-fold cross-validation was used to evaluate the accuracy. Furthermore, the significance of differences in biophysical and biochemical parameters between the two classes (healthy vs. infected) was assessed using the Student t-test or the Mann-Whitney U test after the normality test through the Shapiro-Wilk test.

Expected results (1200 – 1500 characters incl. spaces)

Comparison of the mean spectra from the infected and healthy rice showed higher reflectance in visible, near-infrared and short-wave infrared regions for infected rice than that of healthy rice at the rice stem elongation phase. The separability of each spectral band assessed by linear discriminate analysis demonstrated higher accuracy in the visible and shortwave infrared regions than in the near-infrared region (Figure A). The most sensitive spectral bands are 623nm, 634nm, 657nm, 664nm, 2206nm, 2236nm, and 2238nm, which are in red and shortwave infrared regions. Regarding the assessment of biophysical and biochemical responses, SPAD, LAI, fresh biomass and canopy water content data were tested to be normally distributed, while canopy height and dry biomass were not. Figure B displays the results of the significance test for these biophysical and biochemical parameters. Specifically, student t-

test results of SPAD, LAI, fresh biomass and canopy water content showed above parameters significantly decreased after BLB infection which was explained by the selected sensitive spectral bands. The result of the Mann-Whitney U test showed that canopy height significantly decreased and dry biomass did not.

Outlook for the future (800 - 1000 characters incl. spaces)

This study examined the spectral variation of BLB infection at the rice pre-heading phase using canopy hyperspectral measurements, the potential of red and SWIR regions on BLB detection has been determined using LDA. Although this study was conducted through non-imaging hyperspectral data at canopy level, these findings from the inoculation experiment under control conditions provide a fundamental basis for upscaling to the regional scale using hyperspectral imagery. In addition, some of the sensitive spectral bands selected in this study have similar wavelengths to Sentinel-2 imagery (band 4 and band 12), which demonstrates the applicability of existing multispectral images in BLB detection. The mechanism of detecting BLB using spectral variations has been clarified by assessing the changes in biophysical and biochemical properties. Particularly, the changes in leaf chlorophyll content have great potential to be used for BLB detection using remote sensing, which has been detected by the red region.

Please upload 1-2 figures or graphical abstract (min 300 dpi. jpeg/png)

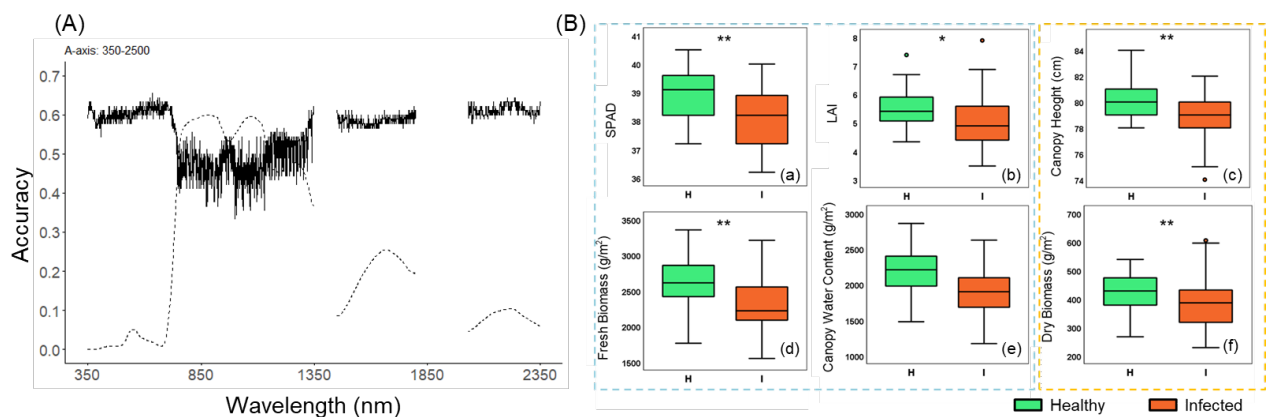


Figure (A) The overall accuracy (OA) of classification per wavelength (B) Comparison of leaf/canopy biochemical and biochemical parameters between the infected and healthy rice, the parameters in the blue frame are normally distributed, while the parameters in the orange frame are not normally distributed

The Spatial Scaling Challenge: ecophysiological variables retrieval and stress detection.

EARSel Valencia 2024
Abstract
Corresponding Author:
jpacheco@bgc-jena.mpg.de

Javier Pacheco-Labrador^{1*}, M.Pilar Cendrero-Mateo², Shari Van Wittenberghe², Itza Hernandez-Sequeira³, Gerbrand Koren⁴, Egor Prikaziuk⁵, Szilvia Fóti⁶⁻⁷, Enrico Tomelleri⁸, Kadmiel Maseyk⁹, Nataša Čereković¹⁰, Rosario Gonzalez-Cascon¹¹, Zbyněk Mollenovský¹², Mar Albert-Saiz¹³, Michal Antala¹³, János Balogh⁶, Henning Buddenbaum¹⁴, Mohammad Hossain Dehghan-Shoar¹⁵, Joseph T. Fennell⁹, Jean-Baptiste Feret¹⁶, Balde Hamadou¹⁷, Miriam Machwitz¹⁸, Ádám Mészáros⁶, Guofang Miao¹⁹, Miguel Morata², Paul Naethe²⁰, Zoltán Nagy⁶⁻⁷, Krisztina Pintér⁷, R. Reddy Pullanagari²¹, Anshu Rastogi¹³, Bastian Siegmann²², Sheng Wang²³⁻²⁴, Chenhui Zhang²⁵.

¹Max Planck Institute for Biogeochemistry, Hans Knöll Straße 10, D-07745, Jena, Germany.

²Laboratory of Earth Observation, Image Processing Laboratory, University of Valencia, C/ Catedrático Agustín Escardino, 46980, Paterna (Valencia), Spain.

³Institute of New Imaging Technologies, University Jaume I, Avda. Sos Baynat, s/n, 12071, Castellón de la Plana (Castellón), Spain.

⁴Copernicus Institute of Sustainable Development, Utrecht University, Princetonlaan 8a, 3584 CB, Utrecht, The Netherlands.

⁵Faculty of Geo-Information Science and Earth Observation (ITC), University of Twente, ITC, P.O. Box 217, 7500 AE, Enschede, The Netherlands.

⁶Department of Plant Physiology and Plant Ecology, Institute of Agronomy, Hungarian University of Agriculture and Life Sciences, Páter K. u. 1, Gödöllő, 2100, Hungary.

⁷HUN-RES-MATE Agroecology Research Group, Páter K. u. 1, Gödöllő, 2100, Hungary.

⁸Faculty of Agricultural, Environmental and Food Sciences, Free University of Bozen/Bolzano, piazza Università 1, 39100, Bozen-Bolzan, Italy.

⁹School of Environment, Earth and Ecosystem Sciences, The Open University, The Open University, Walton Hall, Milton Keynes MK7 6AA, United Kingdom.

¹⁰University of Banja Luka, Faculty of Agriculture, Bulevar vojvode P. Bojovića 1a, 78000, Banja Luka, Bosnia and Herzegovina.

¹¹INIA-CSIC, Department of Environment and Agronomy, Crra. Coruña km 7.5, 28040, Madrid, Spain.

¹²Remote Sensing Research Group, Department of Geography, University of Bonn, Meckenheimer Allee 166, 53115, Bonn, Germany.

¹³Laboratory of Bioclimatology, Department of Ecology and Environmental Protection, Faculty of Environmental and Mechanical Engineering, Poznań University of Life Sciences, Piątkowska 94, 60-649 Poznań, Poland.

¹⁴Environmental Remote Sensing and Geoinformatics, Trier University, 54286, Trier, Germany.

¹⁵School of Agriculture and Environment, Massey University, Tennent Drive, Palmerston North 4414, New Zealand.

¹⁶UMR TETIS, INRAE, Maison de la Télédétection 500, rue Jean-François Breton, 34093, Montpellier cedex 5, France.

¹⁷Laboratoire de Météorologie Dynamique, Sorbonne Université, IPSL, CNRS/L'École polytechnique, 91128, Palaiseau Cedex, France.

¹⁸Remote sensing and natural resources modelling, Department for Environmental Research and Innovation (ERIN), Luxembourg Institute of Science and Technology (LIST), 41, Rue du Brill, 4422, Belvaux, Luxembourg.

¹⁹School of Geographical Sciences, Fujian Normal University, Fuzhou City, FJ 350117, China.

²⁰JB Hyperspectral DeVises, Am Botanischen Garten 33, 40225, Düsseldorf, Germany.

²¹Australian Plant Phenomics Facility (APPF), The Plant Accelerator, School of Agriculture, Food and Wine, University of Adelaide, Waite Campus, Urrbrae, SA 5064, Australia.

²²Institute of Bio- and Geosciences, IBG-2: Plant Sciences, Forschungszentrum Jülich GmbH, Wilhelm-Johnen-Straße, 52428, Jülich, Germany.

²³Department of Agroecology, Aarhus University, Ole Worms Allé 3, 8000, Aarhus, Denmark.

²⁴Agroecosystem Sustainability Center, Institute for Sustainability, Energy, and Environment, University of Illinois Urbana-Champaign, Urbana, IL 61801, USA.

²⁵Institute for Data, Systems, and Society, Massachusetts Institute of Technology, 77 Massachusetts Avenue Cambridge, MA 02139-4307, USA.

Keywords (5): Remote sensing, plant physiology, spatial scaling, temporal mismatch, fluorescence, thermal, hyperspectral, top of the canopy, photosystem, down-scaling.

Challenge (800 - 1000 characters incl. spaces)

Technological advances over the past decade have enabled the development of new remote sensing sensors and platforms capable of collecting data at unprecedented resolutions. These have opened new possibilities for monitoring the ecophysiological status of plants. Traditionally, remote sensing has relied on optical reflectance factors to infer vegetation structure and leaf constituents. In contrast, canopy temperature (*LST*), photochemical reflectance index (*PRI*), and sun-induced chlorophyll fluorescence (*SIF*) provide more direct information about plant physiological state. Extracting ecophysiological information from *LST*, *PRI*, and *SIF* signals is challenging because it requires the integration of information from different scales. This analysis is computationally demanding and requires expertise in a variety of fields, including remote sensing, plant physiology, and data science. To address this challenge, the COST Action CA17134 SENSECO promoted the Spatial Scaling Challenge (SSC).

Methodology (1200 – 1500 characters incl. spaces)

The SSC is a synthetic exercise designed to assess the remote sensing community's maturity and knowledge on ecophysiological variables retrieval from remote sensing data. The challenge consisted of retrieving four ecophysiological variables (leaf area index (*LAI*), leaf chlorophyll content (C_{ab}), maximum carboxylation rate at optimum temperature ($V_{cmax,25}$), and non-photochemical quenching (*NPQ*)) from a synthetic dataset of hyperspectral optical, thermal, and Sun-Induced Fluorescence (*SIF*) imagery.

The SSC presented a number of challenges to the participants, including:

- Scaling the spectral information from the top of the canopy down to the leaf and the photosystem levels.
- Using the spectral information and retrieved variables to diagnose vegetation stress and status.

Uncertainty for each of the required parameters and stress maps were also required to evaluate the quality of the results.

Expected results (1200 – 1500 characters incl. spaces)

The SSC received 15 contributions from 13 groups or individuals. The most used approaches were nonparametric methods combining multiple spectral domains and field measurements. LAI and C_{ab} were obtained acceptably in most cases, but $V_{cmax,25}$, and NPQ were estimated less accurately and required more information than directly provided by remote sensing, such as estimates of other biophysical variables and meteorological data (Figure 1). Canopy-to-leaf scaling was performed mostly indirectly (e.g., statistical approaches), and the remaining explicit (physically based or hybrid) methods were less frequently used. Vertical profiles was mostly ignored, and the temporal mismatch between field sampling and remote sensing acquisition, which is critical for physiological variables that vary throughout the day, was most often ignored or not adequately addressed. Not all participants created stress maps or interpreted the information provided and retrieved.

Outlook for the future (800 - 1000 characters incl. spaces)

The analysis of the SSC allows us to identify the following needs and recommendations. To study plant ecophysiology using remote sensing, researchers should (1) combine data from different spectral domains but consider the daily changes in plant physiology and the corresponding signals and (2) use estimates of biophysical parameters to scale from the canopy to the leaf level, but better account for horizontal and spatial variation, as well as differences in spatial resolution and observational uncertainties across remote sensors.

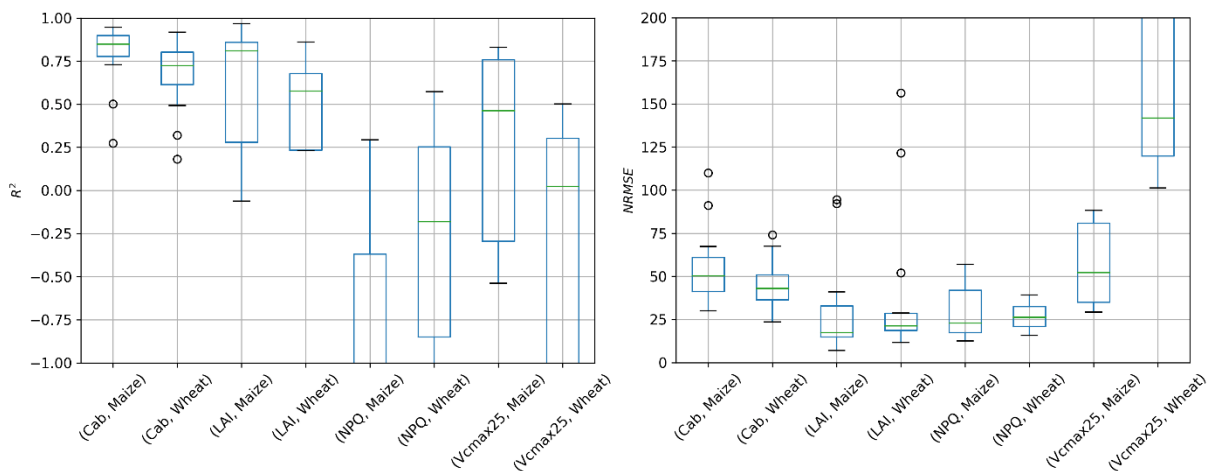


Figure 1. Comparison by means of the coefficient of determination (R^2) and root mean square error (NRMSE) of the ecophysiological parameters retrieved by the SSC participant and the reference simulated data for both the wheat and maize fields. The ecophysiological parameters evaluated were leaf chlorophyll content (C_{ab}), leaf area index (LAI), non-photochemical quenching (NPQ), and maximal carboxylation rate ($V_{cmax,25}$).

**Them.Sess. 3-6: Imaging
spectroscopy for
environmental applications**

First Nighttime VNIR-SWIR Spectra from Space – Mapping Artificial Lights using EnMAP

Martin Bachmann¹, Miguel Pato¹, Tobias Storch¹

¹ German Aerospace Center (DLR), Earth Observation Center (EOC), Germany

Keywords (5): EnMAP, Imaging Spectroscopy, Nighttime Remote Sensing, Lighting Types, Spectral Signatures

Challenge

Artificial nighttime light sources show characteristic spectral behaviour in the spectral range visible to human eyes (VIS). But also in the near infrared (NIR) and in the short-wave infrared (SWIR) narrow-band emission lines of artificial light sources as well as broad-range emissions from fires do exist, allowing for an identification of light sources. These signatures have been studied using field and laboratory spectroscopy, and were also measured and mapped using airborne hyperspectral sensors with a high signal-to-noise ratio (SNR). But from space, the mapping of these artificial light spectra is more challenging as the SNR levels of imaging spectrometers with a reasonably high spatial resolution of ~30 m GSD are low. So far, the only published nighttime light spectra measured by satellite are from EnMAP, which is detailed in this presentation.

Methodology

In this study the standard L1B and L1C products generated by the EnMAP Ground Segment for the area of Las Vegas, USA, are used as inputs (Fig. 1 (a), (b)). It is worth pointing out that neither the EnMAP sensor nor the processors were designed for these low signal levels, so no requirements are applicable regarding *absolute* at-sensor radiance values, SNR and linearity.

For nighttime spectroscopic observations from space, the background noise level in the data is close to the signal level, which requires a noise reduction step before the actual classification. And still many established spectral identification and classification methods show dissatisfying results due to the low signal levels.

In this work, established denoising techniques like an optimized spectral binning as well as a simple cut-off of the typical bandwise noise levels were tested. In order to identify and to map the different light types, a classic spectral signature mapping approach is applied, using documented emission lines of over forty lamps by ELVIDGE et al, 2010 (Elvidge, C.D. et al. 2010. Sensors, 10). For high-temperature emissions, a Planck curve fitting is tested, keeping in mind the expected nonlinearity of radiances at this low signal level. Note that the full VNIR-SWIR range was used as certain lamps also show diagnostic emissions in the infrared.

Results

For the first time ever, full VNIR-SWIR spectra were acquired from space with a sufficient SNR. And based on the reported methods, the identification and the matching of the library spectra of ELVIDGE et al. 2010

to the observed EnMAP night time spectra were possible for the Las Vegas scene. An example is given in Fig. 1 (c) for a metal halide lamp, showing a good agreement of observed and reference spectra.

Due to the good agreement of laboratory and EnMAP-derived spectral signatures, also the mapping of the diverse lamp types was possible (Fig. 1 (d)). The spatial pattern as well as the goodness-of-fit of the spectral signatures (Tab. 1) is showing an overall plausible fit between library and EnMAP spectra.

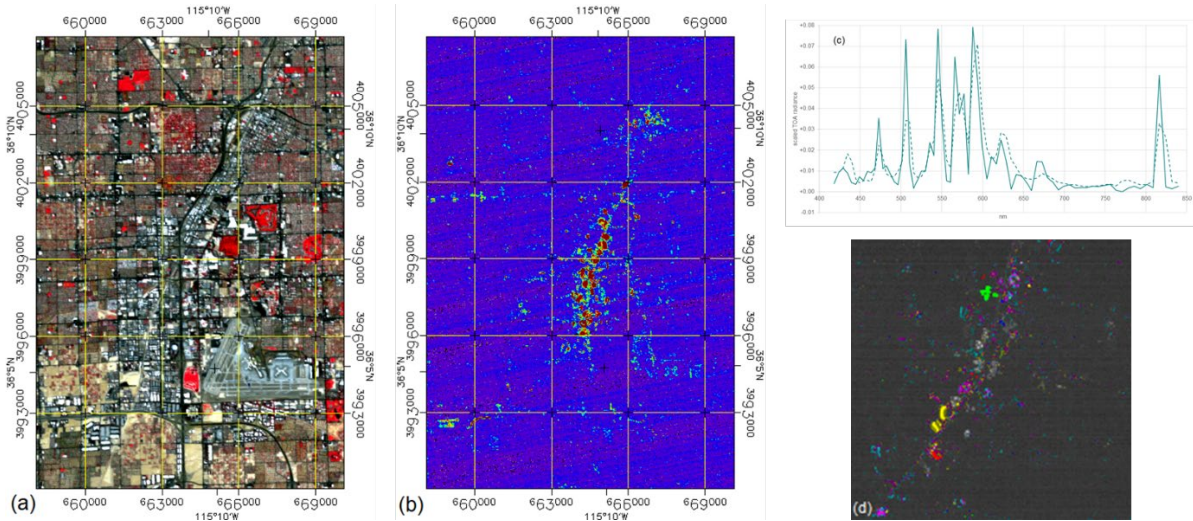


Figure 1: EnMAP "Las Vegas": (a) daytime CIR composite; (b) nighttime composite of representing red, green and blue broadbands; (c) EnMAP nighttime spectrum (solid) of MH and reported lab spectrum by ELVIDGE et al. 2010 (dashed); (d) classification of lighting types - zoom on the Las Vegas Strip (see Tab. 1 for colour key)

Table 1: Identified lighting types based on VIS/NIR and SWIR. The colors relate to Figure 1 (d), and the error relates to the Euclidean distance of the fit against ELVIDGE et al. 2010.

Lighting Type	Color in Figures	Error ≤ 0.5		Error ≤ 0.1	
		VIS/NIR	SWIR	VIS/NIR	SWIR
total		8819	451	2006	448
HPS	dark blue	430	48	165	48
MH	light blue	1479	82	243	82
MV	light green	20	49	0	48
QH	dark green	5	6	0	6
FL	orange	174		26	
LPS	yellow	8		8	
total LED	magenta	6658		1557	
CW	cyan	3311		509	
NW	magenta	2437		740	
Blue	dark blue	90		0	
Green	dark green	69		1	
Red	dark red	69		2	
Yellow	yellow	682		305	
total INC/LIQ/PRES	dark red (VIS/NIR)	45	111	15	108
INC	magenta (SWIR)	45	24	15	21
LIQ	light magenta (SWIR)	0	11	0	11
PRES	dark magenta (SWIR)	0	76	0	76
Temperature	red-orange-yellow (SWIR)		155		155

Lamp types:

- HPS: high-pressure sodium
- MH: metal halide
- MV: mercury vapor
- QH: quartz halogen
- FL: fluorescent
- LPS: low-pressure sodium
- LEDs: light-emitting diodes
- CW: cold white
- NW: natural white
- INC: incandescent
- LIQ: liquid fuel
- PRES: pressured fuel

„Temperature“ relates to fires and other high-temperature sources

Outlook for the future

As of course the illumination levels of Las Vegas are larger than those of many other cities, the transfer of these method will be conducted first to other brightly illuminated metropole areas, but also tests are in preparation for areas with lower illumination levels.

Therefore, an experimental system correction focusing on the improved handling of the Dark Current is currently being developed, with first results being promising. And when achieving a better separation of the nighttime lights from the background noise, then also the mapping of targets with lower illumination

levels can be achieved, as well as in the SWIR the detection of moderately hot targets or high temperature targets covering only a fraction of the pixel.

Finally, for the spectral identification and mapping, a novel knowledge-based approach is in development, allowing for an improved handling of pixels with mixed lighting sources.

Potential of Optical Spaceborne Sensors for the Differentiation of Plastics in the Environment

EARSeL Valencia 2024

Abstract

Corresponding Author: mathias.bochow@gfz-potsdam.de

Toni Schmidt^{1,2,3}, Theres Kuester³, Taylor Smith⁴, [Mathias Bochow](#)³

¹ Department Remote Sensing, Helmholtz-Centre for Environmental Research—UFZ, Leipzig, Germany

² Remote Sensing Centre for Earth System Research—RSC4Earth, Leipzig University, Leipzig, Germany

³ Remote Sensing and Geoinformatics Section, Helmholtz Centre Potsdam—GFZ German Research Centre for Geosciences, Potsdam, Germany

⁴ Institute of Geosciences, University of Potsdam, Potsdam, Germany; tsmith@uni-potsdam.de

Keywords (5): plastic waste; imaging spectroscopy; sensor simulation; machine learning; classification

Challenge (800 - 1000 characters incl. spaces)

Plastics are versatile and inexpensive materials that are part of our everyday life. However, approximately 10 Gt of plastics have been produced to date, and the majority have been accumulated in landfills or spread into the environment in an uncontrolled way. The detection of plastic waste is a pressing research question in remote sensing. In this spectral simulation study, we show that most multispectral sensors are not able to differentiate between plastic types, while hyperspectral sensors are. To resolve absorption bands of plastics with super-spectral sensors, the number, position, and width of the SWIR channels are decisive for a good classification of plastics. Since ASTER and WorldView-3 had/have narrow SWIR channels that match with diagnostic absorption bands of plastics, they yielded outstanding results. Central wavelengths at 1141, 1217, 1697, and 1716 nm, in combination with narrow bandwidths of 10–20 nm, have the highest capability for plastic differentiation.

Methodology (1200 – 1500 characters incl. spaces)

53 plastic samples of five different types (PE, PP, PS, PET, PVC) have been measured in the lab using a HySpex SWIR-320m-e sensor and an ASD FiedSpec 3. They were of different color, transmissivity, structure, thickness, cleanness, and degree of weathering. Based on sample measurements with a dark and bright background the real reflectance (R_r) and transmittance (T) have been derived from the measured apparent reflectance (R_a). Based on the samples' R_r , T, as well as the reflectance spectra of 10 natural surfaces ($R_{r,b}$) apparent reflectance spectra were simulated as if the sample would have been measured on the 10 background surfaces (namely sea water, heathland, green meadow, dry meadow, peat soil, wet sandy soil, sandy soil, sand, asphalt, and concrete).

From former and present multi- and hyperspectral optical spaceborne sensors a subset of 10 sensors have been selected covering a representative range of spectral configurations and the simulated spectra were resampled to the spectral resolutions of these sensors. For additional tests noise was added. Per sensor a k-NN and a Random Forest (RF) classifier was trained and validation was conducted using 8-fold cross validation. We calculated precision, recall, F1 scores, and macro F1 score from the respective confusion matrices.

Finally, the optimal spectral band configuration for the differentiation of plastic types was derived from a feature selection experiment using forward greedy selection and the k-NN classifier.

Results (1200 – 1500 characters incl. spaces)

The classification results demonstrate which sensors enable a differentiation of the types of plastic waste in the environment and how this is affected by different natural background surfaces (Fig. 1). Multispectral VNIR sensors (Pléiades and PlanetScope) output in lowest mean macro F1 scores compared to other sensor types. The achieved low scores are not better than for a random classification, i.e. 0.2 (using five classes), and are the logical consequence of plastics having no diagnostic absorption bands up to ~900 nm.

The results using signals of multispectral VNIR/SWIR sensors show greater variability and can be split into two clusters, i.e. MODIS + Sentinel-2 + Landsat 5/7 and ASTER + WorldView-3 (Fig. 4.2B). Macro F1 scores achieved with sensors of the first cluster are in the range from 0.21–0.37, with means and standard deviations of 0.31 ± 0.05 (MODIS), 0.26 ± 0.05 (Sentinel-2), and 0.26 ± 0.04 (Landsat 5/7). Thus, they are either in the same range of the scores achieved with multispectral VNIR sensors or insignificantly higher. In contrast, the scores achieved with ASTER and WorldView-3 are the highest values among this sensor category, while both range from 0.37–0.56 but have different means and standard deviations, i.e. 0.43 ± 0.05 (ASTER) and 0.48 ± 0.06 (WorldView-3).

Classifications using continuum-removed signals of all hyperspectral sensors were most successful, which is reflected in their relatively high mean macro F1 scores, which are 0.83 ± 0.03 (Hyperion), 0.85 ± 0.03 (EnMAP), and 0.86 ± 0.03 (PRISMA).

A	HIRI (Pléiades-HR 1A/1B)	.30	.26	.21	.14	.23	.18	.19	.14	.25	.18	.21
	PlanetScope (Dove/Flock)	.27	.24	.22	.18	.22	.25	.20	.18	.26	.18	.22
B	ASTER (Terra)	.42	.45	.43	.44	.47	.39	.38	.37	.43	.56	.43
	MODIS (Terra/Aqua)	.32	.37	.36	.29	.30	.32	.29	.21	.35	.27	.31
	MSI (Sentinel-2A/2B)	.30	.29	.21	.25	.29	.32	.21	.21	.32	.21	.26
	TM/ETM+ (Landsat 5/7)	.32	.33	.25	.26	.23	.30	.22	.22	.28	.22	.26
	WV110 (WorldView-3)	.37	.47	.50	.56	.55	.43	.52	.46	.45	.51	.48
C	HSI (EnMAP)	.78	.87	.83	.86	.85	.88	.86	.86	.85	.86	.85
	HYC (PRISMA)	.79	.86	.87	.87	.87	.87	.83	.86	.86	.88	.86
	Hyperion (EO-1)	.74	.86	.85	.84	.84	.82	.83	.82	.84	.83	.83
	Mean	.46	.50	.47	.47	.48	.48	.45	.43	.49	.47	
	Sea water											
	Heathland											
	Green meadow											
	Dry meadow											
	Peat soil											
	Wet sandy soil											
	Sandy soil											
	Sand											
	Asphalt											
	Concrete											
	Mean											

Figure 1 Macro F1 scores in dependence of sensor and background surface using RF. **(A)** are multispectral VNIR sensors, **(B)** are multispectral VNIR/SWIR sensors, and **(C)** are hyperspectral sensors. Here, no noise was added to the simulated reflectance signals.

A	HiRI (Pléiades-HR 1A/1B)	.29	.21	.22	.04	.28	.21
	PlanetScope (Dove/Flock)	.30	.25	.16	.06	.32	.22
B	ASTER (Terra)	.41	.36	.22	.56	.61	.43
	MODIS (Terra/Aqua)	.33	.35	.20	.13	.52	.31
	MSI (Sentinel-2A/2B)	.30	.24	.18	.16	.42	.26
	TM/ETM+ (Landsat 5/7)	.29	.23	.17	.26	.37	.26
	WV110 (WorldView-3)	.51	.56	.22	.54	.58	.48
C	HSI (EnMAP)	.91	.88	.85	.85	.77	.85
	HYC (PRISMA)	.91	.87	.88	.87	.75	.86
	Hyperion (EO-1)	.90	.84	.84	.85	.70	.83
	Mean	.52	.48	.40	.43	.53	
		PE	PET	PP	PS	PVC	Mean

Figure 2 Mean F1 scores in dependence of sensor and plastic type using RF. **(A)** are multispectral VNIR sensors, **(B)** are multispectral VNIR/SWIR sensors, and **(C)** are hyperspectral sensors. No noise was added to the simulated reflectance signals.

Outlook for the future (800 - 1000 characters incl. spaces)

The results showed that multispectral VNIR sensors are generally unable to differentiate between plastics. Multispectral VNIR/SWIR sensors having multiple narrow SWIR channels, such as ASTER and WorldView-3, showed better performance in classifying plastics. Hyperspectral sensors were found to be most capable of differentiating plastics since their absorption bands are sufficiently sampled by the narrow and contiguous spectral channels of these sensors. Classification results could be improved by continuum removal for hyperspectral signals and using only SWIR channels for multi- and hyperspectral sensors. A hypothetical sensor was derived that has four channels in the SWIR range (at 1141, 1217, 1697, and 1716 nm) for optimal plastic differentiation, while narrow FWHMs (10–20 nm) increased its performance. These findings can aid in differentiating plastics on a large scale and investigating global plastic pollution trends.

USING GLOBAL IMAGING SPECTROSCOPY TO DETECT AND MONITOR CLIMATE EXTREMES

Bryce Currey^{1,2}, Benjamin Poulter¹, Shawn P. Serbin¹, David R. Thompson³, Phillip A. Townsend⁴, Arlindo M. Da Silva⁵, Alexey N. Shiklomanov¹

¹ NASA Goddard Space Flight Center, Biospheric Sciences Laboratory, USA

² Montana State University, Department of Land Resources and Environmental Sciences, USA

³ NASA Jet Propulsion Laboratory, California Institute of Technology, USA

⁴ University of Wisconsin-Madison, Department of Forest and Wildlife Ecology, USA

⁵ NASA Goddard Space Flight Center, Global Modeling and Assimilation Office, USA

Keywords (5): Earth Observation, SBG, CHIME, Imaging Spectroscopy, Climate Extremes

Challenge

Extreme climate events such as heatwaves and droughts can have particularly severe impacts on terrestrial vegetation, especially if chronic or prolonged, with an array of cascading impacts on valuable ecosystem services including as carbon storage and biodiversity as well as negatively impact agricultural production and water resources. As climate extremes become more frequent, there is an increasing need for ways to monitor ecosystems and for modeling and tools that can accurately quantify and project the environmental impacts of short- and long-term disturbances, help inform earth system models (ESMs), and guide appropriate management and mitigation efforts. Global imaging spectroscopy (IS) of Earth can help inform our understanding of the surface properties of terrestrial and aquatic ecosystems. By the end of this decade, there will be multiple polar orbiting (i.e., global coverage) IS platforms, including the SBG and the CHIME missions, as well as a host of commercial systems. Evaluating the performance of these missions requires advanced end-to-end simulation tools and observing system simulation experiments (OSSEs).

Methodology

We develop an OSSE framework and demonstrate its utility by exploring the capabilities of global IS to evaluate global climate extremes and their impacts on vegetated ecosystems. Our objectives for this work are three-fold: First, we describe an update to our existing coupled dynamic global vegetation and radiative transfer model testbed, LPJ-PROSAIL. Second, we document and describe the global implementation of the end-to-end OSSE simulation tool *hypertrace*. Finally, we demonstrate the applicability of this work to explore ecosystem impacts and responses to past climate extremes, or "sigma events". We investigated the inclusion of vegetation properties used in land-surface models through the application of global partial least squares regression (PLSR) models as a proof-of-concept and examine how error from the retrieval of at-surface reflectance propagates into higher-level terrestrial plant trait products.

Expected results

We find that global average percent errors between simulated noiseless reflectances and those retrieved by the OSSE are $3 \pm 3\%$, largely due to the atmospheric inversion process and surface model, with the largest errors in regions with high atmospheric aerosol concentrations. The SBG instrument itself contributed ~10% to total error. Downstream PLSR errors were trait-dependent but generally increased total error by an additional ~1-3% when applied to surface reflectances retrieved the OSSE. We emphasize that developing region- or biome-specific plant trait retrievals will be important to preserve accuracy. More generally, we demonstrate that global spectroscopy can detect and help quantify differences in traits under extreme climate scenarios. In the face of projected climate extremes, global imaging spectroscopy will serve as an invaluable asset for monitoring ecosystem changes, understanding their implications, and devising data-driven strategies for sustainable environmental management.

Outlook for the future

Whilst the ecological interpretation of these results is nuanced, our main objective is to provide a simulation exercise and a proof-of-concept use case for global imaging spectroscopy. In the face of projected climate extremes, global IS will serve as an asset for monitoring ecosystem changes, understanding their implications, and devising data-driven strategies for sustainable environmental

management. Recent momentum garnered by current missions like EMIT provide a pathfinder toward deeper exploration and integration of data from imminent missions like SBG and CHIME. More work is needed to understand how to incorporate global spectroscopy data into workflows and analyses, in order to obtain the maximal benefits from current and future missions alike. Global imaging spectroscopy as a discipline hints at a future with opportunities for ecological management and understanding through technology and research.

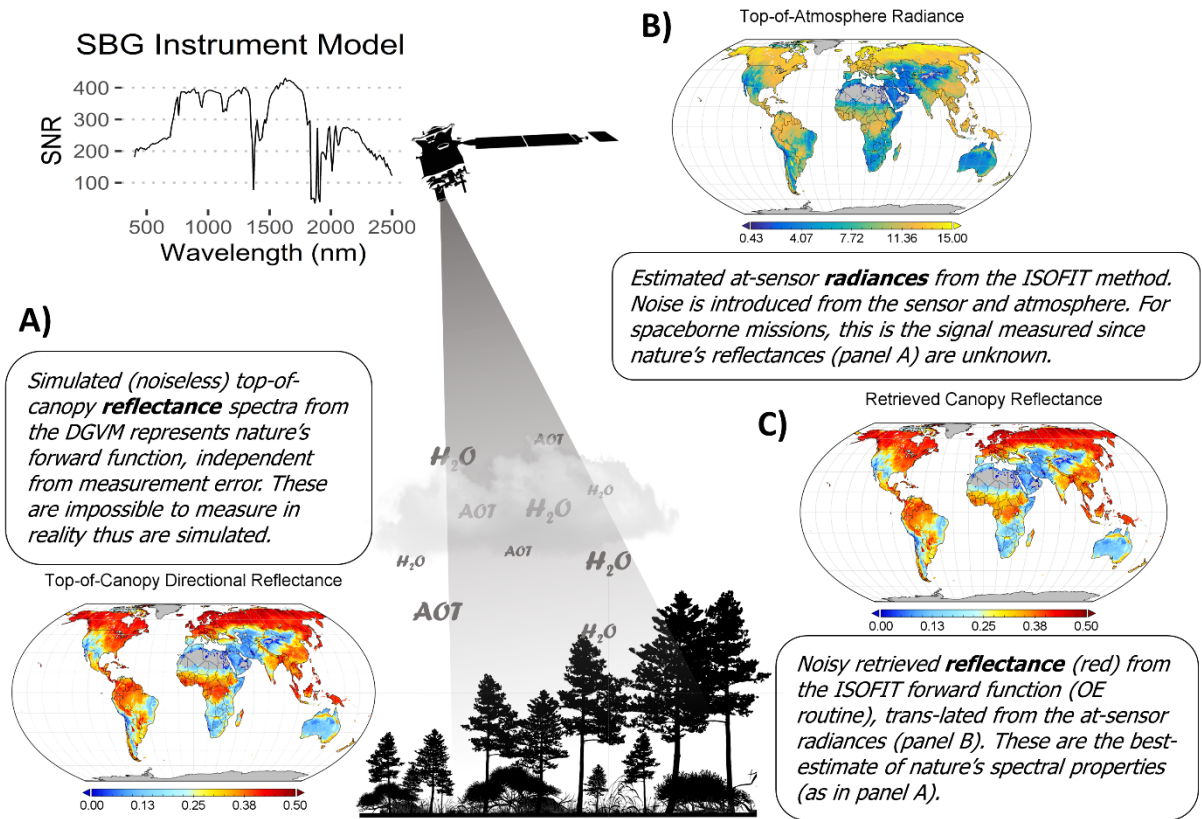


Figure 1. Hypertrace OSSE workflow

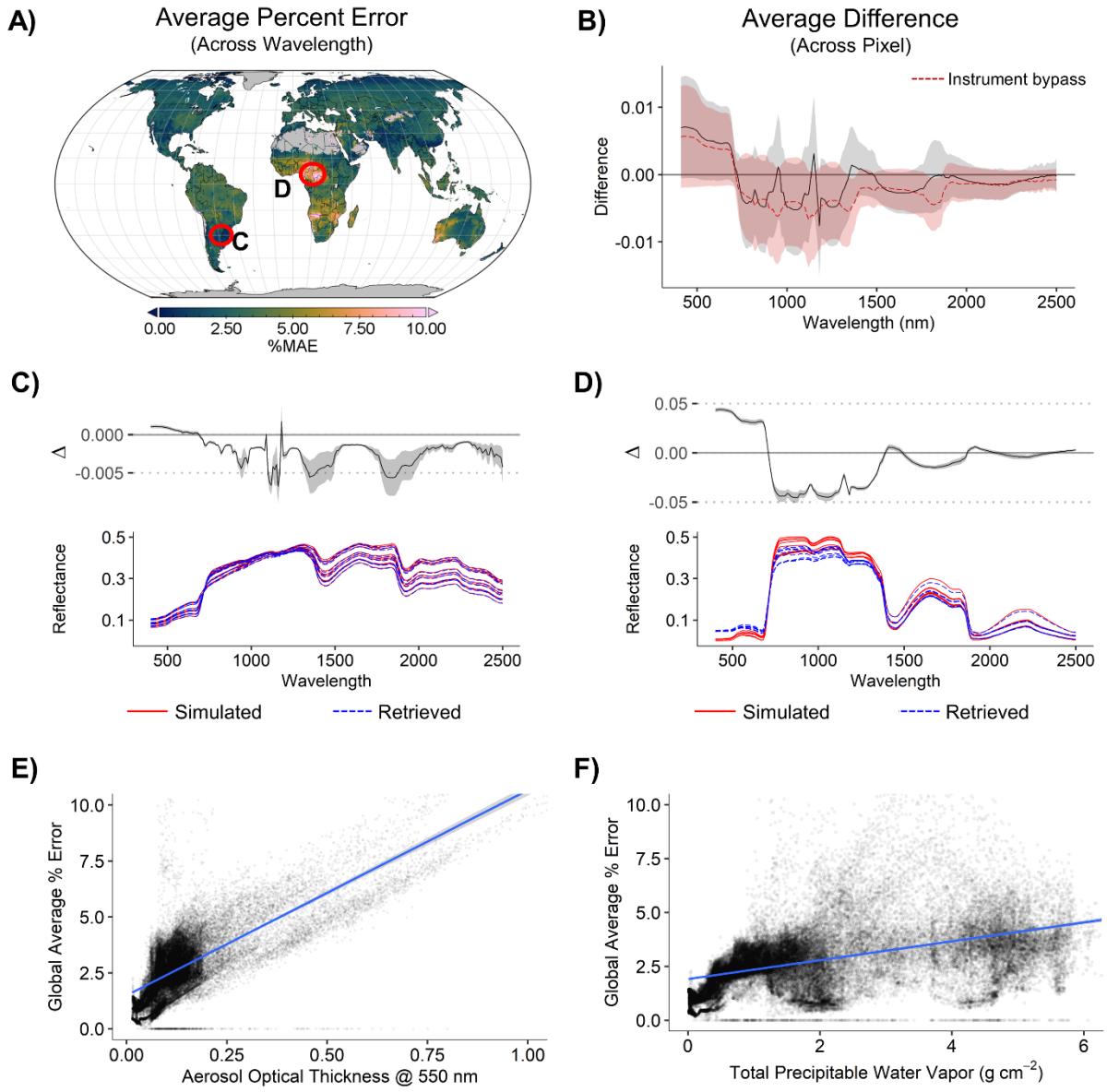


Figure 2. Global distribution of error and per-wavelength average error.

A Physical Method for Optical Characterization of Pollution in Industrial Wastewater Ponds using Imaging Spectroscopy

EARSel Valencia 2024

Abstract

Corresponding Author:

rodolphe.marion@cea.fr

Louis Zaugg¹, [Rodolphe Marion](#)¹, Malik Chami², Xavier Briottet³, Laure Roupioz³

¹CEA/DAM/DIF, F-91297 Arpajon, France

²Sorbonne Université (UFR918) Laboratoire Lagrange, Observatoire Côte d'Azur, Université Côte d'Azur, France

³ONERA, Université Fédérale de Toulouse, F-31055 Toulouse, France

Keywords (5): Imaging Spectroscopy, Inversion Method, Optical Characterization, Water Pollution

Challenge (800 - 1000 characters incl. spaces) 993

Industrial activities are one of the major sources of water pollution worldwide. Water is often used in industrial processes for chemical, physical, or mechanical purposes. It may be contaminated with various undesired by-products. It is therefore necessary to treat the effluents before releasing them back into natural water streams. Industrial settling ponds are often used for such treatment and may contain pollutants in dissolved and/or suspended forms. Current remote sensing methods to study such water bodies are generally site-specific and require in situ measurements to calibrate empirically based inversion models. The absorption and backscattering coefficients of these pollutants, referred to as inherent optical properties (IOPs), are seldom known, unlike those of natural water constituents. The objective of this study is to investigate the feasibility of detecting the presence of water pollutants in industrial ponds using their IOPs derived from imaging spectroscopy data.

Methodology (1200 – 1500 characters incl. spaces) 1502

The proposed methodology, named IWOC (Industrial Wastewater Optical Characterization), consists of retrieving the IOPs of the pollutants using a physically based approach so that it could be applied to a wide range of study areas without prior knowledge on the type of pollutants. For that purpose, the absorption and backscattering coefficients of a pollutant are introduced into the widely used semi-analytical radiative transfer Lee model. Its inversion leads to an ill-posed problem when attempting to invert a single pixel since the number of variables is higher than the number of observations. To minimize this issue, it is assumed that the chemical composition/type of the in-water constituents of a given pond (including the pollutant) is spatially homogeneous. It implies that the absorption coefficient $\alpha_{pol}(\lambda)$ of the pollutant is the same for all the pixels of the pond. On the contrary, the concentrations of the natural constituents and the one of the pollutant C_{pol} , as well as the water column depth and the bottom reflectance scaling factor, vary spatially from one pixel to another. Because the backscattering coefficient $b_{bpol}(\lambda)$ depends on the distribution of particle size, its corresponding parameters (amplitude and spectral shape) also vary from one pixel to another. An alternating multi-pixel inversion jointly estimates the parameters that vary from one pixel to another and the parameters that are the same for all the pixels iteratively and alternatively until convergence.

Results (1200 – 1500 characters incl. spaces) 1423

Figure 1 illustrates the impact of a pollutant on the measured remote sensing reflectance R_{rs} (Figure 1b, blue curve). The simulation of R_{rs} with the Lee model without taking into account the IOPs of the pollutant fails to fit the measurement effectively for the main blue pond of the soda ash plant (Figure 1b, green curve). However, taking the IOPs of the pollutant into account (here coarse gypsum particles) yields a

much more accurate fit (Figure 1b, red curve). This highlights the fact that the IOPs of natural constituents are not sufficient to explain the measured spectrum and that it is necessary to consider the optical properties of the coarse gypsum particles. Figure 2 shows the results of the IWOC inversion method applied to the previous main blue pond. IWOC leads to a highly satisfactory retrieval of R_{rs} (Figure 2a) and provides estimates of the absorption and backscattering coefficients of the pond (Figures 2b and 2c). In particular, the retrieved backscattering coefficient increases with wavelength. Such a spectral shape is consistent with the fact that the suspended matter consists of coarse gypsum particles. Furthermore, the high value of backscattering indicates the high quantity of suspended particles in this settling pond used in the industrial process. The full analysis of the HySpex NEO hyperspectral images is still in progress and the results will be presented during the conference.

Outlook for the future (800 - 1000 characters incl. spaces) 1000

This study demonstrates the feasibility of a generic inversion method for detecting polluted waters and retrieving the IOPs of the pollutants without the need of calibration data as for empirical and site-specific methods. Although a wide range of tests and evaluations of IWOC are carried out in this study (and some are still in progress), further investigations are needed to better evaluate its capabilities. As an example, a chemically oriented study should be carried out and a deeper analysis of the composition and optical properties of the dissolved/suspended matter should be continued with the goal of building a dedicated database to characterize industrial pollutants. Such a database would be relevant for the rapid, large-scale, and low-cost detection of pollution events in aquatic systems. The approach conducted here is a first step towards a generic inversion method for the optical characterization of pollution sources in water, which could further lead to an operational method.

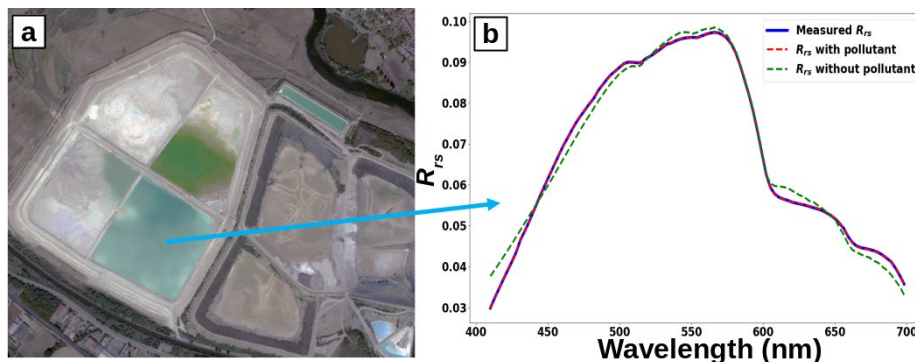


Figure 1. Impact of a pollutant on the measured remote sensing reflectance R_{rs} . (a) Soda ash plant with large water ponds. (b) R_{rs} measured in the main blue pond (blue curve), R_{rs} simulated using the Lee model without pollutant (green curve) and with pollutant (red curve).

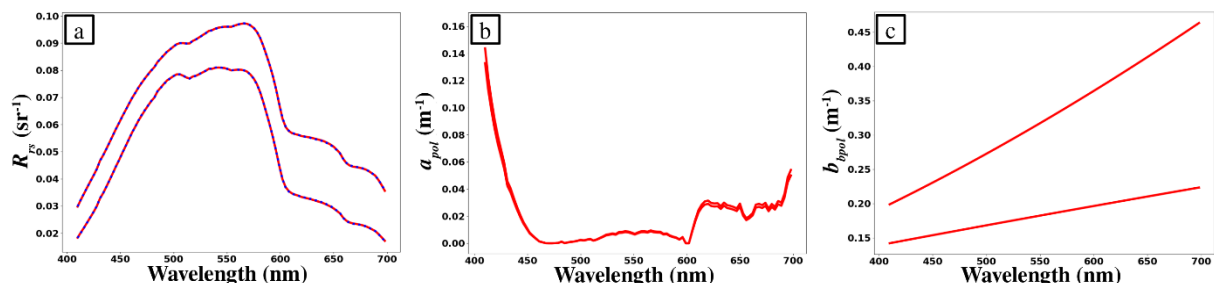


Figure 2. IWOC retrievals for the main blue pond. (a) Remote sensing reflectance R_{rs} retrieved with IWOC for two pixels. (b) Absorption coefficient a_{pol} of the pollutant. (c) Backscattering coefficient b_{bppl} . [Blue curves: image values, red curves: retrieved values].

Detection methane emissions from municipal solid waste landfill using airborne spectroscopy

[Olga Brovkina](#), Adam Bednařík, Daniel Kopkáně, Tomáš Fabiánek
Global Change Research Institute CAS, Brno, Czech Republic

Keywords: Hyperspectral, Methane emission, Airborne, SWIR and LWIR, Urban

Challenge

Detecting methane emissions from airborne hyperspectral (HS) shortwave infrared (SWIR) and thermal long-wave infrared (LWIR) data involves using the unique spectral signatures of methane gas to identify its presence in the atmosphere. Methane has absorption features in SWIR region, typically around 1.65 and 2.3 micrometers (μm), and exhibits an absorption band in LWIR region around 7.7 μm . When methane gas is present, it absorbs infrared radiation at these specific wavelengths, creating absorption lines in the spectrum. The study explored the potential of airborne hyperspectral data acquired by sensors SASI-600 and TASI-600 (Itres®) of FLIS (The Flying Laboratory of Imaging Systems, <https://olc.czechglobe.cz/en/main-page/>) to detect methane emissions. Municipal solid waste landfill was used as a source of methane release from the ground surface in the study.

Methodology

Airborne HS SWIR and HS LWIR data (FLIS) were acquired on August 31, 2022, at 10:00 CET, December 3, 2022, at 20:00 CET, and May 30, 2023, at 10:00 CET for an operated municipal solid waste landfill located near the city of Brno. Field data were acquired simultaneously with the airborne data acquisition in August 2022 and May 2023. Surface temperatures of landfill objects, as well as the concentration and fluxes of CH_4 , were measured using a portable handheld infrared thermometer and a soil chamber connected to a portable greenhouse gas analyzer (Picarro GasScouter G4301, Picarro, CA, USA), respectively. Field spectra were obtained using the ASD FieldSpec 4 spectroradiometer.

The spectral profile of waste with different landfilling period, mixture of waste with soil, and mixture of waste with vegetation from airborne HS SWIR and HS LWIR data were analysed to detect CH_4 absorption features in several landfill parts using HITRAN database methane spectra. Methane indices (Xiao et al., 2020; Thorpe et al., 2021) incorporating specific narrow spectral SWIR regions (1630 - 1690 nm, 2100 – 2300 nm) were calculated to indicate the presence of CH_4 emission spots on the landfill. The landfill surface temperature from airborne HS LWIR data was mapped to identify locations showing "hot spots" in surface temperature. An overlap analysis was then performed with CH_4 emission spots detected from airborne HS SWIR data. This analysis was based on the observation, that intense decomposition of organic matter associated with methane production can lead to localized surface temperature increases. The CH_4 emission spots from airborne data were validated using CH_4 emissions from chamber positions.

Results

The highest CH_4 emissions from chamber positions, ranging from 19 to 38 $\text{g m}^{-2} \text{d}^{-1}$, were observed at several locations within the landfill. These locations coincided spatially with the CH_4 emission spots detected from airborne HS SWIR data. Most of surface temperature "hot spots" identified in the airborne HS LWIR data acquired at 10:00 (August 2022, May 2023) were associated with surface temperature of waste materials and surroundings heating up due to direct sunlight. Surface temperature "hot spots" identified in the airborne HS LWIR data acquired at 20:00 (December 2022) coincided with high CH_4

emissions from chamber positions. CH₄ emissions lower than 1 g m⁻² d⁻¹, were not detected using airborne HS SWIR and HS LWIR methods at the landfill.

Outlook for the future

In the future, the approach can be promised for monitoring methane emissions from landfills. By continuing to use hyperspectral data and advanced spectral analysis techniques, it can be possible to enhance the ability to detect and quantify methane emissions in various environmental conditions. The methodology of mapping landfill surface temperatures to identify "hot spots" associated with methane emissions is a valuable tool for specific areas of interest. Choosing an optimal time for thermal airborne data acquisition to minimize the influence of sun warming and maximize the temperature contrasts of objects should be considered.

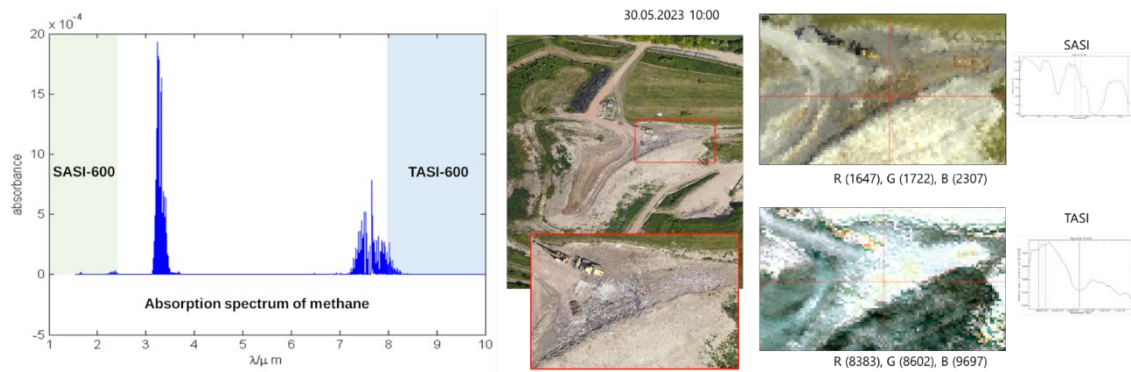


Figure Absorption spectrum of methane (left), and example of methane detection from SWIR (SASI-600) and LWIR (TASI/600) data on municipal solid waste landfill

Attribution of individual methane and carbon dioxide emission sources using EMIT observations from space

EARSel Valencia 2024
Abstract
Corresponding Author:
Andrew.K.Thorpe@jpl.nasa.gov

Andrew Thorpe¹, Robert Green¹, David Thompson¹, Philip Brodrick¹, John Chapman¹, Clayton Elder¹, John Worden¹, K. Dana Chadwick¹, Willow Coleman¹, Claire Villanueva-Weeks¹, Amanda Lopez¹, Daniel Jensen¹, Michael Eastwood¹, Jay Fahlen¹, Charles Miller¹

¹Jet Propulsion Laboratory, California Institute of Technology, Pasadena, CA, United States of America

Keywords (5): Earth Surface Mineral Dust Source Investigation (EMIT), methane, carbon dioxide, emissions, greenhouse gas

Challenge

Carbon dioxide and methane emissions are the two primary anthropogenic climate-forcing agents and an important source of uncertainty in the global carbon budget. Uncertainties are further magnified when emissions occur at fine spatial scales (<1 km), making attribution challenging. We present the first observations from NASA's Earth Surface Mineral Dust Source Investigation (EMIT) imaging spectrometer from the first 30 days of EMIT operations showing quantification and attribution of fine-scale methane and carbon dioxide sources spanning the oil & gas, waste, and energy sectors. EMIT continues to identify methane and carbon dioxide emissions with all results and associated code made publicly available. Identification of large methane and carbon dioxide emissions offers the potential for improving understanding of global greenhouse gas budgets and to inform mitigation strategies.

Methodology

The Earth Surface Mineral Dust Source Investigation (EMIT) is an imaging spectrometer that measures reflected solar radiation for 285 distinct wavelengths from the visible to shortwave infrared (381-2493 nm) at 60 m spatial resolution. At the 7.4 nm EMIT spectral sampling, methane and carbon dioxide have distinct spectral fingerprints between 1900 and 2500 nm (Figure 1). In this study we use a linearized matched filter to identify methane and carbon dioxide plumes and estimate emissions by combining the Integrated Mass Enhancement (IME), plume length, and wind speed. For each plume, an initial assessment of the plume origin was made based on plume morphology and the distribution of concentrations present in a scene and emissions were assigned to broad sector and sub-sector categories, including waste (landfill, wastewater treatment), energy (power plant), and oil & gas (upstream, midstream, downstream).

Expected results

From the first 30 days of EMIT operations, observed emissions ranged from 0.3-73 tonnes CH₄ hr⁻¹ and 1571-3511 tonnes CO₂ hr⁻¹ for plumes observed from the oil & gas, waste, and energy sectors. For selected countries in the Middle East and Central Asia, methane emissions varied at a regional scale with the largest total emissions observed for Turkmenistan (731±148 tonnes CH₄ hr⁻¹), followed by Kazakhstan (207±11 tonnes CH₄ hr⁻¹), Iran (87±48 tonnes CH₄ hr⁻¹), and Uzbekistan (86±22 tonnes CH₄ hr⁻¹). Fig. 2 highlights EMIT's ability to pinpoint multiple emission sources that are in close proximity and to attribute these emissions to different sectors. Methane plumes appear from multiple sources including the Riyadh landfill in Saudi Arabia (8±2 tonnes CH₄ hr⁻¹), a sewage treatment plant (7±1 tonnes CH₄ hr⁻¹), and natural gas fired power plant (30±2 tonnes CH₄ hr⁻¹) where a carbon dioxide plume was also visible (2032±142 tonnes CO₂ hr⁻¹), and a potential source (28±2 tonnes CH₄ hr⁻¹) was identified in close proximity to the Shedgum-Yanbu natural gas liquids pipeline. These results highlight the contributions of current and planned point source imagers in closing global carbon budgets.

All EMIT data products are available through the Land Processes Distributed Active Archive Center (LP DAAC) at the following link, <https://lpdaac.usgs.gov/products/emit11bradv001> and <https://lpdaac.usgs.gov/products/emit12bch4plmv001>. All code is available at <https://github.com/emit-sds> and <https://github.com/emit-sds/emit-ghg>. The plume examples presented in this study are available through the EMIT applications online mapping tool (<https://earth.jpl.nasa.gov/emit/data/data-portal/Greenhouse-Gases/>) and the US Greenhouse Gas Center, with periodic updates reflecting additional observed emissions.

Outlook for the future

EMIT provides important contributions to mapping methane and carbon dioxide emissions through the combination of large area coverage (average daily coverage of 1.3×10^6 km²) and fine spatial resolution (60 m) imaging spectroscopy data, enabling potential future identification of both expected (process-based) and unexpected (fugitive) emissions. Emissions can be quantified and attributed to specific sectors, which is particularly important when multiple emissions from different sectors are present in close proximity. In Nov. 2023 EMIT will complete its primary mission and an extended mission is planned, during which any regions within ISS latitude constraints could be targeted.

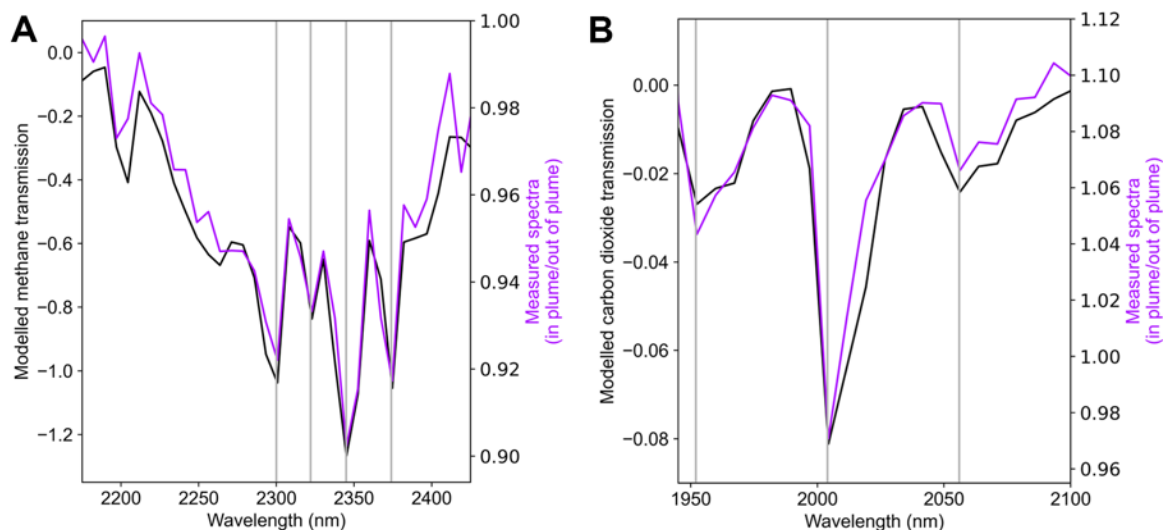


Figure 1 Examples of methane (A) and carbon dioxide (B) spectral fingerprints (purple lines) and modelled gas transmission (black line). The strongest absorption features highlighted by the vertical grey lines.

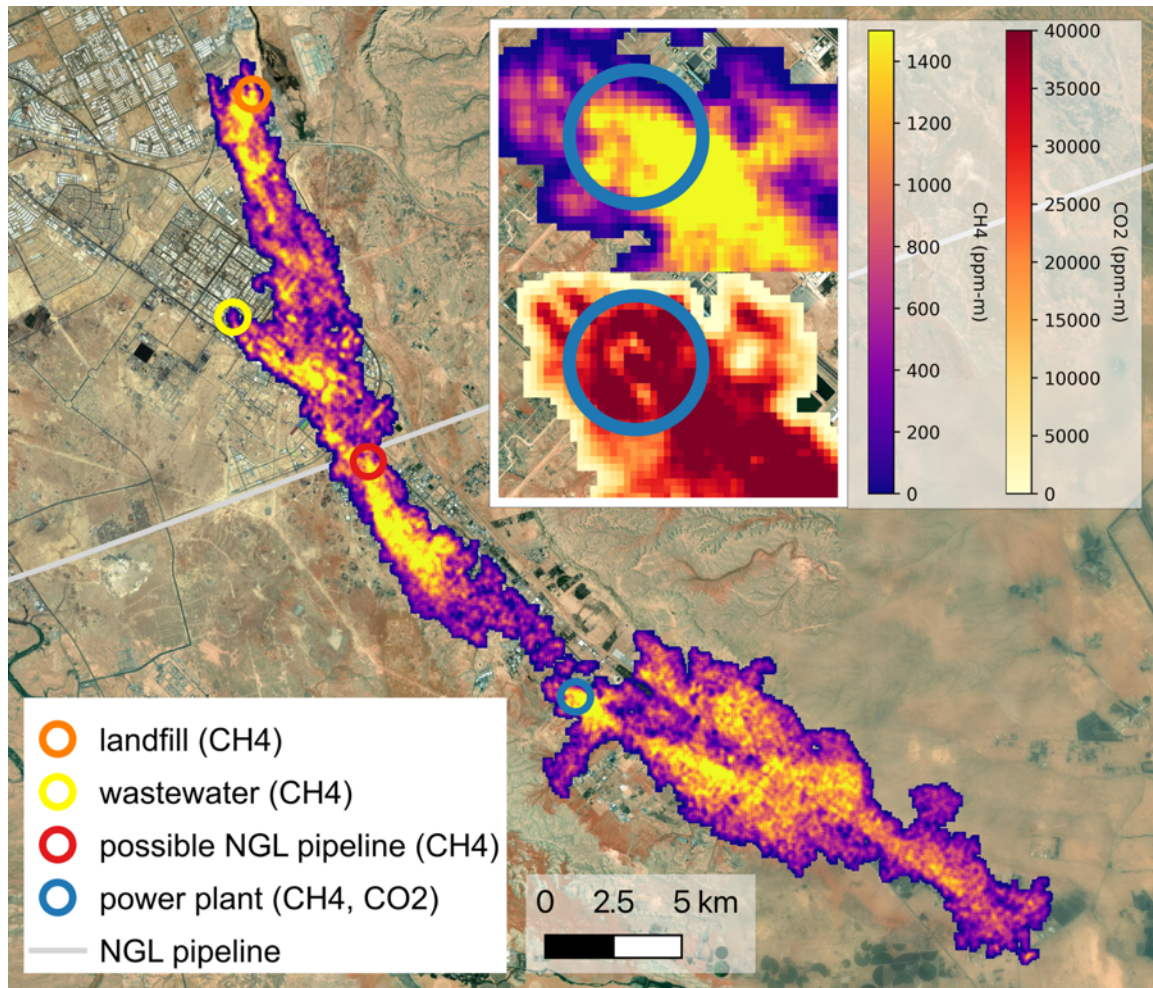


Figure 2 EMIT permits direct attribution of methane and carbon dioxide emissions to specific sectors. This example shows methane emissions from a landfill in Saudi Arabia (28 ± 2 tonnes CH₄ hr⁻¹), wastewater treatment facility (7 ± 1 tonnes CH₄ hr⁻¹), power plant (30 ± 2 tonnes CH₄ hr⁻¹, 2032 ± 142 tonnes CO₂ hr⁻¹) and potentially from a natural gas pipeline (28 ± 2 tonnes CH₄ hr⁻¹). Inlay images show a close up of the power plant source, with co-located methane and carbon dioxide emissions.

YSc: Young Scientist Awards

Quantification and Mapping of Non-Photosynthetic Cropland Biomass Using Hyperspectral Data and Machine Learning

EARSel Valencia 2024
Abstract
Corresponding Author:
Stefanie.Steinhauser@lmu.de

Stefanie Steinhauser¹, Matthias Woche¹, Andrej Halabuk², Svetlana Košanová³ and Tobias Hank¹

¹ LUDWIG-MAXIMILIANS-UNIVERSITÄT MÜNCHEN (LMU), Department of Geography, Germany

² Slovak Academy of Sciences, Institute of Landscape Ecology, Slovakia

³ Constantine the Philosopher University in Nitra, Department of Ecology and Environmental Science, Slovakia

Keywords (5): Agriculture, Machine Learning, NPV, EnMAP-Box, Active Learning

Challenge

This study covers the development of a hybrid modelling approach to quantify non-photosynthetic vegetation (NPV) [g/m²] from hyperspectral data. Due to its influence on nutrient, carbon, and water cycles, NPV plays an essential role in both agricultural and natural systems. For agricultural applications, two forms of NPV are of particular interest: 1) late growth stage senescent crops, and 2) crop residues (CR). Quantification of NPV biomass has rarely been possible due to the lack of large scale and high temporal resolution hyperspectral data. With a new generation of spaceborne spectrometers in orbit, such as the PRecursore IperSpettrale della Missione Applicativa (PRISMA) and the Environmental Mapping and Analysis Program (EnMAP), this data has now become accessible across the Globe and opens up new possibilities for large scale NPV-mapping.

Methodology

Obtaining in-situ data that will satisfy the data demand of machine learning (ML) algorithms is both, time-consuming and expensive. Hybrid approaches offer an independent alternative by using a physically-based invertible Radiative Transfer Model (RTM) (e.g. PROSAIL-PRO) to compile rich and versatile training data bases. The freely available software EnMAP-Box will soon provide a new hybrid retrieval tool under the Agricultural Applications category, which allows training a variety of ML regression algorithms (ANN, GPR, RFR, SVR etc.) across the full range of standard variables within the PROSAIL model. In this study four widely used ML algorithms were applied using a PROSAIL simulated database in combination with internal Active Learning (AL) and PCA. Their quality can be analysed via regression scatterplots of estimated vs. measured AGB_{dry} (NPV) [g/m²]. The AL-optimized ML models now can be applied on different EnMAP images acquired over the Munich-North-Isar (MNI) test site in the northeast of Munich (Germany), resulting in quantitative maps of NPV. For further assessment and to determine spatial and across-sensor transferability, the models are also applied to a PRISMA scene acquired over the Levice area (Slovak Republic), where agricultural land cover validation data, divided into six crop categories (bare soil, crop residues, erectophile NPV, wheat emergence, and green biomass) are available.

Expected results

With the new hybrid retrieval workflow, the initial test with PROSAIL simulated spectra and internal GPR + AL for AGB_{dry} resulted in promising estimations (see Figure 1). By applying the GPR-AL model, saturation can be observed with 800 samples remaining out of the initial 2000 samples, with an RMSE of approximately 190 [g/m²]. High agreement between estimated (y-axis) and measured AGB_{dry} (x-axis) can

be observed with an R^2 of 0.77 and an RMSE of 186 [g/m²] respectively. Based on these first findings assessing the impact and influence of using AL with the help of independent in-situ data in comparison to internal AL appears promising. Furthermore, it is crucial to evaluate the influence of different ML algorithms on the estimated results. Using probabilistic methods, like GPR, has the advantage of providing valuable features such as uncertainty maps based on the standard deviation [g/m²]. The different virtual models will be utilized to generate quantitative NPV maps from actual satellite data (EnMAP and PRISMA). First results indicate that NPV-mapping will be possible in realistic dimensions with this approach. Some quantitative in-situ measurements and qualitative classification data are available for validation from the MNI and the Levice sites.

Outlook for the future

To fully assess the accuracy of the NPV map product, NPV in-situ measurements are required over a wide range of fields with parallel spectrometric imagery. Further endeavours in the field thus will inevitably be necessary in the future. Nonetheless, hybrid approaches in combination with AL, which can reduce the computational costs and potentially improve the quality of the data set by selecting only the most relevant samples, already enable the full use of spaceborne spectroscopic data that is currently acquired across the Globe. The hybrid GPR model will be further applied and tested to map NPV in a spatially continuous way in different agroecological zones. Despite the still limited spatial coverage of hyperspectral data, missions like EnMAP, PRISMA and EMIT thus also pave the way for future refined and more operational multispectral systems that will enable NPV mapping on a global scale.

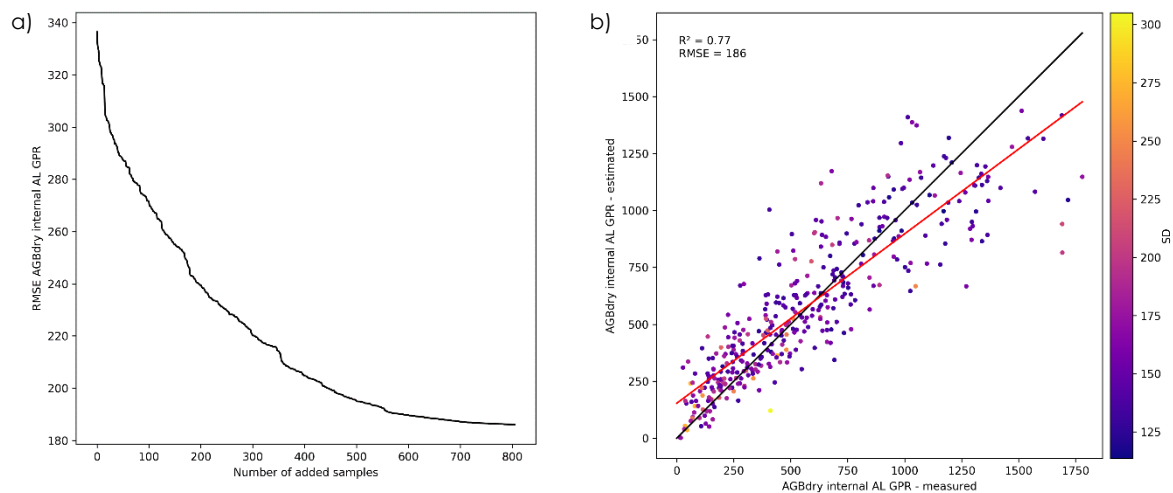


Figure 1 (a) RMSE of the AGB_{dry} data points [m²/m²] as function of the number of data sets selected by AL and (b) AGB_{dry} estimated by the GPR model (y-axis) vs. in-situ AGB_{dry} [m²/m²] (x-axis) with an R^2 of 0.77 and an RMSE of 186 [g/m²]. Yellowish colours indicate high uncertainties of the GPR model (SD = Standard Deviation).

Determining tree diversity indicators in tropical dry forests using orbital hyperspectral sensors

EARSel Valencia 2024

Abstract

Corresponding Author:

lgasanche@ualberta.ca

Patrick B. O'Brien¹, Arturo Sanchez-Azofeifa¹

¹ University of Alberta, Department of Earth and Atmospheric Sciences, Canada

Keywords: Tropical Dry Forests, Hyperspectral, Biodiversity, Phenology, Ecosystem Monitoring

Challenge

The United Nations Convention on Biodiversity (CBD) has set an impetus for monitoring biodiversity globally to best understand the effects of ecosystem changes. Tropical forests are facing changes caused by human development and climate change but their remote locations and extensiveness limit data collection relating to biodiversity. These complex forests contain hundreds to thousands of unique species. Using remote sensing data from orbital hyperspectral sensors allows for extensive coverage of these forests. Indicators have been developed for forests with fewer overall species, but tropical forests have not been well studied in this regard. Tropical dry forests (TDFs) in particular have been less studied than their wet counterparts. The data collected by hyperspectral sensors like DESIS and EnMAP can therefore be used to develop an index to quantify the biodiversity, with frequent return times capable of monitoring changes in biodiversity in the short- and long-term.

Methodology

Tropical dry forests within the northwestern coast of Costa Rica are understudied in terms of biodiversity. Within Santa Rosa National Park (SRNP), only several tens of hectares of forest have been designated for research, leaving the rest of the park (over 45000 ha) unobserved. Within these selected observational plots of varying size, stem maps have been created of all tree individuals with a DBH > 5 cm. Along with the location of the trees, species information has also been determined for each individual. Collection of hyperspectral data has taken place over the park at different points throughout a year using the DESIS, PRISMA, and EnMAP orbital sensors, capturing seasonal phenological differences. Using the Spectral Variation Hypothesis (SVH), which suggests that each unique tree species will reflect light differently in the visible and infrared regions, we can compare indices derived from different regions of the spectra. The sensors used record over 200 bands between wavelengths of 400 and 2500 nm. Several established SVH indicators will be used to identify accurate proxy indices to species richness to test their accuracy in complex TDF ecosystems. These indices will be tested at different phenological stages to determine optimal conditions for future data collection. Given the larger resolution of the orbital sensors (30 x 30 m), once an accurate indicator is produced, a tree species diversity map of the total TDF within a scan area will be created.

Results

The expected results from this project will focus on evaluating the accuracy of different biodiversity indicators for indicating tree species diversity. Several indicators derived from hyperspectral data relating to SVH have proven accurate in predicting species richness for tree species in forests with simpler structures. The use of these established indices will determine the capabilities of these orbital sensors in predicting tree biodiversity, especially at a resolution of 30 x 30 m pixels. A differentiating effect that will be tested is the taxonomic level at which trees are considered. Species of shared origins can have similar spectral signatures, so classification by higher taxonomic levels (genus, family) may provide more accurate indices. These results will also demonstrate the effect that phenology has on the accuracy of the indicators. Since SRNP is composed of TDFs, hyperspectral scans were captured in leaf-off, leaf-on,

and transition periods. This additional level of analysis allows for the comparison of results between different seasonal periods in TDFs. From these results, we can establish an optimal time of year to record hyperspectral data. Overall, this research will demonstrate the capabilities of orbital hyperspectral sensors in predicting tree diversity using ground truth data. A map of the entire scan area of SRNP containing TDF can then be produced that shows the regional tree diversity of the park, indicating overall biodiversity.

Outlook for the future

With the recent launch of several hyperspectral sensors like DESIS and EnMAP, along with several upcoming orbital hyperspectral sensors, the opportunities to monitor changes in biodiversity are increasing. By introducing a method for measuring tree biodiversity in complex TDFs, we establish the ability to accurately monitor changes in tree diversity over the long-term. These changes may result from diseases, pests, or climate change. With the recent goals set by the Convention for Biological Diversity (CBD), defining accurate indicators for measuring biodiversity will help aid in the targets set by the Kunming-Montreal Agreement. Accurate tree biodiversity maps will also aid in the conservation of areas like SRNP. As forests face risks from multiple fronts, their conservation is key for preserving and increasing biodiversity.

Mapping tree species diversity in tropical dry forests using hyperspectral remote sensing

A hyperspectral scan taken by the DESIS sensor aboard the International Space Station of a portion of Santa Rosa National Park. This scan consists of 235 bands from 402 - 1000 nm with the natural colours being presented. At the time of collection, the tropical dry forest was in the midst of its annual drought.

Patrick B. O'Brien
University of Alberta

Hyperspectral imagery data collected from
DESIS (DLR) - February 2, 2022
Background map provided by
OpenStreetMap

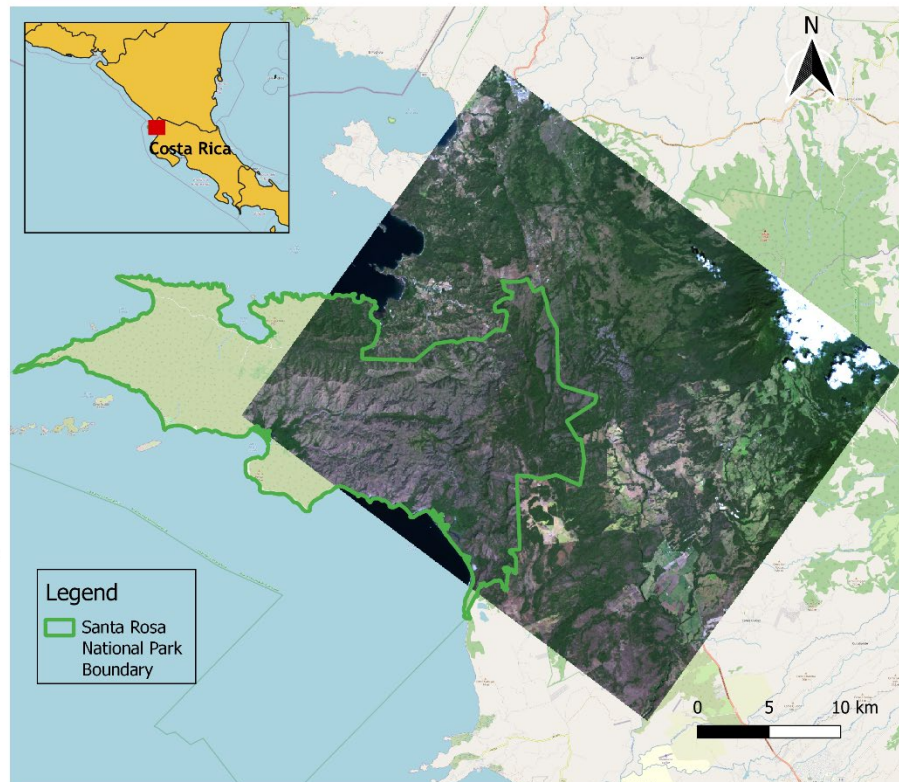


Figure In Costa Rica, hyperspectral scans from the DESIS, EnMAP, and PRISMA sensors are being used to develop indices for tree species diversity in tropical dry forests.

On the potential of principal component analysis for the reconstruction of the full SIF signal to emulate SIF satellite data

Miguel Morata¹, Bastian Siegmann², Juan Pablo Rivera-Caicedo³, Jochem Verrelst¹

¹ University of Valencia, Image Processing Laboratory (IPL), Spain

² Institute for Bio- and Geosciences, Plant Sciences (IBG-2), Forschungszentrum Jülich GmbH, Germany

³ CONACYT-UAN Tepic, Nayarit, Mexico

Keywords (5): Sun-Induced Fluorescence (SIF), Principal Component Analysis (PCA), Emulation, Spectral Fitting Method (SFM), Hyperspectral

Challenge (800 - 1000 characters incl. spaces)

Photosynthesis sustains life on Earth and plays a vital role in regulating the planet's climate. As a residual of photosynthesis, the emission of solar-induced fluorescence (SIF) is a plant strategy developed to release excessive energy. Space-based quantification of SIF as planned with the upcoming Fluorescence Explorer (FLEX) satellite mission thus provides a direct link to the canopy's photosynthetic activity, opening insights into terrestrial vegetation's health and productivity. However, the SIF emission signal is relatively weak compared to the spectral reflectance of vegetation, making it challenging to detect and separate it from background noise. For this reason, retrieving the full SIF emission spectrum typically relies on methods that only allow retrieving the SIF signal in narrow spectral absorption features from recorded radiance in which almost no light is reflected. Recently, emulation became an attractive fast technique to surrogate complex models and to obtain non-linear relations between different types of spectra. In this study, we explore how emulation can be used as an alternative method to reconstruct the full SIF profile from airborne and satellite optical data.

Methodology (1200 – 1500 characters incl. spaces)

The principle of emulation is to train a statistical model that mimics the input-output behaviour of a complex system. In our case, we apply emulation to reconstruct the full spectral SIF emission spectrum through Principal Component Analysis (PCA) dimensionality reduction and SCOPE simulations. The method is based on the spectral auto-correlation of the SIF signatures and applies PCA to preserve the original spectral information in a reduced feature space. A training dataset consisting of SCOPE 10,000 simulations was first generated. SCOPE produces the full SIF spectrum, covering the spectral range from 640 nm to 850 nm. We explored the spectral matrix correlation between the SIF emissions values across the covered spectral range. Subsequently, we used a linear regression technique to establish a linear relationship between SIF at the location of the O₂A and O₂B with the two PCs. The generated regression model allows the reconstruction of the PCs from the two SIF values. As a last step, an inverse PCA was applied to the PCs to reconstruct the full SIF emission spectrum. Additionally, we can propagate the uncertainties of SIF at the two oxygen bands into the linear regression model and the inverse PCA transform, which allows us to obtain uncertainties for each waveband of the reconstructed SIF emission spectrum. Then, we applied the procedure to a HyPlant airborne image data set from northeastern Spain recorded on 17th July 2021. The HyPlant image consists of SIF at the position of the O₂A and O₂B

absorption features, with corresponding uncertainties obtained by the spectral fitting method (SFM). After deriving the full-spectrum SIF map from HyPlant, we trained a Neural Network emulator using 10,000 samples from the two coincident images from HyPlant synthetic SIF spectra and PRISMA radiance data with 231 bands in the range of 402 to 2497 nm.

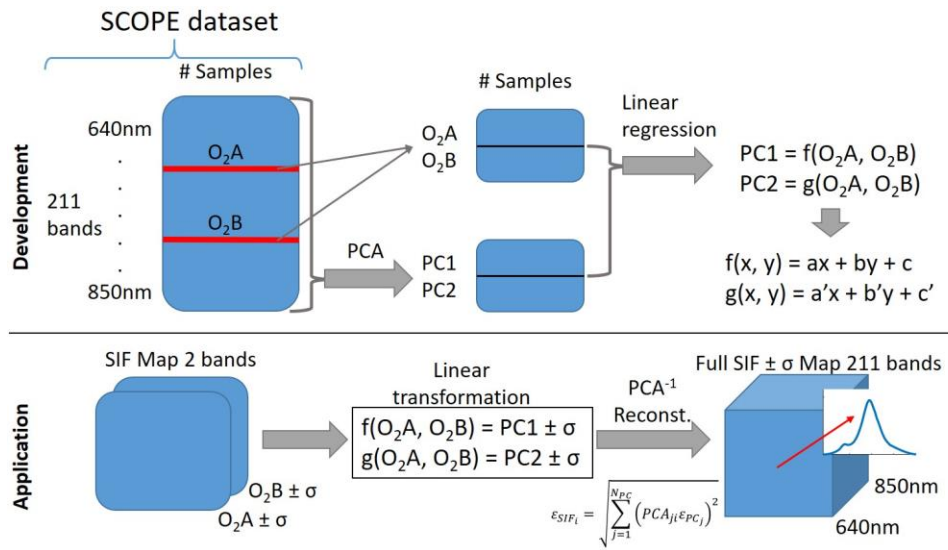


Figure 1 Workflow showing the procedure of full SIF reconstruction using PCA.

Results (1200 – 1500 characters incl. spaces)

The results revealed that the O₂A and O₂B SIF emission signals at 760 nm and 687 nm are highly correlated with the full emission spectrum, providing an R² higher than 0.65. Furthermore, we reduced the dimensionality of the SIF data to two principal components (PCs) that represent 99.38% of the cumulative explained variance. Applying the above-described technique allows us to reconstruct the full-SIF emission spectrum for each HyPlant pixel, including uncertainties for each spectral waveband. Finally, using a hyperspectral PRISMA image, we developed an emulator using the PRISMA top-of-canopy (TOC) reflectance spectra as input and the synthetic full-SIF spectra derived from HyPlant as output. This allows us to emulate synthetic satellite data containing information about the full SIF emission spectrum. Furthermore, as our method is able to reconstruct the full SIF spectrum, we obtained the maximum SIF values at the peak positions of the SIF spectrum (685 and 740 nm) and the full SIF emission (integral under the emission curve), as these values are critical products planned to be delivered by FLEX.

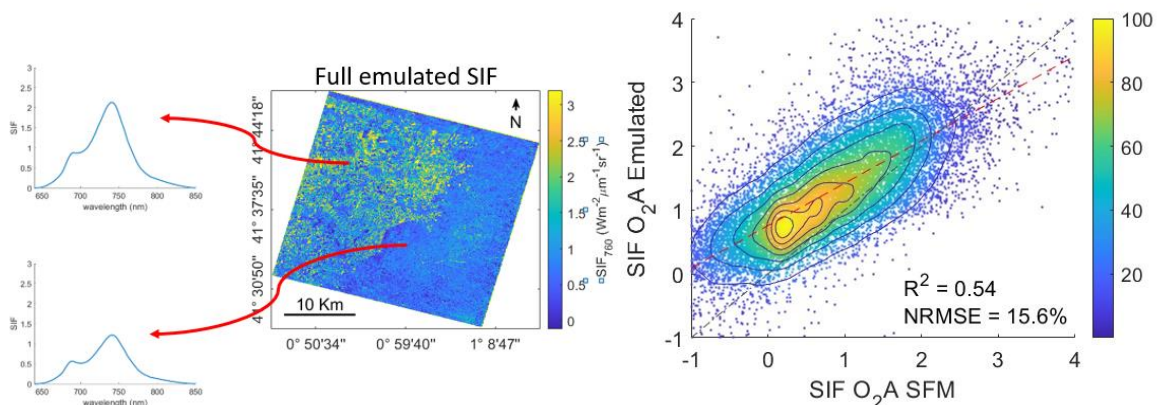


Figure 2 (a) Emulated SIF map from PRISMA. (b) Statistics of the trained emulator applied to PRISMA Test subset.

Outlook for the future (800 - 1000 characters incl. spaces)

Our results demonstrate the potential of the proposed method to emulate the full SIF emission spectrum from hyperspectral TOC reflectance satellite data. Among a variety of other applications, the proposed method has a high potential to be used to produce FLEX-like SIF data and thus can be included in preparatory activities in support of the upcoming satellite mission. We used linear regression methods to be able to propagate uncertainties. Although uncertainty propagation through MLRAs is state-of-the-art, with non-linear regression techniques we could use more than two PCs and thus obtain superior results. We also plan the further exploration of the emulation technique to disengage the PSI and PSII contribution to the full SIF spectrum to obtain unprecedented spatially explicit information on the vegetation's photosynthesis activity.

Detecting methane emissions from palm oil mills using spaceborne imaging spectrometers

Adriana Valverde¹, Itziar Irakulis-Loitxate^{1,2}, Javier Roger¹, Javier Gorroño¹, Luis Guanter^{1,3}

¹ Institute of Water and Environmental Engineering (IIAMA), Universitat Politècnica de València, Valencia, Spain.

² International Methane Emission Observatory (IMEO), United Nations Environment Programme, Paris, France

³ Environmental Defense Fund, Reguliersgracht 79, 1017 LN Amsterdam, The Netherlands

Keywords: methane, palm oil mill, imaging spectroscopy, remote sensing, anthropogenic emissions

Challenge

Methane (CH₄) is a potent greenhouse gas that has become the second most important anthropogenic contributor to climate change after carbon dioxide (CO₂). Its atmospheric concentration has doubled since pre-industrial times and has an 86 times greater global warming potential than CO₂ over 20 years. It is emitted by a diverse range of anthropogenic sources, such as livestock, oil and gas, coal mining, wastewater treatment, etc. The global-scale detection and monitoring of these sources with satellite data represents an important step in implementing methane mitigation strategies. Among the different anthropogenic methane sources, the palm oil industry significantly contributes to the rise of methane emissions. The palm oil produced at mills generates palm oil mill effluent (POME), which requires treatment before discharge into the environment. The treatment includes a ponding system, which releases large quantities of methane due to anaerobic bacteria digestion. The study focuses on the feasibility of satellite imaging spectrometers to detect and quantify methane emissions from the ponds of palm oil mills, mainly in Malaysia and Indonesia. In this context, the challenge for satellite sensors lies in the small and sparse level of methane combined with a low reflectance surface and high scene heterogeneity.

Methodology

We have requested acquisitions of the EnMAP and PRISMA satellite imaging spectroscopy missions and the GHGSat private satellite constellation over palm oil mills in Malaysia and Indonesia. These are the world's largest palm oil producers, significantly increasing their production in recent decades. To identify palm oil mills, we use the Universal Mill List (UML) of Global Forest Watch, which is a database with locations and information about all the mills across the world. Once the infrastructure has been identified, we use hyperspectral data to retrieve methane enhancement maps over the area. PRISMA and EnMAP, at 30m spatial resolution, have been shown to detect various methane point sources from oil and gas infrastructure and landfills (Guanter et al., 2021, Remote Sensing of Environment). We use the Matched-Filter retrieval to obtain methane concentration enhancement maps from EnMAP and PRISMA Level 1 data (Thompson et al., 2016, Geophysical Research Letters). On the other hand, GHGSat is a commercial satellite mission specifically designed for detecting and quantifying methane emissions from point sources. Each satellite is equipped with a wide-angle Fabry-Perot imaging spectrometer capable of producing methane enhancement maps with a spatial resolution of 25m.

Results

Applying the methodology described above, we have mapped different palm oil mills in both countries using PRISMA, EnMAP, and GHGSat observations. In recent years, some mills have installed a biogas system to capture gases such as methane or carbon dioxide. This system can efficiently produce biogas by anaerobic bioreactors and reduces the atmospheric emissions of these gases, which improves POME treatment (Nasrin et al., 2022, Journal of Cleaner Production). In this ongoing study, we have verified that we detect potential methane enhancements in those mills that did not have a biogas system. At the time of writing, we have registered about 20 potential methane enhancements above palm oil mill ponds in Malaysia and Indonesia. In addition, initial estimates of our satellite-based emission detections are in the range of 100-300 kg/h, which agrees with ground-based studies in the literature. The emissions we can detect vary based on the type of installation, the number of anaerobic ponds, and the length of time the POME has been treated. Figure 1 shows an example of methane enhancement in one of the mills we monitor in Indonesia using an EnMAP image.

Outlook for the future

The increase in atmospheric CH₄ concentrations in recent decades is a primary environmental concern due to its growing impact on climate change. Many of these emissions are anthropogenic in origin, including those from the agricultural sector, such as palm oil installations. Our work demonstrates that the detection of methane emissions in the palm oil industry is possible from space, which can help contribute to the improvement of emissions mitigation strategies. In particular, it shows that spaceborne imaging spectroscopy can be highly effective in detecting these emissions, which can be instrumental to better understanding the intensity of the sources and their dependence on external factors. Further research will be focused on extending the sampling of our satellite observations to consolidate our analysis, in particular over palm oil mill sites without a biogas storage system. We will also focus on the identification of leaks or failures in biogas installations, which can significantly help to improve the management of these systems.

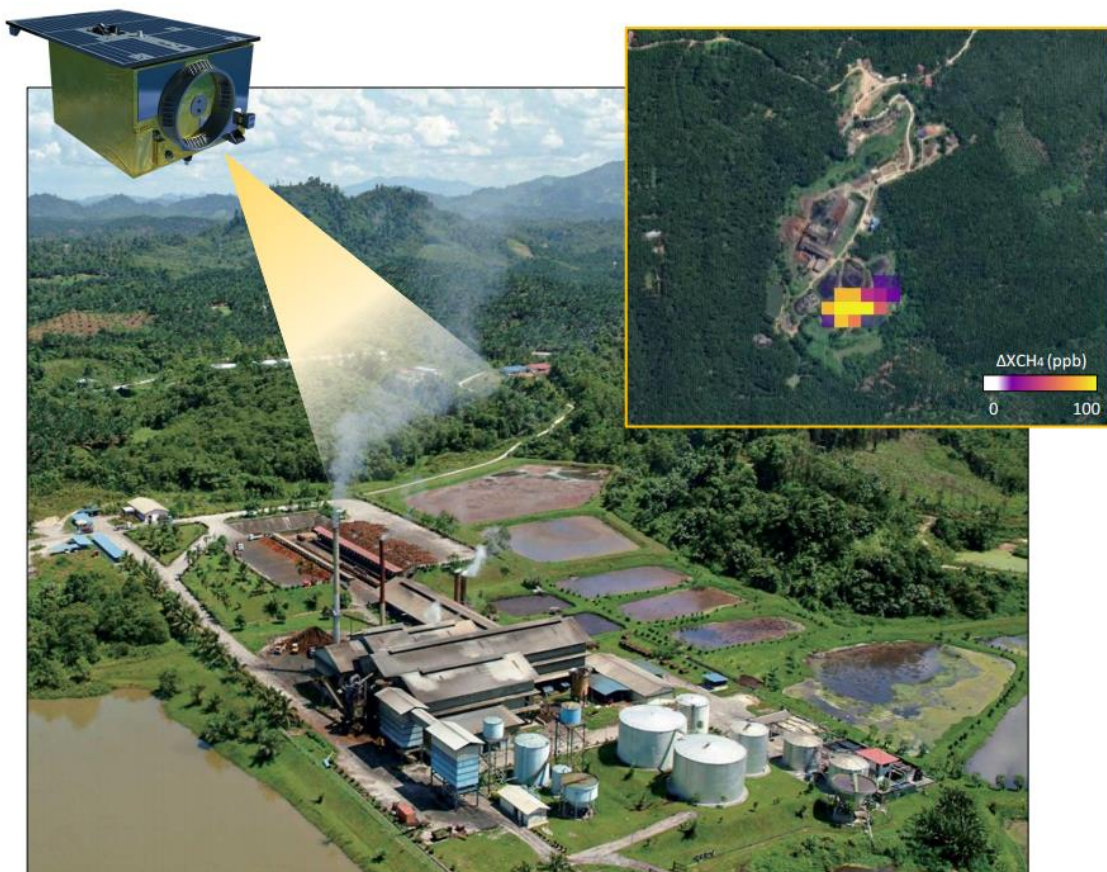


Figure 1 Methane enhancement in a palm oil mill derived from an EnMAP Level 1 acquisition

Early-stress detection in tomato: combining fluorescence and NPQ-related absorption mechanisms

Sara Pescador-Dionisio^{1,2}, *M^a Pilar Cendrero-Mateo*¹, *Sergio G Nebauer*³, *Carolina Rausell*², *Adrián Moncholí-Estornell*¹, *Aida Robles-Fort*², *Dani Gil-Villar*³, *M^a Dolores Real*², *Begoña Renau-Morata*⁴, *Rosa Victoria Molina*³, *Inmaculada García-Robles*², *Shari Van Wittenberghe*¹

¹ UNIVERSITY OF VALENCIA, IMAGE PROCESSING LABORATORY (IPL), SPAIN

² UNIVERSITY OF VALENCIA, DEPARTMENT OF GENETICS, SPAIN

³ POLYTECHNIC UNIVERSITY OF VALENCIA, DEPARTMENT OF PLANT PHYSIOLOGY, SPAIN

⁴ UNIVERSITY OF VALENCIA, BIOTECMED INSTITUTE, SPAIN

Keywords (5): Nonphotochemical quenching, drought stress, nitrogen deficiency, xanthophyll pools, tomato

Challenge

Nutrient and water availability are two critical limiting factors for plant photosynthesis. Early detection of their deficiencies, before damage occurs, has a significant impact on final crop yield. Chlorophyll fluorescence emission is one of the most direct measures of plant photosynthetic activity. However, fluorescence efficiency alone is insufficient to detect early stress or photosynthetic downregulation due to its complex - non-linear and non-constant - relationship with plant photosynthesis, which is mainly induced by non-photochemical quenching (NPQ). NPQ is a protective mechanism in plants that dissipates excess light energy as heat to prevent damage to the photosynthetic apparatus. Carotenoids and xanthophyll pigments play a key role in NPQ. The aim of this study is to lay the foundation for remote estimation of early stress by quantifying the fluorescence quantum efficiency (FQE) and xanthophyll-driven activation of NPQ based on high spectral resolution reflectance in combination with spectral fitting techniques.

Methodology

Tomato plants were grown in a growth chamber for 38 days and subjected to 3 different treatments: control, drought, and nitrogen deficiency. These treatments lasted for 7 days, after which all plants were returned to the initial irrigation and fertilization regime to study the recovery dynamics. During these days, leaf level measurements of net photosynthesis (A_{net}) and active fluorescence as well as the derived NPQ were performed using the Li-Cor 6400 XT portable photosynthesis system (Li-COR Biosciences, Lincoln, USA). Measurements were performed at two illumination levels: 300 $\mu\text{mol}/\text{m}^2/\text{s}$, the illumination under which the plants were grown, and 1000 $\mu\text{mol}/\text{m}^2/\text{s}$, which added an additional light stress to trigger NPQ saturation. In addition, A_{net} and active fluorescence light response curves (0-1800 $\mu\text{mol}/\text{m}^2/\text{s}$) were performed for each treatment. In parallel, leaf passive fluorescence and real reflectance were measured using the FluoWat leaf clip (1) and two QE-pro spectroradiometers. By attaching a block filter to the FluoWat light port, we were able to simulate the growth and light-saturating illumination conditions similar as those used in the Li-Cor 6400 XT protocols. Besides the measurement of passively-induced fluorescence, we applied a spectral unmixing protocol to retrieve Chl a and NPQ-related absorption mechanisms at the two illumination conditions. Finally, pigments, biomass, and enzyme analysis were performed to validate the early stress symptoms observed in this study.

Expected results

A_{net} , ϕPSII and NPQ showed statistical differences between stressed (i.e., drought and nitrogen deficient) and control plants, even on day 2 of the experiment. For fluorescence, FQE, defined as the ratio of fluorescence photons emitted by chlorophyll (F) to the flux of absorbed photons (APAR Chl a), showed

similar trends to the active Fs measurements. However, only when active Fs and passive FQE were combined with NPQ-related absorption mechanisms it was possible to discriminate between the three treatments. In addition, the ϕPSII and Fs/FQE light curves showed the 3 different phases of NPQ activation (i.e., light limitation, NPQ activation, and NPQ saturation), with differences in slope as the stresses progressed. Regarding the discrimination of xanthophyll features using reflectance and spectral fitting techniques, in this experiment, we were able to detect changes in xanthophyll features at day 7 of the experiment, which interestingly correspond to the stress affected plant groups. In conclusion, our results show that the combination of FQE with the spectral fitting of the xanthophyll feature could allow the remote differentiation of the NPQ activation phase, responsible for breaking the linear relationship between photochemistry and fluorescence. The discrimination of the different NPQ phases will ultimately lead to the early detection of stress using remote sensing techniques.

Outlook for the future

Adding potential improvements to the fitting algorithms will allow us to discriminate with a higher sensitivity the spectral changes related to the NPQ activation and saturation mechanisms. Therefore resulting in an earlier remote detection of the stresses and the retrieval of its features in a larger number of samples. Moreover, upscaling this method to larger spatial scales would be the next step. To perform an equivalent experiment, but at the canopy level instead of the leaf level, the spectral unmixing method used should be improved to account for the background contribution to the signal, including soil effects that add absorption in the blue-green region of the spectral range. This future challenge coincides with the upcoming launch of advanced vegetation imaging spectroscopy satellites, such as the European Space Agency's Fluorescence Explorer (FLEX). The presented results demonstrate the current algorithm development aiming for the complex retrieval of photosynthetic energy partitioning based on the key pigment players in the light reactions.

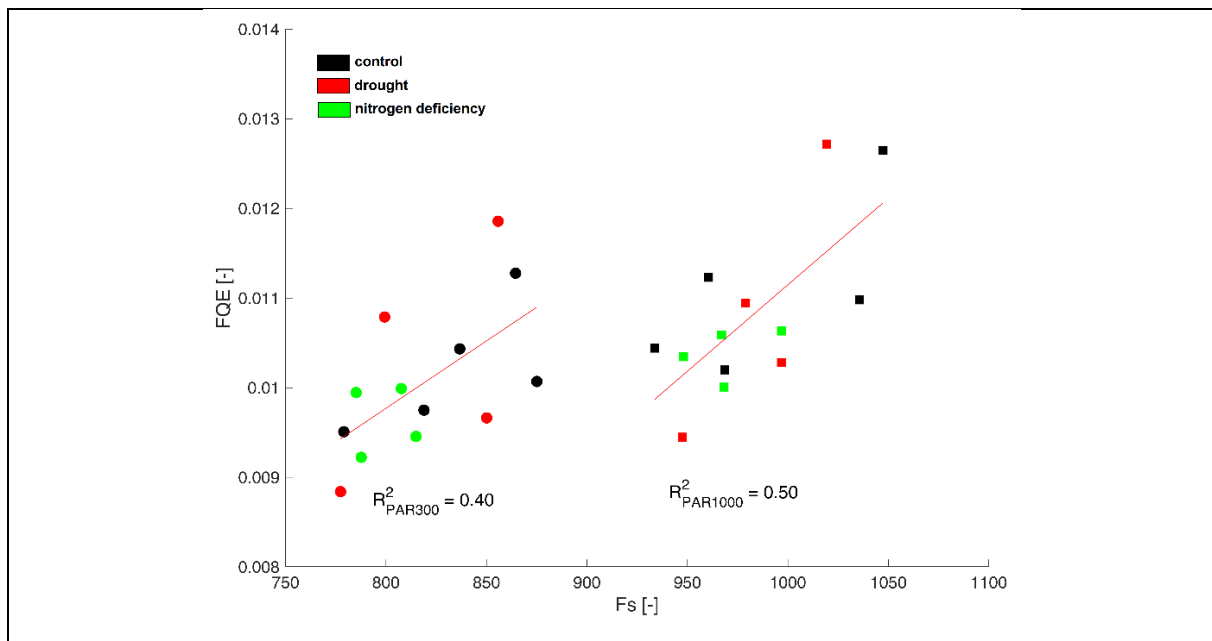


Figure 1. Correlations between the values of Fs (obtained with an active fluorescence technique, Li-Cor 6400 XT) and FQE (obtained with a passive remote technique, FluoWat) in our study. R^2 values are shown for the two different light intensities, PAR300 (filled circles) and PAR1000 (filled squares).

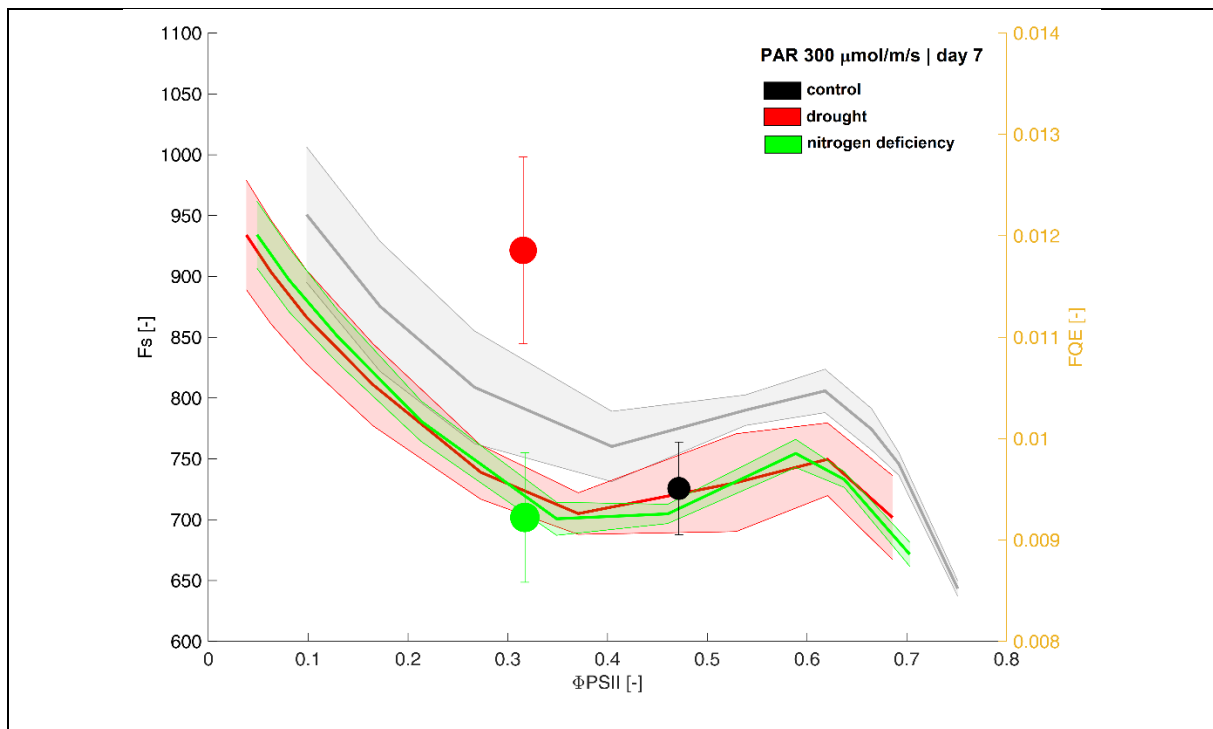


Figure 2. Fv/Fm values for day 7 of the experiment measured at PAR = 300 $\mu\text{mol}/\text{m}^2/\text{s}$ (dots, right axis) with the light curves obtained for each treatment (background, left axis). The size of each dot is proportional to the mean of the NPQ values for each group.

1. Alonso, L. Passive Direct Measurement of Sun-Induced Chlorophyll Fluorescence Spectrum from in vivo Leaves. PhD diss. University of Valencia, 2022.

Temporal and spatial retrieval of Solar-Induced Fluorescence Quantum Efficiency from in-situ and airborne observations with DART modelling

Omar Regaieg¹, Zbyněk Malenovský¹, Bastian Siegmann², Julie Krämer², Juan Quiros Vargas², Nicolas Lauret³, Yingjie Wang³, Valérie Le Dantec³, Jean-Philippe Gastellu-Etchegorry³

¹ University of Bonn, Department of Geography, Germany

² Forschungszentrum Jülich GmbH, IBG-2: Plant Sciences, Germany

³ University of Toulouse III-CNES-CNRS-IRD-INRAe, Centre d'Etudes Spatiales de la Biosphère, France

Keywords (5): 3D structure, Radiative Transfer Modelling, Downscaling, FLoX, HyPlant

Challenge (800 - 1000 characters incl. spaces)

Radiative Transfer Models (RTMs) for Solar-Induced Fluorescence (SIF) that consider the major factors impacting the scaling of the SIF signal from leaves to canopies allow the interpretation and extraction of relevant SIF information from in-situ as well as remote sensing observations through their simulations. The photosystem-level Fluorescence Quantum Efficiency (FQE) is directly linked to the photosystem activity as it represents the fraction of total absorbed photosynthetically active radiation (PAR) which is emitted by plant photosystems as fluorescence. The study objective is to retrieve the temporal (i.e., diurnal) and spatial variation of photosystem-level FQE of an agricultural crop field. These retrievals are downscaling canopy-level SIF signal, acquired as diurnal in-situ measurements and airborne images, to the photosystem level using the 3D Discrete Anisotropic Radiative Transfer (DART).

Methodology (1200 – 1500 characters incl. spaces)

The study was conducted for an agricultural crop field of alfalfa (*Medicago sativa*), in La Cendrosa, Catalonia, Spain (41.6928°N, 0.9282°E). The SIF data of the HiLiaise measurements campaign in summer 2021 include diurnal measurements by a FLoX system (JB Hyperspectral, Germany). Representative 3D mock-ups of individual alfalfa plants were manually built from photographs of real plants using the Blender 3D modelling software. These 3D plant mock-ups were distributed and rescaled to create a field mock-up such that DART simulated RGB images are similar photos taken in the field, and DART simulated top-of-canopy reflectance match the in-situ measured reflectance. Measured leaf optical properties were inverted using the Fluspect-Cx model to estimate leaf biochemical properties and then to forward simulate leaf optical and chlorophyll fluorescence properties. Incoming spectral irradiance measurements were inverted, using DART, into atmospheric optical depths, which were used to simulate direct and diffuse irradiance in DART. Finally, the FQE retrieval is done using a single forward DART simulation of the top-of-canopy SIF radiance. Assuming that top-of-canopy SIF radiance is proportional to the FQE, if all other scene parameters are held constant (the impact of SIF emission induced by SIF radiation is neglected), we applied a proportionality rule to retrieve the FQE value that ensures the equality of simulated and measured canopy SIF radiance.

Results (1200 – 1500 characters incl. spaces)

Downscaling of top-of-canopy SIF measurements using DART simulations allowed us to retrieve the diurnal variation of the steady-state light adapted FQE at photosystem level for six consecutive days (c.f. Figure below). The retrieved FQEs have been shown to significantly correlate with the leaf-level SIF efficiency estimated using other SIF downscaling methods based on spectral indices, e.g., the Fluorescence Correction Vegetation Index (FCVI). The retrieved diurnal variation of FQE was consistent for the six considered days. It tended to decrease from the morning to the afternoon. For the first three days, the FQE stayed nearly constant during the afternoon. For the last three days, after the alfalfa canopy became closed, it increased and showed a local maximum in the late afternoon. Moreover, sensitivity analysis on the canopy geometry showed that the accurate 3D representation is crucial for the FQE retrieval. Compared to the FQE values retrieved using geometrically accurate 3D mock-ups, the FQE values retrieved using 1D representations were systematically underestimated, with higher relative RMSE for earlier growth stages. Contrarily, the FQEs retrieved using randomly distributed 3D plants were overestimated, with nearly constant relative RMSE over the growth stages.

Outlook for the future (800 - 1000 characters incl. spaces)

Using in-situ SIF measurements by a FloX instrument over an alfalfa field, this study shows the potential of RTMs, specifically DART, for downscaling canopy-level SIF observations to the photosystem level by retrieving the diurnal FQE trends. This retrieval can provide insights into diurnal plant photosynthetic activity. Consequently, we aim to develop a similar DART-based approach for SIF data acquired with the HyPlant airborne imaging spectrometer over the same alfalfa field to retrieve spatial patterns (variability) of FQE from HyPlant image pixels. This requires the pre-retrieval of some canopy functional traits (e.g., contents of foliar pigments, LAI, etc.) allowing a per-pixel forward simulation of SIF. The consistency of the retrieved FQE values will be verified with the same leaf-level downscaling methods based on spectral indices. The maps of FQE retrieved at different dates will allow us to study FQE spatiotemporal variations at different scales, including HyPlant resolution.

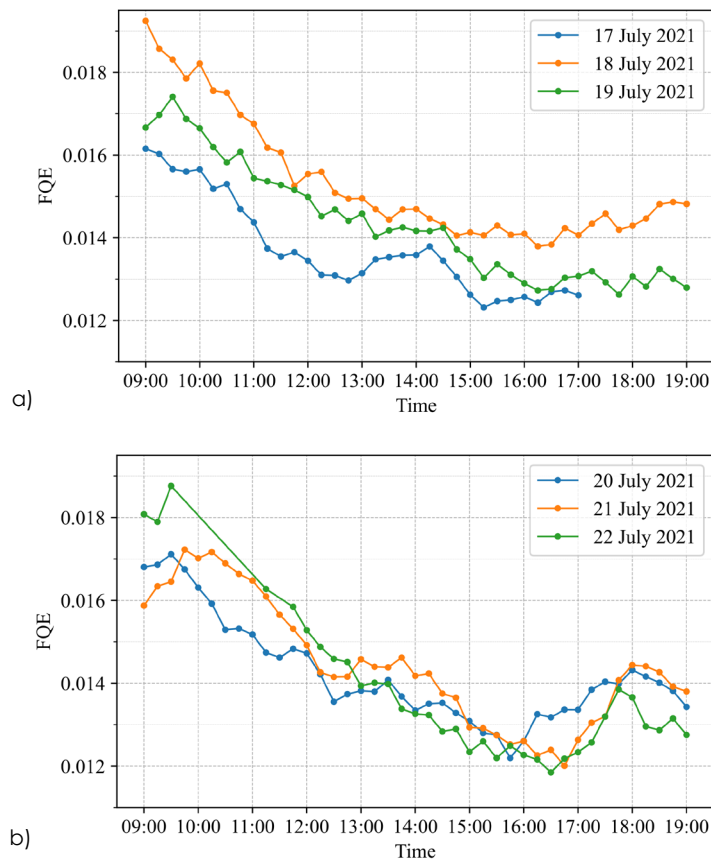


Figure: Diurnal variation of the retrieved FQE with 15 min time step. (a) First three days: open canopy. (b) Last three days: closed canopy

Poster Day 3: Poster session

Investigating Pseudo-Invariant Targets for Validation in SHIFT Time-Series Spectroscopy

Regina Eckert¹, Helena Kuehnle², David R. Thompson¹, Philip G. Brodrick¹, K. Dana Chadwick¹, Kathleen Grant³, Mark Helmlinger¹, Daniel Jensen¹, Raymond Kokaly⁴, Ryan Pavlick¹, Fabian Schneider¹, Robert O. Green¹

¹ Jet Propulsion Laboratory, California Institute Of Technology, United States

² University Of Zurich, Department of Geography, Switzerland

³ University Of Southern California, Department of Earth Sciences, United States

⁴ United States Geological Survey, United States

Keywords: in-situ spectroscopy, uncertainty quantification, validation, pseudo-invariant targets

Challenge

Global imaging spectrometers acquire data across a range of atmospheric and surface conditions. Surface reflectance spectra must be retrieved from calibrated top-of-atmosphere radiance for these spectrometers, and validating the accuracy of these retrievals is key for quantifying the measurement uncertainty for downstream data analysis. Often, validation efforts rely on field teams who must have highly coordinated efforts to measure concurrent in situ spectra with a field spectrometer over the large sampling footprints of orbital instruments, all under clear sky conditions. Given this coordination effort, field teams are often restricted to easily accessible and typically clear regions, leading to systematic biases. Static in situ measurement sites such as RadCalNet can be used for validation, but similarly these sites do not capture the full range of atmospheric and surface conditions measured by orbital instruments.

Methodology

Recent work has suggested that pseudo-invariant targets, or sites with stable spectra over time, could be used in tandem with in situ measurements to bound the uncertainty of surface reflectance retrievals. However, this method relies upon the spectral invariance of targets such as asphalt, gravel, and rock outcroppings over time, which is not well understood. To investigate the degree of change and how change manifests over time for expected pseudo-invariant sites, we undertook a biweekly measurement of three types of pseudo-invariant targets during the SBG High-Frequency Time-Series (SHIFT) campaign in Spring and Fall 2022. In the SHIFT campaign, the AVIRIS-NG instrument overflew an area near Santa Barbara, CA, USA on a weekly basis from February through May 2022, and once in September 2022. We identified seven pseudo-invariant targets in the SHIFT measurement area: three areas of gravel road, two dirt paddocks, and two serpentinite outcrops. We measured the sites with an ASD FieldSpec Pro field spectrometer every two weeks in spring and once in fall, concurrent with the AVIRIS-NG measurements (see Figure 1). We analyzed the changes in these spectra over time and compare them with the spectral variance at a vegetated meadow site (see Figure 2). We have also investigated an invariance metric calculated from the standard deviation over time for each pixel in order to determine what surface types in practice had low variation in the SHIFT dataset.

Results

We compare in situ spectra to remote surface reflectance retrievals obtained using the ISOFIT open source optimal estimation code base in order to validate the stability of the remote retrieval over time. We found that while the pseudo-invariant sites had relatively constant spectral shape, they experienced changes over the course of the SHIFT campaign. In particular, disturbance from cars, changes in sparse vegetation, and variable observation conditions meant that even the relatively pseudo-invariant sites still contained small but meaningful temporal variation. In Figure 2, changes in the overall reflectance in a gravel site can be observed for both the in situ and remote measurements, likely due to differences in atmosphere, spectralon panel, and other observation conditions. Relative spectral changes are also present that are seen with a principle component analysis (PCA) decomposition of the spectra, which reveal small amounts of vegetation in the gravel site that senesced over the course of the campaign. While these changes are small compared to the highly-varying vegetation spectra we measured for comparison, we are continuing to investigate the implications of these changes for use of pseudo-invariant sites for validation of surface reflectance retrievals.

Outlook for the future

With an increasing number of orbital imaging spectrometers, most areas of the globe will soon have repeated measurements under different observing conditions. By understanding the land cover types we expect to be invariant, we can use these repeat measurements to constrain the uncertainty in our reflectance retrievals over pseudo-invariant targets. However, since in most cases we will not have repeated in situ measurements of these pseudo-invariant targets, we will not have knowledge of the small-scale changes in the pseudo-invariant spectra. There is therefore a limit to the uncertainty constraint provided by the invariant target measurement which should be properly accounted for when using pseudo-invariant targets for validation activities.

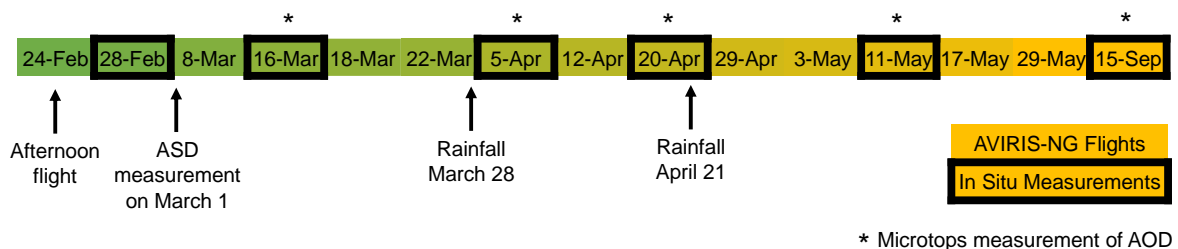


Figure 1: Timing of AVIRIS-NG and in situ ASD measurements during the SHIFT campaign in 2022

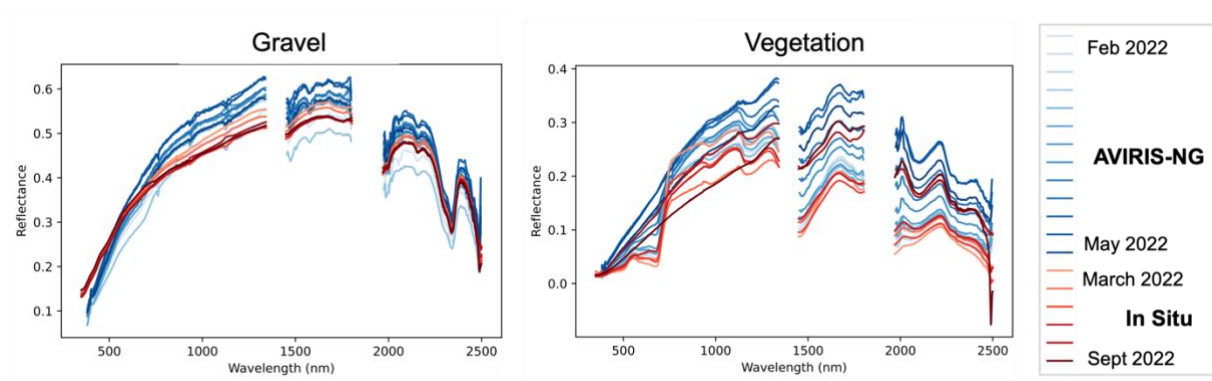


Figure 2: Comparison between in situ and remote measurements over time for a pseudo-invariant gravel parking lot site and a highly time-varying vegetation site.

The role of scale in predicting tree physiology with Hyperspectral data from five mid-European tree species

Ephraim Schmidt-Riese¹, Michael Förster², Fabian Fassnacht³, Pia Kräft⁴, Robert Jackisch⁵, Birgit Kleinschmit⁶,

(Style: Authors, presenting author underlined)

¹ Technische Universität Berlin, Germany

² Technische Universität Berlin, Germany

³ Freie Universität Berlin, Germany

⁴ Technische Universität Berlin, Germany

⁵ Technische Universität Berlin, Germany

⁶ Technische Universität Berlin, Germany

Keywords (5): upscaling, forest health, imaging spectroscopy, scale effects, tree physiology

Challenge

Forest health monitoring is critical to properly manage global forest. Remote sensing is increasingly becoming a capable method for operational monitoring of tree and forest physiology. The bottleneck between currently ample imagery acquisition and operative advice is the transformation of image data to tree vitality information. Here, current analyses mostly rely on a sound understanding of processes at the surface and at the sensor level. However, the influence of temporal and spatial variability of reflectance is often inadequately represented. In this study, we investigate physiological traits of a mixed-stand forest using a composition of biophysical measurement methods and imaging spectroscopy at various scales. Specifically, we examine how spatial and temporal variability of the spectral response of trees alters our capability of consistently mapping tree physiology features.

Methodology

Spectral and physiological measurements are conducted in a temperate, mature forest near Demmin, North-Eastern Germany (Figure 1). Sampled tree species comprise Douglas fir (n = 10), European beech (n = 10), European larch (n = 8), Norway Spruce (n = 3) and Pedunculate oak (n = 10). A gondola platform attached to the crane hook of a tower crane allows for a 3D-access of tree crowns. Physiology measurements include continuous measurements of sap flow, fine root growth, stem growth and tree water deficit. In addition, an array of physiology-related leaf chemicals (e.g. chlorophyll, carotenoids) is measured at a monthly interval. Monthly measurements also include leaf gas exchange, Leaf Area Index and leaf temperature. Simultaneously, leaf spectral response is measured on-leaf (leaf clip device) and from a short distance (30 cm) using an Analytical Spectral Devices (ASD) spectrometer. To understand signal changes with scale, we calculate the direction and magnitude of change in spectral domains from leaf- to forest level. By establishing relationships between spectra from different scales and physiology data via Partial Least Squares Regression, we evaluate how tree physiology is depicted differently across scales. We further consider how seasonal change, as depicted in monthly measurements, as well as tree species identity and tree species traits alter the relationship between small- and large-scale remote sensing observations.

Expected results

Branch exposition (North, East, South, West, Top) did hardly alter overall on-leaf reflectance. However, due to sun and viewing angles, we expect significant differences between branch expositions when comparing on-leaf data with data from coarser scales.

Comparing leaf-level reflectance to gas exchange, we identified a strong correlation between Normalized Ratios of wavelengths from the mid-NIR and Short-wave Infra-red domain and leaf carbon assimilation for Norway Spruce during a diurnal measurement campaign (Figure 1). We expect to find similar relationships to other physiologically relevant variables such as concentrations of related, light-interactive leaf chemicals. However, we expect the relationship between reflectance and leaf-level physiology to deteriorate with increasing scale. We suppose that light-and-shadow-conditions, daily-climate-driven-traits such as leaf angle and increasing spectral mixture add to uncertainties of physiology trait estimation. In contrast, above-leaf Normalized Ratios did show a similarly strong correlation to carbon assimilation as did on-leaf Normalized Ratios ($r = 0.9$). However, above-leaf Normalized-Ratio-correlations are rarely significant (not shown). Also, the maximum correlation shifts from a Near Infra-Red (NIR)-Short-wave Infra-red (SWIR) ratio to a SWIR-SWIR ratio (not shown), illustrating structural differences between scales.

Outlook for the future

With our analyses, we aim to (1) assess which physiological traits can be estimated from spectral responses with sufficient consistency, (2) identify the reason for scale differences in trait estimation. On this basis, we suggest identifying the relative importance of processes that drive scale-dependent capability of physiological trait estimation. With this, we will be able to better frame the actual potential of different remote sensing approaches to operational monitoring of forests. Our results will enable a more thorough evaluation of ongoing monitoring schemes and can critically contribute to a comprehensive interpretation thereof. Lastly, our gained knowledge might spark ideas for improved monitoring designs that take into account the spatially and temporally variable nature of reflectance from living surfaces.

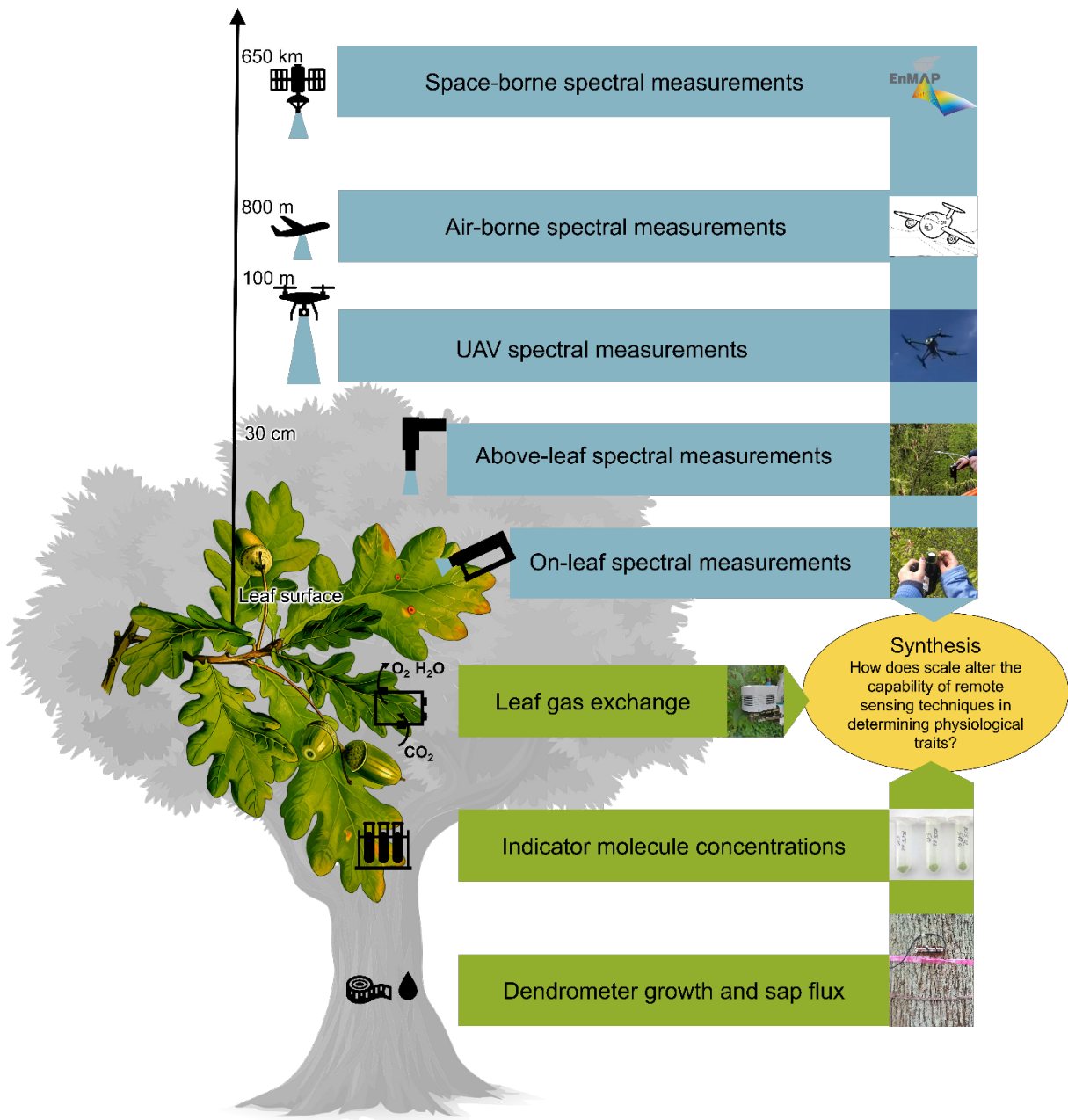


Figure 1 Illustration of measurement setup in order to address scale-effects in physiological trait retrieval from hyperspectral data. Measurements are repeated monthly in 2023 and 2024 on five species (Norway spruce, Douglas fir, European larch European beech and Pedunculate oak) and a total of 41 trees.

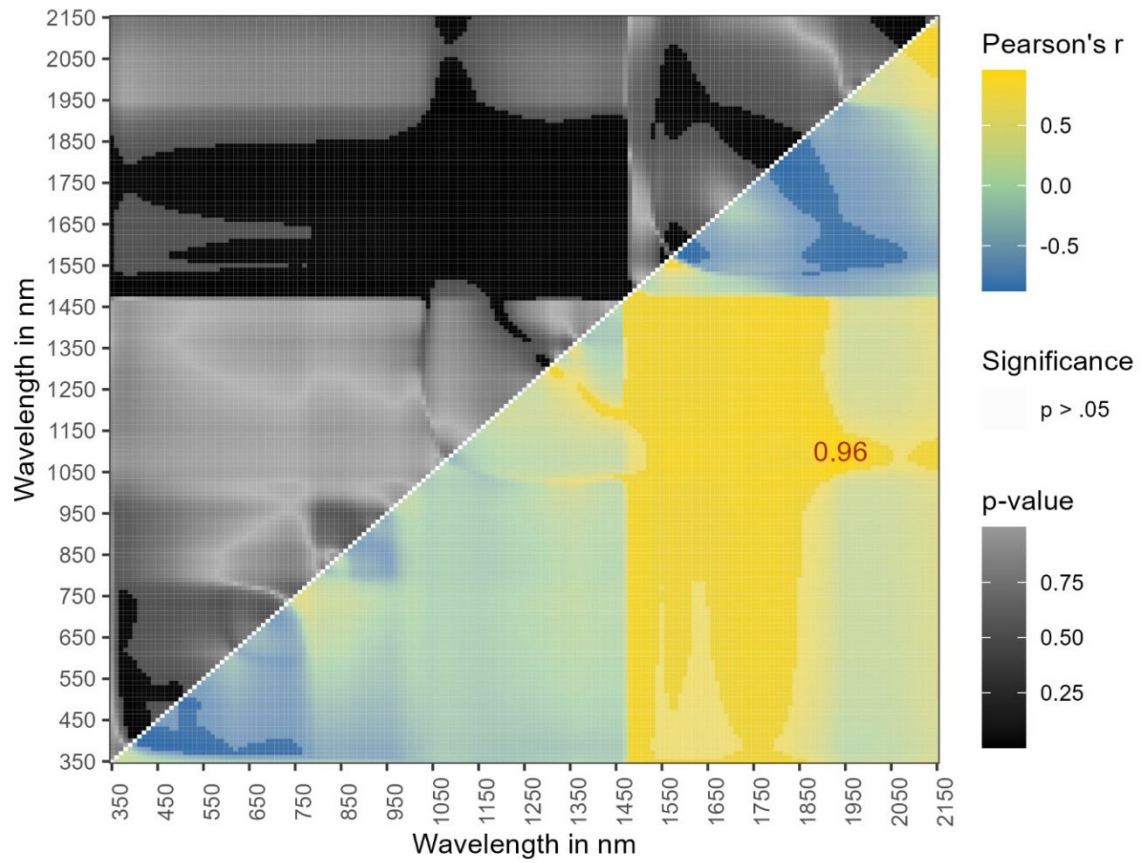


Figure 2 Pearson's correlation between Normalized Ratio Indices of *on-leaf* spectra and corresponding leaf carbon assimilation. The lower triangle displays the correlation coefficient with its maximum value given in red. The upper triangle displays the p-values of correlations. Correlations that are not significant are overlaid with a transparent white layer. Data includes 7 diurnal measurements during a clear-sky hot day in mid-summer (from 7 a.m. to 11 p.m.) from a Norway spruce.

Title: Advancing Plant Trait Estimation using Imaging Spectroscopy: A Bayesian Approach with Enhanced Interpretability and Uncertainty Propagation

Dhruva Kathuria^{1,2}, Yoseline Angel^{1,3}, Evan Lang^{1,4}, Alexey Shiklomanov¹

(Style: Authors, presenting author underlined)

¹ Global Modeling and Assimilation Office, NASA Goddard Space Flight Center, USA

² GESTAR II, Morgan State University, USA

³ ESSIC, University of Maryland - College Park, USA

⁴ Science Systems and Applications, Inc., USA

(Style: Affiliations;)

Keywords (5): Plant Functional Traits, Hyperspectral, Bayesian, Uncertainty quantification, Vegetation

Challenge (800 - 1000 characters incl. spaces)

Imaging spectroscopy, with upcoming satellite missions like Surface Biology and Geology (SBG), provides a promising avenue for assessing plant traits across spatial and temporal scales. Partial Least Squares Regression (PLSR) is a widely used empirical method for predicting traits using reflectance spectra due to its computational efficiency and ability to handle high-dimensional correlated data. PLSR however, transforms the input wavelengths to "latent variables," making interpretation difficult. Besides, PLSR does not rigorously propagate uncertainties from the input reflectance — such as those introduced by Bayesian atmospheric correction algorithms — to the estimated traits. Mapping plant functional traits using PLSR over wide spatial and phylogenetic extents is further challenged by the variability of the relationship between traits and spectra across species, functional types, and biomes.

Methodology (1200 – 1500 characters incl. spaces)

A Bayesian framework that estimates traits directly from reflectance spectra (without any latent transformation), explicitly accommodates variability in the relationship between traits and spectra across different groups (using hierarchical modelling) while propagating uncertainties in a rigorous fashion can address the above limitations. To compare the Bayesian approach with the traditional PLSR algorithm, we first implement a non-hierarchical Bayesian regression algorithm (while assuming no input spectra error) using a special class of shrinkage priors called regularized horseshoe priors to predict multiple plant functional traits (such as leaf mass area, nitrogen content, and carotenoid content) from reflectance spectra data from 400 nm to 2400 nm at 1 nm spectral resolution at leaf scale. The prior shrinks the regression coefficients of the non-important wavelengths to zero while letting the regression coefficients of the important wavelengths escape this shrinkage. To improve the computational efficiency of the Bayesian algorithm, we apply a novel predictive projection technique, which then projects the full Bayesian model to a reduced model with a handful of input wavelengths while preserving predictive accuracy. Finally, we incorporate input spectral error into the Bayesian model, showcasing the inherent capability of Bayesian methods for uncertainty quantification for both parameter estimation and subsequent predictions, in contrast to PLSR.

Expected results (1200 – 1500 characters incl. spaces)

We validate the trait predictions using an independent validation dataset from the Canadian Airborne Observatory spanning a wide variety of plant species. For the non-hierarchical Bayesian algorithm, we find that the RMSE of mean posterior predictions are comparable to PLSR for carotenoid content and LMA, and significantly better than PLSR for Nitrogen. The Bayesian algorithm has the added advantage of providing parameter and prediction uncertainty estimates (Figure 1b). We find that posterior uncertainties are highest for carotenoid content and lowest for the LMA dataset, primarily due to variations in the size of the training data. The reduced model — which uses 8 to 40 wavelengths (depending on the trait) rather than the full spectrum — had similar predictive accuracy to the full model (Figure 1b). Using simulated and real datasets, we further explore the effect of including input uncertainty in spectra while fitting the trait estimation algorithms and show the robustness of the Bayesian approach over the PLSR approach in parameter estimation and subsequent predictions in the presence of noisy spectral data. For the hierarchical model, we expect the accuracy of the Bayesian algorithm to further increase especially for under-sampled groups.

Outlook for the future (800 - 1000 characters incl. spaces)

Our proposed Bayesian model is (a) interpretable, (b) computationally efficient, (c) accounts for uncertainties in input reflectance, and (d) provides parameter and prediction uncertainties. We discuss current and future efforts on extending the Bayesian model to accommodate variability in the relationship between traits and spectra across different groups such as growth forms (e.g., broadleaf tree, needle leaf tree, shrub, grass and herb) and phenology (e.g., deciduous and evergreen) using Bayesian hierarchical modeling (Figure 2a), account for non-linear effects of input spectra on traits (Figure 2b), and model site-specific measurement errors in observed spectra. Additionally, we highlight efforts on developing hybrid physical-empirical methods by combining the proposed Bayesian algorithm with physical-based models such as PROSPECT to upscale the leaf traits to canopy scale.

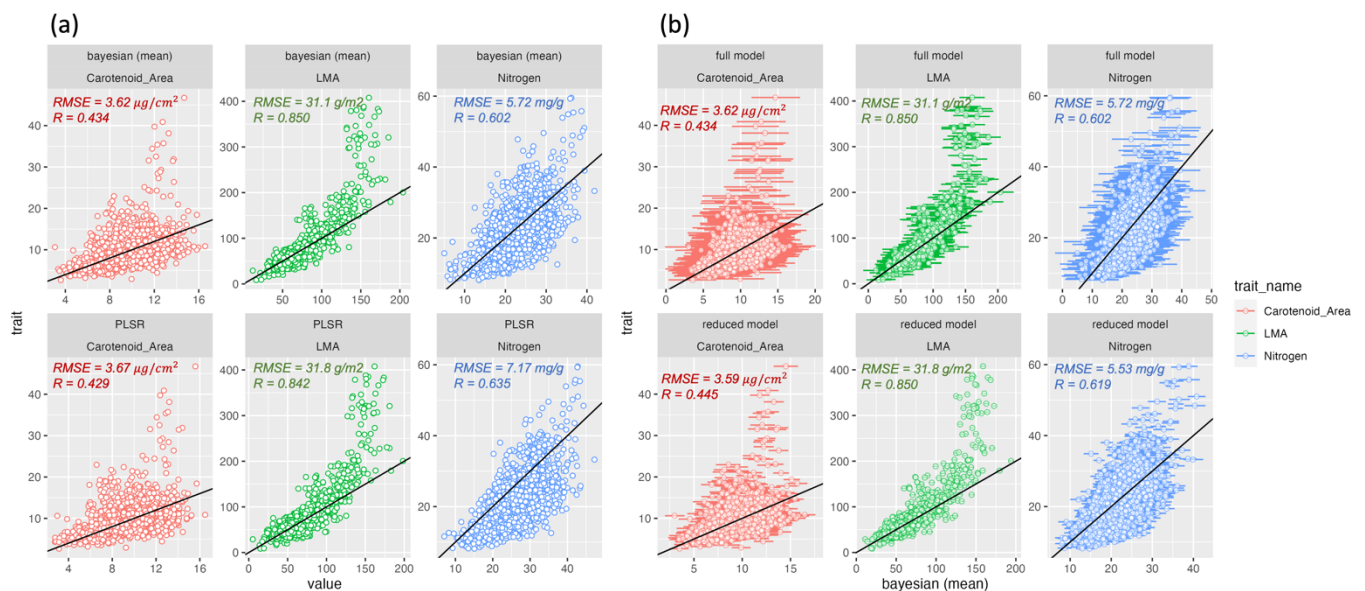


Figure 1. Comparison of the (a) mean posterior predictions of the full Bayesian model with PLSR predictions, and (b) Bayesian predictions of the full model compared with the reduced model. The RMSE and correlation values are given for the mean posterior predictions. Both the Bayesian models also provide uncertainty associated with the predictions (90% quantile intervals shown here).

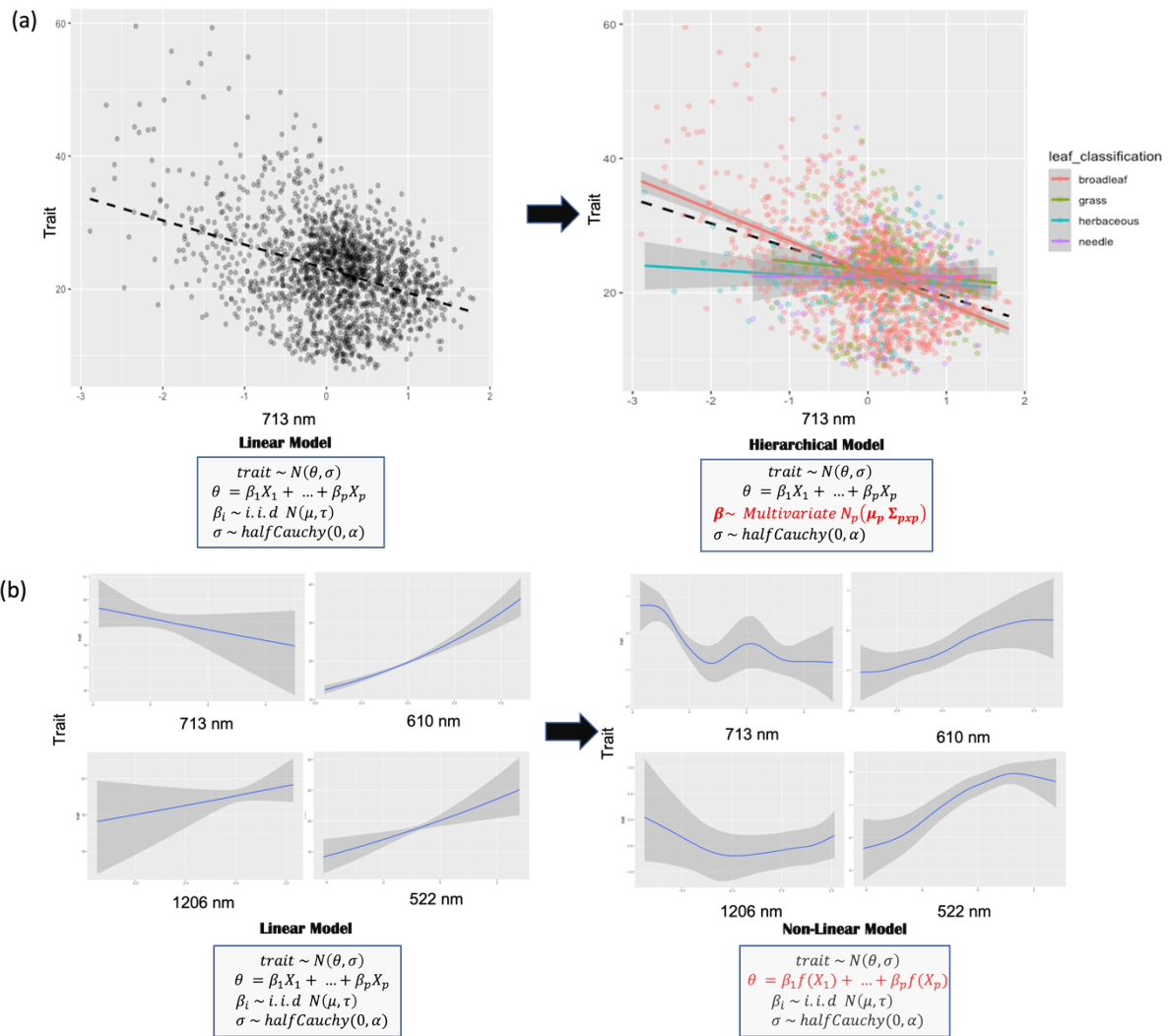


Figure 2. (a) The Bayesian regression model can be extended to model the hierarchical relationship between spectra and traits based on groups such as growth form. The figure shows how the relationship between a trait (Nitrogen) and spectral wavelength (713 nm on a standardized scale) changes with various groups. A hierarchical approach can model such within and across-group variability. (b) The Bayesian model can also be extended from a linear assumption to a non-linear assumption between spectra and trait using a Gaussian additive model.

Target Detection Using UAV-Borne Hyperspectral Imagery (Poster)

[L. Sierra](#)¹, M. Vögtli¹, S. Schreiner², W. Gross², F. Queck², J. Kuester², J. Mispelhorn², W. Middelman², M. Kneubühler¹

¹ UNIVERSITY OF ZURICH, DEPARTMENT OF GEOGRAPHY, SWITZERLAND

² FRAUNHOFER IOSB, IMAGE ANALYSIS GROUP, GERMANY

Keywords (5): Hyperspectral, Airborne (UAV), Target Detection, Camouflage, ISTAR

Challenge

In a recent multi-sensor and multi-temporal campaign, called HyperThun'22, we undertook a comprehensive investigation to address the challenges of camouflage material detection in vegetated environments using UAV-borne hyperspectral technology. Our primary challenge was to design an experimental setup that not only served to assess the limits of security and defence related target detection, but also allowed for a comparative analysis of different hyperspectral sensors under varying circumstances. Our experimental setup entailed simulating gatherings of people, camouflage tactics, and vehicle concealment in open bushland and forest environments. In this study, we present some of our major findings, showcasing the potential of high-resolution UAV-borne hyperspectral data to address complex security and defence challenges.

Methodology

Our campaign was based on two hyperspectral sensors: the Headwall Hyperspec Co-Aligned VNIR-SWIR and the HySpex Mjolnir VS-620. The Headwall system covers the wavelength-regions from 400 – 1000 nm with its VNIR sensor (270 bands) and the region from 900 – 2500 nm with its SWIR sensor (267 bands). The HySpex System provides the spectral range from 400 – 2500 nm in 500 bands. At a flight altitude of 80 m, both sensors acquire data with a ground sample distance of less than 5 cm. Furthermore, we made use of a fixed-wing eBee X drone, delivering auxiliary RGB and thermal data with ground resolutions of 2.5 cm per pixel (RGB) and 15 cm per pixel (thermal) when flying at an altitude of approximately 120 meters. Throughout the campaign, we conducted a total of over 20 flights across three dedicated campaign days, each flight tailored to various experimental configurations. It was important to us to present realistic scenarios to explore the possibilities of our sensors. Using target detection algorithms such as the Adaptive Coherence Estimator (ACE) or the Generalized Likelihood Ratio Test (GLRT), we investigated the possibilities of spectral unmixing to detect hidden targets. We explored the usefulness of different wavelength regions and spatial resolutions flying at varying heights above ground to facilitate performance and comparative evaluations.

Preliminary Results

Our findings demonstrate the versatility and robustness of the acquired data and the applied target detection algorithms, particularly under challenging conditions. We achieved high accuracy in detecting objects hidden by camouflage nets, placed in shaded areas or covered by varying amounts of fresh or dry vegetation. While adding fresh vegetation onto a multi-colored fabric can help concealing it to a certain degree, our algorithms were still able to recognize the concealed object under the vegetation cover. The lowest detection rates were found for a coverage factor of 100% with fresh vegetation, while 100% cover with dry vegetation led to slightly better detection rates than with fresh vegetation. In addition, using the GLRT, we were also able to locate a tent that was in the shade of a tree and was

therefore barely visible to the human eye (see Figure 1). Our two instruments can also be well combined by combining the spectrally higher resolved VNIR range of the Headwall system with the spectrally higher resolved SWIR range of the HySpex system. This gives us a spectrally high-resolved data set with about 570 bands approximately evenly distributed from 400 – 2500 nm. This research has the potential to benefit numerous application fields by validating the utility of hyperspectral data in target detection and spectral unmixing.

Outlook for the future

In the future, we aim to investigate whether we can achieve equally good target detection results with spectrally and/or spatially reduced data. More specifically, we focus on whether we can achieve a faster, less computationally intensive, but still reliable detection of different targets by means of data reduction. The ultimate goal will be to investigate the operability of the ACE and GLRT algorithm in near real-time. Furthermore, it will be interesting to see if we can extend the knowledge gained from our results to other application areas and transfer it to different sensor systems, which entail different spatial and spectral resolutions. In the near future, we also plan to experiment with an airborne hyperspectral sensor, flying simultaneously with our hyperspectral drones, as well as adding multi- or hyperspectral satellite data with which we want to look at various scaling effects for spectral unmixing.

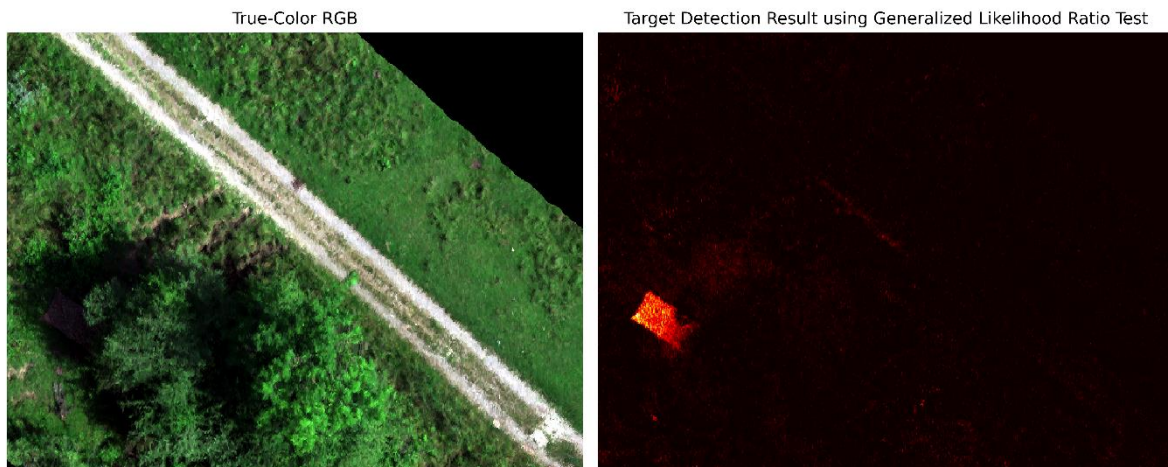


Figure 1 Use of the Generalized Likelihood Ratio Test for the detection of a tent located in the shade of a tree.

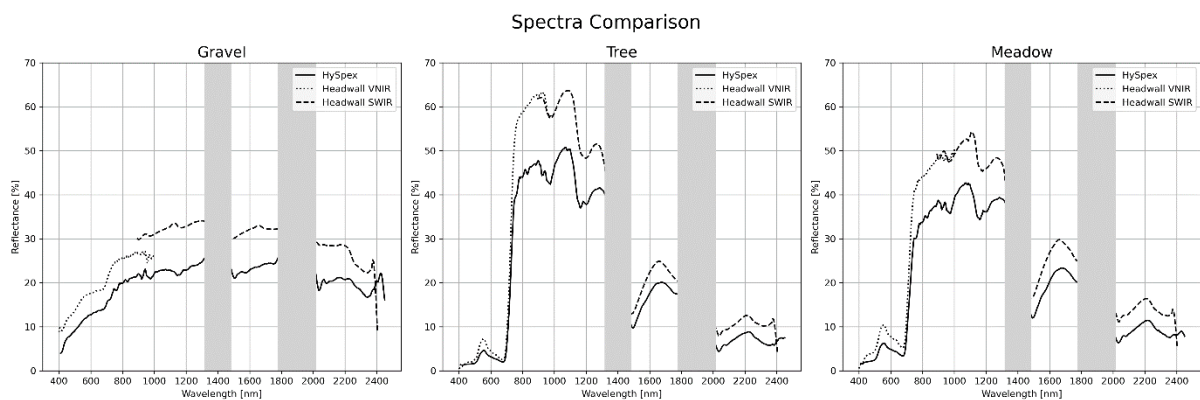


Figure 2 Comparison of different spectra measured by the two UAV-borne hyperspectral systems used.

Comparing Hypex Airborne Hyperspectral Imagery to Multi-Temporal Sentinel-2 Composites for High-Mountain Plant Communities Mapping

Marcin Kluczek¹, Bogdan Zagajewski¹, Marlena Kycko¹

¹ Department of Geoinformatics, Cartography and Remote Sensing, Chair of Geomatics and Information Systems, Faculty of Geography and Regional Studies, University of Warsaw, Poland

Keywords: vegetation mapping, mountain ecosystem, woody tree species, the Tatras, biodiversity

Challenge

Monitoring of non-forest mountain plant communities is now extremely important as a consequence of anthropopressure and climate change which speeds up transformation processes taking place in mountain habitats. The Tatra Transboundary Biosphere Reserve is recognized as one of the most ecologically valuable regions in Central Europe, and it has been the subject of numerous investigations into its plant life. While phytosociological field methods, such as the Braun-Blanquette approach, play a crucial role, they come with the downside of being time-consuming and labor-intensive. Moreover, these techniques are limited to a predefined network of measurement points and can be influenced by the researcher's subjectivity when identifying plant communities. To address these limitations, the utilization of remote sensing technologies offers an objective and scalable approach for collecting comprehensive data on vegetation, allowing for long-term monitoring of plant communities.

Methodology

In our research, we undertook a comparison between multitemporal Sentinel-2 satellite data and airborne hyperspectral images from HySpex for mapping plant communities in the Tatra mountains. Given that high-mountain ecosystems are highly adapted to specific topographic conditions, our study also focused on assessing the impact of various LIDAR derivatives on the accuracy of community classification. Additionally, we explored the influence of the number of training data pixels on classification accuracy, providing valuable insights for optimizing field campaigns with limited time and resources aimed at achieving reliable classification results. Our proposed methodology leverages two machine learning algorithms, namely Random Forest (RF) and Support Vector Machines (SVM) with radial kernels. The classification processes were conducted using the open-source R programming language, with the algorithm's learning parameters optimized through the grid search method, which systematically explores various parameter combinations. We addressed classification bias through an iterative accuracy assessment repeated 100 times. The training and testing datasets were randomly divided in a 50:50 ratio, ensuring their independence based on polygon affiliations. We selected the models with the highest average F1-score across all scenario classes for the final map production.

Expected results

Our results for 13 classes, spanning from rock scree communities and alpine grasslands to montane conifer and deciduous forests, achieved F1-scores ranging from 76% to 90%, depending on the dataset. The inclusion of topographic LiDAR derivatives such as DTM, nDSM, aspect, and slope maps increased the F1-score accuracy of individual datasets from HySpex, MNF, and Sentinel-2 by 5%-15%. Notably, classification maps generated from HySpex data (2 meters resolution, 430 bands) exhibited a high degree of similarity to those produced from multitemporal Sentinel-2 data, with differences of less than 1% for classifications based on 500-1000 pixels. The results we obtained (overall accuracy ranging from 90% to 98%) are consistent with those achieved by other researchers. For instance, Zhang et al. (2020) employed RF and multitemporal satellite data to classify nine classes of mountain vegetation, yielding results like 75%-93% for deciduous forests, 89%-95% for conifer forest types, and 75% for subalpine shrubs and meadows. Mishra et al. (2020) identified 17 classes of mountain vegetation, including eleven forest vegetation communities, using multitemporal Sentinel-2 data and Digital Elevation Model (DEM) in combination with RF, achieving an overall accuracy of 70%-87%. The incorporation of DEM led to a 15% improvement in overall accuracy for eight forest types in the case of Liu et al. (2018), who also utilized multitemporal Sentinel-2 data and the Random Forest algorithm.

Outlook for the future (800 - 1000 characters incl. spaces)

Expanding the application of remote sensing techniques and machine learning algorithms beyond the Tatra mountains offers the potential to address similar challenges in different regions. This approach could be adapted to other mountain ecosystems worldwide, enabling a better understanding of their unique plant communities, adaptive responses, and conservation needs. By customizing the methodology to the specific characteristics of diverse environments, researchers can contribute valuable insights for sustainable land management and biodiversity conservation.

Furthermore, the utilization of alternative datasets, such as those from different satellite sensors or aerial imaging platforms, can enhance the versatility and generalizability of the methodology. Investigating the performance of these methods with varied data sources will enable researchers to better tailor their approach to suit the data availability and quality specific to each study area.

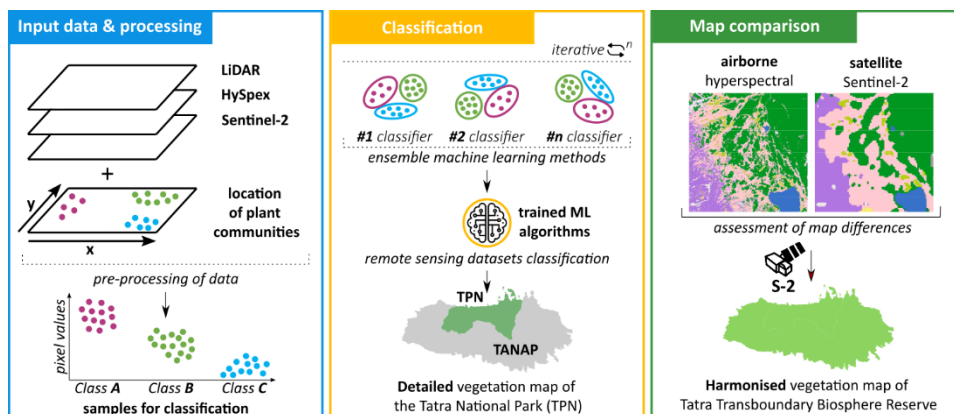


Figure 1. Workflow of classification.

Identification Of Biophysical Traits In Spectral Signatures At The Leaf Level In A Mixed Beech Forest In Northeast Germany

Pia Kräff¹, Ephraim Schmidt-Riese¹, Michael Förster¹, Robert Jackisch¹, Ralf Kätzel², Frank Becker², Anne Clasen³, Kai Jütte³, Fabian Fassnacht⁴, Birgit Kleinschmit¹

¹ Technical University of Berlin, Department of Geoinformation in Environmental Planning, Germany

² State Competence Centre Forestry Eberswalde, Germany

³ Mecklenburg-Western Pomerania State Forestry Office, Department of Forest Geoinformation, Germany

⁴ Free University of Berlin, Institute of Geographical Sciences, Remote Sensing and Geoinformatics, Germany

Keywords (5): Imaging Spectroscopy, ASD Plant Probe, Leaf Clip, leaf reflectance, forest health assessment, tree physiology

Challenge

Forest damage in Germany has been at a very high level since the drought summers of 2018 and 2019. The national terrestrial forest condition survey is only conducted once a year on sample trees, leading to temporal and spatial information gaps on intra-annual changes in tree vitality. Forest remote sensing has great potential to provide complementary information, but there are still uncertainties in species-specific differentiation due to the lack of proven relationships with tree physiology. Spectral signals vary depending on tree species and phenological state or due to possible interferences in the data such as shading. Data of mature trees are often lacking for a true comparison between the spectral signal seen above the canopy and tree physiological parameters indicative of stress (biomarkers) under natural conditions, because a structured leaf sampling is a rather difficult task.

Methodology

To address these challenges, a 40-meter-tall tower crane with a 45-meter radius was installed within a 1-hectare mixed beech forest in Mecklenburg-Vorpommern, Germany. It facilitates leaf sampling for physiological analysis in the upper canopy periphery and imaging spectroscopy at the leaf level, where the spectral detectability of leaf-internal physiological parameters is expected to be highest. In two vegetation periods (2023, 2024), at four phenologically different phases between May and September, imaging spectroscopy contact measurements at leaf level were and will be performed on 41 sample trees of five main tree species (10 European beeches, 10 English oaks, 10 green Douglas firs, 8 European larches and 3 Norway spruces) at five canopy positions (N, S, E, W, top) using the ASD Plant Probe with Leaf Clip. These measurements, using an internal light source, are the most independent of environmental disturbances. Simultaneously, leaf samples will be taken from the same measurement positions and analyzed in the laboratory for a number of selected tree physiological biomarkers (chlorophylls, carotenoids, carbohydrates, proteins, amino acid spectrum, ascorbate, various phenolic compounds, nutrients, etc.) for precise tree vitality diagnostics. Through the utilization of machine learning regression techniques such as PLSR or GPR, a comprehensive examination of the relationships between individual parameters and the reflectance of various wavelength ranges will be implemented.

Expected results

The results of the analysis are expected to provide reliable information on the relation of different biomarkers to the imaging spectroscopy signal using the ASD Plant Probe with Leaf Clip. Strong correlations are expected for the pigment-based biomarkers chlorophyll and carotenoids and the spectral signal in the VNIR wavelength range, so that conclusions on photosynthetic performance and thus energy metabolism can be drawn from the pigment ratios, which can reveal stress states. Strong species-specific differences in pigment ratios are expected, with higher chlorophyll content in English oak compared to European beech. For deciduous trees, multiple measurements during the vegetation period will provide information on species-specific senescence in addition to stress responses. Furthermore, correlations with leaf water content in the SWIR range, indicating drought stress, and phenolic compounds, providing information on secondary metabolism (e.g. tannins) in the VNIR and SWIR range, are expected. Overall, a high variability of biomarker patterns is expected at the individual tree level, so that higher visible stress responses are expected in the sun-exposed areas of the tree tops and southern sample branches than in the shadier northern sample branches.

Outlook for the future

Since the spectral detectability of leaf internal physiological parameters is expected to decrease with the distance between sensor and canopy due to various disturbance variables (e.g. mixing with shadows and branches, tree movements, atmospheric influences), the next step is to investigate to what extent the relationships can be found between the spectral signal or vegetation indices and tree physiological biomarkers, indicating stress also apply to sensors with coarser spatial resolution. For this purpose, four different resolution levels will be investigated: sub-canopy range (crane), canopy range (UAV), stand level (aerial images), and satellite level (e.g., with EnMAP, PRISMA) and use upscaling methods to determine the best possible derivation of stand vitality for comprehensive vitality monitoring.

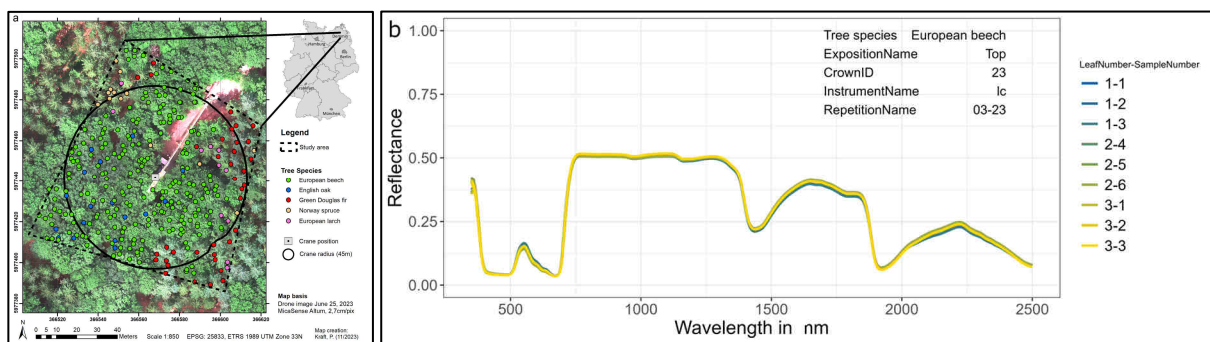


Figure (a) Study area and (b) example of leaf reflectance of European beech (3 leaves, 3 measurements each)

Validation of L2A Surface Reflectances Products Using ROSAS (RObotic Station for Atmosphere and Surface) In-situ Measurements

[Sophie Coustance](#)¹, Jérôme Colin², Arthur Dick¹, Olivier Hagolle^{1,2}, Aimé Meygret¹, Xavier Lenot³, Lucas Landier¹

¹ Centre National d'Études Spatiales, 18 Avenue Edouard Belin, CEDEX 9, 31401 Toulouse, France

² Centre d'Études Spatiales de la Biosphère, UMR 5126 CESBIO (CNRS/CNES/UPS/IRD), 18 Avenue Edouard Belin, CEDEX 9, 31401 Toulouse, France

³ CS GROUP, Zone d'aménagement Concerté de la Grande Plaine, 6 Rue Brindejonc des Moulinais, 31500 Toulouse, France

Keywords (5): ROSAS, surface reflectance, Sentinel-2, PRISMA, in-situ measurements

Challenge

Atmospheric correction is part of the Level-2 processing performed by space agencies for optical Earth observation missions and is essential to deliver Analysis Ready Data to the users. It corrects for aerosol and gas absorption and scattering to generate Level-2 surface reflectance products. At CNES the atmospheric correction of Sentinel-2 products is performed by the MAJA processor within the THEIA land data center and studies are underway to develop an atmospheric correction processor for hyperspectral data called CORATHYP. Significant efforts are also being made to validate the output Level-2 products. ROSAS automated ground stations provide long time series of in-situ surface reflectance measurements in the visible to SWIR spectral range. Validation of surface reflectance against these in-situ measurements provides insightful results on the performance of MAJA (Colin et al. *Remote Sens.* 2023, 15, 2665) and CORATHYP processors.

Methodology

Since 1997, an automated photometric station (ROSAS) has been installed at La Crau (France) by CNES originally for satellite calibration. The current instrumentation is a CIMEL photometer with 12 bands between 414 and 1640 nm mounted on a 10 m high pole. In 2017, a second station was installed at the Gobabeb desert site (Namibia) under the responsibility of ESA and CNES. Both stations are part of CEOS RadCalNet network. In 2021, a third station only dedicated to L2 products validation was deployed by CESBIO and CNES in Lamasquere (France) over cultivated fields. All stations share the same instruments and protocols. If the sky is cloudless, the photometer measures the solar irradiance and the sky radiance to characterize the optical properties of the atmosphere, and the ground upwelling radiances under varying angles corresponding to a 33 m diameter circle footprint. Assuming surface homogeneity, a BRDF model is fitted to the measures. The surface reflectances are then extracted at the satellite's sun and viewing angles and resampled to the satellite bands. To get hyperspectral reference measurements, a spectrum previously acquired with an ASD spectroradiometer for each site is fitted to the photometer measures.

MAJA Sentinel-2 surface reflectances were averaged over a 50 by 50 m square centered on the photometer. PRISMA images were processed with CORATHYP and the pixels corresponding to the photometers extracted. These data were compared to the photometer measurements.

Results

For Sentinel-2, the validation dataset covers the period from July 2017 to December 2021 for the La Crau and Gobabeb sites, and from June to November 2021 for Lamasquere, resulting in respectively 166, 181 and 13 comparison samples. For Sentinel-2 B2 to B4 band surface reflectances, the overall RMSE range from 0.004 to 0.011 on La Crau and Gobabeb sites. This corresponds to the expected uncertainties accounting for both the 3% spectral calibration specification of Sentinel-2 Top Of Atmosphere radiances, the 5% error budget of the ROSAS protocol and the errors of MAJA. For higher wavelengths Sentinel-2 bands, the RMSE are higher and range from 0.01 to 0.021, probably because the aerosol optical thickness is determined by MAJA using blue and red band criteria, so the errors in the aerosol optical thickness estimation are more important for higher wavelengths. The higher RMSE for Lamasquere account for higher uncertainties regarding the ROSAS protocol, that relies on the hypothesis of scene homogeneity which is questionable at the agricultural site of Lamasquere.

The validation comparing PRISMA surface reflectances generated by CORATHYP is still on-going and shows good accordance with in-situ reference measurements.

Outlook for the future

The ROSAS automated ground stations provide long time series of in-situ surface reflectance measurements which are valuable for L2 products validation and give insightful assessments of the performances of the MAJA and CORATHYP atmospheric correction processors. Moreover, the ROSAS instrumentation is evolving to improve the spectral resolution of ground measurements, extend the spectral range and meet the needs of future Earth Observation satellites. A hyperspectral photometer is under development with CIMEL by assembling three spectrometers to cover the 350 - 2500 nm spectral range with a resolution of 2 nm in the visible and up to 10nm in the SWIR. A prototype should be delivered by the end of 2024 and deployed at La Crau. In preparation for the upcoming thermal infrared missions such as TRISHNA (CNES/ISRO), SGB (NASA) or LSTM (ESA), a second 9 m high mast equipped with thermal infrared instruments has been deployed at La Crau.

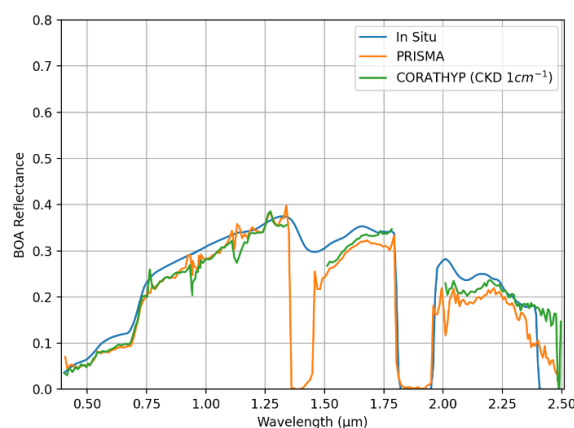


Figure (a) Comparison of surface reflectances retrieved by CORATHYP to the PRISMA L2 ones and to ROSAS in-situ measurements at La Crau

The Invisible Plant: Spectral Feature Analysis of *Tillandsia landbeckii* In The Atacama Desert

[Fabian Reddig](#)¹, Alexander Jenal¹, Christoph Hütt¹

¹ University of Cologne, Department of Geography, Germany

Keywords (5): Shortwave Infrared (SWIR), Upscaling, Atacama Desert, *Tillandsia*

Challenge

Reliable remote sensing of *Tillandsia landbeckii*, endemic to the Atacama Desert, is challenging and has not yet been solved to this day. Due to its morphology and spectral properties, closely resembling the surrounding inorganic environment, the shortwave infrared (SWIR) domain appears to be the most suitable solution for a monitoring approach. For large-scale remote sensing of *T. landbeckii* satellite data is indispensable, as UAV-based methods only capture small-scale areas. Unfortunately, satellite sensors like PlanetScope and Sentinel-2, inadequately represent the SWIR (see figure), leading to missed opportunities. This 'spectral gap' complicates state-of-the-art monitoring. While we collected spectral data at various scales and resolutions, the challenge lies in interpreting and exploiting this data, especially when dealing with lower pixel resolution. Therefore, the challenge was to identify the spectral features unique to this plant species for further analysis approaches.

Methodology

During our extensive field campaign in the Atacama Desert in March 2023, we have operated a comprehensive array of remote sensing instruments. We performed ground-based measurements with an ASD FieldSpec4 and collected different drone-based data sets with an UAV-VIS-NIR, and a unique UAV-SWIR camera sensor (Jenal et al. 2019. *Sensors*, 19(24)). To extend our in-situ measurements into a wider spatial extent, we concurrently requested data from satellite sensors to enhance our data collection: PlanetScope, Sentinel-2, Pléiades-Neo, WorldView3-SWIR, and high spectral and free-to-use EnMAP images. This effort between ground and satellite sources resulted in a multiscale dataset validated by the in-situ spectroradiometer measurements. With our unique SWIR camera system, equipped to capture high-resolution image data in specific SWIR bands using custom filters, we tried to tailor our data acquisition to precisely meet our research requirements, addressing the spectral gaps present in satellite-based systems. This UAV-acquired high-resolution data provides valuable, ground truth-like data for our subsequent analysis and validation of the satellite images. By comparing resampled UAV reflectance data with the original satellite measurements, we can assess the suitability of the respective satellite sensor for capturing the spectral signature of our target plant species. The processing and analysis were executed among with Agisoft Metashape Professional, GIS, R, and Python.

Results

To characterize the unique spectral features of *T. landbeckii* and its adjacent surfaces, we examined over 600 spectral samples collected during the field campaign from the plant itself and three types of surrounding surfaces: sand, roots, and gravel. These spectroradiometric data analyses revealed that *T. landbeckii* displays significant band depth differences from the inorganic materials nearby at

wavelengths of 1156, 1437, and 2090 nm. These results indicate that the detection of *Tillandsia* requires hyperspectral data from the EnMAP sensor, as multispectral sensors, are not feasible to capture its spectral traits, particularly in the SWIR region due to the aforementioned spectral gap. However, the EnMAP sensor's high spectral but rather too low spatial resolution precludes the identification of *Tillandsia*'s fine structures. In a first linear spectral unmixing approach, we could reach moderate results between fraction covers from a support vector machine classifier and a linear mixed model ($R^2 = 0.50$ at 30 m resolution and $R^2 = 0.67$ at 60 m resolution). This method allows for the decomposition of the spectrum of a single pixel with a low spatial resolution into its sub-signals, each symbolizing a unique surface reflection or endmember.

Outlook for the future

As existing large-scale remote sensing approaches reach their limits, our future efforts will be dedicated to improved estimation workflows of *Tillandsia* populations, aiming for detailed mapping and quantification in the Atacama. Understanding the distribution of its biomass could provide insights into the dynamics of fog and atmospheric humidity. Spectral analysis using our SWIR camera will pinpoint the optimal spectral band combinations for accurate species differentiation and canopy moisture estimation. We expect to get a more profound understanding of the role of *Tillandsia* in the Atacama ecosystem by combining structural and spectral characteristics. Therefore, our final objective is to extend the local observations to the broader Atacama region. The role of EnMAP's hyperspectral and WorldView-3's multispectral imagery will be crucial in this upscaling process, effectively linking UAV-based and satellite data sets.

Comparison of Spectral Reflectance across Different Sensors

Note: Resampled from ASD FieldSpec data

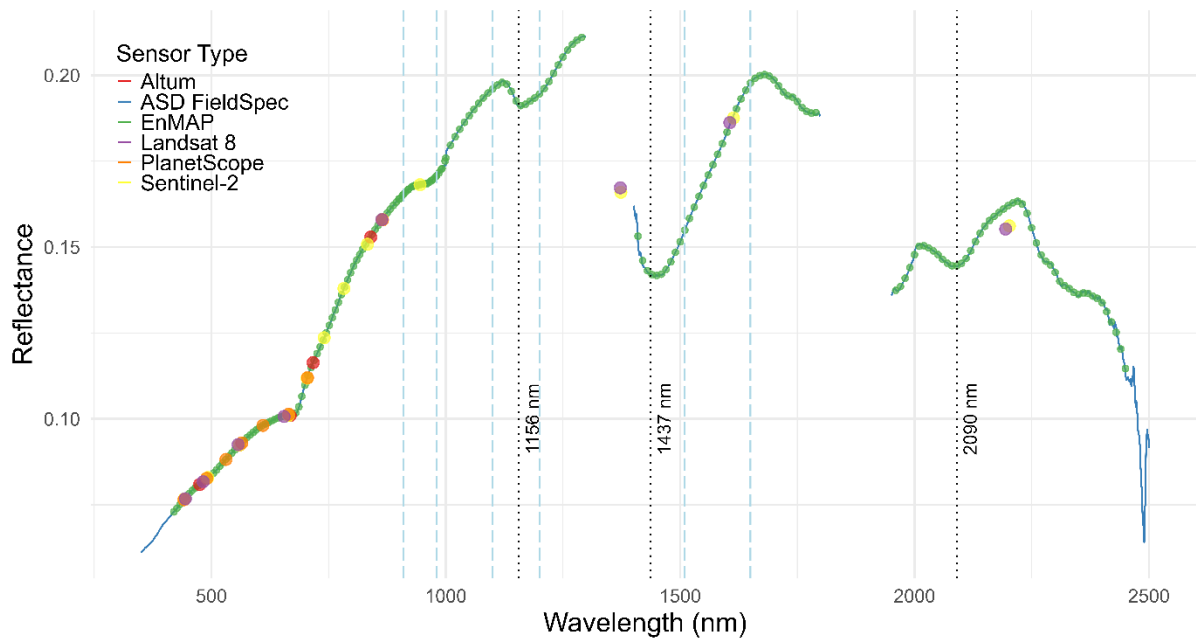


Figure Typical spectral reflectance of *T. landbeckii*. The figure is showing the spectral bands of different satellite sensors, resampled from ASD Fieldspec4 measurements. The black dotted vertical lines indicate the wavelength with the largest band-depth differences from the surrounding inorganic material. The blue dashed vertical lines are representing the SWIR filters flown on the field campaign in 2023.

Nitrogen Monitoring In Specialty Crops Of California; Case Studies In Almond And Grape

EARSel Valencia 2024

Abstract

Corresponding Author: [\[apourreza@ucdavis.edu\]](mailto:apourreza@ucdavis.edu)
<mailto:communication@africanremotesensing.org>

Alireza Pourreza¹, Momtanu Chakraborty¹, Parastoo Farajpoor¹, Sirapoom Peanusaha¹

¹ UNIVERSITY OF CALIFORNIA, DAVIS, DEPARTMENT OF BIOLOGICAL AND AGRICULTURAL ENGINEERING, USA

Keywords (5): Nitrogen, Agriculture, Hyperspectral, Radiative transfer models, Generalizable

Challenge (800 - 1000 characters incl. spaces)

Monitoring crops' nitrogen content is pivotal for precise nutrient management. Conventional lab analysis of Nitrogen is expensive and time-consuming, resulting in a lack of precision and an inability to determine spatial variability that is needed for variable rate application. Many studies using hyperspectral data apply data-driven approaches like machine learning or chemometrics, which rely solely on input-output relationships and need diverse and balanced datasets. Empirical methods can be biased to the specific condition of the dataset that was used to calibrate the model and lack information about important plant traits. Chlorophyll is often used as a proxy for Nitrogen in most studies, and the relationship between CHL and N is inconsistent across plants and phenological stages. In contrast, protein content emerges as a more reliable nitrogen estimator but necessitates the inclusion of SWIR data. Our goal is to construct a robust nitrogen estimation model that can generalize and transfer effectively across datasets from various locations and timeframes, mitigating these challenges.

Methodology (1200 – 1500 characters incl. spaces)

Our study involved the acquisition of an extensive dataset comprising leaf spectra (350-2500 nm) encompassing both reflectance and transmittance measurements across diverse phenological stages and geographical locations. To enhance the precision of our analysis and validate our models, we conducted comprehensive laboratory analyses to quantify essential parameters, including leaf area, fresh weight, dry weight, and nitrogen content of 306 samples for almond and 664 samples for grape. We systematically established and compared a variety of spectral analytics strategies for estimating leaf nitrogen. At the canopy level, we simulated almond tree and grapevine structures using HELIOS, which is a C++ simulation system for 3D geometry and plant canopy analysis. We employed leaf-level insights to generate synthetic hyperspectral imagery mimicking actual aerial view using LESS, a 3D radiative transfer model (RTM). We explored various hybrid modeling that takes advantage of physically based simulation and advanced AI. To assess the effectiveness of these models, we calculated statistical parameters such as R^2 , RMSE, and NRMSE. Throughout our comprehensive analysis, we systematically identified both the strengths and limitations inherent in various methodologies for monitoring canopy-level nitrogen content.

Results (1200 – 1500 characters incl. spaces)

We conducted a model assessment for estimating N mass normalized by either leaf mass or leaf area. Our findings showed a consistent correlation between leaf protein content retrieved by PROSPECT PRO and leaf nitrogen levels measured in the lab across all datasets with a Pearson's correlation coefficient of 0.55 and 0.67 for mass-based almond and grape, respectively. This correlation surpasses that of chlorophyll, which has a correlation coefficient of 0.45 and 0.21 with mass-based Nitrogen for almond and grape, respectively, determining protein as a more reliable nitrogen indicator. Furthermore, our results emphasized the critical role of the SWIR region (2100 – 2179 nm) in nitrogen estimation. Our exploration of various strategies for leaf-level spectral modelling highlighted the consistency of physically based models,

including hybrid models utilizing Random Forest regression with traits retrieved by PROSPECT Pro as input in comparison to empirical approaches. At the canopy level, we generated various tree structures for both grape and almond and employed various plant trait combinations to create simulations of aerial hyperspectral imagery similar to those we collected from actual orchards and vineyards. Our results revealed the substantial impact of tree structure along with the effect of biochemical components on canopy spectral variability.

Outlook for the future (800 - 1000 characters incl. spaces)

Looking ahead, we have multiple important areas of development in our study. By utilizing a larger dataset of labelled hyperspectral data, we are dedicated to further validating and fine-tuning our models. This expansion will enable us to provide more precise and reliable recommendations for improved nitrogen management practices, contributing to enhanced sustainability in agriculture. Overcoming the challenge of limited access to shortwave infrared (SWIR) data for monitoring purposes remains a priority, and we will explore innovative solutions to address this issue. Moreover, we are dedicated to the continued refinement of radiative transfer models (RTMs) to better suit the unique needs of California's specialty crops. Our goal is to provide a comprehensive framework that will provide the agricultural industry with state-of-the-art tools for future nutrient management methods that will be more sustainable and effective.

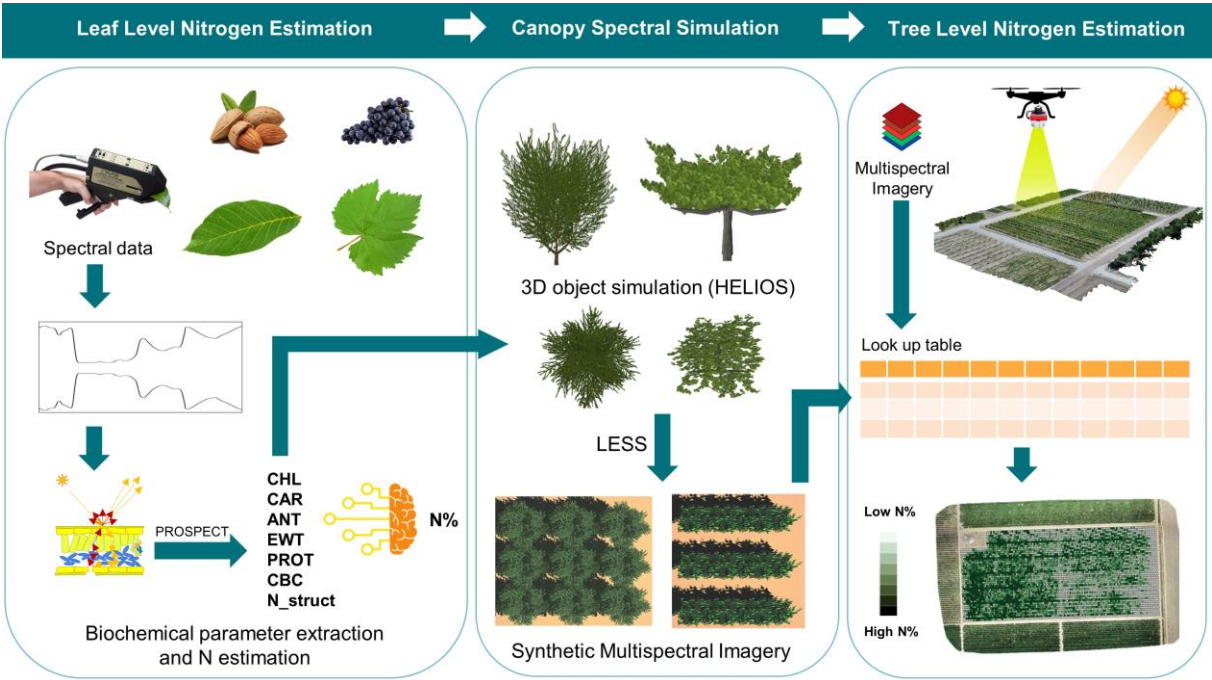


Figure: Graphical abstract for Nitrogen estimation in speciality crops in California

Understanding The Potential For Hyperspectral Remote Sensing Supporting Peatland Restoration Projects

Michael Williams¹, Alice Burrell², Richard Chiles³

¹ CGG U.K. Services Ltd., CGG Crompton Way, Crawley, Surrey, United Kingdom RH10 9QN

Keywords (5): Earth Observation, Peatland Restoration, Hyperspectral, Machine Learning, PRISMA

Abstract: Peatlands are a wetland environment located across many of the world's climates and have a number of ecosystem services, from biodiversity to water purification. They are also vital for the world's carbon budget, covering just 2.84% of global landmass (4 million km²), yet it is estimated that they hold 33% of the world's carbon. However, peatlands are under threat from anthropogenic activities which disrupt the water balance of these ecosystems and change their land-use, resulting in reduced function leading to the loss of carbon storage capabilities and release of GHG emissions into the atmosphere. It is thought that combating the threat against peatlands is one of the most important interventions for halting climate change. Therefore the monitoring of peatland environments is vital for informing management practices which prevent the loss and degradation of peatland environments.

Due to their vast expanse and often remote location, the monitoring and management of peatlands is an ongoing challenge. Current monitoring practices require in-field measurement of peatland depth and peatland condition, often using discrete point sampling. Yet this process is inefficient with poor prospects for high temporal monitoring. Remote sensing could offer a feasible solution which allows larger areas of peatland to be repeatably monitored for changes in peatland depth and peatland condition ensuring restoration activities can be prioritised.

CGG undertook a research study for the capabilities of spaceborne spectroscopy for the monitoring and management of peatland health. The objective of this study was to train a model using hyperspectral and environmental input data to predict peat depth. This model was built upon an extensive Peatland Action dataset collected across Scotland that was acquired through in-field measurements of peat depth and peatland condition (e.g. disturbed, near-natural, forested etc). Hyperspectral data covering approximately 10,000 ground samples was downloaded to temporally match the in-field data collection. Following extensive pre-processing, hyperspectral products including Narrowband Vegetation Indices (NVIs), reflectance and Principle Components were generated from PRISMA data. These hyperspectral outputs along with Digital Elevation Model (DEM) parameters were used as predictor variables for Extreme Gradient Boosting (XGBoost) machine learning.

Model evaluation revealed that the incorporation of hyperspectral data enabled prediction of peat depth with an approximate error of 0.40-0.70m across different PRISMA tiles. The most successful prediction was made across South West Scotland ($R^2=0.67$; Mean Average Error = 0.70m), where peat depth across a number of sites ranged between 0.00m – 7.00m, the model was able to predict the true depth to within ± 0.70 m. Feature importance analysis identified both DEM parameters and NVIs to be highly influential within model iterations.

These results demonstrate the potential that hyperspectral remote sensing could have for the monitoring of peatland condition globally. This methodology could contribute towards a tool for stakeholders to routinely monitor the depth and subsequent condition of peatlands over large geographic areas. Model performance is still limited, and questions could be raised about the accuracy and repeatability of remote sensing in comparison to in-field monitoring. However, with incorporation of further hyperspectral analysis, this methodology could support management decisions and help protect peatland ecosystems.

Exploring Sequential Machine Learning Models Regarding Generalisation Opportunities For Hyperspectral Data Processing

Maximilian Langheinrich¹

(Style: Authors, *presenting author underlined*)

¹ German Aerospace Center, Department Photogrammetry and Image Analysis, Germany
(Style: Affiliations;)

Keywords (5): Earth Observation, Hyperspectral, Machine Learning, Deep Learning, Generalisation

Challenge (800 - 1000 characters incl. spaces)

Currently we are perceiving an advent of a new period of hyperspectral sensing from space. The number of spaceborne spectrometers with very high resolution is constantly increasing, with missions already operational i.e. DESIS, PRISMA, EMIT and EnMAP as well as upcoming missions like NASA's SBG.

With the increasing number of available hyperspectral data from a multitude of different sources, the need for algorithms that are able to tackle the processing of data from different sensors with variable configurations is becoming more and more obvious.

While state-of-the-art machine learning algorithms, in particular models based on neural network architecture, are constantly improving and outperforming traditional approaches, regarding a multitude of different applications i.e. atmospheric correction, classification, spectral unmixing etc., they usually are tightly tailored to one specific sensor configuration / mission.

Taking the high cost in terms of training time and need of data into account, the possibilities of the development of more generalized algorithms should be explored, to exploit the availability of data from different sources and enable better comparison and fusion of data from different hyperspectral missions.

Methodology (1200 – 1500 characters incl. spaces)

The proposed work explores the feasibility of sequential deep learning models, in particular of the transformer architecture, also known as large language models, for the application on hyperspectral data from satellite-based remote sensing missions.

Looking at the individual pixels of that kind of data, the single spectrum can be seen as sequential in nature, similar to i.e. sentences, time series or DNA sequences. Large language models like transformers exhibit certain design concepts that render them very worthwhile for their application on hyperspectral data. Positional encoding and attention mechanism should be able to encode and learn inter-wavelength relations, also known as spectral features of distinctive spectra. Possibilities to provide networks of that particular architecture with sequences of arbitrary input size, facilitate the process of generalisation of one particular algorithm to several different sensor configurations. Probabilistic output layers can inherently catch the accuracy of the trained model on basis of a certain sample distribution of the outputs, which enables simultaneous delivery of uncertainties of the resulting spectral data.

The assess these opportunities hyperspectral data from different satellite missions will be prepared and input into different sequential deep learning models, enabling the comparison of computation performance and result accuracy.

Expected results (1200 – 1500 characters incl. spaces)

It is expected that different architectures will perform differently on the composition of heterogeneous sensor data. The assessment will be based on the performance on specific tasks i.e. atmospheric correction, classification, spectral unmixing.

While the inter-comparison of the network outputs will reveal the aptitude for their application on hyperspectral satellite remote sensing data. Further it will enable to analyse the different architectures in terms of how they learn their specific tasks and data, possible revealing certain spectral correlations within their parametrization, which may facilitate the exploration of new spectral features that may not be easy to grasp by human perception.

The results will be presented in terms of different quality metrics as well as intuitively understandable graphs and visualizations of the underlying processes.

The insights given in this analysis will enable the author to identify potential candidates for further and in-depth development of hyperspectral processing neural networks, with a strong focus on sensor-agnostic performance, transparent and understandable learning strategies, with combined uncertainty and value estimation.

Outlook for the future (800 - 1000 characters incl. spaces)

The identification of certain architectures and successful follow-up development may enable a multitude of applications. Apart from the opportunity to tackle the “classical” before-mentioned tasks for a multitude of sensor simultaneously, the usage of deep neural networks in general, will opens up several deployment and processing scenarios that would hardly be possible by the usage of commonly applied algorithms:

On-platform and real-time processing of hyperspectral data, frequent global scale processing of spatially and spectrally high-resolution hyperspectral data, data exploration in terms of information and knowledge extraction from the networks itself etc.

This development will hopefully facilitate the combined and wide-spread use of the hyperspectral data in the future and enable an easy utilization of all data enable to increase the collective knowledge of the Earth and its surface to a great extent.

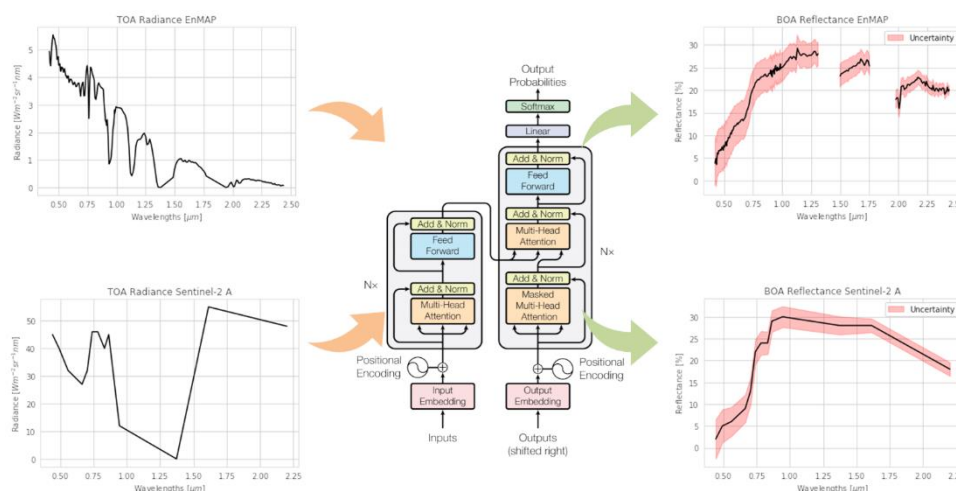


Figure Possible application (atmospheric correction) for sequential neural networks for hyperspectral data

Developing an automatic approach for validating fractional cover of soils in agricultural fields using UAV and cellphone images

Kevin Kühl¹, Paul Karlshöfer¹, David Marshall Ingram¹, Pablo d' Angelo¹, Uta Heiden¹

¹ German Aerospace Center (DLR), Earth Observation Center (EOC), Weßling, Germany

Keywords (5): Fractional Cover, Validation, UAV, EnMAP, CNN, SegVeg

Challenge (800 - 1000 characters incl. spaces)

Fractional Vegetation and Soil Cover (fCover) is an important land surface parameter especially, in agricultural systems. It provides quantitative cover of photosynthetically active vegetation (PV), non-photosynthetically active (NPV), and bare soil (BS) to serve the data needs for soil parameter modeling, soil erosion monitoring and the identification of land degradation. Further, it supports the observation of the impact of climate-friendly tillage practices on carbon stocks in agricultural systems (farming practices). With the increasing accessibility of hyperspectral data, the mapping of fCover is possible with significant accuracy due to the high spectral information content, especially in the SWIR wavelength region. Thus, large-scale validations are becoming necessary. However, validating fCover is challenging because so far ground data availability is very limited and fragmented. Nevertheless, for operational L3 processors, large-scale validation approaches are necessary and required to provide reliable accuracy and uncertainty measures for the land product. At the same time, the validation approach should be easy to implement, operate globally and should be cost and time-efficient. The idea of this study is to test and enhance a fCover validation method that is suitable to validate the separation between bare soils and non-photosynthetically active vegetation (NPV) with the perspective of transferring this approach in space and time.

Methodology (1200 – 1500 characters incl. spaces)

The idea is to use a deep learning model that produces fCover abundance information from RGB images, such as from UAV and cellphone images. Once the model is robust and transferable, it can be used for future validation campaigns by using RGB images from the validation area. Pioneer work has been done by a research group in France (INRAE) that have prepared the VegAnn dataset and developed the two stage SegVeg approach using RGB images (Serouart, Mario et al. 2022, Madec et al., Scientific Data, 2023). First, the whole RGB image is classified into a background and vegetation mask using a U-Net deep learning network with encoder-decoder architecture (semantic segmentation). Second, the predicted vegetation pixels are classified into PV and NPV using SVM. Both binary model outputs are merged to create a 3-class mask that provides pixel-wise information about PV, NPV, and BS.

In this study, we test and adapt this approach with priority to separate NPV and BS. The first step is the development of a suitable database to train the used convolutional neural network (U-Net). The tests start with RGB images of different cellphones and RGB images from the DJI Air 3 UAV camera system. The non-homogeneous images pose a particular challenge to equally capture different brand-specific image software optimization. Further, most of the soils contain stones that additionally need to be considered. To overcome these challenges, preprocessing steps are required. Recorded images have strong geometric distortions which made it necessary to crop the outer margins up to 30% depending on the

acquisition height. Out of each preprocessed image, 10 patches with a size of 256*256 pixels are randomly cut out for labeling. To implement a consistent and standardized labeling workflow the Software "Sample Point" with an equally distributed 7*7 grid was used. In the proposed method it will be tested if the combination of a convolutional neural network and support vector machine can distinguish PV, NPV and BS based on different image sources.

Results (1200 – 1500 characters incl. spaces)

So far, we have just preliminary results. There are fCover results from several EnMAP images across Germany. For this purpose, we used an in-house processor that retrieves NPV, PV and BS on a subpixel level. The validation is done per agricultural field, so we assume to have constant values across a field. This makes it possible to compare these results with an RGB image transect acquired by an UAV. For the model development, we created a database composed of 268 cellphone images from 5 different individuals, areas and times during the day and year with a visible variability in brightness. Further, we used the UAV and tested different flight heights. The best balance between area coverage and separability of fCover was at an acquisition height of about 5 meters. The first results reveal the general suitability of the proposed approach. However, additional classes need to be considered such as stones and shadow. Shadow is creating a large spectral/brightness variety that needs to be incorporated. Since semantic segmentation classifies each pixel, we will first evaluate the model accuracy by, a) using three standard classification metrics, Precision, Recall and F-1Score to quantify the performance at the class level. In addition, the overall F-1 score and the overall accuracy were calculated for a more global evaluation of the segmentation performance. If sufficient model robustness, accuracy and reliability are achieved, we will feed the model with UAV data of large sites for a real accuracy assessment of the outcome of our fCover processor developed at DLR.

Outlook for the future (800 - 1000 characters incl. spaces)

The successful validation of the DLR fCover products is of major importance. It is planned to use the validated fCover abundance maps for several purposes. Bare soils are exposed to erosion effects as well as to carbon sequestration processes that should be prevented for more carbon-conserving agriculture. In contrast, soils with dry vegetation are still protected from erosion due to the root zone. Thus, the duration of soil exposure is one parameter describing the soil quality and health. Additionally, we use the validated fCover products for a data fusion approach in which the EnMAP-based fCover outputs are used to improve Sentinel-2 based fCover products. Since Sentinel-2 does not have enough spectral information in the SWIR to distinguish between BS and NPV, EnMAP-based products can help to develop a deep learning-based model. This work will be presented by P. Schwind et al., 2024 at the EARSeL. In the future, it is planned to increase the data base for the U-Net model, including also the worldwide distributed VegAnn data set and new cellphone images from regions that are still underrepresented.

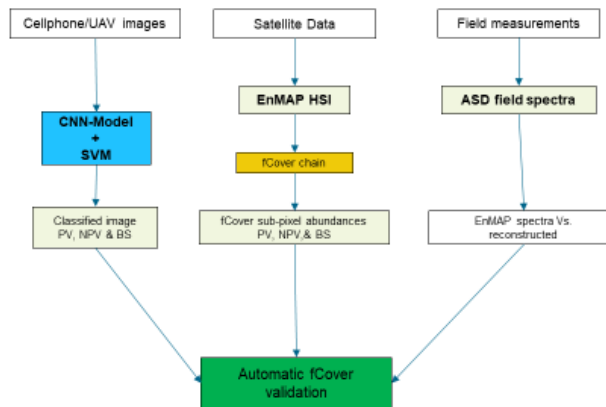


Figure (a) Integration of proposed method in the fCover framework.

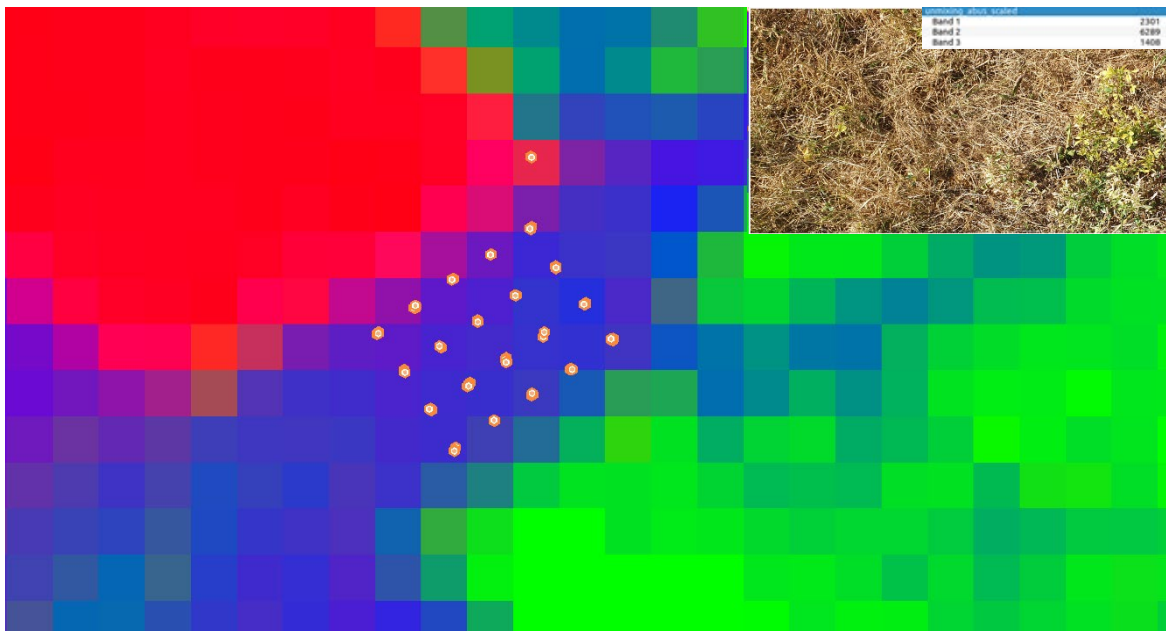


Figure (b) The basemap is a fCover sub-pixel abundance map. Bare Soil (red), NPV (blue) and PV (green). Orange dots represent the location of recorded cellphone RGB images that are used for the validation. Example image top right corner + derived subpixel fraction of each class.

Leaf structure matters for field evaluation of chlorophyll content with portable meters

EARSel Valencia 2024

Abstract

Corresponding Author:

zuzana.lhotakova@natur.cuni.cz

Zuzana Lhotáková¹, Eva Neuwirthová¹, Markéta Potůčková², Lucie Červená², Lena Hunt¹, Lucie Kupková², Petr Lukeš³, Petya Campbell⁴, Jana Albrechtová¹,

¹ Charles University, Faculty of Science, Department of Plant Experimental Biology, Czech Republic

² Charles University, Faculty of Science, Department of Applied Geoinformatics and Cartography, Czech Republic

³ Global Change Research Institute of the Czech Academy of Sciences, Czech Republic

⁴ Joint Center for Earth Systems Technology, NASA/Goddard Space Flight Center, Department of Geography and Environmental Sciences, USA

Keywords (5): SPAD; Dualex; CCM-300; MultispeQ; leaf reflectance

Challenge

Leaf chlorophyll content (Chl) is a widely used indicator of plant physiological status and phenology, which is directly connected to photosynthetic performance. Challenges remain in the field consistent measurements to obtain ground truth at the leaf level, although there are a number of portable devices enabling the non-destructive assessment of Chl and the measurement of a large numbers of samples in remote areas to obtain representative estimates, and save the time and labour required for laboratory pigment assessment. Most instruments are calibrated for flat, dorsiventral leaves. However, less attention has been paid to the performance of portable meters on leaves with special anatomy such as narrow grass leaves and needles. The goal of this study was to evaluate the relationship between optically (Chl_{opt}) and laboratory-determined 'absolute' leaf chlorophyll (Chl_{abs}) content for three groups of leaves differing in anatomical structure from the perspective of remote sensing applications.

Methodology

Three leaf anatomical types were studied: laminar leaves of deciduous woody species (24 species), grass leaves (four wild species), and needles (Norway spruce). Sampling was conducted at least at three times during the growing season: in the Botanical Garden of Charles University in Prague, in a floodplain forest in southern Moravia, in a relict alpine-arctic grass tundra in the Giant Mountains and in a spruce forest in the Beskydy Mountains, Czech Republic. Chl content was measured with four portable meters (CCM-300, SPAD, Dualex, and MultispeQ) and determined biochemically from dimethylformamide extracts. Leaf reflectance was measured using an ASD FieldSpec 4 Wide-Res spectroradiometer with a contact probe and chlorophyll indices were calculated (Datt2, NDChl, RMSR and Vogelmann). Leaf mass per area (LMA) was evaluated for all leaves, and in a sub-sample, leaf anatomy was quantified from cross-sectional images. We used PCA of structural traits (LMA, anatomy), Chl_{abs} and Chl_{opt} to elucidate the effect of internal leaf structure on portable meters readings. Statistical models for relationships between Chl_{abs} , and Chl_{opt} and vegetation indices including linear, logarithmic, and polynomial regression equations were built. The best performing models were selected according to the highest R^2 and lowest RMSE. The models for laminar leaves were validated on the independent dataset.

Results

Leaf anatomy was reflected in the LMA, which increased from laminar leaves to grasses and needles (5.90; 9.62; and 16.66 mg · cm⁻², respectively). For laminar leaves, PCA revealed that portable meter readings were rather independent from LMA, leaf thickness and palisade parenchyma thickness. The relationship between Chl_{obs} and Chl_{opt} measured by fluorescence-based CCM-300 for all leaf types showed weak performance (R²=0.43). When the leaf structure was considered, the models improved for laminar leaves (R²=0.92) but maintained low performance for grass leaves and needles (both R²=0.45). Among the transmittance-based portable meters, only SPAD with the smallest field of view could be used on laminar and grass leaves together and the generic model could be constructed (R²=0.42). The result was similar to CCM-300: the models performed well for laminar leaves (R²=0.86), but for grasses the model performance was weak (R²=0.32) and species-dependent. Chl_{obs} was predicted based on the independent dataset from floodplain forest from portable meter readings and vegetation indices. In all cases, Chl values predicted by the linear models had the lowest RMSE compared to logarithmic and polynomial models. The fit of predicted to measured Chl values of the respective model training and validation reached R² of 0.75 or higher for portable meters (0.75; 0.82; 0.84 and 0.75 for CCM-300, SPAD, Dualex, and MultispeQ, respectively) and over 0.85 for vegetation indices (0.87; 0.86; 0.88 and 0.86 for Datt2, NDChl, RMSR and Vogelmann, respectively).

Outlook for the future

We demonstrated that deriving an accurate generic model for relationship between Chl_{obs} and Chl_{opt} is not possible for such heterogeneous leaf types regardless of the principle of chlorophyll meter measurement (transmittance or fluorescence). Portable meters performed very well for laminar leaves and grasses with wider leaves. However, there are several constraints when used on conifer needles and grasses with narrow leaves. It is good practice in all cases to perform a biochemical pigment assessment on a subset of samples for calibration. We strongly recommend the calibration step especially for needles and narrow grass leaves. The present study was limited to leaf level measurements. Quantitative evaluation of the bias in canopy Chl content assessment using imaging spectroscopy, when ground-truth is obtained only with portable chlorophyll meters, is needed to inform on the trade-off between the speed, feasibility, and accuracy of the chlorophyll ground truth sampling.

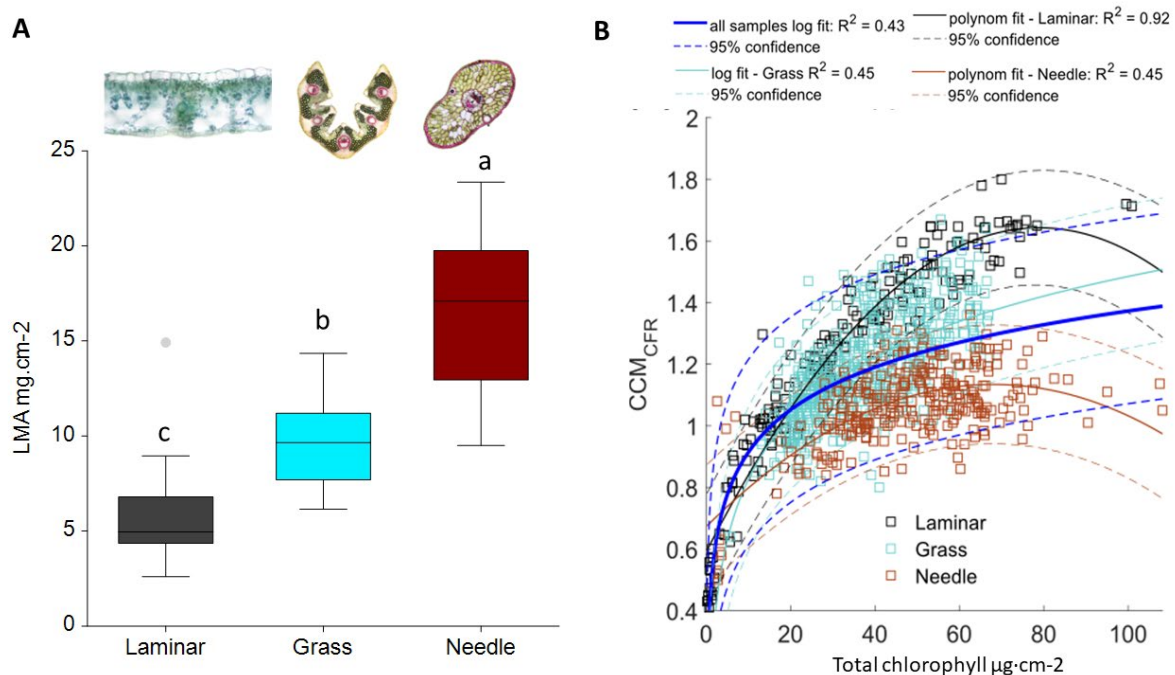


Figure: Representation of the three studied leaf types: laminar and grass leaves, needles, and the relationship between CCM-300 readings (CFR) and laboratory determined total chlorophyll content. (a) Leaf mass per area

(LMA) with illustrative microphotographs of leaf cross section (not in scale). (b) Generic relationships between Chl extracted in the lab (Total chlorophyll) and CCM-300 measurements for all leaf types. The thick blue line in (b) corresponds to the best performing generic model. The black line corresponds to the best performing model for laminar leaves; the cyan line corresponds to the best performing model for grass leaves, and the red line corresponds to the best model fit in needles. Dashed lines of each colours correspond to 95% confidence intervals.

Monitoring Grassland Traits – from Multispectral to Hyperspectral Approaches

Anne Schucknecht¹, Sophie Reiner mann², Francesco Pietro Fava³, Giovanni Argenti⁴, Ralf Kiese⁵, Anita Bayer¹

¹ OHB System AG, Image Simulation and Processing Team, Germany

² University of Würzburg, Department of Remote Sensing, Germany

³ Università degli Studi di Milano, Department of Environmental Science and Policy, Italy

⁴ Università degli Studi di Firenze, Department of Agriculture, Food, Environment and Forestry, Italy

⁵ Karlsruhe Institute of Technology, Institute of Meteorology and Climate Research – Atmospheric Environmental Research, Germany

Keywords: Hyperspectral, EnMAP, Grasslands, Biomass, Plant Nitrogen

Challenge

Climate and land use change affect the provision of ecosystem services of grasslands as well as the dairy and meat production. Remote sensing allows the assessment of regional carbon and nitrogen (N) cycles via spatially explicit information on grassland traits (e.g., biomass, plant N) and thus can support the optimization of grassland management. However, the development and/or validation of retrieval algorithms relies on the availability of remote sensing observations and related in-situ reference data, which is often a challenge. In this study, we aim to explore the potential of the recently launched hyperspectral satellite EnMAP (Environmental Mapping and Analysis Program) for the retrieval of plant traits in grasslands. Due to the lack of corresponding field data for EnMAP acquisitions, we first developed different retrieval approaches based on Sentinel-2 (S2) data. Then, we developed hybrid models for EnMAP data and assessed their plausibility in comparison to S2 models.

Methodology

We used a multi-temporal **field dataset** from 11 differently managed pre-Alpine grasslands in Southern Germany for the development and validation of S2-based retrieval approaches. Sites were sampled during the growing seasons 2019 and 2020 within 20 m x 20 m plots (each sampled at 4 subplots of 0.5 m x 0.5 m) to obtain dry weight of above ground biomass (AGB) and plant N concentration (N%).

Based on field and associated **S2 data**, we developed and compared **empirical machine learning models** (Random Forest, RF; Artificial Neural Network, ANN) for estimating AGB and N% using a 6-fold cross-validation with 10 iterations and testing different predictor variables (reflectance values, vegetation indices, day of year, days since last cut or start of season (SOS)).

Additionally, we developed **hybrid retrieval models for S2 and EnMAP** data, as they do not require field data for training. The radiative transfer model PROSAIL-PRO (parameterized for grasslands based on field data/literature values) was utilized to generate large look-up tables (n=5000) of sensor-specific spectra and associated RTM parameters. AGB, N%, and area-based canopy N content (CNC) were calculated from RTM parameters. The look-up tables were used to train (75%) and test (25%) a machine learning retrieval algorithm (RF). The S2-based hybrid AGB model was validated with pre-Alpine field data.

Trained empirical and hybrid models were applied to S2 and EnMAP images of the study region to compare models on a regional scale.

Results

Empirical S2-based machine learning models can estimate AGB and N% in pre-Alpine grasslands. In general, ANNs show a better performance. The best models using all predictor variables achieved for AGB a R^2_{cv} of 0.62 (ANN) and 0.57 (RF), and a $RMSE_{cv}$ of 59 g m⁻² (ANN) and 64 g m⁻² (RF), and for N% a R^2_{cv} of 0.70 (ANN) and 0.63 (RF), and a $RMSE_{cv}$ of 0.48 wt.% and 0.53 wt.% (RF). The predictor days since last cut/SOS improved the performance of AGB models and was the most important predictor for N%.

First tests with **hybrid modelling** indicate a better performance in testing of **AGB** models when EnMAP data is used ($R^2_{test} = 0.86$, $RMSE_{test} = 70$ g m⁻²) compared to S2 data ($R^2_{test} = 0.76$, $RMSE_{test} = 87$ g m⁻²). The validation of the S2-based hybrid AGB model with field data yielded a R^2_{val} of 0.31 and a $RMSE_{val}$ of 85 g m⁻². The comparison of estimated AGB maps for 27/06/2022 shows a good agreement of spatial pattern for the empirical S2, the hybrid S2 and the hybrid EnMAP model (Fig. 1), with a higher similarity between the two S2 models.

The S2 and EnMAP-based hybrid models in their current parameterization do not work well for the estimation of **N%** ($R^2_{test} < 0.15$, $RMSE_{test} > 0.97$ wt.%), while they yield better results for **CNC** (S2: $R^2_{test} = 0.63$, $RMSE_{test} = 4.3$ g m⁻²; EnMAP: $R^2_{test} = 0.78$, $RMSE_{test} = 3.5$ g m⁻²). The reason might be the scaling with leaf area index, which is well estimated with the hybrid models.

Outlook for the future

Our study showed a good performance of empirical S2-based models for the estimation of AGB and N% in pre-Alpine grasslands, especially when considering the seasonal canopy development via the predictor days since last cut/SOS. First tests with hybrid models indicate that the RTM parameterization is challenging and there is room for improvements. In a next step, we will try to improve the hybrid models. For this, we will test the utilization of data reduction techniques for EnMAP data, the inclusion of active learning techniques and the use of other machine learning approaches like e.g., Gaussian Process Regression.

Furthermore, we will test the temporal and spatial transferability of the developed empirical and hybrid S2 models to grassland datasets from Northern Bavaria, Germany and the Emilia Romagna, Italy.

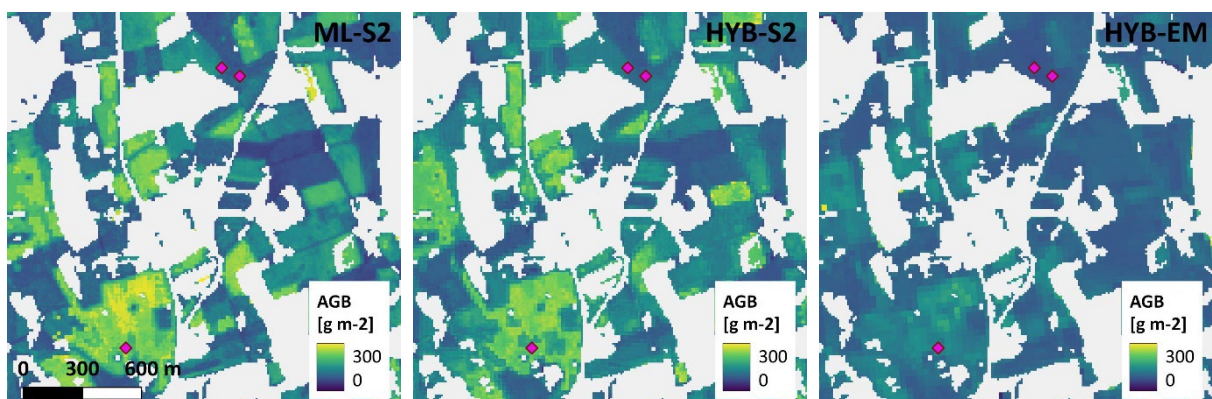


Figure 1 Spatial estimates of AGB for 27/06/2022 with empirical S2-based RF (left), hybrid S2 (middle), and hybrid EnMAP model (right) for a part of the pre-Alpine study region in Southern Germany. Non-grassland areas are masked out with Copernicus High Resolution Grassland Layer 2018.

Deep Learning based Semantic Segmentation for EnMAP-Box

Leon-Friedrich Thomas^{1,2}, Benjamin Jakimow², Andreas Janz², Patrick Hostert², Antti Lajunen¹

¹ University of Helsinki, Department of Agricultural Sciences, Finland

² Humboldt-Universität zu Berlin, Geography Department, Germany

Keywords (5): Artificial Intelligence, QGIS Plugin, Pixel Classification, Spectral Imaging, EnMAP

Challenge

With the growing variety of hyperspectral sensors such as EnMAP, PRISMA, or future missions like CHIME or SBG, as well as the presence of established multispectral sensors like Sentinel-2 and Landsat, there is a growing demand for advanced analytical methods to utilize the increasingly available spectral imaging data. In recent years, deep learning has gained significant attention and delivered impressive results in the realm of computer vision tasks, such as semantic segmentation. These models have also found extensive applications in research related to hyperspectral and multispectral imaging.

In order to ease the accessibility of deep learning models for spectral imaging analysis, we enhance the EnMAP-Box QGIS plugin with a novel application "Spectral Imaging Deep learning mapper - SpecDeepMap" that seamlessly integrates a deep learning-based semantic segmentation workflow. "SpecDeepMap" allows users to harness the power of deep learning with imaging spectroscopy data through a user-friendly graphical interface.

Methodology

Several geospatial and deep learning methods are integrated in this novel toolset. The add-on consists of three distinct processing algorithms, each corresponding to essential stages in the implementation of a deep learning model.

The initial processing algorithm, known as 'RasterSplitter', uses a spectral image raster and a raster label mask as inputs and divides them into tiles. Additionally, users have the option to specify regions of interest via a GeoJSON or shapefile, confining the raster processing to the defined geospatial boundaries.

The second processing algorithm, 'DeepTrain', uses the spectral image and label tiles as input. Users can employ this algorithm to train a U-Net model, featuring a ResNet-50 backbone. A U-Net model is well known for its suitability for semantic segmentation tasks, as well as ResNet-50 is known as a well-performing model backbone.

The third processing algorithm, 'DeepInterference', loads a trained semantic segmentation model and applies interference to the image files. This process predicts pixel classes within the images and generates an Intersection over Union (IoU) metric to assess the model's performance.

Results

The main result of this work is the add-on "SpecDeepMap" for EnMAP-Box including its algorithms, 'RasterSplitter', 'DeepTrain', 'DeepInterference'. It is foreseen to provide the add-on with the EnMap-Box plugin released on github in 2024. The functionalities of the developed plugin are demonstrated with a test dataset, using crop classifications and corresponding EnMAP images for a region of Interest in Germany.

In a first step we illustrate results obtained by utilizing different raster splitting methods, employing the 'RasterSplitter' algorithm. The algorithm allows the exclusion of invalid classification mask labels from further processing. This functionality is particularly relevant to filter larger areas in a satellite image, which don't show any occurrences of the classes for the semantic segmentation task.

The second step displays the training and validation loss of the selected U-Net with the ResNet-50 backbone, which was trained using the developed 'DeepTrain' algorithm. We present an overview of the training parameters used and how training parameters can be adjusted according to the respective classification needs.

The last step provides information on the performance of the trained model. We use the 'DeepInterference' algorithm to apply and evaluate on the test dataset. Mean IoU and IoU per class will be presented.

Outlook for the future

The final application is set to be released in 2024 through the EnMAP-Box. The integration of this semantic segmentation workflow can be viewed as an initial step to promote graphical user interface-based deep learning techniques for hyper- and multispectral imaging.

Future developments of our plugin may include providing different backbones for the U-Net model. I may further provide pretrained backbones tailored to EnMAP or multispectral sensors, such as Sentinel-2. Furthermore, the development of a "merge raster" tool, designed to seamlessly combine predicted image tiles into a continuous orthomosaic, holds significant promise as a prospective feature, moving the add-on towards analysis ready data (ARD) provision. Additionally, there's potential for implementing a tool for comparing different predicted orthomosaics, which would serve the purpose of generating a binary change mask.

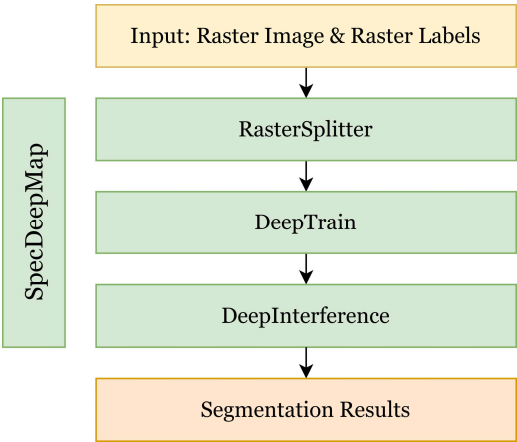


Figure 1 SpecDeepMap - Semantic Segmentation Workflow

Utilizing Hyperspectral Imaging Spectroscopy for the Identification of Potential Toxic Elements (PTE) in the Hyperaccumulator Plant *Brassica juncea*, with a Focus on Remediation.

EARSel Valencia 2024

Abstract

Corresponding Author:

friederike.kaestner@gfz-potsdam.de

Friederike Kästner¹, Theres Kuester¹, Hannes Feilhauer^{2,3,4}, Magdalena Sut-Lohmann⁵

¹ Helmholtz Centre Potsdam, GFZ German Research Centre for Geosciences, Telegrafenberg, Potsdam 14473, Germany

² Remote Sensing Centre for Earth System Research (RSC4Earth), Leipzig University, Talstr. 35, 04103 Leipzig, Germany

³ Helmholtz-Centre for Environmental Research (UFZ), Permoserstraße 15, 04318 Leipzig, Germany

⁴ German Centre for Integrative Biodiversity Research (iDiv), Halle-Jena-Leipzig, Germany

⁵ Institute of Geoecology, Department of Soil Science, TU Braunschweig, Langer Kamp 19c, 38106 Braunschweig, Germany

Keywords (5): potential toxic elements, hyperaccumulator plants, phytoremediation

Challenge (800 - 1000 characters incl. spaces)

Soil contamination with potential toxic elements (PTE) is a worldwide issue resulting from a variety of human activities, including industrial processes, agriculture, and mining. These activities release harmful elements into the environment, which can persist for extended periods and cause adverse impacts on both the ecosystem and human well-being. In response to these concerns, there is a growing demand for efficient and environmentally friendly remediation methods, one of which is phytoremediation. Phytoremediation involves the use of plants to naturally purify, detoxify, and eliminate contaminants from soil, air, or water. Moreover, there is a need for a reliable method to monitor the optimal duration of residence for hyperaccumulator plants like *Brassica juncea* using hyperspectral data, which is currently missing.

Methodology (1200 – 1500 characters incl. spaces)

In our research, we cultivated the hyperaccumulator plant *Brassica juncea* in three distinct greenhouse experiments, each involving different concentration levels. This choice was made due to the plant's remarkable tolerance to the accumulation of zinc (Zn), and nickel (Ni). We utilized a HySpex VNIR-1600 and HySpex-SWIR 320m-e hyperspectral sensor, which covers the spectral range from 408 to 2500 nm, for conducting hyperspectral measurements both in the field and in the laboratory. To monitor the accumulation process through hyperspectral imaging, we computed various vegetation indices (VIs) associated with metal-induced plant stress. These indices included TCARI/OSAVI, Chlorophyll Vegetation Index (CVI), Red-Edge Stress Vegetation Index (RSVI), Normalized Pigments Chlorophyll Index (NPCI), Red-Edge Inflection Point (REIP) and different pigment ratio indices (BGI, BRI, PPR). We applied a range of pre-processing techniques to the data, including using raw, smoothed, and brightness-corrected data. Furthermore, we investigated the relationship between the spectra with the corresponding indices and the measured potential toxic element content in the samples using a multivariate approach, specifically Random Forest Regression (RFR).

Results (1200 – 1500 characters incl. spaces)

The smoothed reflectance data from the hyperspectral image were initially aggregated into a spectral library. Various combinations of spectra, such as VNIR images and VNIR-SWIR images, along with their corresponding Vegetation Indices (VIs), were combined with the concentration of potentially toxic

elements (PTE) for the Random Forest Regression (RFR) model. The VNIR spectral library with the associated nickel concentration were first implemented in the RFR model to determine the spectral pre-processing with the highest R2 and lowest RMSE. The selected RFR parameters were then applied consistently in at least 20 repetitions. The initial outcomes indicated that these 20 repetitions run consistently yielded similar results. The significant spectral features across all models were identified in specific wavelength ranges, notably between 502 to 512 nm, 607 to 632 nm, 749 to 774 nm, 822 nm, 865 to 891 nm, 898 to 913 nm, and 963 nm. Additionally, the Vegetation Index NPCI was also of importance, as it frequently appeared in the top-ranking features among the 20 repetitions. For the VNIR spectral library combined with zinc concentration, the first derivative method emerged as the most effective spectral pre-processing technique, exhibiting the highest R2 values and the lowest RMSE. Subsequent repetitions unveiled important bands and band ranges between 414 nm, 552 to 556 nm, 800 nm, 825 to 840 nm, and 845 to 891 nm, as well as at 949 nm.

Outlook for the future (800 - 1000 characters incl. spaces)

With reflectance data obtained from hyperspectral imaging, we can already identify variations in spectral responses associated with different levels of potentially toxic element (PTE) accumulation within hyperaccumulator plants. As a result, we have the potential to use these crucial wavelengths and wavelength bands to enhance the efficiency of phytoremediation processes. This can be achieved by simplifying the analysis of extensive images for quicker PTE detection and even prediction. Additionally, a closer examination of Vegetation Indices (VI) and the averaged, well-established significant wavelengths bands, contingent upon leaf concentration, may offer insights into PTE-specific thresholds. These insights can help determine the optimal duration for *Brassica juncea*'s residence in the context of phytoremediation processes.

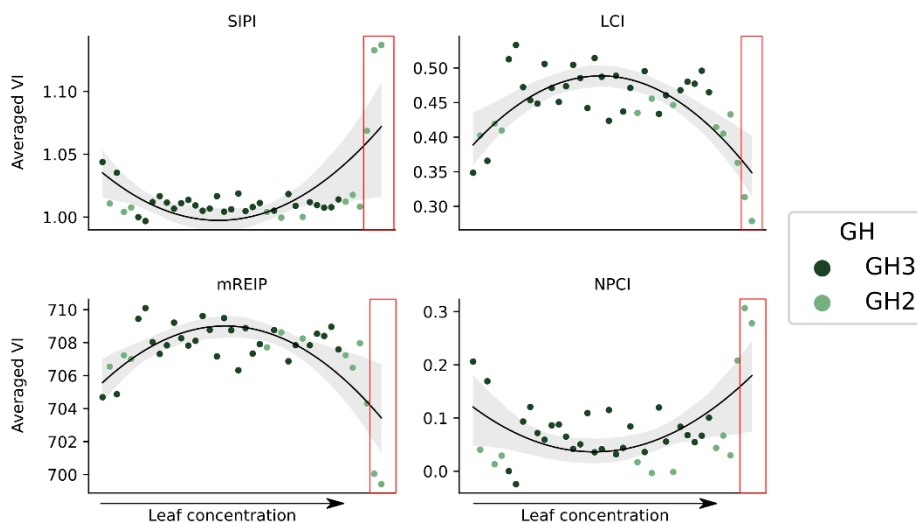


Figure: Four averaged VIs in order of rising leaf concentration and the possible threshold (red square)

Comparison Of Hyperspectral And Multispectral Remote Sensing For Improved Surface Soil Moisture Estimation

[Hadi Shokati](#)¹, Mahmoud Mashal¹, Aliakbar Noroozi², Ali Akbar Abkar³, Thomas Scholten⁴

¹ University of Tehran, Department of water engineering, Iran

² Soil Conservation and Watershed Management Research Institute, Agricultural Research, Education and Extension Organization (AREEO), Iran

³ Geographic Information System and Remote Sensing of Agriwtach Company, Netherlands

⁴ University of Tübingen, Department of Soil Science and Geomorphology, Germany

Keywords: Hyperspectral, Landsat, Multispectral, Sentinel, UAV

Challenge

Surface Soil Moisture (SSM) is a crucial component of soil moisture, encompassing the water content in the top layer of soil. Although this near-surface soil layer contains only a small part of the total soil water storage, it plays a fundamental role in various hydrological, biochemical, physiological, and agricultural processes. Consequently, monitoring the spatial and temporal variability of SSM is an indispensable prerequisite for both mitigating and adapting to the effects of climate change. Conventional methods for estimating SSM are often point-based, and due to the spatial and temporal variability of SSM, extrapolating data from a single point to a larger area result in lower estimation accuracy. An alternative solution is therefore to use remote sensing technology to estimate SSM.

Methodology

The aim of this study was to evaluate the comparative potential of multispectral and hyperspectral remote sensing data for SSM estimation. To this end, a combination of data sources was used, including multispectral imagery from the Sentinel-2, Landsat 8, and Landsat 9 satellites, as well as data acquired by a hyperspectral camera called Spectrocam. The Spectrocam can perform spectroscopic analyses in the wavelength range from 339.6 to 1028.8 nm, offering a spectral resolution of 0.35 nm. In this study, the research farm of the University of Tehran in Iran with an area of 100 hectares was selected as the study area. The study area had a gentle slope and the land use consisted of bare soil, alfalfa, wheat, and maize. While the satellites passed over the study area, the Spectrocam was simultaneously mounted on a Matrice 100 unmanned aerial vehicle (UAV), which conducted aerial imaging spectroscopy over the region. The SSM modeling was carried out for the years 2021 to 2023 using the Random Forest (RF) algorithm. To validate the results, 45 soil samples were taken at each data collection phase.

Expected results

The results showed that the hyperspectral data from Spectrocam outperformed the multispectral data from Sentinel-2 and Landsat in estimating the SSM and had a significantly stronger correlation ($R^2 = 0.87$). In contrast, the Landsat data showed superior performance with an R^2 of 0.66 compared to the Sentinel-2 data, which only achieved an R^2 of 0.49. The lower accuracy of the Sentinel-2 data can be attributed to the lack of a thermal band on this satellite. In addition, the results showed that the models developed in this study tended to overestimate SSM in regions with low moisture content and underestimate it in areas with high moisture content. This tendency is primarily related to the relatively large pixel size of the satellite, which leads to pixel non-uniformity and impurities. It is worth noting that the extent of overestimation and underestimation was less pronounced when using Spectrocam data compared to Sentinel-2 and Landsat.

Outlook for the future

In the future, remote sensing technology will continue to play a significant role in the monitoring of SSM. Advances in hyperspectral cameras and satellite sensors, as well as the integration of UAVs, will improve the accuracy of SSM monitoring. This technology will become increasingly important in precision agriculture and climate change mitigation and adaptation. Addressing accuracy issues will be a focus of future research. It is also worth comparing Spectrocam with existing hyperspectral satellites such as EnMAP, PRISMA, and EMIT, as well as with upcoming missions such as CHIME and PRISMA-2, to make further progress in SSM estimation.

Towards a Unified Data Model for Ground Based Surface Reflectance Measurements

EARSel Valencia 2024

Abstract

Corresponding Author: claas.koehler@dlr.de

Claas H. Köhler¹, David Marshall Ingram¹, Bringfried Pflug¹, Raquel de los Reyes¹

¹ German Aerospace Center, Remote Sensing Technology Institute, Germany

KEYWORDS (5): EARTH OBSERVATION, VALIDATION, HYPERSPECTRAL, DATA FORMATS

Challenge

Reliable earth observation data with known uncertainties have become an indispensable tool for most geoscientists. In particular, long-term time series derived from a combination of satellite instruments are essential to understand the impact of climate change and to devise effective mitigation measures. Satellite products have to be validated continuously to ensure that they are suitable for such datasets, optimally with the help of ground-based or airborne fiducial reference measurements (FRM). Although several networks (e.g. RadCalNet, Hypernets, AERONET) providing high quality FRM to the scientific community on a regular basis already exist, it is often cumbersome to use these data for continuous (automated) product validation. This is mostly due to the lack of a standardised data format including best practices for auxiliary data required for useful selection and integration.

Methodology

As scientists involved in the generation and validation of surface reflectance products from spaceborne instruments (EnMAP, DESIS) we focus our presentation on ground-based measurements suited to validate these products. Currently RadCalNet (<https://www.radcalnet.org>) and Hypernets (<https://www.hypernets.eu>) provide ground-based surface reflectance measurements on a regular basis. Additionally, RadCalNet & AERONET (<https://aeronet.gsfc.nasa.gov>) provide automated measurements of the atmospheric state, which are useful for analysing the performance of atmospheric correction algorithms that correct the apparent reflectance observed at top-of-the-atmosphere for absorption and scattering of atmospheric trace gases and aerosols. We propose a common data model for products similar to those distributed by these networks, which could be extended to include additional datasets if required. The HDF5 derived concept adheres to the CF conventions (<http://cfconventions.org/>) for climate and forecast metadata as closely as possible. The CF conventions define metadata that provide a definitive description of what the data in each variable represents, and of the spatial and temporal properties of the data. This enables users of data from different sources to decide which quantities are comparable, and facilitates integration of the data into applications. We demonstrate this with an exemplary Python implementation capable of extracting data from HDF5 archives relying exclusively on CF metadata, thus enabling users to read CF conform data independent of the specific file layout.

Results

We found that the CF conventions in their current form are well suited to store almost all datasets required within the context of surface reflectance product validation. The unobtrusive nature of the CF conventions leaves a lot of freedom for the actual product layout resulting in a low threshold for adoption. Some remaining questions remain, for example, the CF conventions lack potentially necessary standard names for some quantities specific to the use case at hand. However, this deficiency could be addressed

by cooperating with the CF standards committee and hence defining suitable standard names and best practices on how to store data for which no uniquely defined standard names exist. Additionally, some ambiguities exist, especially for datasets not commonly used in the climate and forecast context. This is especially true for Level 1 data, which is only partially addressed by the CF conventions. Here additional standardisation, either in cooperation with the CF standard committee or in a supplementary effort by the earth observation Cal/Val community, is required to finalise the current concept. On the software development side, we found a comparatively simple way to generalize the HDF5 / CF data model to other file formats. This concept allows to amend existing readers for non-HDF5 data products in such a way that they expose a CF compliant I/O interface to third-party applications. Thus, a thin software wrapper is sufficient to make existing products compatible with the proposed conventions.

Outlook for the future

One essential goal of this contribution is to enter into a discussion with interested parties on how to proceed towards a unified data format for surface reflectance FRM. Any agreed upon standard should allow easy integration of automated surface reflectance measurements into continuous calibration and validation activities for current and future earth observing satellite missions. Since we are aware that there have been a number of previous activities pursuing a similar goal, we would very much like to enter into a discussion regarding the current state of the respective activities with the intention of agreeing upon suitable next steps towards an accepted standard (or best practices). We believe that such a standard would be beneficial to the community and that it could elevate the quality of the data products we deliver. Additionally, it would help to foster the adoption of the excellent data provided by the various ground-based measurement networks even further.

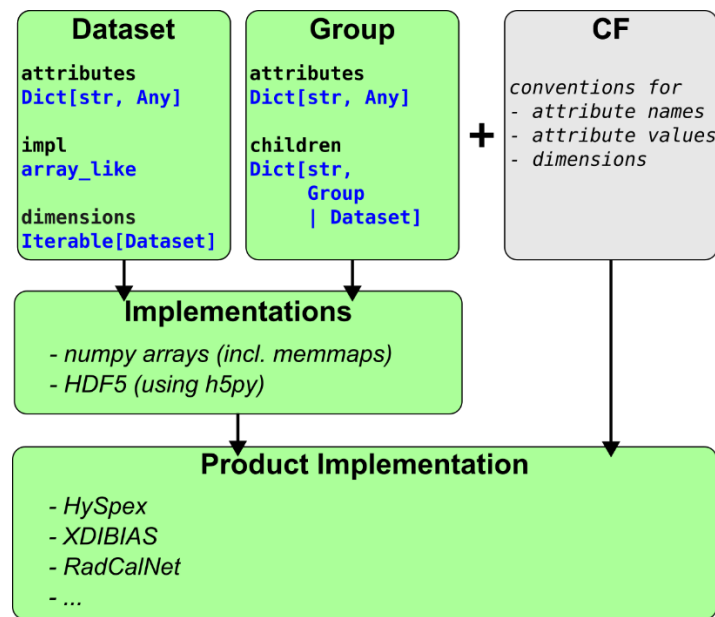


Figure Visualisation of the proposed data model

EUFAR – Current Status and Recent Development

Lucie Homolová¹, Ils Reusen², Jan Hanuš¹, Thomas Rhutz³

¹ Global Change Research Institute CAS (CzechGlobe), Czech Republic

² Flemish Institute for Technological Research (VITO), Belgium

³ Freie University of Berlin, Institute of Space Sciences, Germany

Keywords (5): research infrastructure, airborne, campaigns

Challenge (800 - 1000 characters incl. spaces)

Airborne remote sensing from manned and unmanned platforms play an irreplaceable role in atmosphere and land research, in scaling between in-situ phenomena and satellite observation, in calibration and validation of current and future satellite missions. To better coordinate the airborne research community in Europe, EUFAR – the pan-European network for airborne research infrastructures dedicated to environmental sciences was created in 2000. In 2017, EUFAR was transformed into an AISBL – an international non-profit association under Belgian law. The main objectives of EUFAR is to facilitate and promote transnational access to national airborne research platforms, instruments (including the imaging spectroscopy facilities) and data, reduce redundancy, fill the gaps and optimise the use of innovative airborne research facilities. The goal of this contribution is to present the current status and future activities planned within the EUFAR.

Methodology (1200 – 1500 characters incl. spaces)

Currently, EUFAR consists of 13 members and four partners from eight European countries. EUFAR members operate 13 research aircrafts for troposphere and land surface research. Only a few research aircrafts operate the state of the art imaging spectroradiometers in the European research space. In the context of current hyperspectral satellite missions (EnMAP, PRISMA) and future CHIME it is important to coordinate and facilitate the transnational access to airborne research infrastructures that is important for calibration and validation activities, algorithm testing and development. Besides the facilitation of the transnational access, the other EUFAR activities (Figure 1) include:

- contribution to the European Environmental Research Infrastructures (ENVRI),
- promotion the use of airborne research facilities and providing training opportunities,
- organisation of Expert Working Group meetings, webinars and conference sessions,
- development of protocols and best practice recommendations for airborne operators
- providing access to existing data collected by EUFAR members.

Results (1200 – 1500 characters incl. spaces)

EUFAR maintains the data catalogue hosted by AERSI, the French Data and Services Cluster for Atmosphere, with past campaigns executed by EUFAR research aircrafts. The catalogue allows searching for the principal contact point to retrieve the data for further research use. EUFAR is also developing an online database of planned flight activities of the research aircraft. Such a database would provide users information about the goal, timing, location and type of measurements planned within the future

airborne campaigns. This tool will help to optimise the use of research aircrafts and allow users contacting and joining the future flight campaigns.

Outlook for the future (800 - 1000 characters incl. spaces)

EUFAR is currently joining efforts with the community of balloon- (HEMERA RI) and drone-based research (cost action Harmonious) to submit a proposal to a Horizon Europe INFRADEV call to develop, consolidate and optimise the European research infrastructures landscape related to airborne data acquisitions and research.

THE UNIQUE EUROPEAN RESEARCH INFRASTRUCTURE DEDICATED TO AIRBORNE RESEARCH IN THE ENVIRONMENTAL AND GEO-SCIENCES



Figure 1 EUFAR activities.

Hyperspectral Remote Sensing of Wheat Lodging: An Insight into Its Physiology

Padmageetha Nagarajan¹, Roshanak Darvishzadeh¹, Andrew Nelson¹

¹ FACULTY OF GEO-INFORMATION SCIENCE AND EARTH OBSERVATION (ITC), UNIVERSITY OF TWENTE, ENSCHEDE 7500 AE, THE NETHERLANDS

KEYWORDS (5): WHEAT LODGING, HYPERSPECTRAL MEASUREMENTS, SEVERITY, CHLOROPHYLL, WATER CONTENT

Challenge (800 - 1000 characters incl. spaces)

Cereals are an important source of energy, carbohydrates, proteins, fiber, and a myriad variety of micronutrients and make up a substantial part of the diet in both developed and developing nations. Specifically, as wheat contributes 5% of the daily calories and protein, it plays a significant part in ensuring the food security of the global population. Crop lodging, or the bending of stems from their upright position, is a condition that results in yield reduction and deteriorates grain productivity and quality. Multispectral and synthetic aperture radar data have been used in various studies for lodging detection and severity assessment, yet the use of hyperspectral measurements and the canopy physiological changes associated with lodging remain unknown. Thus, this study aims to use hyperspectral remote sensing data obtained from field measurements of lodged and healthy wheat plots to comprehend the physiology of lodging in wheat at different severity levels.

Methodology (1200 – 1500 characters incl. spaces)

A field campaign was carried out in Bonafische Ferraresi farm located in Jolanda di Savoia, Ferrara, Italy from May 3 to May 18, 2023. To understand the physiological changes that wheat encounters at different severity levels, various lodging parameters including slant height (h_{sl}), vertical lodged height (h_1), lodged area (LA), point of line failure of stem; biochemical parameters such as SPAD and biophysical variables such as Leaf Area Index (LAI), plant density, plant height, leaf area, fresh mass, grain weight were collected. Furthermore, Crop Angle Inclination (CAI) which can be referred to as an angle of the crop stem with respect to the zenith was derived using h_{sl} and h_1 . Then, normalised lodging score index (LS) was derived for each observation using CAI and LA to assign its severity degree. In addition, hyperspectral canopy measurements were collected in a total of 189 plots of size 1.5X1.5m using an ASD spectrometer (VNIR-SWIR), including 115 and 74 measurements for lodged and healthy wheat plots, respectively. The collected spectral measurements were further processed and, the average reflectance spectra in each plot were computed. A Savitzky-Golay filter was then used to smooth the averaged reflectance spectral data. Narrow band vegetation indices, continuum removed spectra and first derivative reflectance were used to study the variability between lodged and healthy wheat plots.

Results (1200 – 1500 characters incl. spaces)

The visible, red-edge, NIR, and SWIR wavelengths, which correspond to plant pigments and water absorption bands, are critical for identifying lodging in wheat. According to the findings, increase in lodging severity lowers water and chlorophyll contents, which in turn increases the overall reflectance (Figure 1). In the NIR region, reflectance increases with severity. We observed that healthy wheat has the lowest reflectance in the NIR region, whereas severely lodged wheat has the highest reflectance. Furthermore, a blue shift was noticed in the red-edge region in lodging classes due to the reduction in chlorophyll content caused by self-shading (Figure 2). Also, a maximal absorption peak was noticed in

healthy wheat at the red-edge region of the continuum-removed spectra, where the chlorophyll content is highest, and the peak lowers with severity as the chlorophyll content declines over time. Similarly, when the water content in wheat declines with severity, the reflectance in SWIR increases, with the severely lodged class exhibiting the highest reflectance and the lowest plant water content. Compared to the lodged wheat, healthy wheat contained the maximum water content and exhibited the lowest reflectance and highest absorbance in the SWIR region.

Outlook for the future (800 - 1000 characters incl. spaces)

This investigation was solely conducted at the field level, utilizing an ASD field spectrometer. With the advent of new hyperspectral satellite missions such as EnMap and PRISMA, this study on detecting wheat lodging can be scaled up to the satellite level for large-scale detection. Furthermore, machine learning and deep learning algorithms can be developed and trained to detect wheat lodging at regional and continental scales. To understand the physiological changes undergone by wheat at various severity levels, retrieval investigations of crop angle, chlorophyll, and plant water can be conducted at the airborne or satellite levels. The results of this study are useful for the launch of new hyperspectral satellites such as the CHIME hyperspectral mission. Utilizing radiative transfer modelling and the knowledge of acquired biophysical and biochemical variables in healthy and lodged wheat, the applicability of CHIME simulated data for lodging studies can be further investigated.

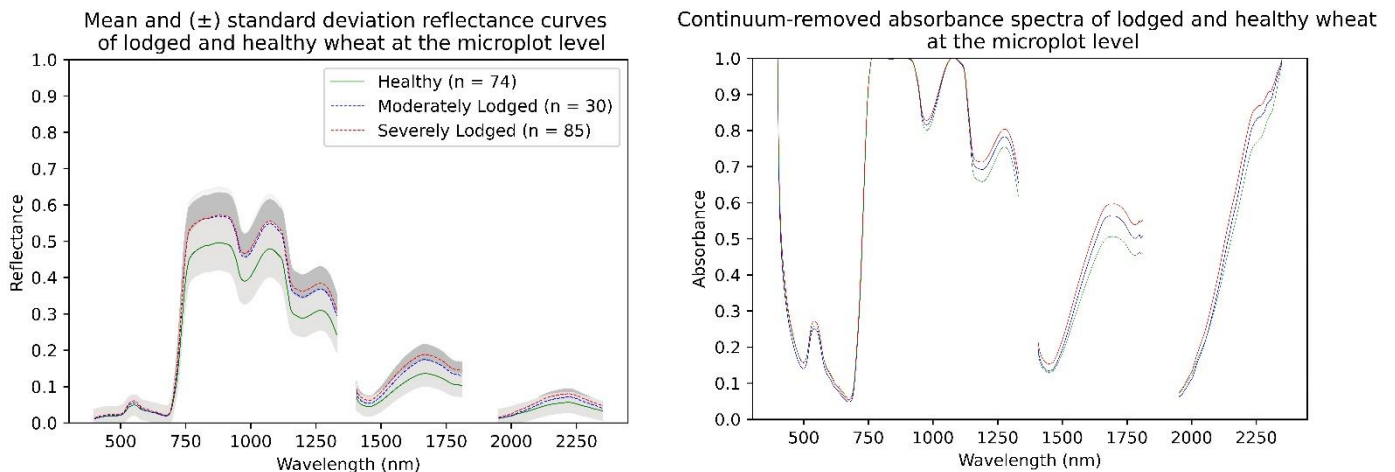


Figure 1 – Mean reflectance and continuum-removed absorbance curves of healthy and lodged at different severity degrees. Green curves represent a healthy condition, blue a moderately lodged condition, and red a severe lodged condition.

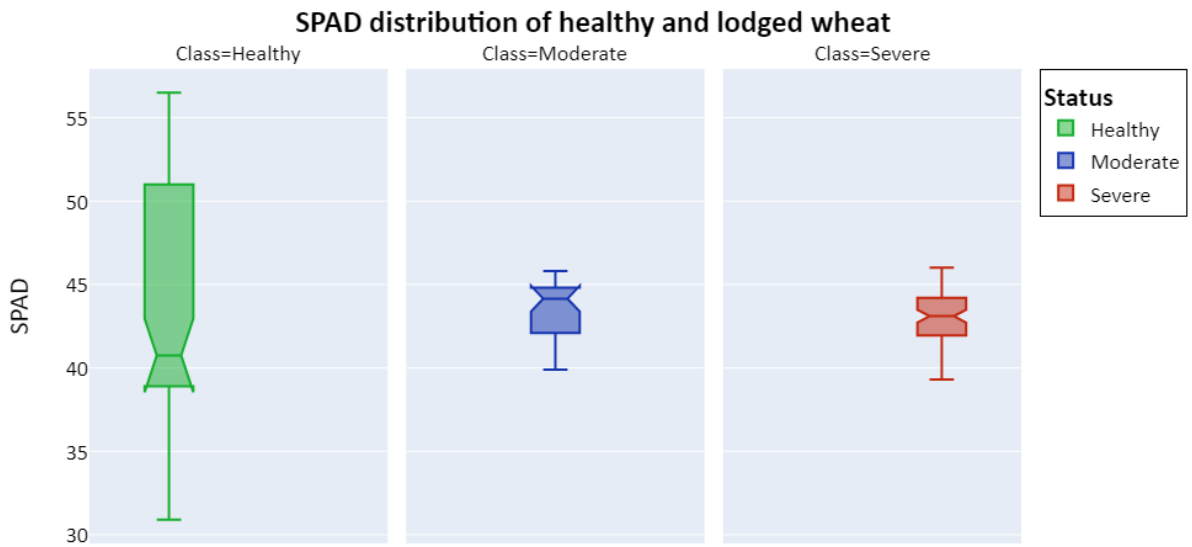


Figure 2 – SPAD distribution of healthy and lodged wheat

Understanding the changes in Maize canopy structure caused by Fall Armyworm (*J.E. Smith Spodoptera frugiperda*) using field hyperspectral spectroscopy measurements

Tatenda Dzurume^{1,2*}, Roshanak Darvishzadeh¹, Timothy Dube², Andy Nelson¹

¹Department of Natural Resources, Faculty of Geo-Information Science and Earth Observation, University of Twente, The Netherlands;

²Institute of Water Studies, Department of Earth Sciences, University of the Western Cape, Private Bag X17, Bellville 7535, South Africa

Keywords (5): Hyperspectral spectroscopy, Fall Armyworm (FAW, *J.E. Smith Spodoptera frugiperda*), Maize (*Zea mays L.*), Pest management, Food security

Maize (*Zea mays L.*) is one of Africa's most popular crops due to its importance as a staple food for the majority of the population. Recurring invasion of Fall armyworm (FAW, *J.E. Smith Spodoptera frugiperda*) caused significant damage to the maize canopy structure and affect maize yield and production. The physical damage caused by FAW varies depending on its larval stage. Superficie feeding can cause semi-transparent patches on the leaves known as 'papery windows'. The larva also causes crop damage by feeding on the leaf tissue and causing holes in the leaf, a common symptom of this pest. Monitoring the changes to maize canopy structure is central to food security and alleviating poverty. Therefore, it is of critical importance to monitor these changes. Studies have used traditional and remote sense-based techniques. Traditionally, direct field and laboratory measurements, which are spatially and temporally limited, costly, and time-consuming have been used to measure the biophysical changes that have been used by FAW. Whereas remote sensing (RS) techniques can be used to explain the spatial, spectral, and textural features of canopy structures in a cost-effective and timely manner. This study aimed to understand the effects of FAW infestation on maize canopy structure in Mpumalanga, South Africa, using field hyperspectral spectroscopy measurements and machine learning algorithm (random forest (RF)). These were used to classify and model the spectral behaviours of maize crop biophysical changes under FAW. Spectral measurements were also taken in the field to observe the spectral difference between the infested and non-infested maize crops. The study hypothesised that changes in canopy biophysical variables (e.g., leaf area index, stem and leaf length, and biomass) can be used to study the changes in maize canopy structure caused by FAW infestation using field hyperspectral spectroscopy measurements. The preliminary results from this study show that structural changes (e.g., leaf area index, stem and leaf length, and biomass) caused by FAW can be mapped with high accuracy using field hyperspectral spectroscopy measurements. This study underscores the significance of comprehending maize canopy structure alterations for two primary purposes: enhancing crop yield and optimizing agricultural production to ensure food security.

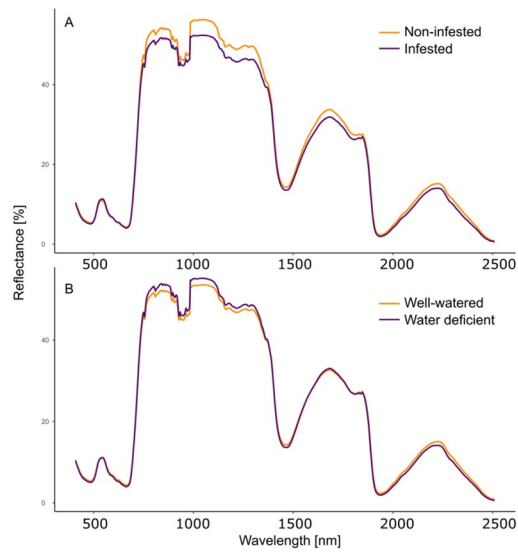


Figure 1: An example of the expected spectral reflectance: **(A)** non-infested and infested crops; **(B)** well-watered and water-deficient crops (Praprotnik et al., 2023; *agronomy*).

Sharing in-situ Measurements for Surface Reflectance Product Validation: a Proposal for Content, Format and Tools

Jérôme Louis¹, Bringfried Pflug², Sébastien Saunier³, Raquel De Los Reyes⁴

¹ Telespazio France, Image Processing Unit, France

² German Aerospace Centre (DLR), Remote Sensing Technology Institute, Germany

³ Telespazio France, Image Processing Unit, France

⁴ German Aerospace Centre (DLR), Remote Sensing Technology Institute, Germany

Keywords (5): Earth Observation, Copernicus, In-situ, Product Validation, Atmospheric Correction

Challenge (800 - 1000 characters incl. spaces)

Surface reflectance products from optical EO missions have become a standard for delivering final products compensated from atmospheric effects, ready to be used in the analysis of bio- and geophysical variables.

Their validation is usually performed in two steps, first by assessing the accuracy of the atmospheric parameters retrieved during the atmospheric correction, then by performing a direct validation of the surface reflectance against in-situ measurement.

Whereas CEOS, ESA and EU support initiatives like HyperNETs or RadCalNet, providing in-situ surface reflectance measurements, there is still the need for supplementing these validation data by in-situ measurements from ad-hoc campaigns.

The objective of this presentation is to present a proposal for the in-situ measurements contents, a data format for exchange and processing and possibly a set of readers for this data in Python language. This would help fostering the sharing and usage of existing and future in-situ measurements.

Methodology (1200 – 1500 characters incl. spaces)

For the validation of Atmospheric Correction (AC) processors, although the surface reflectance is the most important measurement, additional in-situ measurements like Aerosol Optical Thickness (AOT), Aerosol type, Water Vapour (WV), Ozone and bidirectional reflectance function (BRDF) are important and allow validation teams to perform exercises that determines the source of the discrepancies.

The contents and format of the two principal existing validation networks, i.e. RadCalNet and HyperNETs see Fig.1, will be reviewed and assessed. RadCalNet was initially designed to provide SI-traceable Top-of-Atmosphere (TOA) spectrally-resolved reflectances for radiometric calibration and validation of optical imaging sensor data, mostly on bright surfaces with low aerosol content conditions. HyperNETs network is quite recent and should help to extend the diversity of in-situ ground targets, e.g. with more vegetated areas and variety of aerosol content, required for the validation of the AC processors.

Concerning the ad-hoc campaigns, the contents and format of several campaigns are of interest: SRIX4Veg but also DLR campaigns and CSIRO-campaigns, the latter ones looking for coincidence with overpasses of Sentinel-2, Landsat, DESIS, EnMAP.

The conclusions of former and on-going projects like Copernicus CAL/VAL Solution (CCVS) and Fiducial Reference Measurements (FRM) will serve as guidance for establishing the contents and associated metadata of the proposed common format.

Results (1200 – 1500 characters incl. spaces)

AC processors have performance requirements in the form of products uncertainties. These required uncertainties need to be validated among a large diversity of atmosphere conditions (e.g. AOT > 0.1) and ground surface reflectances. Therefore, it is important that the file providing the in-situ measurements contain information about the surface reflectance itself as well as information of the atmospheric conditions and stability at the time of the in-situ measurements, with some optional information (e.g. characterization, homogeneity and BRDF of the site). For each measurement provided, the related metadata and associated uncertainties should be provided in line with the FRM guidelines.

The following content has been identified:

- Spectral Surface reflectance
- Column integrated Water Vapour
- Aerosol Optical Thickness
- Viewing angles
- Solar angles
- all information necessary for TOA reflectance computation
- Time of the measurement
- Coordinates of the region of interest of the measurements

Once the in-situ measurements contents and file format would have been defined, it would be interesting to develop, within an open source EO collaboration, a reader for those in-situ files, structured in a light software library. The programming language to be adopted should be easily readable by the non-computer expert community and allow to read-in the in-situ measurements in the adopted format and optionally existing HyperNets, Radcalnet formats. The reader would output a set of data arrays ready to be analysed in the frame of surface reflectance validation activities.

Outlook for the future (800 - 1000 characters incl. spaces)

This initiative of the common format and content should contribute to the efficiency of the teams of the ESA Optical MPC involved in surface reflectance product validation, when it is anticipated that the validation activities will continue with the maintenance of the Sentinel-2 and 3 constellations, and extend in the future with the addition of other Copernicus missions like LSTM and CHIME hyperspectral mission.

Considered so far as optional, the BRDF should also be addressed in the future as this information is essential to maximize the usage of in-situ measurements for EO missions acquiring images with viewing angles off Nadir.

We are confident that a global joint effort for sharing the data from these ad-hoc campaigns would be very helpful to all the science community. Starting from a need from the surface reflectance validation for land applications this approach could be extended and evolve, in collaboration with the teams in charge of validation of water products.



Figure 1 (a) RadCalNet Gobabeb test site © NPL (b) HyperNETS Soontage test site © TARTU

PRISMA and EnMAP comparison in the context of wheat nitrogen status assessment

M. Troiani¹, J. Bouchat¹, L. Leclère², Y. Curnel², P. Vermeulen³, F. Stevens³, B. Scaut³, D. Malice², V. Baeten³, N. Chamberland⁴, V. Planchon², P. Defourny¹

¹ UCLouvain, Earth and Life Institute, Belgium

² CRA-W - Agriculture, territory and technologies integration Unit, Belgium

³ CRA-W - Quality and authentication of agricultural products Unit, Belgium

⁴ ConstellR GmbH, Germany.

Keywords (5): Agriculture, Hyperspectral, PRISMA & EnMAP, Biophysical variables, Nitrogen concentration.

Challenge

Over the past few decades, spaceborne hyperspectral imagery has evolved significantly, opening up new possibilities for agricultural research and monitoring. Despite this growing potential, many agricultural challenges remain as pressing as ever. Farmers are caught between growing production demands and ever-increasing environmental pressures. On the one hand, despite having a very high economic cost for farmers, nitrogen fertilization enables them to maintain high levels of productivity. On the other hand, many Belgian and European regions are facing nitrogen pollution of groundwater. In order to guarantee an optimum level of production while minimizing the environmental impact, the development of applications to monitor the nitrogen status of wheat, a prominent crop worldwide, is essential and in line with several of the United Nations' "Sustainable Development Goals".

Methodology

A first field campaign was carried out from March to July 2023, i.e., during the nitrogen fertilization period. Winter wheat samples were taken from trials plots and several farmers' fields. For each of these plots, dry matter and nitrogen content measurements were carried out in laboratory. Due to the difficulty to match ground measurements with EnMAP and PRISMA acquisitions, reference Canopy Nitrogen Content (CNC) data have been derived from operational nitrogen status products based on Sentinel-2 MSI (Delloye et al., 2018). This method is based on the inversion of the radiative transfer model PROSAIL using an artificial neural network. Regarding the estimation of the CNC, two different methods have been designed and are currently being implemented. The first method relies on the use of hyperspectral vegetation indices. The second method relies on the inversion of the radiative transfer model PROSAIL. For the first method, Normalized Difference Index (NDI) $\frac{Band\ 1 - Band\ 2}{Band\ 1 + Band\ 2}$ and Simple Ratio Index (SRI) $\frac{Band\ 1}{Band\ 2}$ have been computed for all possible combinations of spectral bands. The indices that are the most correlated to the CNC are then used as explanatory variable with a simple parametric regression. The CNC and indices values have been aggregated at the parcel level. Parcels were selected based on the Walloon IACS (Integrated Administration and Control System).

Results

Based on the IACS and the extent of the PRISMA and EnMAP acquisitions, 2659 and 1279 parcels have respectively been selected. The indices have then been compared to the Sentinel-2 derived CNC based on the Pearson correlation formula (see fig. 1,2,3,4). The most correlated indices have been derived from spectral bands within the Sentinel-2 spectrum, but other indices showed similar correlation coefficient with the CNC. The red-edge region appears to be particularly sensitive to the CNC which confirms the high correlation between the chlorophyll content and the nitrogen concentration. However, heatmaps exhibit numerous other sensitive spectral bands, especially in the SWIR region. This could be explained by the fact that the SWIR region is particularly sensitive to protein content, inherently linked to the plant nitrogen

content. For the NDI and SRI, the correlation matrices from the EnMAP and PRISMA images look similar. However, for both EnMAP correlation matrices, several bands in the NIR region appear to have questionable behavior. It is important to note that no pre-processing was carried out a priori in order to preserve the readability of the signal physics. This could therefore explain the perturbations observed. Regarding the results obtained with a linear regression model, the performance achieved with EnMAP data are slightly better in terms of R^2 . The associated RMSE is significantly lower as compared to the model using PRISMA data (see table 1). The results obtained from a simple linear regression suggest that there is a room for improvement regarding the accuracy of CNC estimation.

Table 1: linear regression results for EnMAP and PRISMA NDI and SRI most correlated indices

	Band 1 (nm)	Band 2 (nm)	R	R ²	RMSE [kg/ha]
EnMAP (NDI)	778	749	0.87	0.76	49.96
PRISMA (NDI)	786	734	0.83	0.68	132.58
EnMAP (SRI)	764	742	0.87	0.76	46.71
PRISMA (SRI)	786	724	0.83	0.69	129.72

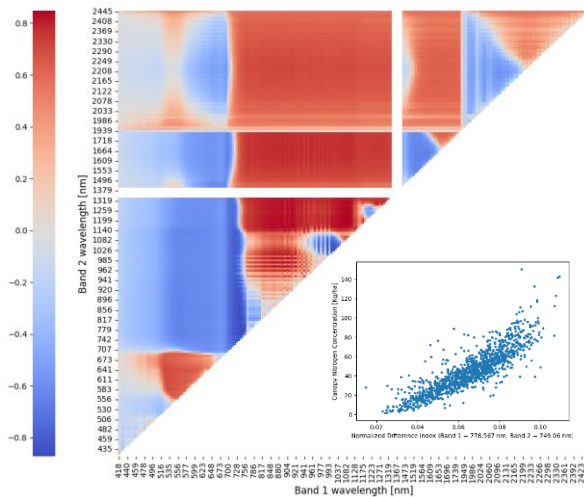


Figure 1: Heatmap correlation matrix, EnMAP NDI

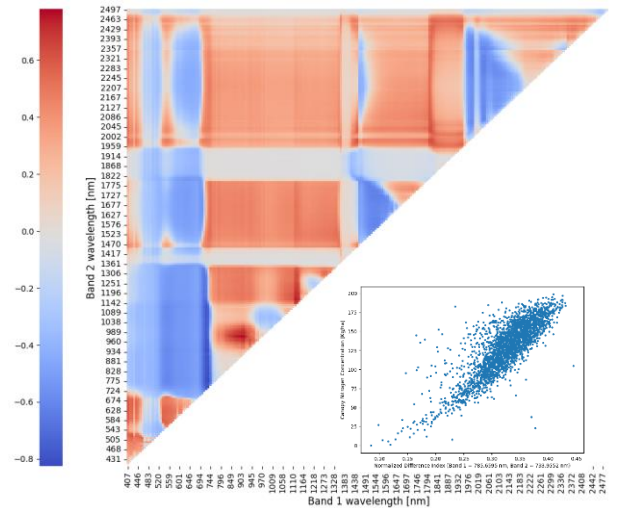


Figure 2: Heatmap correlation matrix, PRISMA NDI

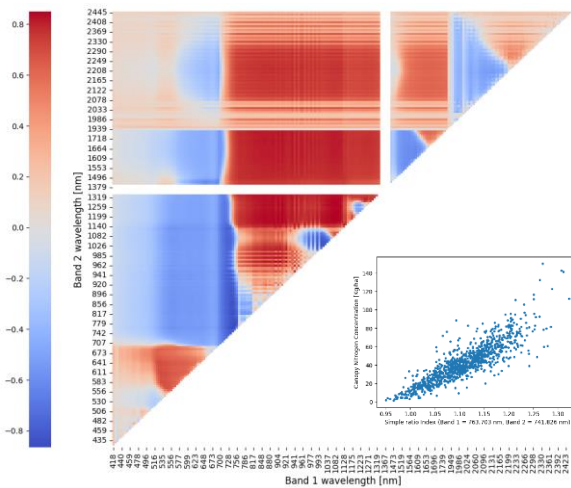


Figure 4: Heatmap correlation matrix, EnMAP SRI

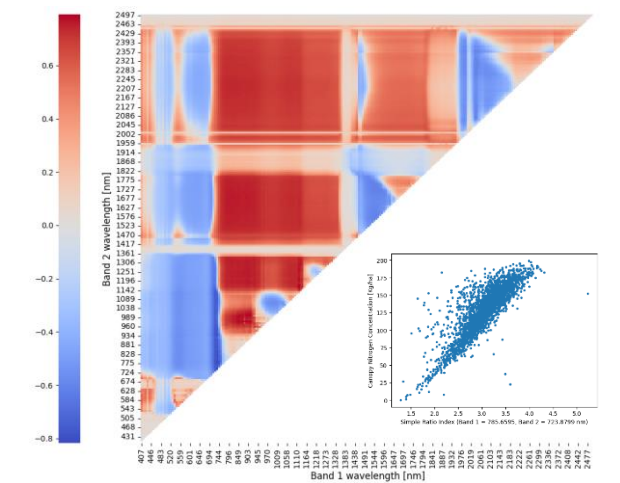


Figure 3: Heatmap correlation matrix, PRISMA SRI

Outlook for the future

As mentioned in the previous section, the lack of ground-truth measurements has been the most limiting factor. To leverage this, estimated CNC has been used as reference data. The organization of the 2024 forthcoming campaign will therefore be crucial. A special attention will be put on satellite tasking and on ground measurements. Moreover, an analysis will be performed to quantify the signal-to-noise ratio and its impact on the signal coming from vegetated surfaces. Regarding the use of a physically-based model to estimate the CNC, different methods are currently being assessed. In addition, the potential complementarity between frequent Sentinel-2 data and precise hyperspectral data will be investigated.

An Integrated Atmospheric-Terrain Correction Method for Imaging Spectroscopy

Yujie Zhao^{1,3}, Guorui Jia^{1,3}, Huijie Zhao^{1,2,3}

¹ Beihang University, School of Instrumentation and Optoelectronic Engineering, China

² Beihang University, Institute of Artificial Intelligence, China

³ Key Laboratory of Precision Opto-Mechatronics Technology, Ministry of Education, China

Keywords : Hyperspectral Remote Sensing, Atmospheric Correction, Topographic Correction, Geometric Correction, Integrated Correction

Challenge

Correction for atmospheric and terrain effects is a critical step in the pre-processing chain of remote sensing data. With the improvement of satellite sensor performance, high-precision pre-processing methods are necessary to meet the new applications of remote sensing in many fields. Although it is currently a routine operation to perform terrain correction and atmospheric correction separately and treat them as two independent processes, this cannot truly reflect the radiation transfer mechanism between the atmosphere and the surface, leading to over-correction or under-correction of reflectance in some regions. Therefore, the trend of land reflectance inversion is moving towards an integrated model of atmospheric-terrain joint correction. Although some methods have established coupled models of atmospheric and terrain, the model construction is not precise enough, resulting in inaccurate calculation of some radiative quantities and rough estimation of initial reflectance values.

Methodology

To address the challenge of high-precision surface reflectance inversion caused by complex illumination conditions in undulating areas, an integrated correction method for geometric, atmospheric and terrain effects (ATGCOR) is proposed. By establishing a coupled radiative transfer model for the atmosphere and terrain, and breaking through the high-precision automatic registration technology between high-precision digital surface models and hyperspectral images, the method performs high-precision iterative calculations of components such as direct solar irradiance, sky scattering, coupled radiative transfer between the atmosphere and surface, and surrounding background reflection along the sun-terrain-target-sensor geometric path. The model takes into account the coupling radiation components between the surface and the atmosphere. The influences of both the target and the background are considered during the calculation of initial reflectance values. Subsequently, the reflectance is solved through fixed-point iteration. It then reconstructs the reflectance characteristics of ground pixels on a regular grid, ultimately obtaining radiometrically and geometrically corrected hyperspectral surface reflectance.

Results

The ATGCOR algorithm proposed in this paper has demonstrated its effectiveness in both flat and undulating terrains, as well as for various land cover types including vegetation and rocky surfaces. The key findings are as follows:

(1) Visually, the ATGCOR algorithm significantly reduces the terrain effects, particularly enhancing the spectral consistency of the same land cover on both sunny and shady slopes, with a reduction of over 30% in normalized spectral distance compared to traditional SCS+C and atmospheric sequential correction methods.

(2) In terms of the correlation between reflectance images and topography, the ATGCOR method exhibits the lowest overall correlation across different spectral bands.

(3) Regarding land cover classification, the ATGCOR method reduces the intra-class spectral variability of reflectance, leading to improved classification results.

In conclusion, visual analysis and indirect verification methods have been adopted for validation purposes. As mentioned in the **Challenge** part, previous studies have mainly applied separate terrain correction, atmospheric correction, and geometric correction methods. The integrated ATGCOR method proposed in this study conforms better to the law of objective radiative transfer and effectively improves the accuracy of reflectance, overcoming the problem of over- or under-correction in fluctuating terrain encountered in previous reflectance inversion methods.

Outlook for the future

It should be noted that the effectiveness of the proposed algorithm in terrain and atmospheric correction has not been validated using field-collected data. This is mainly due to the difficulties in obtaining high-quality field reflectance measurements in rugged areas. Hence, it is essential to devise an approach for validating the precision of reflectance in inaccessible regions going forward. Furthermore, the uncertainty evaluation from the field of metrology into the preliminary accuracy evaluation of reflectance should be considered. In addition, reflectance inversion for non-Lambertian surfaces will be a future research direction, such as BRDF correction for vegetation at different observation angles.

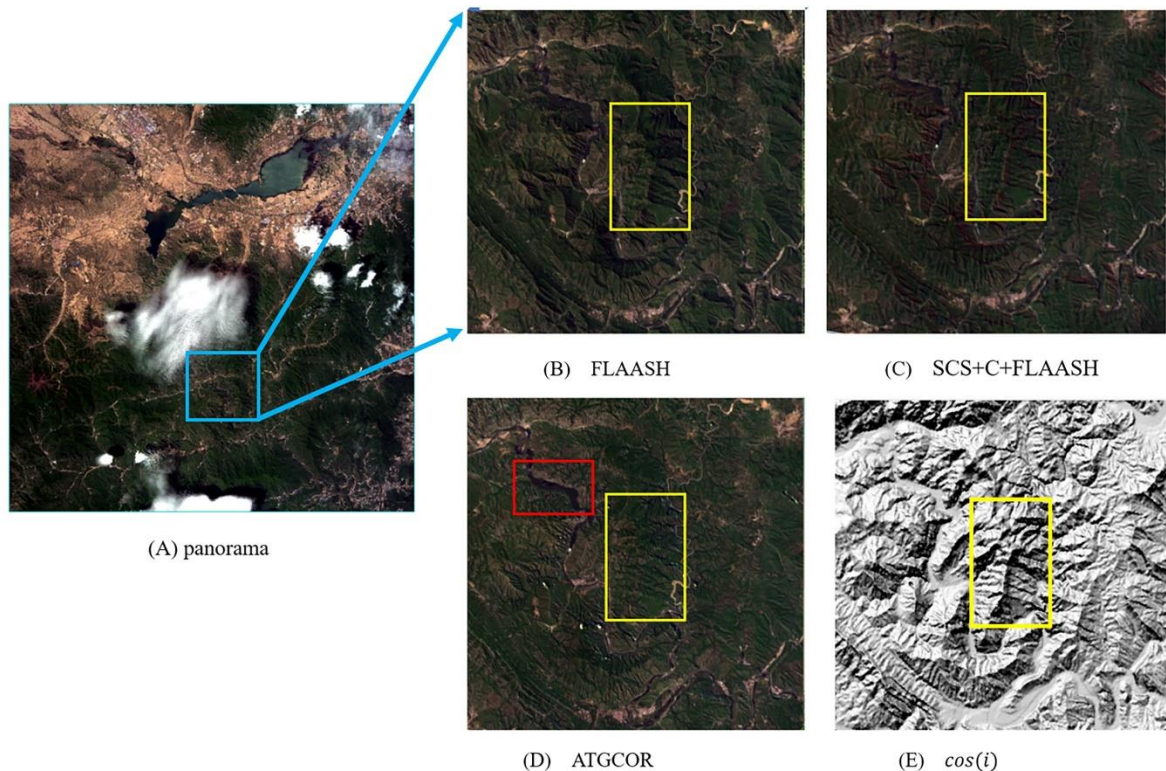


Figure (A) panorama of GF-5 hyperspectral image (B) the result of FLAASH atmospheric correction (C) the result of SCS+C+FLAASH and (D) the result of ATGCOR (the method adopted in this paper) and (E) cosine of solar incidence angle. The relief effect in the yellow area is obviously improved, and the pearl Lake in the red area is obviously distinguishable.

Soil Organic Carbon Estimation using VNIR–SWIR Spectroscopy And Machine Learning

[Ashfak Mahmud](#)¹, Markku Luotamo ², Kristiina Karhu³, Petri Pellikka¹, Juuso Tuure³, Janne Heiskanen^{1,4}

¹ University of Helsinki, Department of Geosciences and Geography, Helsinki, Finland

² University of Helsinki, Department of Computer Science, Helsinki, Finland

³ Department of Agricultural Sciences, University of Helsinki, Helsinki, Finland

⁴ Finnish Meteorological Institute, Helsinki, Finland

Keywords (5): Soil Organic Carbon, Machine Learning, Hyperspectral, Spectroradiometer, Proximal Sensing

Challenge (800 - 1000 characters incl. spaces)

Soil organic carbon (SOC) is an important indicator of the physical, chemical, and biological functions of the soil. Higher SOC contents improve soil fertility, while the depletion of SOC contributes to soil degradation. SOC reduction and accumulation are associated with climate change with the release of CO_2 to the atmosphere and capturing CO_2 through carbon sequestration. SOC enhances the soil water and nutrient-holding capacity which results in increased agricultural productivity. The spatial variation of the SOC can be attributed to factors such as land cover, vegetation type, topography, and anthropogenic activities. For sustainable soil management practices in agricultural settings, accurate estimation of SOC is necessary. Laboratory measurement of SOC is a costly and time-consuming procedure for analyzing large numbers of samples in remote areas.

Methodology (1200 – 1500 characters incl. spaces)

SOC modelling using hyperspectral sensing coupled with machine learning offers an effective solution to the limitations of laboratory measurement. We collected 157 soil samples from four different landcovers (sisal, cropland, shrubland and agroforestry) in Taita Hills in Kenya. The SOC content (%) was retrieved from the oven-dried samples using a dry oxidization analyzer in the laboratory. We took spectral measurements of the soil samples using a field spectroradiometer (SVC HR-1024i, 350-2500 nm). We placed the soil samples in petri dishes and measured spectra in controlled light conditions using SVC Leaf Clip and Reflectance probe (LC RP PRO). We pre-processed the data to remove the bands having noise and inconsistent spectra due to overlapping sensors. Finally, we utilized three machine learning algorithms, namely Lasso Regression (LR), Partial Least Squares Regression (PLSR), and Gaussian Process Regression (GPR) to predict SOC using different wavelength ranges: full wavelength range (FWR: 400-24000 nm), visible-near infrared (VNIR: 400-1000 nm) and shortwave infrared (SWIR: 1000-2400 nm). We cross-validated our models with k-fold cross-validation approach to calculate model performance metrics.

Results (1200 – 1500 characters incl. spaces)

All the tested models (LR, PLSR and GPR) yielded very good accuracy having R^2 between 0.82-0.83 and RMSE between 0.36-0.38 % in FWR and SWIR range. However, in the VNIR range, all the models

showed less accuracy having the R^2 between 0.52 to 0.61 and RMSE between 0.55 to 0.61 %. LR achieved the highest ratio of performance to deviation (RPD) and ratio of performance to inter-quartile distance (RPIQ) of 2.43 and 3.72, respectively over FWR, and GPR yielded the highest RPD and RPIQ of 2.47 and 3.78, respectively when predicting SOC with SWIR. On the other hand, all the models yielded $RPD < 1.61$ and $RPIQ < 2.46$ over the VNIR range.

SOC estimation with all the models achieved competitive performance when SWIR was included as predictor. Although very few studies employed the GPR model in soil properties prediction from hyperspectral sensing, we found that GPR achieved the highest accuracy in SOC prediction over SWIR wavelength range. We also identified important bands over 10-fold iterations utilizing LR in FWR for estimating SOC. We noticed that selected bands having good correlation with SOC are located between 950 to 1350 nm and 2100 to 2400 nm. Most of the highly correlated selected bands are located in SWIR range, which illustrates the importance of SWIR for SOC modelling.

Outlook for the future (800 - 1000 characters incl. spaces)

The future studies will look into the transferability of the models to different areas and measurement conditions but also to hyperspectral remote sensing data from airborne and satellite platforms. We aim to test the performance of our SOC modelling approach on the spectral measurement done on-site to accelerate the process of determining SOC. The spatial variability of SOC is quite large even at an intra-field level. The point measurements are not enough to support sustainable soil management practices and better spatial representation of SOC variation is needed. To address this, we plan to conduct a flight campaign with airborne hyperspectral sensor to cover a larger area in the study area. Reference SOC content can come from the predicted point measurement from the field campaign done with a field spectroradiometer. Finally, the output will be a SOC distribution map showing SOC variation spatially predicted using machine learning or deep learning approaches.

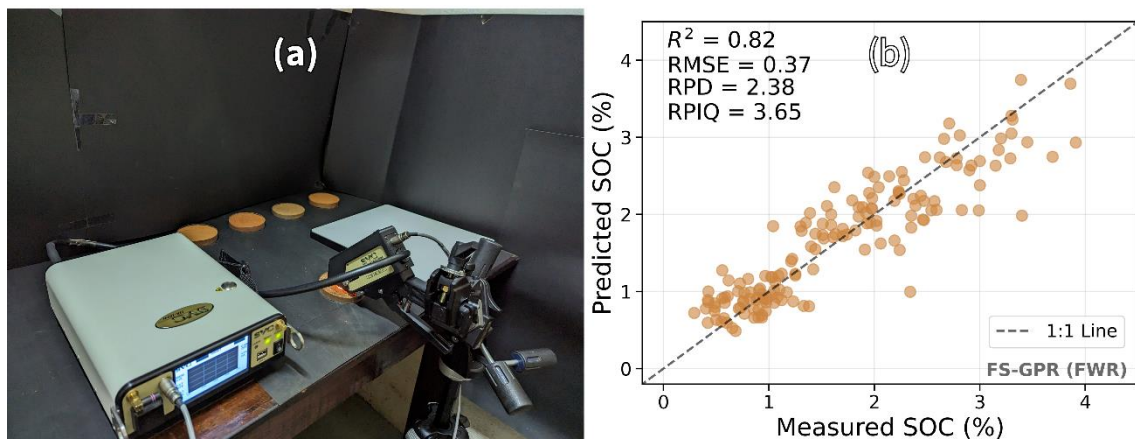


Figure (a) Soil spectral measurement protocol and (b) SOC modelling results based on Gaussian Process Regression (GPR).

The impact and correction of illumination and view geometry (I&VG) on spectral reflectance measured in situ

Ziwei Wang¹, Guorui Jia¹, Huijie Zhao^{1,2}

¹ Beihang University, School of Instrumentation and Optoelectronic Engineering, Ministry of Education Key Laboratory of Precision Opto-Mechatronics Technology, Beijing 100191, China

² Beihang University, Institute of Artificial Intelligence, Aerospace Optical-Microwave Integrated Precision Intelligent Sensing, Key Laboratory of Ministry of Industry and Information Technology, Beijing 100191, China

Keywords (5): In situ measurements; illumination and view geometry (I&VG); Standard uncertainty; Sensitivity analysis; Spectral reflectance correction

Challenge

In situ measurements are used as the “truth” and plays a significant role in the applications of earth observation. In situ measurements are easily impacted by illumination and view geometry (I&VG), resulting in the same objects with different spectra. The uncertainty of reflectance measured in situ caused by I&VG has been extensively studied. A main problem is that I&VG are uncontrollable which leads to inconsistent uncertainty of measurement data under different I&VG. Moreover, it is unfeasible to collect data under all I&VG conditions, which leads to a lack of comprehensive quantitative evaluation of uncertainty. A further problem is that the uncertainty caused by I&VG is formed by the coupling of multiple I&VG parameters. Since it has remained a challenge to decouple multiple I&VG parameters, the impact mechanism of single I&VG parameters is still poorly understood. Furthermore, how to correct the impact of I&VG on reflectance is another urgent issue that needs to be addressed.

Methodology

This work conducted extensive experiments using our innovative facility MHSRS²F to investigate the impact of I&VG (solar zenith and azimuth angles, view zenith and azimuth angles, and observation height) on the measurement of reflectance spectra. The SpectralonTM white diffuse reflectance standard (99%) panel is used to separate I&VG from the surface heterogeneity of objects and analyze the impact of different I&VG on reflectance. Rock samples are used to explore the effects caused by the coupling of different I&VG and surface heterogeneity of rocks. Based on the experimental results, an uncertainty evaluation model was constructed for I&VG. This work quantifies the uncertainty caused by a single I&VG parameters and the coupling of multiple parameters. Moreover, this work use the spectral reflectance collected by MHSRS²F to replace the results of the in situ measurement model. And the sensitivity of spectral reflectance to I&VG at different wavelengths was explored based on Sobol’s Global Sensitivity Analysis method. On the basis of understanding the impact of I&VG, a correction model for reflectance under different I&VG conditions is proposed. The core concept is to correct the impact of different I&VG parameters on the reference panel to eliminate the partial of impact of I&VG on the reflectance of objects.

Results

The statistical results indicate that the uncertainty caused by I&VG is around 0.86%. The uncertainty caused by the coupling of I&VG and surface heterogeneity of rocks samples is 12.98-27.69%. The uncertainty and sensitivity caused by different I&VG are closely related to the surface heterogeneity of the object. The greater the surface heterogeneity, the greater the uncertainty. Regardless of surface heterogeneity, the uncertainty and sensitivity caused by observation height are relatively greater than those by solar zenith and azimuth angles, view zenith and azimuth angles. For approximate Lambertian objects, the uncertainty and sensitivity have relatively consistent results. The uncertainty and sensitivity caused by the solar and view zenith angles are relatively high. This indicates that the selection and variation of the zenith angle are crucial. When there is surface heterogeneity on the measured object, the uncertainty caused by the solar and view azimuth angles is relatively high, but it is more sensitive to the solar azimuth angle and solar zenith angle. This indicates that the selection of the solar azimuth angle and the avoidance of changes during the experimental process are crucial. And more attention should be paid to the changes in the solar zenith angle and the selection of view azimuth angle. The correction method for reflectance data under different I&VG conditions proposed in this study has been applied to correct the view zenith angle and achieved good results, with a correction ability of 41.25%.

Outlook for the future

A limitation of this study is the unified use of surface heterogeneity to represent differences in physicochemical properties between objects. Experimental results shows that the uncertainty caused by the coupling of surface heterogeneity with I&VG is much greater than that caused only by I&VG. Therefore, we will continue to conduct experiments on objects of different materials such as soil, vegetation, and artificial targets. On the basis of understanding the impact of I&VG on spectral reflectance, exploring the impact of coupling different physicochemical properties with I&VG will be a fruitful field for further work. It can help us better understand the impact mechanism of I&VG for the spectral reflectance of objects. In addition, atmospheric conditions are also one of the important factors affecting in situ measurements. We have established a larger set of facility, and will conduct simulation experiments and research on the impact of atmospheric conditions in the future.

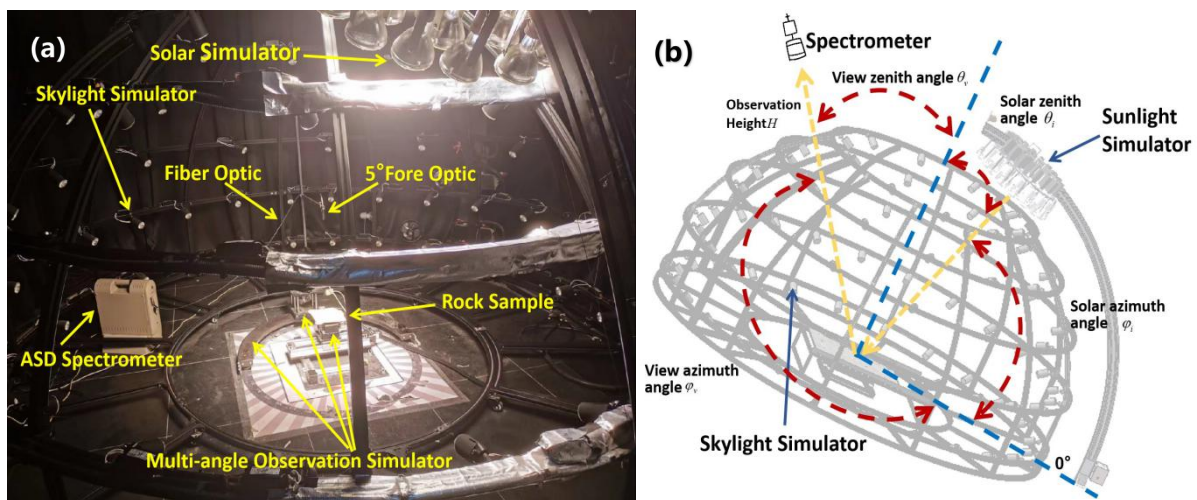


Figure 1 (a) actual picture of the components and structure of MHSRS²F and (b) adjustment trajectories of different I&VG parameters in the MHSRS²F

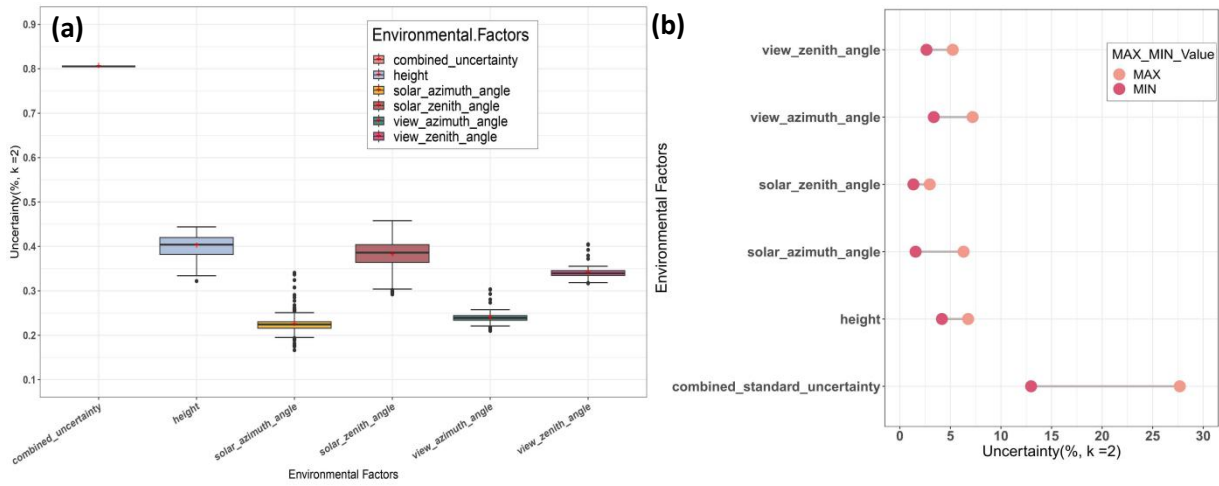


Figure 2 (a) The Box-plot shows the uncertainty distribution of reference panel within the 400 nm-900 nm range, and the red cross represents the average value and (b) The Dumbbell-plot shows the uncertainty range of 10 rock samples at different single I&VG parameters and coupling of multiple parameters.

A Prototype for Physiologically Based Retrieval of Landscape-scale Crop Growth and Development from Spaceborne Imagery

EARSel Valencia 2024

Abstract

Corresponding Author:

lukasvalentin.graf@usys.ethz.ch

Lukas Valentin Graf^{1,2}, Flavian Tschurr¹, Quirina Noëmi Merz¹, Raphael Portmann³, Achim Walter¹, Helge Aasen^{1,2}

¹ ETH Zürich, Crop Science, Institute for Agricultural Science, Switzerland

² Agroscope Reckenholz, Earth Observation of Agroecosystems Team, Division Agroecology and Environment, Switzerland

³ Agroscope Reckenholz, Climate and Agriculture Group, Division Agroecology and Environment, Switzerland

Keywords (5): Leaf Area Index, Phenology, Physiology, Radiative Transfer Modeling, Field Phenotyping

Challenge

Understanding plant growth and development is critical to maintaining future crop productivity. Space-based imaging sensors have proven to be an invaluable tool for monitoring crops on a large scale. In this context, growth is typically measured as an increase in leaf area or biomass over time, while development refers to the timing of events in the plant's life cycle, such as germination, flowering and maturity. Long-term experiments at field phenotyping stations have clearly shown that growth and development are closely linked. These processes are influenced by various environmental factors, with air temperature being particularly important. Surprisingly, in the field of imaging spectroscopy, plant growth and development are often treated separately and the potential relationship with environmental factors is not fully exploited. As a result, the physiological plausibility of crop growth and development derived from imaging spectroscopy remains a challenge.

Methodology

We propose a prototype framework for an integrated assessment of growth and development of winter wheat, with particular emphasis on the Green Leaf Area Index (GLAI). The framework consists of three components (Figure 1).

First, we use the crop model WOFOST, which is calibrated using field phenotyping data collected over multiple years and sites. WOFOST uses mean air temperature, day length and vernalisation requirements to simulate the daily phenological development of winter wheat from sowing to maturity.

Secondly, we use phenology to retrieve GLAI from space-borne Sentinel-2 imagery by inverting the PROSAIL radiative transfer model. We adjust the ranges of leaf and canopy traits input into PROSAIL over time to capture the relationship between GLAI and phenology established by field phenotyping. In addition, we incorporate empirical correlations between GLAI and leaf chlorophyll and carotenoid content. This ensures that physiologically unrealistic trait combinations are excluded from the inversion routine.

Finally, we fill temporal gaps between individual Sentinel-2 GLAI observations by exploiting the relationship between plant growth and air temperature. This relationship is captured by dose-response curves (DRCs) calibrated using field phenotyping data, which allow daily GLAI growth rates to be simulated. Using a probabilistic data assimilation scheme, we can link DRCs and GLAI observations to obtain a continuous representation of winter wheat growth and development.

Expected results

We validated the proposed prototype by using independent in-situ data collected in Switzerland in 2019, 2022, and 2023 from farmers' fields.

The timing of phenological stages, such as stem elongation and heading, was estimated with a high level of accuracy. For example, the root mean squared error (RMSE) for predicting the timing of heading was 2 days.

Next, we investigated the impact of incorporating phenological knowledge into the RTM inversion process. We observed that utilizing phenological information significantly improved the accuracy of GLAI (Green Leaf Area Index) retrieval. In a standard RTM setup without considering phenology, the RMSE was found to be 1.15 m² m⁻² (relative error: 18.9%). However, when we took into account the GLAI dependency on phenology, the RMSE decreased to 0.85 m² m⁻² (relative error: 14.0%). These results were obtained based on in-situ samples collected during a Sentinel-2 overpass, with a total of 177 samples analyzed.

Moreover, when we employed the DRCs and a probabilistic data assimilation scheme to reconstruct daily GLAI values, we found that the overall retrieval accuracy remained consistent in terms of RMSE. Still, we were able to reduce the underestimation of in-situ GLAI values above 5 m² m⁻². This reduction in underestimation can be attributed to the use of physiologically-based growth rates derived from the DRCs, helping to address the saturation effects typically encountered when using RTM inversion techniques.

Outlook for the future

We have demonstrated the potential of an integrated prototype to estimate the growth and development of winter wheat using Sentinel-2 imagery and air temperature data. As the prototype is based on physiological and phenological knowledge from multi-year and -site phenotyping data, we expect it to be geographically transferable to agricultural regions with similar climate and day length conditions. In addition, it can be applied to other crops (e.g., maize) if sufficient field phenotyping data are available for calibration. As we used PROSAIL for GLAI retrieval, it can be easily applied to other (future) imaging sensors such as EnMAP or CHIME. Furthermore, the use of DRCs could eliminate the need for complex crop growth models, which are currently used in data assimilation schemes and crop growth simulations. Thus, the prototype has great potential to become operational in the near future, providing a physiologically based perspective on crop growth and phenology at the landscape scale.

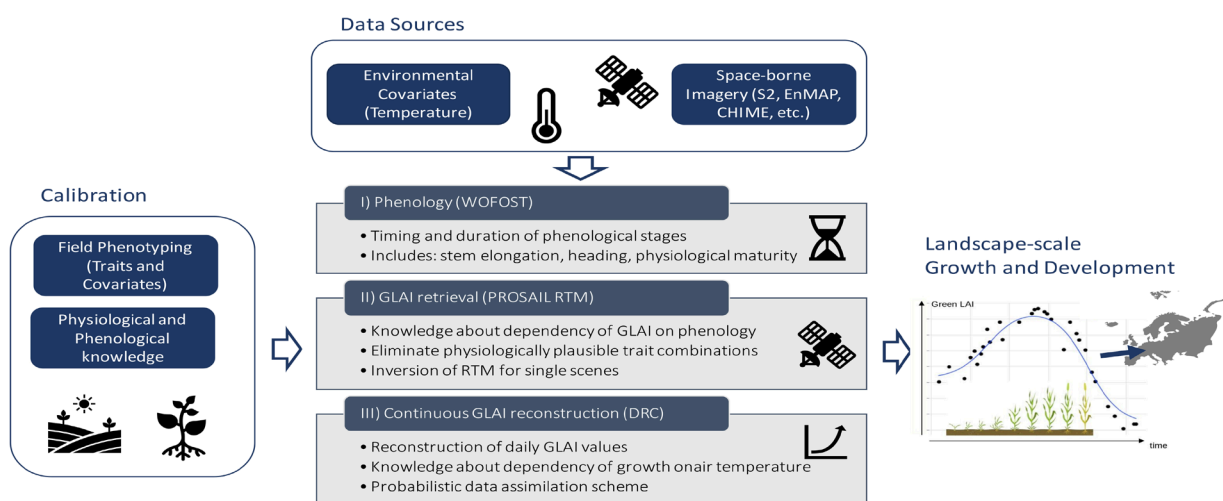


Figure 1 The proposed prototype uses spaceborne imagery, physiological and phenological knowledge from field phenotyping, and environmental covariates to provide an integrated view of crop growth and development at the landscape scale.

The accuracy of European dry heaths identification dependent on the feature reduction method of hyperspectral images

Anna Jarocińska¹, [Marlena Kycko](#)¹, Dominik Kopeć^{2,3}

¹ University of Warsaw, Faculty of Geography and Regional Studies, Department of Geoinformatics, Cartography and Remote Sensing, Poland

² University of Lodz, Faculty of Biology and Environmental, Department of Biogeography, Paleoecology and Nature Conservation, Poland

³ MGGP Aero sp. z o.o., Poland

Keywords: Feature Selection, Feature Extraction, Natura 2000 habitats, Random Forest

Challenge

One of the challenges for nature conservation is monitoring the conservation status of protected habitats and searching for new potential areas that should be protected. For these remote sensing can offer a solution. Identification of the Natura 2000 habitats including European dry heaths using remote sensing techniques was proven in previous studies (Jarocińska et al. 2023. Scientific Reports, 13, Marcinkowska-Ochtyra et al. 2018. Remote Sens., 10(4)). In very few studies feature selection method was used. An essential problem of classification is the optimization of data, time and costs of the process with the acquisition of high accuracy. It is also necessary to adjust the data and methods to the expected level of detail of the results. The aim of the study is to evaluate the accuracy of heath (code 4030) identification using different Feature Reduction methods. The study area was located in Poland in Lasy Janowskie, where is located Natura 2000 site. The heaths 4030 are shrub communities, with a small number of species and quite varied cover often associated with sandy substrate.

Methodology

The images were acquired on the 1st of June 2017 using two HySpex scanners from the NEO: VNIR-1800 (0.4–0.9 μm) with 182 spectral bands, and SWIR-384 (0.9–2.5 μm) with 288 bands. At the same time as the overflight were acquired ground truth polygons of the dry heaths and other vegetation types as a background. The airborne data were radiometrically, geometrically and atmospherically corrected. Based on the spectral reflectance Minimum Noise Fraction and Principal Component analysis were calculated. The first 30 PCA and MNF bands were extracted.

As a first step, ten polygons were randomly selected for each class to analyse the find the most separative layers. For each pixel in polygons, the values from spectral reflectance, MNF and PCA images were collected (Figure 1). To estimate the most separative bands Linear Discriminant Analysis was performed in the iterative mode (100 iterations). Based on the correctness rate and frequency of occurrence differentiating bands were selected. Based on the information six different datasets were created: (SB1) the most separative spectral bands for 4030 habitat estimated based on study area; (SB2) most separative spectral bands for 4030 habitat; (30MNF) 30 MNF bands; (MNF_FS) the most separative MNF bands; (30PCA) 30 MNF bands; (PCA_FS) the most separative PCA bands.

As a second step, the Random Forest algorithm was performed 50 times with stratified random sampling of reference polygons for each dataset and F1 values were calculated for the dry heaths class. Based on

the tests, it was checked whether the differences between F1 accuracy for each dataset were statistically significant. The results were visualised based on majority voting from 50 iterations.

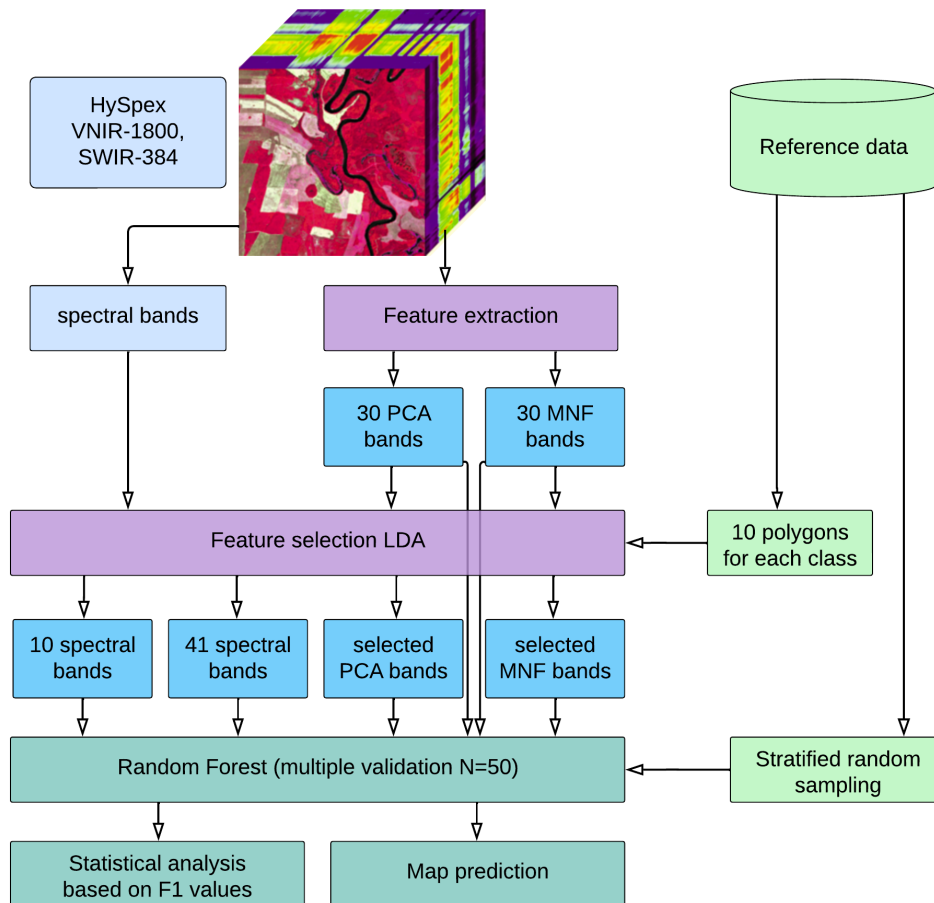


Figure 1 The scheme of the method

Expected results

The correctness rate values were very high. Based on LDA bands were found differentiating habitat 4030 from the background: 10 bands were the most separative based on previous studies and 41 were noticed as differentiating based on the study area. These bands were used to create two datasets. Also, the selected bands from MNF and PCA datasets were used in the classification.

The results of the analysis will be differences in the F1 accuracy between different datasets. Based on the differences in F1 accuracy and the dry heaths distribution maps it will be possible to determine whether feature extraction methods such as MNF and PCA provide high accuracies and whether the use of LDA feature selection increases accuracy.

Outlook for the future

Based on the results, it will be possible to define which feature reduction methods should be used to achieve the best accuracy in identifying dry heaths. Feature reduction methods are necessary to use for hyperspectral data, especially for the classification of large study areas. The idea is to reduce the amount of data and time for acquiring, preprocessing and classification while maintaining accurate classification results. Each feature reduction method is time-consuming, but in the case of multiple classifications it is profitable, and the selection or extraction based on the transformation of appropriate information can also increase classification accuracy.

Thank you to our sponsors and participants who were part of the 13th EARSeL.

PLATINO SPONSORS



GOLD SPONSORS



SILVER SPONSORS



BRONZE SPONSORS

